NUREG/CP–0076
SAND86–0618
R1, RD, RM
Printed August 1986

Proceedings of the Third Workshop on Containment Integrity

Toni Molina, Ruby Cochrell, Editors

Prepared by
Sandia National Laboratories
Albuquerque, New Mexico 87185 and Livermore, California 94550
for the United States Department of Energy
under Contract DE-AC04-76DP00789



Prepared for
U. S. NUCLEAR REGULATORY COMMISSION

SF2900Q(8-81)

8610290251 860831
PDR NUREG
CP-0076 R PDR

NOTICE

This report was prepared as an account of work sponsored by an agency of the United States Government. Neither the United States Government nor any agency thereof, or any of their employees, makes any warranty, expressed or implied, or assumes any legal liability or responsibility for any third party's use, or the results of such use, of any information, apparatus product or process disclosed in this report, or represents that its use by such third party would not infringe privately owned rights.

Available from

Superintendent of Documents
U.S. Government Printing Office
Post Office Box 37082
Washington, D.C. 20013-7982

and

National Technical Information Service
Springfield, VA 22161

NUREG/CP-0076
SAND86-0618
R1, RD, RM

PROCEEDINGS OF THE THIRD WORKSHOP ON CONTAINMENT INTEGRITY

Toni Molina* and Ruby Cochrell, Editors

August 1986

Sandia National Laboratories
Albuquerque, NM 87185
Operated by
Sandia Corporation
for the
U.S. Department of Energy

Prepared for
Division of Engineering Technology
Office of Nuclear Regulatory Research
U.S. Nuclear Regulatory Commission
Washington, DC 20555
Under Memorandum of Understanding DOE 40-550-75
NRC FIN A1249

The views and conclusions contained in this document are those of the authors and should not be interpreted as necessarily representing the official policies, either expressed or implied, of the United States Government or Sandia National Laboratories. Any use of trade names and trademarks in this publication is for descriptive purposes only and does not constitute endorsement by the U.S. Nuclear Regulatory Commission.

*Technadyne Engineering Consultants, Inc.

PREFACE

The Third Workshop on Containment Integrity was held in Washington, DC, on May 21-23, 1986. The workshop provided a forum for exchanging information on the integrity of containments at nuclear power plants. The behavior of containments during severe accidents was of primary interest to the over 140 participants. Thirty-seven oral presentations were made at the workshop. Written contributions that correspond to each of the presentations make up the body of this report. Sessions were held on (A) Containment Integrity as a Part of Risk Assessment, (B) Operational Experience and Its Relationship to Containment Performance During Accident Conditions, (C) Containment Environment and Loading Conditions During Severe Accidents, (D) Analysis/Testing of Containment Systems, Part 1, and (F) Analysis/Testing of Containment Systems, Part II.

The workshop was hosted by Sandia National Laboratories under the sponsorship of the U.S. Nuclear Regulatory Commission. Principal organizers for the workshop were W. A. von Riesemann of Sandia, T. D. Molina of Technadyne, and J. F. Costello of the U.S. Nuclear Regulatory Commission.

CONTENTS

Page

Program Schedule..... 1

List of Attendees..... 5

SESSION A--CONTAINMENT INTEGRITY AS A PART OF RISK ASSESSMENT... 13

Structural Reliability of Containment Structures, CANDU Nuclear Power Plants..... 15

The Modelling of a Negative-Pressure, Filtered-Vented Containment System as Part of a Probabilistic Safety Evaluation..... 33

Secondary Containment Building Loads Performance in Severe Accidents..... 43

Risk Analyses of the Ringhals Plants: Containment Behavior and Filtered Vent..... 55

Containment Integrity is a Major Part of KKL-Safety Systems PRA..... 69

Analysis of Strategies for Containment Venting in Case of Severe Accidents..... 85

Evaluation of Uncertainties in Risk Emanating From a Number of Severe Accident Issues..... 97

SESSION B--OPERATIONAL EXPERIENCE AND ITS RELATIONSHIP TO CONTAINMENT PERFORMANCE DURING ACCIDENT CONDITIONS... 127

New Belgian Position on Containment Leakage Testing..... 129

Alternative Containment Integrity Retesting Requirements and Local Leakage Calculation Methods..... 139

Preservice and Inservice Requirements for Containment Structures--A Status Report..... 153

Review of Containment Examination and Testing Requirements.. 167

Containment Systems Leakage Testing Requirements..... 173

Methods for Determining Integrated Leakage Rate Test Duration..... 185

Alternative Containment Integrity Test Methods, An Overview of Possible Techniques..... 205

CONTENTS (Continued)

Page

SESSION C--CONTAINMENT ENVIRONMENT AND LOADING CONDITIONS DURING SEVERE ACCIDENTS 221

Integrated Analysis of Core Debris Interactions and Their Effects on Containment Integrity Using the CONTAIN Computer Code 223

Hydrogen Deflagration Tests in Hydro-SC Facility 237

Scaling and Extrapolation of Hydrogen Distribution Experiments 251

On Two Aspects of Hydrogen Risk 267

Impact of a Hydrogen Ignition System on Degraded Core Accident in a Mark-III Containment 285

Hydrogen Burn Assessment With the CONTAIN Code 301

Containment Response and Radiological Release for a TMLB' Accident Sequence in a Large Dry Containment 317

SESSION D--ANALYSIS TESTING OF CONTAINMENT SYSTEMS, PART I 333

Plastic Analysis of Concrete Containment Structure 335

A Simplified Model for Concrete at Low Confining Pressures .. 351

Effect of High Temperature on Integrity of Concrete Containment Structures 367

Results of Large Scale Test of Discontinuity Region in a Prestressed Concrete Containment 377

Analytical Correlation and Interpretation of Full-Scale Containment Specimen Tests 391

Construction and Analysis of a 1/6th Scale Concrete Containment Model 407

An Evaluation of Structural Failure Modes for Prestressed Concrete Containments 429

The Influence of Non-Linearity and Foundation Behaviour on Containment Integrity 445

CONTENTS (Continued)

Page

SESSION E--ANALYSIS/TESTING OF CONTAINMENT SYSTEMS, PART II..... 461

Structural Analysis of a Japanese BWR MARK-I Containment Under Internal Pressure Loading..... 463

Crack Propagation in High Strain Regions of a Steel Containment..... 479

Failure Mechanisms for LWR Steel Containment Buildings Subject to Severe Accident Loadings..... 495

Failure Pressure and Failure Mode of the Latest Type of German PWR Containments..... 511

Analysis of Severe Accidents and Estimates of Ultimate Loading Capacity of the Steel Containment..... 527

Small Scale Model for Experimental Investigations of the Dynamic Behaviour of Spherical Steel Containments..... 549

Leakage Potential Through Mechanical Penetrations in a Severe Accident Environment..... 557

Leak Behavior Through EPAs Under Severe Accident Conditions. 569

CONTAINMENT INTEGRITY

May 21-23, 1986

Washington Marriott
Washington, D.C.

Hosted by: Sandia National Laboratories
Sponsored by: U.S. Nuclear Regulatory Commission

Third Workshop on CONTAINMENT INTEGRITY

Conference Organizers:

James F. Costello, U.S. Nuclear Regulatory Commission
Walter A. von Riesemann, Sandia National Laboratories
Toni D. Molina, Sandia National Laboratories

PROGRAM SCHEDULE

TUESDAY, MAY 20

6:30 - 8:00 p.m. Registration

WEDNESDAY, MAY 21

7:30 - 8:30 a.m. Registration

8:30 - 8:50 a.m. Opening of the Workshop

8:50 - 11:20 a.m. **SESSION A**

CONTAINMENT INTEGRITY AS A PART OF RISK ASSESSMENT (p.13)

Chairpersons: Joseph Murphy — U.S. Nuclear Regulatory Commission
Michael Bohn — Sandia National Laboratories

"Containment Structural Reliability Analysis in Ontario Hydro CANDU Nuclear Power Plants" (p.15)
M.A. Osman — Ontario Hydro, Canada

"The Modelling of a Negative-Pressure, Filtered-Vented Containment System as Part of a Probabilistic Safety Evaluation" (p.33)
K. S. Dinnie — Ontario Hydro, Canada

"Secondary Containment Building Loads and Performance in Severe Accidents" (p.43)
R. Denning, P. Cybulskis — Battelle Columbus Laboratory

"Risk Analyses of the Ringhals Plants: Containment Behaviour and Filtered Vent" (p.55)
R. Espefaelt, L. Gunsell, G. Loewenhielm — Swedish State Power Board
G. Kaiser, P. Fulford — NUS Corporation

"Containment Integrity is a Major Part of KKL-Safety Systems PRA" (p.69)
T. Schaub — Kernkraftwerk Leibstadt
H. Haenni — Motor Columbus, Switzerland

"Analysis of Strategies for Containment Venting in Case of Severe Accidents" (p.85)
K. Bracht, M. Tiltmann — Gesellschaft fuer Reaktorsicherheit, Federal Republic of Germany

"Evaluation of Uncertainties in Risk Emanating from a Number of Severe Accident Issues" (p.97)
A. S. Benjamin — Sandia National Laboratories, Albuquerque, NM
G. R. Boyd — Safety & Reliability Optimization Services, Knoxville, TN
W. B. Murfin — Technadyne Engineering Consultants, Albuquerque, NM
D. M. Kunsman — Sandia National Laboratories, Albuquerque, NM

11:20 - 11:50 p.m. Session A Discussion

12:00 - 1:30 p.m. Lunch

1:40 - 4:30 p.m. **SESSION B**

OPERATIONAL EXPERIENCE AND ITS RELATIONSHIP TO CONTAINMENT PERFORMANCE DURING ACCIDENT CONDITIONS (p.127)

Chairpersons: Frank Jape — U.S. Nuclear Regulatory Commission
Patrick Ervin — Stone & Webster

"New Belgian Position On Containment Leakage Testing" (p.129)
B. DeBoeck — Vincotte, Belgium

"Alternative Containment Integrity Retesting Requirements and Local Leakage Testing Methods" (p.139)
J. Glover — Commonwealth Edison

"Preservice and Inservice Requirements for Containment Structures — A Status Report" (p.153)
R. Sammataro — General Dynamics, Electric Boat Division

"Review of Containment Examination and Testing Requirements" (p.167)
J. Cook — Idaho National Engineering Laboratory

Pending Revisions to ANS 56.8-81 *"Containment Systems Leakage Testing Requirements"* (p.173)
T. Brown — Wiss, Janney, Elstner Associates

"Methods for Determining Integrated Leakage Rate Test Duration" (p.185)
L. Young — Bechtel Power Corporation

"Alternative Containment Integrity Test Methods" (p.205)
B. Spletzer — Sandia National Laboratories

4:30 - 5:00 p.m. Session B Discussion

6:00 - 7:00 p.m. No-host Reception

THURSDAY, MAY 22
8:30 - 11:20 a.m. **SESSION C**

CONTAINMENT ENVIRONMENT AND LOADING CONDITIONS DURING SEVERE ACCIDENTS (p.221)

Chairpersons: Jocelyn Mitchell — U.S. Nuclear Regulatory Commission
Kenneth Bergeron — Sandia National Laboratories

"Integrated Analysis of Fuel-Concrete-Coolant Interactions and Their Effects on Containment Integrity Using the CONTAIN Code: Current and Proposed Capabilities" (p.223)
D. Carroll — Sandia National Laboratories

"Hydrogen Deflagration Tests in Hydro-SC Facility" (p.237)
M. Carcassi, F. Fineschi — Universita di Pisa, Italy
G. Lombardi — ENEA, Italy

"Scaling and Extrapolation of Hydrogen Distribution Experiments" (p.251)
H. Karwat - Technical University, Munich, Federal Republic of Germany

"About Two Aspects of Hydrogen Risk" (p.267)
A. Forestier, S. Goldstein — Commissariat a l'Energie Atomique, France

"Impact of a Hydrogen Ignition System on Degraded Core Accident in a Mark-III Containment" (p.285)
C. Centanaro — Ansaldo Divisione Impianti, Italy

"Hydrogen Burn Assessment With the CONTAIN Code" (p.301)
H. van Rij — Netherlands Energy Research Foundation

"Containment Response and Radiological Release for a TMLB' Accident Sequence in a Large Dry Containment" (p.317)
R. Gasser — Sandia National Laboratories
P. Bieniarz — Risk Management Associates
J. Tills — Jack Tills & Associates

11:20 - 11:50 a.m. Session C Discussion

12:00 - 1:30 p.m. Lunch

1:40 - 4:30 p.m. **SESSION D**

ANALYSIS/TESTING OF CONTAINMENT SYSTEMS, PART I (p.333)

Chairpersons: Hans Ashar — U.S. Nuclear Regulatory Commission
Joseph Ucciferro — United Engineers

"Plastic Analysis of Concrete Containment Structure" (p.335)
A. Hindy, A. Danay — Ontario Hydro, Canada

"A Simplified Model For Concrete At Low Confining Pressures" (p.351)
H. Hibbitt — Hibbitt, Karlsson & Sorensen, Inc.

"Effect of High Temperature on Integrity of Concrete Containment Structures" (p.367)
P. Bhat — Ontario Hydro, Canada

"Results of Large Scale Test of a Discontinuity Region in a Prestressed Concrete Containment" (p.377)
N. Hanson, D. Schultz, J. Roller — Construction Technology Laboratories

"Analytical Correlation and Interpretation of Full-Scale Containment Specimen Tests" (p.391)
Y. Rashid, R. Dunham — ANATECH International Corporation
H. Tang — Electric Power Research Institute

"Construction and Analysis of a 1/6th Scale Concrete Containment Model" (p.407)
D. Horschel, J. Jung — Sandia National Laboratories

"An Evaluation of Structural Failure Modes for Prestressed Concrete Containments" (p.429)
P. Shunmugavel, O. Gurbuz — Bechtel Power Corporation

"The Influence of Non-Linearity and Foundation Behaviour on Containment Integrity" (p.445)
J. Evans, P. Keogh — Ove Arup & Partners, United Kingdom

4:30 - 5:00 p.m. Session D Discussion

FRIDAY, MAY 23
8:30 - 11:20 a.m.

SESSION E

ANALYSIS/TESTING OF CONTAINMENT SYSTEMS, PART II (p.461)

Chairpersons: James Costello — U.S. Nuclear Regulatory Commission
Hiroshi Akiyama — University of Tokyo

"Structural Analysis of a Japanese BWR MARK-1 Containment Under Internal Pressure Loading" (p.463)
J. Isozaki, K. Soda, S. Miyazono — Japan Atomic Energy Research Institute

"Crack Propagation in High Strain Regions of a Steel Containment" (p.479)
L. Greimann, F. Fanous — Ames Laboratory, Iowa State University

"Failure Mechanisms for LWR Steel Containment Buildings Subject to Severe Accident Loadings" (p.495)
D. Clauss — Sandia National Laboratories

"Failure Pressure and Failure Mode of the Latest Type of German PWR Containments" (p.511)
R. Krieg, B. Goeller, G. Messemer, E. Wolf — Kernforschungszentrum Karlsruhe, Federal Republic of Germany

"Analysis of Severe Accidents and Estimates of Ultimate Loading Capacity of the Steel Containment" (p.527)
A. Hoefler, F. Heuser — Gesellschaft fuer Reaktorsicherheit, Federal Republic of Germany

"Small Scale Model for Experimental Investigations of the Dynamic Behaviour of Spherical Steel Containments" (p.549)
E. Wolf, B. Goeller — Kernforschungszentrum Karlsruhe, Federal Republic of Germany

"Leakage Potential Through Mechanical Penetrations in a Severe Accident Environment" (p.557)
L. Koenig — Sandia National Laboratories

"Leak Behavior Through EPAs Under Severe Accident Conditions" (p.569)
J. Keck, F. Thome — Sandia National Laboratories

11:20 - 11:50 p.m. Session E Discussion

11:50 - 12:10 p.m. Closing Comments

CONFERENCE HOTEL: Washington Marriott
22nd and M Streets, NW
Washington, D.C. 20037
Telephone (202) 872-1500

The proceedings of this workshop will appear as NUREG/CP-0076.

THIRD WORKSHOP ON CONTAINMENT INTEGRITY

HOSTED BY SANDIA NATIONAL LABORATORIES

Washington, DC
May 21-23, 1986

LIST OF ATTENDEES

Tom Ahl
Chicago Bridge & Iron
800 Jorie Blvd.
Oak Brook, IL 60521

Hiroshi Akiyama
University of Tokyo
Engineering Research Institute
Yayoi, Bunkyo-ku
Tokyo
Japan

N. Anderson
U. S. Nuclear Regulatory Commission
Mail Stop 144
Washington, DC 20555

Gunter Arndt
U. S. Nuclear Regulatory Commission
Office of Research
Mail Stop 1130 SS
Washington, DC 20555

Leonardo Arru
ENEA-DISP
via Vitaliano Brancati 68
00166 Roma
Italy

Hans Ashar
U. S. Nuclear Regulatory Commission
Mechanical/Structural Engineering Branch
Washington, DC 20555

Bernard Barbe
Commissariat a l'Energie Atomique
CEN-FAR
92260 Fontenay-Aux-Roses Cedex
France

Peter Barr
United Kingdom Atomic Energy Authority
Safety & Reliability Directorate
Warrington, WA3 4NE
United Kingdom

Richard Barrett
U. S. Nuclear Regulatory Commission
Mail Stop 266
Washington, DC 20555

Peter Beament
Virginia Power Company
P. O. Box 26666
Richmond, VA 23261

J. C. Belote
U. S. Nuclear Regulatory Commission
Washington, DC 20555

A. S. Benjamin
Division 6411
Sandia National Laboratories
Albuquerque, NM 87185

Kenneth Bergeron
Division 6449
Sandia National Laboratories
Albuquerque, NM 87185

Param Bhat
Ontario Hydro, H17
700 University Ave.
Toronto, Ontario
M5G1X6 Canada

Storrs Bigelow
General Electric Company
P. O. Box 1072
Schenectady, NY 12301

Cheryl Bly
International Energy Associates, Limited
2600 Virginia Ave. NW
Washington, DC 20037

Michael Bohn
Division 6412
Sandia National Laboratories
Albuquerque, NM 87185

Ted Brown
Wiss, Janney, Elstner Associates
330 Pfingsten Rd.
Northbrook, IL 60062

Jack Burns
U. S. Nuclear Regulatory Commission
Structural Engineering Section
Washington, DC 20555

Daniel Carroll
Division 6449
Sandia National Laboratories
Albuquerque, NM 87185

Carlo Centanaro
Ansaldo S.p.A. Divisione Impianti
via Gabriele D'Annunzio 113
16121 Genova
Italy

Kenneth Chao
Consumer Powers Company
1945 W. Parnall Road
Jackson, MI 49201

John Chen
U. S. Nuclear Regulatory Commission
Mail Stop 266
Washington, DC 20555

Nilesh Chokshi
U. S. Nuclear Regulatory Commission
Mail Stop 144
Washington, DC 20555

J. Chung
U. S. Nuclear Regulatory Commission
631 Park Ave.
King of Prussia, PA 19406

Dave Clauss
Division 6442
Sandia National Laboratories
Albuquerque, NM 87185

Jeffrey Cook
EG&G Idaho, Inc.
P. O. Box 516
Idaho Falls, ID 83415

Carl Costantino
Brookhaven National Laboratories
Upton, NY 11973

James Costello
U. S. Nuclear Regulatory Commission
Mechanical/Structural Engineering Branch
Washington, DC 20555

Robert Curtis
U. S. Nuclear Regulatory Commission
Mail Stop 1130 SS
Washington, DC 20555

Peter Cybulskis
Battelle Columbus Laboratory
505 King Ave.
Columbus, Ohio 43201

Dirk Dahlgren
Department 6440
Sandia National Laboratories
Albuquerque, NM 87185

Robert Dameron
ANATECH International Corp.
3344 N. Torrey Pines Court
Suite 320
La Jolla, CA 92037

Marwan Daye
Bechtel Power Corp.
15740 Shady Grove Rd.
Gaithersburg, MD 20877

Moni De
U. S. Nuclear Regulatory Commission
Mail Stop H-1016
Washington, DC 20555

Benoit DeBock
Association Vincotte
157 Ave. Du Roi
1060 Brussels
Belgium

Keith Dinnie
Ontario Hydro
700 University Ave.
Toronto, Ontario
M5G1X6 Canada

Rod Eagles
New Brunswick Power
Box 10
Lepreau New Brunswick
EOG2HO Canada

Farouk Eltawila
U. S. Nuclear Regulatory Commission
7920 Norfolk Ave.
Bethesda, MD

Patrick Ervin
Stone & Webster
P. O. Box 5406
Denver, CO 80013

Ralf Espefaelt
Swedish State Power Board
S-16287 Vallingby
Sweden

F. Fanous
Iowa State University
325 Town Engineering Building
Ames, Iowa 50011

Fabio Fineschi
Universita' di Pisa
Dipartimento Di Costruzioni
Meccaniche E Nucleari
via Diotisalvi 2
56100 Pisa
Italy

M. Fleishman
U. S. Nuclear Regulatory Commission
Mail Stop 1130 SS
Washington, DC 20555

A. Forestier
Commissariat a l'Energie Atomique
Centre D'Etudes Nuclearies
de Fontenay-Aux Roses
B P no. 6
92265 Fontenay-Aux-Roses Cedex
France

P. J. Fulford
NUS Corporation
910 Colpper Rd.
Gaithersburg, MD 20898

Philip J. Galanti
Bechtel Power Corporation
P. O. Box 3965
San Francisco, CA 94119

Ron Gasser
Division 6411
Sandia National Laboratories
Albuquerque, NM 87185

Nahas Georges
Socotes Industrie
1 Avenue du Parc
78180 Montigny Le Bretonneux
France

J. Giitter
U. S. Nuclear Regulatory Commission
Mail Stop 3302
Washington, DC 20555

James Glover
Commonwealth Edison
72 W. Adams
Chicago, IL 60603

Joseph Golla
U. S. Nuclear Regulatory Commission
302B Saybrook Lane
Wallingford, PA 19086

H. Graves
U. S. Nuclear Regulatory Commission
Mail Stop 1130 SS
Washington, DC 20555

Lowell Greimann
Ames Laboratory
Iowa State University
Ames, Iowa 50010

J. S. Guo
U. S. Nuclear Regulatory Commission
Mail Stop P-1132
Washington, DC 20555

A. H. Hadjian
Bechtel Power Company
12440 Imperial Highway
Norwalk, CA 90650

H. Haenni
Motor Columbus
Parkstr. 27
5401 Baden
Switzerland

Lyman Heller
U. S. Nuclear Regulatory Commission
Mail Stop 144
Washington, DC 20555

Dave Hibbitt
Hibbitt, Karlsson & Sorensen
100 Medway St.
Providence, Rhode Island 02906

Howard Hill
Bechtel Power Company
P. O. Box 3965
San Francisco, CA 94119

Aly Hindy
Ontario Hydro
700 University Ave.
Toronto, Ontario
M5G1X6 Canada

Malcolm Hinley
National Nuclear Corp.
Booths Hall Chelford Rd.
Knutsford
Cheshire WA16 8Q2
United Kingdom

A Hoefler
Gesellschaft fuer Reaktorsicherheit
Schwertnergasse 1
5000 Köln
Federal Republic of Germany

Dan Horschel
Division 6442
Sandia National Laboratories
Albuquerque, NM 87185

Dean Houston
U. S. Nuclear Regulatory Commission
ACRS, Mail Stop H-106
Washington, DC 20555

E. G. Igne
U. S. Nuclear Regulatory Commission
ACRS, Mail Stop H-1016
Washington, DC 20555

Toshikuni Isozaki
Japan Atomic Energy Research Institute
Tokai-mura, Ibaraki-ken
319-11 Japan

Frank Jape
U. S. Nuclear Regulatory Commission
101 Marietta St.
Atlanta, GA 30323

J. Jemielewski
Motor-Columbus Consulting Engineers
Parkstr. 27
5401-Baden
Switzerland

Joe Jung
Division 1524
Sandia National Laboratories
Albuquerque, NM 87185

Helmut Karwat
Technical University Munich
8046 Garching
Federal Republic of Germany

Roger Kenneally
U. S. Nuclear Regulatory Commission
Mail Stop 1130 SS
Washington, DC 20555

Peter Keogh
Ove Arup & Partners
13 Fitzroy Street
London W1P 6BQ
United Kingdom

Don Kirkpatrick
U. S. Nuclear Regulatory Commission
Mail Stop EW/W 507
Washington, DC 20555

Larry Koenig
Division 6442
Sandia National Laboratories
Albuquerque, NM 87185

Philip Kohn
Wisconsin Electric Power Company
231 W. Michigan, Room 500
Milwaukee, WI 53201

Rolf Krieg
Kernforschungszentrum Karlsruhe
Postfach 3640
7500 Karlsruhe
Federal Republic of Germany

P. T. Kuo
U. S. Nuclear Regulatory Commission
Mail Stop P-712
Washington, DC 20555

John Lane
U. S. Nuclear Regulatory Commission
Mail Stop 266
Washington, DC 20555

R. E. Lipinski
U. S. Nuclear Regulatory Commission
Mail Stop P-712
Washington, DC 20555

C. Lomas
Central Electricity Generating Board
Booths Hall
Knutsford, Cheshire WA16 8QG
United Kingdom

Giovanni Lombardi
ENEA
via Diotisalvi 2
56100 Pisa
Italy

Dan Lurie
U. S. Nuclear Regulatory Commission
Mail Stop 7602 NMBB
Washington, DC 20555

Al Marchertas
Argonne National Laboratory
9700 S. Cass Ave.
Argonne, IL 60439

Marty Marugg
American Nuclear Insurers
The Exchange
270 Farmington Ave.
Farmington, CT 06032

Tim Margulies
U. S. Nuclear Regulatory Commission
Mail Stop 1130 SS
Washington, DC 20555

Mario Mazza
Ontario Hydro, H17F23
700 University Ave.
Toronto, Ontario
M5G1X6 Canada

Craig McWhorter
Southern Company Services
P. O. Box 2625
Birmingham, AL 35202

Peter Medina
Ontario Hydro
Attn: RMED A2F1
700 University Ave.
Toronto, Ontario
M5G1X6 Canada

Jim Metcalf
Stone & Webster
245 Summer St.
Boston, MA 02107

Alain Millard
CEA/DEMT
Cen Saclay
B P No. 2
91191 Gif Sur Yvette Cedex
France

Charles Miller
Brookhaven National Laboratories
Upton, NY 11973

Jocelyn Mitchell
U. S. Nuclear Regulatory Commission
Mail Stop 1130 SS
Washington, DC 20555

Glenn Morris
Tennessee Valley Authority
Lookout Place 5S123D
Chattanooga, TN 37401

Joseph Murphy
U. S. Nuclear Regulatory Commission
Mail Stop 1130 SS
Washington, DC 20555

Stephanie Murphy
Nuclear Information
1616 P St., Suite 160 NW
Washington, DC 20036

Dan Naus
Oak Ridge National Laboratory
P. O. Box Y, Building 9204-1
Oak Ridge, TN 37831

P. K. Niyogi
U. S. Nuclear Regulatory Commission
Mail Stop 1130 SS
Washington, DC 20555

Allen Notafrancesco
U. S. Nuclear Regulatory Commission
7920 Norfolk Ave.
Mail Stop P-1114
Bethesda, MD

Mohamed A. Osman
Ontario Hydro, H17F23
700 University Ave.
Toronto, Ontario
M5G1X6 Canada

Giampiero Orsini
ENEA-DISP
via Vitaliano Braucati 48
00144 Rome
Italy

A. J. Philippacopoulos
Brookhaven National Laboratories
Upton, NY 11973

Giuseppe Pino
ENEA-DISP
via Vitaliano Braucati 48
00144 Rome
Italy

D. Pyatt
U. S. Nuclear Regulatory Commission
Mail Stop 5650 NL
Washington, DC 20555

M. S. Quraisipi
Atomic Energy of Canada
Sheridan Park Research Community
Mississauga, Ontario
L5K1B2 Canada

Y. R. Rashid
ANATECH International Corp.
3344 N. Torrey Pines Court
Suite 1320
La Jolla, CA 92037

Terry Renton
Testing, Engineering, & Research Services
3009 E. Knoxville
Broken Arrow, OK 74014

Frank Rinaldi
U. S. Nuclear Regulatory Commission
Mail Stop 316
Washington, DC 20555

Zoltan Rosztoczy
U. S. Nuclear Regulatory Commission
Mail Stop 266
Washington, DC 20555

Robert Sammataro
General Dynamics
Nuclear Eng./Dept. 474
Eastern Point Road
Groton, CT 06340

Theo Schaub
Kernkraftwerk Leibstadt
4353 Leibstadt
Switzerland

Donald Schultz
Construction Tech. Laboratories
5420 Old Orchard Rd.
Skokie, IL 60077

Rick Sherry
JAYCOR
P. O. Box 85154
San Diego, CA 92138

Kelvin Shiu
Brookhaven National Laboratories
Building 130
Upton, NY 11030

P. Shunmugavel
Bechtel Power Corp.
12440 E. Imperial
Norwalk, CA 90650

C. P. Siess
ACRS/U. S. Nuclear Regulatory Commission
805 Hamilton Drive
Champaign, IL 61820

Barry Spletzer
Division 6447
Sandia National Laboratories
Albuquerque, NM 87185

John Stevenson
Stevenson & Associates
9217 Midwest Ave.
Cleveland, OH 44125

William Suslick
Duke Power Company
P. O. Box 33189
Charlotte, NC 28210

Steve Swartz
Illinois Department of Nuclear Safety
1035 Outer Park Dr.
Springfield, IL 62704

C. P. Tan
U. S. Nuclear Regulatory Commission
Mail Stop P-1132
Washington, DC 20555

H. T. Tang
EPRI
3412 Hillview Ave.
Palo Alto, CA 94303

Joe Tapia
U. S. Nuclear Regulatory Commission
611 Ryan Plaza, Suite 1000
Arlington, TX 76010

M. Tiltmann
Gesellschaft fuer Reaktorsicherheit
Schwertnergasse 1
5000 Köln
Federal Republic of Germany

Charles Tinkler
U. S. Nuclear Regulatory Commission
Mail Stop 416
Washington, DC 20555

Iain Todd
HM Nuclear Installations Inspectorate
Thames House South
Millbank
London SW1P 4QJ
United Kingdom

A. N. Tse
U. S. Nuclear Regulatory Commission
Mail Stop 1130 SS
Washington, DC 20555

Joseph Ucciferro
United Engineers & Constructors, Inc.
305 17th St.
Philadelphia, PA 19101

H. M. van Rij
Netherlands Energy Research Foundation
ECN
P. O. Box 1
1755 ZC Petten
The Netherlands

Walter von Riesemann
Division 6442
Sandia National Laboratories
Albuquerque, NM 87185

Robert Walker
Grove Engineering
P. O. Box 720
Washington Grove, MD

Thomas Walker
U. S. Nuclear Regulatory Commission
Mail Stop 1130 SS
Washington, DC 20555

H. B. Wang
U. S. Nuclear Regulatory Commission
EWS 305B
Washington, DC 20555

Randy Weatherby
Division 1521
Sandia National Laboratories
Albuquerque, NM 87185

Michael Weinstein
American Nuclear Insurers
The Exchange
270 Farmington Ave.
Farmington, CT 06032

Peter Wiebe
Ontario Hydro
700 University Ave.
Toronto Ontario
M5G1X6 Canada

Ed Yachimak
U. S. Nuclear Regulatory Commission
Mail Stop EWW 332
Washington, DC 20555

SESSION A

CONTAINMENT INTEGRITY AS A PART OF RISK ASSESSMENT

STRUCTURAL RELIABILITY OF CONTAINMENT STRUCTURES - CANDU NUCLEAR POWER PLANTS

M.A. Osman, Structural Design Engineer - Specialist
Ontario Hydro, Toronto, Canada

ABSTRACT

This paper identifies three types of structural failure for the containment, based on the definition of failure as "the termination of the ability to perform a required function".

It describes a proposed methodology for modelling structural reliabilities for containment and methods to improve such reliabilities through design, specifications and construction controls.

1.0 INTRODUCTION

Canadian Deuterium Uranium (CANDU) multiunit Nuclear Power Plants have the containment typically in the form of a Vacuum Building (Structure), connected through reinforced concrete ducts to the Reactor Buildings. In case of a loss of coolant accident (LOCA), the released radio-nuclides will be drawn by the Vacuum Building (VB), through the ducts, without being released to the environment.

Thus the containment structures represent a major safety mechanism against LOCA. Because traditional reliability models cannot be used to quantify structural reliability, a methodology by which this can be done is being proposed.

Reliability will be considered here as the compliment of probability of failure. Failure is defined as "the termination of the ability to perform a required function".

2.0 MODES OF FAILURE

Containment structures will be considered as having a failure when one or more of its components has a structural failure. A component has structurally failed if it

(a) has a structural collapse;

(b) gets deformations, large enough that one or more of the enclosed systems is rendered inoperative or

(c) cracks to an extent allowing leakage beyond specified limits.

A component could have structural deformation failure, without necessarily having extensive cracking or a structural collapse. Cracks, causing a leakage type structural failure may not necessarily be accompanied by "deformation failure" or "structural collapse". However, a "structural collapse" is assumed to have got both "cracks beyond specified limits" as weld as "deformation failure". It also renders all equipment included

not functioning, i.e., what is called common mode. Due to continuity of the containment envelope, the whole containment is rendered as failed if one of its components has a structural collapse.

3.0 RELIABILITY MODELS

3.1 General Reliability

For reliability modelling, we will model the probabilities of failure and have the reliability values as being their compliments or 1.0 - P_f.

The basic definition of probability of failure is "the termination of the ability to perform a required function".

As such, it can be defined as the total probability of a "loading" exceeding the "available resistance".

The "loading", in this case, may be forces, pressures, temperatures, etc.

The "resistance" is either mechanical (strength), resistance to leakage or resistance to deformation, etc.

In essence, then, the probability of failure can be illustrated as the area under the convolution curve of the probability

$$P_f = \int_{-\infty}^{\infty} F_R(x)\, f_S(x)\, dx$$

$$= \int_{-\infty}^{\infty} \left[\int_{-\infty}^{S} f_R(r)\, dr \right] f_S(s)\, d_S$$

where f_S and F_S are probability density function (PDF) and cumulative distribution function (CDF) of load effect,
f_R and F_R are PDF and CDF of the resistance and
P_f = Probability of failure which is used in the proposed PDF models shown in Figures 2 to 5.

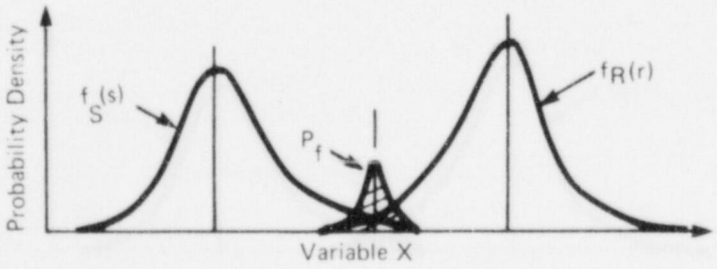


FIGURE 1

This is just a simplification of the process. Many more sophisticated forms exist like the Rainflow Algorithm, Peak Counting Method, Level Crossing Count Method, Mean Crossing Peak Count Method (Zero Crossing Method), Range Count Method, etc., particularly under repeated loading and especially when there are load reversals [Reference 2].

Depending on how much the detail analysis is required, the loading model could be a simple Gaussian (Normal) distribution, or a Weibull or Frechet, if biased. However, in almost all loading models, the loading is from components that are probabilistically additive [$P(A \cap B \cap C)$ etc.], which require more analysis of the load dependencies.

In containment structures for CANDU Nuclear Power plants, the following probabilistic models of failure are considered.

(a_1) Structural Collapse - Concrete Structures

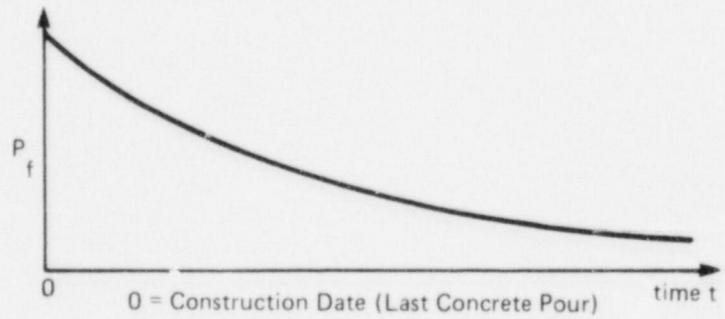


FIGURE 2

(a_2) Structural Collapse - Steel Structures

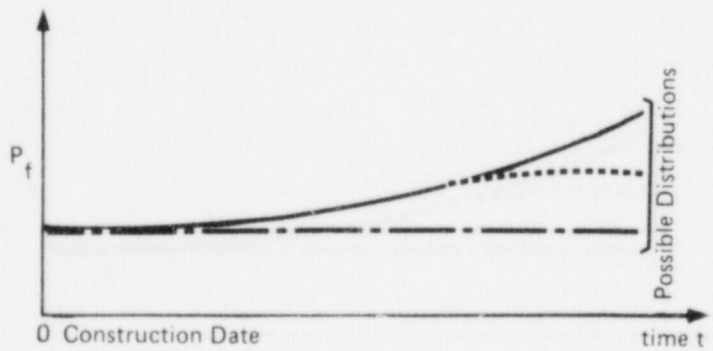


FIGURE 3

Figure 2 represent concrete structures with strength increasing with time to beyond t_e, the economic design life of the plant (t_e is commonly 30 to 40 years).

Figure 3 is for a metallic material, with only slight probabilistic failure increase (deterioration) beyond the initial value "t_o". It could even be constant, or returning almost to its original reliability level, with some preventive maintenance. Most of the decrease in reliability here is due to corrosion and loss of torquing in connections.

Normally, very few structures in CANDU containment are of this category. Therefore, its analysis would not be treated in detail.

(b_1) Serviceability Limits - Deformation



FIGURE 4

Figure 4 shows the probabilities related to deformation beyond serviceability limits. Mostly, in containment, this is due to creep of concrete material. It may or may not be due to load variance, although the seismic forces (Design Basis Earthquake) may have a contributory effect.

(c) Leakage Failure

Figure 5 represents the "recurrence" phenomenon, where the probability of failure increases to a point where the maintenance starts ($t_{i,s}$) and then the curve is not continuous (during maintenance window, from $t_{i,s}$ to $t_{i,e}$).

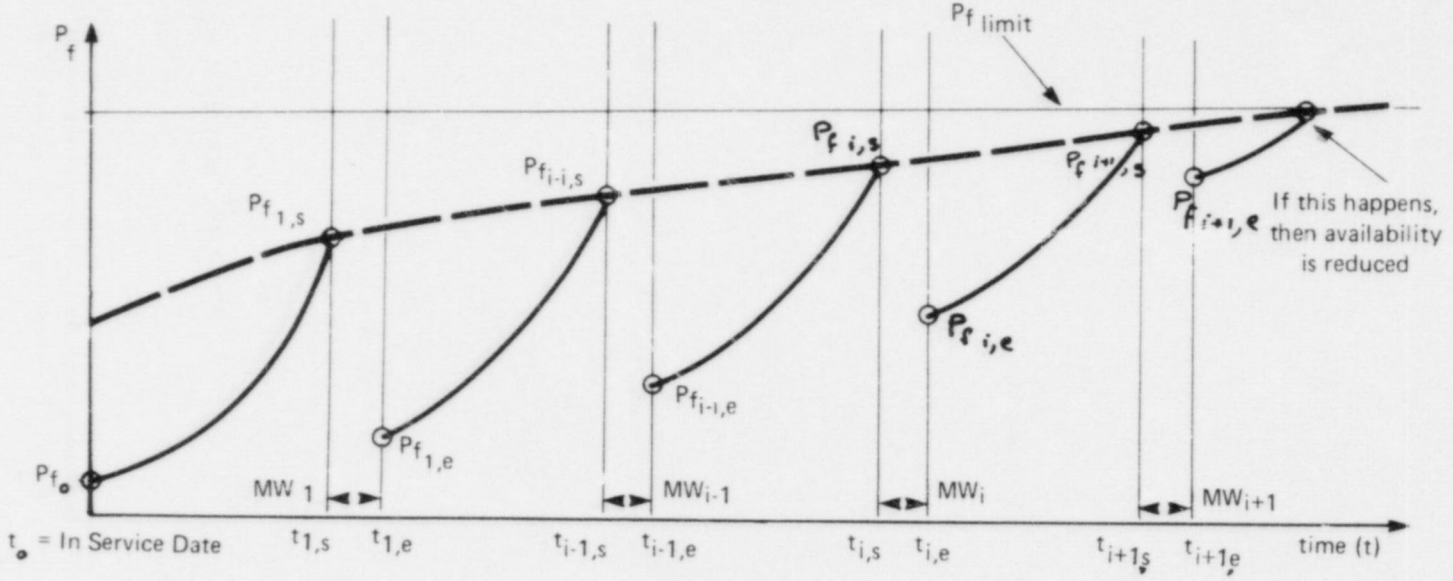

P_f
$P_{f\ limit}$
$P_{f\ 1,s}$
$P_{f\ i-i,s}$
$P_{f\ i,s}$
$P_{f\ i+1,s}$
$P_{f\ i+1,e}$
If this happens, then availability is reduced
$P_{f\ i,e}$
$P_{f\ i-i,e}$
$P_{f\ 1,e}$
P_{f_o}
MW 1
MW_{i-1}
MW_i
MW_{i+1}
t_o = In Service Date
$t_{1,s}$
$t_{1,e}$
$t_{i-1,s}$
$t_{i-1,e}$
$t_{i,s}$
$t_{i,e}$
t_{i+1_s}
t_{i+1_e}
time (t)

FIGURE 5

As the unit ages, $P_{f_{i,e}}$, in general, cannot be maintained to the same previous low level, so, we get

$$P_{f_{i,e}} > P_{f_{i-1,e}}, \text{ for any value of } i.$$

But the corrections required, for efficiency, or acceptable performance criteria, has to be maintained, i.e., $P_{f_{i,s}}$ has to be within the limits of requirements, i.e.,

$$P_{f_{i,s}} < P_{f_{lim}} \text{ for all values of } i.$$

We have the maintenance effect also decreasing with age, i.e.,

$$P_{f_{i,s}} - P_{f_{i,e}} < P_{f_{i+1,s}} - P_{f_{i+1,e}}$$

The lower bound for P_f is determined by achievable maintenance criteria, while the upper bound is determined by economic and performance requirements. Also these could be the limits imposed by the licensing authorities.

Maintenance is mainly to be during a scheduled outage, i.e., a preventive maintenance (PM). Some maintenance, mostly corrective (CM) could be on-line, which then reduces the rate of deterioration.

In general "Time to Maintenance", TTM_i or $(t_{i,s} - t_{i-1,e})$ is not constant and the "Maintenance Window" (MW_i) or $(t_{i,e} - t_{i,s})$ is variable.

The mathematical formulations for each of these structural reliability models may look different, but noting the type of failure and the affected component(s), we find, basic similarities affecting them.

Obviously for operating any plant, the selection of time to maintenance and maintenance duration should enable the owner to minimize his costs. This means that TTM_i should be maximized, and MW_i is to be minimized. However, MW_i cannot be reduced below a limit imposed by construction/maintenance operational constraints, e.g., getting temporary platforms, opening temporary sealing hatches, curing of sealants, etc. Therefore, a practical bottom limit is MW, which includes both structural as well as other maintenances in the same maintenance window, i.e., even for this structural model $t_{i,e} - t_{i,s} \sim MW \sim$ constant - an operational experience.

4.0 MODELS FOR RELIABILITY EVALUATION

4.1 Analytical Models

(i) We notice from the subjective distribution, which is a highly reliable representation of these probabilities, based on the known factors affecting each, that they all conform with the two parameter exponential upper band model [References 2 and 9].

Namely, the probability density function (PDF) is:

$f_X(x) = \lambda \exp [-\lambda (x-a)]$, for $a \leq x \leq \infty$

$= 0.0$, for $x < a$

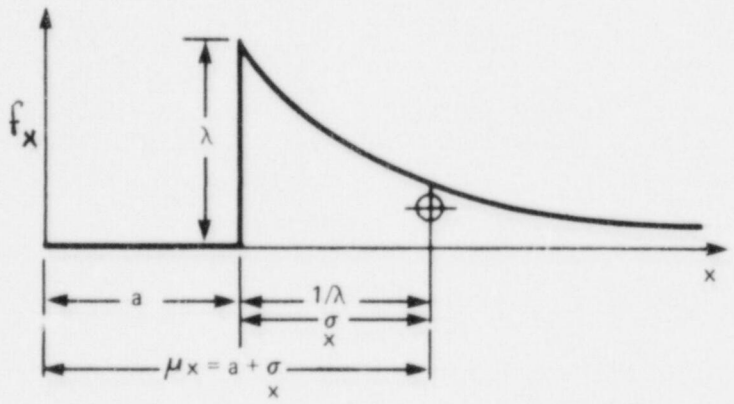


FIGURE 6

and the cumulative density function is then

$F_X(x) = 1 - \exp [-\lambda (x-a)]$, for $a < x < \infty$

$= 0.0$, for $x < a$

This function has three useful features simplifying the use of available data in predictions of probabilistic failure.

(a) The c.g. of the PDF, its mean value (μ_X) is $1/\lambda$ from $x = a$;

(b) The standard deviation σ_X is also $1/\lambda$ and

(c) The starting point, at $x = a$, or $\lim_{\delta \to 0} \{f_X(x + \delta)\} = \lambda$

Since the data available are scarce, the starting point, using fuzzy theorm, would be easily evaluated, using these assumptions, μ_X and σ_X.

(ii) However, where the changes in values of f_X are so small, that the PDF curve will be almost flat, we can use the power model:

$$f_X(x) = \alpha b^{-\alpha} x^{\alpha-1}, \text{ for } 0 < x < b$$
$$= 0., \text{ for } x > b$$

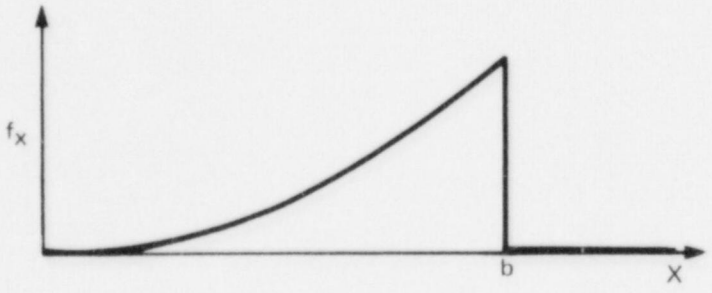


FIGURE 7

The relationships between the parameters of the power model are as follows:

$$C_X = \sigma_X/\mu_X$$

$$\alpha = \sqrt{1 + (1/C_X{}^2)} - 1$$

$$b = \mu_X\ (\alpha + 1)/\alpha$$

These will be used for each of the segments, with different μ_X and σ_X, i.e., for every part of the PDF starting after the maintenance window.

4.2 Evaluation (the three modes of failure)

The data required for this analysis is, first for subjective (fuzzy) models, for which the exponential or power distribution can be used.

The PDF will then be the total probability of "load" exceeding "available resistance" rather than the detail probability of each.

4.2.1 Structural Collapse - Common Mode

For this model, the analysis is based on loading and material (structural) strength.

(a) Concrete Strength

The construction material in CANDU stations is mostly reinforced concrete. The reinforcement is normally not less than 200 kg/m^3 and in some areas exceeds 400 kg/m^3.

Concrete strength plays the major role in strength models (except for errors of reinforcing steel splices). Therefore, the material strength model will have to concentrate on the concrete data.

In Ontario Hydro, every concrete pour has a minimum of three test cylinders and, in many cases, it has 6 test cylinders, to help evaluate the concrete strength of the pour.

These will normally give, for the containment, a Gaussian (Normal) distribution, since there is no bias known to affect such distribution.

The PDF could be easily plotted, for the cylinder strength (f_c') of a specific age, e.g., the common 28 days.

For a long term evaluation, considering strength vs time, a non-destructive examination (NDE) or test cylinder program will be required. This should evaluate concrete strength after six months, 1, 3, 5, 10, 20 and 30 years. NDE should start with measurements at the concrete strength testing dates, to enable us to relate the NDE relative measurements to the common strength base (i.e., to calibrate the NDE measurements to produce strength values).

Since concrete gains strength with age, within some limits, the data will give a reference strength (average-each) and a variant. This will be used to establish the strength PDF.

(b) Loading Data

Loading PDF is not as easy to evaluate. It requires creating some databases that have not been assembled earlier (e.g., the designer specifies a live load - what is the actual live load there on a floor? What mean? What variance? What distribution?).

Next we have to consider the load combinations and dependencies. What probable live load to be used with what LOCA level? What maximum likelihood event (MLE) would be for a specific combination and how critical would it be?

Obviously, these data will have to be evaluated for the critical combinations only. (If a load combination is less severe than another, it does not need to be detail analyzed.) On a probabilistic basis, these critical combinations may surprise those accustomed to deterministic approaches. (Using the definition before, of the convolution integral, it may be not the one that has "added maximum components".)

Collected data has to cover an operation span of 10 years or more. The reliability analyst will have to use a lot of load histories (e.g., during construction - as concrete cracks, e.g., due to a higher loading at a lower strength than if it were at 15 year age).

Reference 3, Table 16, e.g., shows that concrete strength has a log normal distribution and the live load, has an "Extreme Type I", for a two way slab element. It gives also a normal distribution (Gaussian) for concrete columns (Table 19).

The same reference also gives in Table 11 the comparative death risk/hour per 10^8 persons exposed in UK to 0.002 for structural failures, versus 0.7 such event units due to accidents at home (able bodied). This illustrates only the very low risk expected from structural failure at a nuclear power plant, where the risk is even less, due to larger shifts of design strengths from means. (Most commonly, it is $\mu \pm 3\sigma$ in the nuclear design codes - although there is no formal code calibration at present.)

Under LOCA load combinations, P_f is expected to be in the range of 1.0×10^{-7} to 1.0×10^{-6} events/year. This is close to the null event (the event in probabilistic failure analysis equivalent to zero in deterministic mathematics).

Professor E.G. Haugen of the University of Arizona [Reference 4] gave values for ultimate and yield tensile strengths, mean and standard deviations for many ASTM specified materials - with different specified conditions as well as variability of tolerances.

Professor T.V. Galambos of the Washington University, St. Louis, [Reference 11] gave the load type, mean, COV and distribution as well as structural steel material property statistics, as were then suggested for use by the AISC-LFRD steel design code.

Lind et al [Reference 5] gave the mean, nominal and COV for both loads and material strengths. Taylor [Reference 6] published similar values for concrete as early as in 1965.

These data, and the load factors given by the Canadian Nuclear Design Code [Reference 7], would suggest probabilities of failure less than even the values indicated above, due to the very low probability of exceedance of LOCA loads given for design. (LOCA has a load factor of 1.5 under Canadian Standard N287.3-M82.)

4.2.2 Structural Deformations - Serviceability Limits

These probable deformations are due to either long term (e.g., creep) or short term, but extreme effects.

The design for abnormal/environmental loads of a low probability of exceedance like seismic (Design Basis Earthquake (DBE), Tornadic and Explosion loads) uses load factors of 1.0. This implies that the "yield", i.e., deformation beyond elastic limits is allowed under small probabilities. This condition, when evaluated, will give us the probability of having non-elastic deformations, exceed some "specified" limits.

If we consider here these "load" variables, affecting structural materials (components), we have

(a) Creep which commonly has a log normal distribution - long term;

(b) Tornadic and Earthquake design loads. These normally follow an EVD analysis (Weibull) with

$$\mu_X = \beta + \frac{0.577}{\alpha} \text{ and } \sigma_X = 1.283/\alpha \quad \text{[Reference 2]}$$

Using the basic probability axioms (posteriori probabilities)

$$P(\text{LOCA} \cap \text{Earthquake}) = P(\text{LOCA} \mid \text{Earthquake}) \cdot P(\text{Earthquake})$$

(Probability of an earthquake immediately after a LOCA is unplausible structural event due to the time required for repairs, checks and inspections during which the plant is not operating.)

Noting that generally $P(\text{Earthquake} > \text{DBE})$ is not larger than 1.0×10^{-3}

and $P(\text{LOCA} > \text{Design LOCA})$ is normally less than 1.0×10^{-3}.

If we can conservatively start with an initial estimate that a LOCA due to an earthquake or P(LOCA|Earthquake) is as high as 0.3, we get the probability $P(\text{LOCA} \cap \text{Earthquake})$, being non-independent events as 3×10^{-4}.

With Weibull distributions, assuming COV of 10 percent and 25 percent, we see that it is at the upper tail probability of $\mu - 2.2\sigma$ [Reference 2]. (Initially we have to start with some assumptions (subjective) before we may collect a data base).

However, we can see that the probability of failure for this mode is less than the acceptable margin of 1×10^{-3} events/year. Such an event is not considered to produce any damage to the environment, and is of significance only to economic (cost benefit) analysis.

The same general analysis could extend to other load combinations that may produce probabilistic failures.

4.2.2.1 Shrinkage and Creep

At Ontario Hydro, we have a shrinkage and creep analysis program for concrete structures. It quantifies shrinkage and creep predictions, as being function of concrete age, loading age, concrete mix and relative humidity.

For concrete mix, it considers the concrete strength, amount and type of cement, water content, quantities of fine and coarse aggregates, concrete mass (density) and the exposed surface(s). This elaborate model, was initially suggested by Professor Z.P. Bažant et al, at North Western University [Reference 8] and when we compared its predictions with actual field measurements gave values within 18 percent margin. [Reference 10].

4.2.2.2 Suggested Work Program

For this model the data bases required are for loading and material properties. Loading data base should primarily be for the long term effects (e.g., small negative pressure at which our CANDU multi-units are operated and dead load) and short term, like accident pressures, seismic and tornado effects.

For material properties, concrete mix data are available or can be obtained from tests. Loading can be evaluated (dead load of material - from same tests, equipment from already supplied manufacturers data). Using known seismic, tornadic and other extreme events and assuming occurrence is 100 percent all the time. If the probabilities of deformation, long or short term are very small compared to acceptable limits (e.g., less than 10 percent of acceptable), then no more analysis is required.

If the limit of 10 percent is exceeded, we have to refine our calculations by using a probabilistic model. A starting point can be the main loading assumptions 1.0×10^{-3} for seismic (DBE), 1.0×10^{-4} for tornadic (DBT) with some measurements for mean and variance of other loading parameters. These can give us probabilities of occurrence (or being exceeded) and then we calculate, on probabilistic basis the values of deformation. These probabilities help us accept such limits or determine whether they are worth further pursuing. The analysis when made then, should be for various time elements, to give us its PDF.

4.2.3 Leakage Failure

Ontario Hydro has both commissioning testing of the containment, as well as in service testing.

Testing, in both cases, has an objective, namely to prove that the maximum recorded leakage is less than a target limit (often 1 percent of the mass of the containment air per hour under specified maximum test pressure).

Containment ranges from unlined, partially or fully lined (carbon steel 7 mm - 1/4" welded plates). Welds, between adjacent plates, are full penetration welds to a concrete embedded steel channel. All welds are non-destructively examined by two methods, one of them is vacuum box. (The others are radiography, liquid penetrants, etc.)

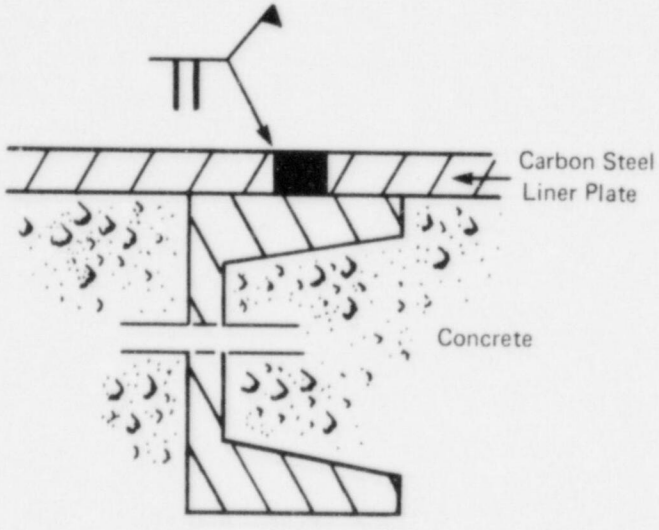


FIGURE 8

The expansion joints (EJ) at the containment have steel bellows at the steel liner. In newer projects there are water stops, in addition.

Where it was not justifiable to steel line, reinforced concrete was generally thick, with its containment surface epoxy lined.

Thus, the leakage is then through one or more of:

(a) Welds, between liner plates;
(b) Expansion joints;
(c) Embedded parts; or
(d) Through concrete in the non-steel lined areas, particularly at EPs and Construction Joints (CJ).

Both commissioning tests and in-service tests may identify leak sites requiring repairs. These repairs (maintenance) have the objective of reducing leakage enough that even after some expected deterioration, will be still within acceptable limits. Modelling for this mode of failure is as shown in Figure 5.

4.2.3.1 Data

Much of the data for this analysis are from commissioning, in-service tests and significant events reports (SER). The last, is not too common at present and should be taken only as a refinement in the later cycles of this analysis, for correction.

For future modelling, however, more parameters will be required to evaluate μ and σ, with a better precision from larger data. The properties of concrete (permeability of concrete), leakage paths, number (of each size/type) of penetrations per unit, number of welds (butt welds) per unit area of steel liner and the number of expansion joints as well as the construction joints will be considered.

These, when evaluated, may affect the general shape of the suggested PDF. However, each of these refinement components will have to follow one of the referenced PDF models.

5.0 FUTURE PROJECTS - DESIGN AND PROCUREMENT

Emphasis should be on the probabilistic behaviour in both design and procurement.

Design should use the probabilistic model in loading rather than the current deterministic methods based on quasi-probabilities.

These lead to following the probabilistic relationships from start to end. An occurrence, of a very small probability of exceeding a specific limit, might be tolerated. Once the designer knows the real effect of a hazard on his design, he wil not fear the unknown and will not have to hide behind codes for protection.

Safety of the public and station personnel, sound economical cost/benefit analysis should govern his decisions. He will not fear accepting a small risk, having no effect on the safety of the public and the operators. If the probable cost of repairs for such occurrence is far less than the capitalized cost, his design should be based on taking that calculated risk.

On that basis, for example it may be unnecessary to use steel lining, if concrete can be procured and designed to have an air tightness, at a small cost above the current practice, capable of providing the same probabilistic protection.

Acknowledgement

The author would like to thank Mr. Z.M. Beg, Supervising Design Engineer and Mr. R.I. Chen, Structures Engineer, for their valuable review and comments. They helped the author simplify this paper, particularly from having to repeat the already known structural analyses and already known techniques.

The author would like also to thank Prof. Paul W. Wirsching, of the University of Arizona at Tucson. His guidance during his valuable professional course (on Structural Reliability) and many discussions, had a major contribution on having the author look at these models. They helped the author go beyond theoretical structural analysis and helped "see the forest rather than the trees".

References

1. Reliability Engineering for Nuclear and Other High Technology Systems by A.A. Lakner and R.T. Anderson, Elsvier Applied Science Publisher, 1985.

2. Reliability Methods in Mechanical and Structural Design, January 1985 (Paul H. Wirsching, Colleen K. Vance and Yih-T. Wu, University of Arizona).

3. Rationalization of Safety and Serviceability Factors in Structural Codes, Construction Industry Research and Information Association (CIRIA) Report No. 63, London, UK (1977).

4. Probabilistic Mechanical Design, E.G. Haugen, Wiley (1980).

5. Practical Approach to Code Calibration by Siu, Parimi and Lind, Journal of Struct Div, ASCE, July 1975.

6. Concrete Technology and Practice, W.T. Taylor, Elsevier Publishers, 1965.

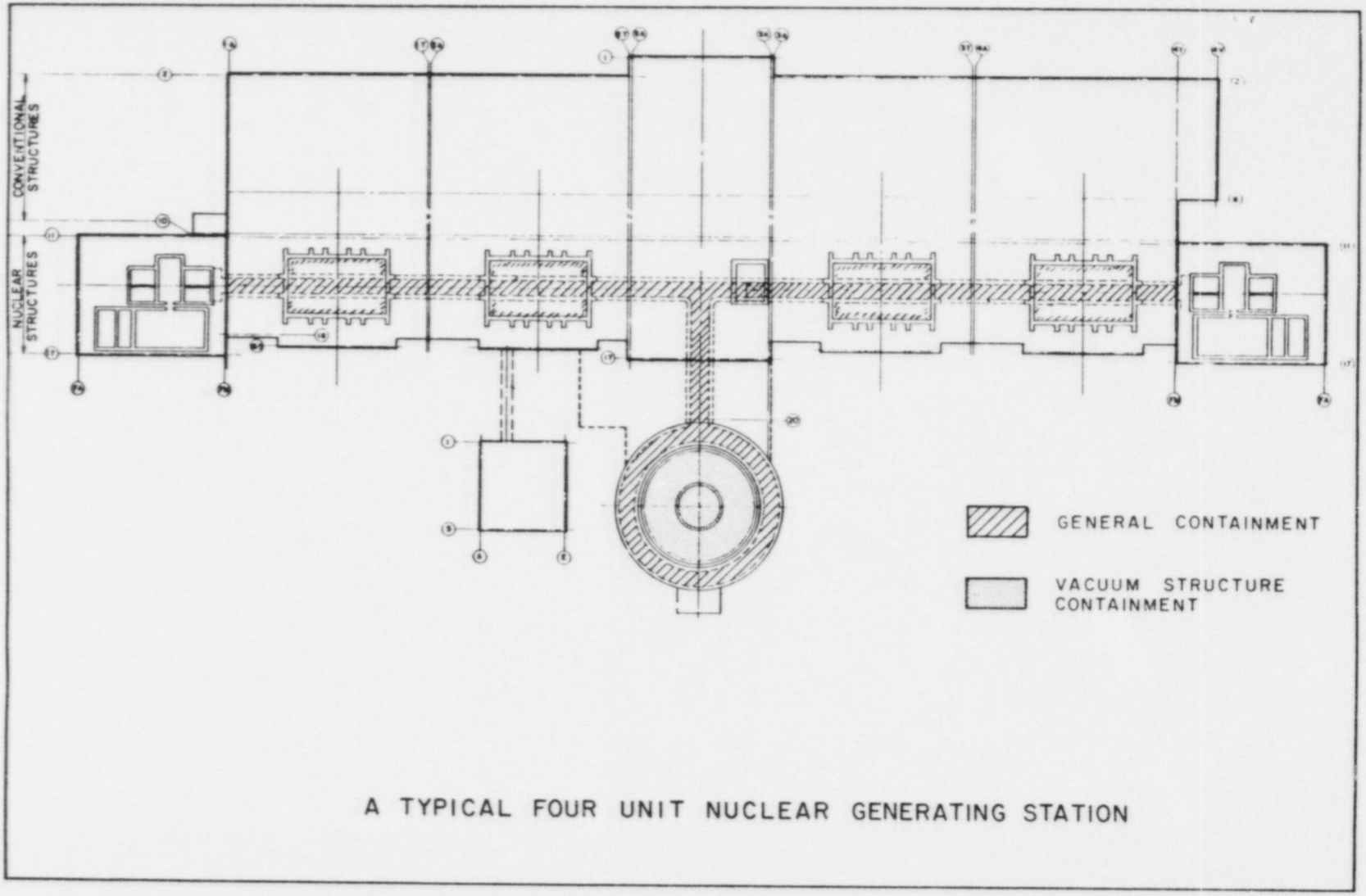
7. Design Requirements for Concrete Containment Structures for CANDU Nuclear Power Plants, CAN3-N287.3-M82, published by Canadian Standards Association.

8. Input of Creep and Shrinkage Characteristics for Structural Analysis Program, Z.P. Bažant, Materiaux et Construction, Vol 15/88 (1982). This is based on the Bazant/Panula model.

9. Probabilistic Methods in the Theory of Structures, by Isaac Elishakoff, John Wiley & Sons, 1983.

10. Design for Creep and Shrinkage Effects in Overpressure Containment Structures of Darlington GS, J. Huterer and E.C. Ha presented at the ACI October 1985 Convention, Chicago, Illinois (accepted for publication by the ACI in Concrete International Design and Construction).

11. Structural Safety and Reliability, edited by T. Moan and M. Shinozuka, Elsevier Publishing, 1981.



A TYPICAL FOUR UNIT NUCLEAR GENERATING STATION

THE MODELLING OF A NEGATIVE-PRESSURE, FILTERED-VENTED CONTAINMENT SYSTEM AS PART OF A PROBABILISTIC SAFETY EVALUATION

Keith S. Dinnie
Ontario Hydro
Toronto, Canada

ABSTRACT

The modelling of a negative-pressure, filtered-vented containment system as part of the Darlington Probabilistic Safety Evaluation is addressed. The approach taken to containment modelling has been influenced by both the containment design and the scope of the study as a whole. This paper describes the development of the containment event tree and outlines its role in the overall containment analysis.

1.0 INTRODUCTION

The modelling of containment in probabilistic risk and safety evaluations is crucial to the realistic assessment of potential public health effects arising from reactor accidents. The modelling of a multi-unit, negative-pressure, filtered-vented containment design, such as is employed at Ontario Hydro's Darlington station, represents a markedly different challenge to that for other commercial reactor containment systems.

The purpose of this paper is to describe the approach to containment modelling being used in the Darlington Probabilistic Safety Evaluation (Reference 1). The considerations leading to the development of the containment event tree are outlined together with a general description of its role in the overall containment analysis. Since the study is not yet complete, the information contained in this paper is subject to review and change, and should be considered preliminary.

2.0 THE DARLINGTON PROBABILISTIC SAFETY EVALUATION

The Darlington Probabilistic Safety Evaluation (DPSE) is currently being carried out on Ontario Hydro's Darlington station, a 4-unit CANDU PHWR, the first unit of which is scheduled to come into service in 1988. The main purpose of the DPSE is to provide a thorough review of station design adequacy using risk assessment methods. The DPSE Final Report is scheduled for publication in December 1986.

The DPSE will generate estimates of both off-site public health and on-site economic risk arising from reactor accidents. The study does not address initiating events arising outside the plant, such as natural phenomena (other than the loss of off-site electrical power). The study objectives require risk estimates to include

contributions from events involving widely varying degrees of core damage.

A fundamental concept of the DPSE approach is that, at some low cutoff frequency, events cease to be of safety or economic concern irrespective of their calculated consequence. A category of events has been defined for which a cumulative frequency will be estimated but no consequence analysis performed. Any event can be allocated to this category, provided that the calculated frequency remains below the cutoff criterion. Because of unique features of the CANDU design, the DPSE expects to demonstrate that all events which might involve large scale fuel melting can be included in this category. The DPSE containment analysis, therefore, does not address LWR-type core melt events. The derivation and justification of the frequency criterion is beyond the scope of this paper. It should be added that the most severe DPSE fuel damage category involves substantial fission product release and hydrogen production.

The DPSE has identified nine fuel damage categories (FDCs) ranging from events involving the initiation of emergency coolant injection but without significant fuel damage to a total loss of all direct fuel cooling resulting in up to 30% of the core inventory of fission products being released to containment. Each FDC possesses unique characteristics describing the magnitude and timing of radionuclide releases from the heat transport system, together with the associated thermal hydraulics. These characteristics determine the required containment response.

3.0 THE DARLINGTON CONTAINMENT DESIGN

The Darlington containment includes four reactor vaults connected by a common duct, which connects through an isolation manifold to a large vacuum building (Figure 1). During normal operation the vacuum building is maintained at a low pressure (7 kPa absolute), while the remainder of containment is slightly sub-atmospheric. Design pressure is about 100 kPa (gauge), total containment volume including the vacuum structure approximately $2 \times 10^5 m^3$. The containment envelope contains 29 airlock/transfer chambers and about six hundred other penetrations.

In the event of a significant overpressure on the reactor vault side of the manifold (e.g., resulting from a heat transport system pipe break), pressure relief valves open automatically, venting steam to the vacuum building, where dousing occurs. Containment button-up takes place automatically on high pressure or high activity, or it may be manually initiated. Following the condensation of the steam, containment is maintained at a sub-atmospheric pressure to prevent out-leakage of any airborne radioactivity by venting air from the reactor vault to the vacuum building.

Due to air inleakage through the containment boundary and instrument air discharge into containment, the vacuum reserve is slowly used up and containment gradually repressurizes until the internal pressure approaches atmospheric. To avoid the possibility of uncontrolled leakage of radioactivity in the long-term, the containment atmosphere is slowly vented to atmosphere via a filtration system connected to the vacuum building. The repressurization time and the rate at which venting takes place is a function of, among other things, containment integrity.

4.0 IDENTIFICATION OF CONTAINMENT FAILURE MODES

In the event of the occurrence of one of the FDCs, some release of radioactivity to the environment will result. The release can occur in either of two phases of the accident sequence:

- During the period of steam blowdown when containment internal pressure is above atmospheric (by pressure driven flow through impairments in the containment boundary), or

- In the long term when containment repressurizes and contaminated air must be exhausted through the filtration system to maintain a slightly sub-atmospheric pressure inside containment.

Even when no fuel damage is predicted, the potential for off-site release still exists because of the presence of tritium in the containment atmosphere. Containment failures which can cause an increase in either or both these modes of release are of potential significance.

The most important failure modes are those affecting containment envelope integrity. Undetected impairments may exist prior to the initiating event or may be caused as part of the accident sequence. Certain types of impairment can lead to liquid release, which can be equally important if the liquid is radioactive or fuel cooling is threatened.

Failure to relieve steam pressure from the reactor vault to the vacuum building can enhance the early releases. There are three components to this function; pressure relief valves, vacuum pressure and dousing capability. Finally, in the long-term, failure to minimize airborne fission product concentrations by control of coolant chemistry, failure to maintain a filtered pathway for containment exhaust flow and inefficiencies in filter performance can also lead to releases beyond design expectation.

From these considerations, eight basic failure modes were identified prior to the development of the containment event tree:

(1) Containment integrity failure from any cause leading to increased air leakage.

(2) Containment integrity failure due to a hydrogen burn.

(3) Containment integrity failure from any cause leading to liquid release.

(4) Failure of sufficient containment pressure relief valves (PRVs) to lift to relieve overpressure.

(5) Initial vacuum building pressure too high.

(6) Failure of the vacuum building dousing system.

(7) Failure to minimize airborne fission product concentrations.

(8) Failure of filtered air discharge.

5.0 THE CONTAINMENT EVENT TREE

The structure of the containment event tree bears a close resemblance to other DPSE plant event trees in that the top event definitions involve failures which can be modelled by fault tree analysis. The vacuum system and the large containment volume combine to effectively eliminate the possibility of a large-scale overpressure failure of containment integrity other than by localized hydrogen combustion.

In developing the detailed tree and top event failure definitions, two further considerations must be taken into account. First, for some failure modes the change in consequence can be very large if the representation is limited to total success or total failure. In such cases, intermediate failure modes have been introduced to improve the discrimination between levels of consequence and reduce the assumed consequence of relatively minor system impairments.

Second, because the containment event tree is to be used in conjunction with each of the FDCs, the top event definitions must vary depending on the particular characteristics of the FDC (such as the number of valves needed to provide pressure relief for different sizes of pipe break). The fault tree logic for each top event must include suitable conditioning where all or part of a fault tree may be inapplicable to one or more FDCs.

The event tree is shown in Figure 2 and the associated top event failure definitions in Table 1. The status of containment envelope integrity can be represented by any of five levels of impairment or the success state. Three equivalent hole size ranges model failures involving increased air leakage (CIA1, CIA2, CFS) plus hydrogen burn (CFH) and liquid release (CIL). The effects on accident consequences include increased overpressure releases, reduced repressurization times and increased filter exhaust rates.

Only three of the thirteen top events are considered sufficiently severe for the subsequent logic to bypass the remainder of the

tree. Combined with the nine FDCs, a large number of end-states are generated for inclusion in the subsequent consequence analysis.

6.0 OVERALL CONTAINMENT ANALYSIS

Three further steps are required to complete the containment analysis; the identification and classification of events that can lead to containment bypass, the categorization of all containment event tree end-states for ex-plant consequence analysis and the evaluation of time-dependent radioactive releases to the environment for each ex-plant release category (EPRC).

Containment bypass events are identified either by initiating event (e.g., steam generator tube ruptures) or by suitable flags in the FDC logic (a LOCA via failures in the pressure and inventory control system). These events are collected together depending on which FDC they contribute to and given a composite event name indicating that they bypass containment. These composite events are then included directly in the EPRC structure, together with the containment event tree end-states.

It is not possible to categorize the end-states by engineering judgement based on a few major sequence characteristics. The wide range of fission product release from the core represented by the FDCs and the varying response of containment subsystems requires that some form of consequence assessment be performed for each candidate sequence. A simplified form of consequence analysis was used to predict a "categorization dose", an estimate of population dose using average weather and dispersion assumptions. Events were then categorized based on similarity of consequence magnitude and duration of release.

The proposed ex-plant categorization scheme contains six categories. The structure consists of four main categories (EPRC1-4) plus two special categories (EPRC0 and EPRC5) which bound the scheme (Figure 3). EPRC0 is the embodiment of the DPSE approach to low frequency/high consequence events, for which it is simply necessary to ensure that the frequency is below the cutoff criterion to demonstrate design adequacy. EPRC5, at the other extreme, contains all events whose public dose consequences are considered to be too small to constitute a public safety concern. No detailed offsite consequence analysis will be performed for either category.

The final step is to take representative events from each of the four main categories and evaluate the time-dependent radionuclide releases from containment. Since these categories do not include any events which involve significant fuel melting, existing analytical methods may be used, at greatly reduced cost and complexity. Each release will be analyzed to determine individual and collective dose to the public as a measure of the potential for adverse health effects.

7.0 REFERENCES

1. F.K. King and V.M. Raina. "The Benefits of Pre-operational Risk Assessment Based on Experience with the Darlington Probabilistic Safety Evaluation." Proceedings of the International ANS/ENS Topical Meeting on Probabilistic Safety Methods and Applications, San Francisco, February 1985.

TABLE 1

Top Event Failure Definitions

CIA1	An impairment exists which, if detected at the pressure test and linearly extrapolated, would predict a leak rate of up to 3 percent of containment volume per hour at full positive design pressure.
CIA2	An impairment exists, greater than CIA1, up to the equivalent hole size associated with a failed airlock seal (0.113 m^2).
CFS	Failure of containment envelope integrity resulting in effective loss of pressure control (any hole size greater than 0.113 m^2).
VAC1	Vacuum building main chamber pressure between 15 and 39 kPa absolute.
VAC2	Vacuum building main chamber pressure between 39 kPa absolute and atmospheric.
DOUS	Failure of dousing when vacuum structure main chamber pressure exceeds 39 kPa absolute.
PRV	Failure of sufficient PRVs to operate to minimize overpressure adequately.
CIL	Failure of containment integrity resulting in significant contaminated liquid release outside containment.
CFH	Failure of containment integrity caused by an overpressure transient that peaks above 250 kPa gauge (2.5 times containment design pressure) as a result of a hydrogen burn.
FTR1	Filter efficiency within the range 99.8 percent and 99 percent (for all nuclides).
FTR2	Filter efficiency within the range 99 percent and 90 percent (for all nuclides).
AFPC	Failure of chemical addition to minimize airborne fission product concentrations inside containment.
LTPC	Failure to maintain an adequate filtered flow from the reactor vault to the stack to maintain containment at a sufficient negative pressure to prevent out-leakage for the duration of significant fission product release (30 days).

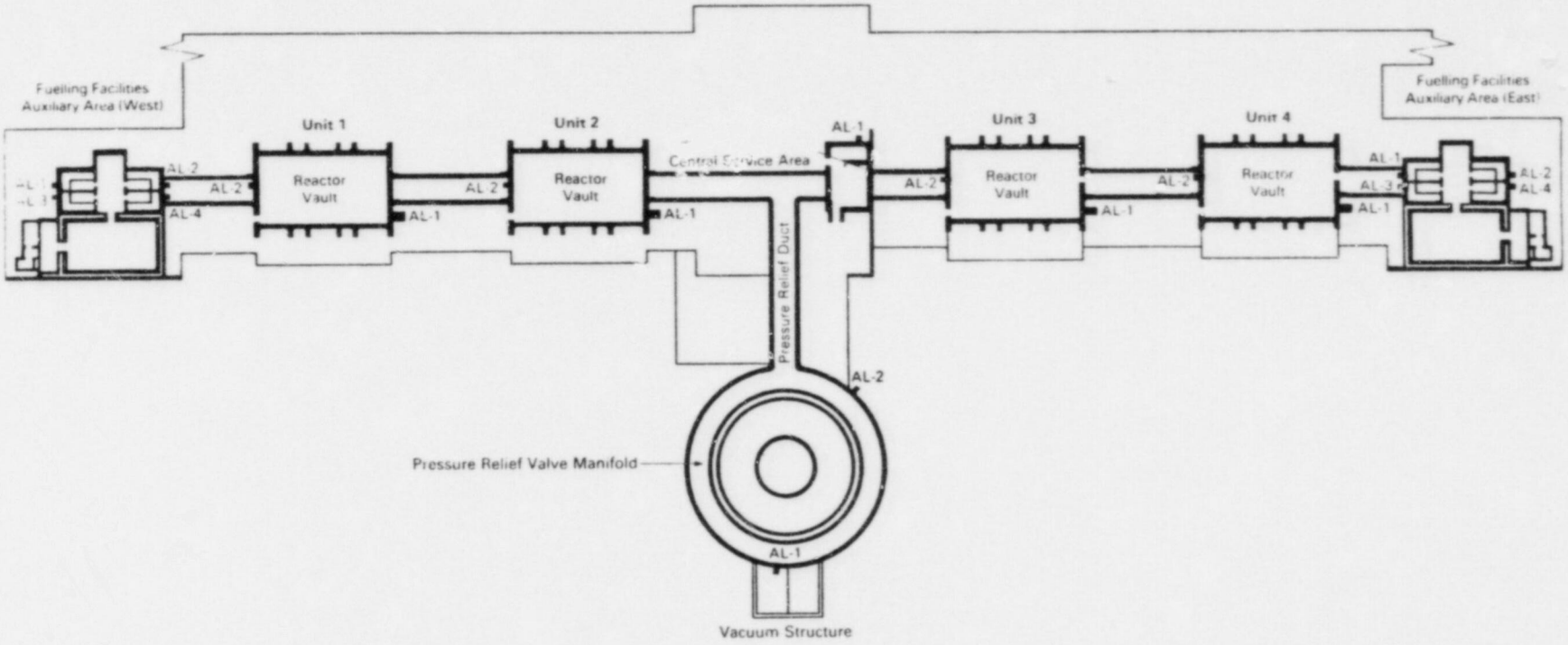


FIGURE 1

Darlington Containment

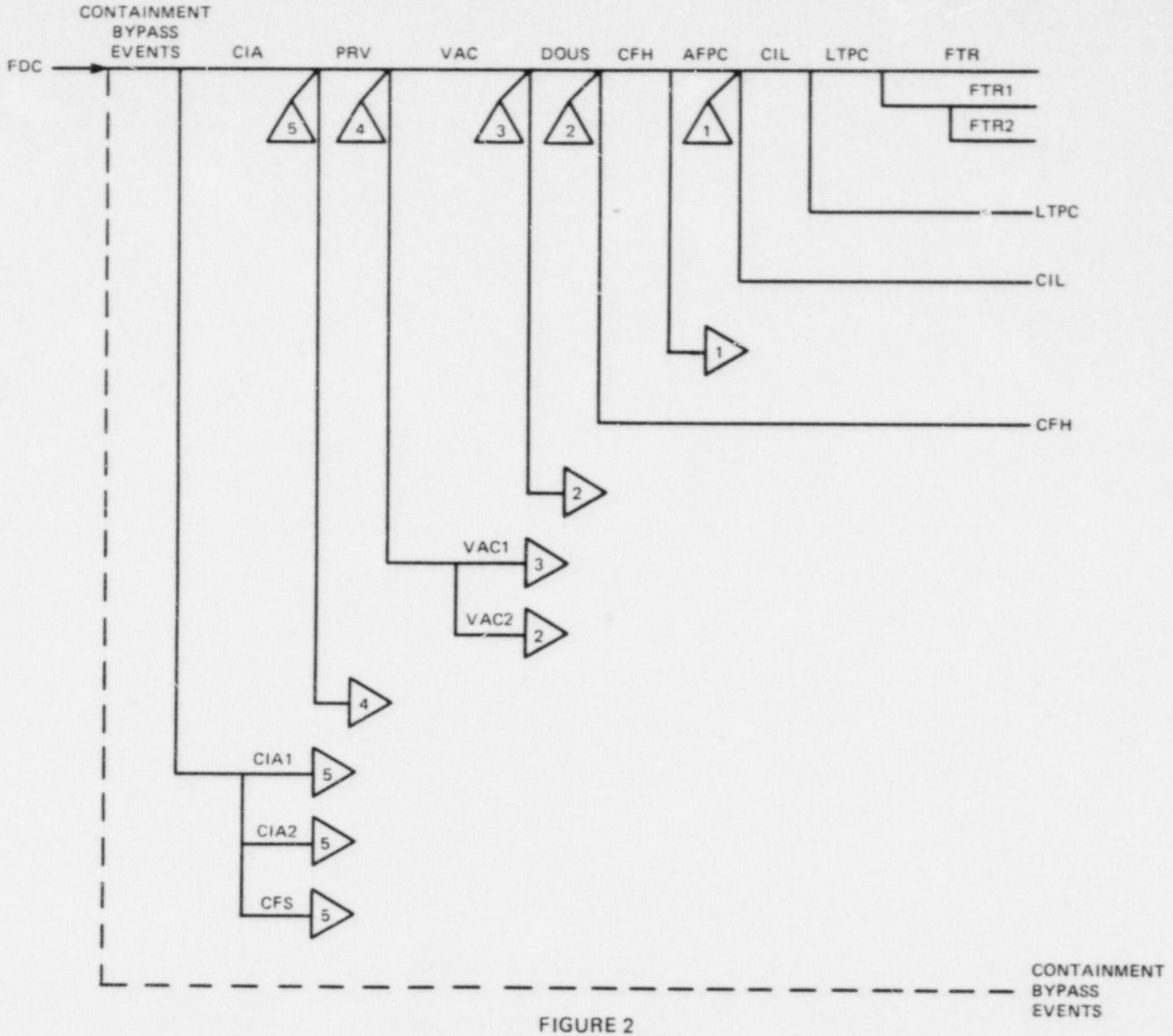


FIGURE 2
Containment Event Tree

EPRC 0 (very low frequency events)
EPRC 1
EPRC 2
EPRC 3
EPRC 4
EPRC 5 (Very low consequence events)

Figure 3: Ex-Plant Release Categories

SECONDARY CONTAINMENT BUILDING PERFORMANCE IN SEVERE ACCIDENTS

R. S. Denning and P. Cybulskis
Battelle Columbus Division

ABSTRACT

In evaluating the potential consequences of severe accidents in nuclear power plants, principal emphasis has been on the performance of the primary containment building. For the most severe accident scenario in which the primary containment may be predicted to fail early in the accident or in which containment is bypassed, the behavior of a secondary containment building could be important in reducing the potential consequences of the accident. In this paper, some example analyses are presented in which the behavior of the secondary building was considered. The predicted effect on accident consequences are discussed. Key uncertainties regarding the analysis of secondary containment performance are identified and recommendations are made to improve future analyses.

1.0 INTRODUCTION

In recent years the U.S. Nuclear Regulatory Commission has undertaken a reassessment of the methods used to predict the release of radioactive fission products to the environment in severe accidents. In 1985 a draft report "Reassessment of the Technical Bases for Estimating Source Terms" NUREG-0956[1] was issued in which an approach was presented for the evaluation of severe accident source terms in a consistent, mechanistic manner. The methodology currently being used by the NRC for the implementation of this approach is referred to as the Source Term Code Package.[2] The first major application of the Source Term Code Package is in the NRC's evaluation of the risk from five reference nuclear power plants which is to be issued as NUREG-1150 in September of 1986.[3] One of the major issues identified by the NRC in the estimation of severe accident source terms is the performance of the secondary buildings of nuclear power plants as an area of fission product retention. This issue has been the subject of discussions between the NRC and the industry severe accident program, IDCOR, in an attempt to understand differences obtained between the NRC analyses and those performed with the IDCOR computer code package, MAAP.

The purpose of this paper is to review some of the results obtained with the Source Term Code Package, to identify the principal sources of uncertainty in the analysis, and to suggest means by which the behavior of secondary buildings can be better predicted in the future.

2.0 SIGNIFICANCE OF SECONDARY BUILDING RETENTION

The secondary containment buildings, adjacent to or in some cases surrounding the primary containment are in many severe accident sequences the last confinement volumes in the flowpath of fission products to the environment. The structural response of the primary containment to severe accident loads is a major element of the prediction of source terms and accident risk. The subject of most of the papers at this conference is related to predicting the integrity of the primary containment under these conditions. Comparatively little attention has been paid to secondary containment response. In the design philosophy used in the construction and licensing of nuclear power plants the primary containment is the principal barrier to the release of fission products. The integrity of the containment under design basis loads is the focus of regulatory review in the licensing of nuclear power plants. Although severe accident conditions differ from design basis conditions, the primary containment structural behavior is comparatively well known. In contrast, secondary containments were not intended to provide an additional level of confinement under these conditions. The extent to which they do provide this function is to a degree serendipitous.

Even a small decontamination factor for a secondary building (DF = quantity entering the volume/quantity escaping the volume) can have a significant impact on offsite consequences, particularly if calculated doses are close to a threshold value such as that for early fatalities. The sequences in which this occurs are those in which there is little other retention. Cases of particular interest are:

i. Containment isolation failure - In these sequences a leak path from the containment exists from the start of the accident. These scenarios show prominently in some PRAs because of the poor history of assuring containment integrity that has existed in the past. Secondary building retention is particularly relevant because most of the isolation failures involve leak paths through penetrations to secondary buildings rather than directly to the environment. Loads on the secondary building are typically not large initially in these sequences since the leakage is not induced suddenly and the leak path will not transmit rapid pressure changes from the primary containment. Hydrogen burns in the secondary building are a potential problem later in the scenario, however.

ii. Containment bypass - These sequences, V sequences in the WASH-1400[4] nomenclature, involve failures leading to a direct pathway from high pressure piping in the reactor coolant system to low pressure piping in a secondary building at a time when the RCS is pressurized. Failure of the low pressure piping results in the bypass of the containment. This sequence was found to be a major risk contributor for the WASH-1400 PWR. Although the likelihood of the sequence has been reduced by improved testing procedures for the isolation valves separating the high pressure and low pressure systems, the sequence may still be an important risk contributor because of the potential for high consequences. Because of the occurrence of low pressure piping overpressure incidents that could

be precursors to containment bypass sequences, consideration is also being given to the potential for bypass sequences in BWRs. The magnitude of the loads on the secondary building in this type of sequence depend on the mode of failure of the piping. The potential for hydrogen burns is again a major consideration which could affect the integrity of the secondary building, the residence time available for fission product removal, or result in resuspension of fission products.

iii. Early disruptive failure of the containment - In these scenarios the containment fails by overpressurization before core melting begins, during the in-vessel core melting phase or approximately at the time of vessel failure. If the containment remains intact for a number of hours after containment failure the estimated release to the environment is usually small. The mode of primary containment failure in these sequences can be very important. The loads imposed by primary containment failure can lead to failure of the secondary building before there is an opportunity for fission product attenuation.

iv. Delayed release scenarios - As methods for the analysis of source terms have become more sophisticated, the potential for delayed release of fission products after containment failure has been recognized. One possible mechanism of this type is the revaporization of fission products from surfaces in the reactor coolant system which are heated by the decay heat of deposited radioactive materials. Another possibility is the dryout of quenched debris beds and the delayed attack of concrete. In these cases, the long term driving force for sweeping the fission products to the environment is quite reduced and the potential for enhanced retention in a large secondary building can be significant.

3.0 CHARACTERISTICS OF SECONDARY BUILDINGS

There are a variety of different buildings external to the primary containment that can potentially attenuate the source term. The design of these buildings is completely within the domain of the architect-engineer. Plants with very similar reactor and primary containment designs can have significant differences in secondary buildings. Even in a given plant, there may be a variety of paths through the secondary containment with varying potential for fission product retention. As a result it is very difficult to make generalizations about secondary building performance or to treat behavior for different plants as an extension of a reference plant analysis. The buildings of interest could house critical safety equipment, such as the safeguards building at Surry, or could merely house conventional equipment used to generate electricity such as the turbine building. As a result the design criteria of the buildings vary. Some of the structures are designed to withstand tornado loads and may be quite robust. Other buildings are designed to conventional standards without consideration of special safety significance.

Some of the features of secondary buildings that can affect their ability to retain fission products are: the size of the building, the strength of the building, the amount of surface area available for deposition, and the availability of fire protection and ventilation systems. Some plants have gas treatment systems which could filter the exhaust from the building before releasing to the environment. Special consideration must be given to the limitations of the system, however, before giving large credits for retention. For example, the gas flow rate of the system may not be adequate to keep up with the in-leakage from the primary containment so that some fraction of the leakage will not be filtered. Usually the filter systems are not designed to cope with either the level of moisture or aerosol loading that would accompany a core meltdown accident. Thus the system might operate for a period of time before failing. In the ORNL Severe Accident Sequence Analysis program[5] consideration has been given to the effectiveness of fire protection systems in secondary buildings to act as fission product scavengers. The availability of these systems and their potential effectiveness in severe accidents is quite design dependent and would have to be carefully examined for each plant.

4.0 EXAMPLE RESULTS

A number of source term analyses have been performed with the Source Term Code Package for the NUREG-0956 and NUREG-1150 efforts. Two examples will be described to provide an indication of the types of results obtained when including secondary buildings in source term analyses and to identify some of the principal sources of uncertainty in the analysis.

4.1 Mark I BWR Secondary Containment

The reference plant for the Mark I BWR containment design for NUREG-1150 is the Peach Bottom 2 plant. A number of sequences have been analyzed for this design. In some of the more important station blackout and anticipated transient without scram scenarios that have been analyzed, the primary containment is predicted to fail in the drywell prior to the beginning of core concrete attack. Although the fission products that escape the reactor coolant system prior to reactor vessel failure are predicted to be scrubbed quite effectively by the suppression pool, fission products released to the drywell after containment failure would not be transported into the pool. Because the drywell volume is small and the gas generation rate is significant, the residence time in the drywell is too short for effective retention. Thus a large fraction of the fission products released to the drywell after containment failure leak from the drywell into the secondary building.

Figure 1 illustrates the configuration of the primary containment, the surrounding reactor building and the overlying refueling bay. The volume of the reactor building is 1.5×10^6 ft^3. The design pressure is 3 psig. There are three principal floors in the building. An open shaft with an area of about 400 ft^2 connects the floors and opens into the overlying refueling bay.

The refueling bay has a volume of 1.0×10^6 ft^3. The design pressure of this sheet metal structure is very small. Blowout panels are provided with a total area of 240 ft^2.

The Peach Bottom secondary containment has a Standby Gas Treatment System but fire dampers would operate to shut off the system at the time of primary containment failure. The fire protection system is localized to cover the cable trays and would not provide general area coverage.

In the analysis with the Source Term Code Package, the reactor building and the refueling bay were each treated as single volumes. Based on the thermal-hydraulic calculations it was felt that the refueling bay structure would be severely damaged in the accident and no credit was taken for retention of fission products in this volume. Furthermore in the analysis of gravitational settling the horizontal area of only one floor was taken into account since the large area connecting the floors could act as a chimney, bypassing the other floors.

For each of the cases analyzed, the decontamination factor for the building was found to be about a factor of two. The principal retention mechanism was diffusiophoresis (the flow of aerosols to the wall with condensing steam). The secondary retention mechanism was gravitational settling. The period of high steam condensation was found to occur shortly after failure of the primary containment. In this time period the e-folding time for deposition was 17 minutes. Later, during periods of moderated steam condensation the e-folding time became approximately two hours. If a larger area is actually available for gravitational settling this characteristic time could be shorter. It is noteworthy, however, that in the cases considered, the principal fission product releases are predicted when deposition rates are low.

In each case hydrogen burning events were predicted to occur in the secondary buildings. Not only were the predicted pressures high enough to threaten the integrity of the buildings but the burns also had a profound effect on the residence time in the building. The predicted pressure pulses were typically in the range of 8 psig as indicated in Figure 2. The impact of pressures in this range on the reactor building are not clear. Certainly some damage would be expected. The refueling bay structure would not survive these loads. As indicated in Figure 3, however, each time a burn is predicted to occur the integral leakage of gas to the environment increased by approximately 1.0×10^6 and the airborne contents of the building would effectively be released to environment. This is the principal reason the decontamination factors for the building are as small as they are.

What if the hydrogen did not burn? There is considerable uncertainty in the quantity of hydrogen produced and in the manner in which the hydrogen burns in the analyses. The peak gas generation rate predicted in the analysis (which happens to coincide

with the peak period of fission product release from the fuel) is 250-500 moles/sec, corresponding to an e-folding time for leakage of 1 to 2 hours. Thus during the period of highest release from the fuel ex-vessel, when the level of steam condensation would be moderate, the expected decontamination factor would be in the neighborhood of two. At later periods when the gas generation rate is substantially reduced the decontamination factor could be substantially higher.

4.2 PWR Safeguards Building

The Surry plant is used as the reference for PWR subatmospheric designs in NUREG-1150. Two cases were analyzed in which the fission product flow path included the safeguards building which houses some of the engineered safety features equipment. In the V sequence the rupture of low pressure piping was assumed to occur in the safeguards building. Before reactor vessel meltthrough the fission products released from the fuel are carried through ECCS piping to the safeguards building. Although this building is quite small it is connected to another building called the Main Steam Valve House and Quench Spray Pump House. The combined volume of the two buildings is 2.74×10^5 ft^3. A major question affecting the source term for the V sequence is whether the pipe break occurs under or above the water level in the building that may result from the drainage of water from the refueling water storage tank.

The other case involved containment isolation failure in combination with a large loss of coolant accident and loss of all AC power. The location of the leakage was assumed to be associated with penetrations connecting the safeguards building with the primary containment. It is interesting to compare the decontamination factors associated with each case. Although the building was characterized the same way, the amount of retention predicted varied substantially. For example in the V sequence the decontamination factor for the volatile fission products released during the in-vessel melting phase was quite small (DF=1.2 for iodine) for the break occurring above the water level. However, when the break was assumed to occur below the water level the environmental release of iodine was reduced by an additional factor of 5.2.

The effectiveness of the secondary buildings was found to be substantially greater for the containment isolation case than for the interfacing LOCA case. For iodine the decontamination factor was calculated to be 4.3. The principal reason for the difference was residence time. In the isolation failure case the flow of gases into the secondary building was steady with time. In the V sequence, however, the rapid rate of steam generation that occurs following core collapse acted to drive fission products from the secondary building to the environment. The effectiveness of the secondary buildings is found to vary not only between sequences but

also as a function of time within a sequence. For example, the decontamination factor predicted for tellurium in the containment isolation case was somewhat lower than for iodine (2.4 versus 4.3) because it was released later in time from the fuel. A number of factors affect the time dependence of secondary building retention. Usually steam condensation is most effective early in an accident sequence. This is partly because there is more steam present from the loss of inventory of the reactor coolant system and partly because the structures in the building become thermally saturated with time. A compensating effect is the trend toward decreasing gas generation rates and increased residence times as the decay heat in the core decreases and the rate of core-concrete attack decreases. Another important effect is the decrease in aerosol size that occurs with time. Early in the accident, when a large quantity of material is being vaporized and condenses to form aerosols, the aerosols agglomerate to large size and settle rapidly. Late in the accident, when the vaporization rate is low, (such as during revaporization from the primary system) the density of aerosols is too low to promote agglomeration and the settling rate decreases.

5.0 COMPARISON WITH OTHER ANALYSES

Using the MAAP code the IDCOR program has also analyzed the effectiveness of secondary buildings in retaining fission products in severe accident sequences. In general the IDCOR results have indicated a greater potential for secondary building retention than the examples described above. In the example provided in the IDCOR Technical Report 85.2 "Technical Support for Issue Resolution"(6) a decontamination factor of 8.6 was obtained for the Peach Bottom reactor building. There are a number of reasons why the IDCOR values are typically higher than the examples cited here:

i. In the IDCOR analyses the failure of containment is typically later than in the NRC analyses and the associated leak rate is much smaller. Both of these tend to result in longer residence times in the secondary building.

ii. IDCOR has not accounted for hydrogen burning in the secondary building. This is to some degree because IDCOR predicts less generation of combustible gases.

iii. IDCOR predicts a less rapid attack of concrete by core debris and as a result a lower generation rate of gases and less driving force for release.

iv. IDCOR accounts for the revaporization of volatile fission products from RCS surfaces explicitly in their analyses. In the example presented in the IDCOR report the iodine source term to the environment is dominated by the revaporization source term which occurs over tens of hours. It is not surprising that in this time

period the decontamination factor would be higher than early in the accident.

6.0 MODELING UNCERTAINTIES

In general the source term methods that are used to predict transport and deposition in the reactor containment are equally valid for predicting these processes in secondary containment. The principal uncertainties in treating secondary building effectiveness in retaining fission products are associated with defining the physical state of the containment building and the secondary buildings after containment failure. The most difficult aspect of predicting containment performance is determining the mode and location of failure. In order to assess secondary building effectiveness, however, these are the initial conditions that must be defined.

From the view point of predicting thermal-hydraulic behavior and fission product transport in secondary buildings, the multicompartment aspect of secondary buildings is more challenging than primary containment analysis in most cases. It is more likely that a primary containment can be analyzed adequately with one or a few volumes than a secondary building. The inability of the Source Term Code Package to predict natural convection between control volumes could be a serious deficiency. In the ORNL Severe Accident Sequence Analysis program the CONTAIN code is being used to examine the importance of a multi-volume treatment of secondary buildings. The compartmentalized nature of secondary buildings is also recognized to have a potential impact of the behavior of hydrogen combustion, its effect on secondary building integrity and its effect on residence time.

Although research on the failure of primary containments can be expected to improve understanding of how they fail, where they fail and the resulting leakage, this is an area that will continue to have significant uncertainty after all the research is completed. It will be necessary to continue to treat secondary building performance in a probabilistic manner in which alternative modes of failure are considered. Having determined the mode and location of primary containment failure, it is not a simple exercise to determine how and where the secondary building will fail. Little consideration has been given to date regarding the methods of analysis that are applicable to predicting the structural performance of secondary buildings.

In order to put the importance of secondary building retention into proper perspective, it is necessary to determine the contribution of sequences such as V, in which secondary retention is a potentially important mitigating factor, to plant risk. Based on results presented previously by Sandia, it can be assumed that uncertainties associated with secondary performance will have an important impact on the uncertainty in plant risk at least for some plant design types.

7.0 RECOMMENDATIONS

Inadequate attention has been placed to date on evaluating the structural response of secondary buildings to severe accident loads. Depending on the accident conditions, secondary building retention does have the potential to change risk perspectives. It can be expected that in the future more effort will be placed in PRAs on including the effect of secondary buildings on source terms. A better technical basis is required for these analyses, however, as an aid to the analyst in performing the analyses or as guidance to the NRC in evaluating the credibility of PRA analyses in which credit for secondary building retention is claimed. While neglect of secondary containments, as has been the case in many past studies, may be overly conservative, oversimplified treatments may lead to unrealistic conclusions of secondary containment effectiveness.

REFERENCES

1. U.S. Nuclear Regulatory Commission, "Reassessment of the Technical Bases for Estimating Source Terms", NUREG-0956, Draft Report for Comment (July, 1985).

2. Gieseke, J. A., Cybulskis, P., Jordan, H., et al., "Source Term Code Package: A User's Guide", NUREG/CR-4587, BMI-2138, (Draft) (April, 1986).

3. U.S. Nuclear Regulatory Commission, "Nuclear Power Plant Risks and Regulatory Applications", NUREG-1150, to be published September, 1986.

4. U.S. Nuclear Regulatory Commission, "Reactor Safety Study - An Assessment of Accident Risks in U.S. Commercial Nuclear Power Plants", WASH-1400 (NUREG 75-104) (October, 1975).

5. Wichner, R. P., et al., "Noble Gas, Iodine and Cesium Transport in a Postulated Loss of Decay Heat Removal Accident at Browns Ferry", NUREG/CR-3617 (August, 1984).

6. Fauske and Associates, "Technical Report 85.2, Technical Support for Issue Resolution" (July, 1985).

ORNL-DWG 82-5181 ETD

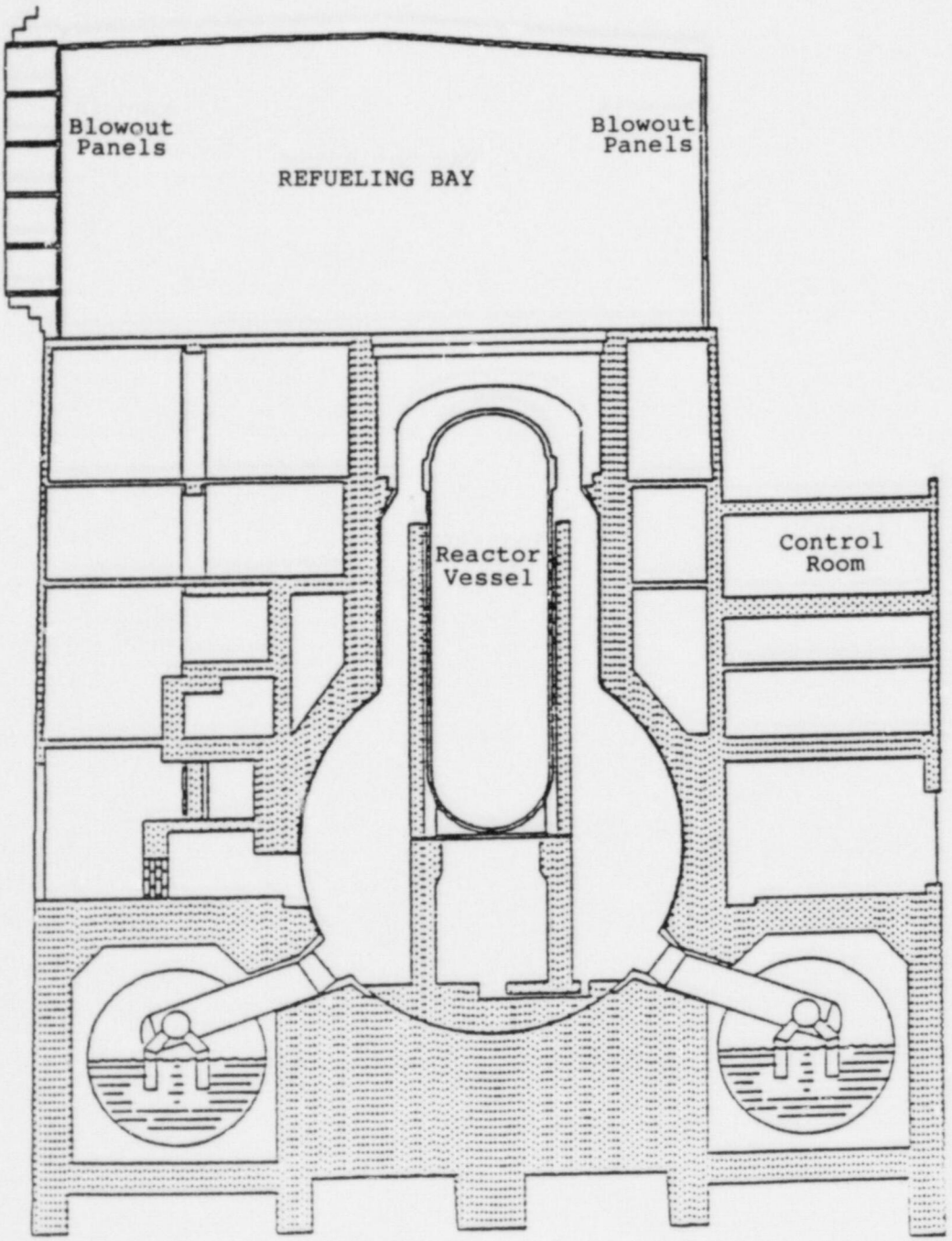


FIGURE 1. LOCATION OF THE MK I PRIMARY CONTAINMENT WITHIN THE SECONDARY CONTAINMENT (REACTOR BUILDING)

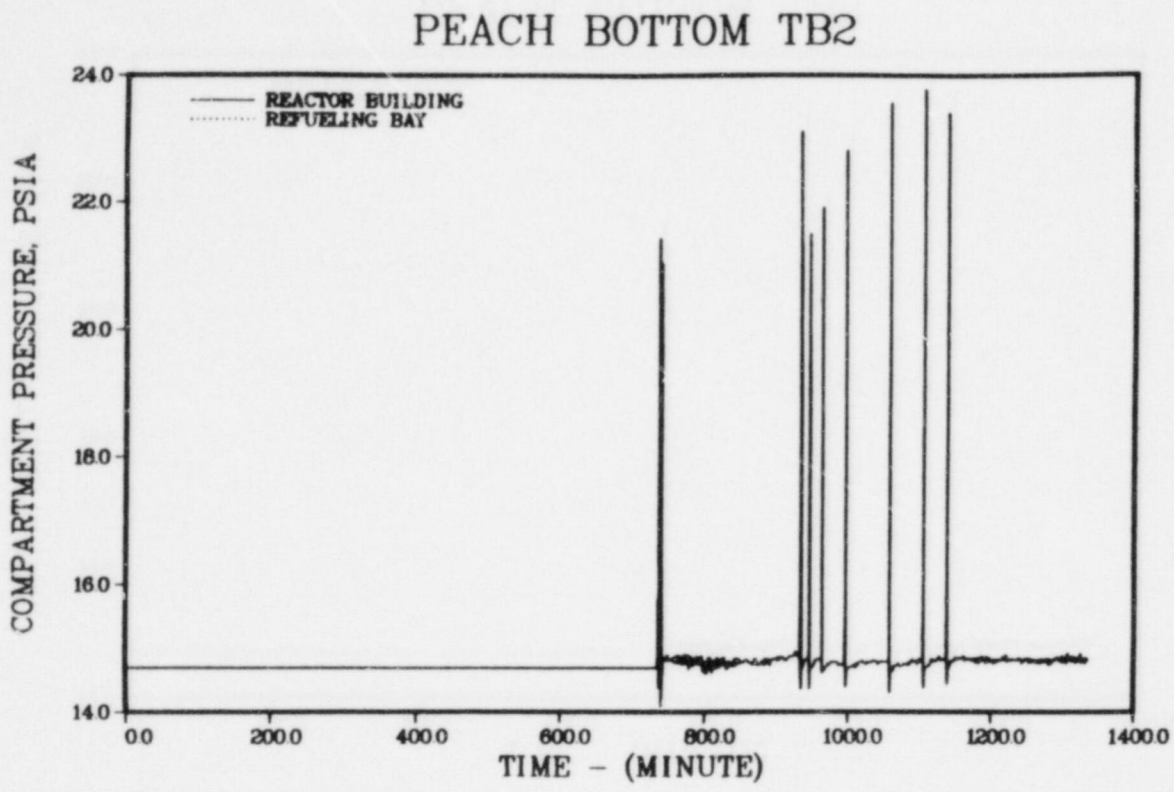


FIGURE 2. SECONDARY CONTAINMENT PRESSURE RESPONSE FOR TB2

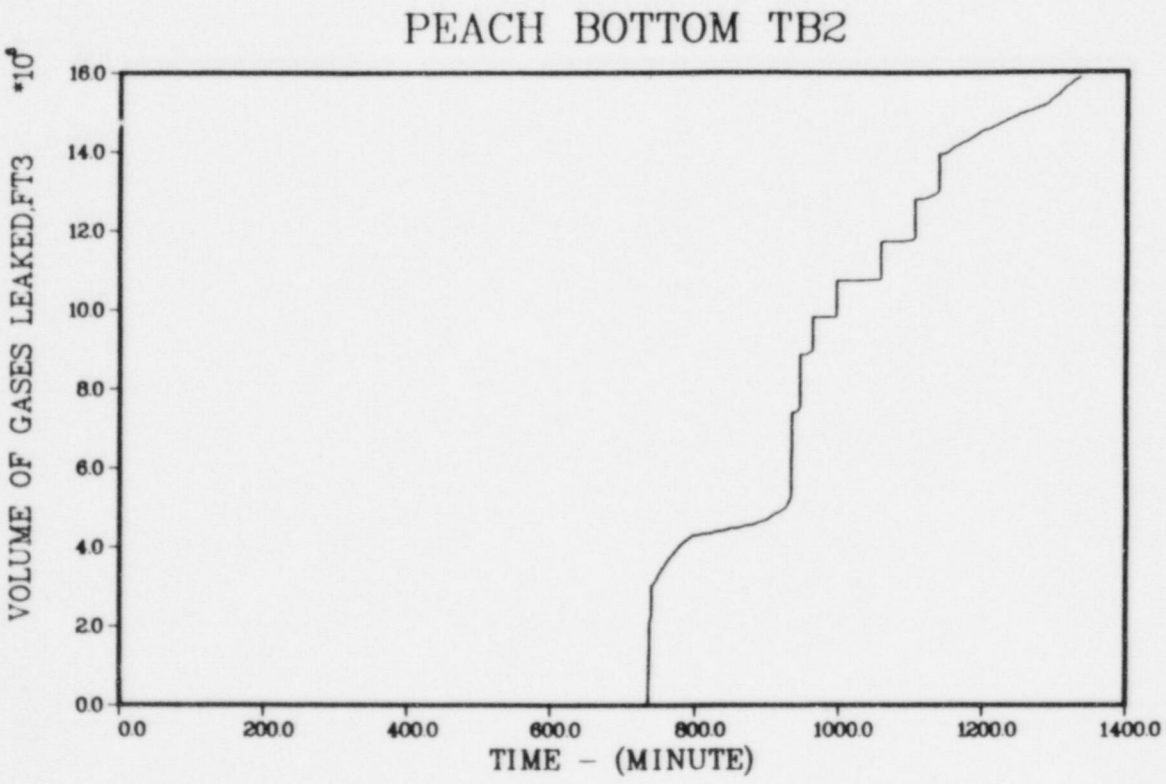


FIGURE 3. TOTAL VOLUME OF GASES LEAKED FOR TB2

RISK ANALYSES OF THE RINGHALS PLANTS: CONTAINMENT BEHAVIOUR AND FILTERED VENT

R Espefält, L Gunsell, G Löwenhielm
Swedish State Power Board, S-162 87 Vällingby, Sweden

G Kaiser, P J Fulford
NUS Corporation, 910 Clopper Road, Gaithersburg,
Maryland 20878, USA

1. INTRODUCTION

In 1981, the Swedish Government requested that the potential for the accidental release of radioactive materials from Swedish Nuclear Power Plants should be investigated, and that the need for filtered vents or other mitigative devices should be evaluated. In the case of the Barsebäck plant, a request was made for a filtered vent to be built and made ready for operation by 1985. This has been constructed already. For the other plants the time limit was set to the end of 1988.

The investigation was organized in two separate projects:

- RAMA, where generic issues were studied and analytical tools were developed in a joint Swedish effort, with participation from both the authorities and utilities

- MITRA, a strictly SSPB project for plant specific analyses of SSPB Ringhals and Forsmark plants.

For the Ringhals plant, the MITRA investigations comprise a probabilistic safety analysis for each of the units No 1 (ASEA-ATOM BWR 750 MWe) and No 2 (Westinghouse PWR 800 MWe) and some additional analyses for units No 3 and 4, which are similar to No 2. The results of the analyses were supplied to the Swedish Nuclear Power Inspectorate for review in April 1985 (ref 1).

As a result of the review, regulatory requirements were proposed by the authorities in a report to the Swedish Government. In the report, the results of the risk analyses described in this paper are combined with requirements for the further development of accident management. The adopted strategy puts a strong emphasis on both hardware and procedural measures aiming at bringing the reactor core back to stable cooling and maintaining containment integrity during an accident. The requirements include improved protection against overpressure (both early and late) and means for controlled venting of the containment. For controlled venting and pressure relief a limit is set on the radioactive release at 0.1% of core fission product inventory excluding noble gases. The basic idea is to allow flexibility for the operator to act and maintain the containment

integrity. It is not considered acceptable to keep the containment at high pressure for a long time.

In the following chapters, the role of the containment behaviour in the risk analyses for the Ringhals plant is discussed. Finally, the presently visualized strategy for meeting the requirements is briefly outlined.

2. CONTAINMENT EVALUATION

2.1 Ringhals 1 BWR

2.1.1 Brief Description of Plant and Containment

Ringhals 1 is an ASEA-ATOM BWR with external main recirculation pumps and with a power of 750 MWe.

The containment is typical of the second generation ASEA-ATOM design and is shown in Figure 1. The pressure suppression pool covers the bottom area of the containment and can be reached by molten core material from the pedestal region via a drain pipe. The volume (excluding the pool) is 8 300 cubic meters.

Basically, the pressure retaining reactor containment vessel is composed of a load bearing concrete structure, a steel liner embedded in concrete, serving as the primary leaktight barrier, a bolted steel dome as the containment lid above the reactor vessel and a large number of penetrations. The base of the containment consists of a reinforced concrete slab. The cylindrical wall is a concrete shell prestressed in the vertical as well as the horizontal direction. The design pressure is 0.4 MPa (internal overpressure).

2.1.2. Containment Failure Modes

An evaluation of the containment has been performed to determine its probable failure modes and its ability to resist overpressure. The evaluation was based on both the original design calculations and additional calculations in specific areas, taking into account known deviation from design values. Estimation of the probability of large leakage before gross rupture of the containment was included.

The results of the calculations show that the most probable location of a rupture is at the intersection between the cylindrical wall and the roof. The mode of failure identified is overloading and break in one of the vertical tendons, causing adjacent tendons to be overloaded and resulting in rapidly propagating breaks in the vertical tendons. In this way a large opening is expected to be formed in the containment. A somewhat conservative lower pressure limit for this to occur is 0.65 MPa(g).

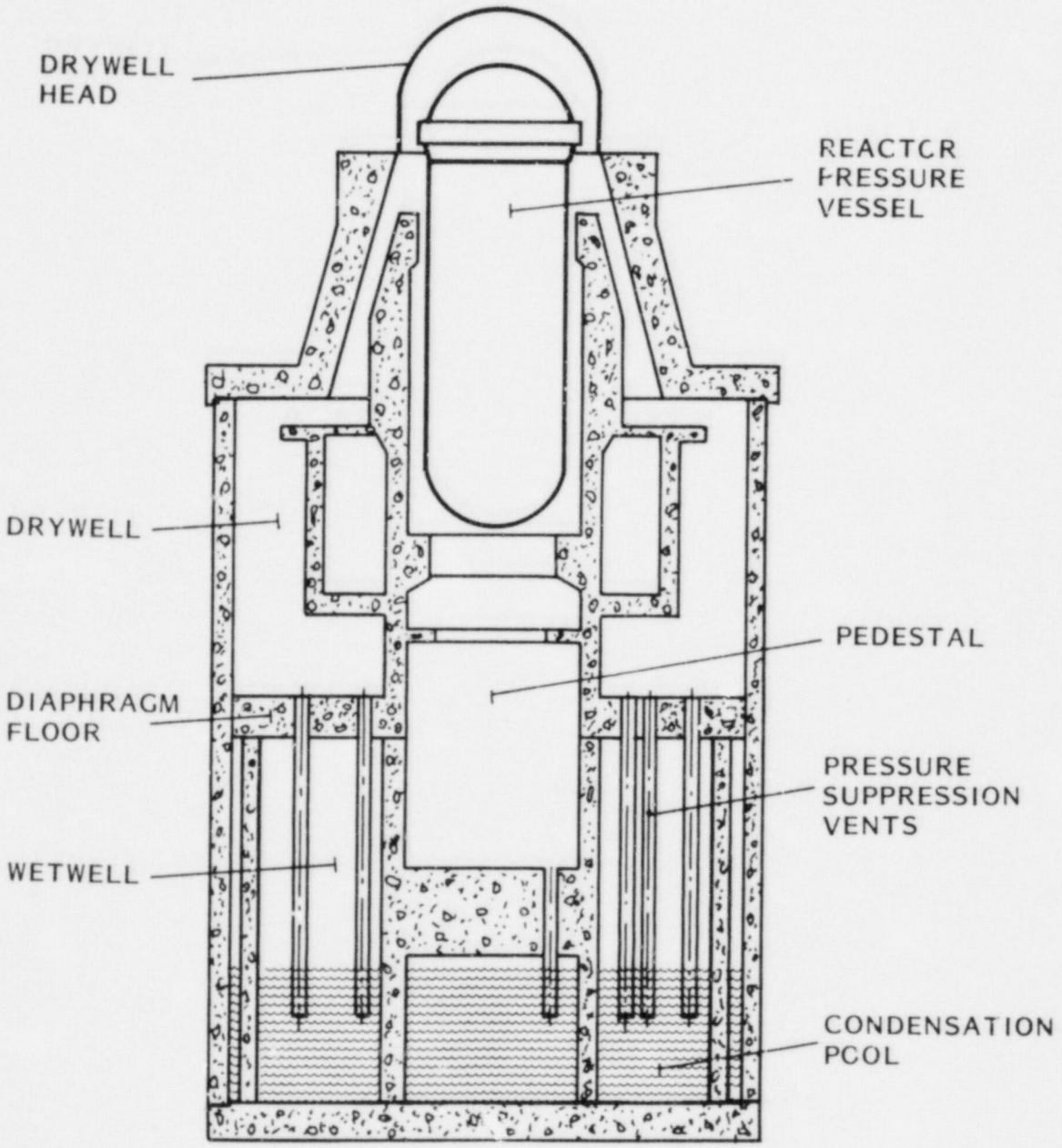


Figure 1. Ringhals 1

Containment
Configuration

It is not considered likely that significant leakage will occur before gross rupture. This is due to the design of the steel liner, which is equipped with a flexible, torus-shaped, connecting plate between the wall and the roof, which will allow wall displacements without leakage. At the temperatures considered - up to 300°C - leakage is also not considered probable at the wall penetrations.

A second probable failure location is at the intersection between the concrete structure and the steel dome, where the concrete structure would crack and the anchoring of the steel flange, to which the dome is bolted, would fail. This failure mode is less likely than the one described above and the failure pressure estimated to be at least 50 kPa higher. All other structures have been found to have larger failure pressures.

The evaluation has shown that the most probable failure mode is a large rupture of the drywell with negligible preceding leakage. The consequent rapid depressurization of the drywell will cause a transient pressure difference between wetwell and drywell. No detailed analysis has been made of the consequences of this transient. It is possible, however, that it would cause a vertical displacement of the internal structures of the containment, including the pedestal and the reactor tank, since these structures are not fixed to the walls or bottom slab. Since such a displacement could cause damage to the core cooling systems it has been conservatively assumed in the risk assessment that gross rupture of the containment will cause loss of core cooling in sequences, where this has not yet occured.

2.2 Ringhals 2, 3 and 4 PWR's

The leakage probability for the Ringhals 2 PWR has been extensively evaluated and is summarized in Appendices C and D of ref 2.

2.2.1 Brief Description of Plant and Containment

Ringhals 2 is a three-loop Westinghouse PWR with a power of 800 MWe. There are two other PWRs on the site, Ringhals 3 and Ringhals 4, with power levels of 900 MWe.

Ringhals 2 has a large, dry containment consisting of a post-tensioned reinforced concrete structure with a gross volume of 58 000 cubic meters and a net volume of 51 000 cubic meters. The containment structure has an interior radius of 17.7 m and a height of 73.6 m from the top of the containment dome. The height of the cylindrical wall of the containment is 58.5 m, its thickness is 1.1 m, and the dome thickness is 0.8 m. The basemat is 3.05 m thick in the cavity region and 3.85 m elsewhere. The steel liner has a thickness of 7 mm. The design pressure of the containment is 0.414 MPa (internal overpressure).

2.2.2 Gross Rupture

SSPB has carried out a numerical analysis of the response of the Ringhals containment using the methods of stress analysis described by Frid (ref 3). Tendon capacities in the the cylinder, dome, and ring girder were investigated. Potential modes of failure in the base slab were also considered. The slab was found to have a higher capability than the cylinder. The most likely mode of containment failure is gross rupture in the cylinder upon reaching the ultimate capacity of the prestressing tendons, which for Ringhals 2 corresponds to a strain of about 3.5 percent. Once failure of a few neighboring tendons has occurred, the remaining tendons, reinforcing steel, and containment liner do not have sufficient reserve strength to withstand the internal pressure, and a large rupture of the structure and liner is expected. This rupture could be between 1/3 and 1 meter wide, and could extend for 3/4 of the height of the cylinder, that is, an area of several square meters.

The properties of the prestressing cables under tension are well understood. It is expected that there will be a structural failure by the time the internal pressure has reached 1.3 MPa (abs). The uncertainty in this estimate is quite small. SSPB has provided an assessment of the probability as shown in Figure 2. The probability is unity at a pressure of 1.3 MPa, and is "small" at 1.2 MPa, with a linear interpolation between these two values on a log probability vs linear pressure plot. SSPB's assessment is thought to be somewhat conservative in the sense that the median failure pressure is probably somewhat higher than shown in Figure 2.

It is pertinent to note that, with such a high failure pressure, it is not possible for a hydrogen burn to fail the containment early.

2.2.3 Pressure Induced Leakage Before Rupture

Several ways in which the buildup of pressure may cause the containment to leak before gross rupture occurs have been considered. All of these are expected to have a small probability of occurrence.

2.2.3.1 Liner Failure Near Leak Chases

SSPB has analyzed a number of different kinds of penetrations and has concluded that the most likely locations for liner failure are backed by leak chases that were installed at the time of construction. This is illustrated by Figure 3, which shows the liner butt weld with a leak chase behind. The most likely location of liner failure is judged to be at a defective butt weld, in which case the leak chase would provide pressure retention capability.

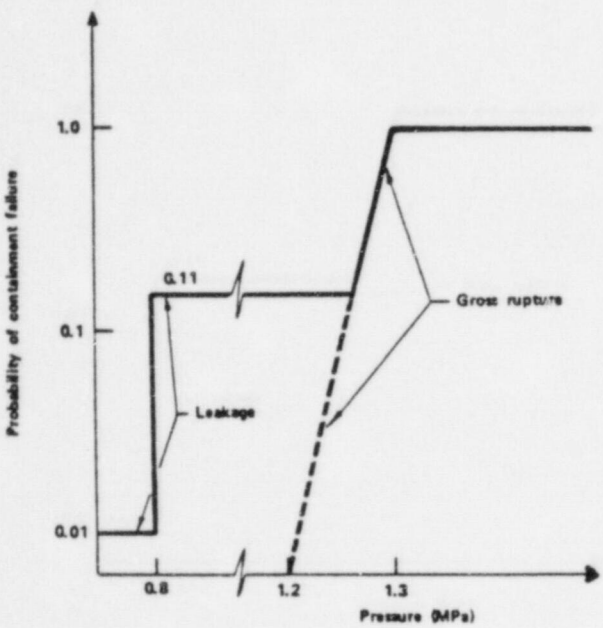


Figure 2 - Ringhals 2
Containment Failure
Pressure Distribution

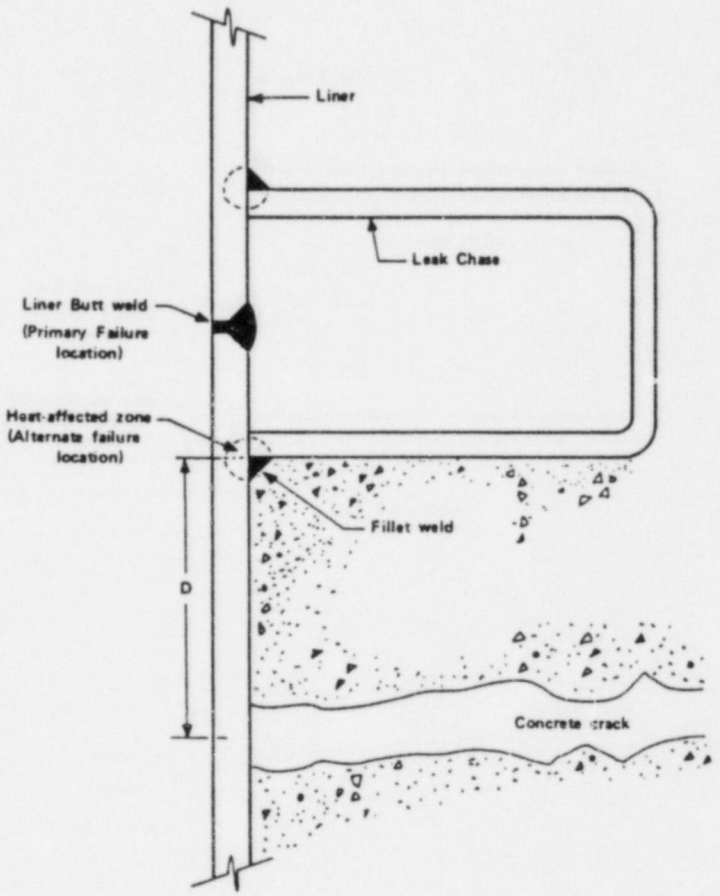


Figure 3
Potential Liner Failure
Locations

Note: If the concerete crack as shown, the leak chase tends to act as a shear anchor and concentrate the strains over the length "D" (unless the fillet welds fail in shear). Stresses in the liner butt weld are reduced compared to the stress in the liner beyond the leak chase, and failure may occur in the heat-affected zone of the leak chase to liner fillet weld. Failure in this location can result in leakage behind the liner and through the concrete crack.

2.2.3.2 Failure due to Pipe Loads

Failure of the liner near a penetration can also occur due to pipe loads caused by the radial deflection of the containment structure at high strain levels but before tendon failure. Such failures are only possible near thick walled pipes (i.e.sch.160) which are anchored very close to the containment. As the containment deforms outward under pressure, it may effectively slide over the pipe and thus cause a leak. Since this type of failure requires a very specific combination of pipe strength and anchorage configuration, it is considered to be very unlikely; that is, it is less probable than the butt weld failure discussed above.

2.2.3.3 Failure of Major Penetrations

SSPB has investigated the potential for failure of the major penetrations in the Ringhals 2 containment and has concluded that failure in these locations is unlikely. This is also generally consistent with U S experience. Major penetrations are normally over-reinforced compared to the remaining structure and tend to behave as essentially rigid inclusions in the shell.

2.2.3.4 The "Rashid" Mode of Failure

Rashid (ref 4) has proposed a mechanism whereby local liner failures are possible. Experimental data on the way in which reinforced concrete vessels respond to internally generated pressures show that the concrete tends to crack in a regular, widely spaced pattern, with a spacing of about a meter being possible for reactor containment structures. After the cracking has occurred, the behavior of the liner will depend on how strongly it is bonded to the concrete. If it is firmly bonded, then the liner may "stick" to the concrete and the strain will be confined to the length of liner adjacent to the crack. Thus, if there is a 1% strain in the tendon over 1 m, there would be a 20% strain over 5 cm. This is the "Rashid" mechanism leading to local liner failure. However, it is judged that the Ringhals 2 liner is not firmly enough bonded to the concrete for this mechanism to be plausible.

2.2.4 Leakage of Electrical Penetrations

The electrical penetration assemblies (EPAs) through the Ringhals 2 containment are of the Westinghouse Canister type and are constructed as follows. The penetration is built into a stainless steel pipe with a diameter of 8 inches (20 cm) and a total length of 62 inches (1.6 m). At each end, some inches into the pipe, stainless steel headers are fitted for the conductors. The cables are crimped to the conductors. The outer parts of the pipe where the crimps are located are potted with epoxy, except for the 6 kV cables. Flame resistant spacers are located on the potting at the ends of the pipe.

The 6 kV penetrations have no potting; they have a ceramic-metal seal assembly. The compartment between the headers can be pressurized for leak detection.

Sebrell (ref 5) has reviewed design information on Westinghouse EPAs and concluded that "...there is a very low probability of loss of integrity below 340° - 350°F (440-450K) and 100 to 115 psig (0.8 to 0.9 MPa abs)". In accident sequences in which leakage before rupture could be important, such temperatures are not seen in the containment until close to the expected time of gross rupture: furthermore, the outboard end of the EPA would be exposed to lower temperatures. Overall, it seems unlikely that the canister EPA will leak. Nonetheless, a conservative probability of 0.1 has been assigned to the probability of EPA leakage late in the sequence.

2.2.5 Failure to Isolate Containment

The probability that the containment will not be isolated has been covered in detail in Appendix B of ref 2. There, on the basis of a review of US PWR experience, it was concluded that the most probable way in which an isolation failure might occur would be as a result of small leakages from airlocks and the equipment hatch or arising from miscellaneous causes such as missing gaskets, flange caps and inadvertently opened lines. The probability of such leakages is estimated to be 2.5E-2. However, for rates of leakage that are significantly above the design basis (0.1% per day) the probability is lower, about 1.0E-2, corresponding to openings with effective diameters in the range 2.5 through 10 cm (diameters from 1" through 3", 2.5 through 7.5 cm, and leak rates from 7% through 100% per day). This failure to isolate is judged to be more likely than pressure induced leakage. This diameter is sufficient to prevent gross rupture of the containment.

2.2.6 Summary for Ringhals 2

Figure 2 summarizes the results of the analysis of the leaktightness of the Ringhals 2 containment. There is a probability of 1% that the containment will not be isolated. At 0.8 MPa, there is a step up to 11% to allow for possible leakage of an EPA. Finally, at around 1.2 MPa, the curve rises steeply, representing the cumulative probability of failure due to gross rupture.

2.2.7 Ringhals 3 and 4

The Ringhals 3 and 4 containments have not been investigated in as much detail. The probability of failure to isolate should be the same as for Ringhals 2. However, the containment designs differ and the pressures at which gross rupture would occur are lower. This is due to a different construction of the intersection between the cylindrical wall and the base slab. Finite element calculations have shown that at a pressure of about 0.6 MPa (abs) cracks will appear in the base slab, become extensive at 0.67 MPa and cause rupture at

a slightly higher pressure. Therefore, it is less likely than for Ringhals 2 that EPAs would leak before gross rupture, or that other modes of pressure induced leakage as discussed above would occur.

3. RISK ANALYSIS

3.1 Ringhals 1 BWR

The probabilistic risk assessments in the MITRA investigations were completed at the beginning of 1985. The release of radioactive material for the dominant accident sequences was calculated using the MAAP 1.0/RETAIN-S codes, which were developed by IDCOR and further developed and modified by the RAMA project in Sweden. On the basis of these calculations, the potential for reduction of the release was estimated for different measures to protect the containment integrity: a safety valve with or without filtering and an alternative containment cooling system.

The results of the analysis have been summarized in curves showing the cumulative release frequency as a function of the release amplitude (frequency of release larger than X%). The release is expressed in terms of percent of core inventory of radioactive iodine and cesium, which are treated as one group in RETAIN-S. These isotopes are considered to dominate environmental consequences, in particular the long term land contamination which is a special concern in Sweden.

The cumulative release frequency for Ringhals 1 is shown in Figure 4, where the corresponding curves calculated from WASH-1400 data are also drawn for comparison. The two curves for Ringhals 1 show the present situation and the one where containment rupture is prevented by means of a pressure relief device, e.g. safety valve (without filtering).

The safety valve will prevent accident sequences like:

- LOCA with failure of the pressure suppression function
- Transient or LOCA with loss of containment cooling.

Several sequences in this group represent containment failure before core melt, where core melt is caused by the assumed damage to core cooling systems in connection with containment rupture, as described in chapter 2.1. In these cases, core melt has not occured at the time of pressure relief and will not occur since core cooling is maintained. No fission products are available for release and, therefore, filtering gives no extra benefit. In those cases where late overpressurization after core melt is prevented the release was calculated to be reduced by the controlled, slow pressure relief.

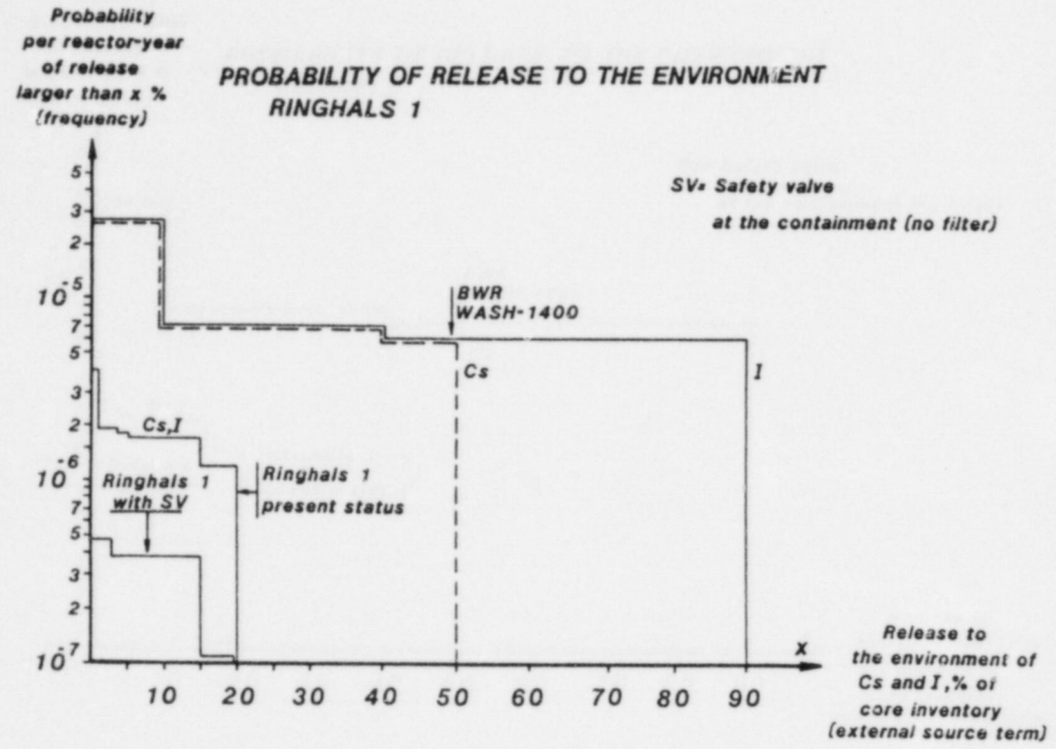


Figure 4

The reason for this is the extra residence time for agglomeration and deposition of aerosols. A further reduction of the release by filtering was estimated to have a small influence on the overall risk.

The residual risk is mainly due to reactor pressure vessel rupture, LOCA outside the containment and some ATWS sequences.

A similar evaluation has been made for an alternative containment cooling system. By providing a reliable back-up water source for containment spray and preventing gross containment rupture, a significant reduction of large releases can be achieved. The reason is the same as discussed above: The loss of core cooling caused by the containment overpressurization is prevented in those cases, where containment cooling is lost but core cooling is intact. The main difference as compared to a safety valve would be the LOCA sequences containing failure of the pressure suppression system, which causes an initial very rapid containment pressure increase.

The calculations cited above were performed with the first generation of IDCOR codes, where internal natural circulation and revaporization of volatile fission products in the primary system could only be handled very approximately. The results are therefore

subjected to considerable uncertainty, although conservative assumptions have been made in several instances, where knowledge was insufficient.

The main conclusion drawn from the above results is that a pressure relief device, e.g.a safety valve, preventing gross rupture of the containment leads to a significant reduction of the frequency of large releases and of core melt. With respect to the need for filtering, the uncertainties in the analytical methods, in particular regarding revaporization, and the new requirements for controlled venting discussed in the introduction have to be taken into account. No results are presently available with the new generation of codes for these cases, but in order to meet the strict 0.1% limit in all venting scenarios, it seems likely that some filtering device will be required in the venting line.

3.2 Ringhals 2, 3 and 4 PWR - Filtered Vent

The advantages and disadvantages of a filtered vent of a design similar to that used for Barsebäck for the Ringhals 2 containment were considered in the MITRA project (ref 1 and 2). The assumed failure pressure of the bursting disc was 0.65 MPa, in contrast to the 1.2 - 1.3 MPa for gross rupture. The cumulative release frequency for Ringhals 2 with and without the filtered vent is shown in Figure 5.

The principal conclusions about the filtered vent are as follows:

- The filtered vent has no impact on bypass sequences or sequences with failure to isolate containment because the pressure in the containment never rises to the set point and the releases therefore bypass the filtered vent system. These are the sequences that are likely to be risk dominant as far as early health effects are concerned. However, none of these sequences has a predicted point estimate frequency exceeding 10^{-7} per reactor year.

- For sequences in which the core melts before overpressure failure of the containment occurs, source terms without the filtered venting system are already very small. If a filtered venting system was installed, source terms would be reduced but not in such a way as to make a significant reduction in the impact on the public, since the source terms with and without a filtered vent are both expected to be small, with the noble gases dominating the offsite doses. The filtered vent would affect sequences with a total frequency of about 10^{-6} per reactor year, about half the core melt frequency. *

* Note - about half of the core melt sequences for Ringhals 2 do not cause containment failure because long term containment heat removal is available.

o Possible advantages of the filtered vent include forestalling the violence of a gross rupture, which is expected to be the most likely mode of containment failure. Possible disadvantages include the rupture of the disc many hours before the containment would be expected to fail from overpressure, thus reducing the time available to recover long term cooling of the containment, and the possibility that an early hydrogen burn could rupture the disc.

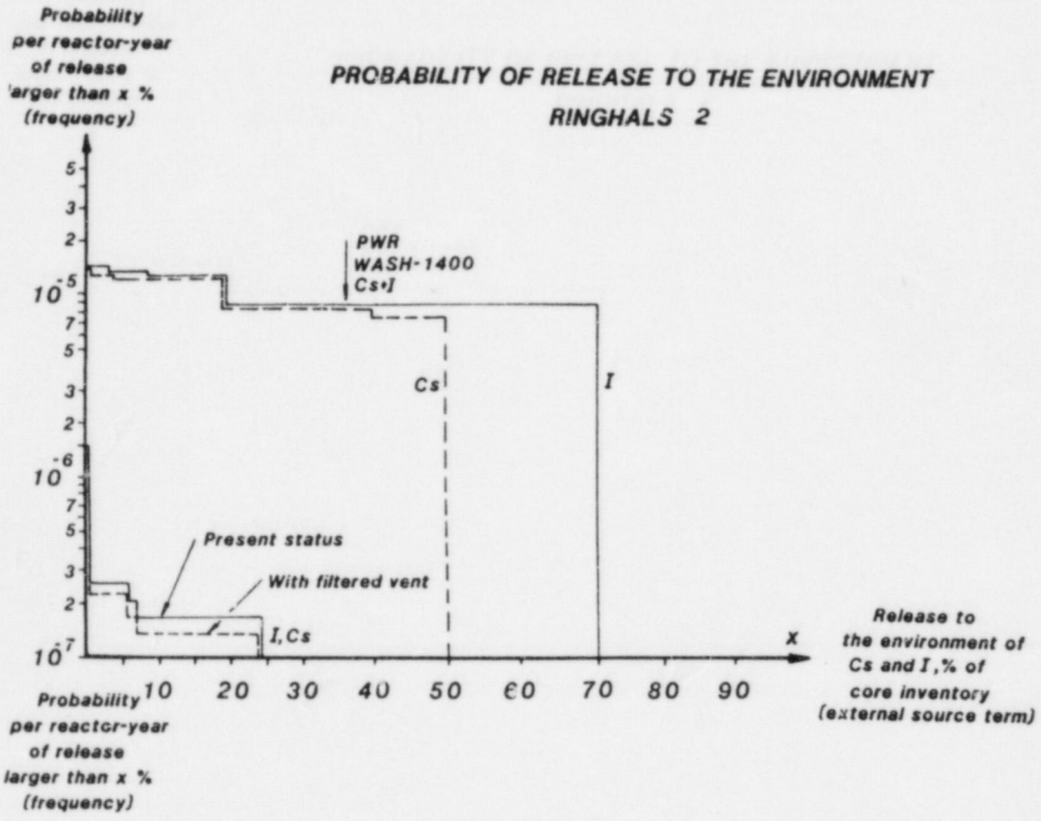


Figure 5

An alternative containment cooling system was studied also for the Ringhals 2 and the effect on the source term evaluated. The resulting influence on the release frequency was found to be similar to that of the filtered vent.

Ringhals 3 and 4 are similar to Ringhals 2, except that, as noted above, the failure pressure of their containment was found to be lower for construction - specific reasons. Nonetheless within the framework of the MITRA project (ref 1) it was possible to estimate the influence of the lower failure pressure on the source terms and to use the same basic assessment for all three units. The overall

conclusion drawn by SSPB is that from the point of view of risk it is not justified to introduce a large scale filtered vent for Ringhals 2, 3 or 4. However, in order to meet the accident management requirements, facilities for venting of the containment will have to be installed for the PWR units as well.

4. CONCLUSION

The risk analysis performed for the Ringhals plants has demonstrated the importance of the containment with respect to preventing releases of radioactive material during severe accidents. The importance of plant specific features when evaluating the containment behaviour and influence on accident sequences is also evident.

Work is presently going on to implement the new Swedish strategy for handling severe accidents. This will include new installations to protect the containment by pressure relief and controlled venting, probably combined with means for providing a back-up source of water for the containment sprays.

In parallel, a strong effort will be made to develop accident management instructions, analytical validation of these instructions, operator training etc.

The ultimate aim of this work is to ensure that, in the case of a severe accident, there will be options and time available for the operator to restore cooling of a damaged core and keep the containment intact at low pressure, while releases are restricted to less than 0.1% of the core inventory of fission products excluding noble gases.

5. REFERENCES

1. MITRA Final Report, 1985
   Swedish State Power Board (April 1985)

2. NUS Corporation, 1984. Ringhals 2 Probabilistic Safety Study Phase II, Gaithersburg, Maryland, USA; prepared for the Swedish State Power Board.

3. Frid, W, 1981. A Study of Hydrogen Combustion and Containment Building Response at Ringhals Power Plant Unit No 3. Presented to the Workshop on the Impact of Hydrogen on Water Reactor Safety, Albuquerque, New Mexico, USA, January 1981: SAND-0661 (NUREG/CR-2017). Vol III p, 281 et seq.

4. Rashid, Y R, 1983. Review of the WASH-1400 Surry Containment Capability, Electric Power Research Institute Project 2288-2, ANATECH International Corporation, La Jolla, California, USA.

5. Sebrell, W, 1983. The Potential for Containment Leak Paths Through Electrical Penetration Assemblies Under Severe Accident Conditions, NUREG/CR-3234 (SAND83-0538), Sandia National Laboratories, Albuquerque, NM.

CONTAINMENT INTEGRITY IS A MAJOR PART OF KKL-SAFETY SYSTEMS PRA

Th. Schaub
Kernkraftwerk Leibstadt AG
4353 Leibstadt, Switzerland

H.P. Hänni
Motor-Columbus, Consulting Engineers Inc.,
5401 Baden, Switzerland

ABSTRACT

Assuming a hypothetical accident with core meltdown, hardware changes are described with which the containment integrity of the Leibstadt NPP can be secured. Venting of the containment through the standby gas treatment system is initiated manually. This system is called COSA (Containment Safegard).

The pressure margins for the containment failure are determined and compared with the design pressure.

The expected population doses without and with COSA are presented.

On the basis of a fault tree PRA the gain in overall safety is derived. A cost-benefit analysis on the three safety levels 1, 2 and 3 leads to a general formula as a proposal to minimize the ratio of investment cost to safety gain.

CONTAINMENT INTEGRITY IS A MAJOR PART OF KKL-SAFETY SYSTEMS PRA

1. INTRODUCTION

Several publications have shown that the safety defense-in-depth method using PRA is a promising tool for improving safety in a economical way. This method has been especially applied on safety level 1, 2 and 3 for KKL Leibstadt.

Before any measures will be taken to lower the probability of occurrence of severe accidents it is obvious to improve first the reliability of the safety-related systems; that is exactly what has been done for the Leibstadt Nuclear Power Plant in applying the Project Planning Rules of the Swiss Licensing Authority (KSA 22/1, Ref. 3). In addition to the General Electric Standard ECCS a new system called SEHR (Special Emergency and Heat Removal) has been installed which can be used for low pressure injection and/or containment cooling. The realization of this system was a great step forward to improving overall safety and especially containment integrity.

Containment integrity is a fundamental requirement for nuclear power plants. If it cannot be maintained for design basis accidents or performed during unlikely severe accidents the "nuclear society" would not be credible anymore. Therefore, any effort which will be made to improve the integrity of a containment with reasonable cost is a step in the right direction. NPP Leibstadt is soon installing a containment venting system called COSA (Containment Safeguard) which together with "emergency procedure guidelines" (EPG) is capable to ease the situation for accidents beyond DBA and to fulfil criteria which are in the limits of the ordinance for radiation protection (accident dose of 10 rem near the fence of the plant).

The authors extend the cost-benefit method/formulae [9] for all safety levels. This method could be generally applied for other nuclear power plants or industrial plants.

A section of NPP Leibstadt (KKL) is shown in Fig. 6.

2. PRA Study for NPP Leibstadt by Improvement of Safety Features on Level 1 and 2

NUREG-1050 [1] and NUREG-2300 [2] describe how a PRA study can be performed on the safety levels 1, 2 and 3.

2.1 Definition of Safety Level 1, 2 and 3 [1,2]

For level 1 PRA only the system accident sequences are developed. It identifies the potential accident sequences that may lead to core damage. The containment analysis for a level 1 PRA is limited to an analysis of core containment and safety systems

to determine impacts on sequences leading to core damage (core melt sequences).

Level 2 PRA must include a detailed evaluation of containment response to system accident sequences. When such PRA are performed, both systems event trees and containment event trees are used to describe complete accident sequences. Level 2 analyses the transport and release of radionuclides from the core to the environment. It provides insights into the risk by generating the frequencies and magnitudes of the release categories.

A level 3 PRA analyses the transport of radionuclides to the environment and assesses the public health and economic consequences of accidents. Thus a level 3 study provides an assessment of public risk.

2.2 Improvement of ESF (Engineered Safety Feature) on Level 1

Before any measure will be taken to lower the risk of severe accidents to the environment (back end), it is obvious to improve first the reliability of the safety-related systems (front end); that is exactly what has been done for the Leibstadt Nuclear Power Plant in applying the Project Planning Rules of the Swiss Licensing Authority (KSA 22/1, Ref. 3). In addition to the General Electric Standard ECCS a new system called SEHR (Special Emergency and Heat Removal) has been installed which can be used for low pressure injection and for containment cooling (Fig. 1). Generally speaking, with the implementation of SEHR, the core melt frequency has been lowered for all events which have been discussed in GESSAR II [4].

2.3 Improvement of ESF on Level 2

Containment integrity is a fundamental requirement for nuclear power plants (back end). If it cannot be maintained for design basis accidents or performed during unlikely severe accidents the nuclear society would not be credible anymore. Therefore any effort which will be made to improve integrity of a containment with reasonable cost is a step in the right direction. NPP Leibstadt is about to install a containment venting system called COSA (Containment Safeguard) which is capable - together with "Emergency Procedure Guidelines" (EPG) - to ease the situation for accidents beyond DBA and to fulfil criteria which are within the dose limits of the ordinance for radiation protection.

In an early stage of the project discussions with the authority took place with respect to the capabilities of the containment in view of hypothetical accidents exceeding the design pressure in the containment. The mishap at Three Mile Island reactivated these discussions.

One of the consequences was the necessity to install a hydrogen recombiner. The thermal type was chosen. One of the reasons

of this choice was the possibility that the equipment could be installed outside of the containment, utilizing two containment penetrations.

The recombiners themselves have been disposed in the adjacent fuel handling building. The authority required only one recombiner unit to be readily operable. We therefore shared a spare unit with another nuclear power plant, as a couple of hours could be allowed for the transport.

A major advantage of this arrangement consisted in the possibility to branch the recombiner system to the standby gas treatment system (SGTS). Fig. 2 shows the simplified schematic of the two systems. A number of locked closed valves and test vent nozzles are necessary in order to check the permanent tightness throughout the life of the plant. The first idea to complete the connection with the aid of a separate spool piece-only in case of necessity-did not find the approbation of the authority. We therefore had to provide a fixed connection.

The size of the connecting pipe is partly 80 mm and partly 100 mm. Starting from a containment differential pressure of 1 bar, a mass depletion of about 1 kg/s can be expected. The design mass flow rate of the SGTS is 2.4 kg/s. Suction is taken from the containment annulus at slightly less than 1 bar i.e. at underpressure. Under these conditions the vent mass flow can be taken over by the SGTS. However the valve in the connecting pipe has to be opened carefully to avoid a pressure peak which could endanger the check valve and dampers. Further it has to be considered, that during the venting of the containment only reduced suction can be taken from the annulus by the SGTS. Containment leakage could thus be carried to the environment without charcoal filter. With the low leak rates which - owing to the COSA - still can be supposed, its contribution to the population dose is not very significant.

2.4 The Pressure Margins of the Containment

It has been indicated above that we shall have recourse to the COSA when the containment pressure tends to overpass the ultimate safe pressure. As this is a very severe decision one has to have a clear understanding of the endangered parts and their safety margins. The venting of the containment being the last resort, one would risk a marked infringement of the design pressure. However a culmination point should be expectable within the pressure margin.

Personnel lock

A differential pressure of 2.55 bar can be borne without exceeding the design stresses. At a differential pressure of 1.42 bar however the joint at the inner door starts to leak. As both doors are of equivalent design an overall pressure difference over the lock of 2.84 bar could just be held.

Penetrations

At a temperature of 120° C a differential pressure of 2.18 bar is admissible if the material corresponds to its specifications. As the actual values are higher the pressure might even rise to 2.55 bar.

Containment Shell

The cylindrical part can bear 3.34 bar and the spherical dome 5.6 bar differential pressure. Stiffening rings and the base plate neither represent limiting components.

Material Hatch

The limiting differential pressure at 120° C is 2.55 bar.

Drywell Head

The drywell head would suffer a transient buckling load if a hydrogen-oxygen reaction would occur in the containment. This is very unlikely due to the hydrogen recombiner. Thus, there will be a very close pressure equilibrium.

Summary

The conservative maximum pressure differential is governed by the penetrations and reaches 2.18 bar. Compared to the design pressure of 1.034 bar, this represents a load increase by a factor of 2.1. (Table 1)

Location	p_{max} (bar)
Spherical shell	5.60
Cylindrical shell	3.34
Crane rail region	3.50
Nozzles	2.18
Ankering region in concrete	4.50
Ankering region, free part	3.00
Base plate	3.00
Base plate liner	2.55
Personnel lock, tightness	2.84
Personnel lock, stress	2.55
Material hatch, tightness	2.94
Material hatch, stress	2.55
Drywell head	4.75
Drywell ankering	3.75
Isolation dampers	3.90
Containment system	2.18

Table 1: Allowable Differential Pressures of Particular Regions of the Containment.

2.5 Risk to the population by installing the above ESF (Level 3)

In GESSAR II [4] a few examples are given for the impact to the

environment with short and long term consequences.

Input data for sample case:

Containment failure time	4 h
Duration of release	8 h
Overall decontamination factor	10^4-10^5*
Release height	40 m

* Decontamination factor for path through suppression pool.

Comparing the risk for the WASH-1400 BWR and the GESSAR BWR 6 there will be reduction for late fatalities of three orders of magnitude (Fig. 6.1-1 in Ref. 4).

The latest results show that a short term failure of the Mark III containment will be very unlikely [5]. Therefore a containment failure can only be expected after several days. COSA will release the containment pressure such, that the failure of the containment does not happen, i.e. the release of radioactivity will be controlled. The reduction of the source term reaches at least a factor of 100 for the isotopes I, Cs, Rb, Te, Sb, Sr, Ba and 1000 for Y, Zr and Nb [7]. With a reduction factor of 1000 only the radioactivity of noble gases starts to play an important role for the dose in the environment.

Assuming a similar accident in NPP Leibstadt as described and calculated in GESSAR II [4], the whole body doses (under similar weather conditions) will be reduced by a factor of about 30.

Distance	DBA (LOCA) KKL	Core Melt Accident GESSAR II	KKL
2.0 km (Leibstadt)	0.07	13 rem	0.4*
6.8 km (Koblenz)	0.03	5 rem	0.16*

* Independent KKL calcultion

Table 2: Accident Population Doses in rem.

Table 2 shows that the dose values for DBA and Core Melt Accident are comparable. Therefore a severe accident produces a similar radiation dose in the environment as a design basis accident. Hypothetical accidents with a frequency of occurrence $< 10^{-6}$/reactor year fulfil the requirements of the Swiss radiation protection ordinance (< 10 rem [8]).

3. Cost-Benefit Considerations / Proposed Criteria

It has been shown in an earlier paper [9] that with the implementation of SEHR and COSA a considerable safety gain in the NPP is possible.

3.1 Cost-Benefit-Criteria for Additional Safety Systems in Leibstadt

The two reliability studies [10, 11] show that there is a considerable drop of unavailability of the ECCS - especially the reliabi-

lity of the heat removal systems of the containment - by using the SEHR system. Assuming a transient event which is leading to a core melt down in Fig. 3 a cost-benefit criterion has been developed:

The cost-benefit general formulae for the reduction of core melt down frequency on level 1 can be written,

$$\frac{\text{Investment}}{\text{Reciprocal Unavailability } (1/U)} = \frac{I}{(I \times U)} \rightarrow \text{Min.}$$

Example: $I_0 = 100$ Mill. \$ $\qquad I_1 = 150$ Mill. \$

$U_0 = 10^{-4} \qquad U_1 = 10^{-6}$

$$\left[\frac{I_1 \times U_1}{I_0 \times U_0}\right]' = \frac{150}{100} \times \frac{10^{-6}}{10^{-4}} = \frac{3}{2} \times 10^{-2} = 1.5 \times 10^{-2}$$

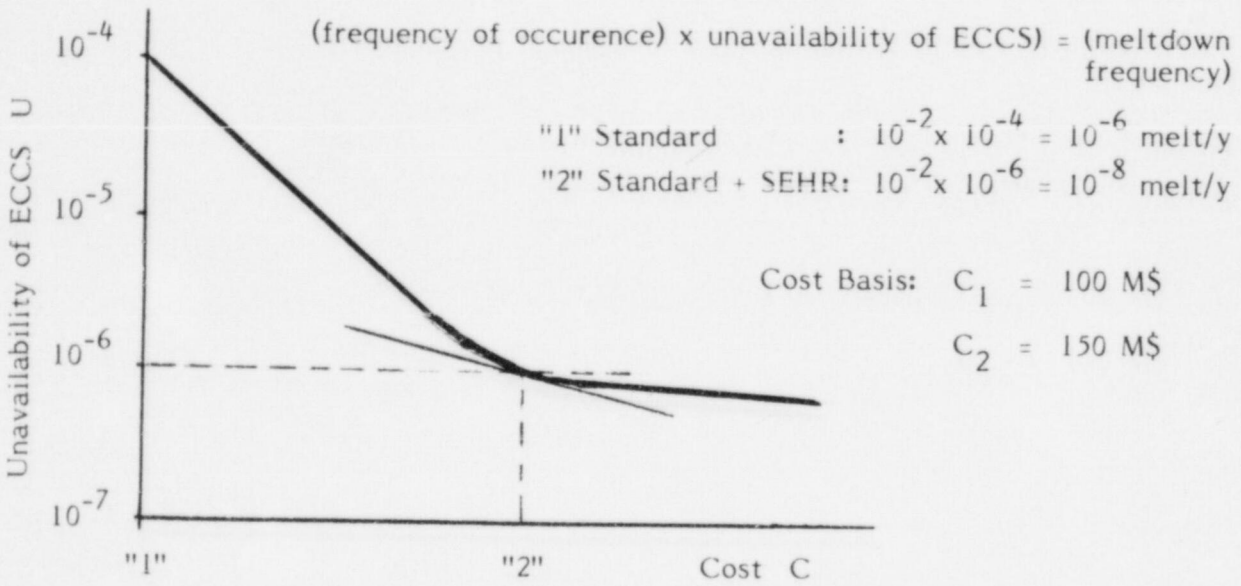


Fig. 3 Unavailability Reduction with SEHR (Level 1)

The containment failure due to slow pressure build-up can be avoided by implementing the COSA system which discharges non-condensable gases and fission products from the containment to the standby gas treatment system. It has to be taken care that the differential pressure of 40 mbar across the annulus filters is not overpassed. In Fig. 4 we evaluate the same way a cost-benefit-criterion for the COSA system.

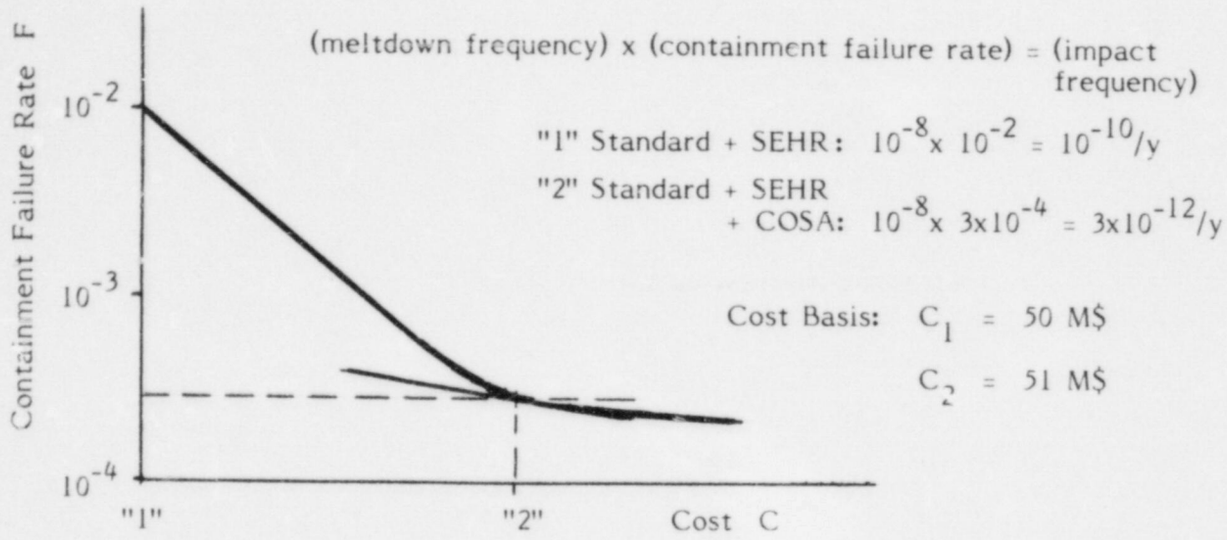


Fig.4 Containment Failure Reduction with COSA (Level 2)

The cost-benefit criterion on level 2 would be the following:

Investment I x Failure Rate = (I x F) → Min.

Example: $$\left[\frac{I_1 \times F_1}{I_0 \times F_0}\right]'' = \frac{51}{50} \times \frac{3 \times 10^{-4}}{10^{-2}} = 3 \times 10^{-2}$$

We have shown in chapter 2.4 that on level 3, a risk (radiation dose) reduction of a factor of $R_1/R_0 = 30$ is possible with COSA. The overall characteristic reduction in the cost times risk figure is therefore

$$\left[\frac{I_1 \times U_1}{I_0 \times U_0}\right]' \times \left[\frac{I_1 \times F_1}{I_0 \times F_2}\right]'' \times \left[\frac{R_1}{R_0}\right]''' \rightarrow \text{Min.}$$

$$1{,}5 \times 10^{-2} \times 3 \times 10^{-2} \times 3 \times 10^{-2} = 1.35 \times 10^{-5}$$

An uncertainty estimate shows that the product of the minima varies approximately by a factor of 10.

3.2 Conclusions

The installation of SEHR has lowered the probability of core meltdown frequency and therefore of a substantial impact to the environment, which was anyway quite low. Applying the French rule for severe accidents which lead to a loss of an essential safety function, i.e. loss of the integrity of the containment, must be less than $10^{-7}/y$: Fig. 3 and 4 show that both the standard and the standard + SEHR would fulfil this requirement.

The obvious question would now be: Was the SEHR installation necessary? If we consider accidents beyond DBA, we would say yes, because the probability of all the scenario for core meltdown are dropping (see Table 3.3-4/5 in Ref. 4).

The PRA of GESSAR II is the state-of-art for GE Mark III safety aspects which are treated on a probabilistic basic. The results are impressive: The risk of BWR/6 (PRA GESSAR II) is more than three orders of magnitude less than the calculated risk for a BWR in WASH-1400. This results mainly from the knowledge of "beautiful" scrubbing factors in the suppression pool.

With the installation of the depressurization or venting system COSA another step of improvement of safety has been made at low cost. This has produced an overall reduction of unavailability on the safety levels 1 and 2 and on overall risk reduction of a few orders of magnitude. In chapter 2.5 is shown that a severe accident in the nuclear power plant Leibstadt would correspond to a similar radiation dose to the population like a design basis accident.

Major problems are left which will be treated in chapter 4.

The failure of the containment with COSA can also be demonstrated by the fault tree shown in Fig. 5.

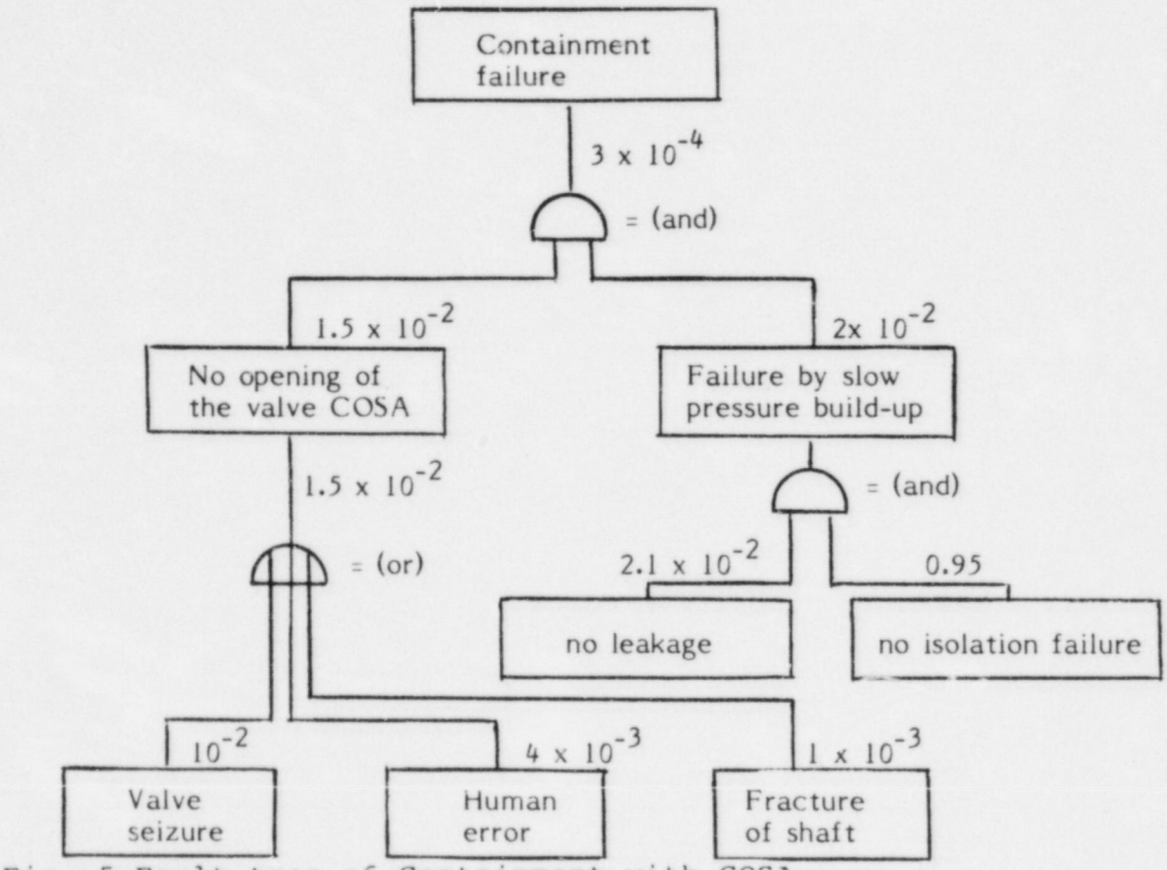


Fig. 5 Fault tree of Containment with COSA

4. The Hydrogen and the Corium Concrete Problem in Case of Severe Accidents

The GESSAR II PRA report treats the hydrogen problem in all details and it seems that local deflagration in the containment is of no importance but a detonation with a mean concentration of 18 % could be dangerous. It is likely that this will never happen.

In Ref. 12 special studies have been carried out to investigate the behaviour of the KKL containment shell under severe accident conditions, beyond the design basis. These indicate that even with suppression pool temperatures as high as 120° C an internal pressure difference of 2.18 bar can be sustained.

The integrity of the containment shell is determined by stresses at the weakest components, namely the containment penetration (s. chapter 2.4). Above overpressure corresponds also to the peak pressure following a hydrogen deflagration in the containment with a hydrogen concentrantion of 6 % vol. and an initial pressure difference of 1 bar.

The conclusion is: Even in a low pressure containment hydrogen deflagration peaks are not dangerous.

A further concern is the corium interaction with the foundation. The German KWU and others have studied the penetration of core melt in the concrete foundation . Artnik [13] shows that the spherical shaped melt stops at a maximum of 9 m radius (from a 1'300 MW reactor) and this after 200 days. Therefore, the reaction is very slow. That helps by using the COSA-system. The influence of the frozen core concrete mass on the ground water below the foundation will be negligible. But is it sure that the weakened pedestal will not endanger the integrity of the drywell? - This still open question could also have an influence on the integrity of the containment.

5. Final Conclusions

Reliability analyses of ECCS have shown that KKL Mark III has a considerable improvement in comparison to the standard Mark III plant. A cost-benefit-study combined with a safety goal shows that both designs are acceptable.

The installation of an additional heat removal system (SEHR is also designed against third party) and the COSA system (containment venting) lowers the probability of the core melt scenario by about a factor of 100.

The scenario BWR 1/2 resp. PWR 1/2 (WASH-1400) and FK 1/2 (German Risk Study) are not risk dominant, they can be neglected.

The controlled and slow release by COSA in a severe accident will be of no harm to the environmental population.

Two important criteria can therefore be satisfied:

Criterion 1:

The leakage of the containment is such that the release is controlled by the SGTS which is fed from the secondary containment and the probability of early release is negligible.

Criterion 2:

The release of radionuclides to the environment and its control is such that during a severe accident the dose limit of the Ordinance of Radiation Protection is not reached. Early fatalities are not and late fatalities might not be expected.

The cost-benefit-study shows that investment and safety gain are in a reasonable ratio. A general formulae has been deduced for the three safety levels and the overall risk reduction.

References:

[1] NUREG-1050,
Probabilistic Risk Assessment (PRA)
Reference Document, Final Report, USNRL, Sept. 1984.

[2] NUREG/CR-2300,
A Guide to the Performance of Probabilistic Risk Assessment for Nuclear Power Plants, Final Report, USNRC Vol. 1 and 2, Jan. 1983.

[3] KSA 22/1
Projektierungsregeln der KSA für Kernkraftwerke mit Leichtwasserreaktoren, Febr. 1978.

[4] PRA GESSAR II, 238 Nuclear Island, Appendix 15D: Severe Accidents, Rev. 4, 1984: Table 3.4-1, Assessed frequency of Core Damage per Plant Year, Class I to VI.

[5] Fontana M.H., Buhl A.R., Carter J.C., Henry R.E., Mitchell H.A.
The IDCOR Programm - Severe Accident Issues,
Individual Plant Examinations and Source Term Developments.
Int. Symp. on Source Term Evaluation for Accident Conditions,
IAEA-SM-281, Columbus, 28.10. - 1.11.1985.

[6] SB, Sicherheitsbericht KKL, Rev. 1984, Table 15.6.-4.

[7] I.R. Brearley, W. Nixon and M.K. Hains,
An Investigation of the Closure Problem Applied to Reactor Accident Source Terms,
IAEA-SR 111/37, Int. Seminar on Implications of Probabilistic Risk Assessment, Blackpool, March 18-22, 1985.

[8] Schweiz. Verordnung über den Strahlenschutz, Stand Juli 1984.

[9] H.P. Hänni, Th. Schaub
How Can Containment Integrity of a NPP be Performed in a Case of Severe Accident?
IAEA-SM-281/05P, Int. Symposium on Source Term Evaluation for Accident Conditions, Columbus, Ohio, USA, 28. Oct. - 1. Nov. 1985.

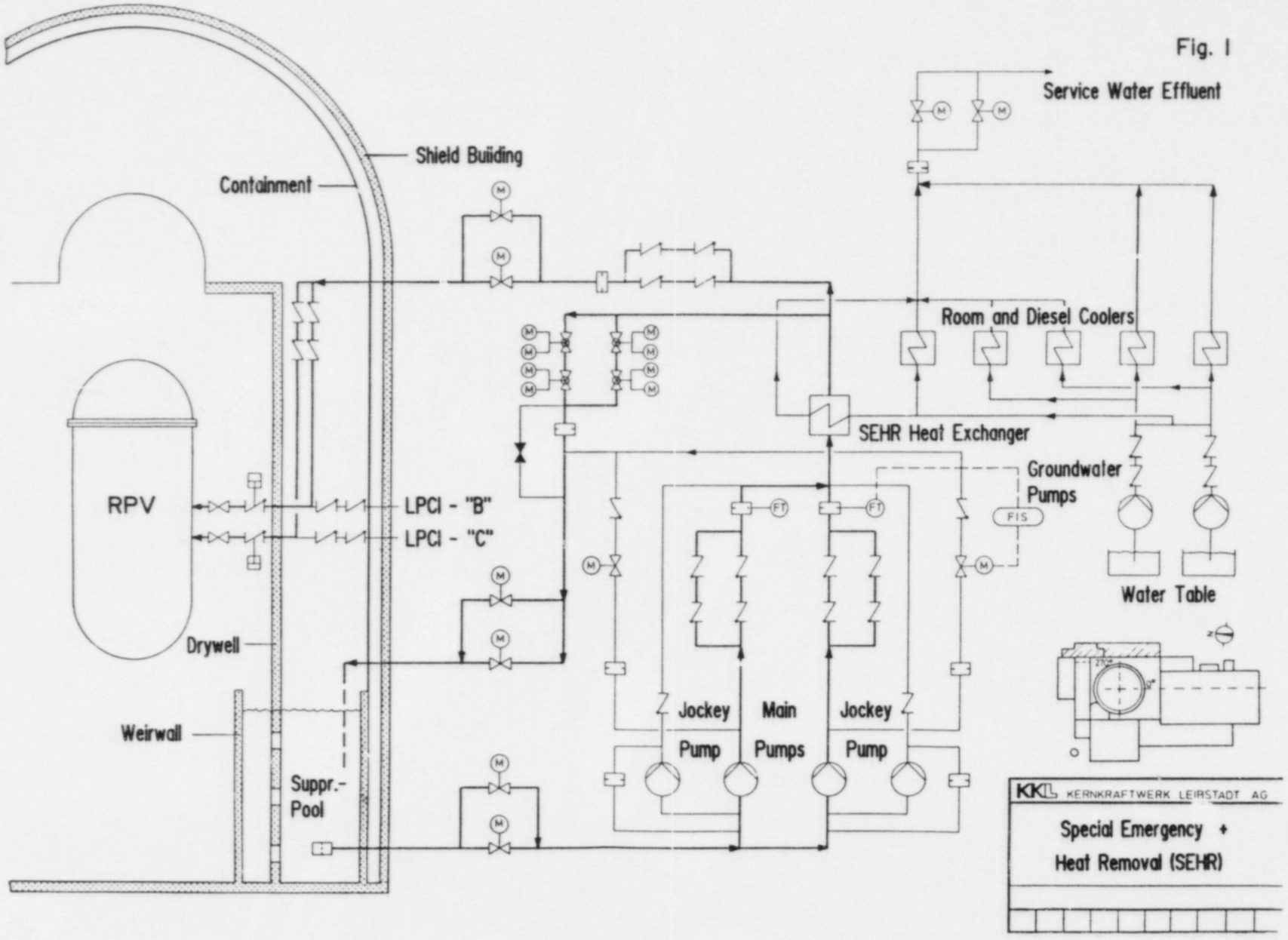
[10] GRS-A-96,
v. Albertz, K. Boesebeck, E. Lindauer,
Zuverlässigkeitsanalyse für das Not- und Nachkühlsystem KKL, Jan. 1978.

[11] Electrowatt Engineering Services Ltd.
System Reliability Studies, ECCS Performance, 29.4.1982.

[12] HSK Evaluation of the Leibstadt GE Mark III Containment, December 1984.

[13] J. Artnik,
Ueberlegungen zur Ausbreitung einer hypothetischen Kernschmelze im Betonfundament bis zu ihrem Stillstand, Reaktortagung Kerntechnik, 1984.

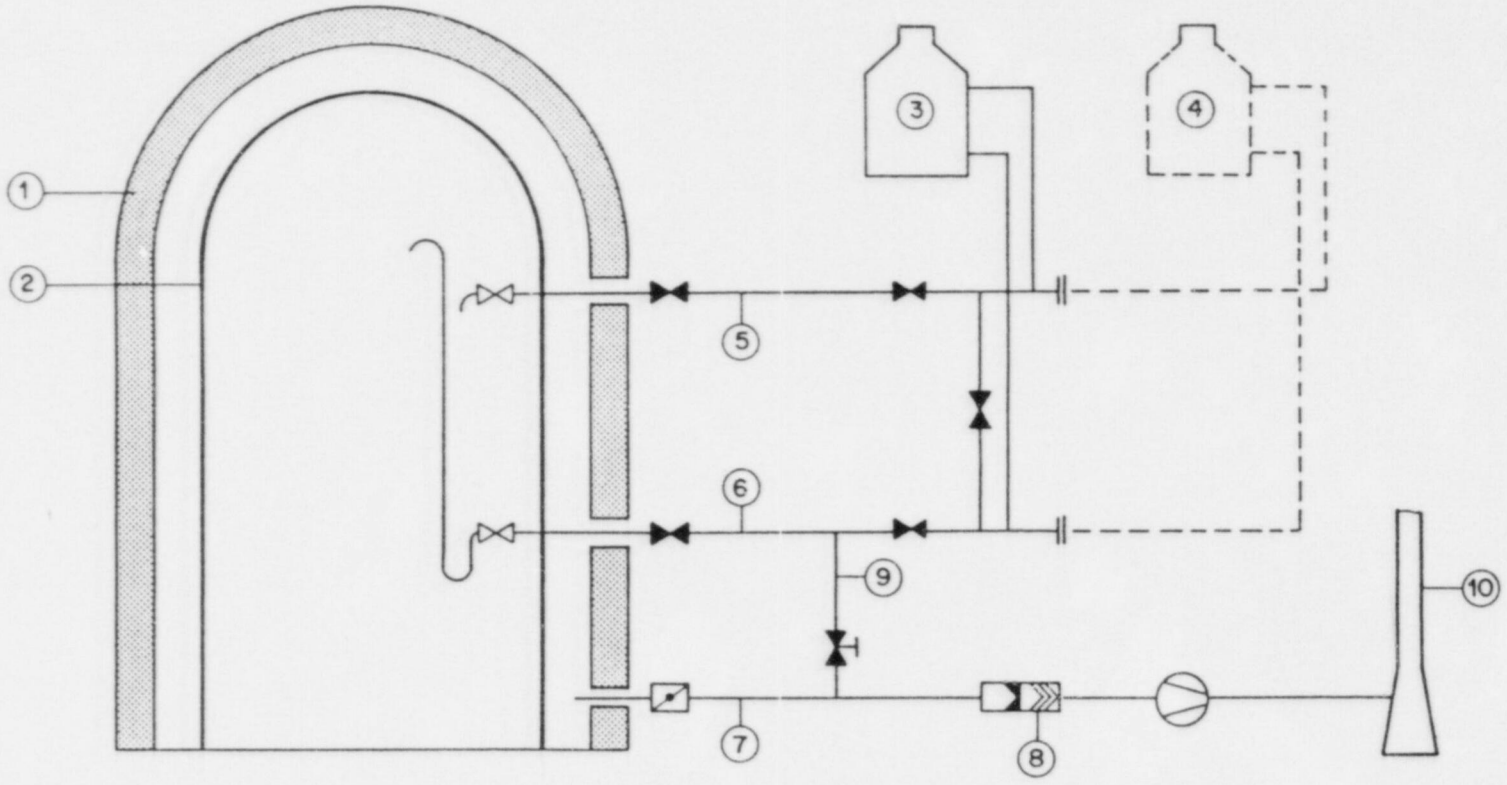
Fig. 1


Service Water Effluent
Shield Buiiding
Containment
Room and Diesel Coolers
SEHR Heat Exchanger
Groundwater
Pumps
FIS
RPV
LPCI - "B"
LPCI - "C"
Water Table
Drywell
Weirwall
Suppr.-
Pool
Jockey
Pump
Main
Pumps
Jockey
Pump
KKL KERNKRAFTWERK LEIBSTADT AG
Special Emergency +
Heat Removal (SEHR)

KKL

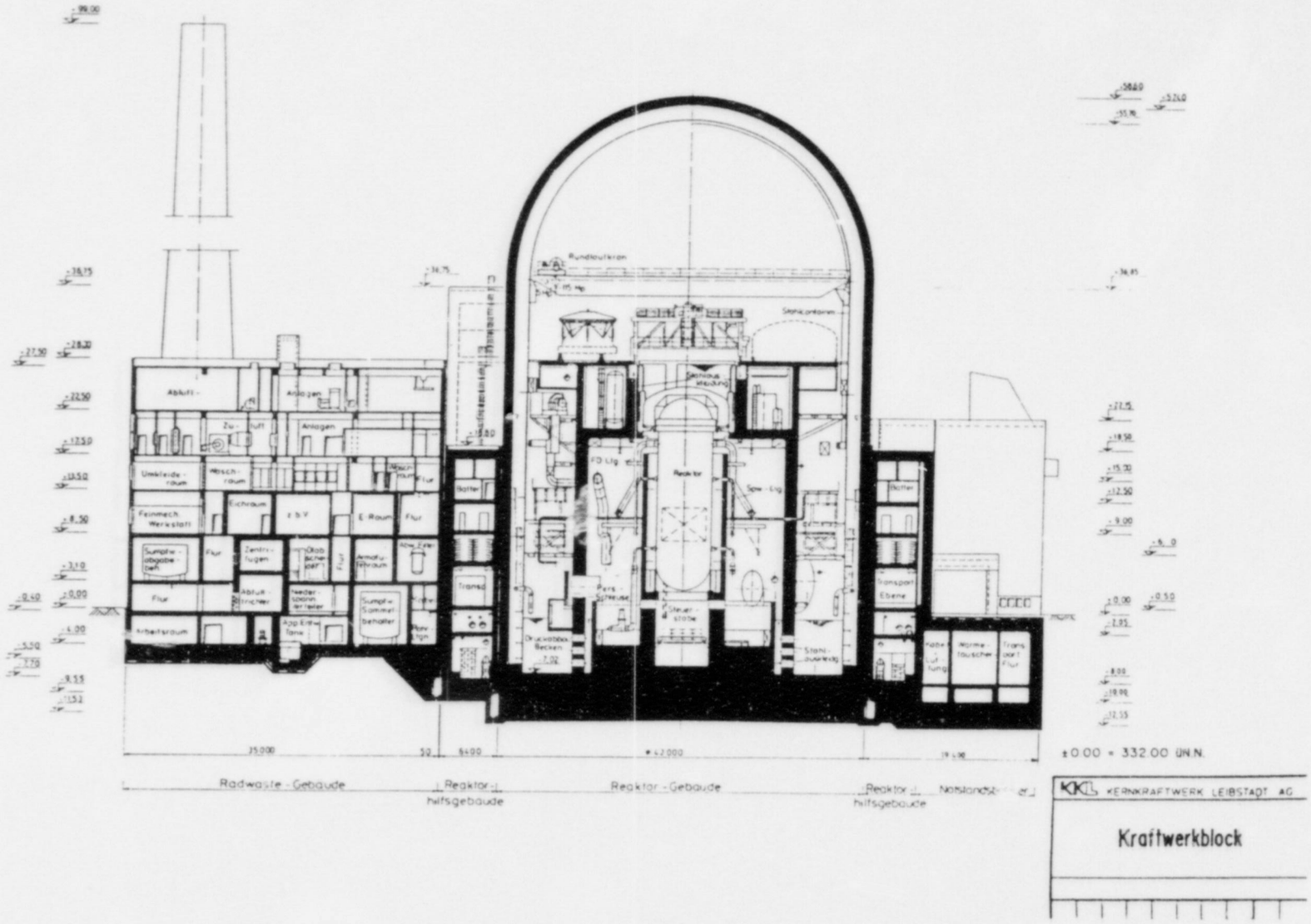
Containment Venting System COSA

Fig. 2



1 Shield Building
2 Containment
3 Main Hydrogen Recombiner
4 Spare Hydrogen Recombiner
5 Recombiner Return
6 Recombiner Suction
7 Standby Gas Treatment System (SGTS)
8 Charcoal Filter and Absolute Filter of SGTS
9 Connection Pipe
10 Stack

Fig. 6



KKL KERNKRAFTWERK LEIBSTADT AG

Kraftwerkblock

ANALYSIS OF STRATEGIES FOR CONTAINMENT VENTING IN CASE OF SEVERE ACCIDENTS

K. Bracht and M. Tiltmann

Gesellschaft fur Reaktorsicherheit (GRS)
mbH Schwertnergasse, D-5000 Cologne, Germany

Abstract

During a core melt accident, a pressurization of the containment has to be expected, which could lead to a failure of the containment due to overpressurization. This failure mode is expected to be the most likely one for large dry containments under accident conditions. Also during a core melt accident, a large quantity of hydrogen may be generated, giving the potential of a loss of containment integrity due to violent hydrogen combustion. Timely venting of the containment atmosphere can prevent overpressurization and may perhaps make the hydrogen situation in the containment less severe. This paper discusses the thermodynamic consequences of different vent strategies for a large German PWR during core melt accidents.

1.0 INTRODUCTION

In a PWR accident with core melt, there are several possibilities that the containment may lose its functional capability or its integrity to act as the last barrier against fission product release into the environment:

- containment-isolation failure, or preexisting openings at the beginning of the accident;
- containment by-pass (V-sequence);
- early containment failure due to transient events such as violent hydrogen (H_2) combustion;
- basemat penetration.

Finally, the containment may lose its specified function due to overpressurization as a consequence of long-term steam and gas generation (H_2, CO_2, CO). As calculated in different risk studies (e.g., Reference 1), containment failure due to overpressurization has to be expected to be the most probable reason for fission product release into the environment. Due to the long-term generation of noncondensible gases during the melt-concrete interaction, which is expected generally after failure of the RPV, overpressurization can be prevented only by timely venting of the containment atmosphere,[2] if the gas-generation cannot be stopped before overpressurization.

While containment overpressurization will only occur late during an accident (several days after accident initiation in a PWR of German design), violent combustion of hydrogen (H_2-deflagration, eventually local detonation) may take place quite early. Presuming sufficient accumulation of H_2 within the containment atmosphere, violent combustion of H_2 has the potential to cause containment failure within some hours after beginning of an accident.[3]

With this background, a study was performed in which the effect of several strategies of filtered containment venting was analyzed with respect to the following questions:

- Is it possible to mitigate the H_2 situation in the containment atmosphere by venting?
- What is the effect of different vent strategies on the H_2 situation and the overall containment thermodynamics?
- Which are the requirements on a vent system to prevent late overpressurization?
- Which are the necessary dimensions of vent systems with respect of the strategies?

The analyses of the containment thermodynamics were performed for a 1300 MWe-PWR with a large dry containment.

2.0 ACCIDENT SEQUENCES AND CODES

The effect of containment venting was analyzed for two accident sequences, which are expected to envelope sufficiently the relevant scenarios of core-melt accidents:

- Loss of coolant accident (LOCA) caused by a double-ended break of a main coolant pipe and complete failure of all low-pressure recirculation systems.
- Emergency power case and complete failure of the auxiliary power supply ("Station Blackout").

The first case may be regarded as characteristic for accidents with core meltdown under low system pressure ("Low-Pressure Case"), the second for meltdown under high pressure ("High-Pressure Case"). For the analysis of the accident sequences with and without containment venting, the codes MARCH (for primary circuit and core heatup calculations), KAVERN (melt-concrete interaction), and CONDRU (containment analysis) were used.[3]

Concerning the simulation of a vent system, exemplarily a pressure suppression system was chosen similar to that of a BWR (Figure 1). Only a filtered vent system seemed to be admissible. The dimension of the system was varied. With respect to the volume flow rates via the system, they are called the following "High Volume (HV)" or Low Volume (LV)" systems, respectively.

3.0 COURSE OF THE CORE MELT ACCIDENTS WITHOUT VENTING

In the following a general view is given of the course of the accident sequences defined before, without any countermeasures.

3.1 Low-Pressure Case

The accident sequence presumes a complete failure of all low-pressure recirculation systems about 20 min after the break of a main coolant pipe and the subsequent blowdown. At this time the core region is assumed to be completely reflooded.

After about 0.7 h, the water level has decreased to the top of the active core as a consequence of the evaporation of the coolant by decay heat. Core meltdown will start about 1.1 h after blowdown. At about 1.4 h, the lower grid plate of the core is assumed to fail. The molten material is expected to slump into the lower plenum of the RPV. Residual water inside the plenum will be evaporated, before about 2.5 h after blowdown; also the RPV is supposed to fail due to the attack of molten material.

The failure of the RPV marks the end of the in-vessel melt phase of the accident.

In the subsequent ex-vessel melt phase, melt-concrete interaction will decompose thermally the concrete of the basemat of the reactor building. Besides the erosion of the concrete, the release of steam and gases like CO_2, CO, and H_2 has to be expected from the melt.

Figure 2 shows the pressure of the containment atmosphere versus time in the "Low-Pressure Case." Additionally, the partial pressures of several components of the containment atmosphere are shown.

According to Figure 2 the expected failure pressure of the containment steel shell will be exceeded after nearly 5 days. The long-term pressure increase is mainly a consequence of the increase of the partial pressure of steam after the contact between melt and sump water as a result of melt-concrete interaction. This contact happens when the innermost shield inside the reactor cavity, which initially separates sump water from melt, has been penetrated by the melt. At the expected failure time, the contribution of noncondensible gases (H_2, CO_2, CO) to the pressure of containment atmosphere is of minor importance.

3.2 High-Pressure Case

Core meltdown under high system pressure can occur if in an emergency power case the redundant auxiliary power supply is also assumed to fail completely. Such an event would cause loss of feedwater supply. Therefore, the secondary side of the steam generators would become dry after some time. The loss of the heat sink will increase the pressure in the primary circuit until relief valves will open. Energy produced in the core will be transferred out of the primary circuit by coolant via the relief valves and the

pressurizer-drain tank into the containment. In this way the primary circuit becomes more and more empty, while the relief valves keep the pressure high all the time. About 2.4 h after the beginning of the accident, core uncovery starts followed by the meltdown of the core. After failure of the lower core support structure and slumping of the core into the lower plenum, the RPV is expected to fail after about 3.2 h.

The characteristic feature of this accident sequence is that in comparison to the "Low Pressure Case," the in-vessel melt phase of the accident takes places under high system pressure.

The high-pressure (HP) failure of the RPV can initiate a rapid release of a large amount of superheated steam and of H_2 (due to Zr-H_2O reaction) into the containment. Additionally, a discharge of coolant from accumulators on the hot core fragments may occur, triggered by the depressurization of the primary circuit, and/or contact between core material and sump water may take place. Both events result in steam generation. Thus as a consequence of the HP failure of the RPV, a rapid increase of the pressure (steam spike) in the containment atmosphere is expected.

As in the "Low Pressure Case," the ex-vessel melt phase of the accident is expected to continue most likely in melt-concrete interaction. Only if the core material would be fragmented in small particles and would be dispersed sufficiently in the sump water, could the core material become completely coolable. Generally this is not expected.

Figure 3 shows the pressure-time history within the containment for the "High Pressure Case."

The depressurization of the primary circuit after RPV failure will result in a pressure spike ("steam spike") well below the failure pressure of the containment.

The long-term pressure increase inside the containment is again mainly a consequence of the steam generation, following sump water ingression on melt or on hot core debris. This event is expected to happen immediately after the high pressure failure of the RPV due to pressure load on the inner biological shield and its subsequent failure, and not due to melt-concrete interaction like in the "Low Pressure Case."

Assuming the most likely case of incomplete coolability of the core material, i.e., melt-concrete interaction will be established, the expected failure pressure of the containment will be reached after nearly 5 days after the accident has started, similar to the "Low Pressure Case."

4.0 RESULTS FOR DIFFERENT STRATEGIES OF CONTAINMENT VENTING

The following strategies of containment venting were analyzed:

- early but in time limited venting before the start of core heatup.
- early but in time limited venting during core melt.
- late venting of the containment beyond its design pressure (continuously or discontinuously); limitation of pressure-increase before overpressurization.
- direct venting into the annulus of the reactor building immediately before overpressurization only using already existing systems.

4.1 Early Venting

Venting Before Core Heatup

Figure 4 gives an example for the effect of an early but in time limited venting, initiated before start of core heatup ("Low Pressure Case"). Depending on the capacity of the system, the time over-pressurization may occur (p cont > 0.85 MPa) is delayed on the order of one day. No significant reduction of the accident consequences is expected by that delay. In addition to Figure 4, Figure 5 shows the course of the H_2 enrichment during the accident in the H_2-air-steam diagram. Homogeneous mixing of the containment atmosphere has been presumed. Thus this simplified treatment can only indicate the overall potential for the possibility of violent H_2 combustion.

Venting limited in time and before core heatup, reduces the content of steam and air of the containment atmosphere. After core melt the enrichment of steam and H_2 is shifted to higher values in case of venting. This means that in long term the containment atmosphere becomes more inerted in case of venting (due to the increase of the steam content), but on the other side, the H_2 enrichment increases also and may make the consequences of an H_2 combustion more severe. In no case will the detonation area as marked in the diagram be reached.

If an H_2 deflagration should occur during the accident, the pressure increase is obviously smaller in case of a preceding venting than without the measure due to the lower pressure level before the combustion. On the other hand, the temperature of the containment atmosphere may reach significantly higher values than without venting, and may locally lead to a severe challenge to the containment integrity or to important equipment inside the containment. The higher temperature increase of the containment atmosphere due to a deflagration after previous venting is a consequence of the reduction of the heat capacity of the containment atmosphere due to the venting process.

For the "High-Pressure Case" the results are, in general, similar to those of the "Low-Pressure Case" discussed before. By venting before core heatup, a small but not significant reduction of the

steam spike after failure of the RPV may be obtained. The effect on the H_2 enrichment in the containment by the venting process is similar as shown in Figure 5.

The advantages of venting before core heatup are that no combustible gases (H_2, CO) and fission products can be released into the vent system and the environment. Venting limited in time does not necessarily require cooling of the system.

Venting During Core Melt

The largest portion of the H_2 mass generated during the whole accident is produced within the first hours after start of core degradation. At that time a severe H_2 deflagration seems to be most likely. Thus venting of the containment atmosphere during that period could be taken into account. The calculation performed for this strategy showed that indeed the H_2 situation in the containment will become less severe. On the other hand, the H_2 enrichment within the vent system will exceed critical values to make a deflagration or even a detonation possible if no countermeasures are realized. The realization of those measures seems to be not impossible for the confined vent system from the technical point of view. The disadvantage of such a vent strategy seems to be that the depressurization occurs at a time when the fission product level in the containment is extremely high and aerosol settlement has just started. Therefore, the loading of the filter of a vent system may be extremely high in that period and a failure of the vent system could have extreme severe consequences to the public and to the environment. Thus the value of early venting during the core melt accident seems to be highly questionable and should not be taken into account.

4.2 Late Venting

Continuous and Cyclic Venting

Figure 6 shows the pressure-time history for continuous and cyclic venting via systems of different capacities. With continuous venting via the high-volume vent system, depressurization of the containment from 0.7 MPa to 0.2 MPa can be obtained within about half an hour (using the low-volume system would require more than 6 hours). Generally, cooling of the systems will become necessary.

The total mass flow rate through the vent system (HV) is in the order of some hundred kilograms per second at the beginning of the vent process. Obviously, late venting has no effect on the H_2 situation in the containment, while the H_2 enrichment inside the vent system will become high enough for violent H_2 combustion (see later), if no countermeasures are performed (e.g., continuous combustion of the entering H_2).

Prevention of overpressurization is also possible by cyclic venting (Figure 6), using a safety valve for example. A system of small capacity is sufficient in that case. (In the system used for the

calculations, cooling of the waterpool becomes necessary after two cycles, i.e., after about one day. Because cooling was not simulated, the venting process was finished then.) As in the case of continuous venting the H_2 enrichment within the vent system (Figure 7) may exceed critical values with respect to violent H_2 combustion (presuming no countermeasures).

Limitation of Pressure Increases

Limitation of the pressurization of the containment can also be obtained by using a vent pipe of a diameter sufficiently large that only the additional energies and masses that are released into the containment at a certain pressure level are transferred into the vent system. Easily, it can be shown that theoretically (no pressure resistance) a pipe with an effective cross section of only about 15 cm^2 (~2.3 in^2) is sufficient to limit the pressure at a level of 0.85 MPa* (in the Low- as well as High-Pressure Case). Calculations performed for the vent arrangements of Figure 1 showed that by using a vent pipe with an effective cross section of 25 cm^2(~3.8 in^2) overpressurization of the containment steel shell can be prevented in any case. A further reduction of the size of the vent system used is still possible.

Direct Venting

The idea of direct venting into the annulus of the containment without any additional vent system was to use the possible potential for fission product retention of the annulus (its volume is nearly about half the volume of the containment steel shell), of the auxiliary building, and of the capacity of the air exhausting system. (The air exhausting system is to handle leakages of the containment steel shell during design basis accidents.[4])

Calculations for both accidents sequences showed that under optimum conditions (i.e., vent-pipe diameter as small as possible for pressure increase limitation, etc.), there is indeed a potential of fission product retention by existing features. Nevertheless, it has to be expected that a significant part of the fission products will be released directly into the environment due to leakages from the annulus and the auxiliary building. Thus without additional backfitting, this measure should not be taken into account presently.

* 0.85 MPa is the expected failure pressure of the containment steel shell.

5.0 SUMMARY AND CONCLUSIONS

The results and our conclusions are:

- Early but in time limited venting
  - can improve the H_2 situation in a limited but only equivocal extent (additional inerting of the containment atmosphere; in case of H_2 deflagration, smaller pressure increase but significantly higher increase of the temperature of the containment atmosphere is possible);
  - can delay overpressurization only on the order of one day;
  - in general, a vent system of large dimension is necessary to obtain a sufficiently quick depressurization;
- Late venting
  - prevents overpressurization;
  - has no influence on the H_2 situation in the containment;
  - requires additional measures against violent H_2 combustion in the vent system (always necessary in case of venting after the start of core melt);
  - for the limitation of containment pressurization and finally depressurization, a vent system of relatively small dimension is sufficient.
- Venting of the containment atmosphere directly into the annulus of the reactor building is problematic and requires additional backfitting.

Our conclusion is that it is only useful to pursue the concept of a late limitation of the pressure increase and subsequent depressurization of the containment. Possible advantages are:

- presently the failure mode of the containment steel shell due to overpressurization is still uncertain (small or large leak?) and becomes controllable by the measure;
- it enables accident management action (e.g., controlled confinement of the fission products);
- the core material can be kept covered by sump water as long as possible (advantages: partial cooling of the material; impediment of the melt-concrete interaction; prevention of additional aerosol generation from the melt);
- venting may be favorable if uncontrolled containment leakage occurs.

Meanwhile, an uncomplicated filtered vent system has been developed in FRG at the Kernforschungszentrum Karlsruhe (KFK), which meets the requirements for late limitation of containment pressurization (Figure 8). An important part of this system is newly developed filters to retain aerosol and iodine. They are already tested for accident conditions (details are given in Reference 5).

Nevertheless, implementation of a vent system is only one possibility with respect to achieve risk reduction. Due to the fact that over-pressurization of a German plant is expected to occur not before several days after the start of the accident, there is an additional potential to mitigate the consequences of an accident by an adequate accident management using still operable systems.

ACKNOWLEDGMENT

The study was supported by the Ministry of Interior (BMI) of the Federal Republic of Germany as part of the project SR 271/2.

6.0 REFERENCES

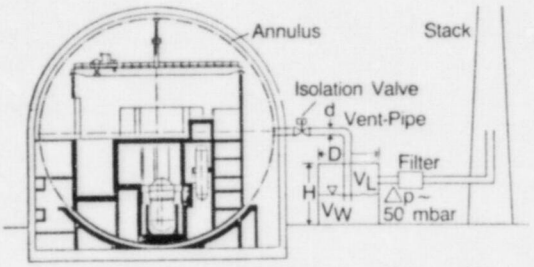
1. The Federal Ministry of Research and Technology (BMFT), "The German Risk Study," A Study of the Gesellschaft fuer Reaktorsicherheit (GRS) Cologne, 1979, Germany.

2. K. Bracht, J. Rohde, "Measures Against Containment Over-pressurization and Their Thermodynamic Efficiency," Int. Meeting on LWR Severe Accident Evaluation, Cambridge, MA, USA, August 22 - Sept. 1, 1983.

3. K. Bracht, M. Tiltmann, "Analysis of Containment Loading by Hydrogen Burning During Hypothetical Core Meltdown Accidents," SMIRT 7, Chicago, IL, USA, 1983.

4. M. Tiltmann, "Thermodynamic Consequences of Leakages in a Double Containment During Severe Accidents," Nuclear Engineering and Design, 90 (1985) 161-165.

5. H. Dillmann, H. Pasler, "A Containment-Venting Filter Concept and Its Implementation," 5th Int. Meeting on Thermal Reactor Safety, Karlsruhe, Germany, 1984.



	High Volume (HV)	Low Volume (LV)
Vent-Pipe Ø = d	600 mm	250 mm
Air space V_L	2300 m^3	250 m^3
Waterpool V_W	2250 m^3	250 m^3
D	Ø 18 m	Ø 8 m
H	18 m	10 m

Fig. 1: VENT-SYSTEM IN PRIN - CIPLE FOR CALCULATION

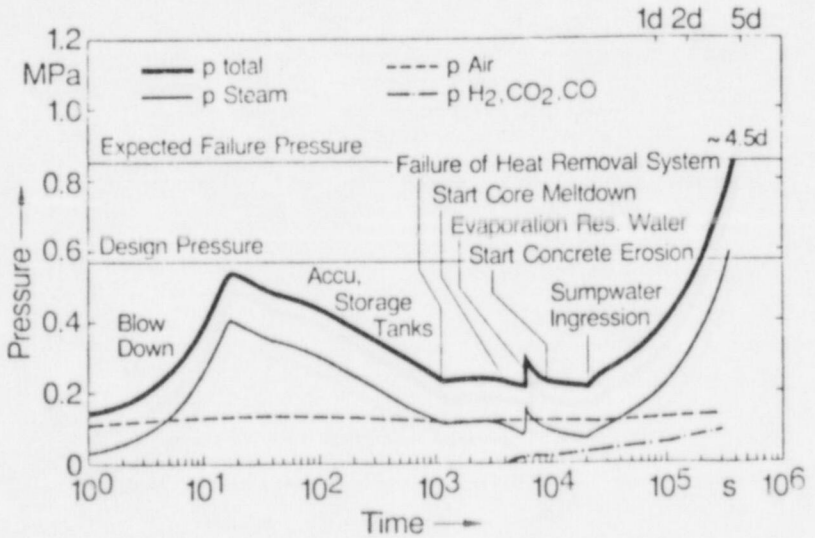


Fig. 2: CONTAINMENT PRESSURE-TIME HISTORY (LOW PRESSURE CASE)

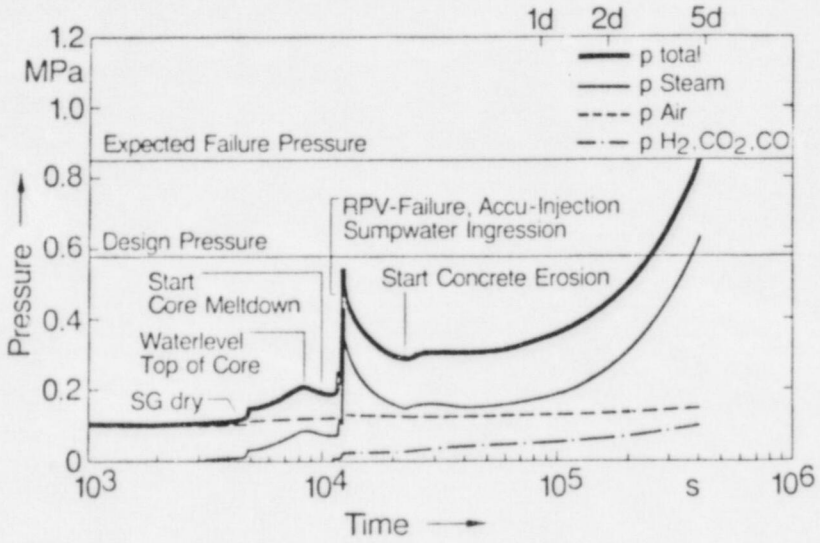


Fig. 3: CONTAINMENT PRESSURE-TIME HISTORY (HIGH PRESSURE CASE)

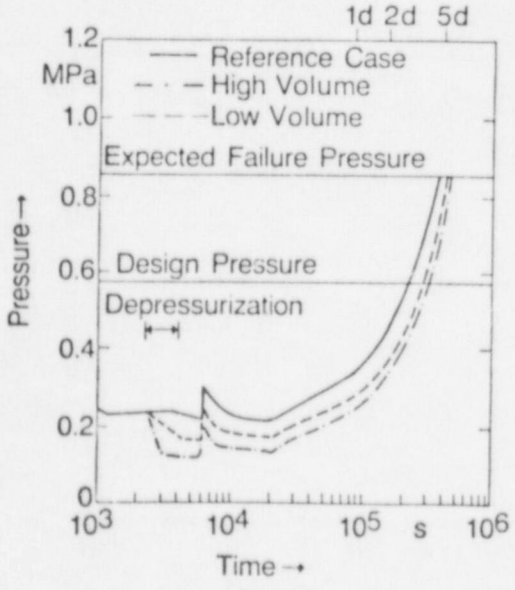


Fig. 4: CONTAINMENT PRESSURE-TIME HISTORY; EARLY VTG.

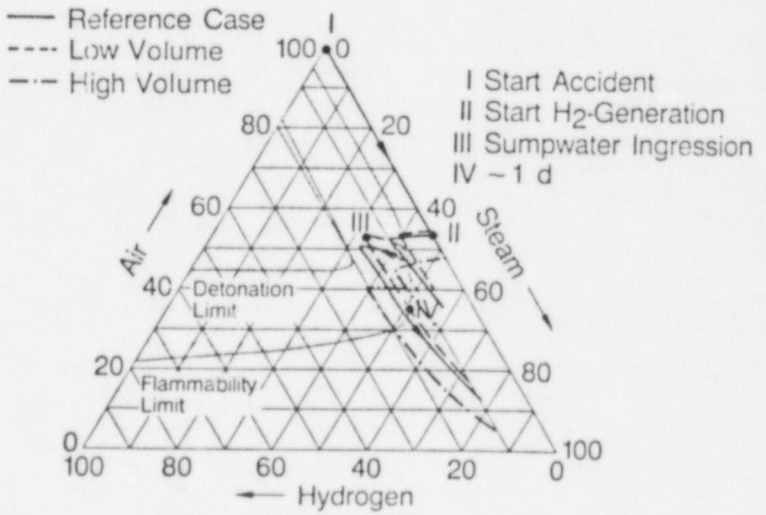


Fig. 5: HYDROGEN ENRICHMENT WITHIN CONTAINMENT; EARLY VENTING (LP)

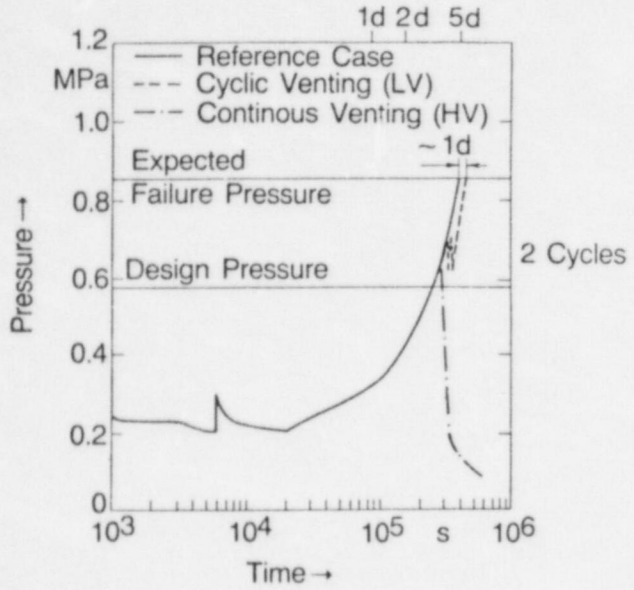


Fig. 6: CONTAINMENT PRESSURE-TIME HISTORY; LATE VENTING

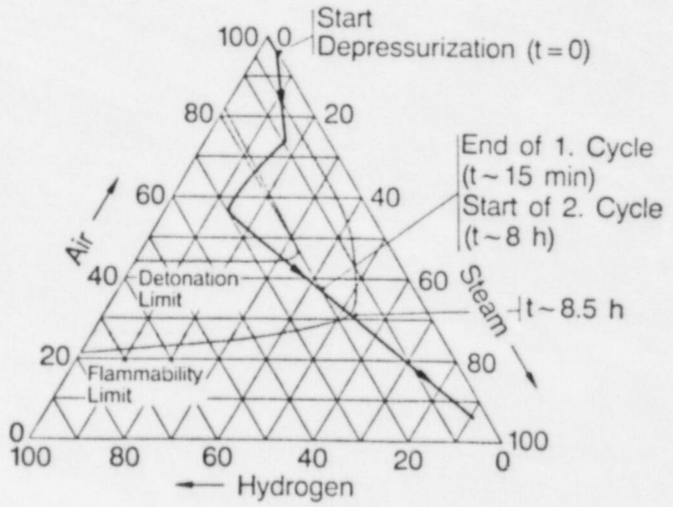


Fig. 7: HYDROGEN ENRICHMENT WITHIN THE VENT-SYSTEM; LATE CYCLIC VENTING (LP-CASE)

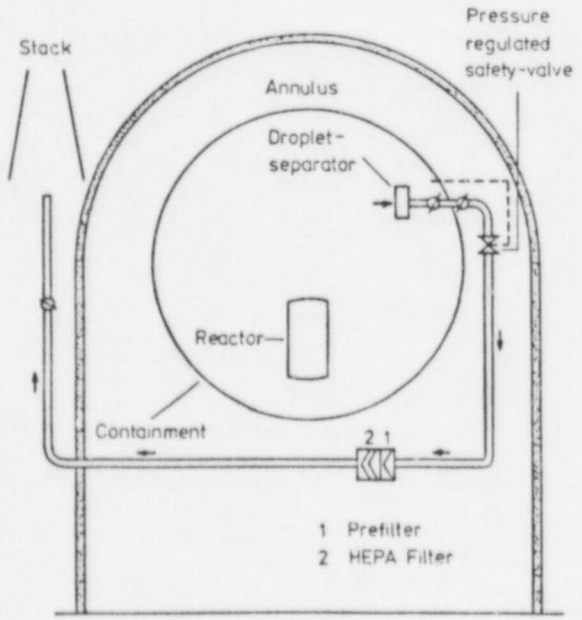


Fig. 8: CONCEPT OF AN ACCIDENT FILTER SYTEM FOR CONTAINMENT VENTING AGAINST BURSTING /5/

EVALUATION OF UNCERTAINTIES IN RISK EMANATING FROM A NUMBER OF SEVERE ACCIDENT ISSUES*

A. S. Benjamin, Sandia National Laboratories, Albuquerque, NM
G. R. Boyd, Safety & Reliability Optimization Services, Knoxville, TN
W. B. Murfin, Technadyne Engineering Consultants, Albuquerque, NM
D. M. Kunsman, Sandia National Laboratories, Albuquerque, NM

ABSTRACT

A study has been performed to estimate, for a particular pressurized water reactor, the uncertainty in risk associated with a number of key phenomenological issues. A second objective was to distinguish the individual importance of the various issues as contributors to the overall uncertainty in risk. The issues considered touched upon the areas of system behavior, containment loading, containment performance, and fission product source term behavior. It was found that direct heating was the most important issue for the plant in question (Surry). Other important containment issues included the potential for hydrogen burning during direct heating scenarios and the containment failure pressure.

INTRODUCTION

A number of research activities are currently engaged in extensive efforts focused on better characterizing the hazards associated with the operation of nuclear power plants. These efforts typically focus on one or more of the following areas of reactor safety:

- The likelihood and nature of accidents severe enough to liberate substantial quantities of fission products from the reactor fuel;
- The challenges such accidents would present to the integrity of the reactor containment;
- The quantities and physical properties of fission products that could be released to the environment; and
- The ultimate consequences of these accidents, both in terms of their effects on public health, and their associated costs to society and to the plant owners.

*This work is supported by the United States Nuclear Regulatory Commission and performed at Sandia National Laboratories which is operated for the U.S. Department of Energy under contract number DE-AC04-76DP00789.

The first attempt to incorporate the state-of-the-art in all of these areas into an integrated perspective on the risk associated with the operation of nuclear power plants culminated in the Reactor Safety Study, which was published in 1975. Although that study produced the first comprehensive assessment of plant risk, it also focused attention on a number of gaps in the understanding of accident processes.

Since that time, many risk assessments of specific plants have been performed. In general, each of these has progressively reflected at least some of the advances that have been made in the ability to predict accident behavior. In order to investigate the significance of more recent developments in a comprehensive fashion, it was concluded that the current efforts of research programs being sponsored by the NRC should be coalesced to produce an updated representation of risk; this led to the current program definition for the Severe Accident Risk Rebaselining and Risk Reduction Program (SARRP).

The results of the specific research programs, including their significance with respect to various questions concerning reactor safety, are, of course, documented individually. It is the objective of SARRP to integrate these results and to cast them in the context of their implications with respect to risk. This includes not only an estimate of risk as measured by a number of health effects and financial consequences, but also a thorough understanding of the important sensitivities and uncertainties associated with the state-of-the-art in reactor safety assessment. This risk context also provides a mechanism to investigate the effects on risk that would be anticipated to result from the modification of existing plants, and the associated costs incurred as a consequence of such modifications, providing additional information useful to the NRC's decision-making process.

This paper focuses upon one of the five reference reactor plants being considered by SARRP, and explores for that plant the uncertainty in risk associated with a number of issues. The issues under consideration can be conveniently grouped into four categories: (1) system behavior, (2) containment loading, (3) containment performance, and (4) fission product behavior. For purposes of this paper, issues in the second and third category will be emphasized; however, all the issues will be included in the presentation of results. The plant under consideration is Virginia Electric Company's Surry Unit 1, a Westinghouse PWR with a dry, subatmospheric containment. Details of the analysis may be found in References [1] and [2].

METHODOLOGY FOR THE EVALUATION OF UNCERTAINTIES

The principal method of uncertainty analysis in SARRP is a limited Latin Hypercube (LLH) approach, limited because not all uncertainties are addressed. Particular issues selected by the SARRP analysts and an expert review group are investigated by determining the range of outcomes that might be expected and sampling the outcomes

based on the assignment of weighting factors by the experts. The expert review group consisted of representatives from Sandia, Brookhaven, and Oak Ridge National Laboratories, Battelle Columbus Laboratories, University of Wisconsin, and Pickard, Lowe & Garrick.

The basic interest here is the uncertainty in risk due to the uncertainty in the input information. Risk can be defined by the equation given below.

$$RISK_k = \sum_i \sum_j FREQ_i * CRMP_{ij} * CONS_k(FP_{ij})$$

where

$RISK_k$ = the risk associated with consequence measure k

$FREQ_i$ = the frequency of accident sequence i

$CRMP_{ij}$ = the probability of containment release mode j, given accident sequence i

FP_{ij} = the fission product source term for containment release mode j of accident sequence i

$CONS_k$ = the magnitude of consequence k, given fission product source term (FP) for sequence ij

There are unknown uncertainties in each of the inputs to this risk equation. As already described above, a full uncertainty analysis would involve sampling of the range of potential outcomes for every detailed element of every input to the risk equation. The goal here was to identify the major uncertainties in each of the inputs and then determine the effect of the uncertainty on the risk measures due to a reasonable variation of those inputs.

The entire LLH process used in this study is represented schematically in Figure 1. The first feature which must be recognized is that the uncertainty analysis was not complete. The word "limited" in the title refers to the number of issues selected--only a few major uncertainties were addressed (approximately 20). These uncertainties are defined in terms of "issues" which are high-level representations of uncertainties in the input. For example, one "issue" is the magnitude of pressure increase due to direct heating, the phenomenon which occurs when core debris is ejected at high pressure from the reactor vessel and dispersed throughout the containment atmosphere. This obviously involves many other uncertainties (heat generation rates, thermal-hydraulic uncertainties, amount of debris involvement, particle sizes, physical structure effects on debris transport, chemical reaction uncertainties, etc.) which were not considered individually but rather in terms of their overall effect--the pressure rise due to direct heating. The source term uncertainties involve even broader issues; for example, one fission product issue is concerned with all uncertainties affecting the release of all radionuclides from the fuel during the in-vessel

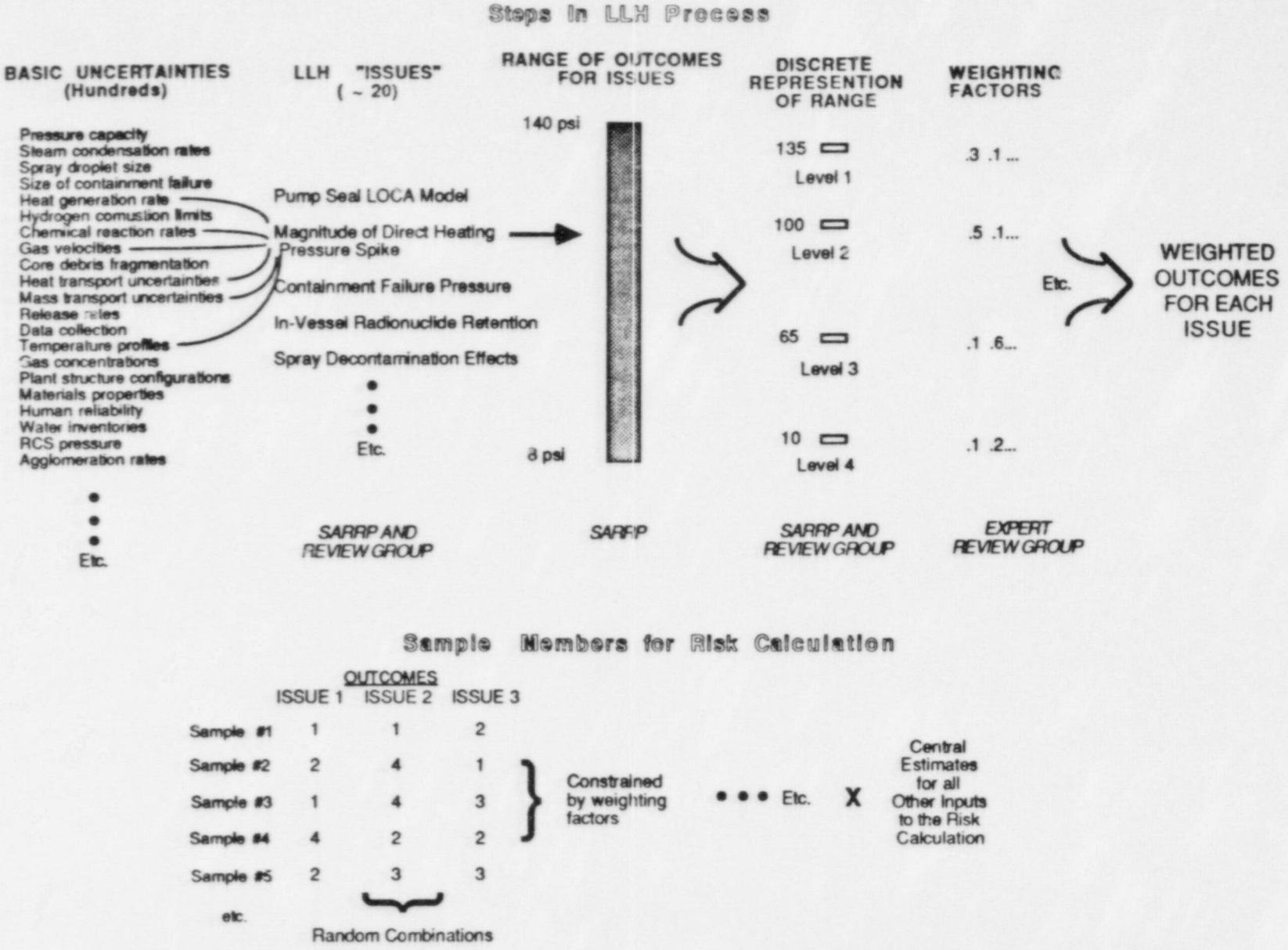


Figure 1. Overview of the LLH Process

phase of the accident. The issues were initially selected by the SARRP team but were then reviewed by the groups of experts in each area of the analysis.

The second step of the analysis was the generation of a range of outcomes for each individual issue. This was intended to represent a reasonable variation of the outcome (e.g., pressure rise) considering all of the uncertainties in the input parameters of the modeling. The ranges were developed by examining the applicable information developed by the reactor safety community through various studies. In order to allow efficient manipulation of the information, and to allow expert input in a consistent manner, the ranges were then discretized and represented by specific outcomes (called levels), usually three to five per issue. Where possible, the levels represented the results of particular analyses performed by various organizations in the reactor safety community. This step was also done by the SARRP analysts but the expert review groups provided additional input and changed the levels where appropriate.

For each level of an issue, each individual reviewer supplied weighting factors to express his opinion of the relative likelihoods of the outcomes represented by that level. Essentially the reviewers provided their "degree of belief" for each level, with the constraint that the total weighting factors sum to one for the issue.

After collection of all of the input, the groups' weighting factors were combined into composites to represent the issue in the LLH sample. The process of creating composites to represent the group depended on the type of input for the issue. Some of the issues involved the specification of discrete distributions to approximate a continuous variable (e.g., pressure rise from direct heating). For these issues, each reviewer gave his view of the distribution by providing weighting factors on parameter values. The composite represented a distribution comprised of the average of the individuals' responses. Other issues required probabilistic input for a branch point (e.g., probability of ignition of hydrogen for a given sequence), and since a composite would not represent the uncertainty, each reviewer's input was weighted equally and assigned as an issue outcome for the sampling process.

A typical result is illustrated in Figure 2. All of the samples are calculated and plotted. The specific combinations of issue outcomes associated with each sample are also available to enhance understanding of particular sample members. For display and discussion purposes, the plot of the results includes a bar that illustrates the 5th and 95th percentile of the sample. It must be recognized that this bar does not have statistical meaning concerning the uncertainty in risk. The results of this task are limited to a representation of the uncertainty in the risk measures attributable to the limited number of specific issues selected, and are further limited to the input of those providing the weighting factors.

DEVELOPMENT AND QUANTIFICATION OF CONTAINMENT EVENT TREES

A major focus in SARRP was the development of a containment event tree for each of the reference plants under investigation. These event trees delineated the pathways that could lead to releases of

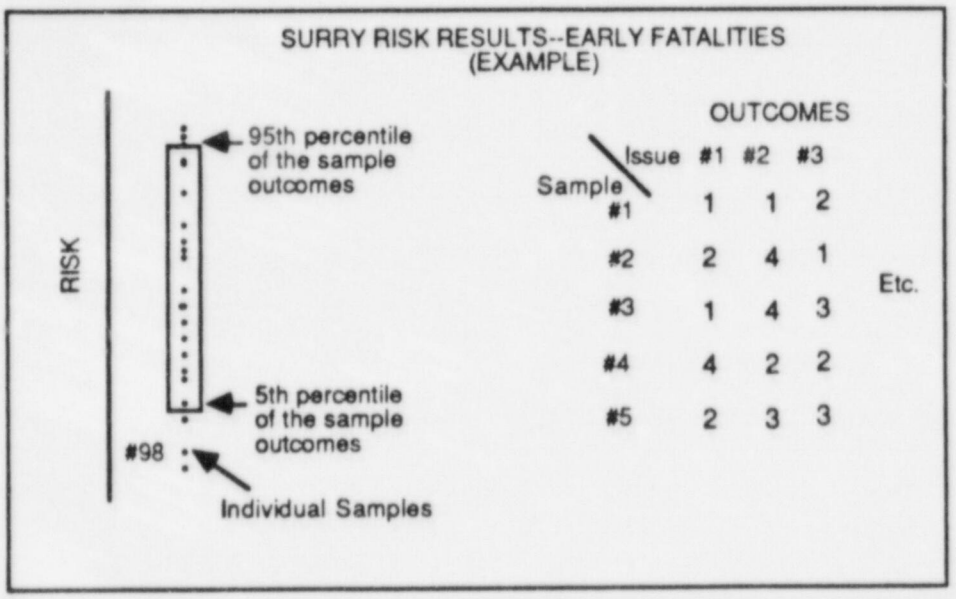


Figure 2. Example of LLH Output for Risk Measures

fission products as a consequence of core-damage accidents. The containment event tree for Surry was developed by identifying the types of containment responses that might be expected to impact risk and the various events and conditions that could affect those responses, at a level of detail that could reasonably be supported by the information currently available. This led to the construction of an event tree that is significantly expanded beyond those previously used in PRAs; the Surry containment event tree contains 59 questions, many of which have more than two branching options. The event tree is composed of the following types of questions:

1. Entry states. What are the conditions in the reactor coolant system and containment prior to melting of the core that could influence the accident progression?

2. Phenomenological events. What are the phenomena that could affect the progression of severe accidents, at what points during the accident timeline do they occur, and what are their subsequent effects on the accident development?

3. Reactor coolant system failure modes. What are the size and location of the reactor coolant system breach and the corresponding pressure during core meltdown?

4. Survivability of containment systems. Do the containment spray systems survive the conditions occurring during severe accidents that exceed their design bases?

5. Containment failure modes. What are the loads that challenge containment, does containment survive these loads, what is the nature of the failure (approximate size and location), and what is the subsequent pathway for release of fission products to the environment?

Because of the number of possible branching points, the event tree is too large to depict graphically. The questions are listed in Table I.

Rank regression techniques were used to evaluate the relative importance of specific issues. The regression calculated the fraction of the total variance explained by the individual issue.* These techniques are a good supplement to detailed review of the results; however, the statistics of the sample sizes used for SARRP do not always allow for meaningful regression analyses.

The questions are posed in ways that require the answers to be expressed in terms of likelihoods. The estimation of these likelihoods is often a highly uncertain process, and requires that information from a large number of sources be examined and incorporated in order to reflect the current level of understanding most appropriately. Table II lists many of the key issues represented by the questions in the event tree, and identifies some of the major research and analysis programs from which information was drawn to evaluate the corresponding questions. Among the sources of information used in the analysis are the following:

1. Containment Loads Working Group (CLWG) [4-5];

2. Containment Performance Working Group (CPWG) [6];

3. Battelle calculations for the Accident Source Term Project Office [7] and subsequently for SARRP;

4. Quantitative Uncertainty Estimation for the Source Term program [8];

5. Industry Degraded Core (IDCOR) program [9];

6. Severe Accident Sequence Analysis program [10-14];

7. Severe Accident Uncertainty Analysis [15];

8. Accident Sequence Evaluation Program (ASEP) [16-17];

9. SARRP Phenomena Assessment Task Force [18];

*If all issues were independent, the sum of the fractional variances for the individual issues would be unity. However, the correlations in the sample cause some issues to explain variance due to a correlation with another issue,and the total variance fraction sometimes exceeds one.

Table I

SUMMARY OF TOP EVENTS FOR SURRY CONTAINMENT EVENT TREE

	Question Posed by the Event Tree	Dependencies on Prior Questions
1.	Is ac power available after the initiating event?	None
2.	Does emergency core cooling fail prior to overpressurization of containment?	None
3.	What is the level of pre-existing containment leakage or isolation failure?	1
4.	Where is the initial reactor coolant system break?	None
5.	What is the size of the initial reactor coolant system break?	None
6.	Is the containment initially bypassed?	4
7.	Are the steam generators wet or dry?	None
8.	Do the fan coolers fail to actuate before core degradation	N/A*
9.	Do the containment sprays fail to actuate in the injection mode before core degradation?	1,3,5,6
10.	Do the containment sprays fail to actuate in the recirculation mode before core degradation?	1,9
11.	To what degree, if any, is the auxiliary building initially bypassed?	3,4,7
12.	Where, if at all, is there a temperature-induced failure of the reactor coolant system during the period of core degradation?	5
13.	What is the size of the temperature-induced reactor coolant system failure?	12
14.	What is the primary system pressure during core degradation? Also, what would be the containment pressure increment from a primary system blowdown?	5,12,13
15.	At what level, if any, is containment bypassed during core degradation?	4,5,12,13
16.	What is the rate of blowdown to containment during core degradation?	5,6,13,15
17.	Do the contianment sprays fail to actuate during the period of core degradation?	1,3,10,16
18.	Is there containment heat removal during core degradation?	8,17
19.	At what level, if any, does containment fail due to steam pressurization before vessel breach?	2,3,15,18
20.	What is the containment pressure before vessel breach?	3,16,18,19
21.	Is there a hydrogen burn before vessel breach? Also, what is the pressure increment from such a burn?	3,16,18
22.	Does containment fail because of a hydrogen burn before vessel breach? Also, what is the associated failure pressure and standard deviation?	20,21
23.	To what degree, if any, is the auxiliary building bypassed before vessel breach?	7,11,12,19,22
24.	Do the fan coolers fail after the early hydrogen burn?	N/A*
25.	Do the containment sprays fail after the early hydrogen burn?	1,17,21,22
26.	Is there containment heat removal after the early hydrogen burn?	24,25
27.	What is the mode of vessel breach?	14
28.	Does direct heating of the containment atmosphere occur just after vessel breach? Also, what is the pressure increment from a steam spike alone and from a steam spike plus direct heating?	14,17,27

*The event tree was developed to be generally applicable to plants with large, dry containments. Since Surry does not have fan coolers for emergency operation, these questions are not applicable.

Table I

SUMMARY OF TOP EVENTS FOR SURRY CONTAINMENT EVENT TREE (Continued)

	Question Posed by the Event Tree	Dependencies on Prior Questions
29.	Is there a hydrogen burn just after vessel breach? Also, what is the pressure increment from such a burn?	3,16,21,26
30.	Does containment fail due to a steam spike, direct heating, and/or hydrogen burn just after vessel breach?	14,20,28,29
31.	What is the mode of containment failure, if any, just after vessel breach?	3,19,22,27,28,29,30
32.	To what degree, if any, is the auxiliary building bypassed just after vessel breach?	23,31
33.	Do the fan coolers fail after vessel breach?	N/A*
34.	Do the containment sprays fail after vessel breach?	1,25,31
35.	Is there an oxidation release?	27,28
36.	Is ac power restored after vessel breach?	1
37.	Do the fan coolers fail late in the accident?	N/A*
38.	Do the containment sprays fail late in the accident?	34,36
39.	Is there containment heat removal late in the accident?	37,38
40.	Has the inventory of the refueling water storage tank been injected into containment?	9,17,25,34,38
41.	What is the amount of water injected into containment?	2,14,16,40
42.	Do significant core-concrete interactions occur after vessel breach?	14,18,27,34,41
43.	Is ac power recovered late in the accident?	1
44.	What is the containment pressure late in the accident?	3,15,19,22,31,41,43
45.	Has a large leak or gross failure occurred late in the accident?	3,15,19,22,31,44
46.	Does a late hydrogen burn occur?	21,29,39,44,45
47.	What pressure rise would occur if combustible gases were to burn late in the accident?	28,42,43,46
48.	Would containment fail due to a late hydrogen burn or steam production?	18,21,26,29,37 39,42,45,46,48
49.	In what way, if at all, does containment fail due to gradual pressurization from boiloff of water or non-condensible gases or hydrogen burning (leakage or gross rupture)?	45,46,48
50.	To what degree, if any, is the auxiliary building bypassed late in the accident?	32,44,49
51.	Do the fan coolers fail after the late hydrogen burn?	N/A*
52	Do the containment sprays fail after the late hydrogen burn?	36,38,49
35.	Is there containment heat removal very late in the accident?	51,52
56.	Does basemat melthrough occur, given no prior containment failure?	26,38,39,45, 49,53,54,55
57.	Does containment depressurize after basemat melthrough?	26,39,53,56
58.	What is the ultimate containment failure mode, if any, resulting from core-concrete interactions?	42,45,49,53, 55,56,57
59.	To what degree, if any, is the auxiliary building bypassed very late in the accident?	50,55,57

Table II

Use of Information Sources in Addressing the Issues in the Containment Event Tree

ISSUE	INFORMATION SOURCES*													
	CLWG	CPWG	BMI-2104	QUEST	IDCOR	SASA	SAUNA	PATF	SERG	HIPS	PRA	AE	FVCS	Others
1. Size of Preexisting Containment Leakage.	–	X	–	–	X	–	–	–	–	–	X	–	–	X
2. Size and Location of the Primary System Break During the Melt Release (e.g., Hot Leg vs. Cold Leg).	–	–	–	–	–	–	–	–	–	–	–	–	–	–
3. Timing of Accumulator Discharge Relative to Timing of Reactor Vessel Breach.	–	–	X	–	X	–	–	–	–	–	–	–	–	–
4. Occurrence of In-Vessel Steam Explosion Large Enough to Fail the Reactor Vessel.	–	–	–	–	X	–	X	–	X	–	X	–	–	X
5. Occurrence of In-Vessel Steam Explosion Large Enough to Fail the Containment.	–	–	X	–	X	–	X	–	X	–	X	–	–	X
6. Timing and Magnitude of Early Hydrogen Burns.	X	–	X	–	X	X	–	X	–	–	X	–	–	X
7. Magnitude of the Ex-Vessel Steam Spike.	X	–	X	X	X	–	–	–	–	X	–	–	–	–
8. Extent of Direct Heating of the Atmosphere Following Vessel Breach.	X	–	–	–	–	–	–	–	–	X	–	–	–	–
9. Containment Structural Failure Pressure.	–	–	–	–	X	–	–	–	–	–	X	X	–	–
10. Size of Containment Leakage Induced by Temperature or Pressure.	–	X	–	–	X	–	–	–	–	–	–	–	–	–
11. Survivability of Containment Sprays and Fan Coolers at Various Times During the Accident.	–	–	–	–	X	–	–	–	–	–	X	–	–	X
12. Survivability of Suppression Pools and Ice Condensers at Various Times During the Accident.	–	–	–	–	–	–	–	–	–	–	–	–	–	–
13. Extent of Core-Concrete Interaction.	X	–	X	–	X	–	X	–	–	X	X	–	–	–
14. Timing and Magnitude of Late Hydrogen Burns.	X	–	X	–	X	–	–	–	–	–	–	–	–	X
15. Potential for Direct Core Debris Attack on Containment Structures.	X	–	–	–	–	–	–	–	–	–	–	–	–	–
16. Potential for Core Debris to Melt Through the Basemat.	–	–	X	–	X	–	–	–	–	–	X	–	–	X
17. Potential for Basemat Meltthrough to Cause a Depressurization of Containment.	–	–	X	–	–	–	–	–	–	–	X	–	–	–
18. Potential for Effluent to Pass Through Adjacent Structures, Such as the Auxiliary Building.	–	–	X	–	X	–	–	–	–	–	–	–	–	–

*Information sources used in evaluating a particular issue are denoted by an "X."

10. Steam Explosion Review Group [19];

11. High-pressure ejection test series [20];

12. Available probabilistic risk assessments [21-26];

13. The Final Safety Analysis Report [27];

14. Architect-engineer and other estimates of containment failure pressure [28-29];

15. Filtered-Vented Containment System reports [30-31]; and

16. Others [32-40].

CONTAINMENT LOADING AND PERFORMANCE ISSUES

The following containment loading and response issues were included in the LLH study for Surry:

1. Probability and location of induced failure of the RCS pressure boundary;

2. Mode of reactor vessel breach;

3. Magnitude of pressure loading at vessel breach due to direct heating and steam spike;

4. Magnitude of hydrogen burn pressure increment at vessel breach;

5. Containment failure pressure;

6. Size of containment failure;

7. Probability of late containment spray system failure; and

8. Probability of submergence of the interfacing systems LOCA failure location.

Each of these issues is defined in the following subsections. It should be noted that the consideration of several of the issues involves a level of detail considerably greater than that presented here and that further details are given in a separate report [1].

Probability and Location of Induced Failure in the RCS Pressure Boundary

Recent analyses have indicated the potential for very high gas temperatures in the primary system for core damage sequences involving high pressure in the RCS prior to vessel breach. These results have prompted the consideration of induced failures of the

pressure boundary that would lead to a change in the scenario phenomenology due to RCS depressurization or containment bypass through the occurrence of a steam generator tube rupture. These failures have not been included in previous studies but were found to be of sufficient significance that they were included in both the SARRP central estimate and the LLH study. Six potential LOCA outcomes (and one outcome for no induced LOCA) were considered based on location and size of the failure:

- Large hot-leg LOCA
- Small hot-leg LOCA
- Large seal LOCA
- Small seal LOCA
- Large steam generator rupture
- Small steam generator tube rupture
- No induced failure

The expert review group overall felt that an induced failure was fairly likely. Figure 3 illustrates both the composite weights, denoted by X's, as well as the range of responses for the individual reviewers for each outcome for a particular set of boundary conditions.

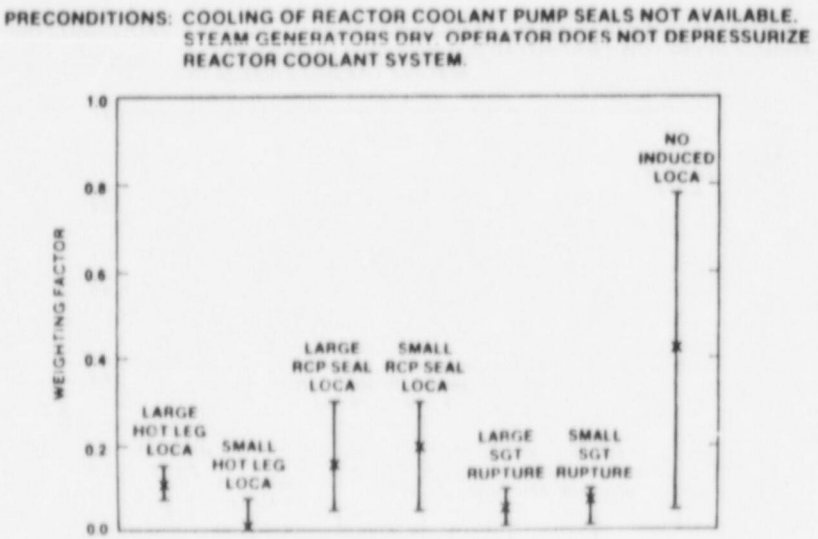


Figure 3. Outcomes and Weighting Factors for Location and Size of Induced LOCA

Mode of Reactor Vessel Breach

This issue includes the rather controversial containment failure mode of direct containment failure by a steam explosion-induced missile (the mode). The issue also addresses the potential for high pressure ejection of the core material, gravity flow after

vessel breach, and in-vessel steam explosions leading to vessel failure but not containment failure. Figure 4 illustrates the ranges of the expert review input for this issue.

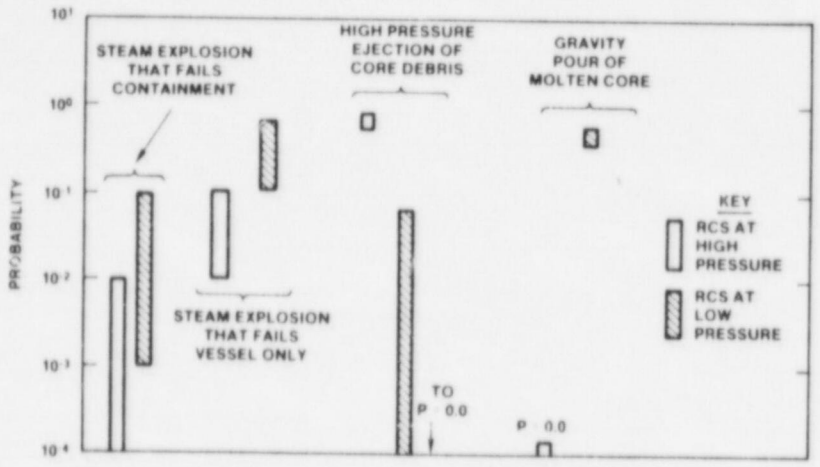


Figure 4. Outcomes and Weighting Factors for Mode of Reactor Vessel Breach

Magnitude of Pressure Loading at Vessel Breach Due to Direct Heating and Steam Spike

This issue deals primarily with the phenomenon of direct heating--the addition of substantial heat directly to the containment atmosphere caused by the dispersal throughout containment of finely divided core material. To limit the detail considered in the LLH study, the issue was defined in terms of the pressure loading of containment at vessel breach due to the generation of steam and the possibility of direct heating. Reviewers were asked to incorporate all their considerations about the uncertainties in these phenomena into the final pressure increment. Thus, the issue includes uncertainties in the:

- Amount of core initially ejected
- Amount of core exiting the cavity
- Efficiency of energy transfer
- Probability of the phenomenon itself

The input of the review group for the most significant case, high pressure sequence with no water in the reactor cavity, is illustrated in Figure 5. The reviewers based their input on previous discussions of this issue by the Containment Loads Working Group (CLWG) and recent experimental evidence. As the figure illustrates, there was fairly wide uncertainty indicated by the inputs of the individual expert reviewers, but the overall conclusion was that direct heating was likely to produce very large pressure loadings at

vessel breach--one-half of the LLH samples for these conditions have pressure increments of 75 psi or greater at vessel breach, not including any hydrogen burn contribution.

A further interesting input of the review group (not shown on the figure) was that the phenomenon of direct heating would be almost as severe for intermediate pressure sequences as for high pressure. For the Surry plant, the reviewers also thought that a reactor cavity full of water would have a relatively small impact on the resulting pressure increments due to direct heating (a 25% reduction in the peak pressures on the average). No reviewers thought that the phenomenon was possible at low pressure.

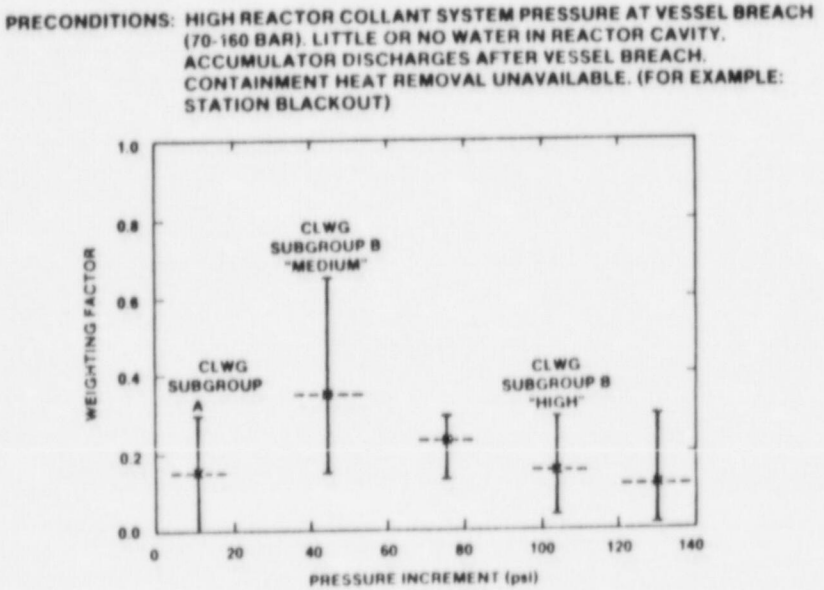


Figure 5. Outcomes and Weighting Factors for Magnitude of Pressure Loading at Vessel Breach Due to Direct Heating and Steam Spike

Magnitude of Hydrogen Burn Pressure Increment at Vessel Breach

All of the uncertainties relative to hydrogen generation and burning at vessel breach were included in this issue in which the reviewers were asked to weight pressure increments due to hydrogen burning at vessel breach. The most significant uncertainty in the issue is the amount of hydrogen generated up to the time of vessel breach, although there is also uncertainty in the amount left in the vessel at vessel breach as well as the ignition characteristics of the hydrogen steam mixture. This issue required a considerable number of cases to account for important boundary conditions: steam concentration, the occurrence of direct heating, and the magnitude of the steam spike.

One case is illustrated in Figure 6. The pressure increment corresponding to 50% equivalent Zr oxidation was weighted most heavily,

but the range of pressure increments with weighting factors greater than 0.1 was still quite large: 0 to 70 psi. One other important factor was determined by the review group input for other cases: the potential for significant pressure increments associated with hydrogen when direct heating occurs, even when the containment is steam inert relative to large scale burning. These increments were attributed to recombination reactions of hydrogen and oxygen in the local vicinity of the hot fuel particles dispersed in containment.

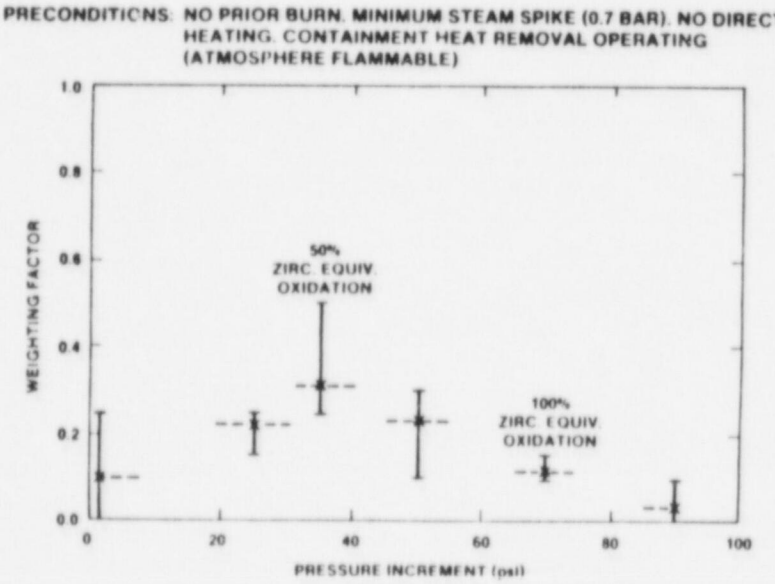


Figure 6. Outcomes and Weighting Factors for Magnitude of Hydrogen Burn Pressure Increment at Vessel Breach

Containment Failure Pressure

For Surry, two previous studies of containment structured capacity were directly applicable: The RSS and a Stone and Webster Study. In addition, the experts cited other studies of similar containments that provide insight into the expected capacity of the Surry containment. The input of the review team is illustrated in Figure 7. As indicated, the Stone and Webster value was weighted most heavily, but there was also significant weight attached to the next highest pressure capacity because the Stone and Webster evaluation only considered yield strength of materials rather than ultimate strength. It should be noted that the values indicated are only the mean values of a distribution: the uncertainty in materials parameters was also included in the study through the selection of standard deviations of the failure pressure distribution.

Containment Failure Size

The LLH study also included consideration of the size of the containment failure opening. The reviewers thought that there were two

principal correlations associated with this issue: (1) the size would be correlated with the ultimate pressure capacity assumed, and (2) the size would also be dependent of the level of pressurization relative to the mean failure pressure. This latter correlation could not be accommodated within the constraints of the schedule and

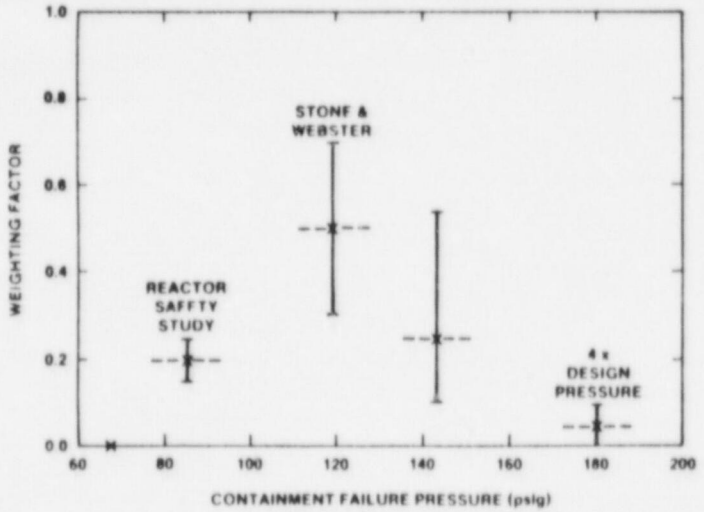


Figure 7. Outcomes and Weighting Factors for Containment Failure Pressure

the reviewer input had to be redefined in terms of only two failure sizes for the same reason. The original input is illustrated in Figure 8 for two cases of containment failure pressure. As illustrated, for the low pressure capacity the reviewers assigned a very high weighting factor to small openings based on a belief that a low pressure capacity would be due to an anomaly that would result in a local failure. The second case for a higher ultimate capacity illustrates a shift to larger openings based on the view that the higher the capacity, the more likely a gross rupture would occur since all materials would approach their ultimate strength together.

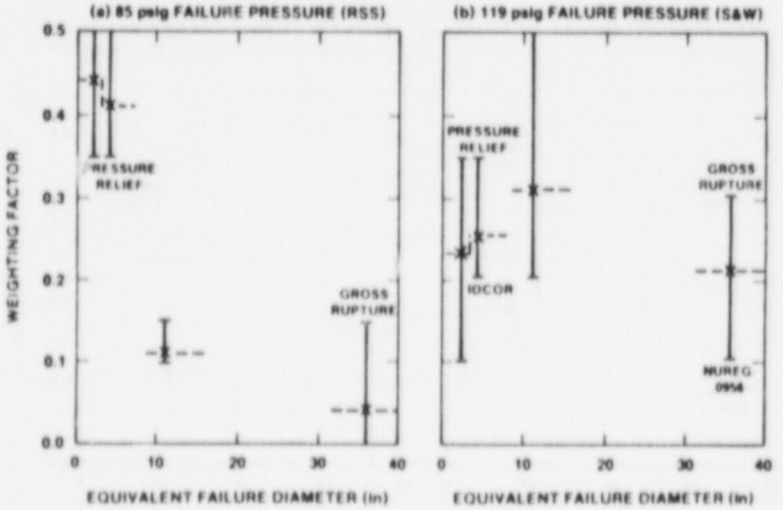


Figure 8. Outcomes and Weighting Factors for Containment Failure Size

Probability of Containment Spray Failure

This issue deals with the late failure of the containment sprays due to phenomena in the containment. The review group was asked to provide weighting factors for three containment states. The first case was for no containment failure and was intended to account for failures due to debris in the sump or possible damage due to hydrogen burns. All of the reviewers except one thought that there would be no increase in failure rate over the basic spray failure unreliability for no severe environment, and the other reviewer thought that the failure probability would be 0.05. The results for the case of a containment failure with a small failure opening were similar. The reviewers did assess a significant failure probability (0.25 average) for the case of containment failure by gross rupture.

Probability of Submergence of the V Sequence Failure Site

The interfacing systems LOCA, or V sequence, was determined early in the analysis to be a very significant risk contributor. There are a number of uncertainties associated with this sequence and this issue deals with the physical conditions associated with the failure in the auxiliary building--whether or not the failure site is covered by water after the initial blowdown of the primary system. This issue is actually important to the assessment of the radiological source term but the input was more appropriate to the containment performance experts than the source term experts. Based on a several analyses of the situation, the reviewers assigned a probability of submergence. There was limited variation in the input and the average submergence probability was approximately 0.8.

SEQUENCE FREQUENCY AND SOURCE TERM ISSUES

Issues involved in systems analysis and fission product source term analysis were also included in the LLH uncertainty evaluation. These issues are listed below but not elaborated upon. Reference [1] contains a detailed discussion of these issues and describes the development of outcomes and weighting factors.

Five issues affecting only the assessment of the core-damage sequence frequencies were included in the LLH study. They are as follows:

1. The likelihood and timing of early reactor coolant pump seal LOCAs during station blackout.

2. Use of the gas turbine generator for offsite power recovery.

3. Manner of application of beta factors to characterize common mode failures.

4. Failure rates for interfacing system check valve (V sequence).

5. Effect of containment failure on operability of emergency core cooling systems.

The following radiological source term issues were included in the LLH analysis of Surry:

1. Magnitude of in-vessel release from the fuel;

2. Amount of CsI decomposition in the reactor coolant system (RCS);

3. Amount of RCS retention due to deposition;

4. Decontamination factor for V sequence release under water;

5. Fraction of species released from the RCS that are subsequently released from containment;

6. Magnitude of core-concrete interaction release;

7. Fraction of core-concrete interaction species that are subsequently released from containment;

8. Decontamination factor for the containment sprays;

9. Aerosol agglomeration uncertainties;

10. Amount of iodine released late in the accident from containment sources;

11. Revolatilization from the RCS after vessel breach;

12. Release associated with the high pressure ejection vessel failure mode; and

13. Release associated with direct heating.

RISK RESULTS

Sequence Frequencies

The study of the Surry plant by the Accident Sequence Evaluation Program (ASEP) resulted in a new estimate of the total frequency of core damage emanating from internal events as well as the individual accident sequences contributing to that total [3]. The dominant accident sequences are listed in Table III. As illustrated, there are about 15 sequences that contribute to make up 95% of the total frequency. There were no single sequences found to dominate the result. The table also illustrates the importance of one initiating event--loss of offsite power. This initiator is involved in sequences contributing one-half of the total.

Table III

DOMINANT CORE-DAMAGE SEQUENCES FOR SURRY

Sequence	Description	Frequency*
$T_1SL\text{-}D_1CF_1$	Loss of offsite power, resulting in a reactor-coolant pump (RCP) seal LOCA due to the failure of all seal cooling. High-pressure injection, containment spray injection, and spray recirculation are all unavailable (all caused by the extended unavailability of all electric power).	5.6×10^{-6}
$T_{4J}QH_1$	Loss of 4 kv bus J, followed by failure of a pressurizer relief valve to reclose, and failure of low-pressure recirculation.	1.5×10^{-6}
$T_{4H}QH_1$	Loss of 4 kv bus H, followed by failure of a pressurizer relief valve to reclose, and failure of low-pressure recirculation.	1.3×10^{-6}
T_1LP	Loss of offsite power, followed by failure of auxiliary feedwater and failure of the power-operated relief valves to be opened to permit feed-and-bleed cooling.	1.2×10^{-6}
$T_1L(LT)D_1CF_1$	Loss of offsite power and failure of auxiliary feedwater in the long term due to the extended unavailability of electric power and eventual depletion of the batteries. The unavailability of power also results in unavailability of high-pressure injection and containment sprays.	1.1×10^{-6}
$T_1L(ST)D_1CF_1$	Loss of offsite power and failure of auxiliary feedwater in the short term due to failure of the turbine-drive pump. The unavailability of power also results in failure of high-pressure injection and containment sprays.	1.1×10^{-6}
$T_{4J}QH_2$	Loss of 4 kv bus J, followed by failure of a pressurizer relief valve to reclose, and failure of high-pressure recirculation.	1.1×10^{-6}
$TKRD_4$	Transient followed by failure to scram and failure of high-pressure injection for emergency boration.	9.8×10^{-7}
$T_{4H}QH_2$	Loss of 4 kv bus H, followed by failure of a pressurizer relief valve to reclose, and failure of high-pressure recirculation.	9.2×10^{-7}
V	Interfacing-systems LOCA.	9.0×10^{-7}
S_2D_1	Small LOCA with failure of high-pressure injection.	7.7×10^{-7}
S_1D_1	Intermediate LOCA with failure of high-pressure injection.	7.7×10^{-7}
S_2H_1	Small LOCA followed by failure of low-pressure recirculation.	7.2×10^{-7}
S_2H_2	Small LOCA followed by failure of high-pressure recirculation.	5.5×10^{-7}
S_1H_1	Small LOCA followed by failure of low-pressure recirculation.	5.1×10^{-7}
	Total (95% of frequency)	1.9×10^{-5}

* Point estimate values derived by propagating mean values of individual events.

Risk of Early and Latent Cancer Fatalities

The basic risk results for early and latent cancer fatalities are shown in Figures 9 and 10. Included on these charts is the following information:

1. The mean risk for the plant in question as reported in 1975 by the Reactor Safety Study [21].

2. A current central estimate of risk based on the use of fission product source terms with "best guess" estimates of sequence frequencies and containment failure mode probabilities obtained from ASEP and SARRP analyses.

3. A measure of the uncertainty about the central estimate associated with data (i.e., the uncertainty caused by incomplete or inconsistent data pertaining primarily to equipment failure rates).

4. The uncertainty in risk associated with issues covered by the limited Latin Hypercube analysis (i.e., those issues associated primarily with incomplete or incorrect modeling of phenomena or system behavior). The first of the three bars depicts the uncertainty attributable to system issues only, the second includes system, containment loading, and containment performance issues, and the third includes all of these plus fission product source term issues. The medians and means of the distributions are also shown.

The current central estimates of risk for Surry are generally lower than those presented in the Reactor Safety Study. There are several reasons:

- The frequency of sequences for which containment is bypassed (e.g., the V sequence) is lower.

- Early containment failures are less likely.

- Advances in fission product modeling have resulted in generally lower source terms.

- Siting and emergency response assumptions are different. (The current study used site-specific demography and meteorology and assumed that 5% of the population did not evacuate.)

On the other hand, the uncertainties are mostly in the upward direction. The tops of the LLH uncertainty bands with all issues included portray values which are comparable to the Reactor Safety Study risk estimates.

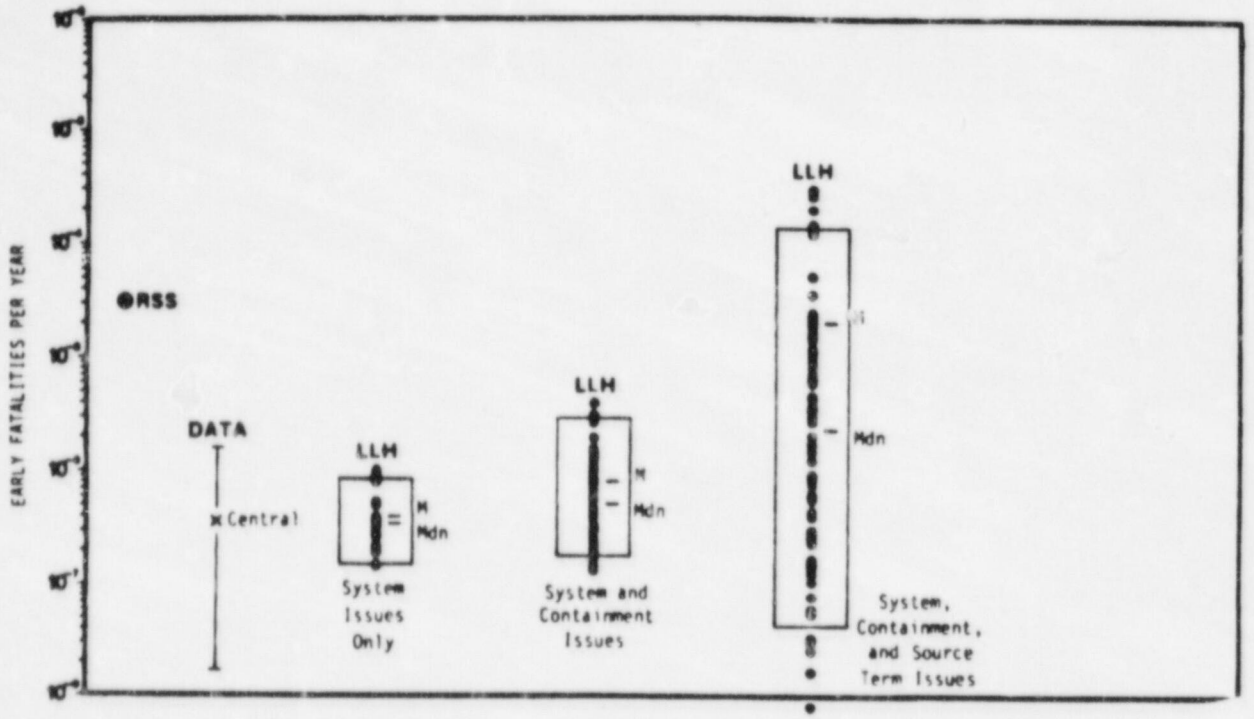


Figure 9. Comparison of Risk Results Including Uncertainties: Early Fatalities

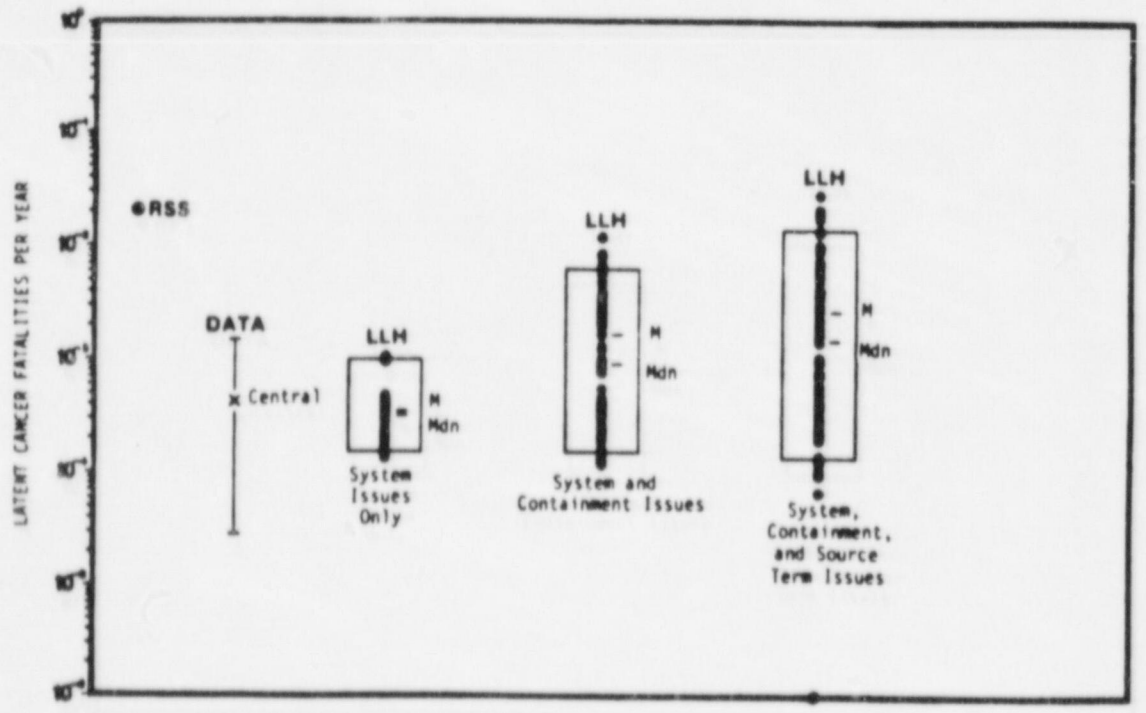


Figure 10. Comparison of Risk Results Including Uncertainties: Latent Cancer Fatalities

RELATIVE CONTRIBUTION OF THE VARIOUS CONTAINMENT ISSUES TO THE UNCERTAINTY IN RISK

The first method used to examine the relative importance of the LLH issues was a rank regression analysis of the results. Thus, the contribution of each issue to the overall variance is calculated (including contribution due to correlation with other issues). The results of these regressions are plotted in Figures 11 and 12. Unfortunately, the statistical sample is small and fractional contributions less than 10% are not significant. From both of the figures it is obvious that the direct heating issue is far and away the most important uncertainty.

Since the limited sample size and the dominance of the direct heating issue did not allow for additional insight through the rank regression technique, the sample members at either end of the range were reviewed in detail to understand the contributing uncertainties more fully. Of the 100 LLH samples, the top 20 and bottom 20 contributors to early and latent fatalities were examined individually and compared to each other. Those issues found to have the same distribution of outcomes in the top 20 risk samples as the bottom 20 risk samples probably are not significant to the overall uncertainty. However, those issues with substantially different outcome distributions in the top 20 versus bottom 20 probably are important to risk uncertainty. This method of review is limited in statistical meaning but was performed to help provide qualitative insights. Table IV summarizes the results of this process for the containment issues as applied to the early fatality risk measure. Only the issues with different distributions in the top and bottom regimes are indicated (variation less than 15% was assumed to be negligible).

The results of this analysis indicated that after direct heating the next most important issue determined was the containment failure pressure. Note that the high risk samples have the two lowest levels of pressure capacity 90% of the time while the low risk samples have these two levels in only 65% of the samples. Containment failure size is correlated with the failure pressure and therefore shows some effect although it is not of great significance.

The issue of hydrogen burn at vessel breach is also important but the reason is more subtle. The table indicates that the highest risk samples never have the lowest level of hydrogen burning. Therefore, all of the risk dominant scenarios of direct heating have some level of hydrogen burn pressure increment. Prior to the input of the LLH review group, hydrogen burns were not allowed for most of these cases since nearly all of the important scenarios are station blackout accidents with no containment heat removal. These scenarios were thought to involve a steam inerted containment, precluding the possibility of hydrogen burning. The review group assigned fairly high likelihood of significant pressure increments due to hydrogen in direct heating scenarios, regardless of the steam concentration. The phenomenon cited was the possibility of local burning or recombination of hydrogen in the vicinity of the hot fuel

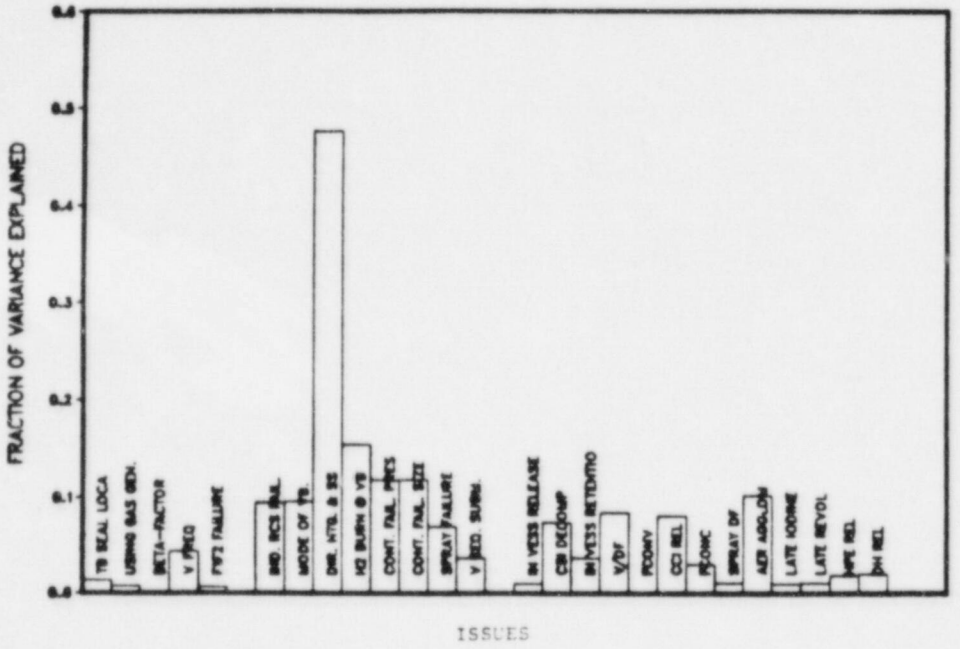


Figure 11. Rank Regression Analysis for Risk of Early Fatalities

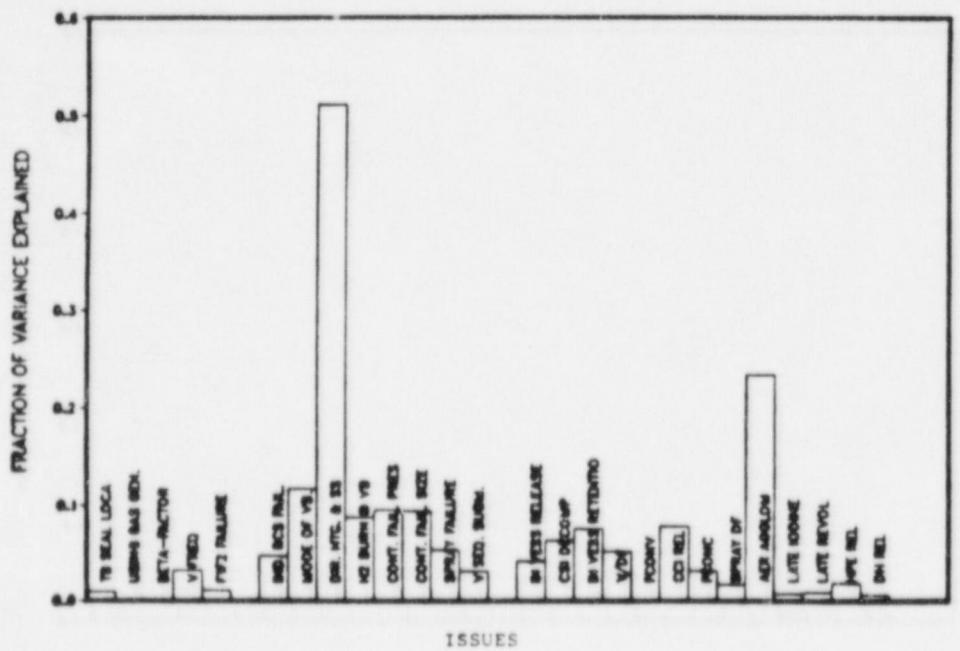


Figure 12. Rank Regression Analysis for Risk of Latent Fatalities

Table IV

LLH UNCERTAINTY ISSUE IMPORTANCE TO EARLY FATALITY RISK

Issue & Outcome	# In 20 Lowest Risk Samples	# In 20 Highest Risk Samples	% In 20 Lowest Risk Samples	% In 20 Highest Risk Samples	% Difference	Discussion
Issue 6	Location and Size of Induced RCS Failure					
Level 1	2	3	10	15	5	A review of the level definitions indicates that there is no significance to this arrangement of samples except that Level 4 is tube rupture which only appears in high risk samples.
Level 2	6	2	30	10	20	
Level 3	4	5	20	20	0	
Level 4	0	3	0	15	15	
Level 5	0	0	0	0	0	
Level 6	8	7	40	30	10	
Issue 7	Mode of Vessel Breach					
Level 1	4	4	20	20	0	The level definitions were reviewed to discover that there is no real significance to this level distribution. The Level 5 difference is random because the meaning of Level 5 is nearly the same as Levels 1 and 9 which do not have the same anomaly.
Level 2	3	1	15	5	10	
Level 3	1	5	5	25	20	
Level 4	0	2	0	10	10	
Level 5	5	0	25	0	25	
Level 6	1	2	5	10	5	
Level 7	2	0	10	0	10	
Level 8	2	4	10	20	10	
Level 9	2	2	10	10	0	
Issue 8	Direct Heating					
Level 1	5	1	25	5	20	This is overwhelmingly the most significant issue. Levels 1&2 involve little or no direct heating and appear in nearly all the low risk samples and vice versa.
Level 2	13	1	65	5	60	
Level 3	2	6	10	30	20	
Level 4	0	7	0	35	35	
Level 5	0	5	0	25	25	
Issue 9	Hydrogen Burn at Vessel Breach					
Level 1	5	0	25	0	25	This issue is important in tandem with direct heating. Note that the least significant levels (1-3) are weighted most heavily in the low risk samples while the high risk samples are skewed to higher levels. Further, no high risk samples have no hydrogen burn (Level 1). This is very important because the hydrogen pressure increment is adding to the direct heating pressure to bring about failure. See the discussion in this section.
Level 2	5	7	25	35	10	
Level 3	4	5	20	25	5	
Level 4	2	4	10	20	10	
Level 5	3	3	15	15	0	
Level 6	1	1	5	5	0	
Issue 10	Containment Failure Pressure					
Level 1	2	9	10	45	35	This is relatively important. 95% of the high risk samples have the lowest two levels of containment capacity.
Level 2	11	10	55	50	5	
Level 3	5	1	25	5	20	
Level 4	2	0	10	0	10	
Issue 11	Containment Failure Size					
Level 1	4	0	20	0	20	The levels increase in the frequency of large hole sizes. Note that the high risk samples are skewed to the higher levels. This is of moderate importance
Level 2	4	1	20	5	15	
Level 3	5	5	25	25	0	
Level 4	4	8	20	40	20	
Level 5	2	2	10	10	0	
Level 6	1	4	5	20	15	

particles with a pressure increment similar to the case of global hydrogen deflagration. For many of the accidents, it appears that this additional pressure increment is the actual cause for exceeding the containment pressure capacity. Direct heating alone does not always result in the failure probabilities seen in the LLH result. Of course, both hydrogen burning and direct heating pressure increments are intimately coupled with the containment failure pressure issue.

LIMITATIONS

The limitations associated with probabilistic risk assessment have been discussed in many forums and a reiteration of the entire subject would not be useful here. There are a few specific limitations of importance that should be recognized when interpreting the results of this paper:

- The results apply to one reactor plant only and should not be inferred as being generally applicable to other reactor plants.
- The results are based on internal initiating events only as external events were out of scope.
- The number of issues considered was limited and, while an attempt was made to focus upon important issues, there is no guarantee that the ones considered are the most important.
- The consideration of operator actions was limited to actions associated with written procedures. During severe accidents, operator actions outside the formal procedures, both positive and negative, could occur.
- Accident sequences resulting in core damage were assumed to proceed to core melting and subsequent breaching of the reactor vessel. It is anticipated that some of the sequences would be arrested prior to reactor vessel breach.

REFERENCES

1. Benjamin, A. S., et al., "Evaluation of Severe Accident Risks and the Potential for Risk Reduction: Surry Power Station, Unit 1," Sandia National Laboratories Report (Draft), Albuquerque, NM: May, 1986.

2. Benjamin, A. S., et al. "Containment Event Analysis for postulated Severe Accidents at the Surry Nuclear Power Plant." Sandia National Laboratories Report SAND86-0119 (Draft), Albuquerque, NM: January 1986.

3. Bertucio, R. C., et al., "Analysis of Core Damage Frequency from Internal Events: Surry, Unit 1," Sandia National Laboratories Report (Draft), Albuquerque, NM: April, 1986.

4. "Estimates of Early Containment Loads from Core Melt Accidents, Report of the Containment Loads Working Group." U.S. Nuclear Regulatory Commission Report NUREG-1079 (Draft for Comment), Washington, DC: December, 1985.

5. Containment Loads Working Group, "Consensus Summaries for Standard Problems 1 through 6." Letter Reports to J. Telford, U.S. Nuclear Regulatory Commission, May-June, 1984.

6. Containment Performance Working Group, "Containment Leak Rate Estimates." U.S. Nuclear Regulatory Commission Report NUREG-1037 (Draft for Comment), Washington, DC: May, 1985.

7. Gieseke, J. A., et al. "Radionuclide Release Under Specific Accident Conditions." Battelle Columbus Laboratories Report BMI-2104, Columbus, OH: 1984.

8. Lipinski, R. J., et al. "Uncertainty in Radionuclide Release Under Specific LWR Accident Conditions." SAND84-0410, Sandia National Laboratories, Albuquerque, NM: 1985.

9. IDCOR Task 23.1: "Integrated Containment Analysis." Technology for Energy Corporation, Knoxville, TN: 1984.

10. Haskin, F. E., et al. "Analysis of Hypothetical Severe Core Damage Accidents for the Zion Pressurized Water Reactor." U.S. Nuclear Regulatory Commission Report NUREG/CR-1989, Sandia National Laboratories, Albuquerque, NM: 1982.

11. Camp, A. L., et al. "MARCH-HECTR Analysis of Selected Accidents in an Ice-Condenser Containment." U.S. Nuclear Regulatory Commission Report NUREG/CR-3912, Sandia National Laboratories, Albuquerque, NM: December, 1984.

12. Cook, D. H., et al. "Loss of Decay Heat Removal Sequences at Browns Ferry Unit One - Accident Sequence Analysis." U.S. Nuclear Regulatory Commission Report NUREG/CR-2973, Oak Ridge National Laboratory, Oak Ridge, TN: May, 1983.

13. Harrington, R. M., et al. "ATWS at Browns Ferry Unit One - Accident Sequence Analysis." U.S. Nuclear Regulatory Commission Report NUREG/CR-3470, Oak Ridge National Laboratory, Oak Ridge, TN: July, 1984.

14. Bruske, S. Z., et al. "Severe Accident Sequence Analysis (SASA) Program Sequence Event Tree: Boiling Water Reactor Anticipated Transient Without Scram." U.S. Nuclear Regulatory Commission Report NUREG/CR-4165, Idaho National Engineering Laboratory, Idaho Falls, ID: February, 1985.

15. Rivard, J. B., et al. "Identification of Severe Accident Uncertainties." U.S. Nuclear Regulatory Commission Report NUREG/CR-3440, Sandia National Laboratories, Albuquerque, NM: September, 1984.

16. Kolaczkowski, A. M., et al. "Interim Report on Accident Sequence Likelihood Reassessment." (Draft Report), Sandia National Laboratories, Albuquerque, NM: August, 1983.

17. Harper, F. T., et al. "Accident Sequence Likelihood Information." U.S. Nuclear Regulatory Commission Report NUREG-0956 (Appendix), Washington, DC: August, 1985.

18. Benjamin, A. S., et al. "SARRP - Risk Rebaselining and Risk Reduction Analysis." Proceedings of the 11th Water Reactor Safety Research Information Meeting. U.S. Nuclear Regulatory Commission Report NUREG/CP-0048, Vol. 3, Washington, DC: January, 1984.

19. Steam Explosion Review Group. "A Review of the Current Understanding of the Potential for Containment Failure Arising from In-Vessel Steam Explosions." U.S. Nuclear Regulatory Commission Report NUREG-1116, Washington, DC: February, 1985.

20. High-Pressure Ejection Test Series, Sandia National Laboratories, Albuquerque, NM: 1985.

21. "Reactor Safety Study--An Assessment of Accident Risks in U.S. Commercial Nuclear Power Plants." U.S. Nuclear Regulatory Commission Report WASH-1400 (NUREG-75/014), Washington, DC: 1975.

22. "Reactor Safety Study Methodology Applications Program." U.S. Nuclear Regulatory Commission Report NUREG/CR-1659 (Volumes 1 through 4), Sandia National Laboratories, Albuquerque, NM: 1981-1982.

23. Commonwealth Edison Company. "Zion Probabilistic Risk Assessment." Chicago, Illinois: 1980.

24. "Sizewell B Probabilistic Safety Study." Westinghouse Electric Co. Report WCAP-9991, Monroeville, PA: 1982.

25. "Seabrook Plant Probabilistic Safety Study." Yankee Atomic Electric Co., Seabrook, NH: December, 1983.

26. "GESSAR-II BWR/6 Standard Plant Probabilistic Risk Assessment." General Electric Co., San Jose, CA: 1982.

27. "Final Safety Analysis Report for Surry Unit 1." Virginia Electric Power Company, Richmond, VA: 1971.

28. Drozd, A., et al. "Parametric Study of Aerosol Behavior Following AB and TMLB Accidents, "Proceedings of the American Nuclear Society 1984 Annual Meeting. TP84-54, Stone and Webster Engineering Corp.: 1984.

29. Griesmann, L., et al. "Final Report, Containment Analysis Techniques, a State-of-the-Art Summary." U.S. Nuclear Regulatory Commission Report NUREG/CR-3653, Ames Laboratories, Ames, IA: March, 1984.

30. Harper, F. T. "The Effect of Filtered-Vented Containment Systems on Severe Accident Frequencies and Consequences for a Mark III Boiling Water Reactor." U.S. Nuclear Regulatory Commission Report NUREG/CR-4066, Sandia National Laboratories, Albuquerque, NM: (to be published).

31. Benjamin, A. S., et al. "Value Impact Assessment of Filtered-Vented Containment Systems and Other Safety Options for a BWR Mark I Containment." U.S. Nuclear Regulatory Commission Report NUREG/CR-4065, Sandia National Laboratories, Albuquerque, NM: (to be published).

32. Weinstein, M. B., et al, "Primary Containment Leakage Integrity: Availability and Review of Failure Experience." Nuclear Safety: 21, 1980.

33. Pratt, W. T., et al. "Containment Response During Degraded Core Accidents Initiated by Transients and Small Break LOCA in the Zion/Indian Point Reactor Plants." U.S. Nuclear Regulatory Commission Report NUREG/CR-2228, Brookhaven National Laboratories, Upton, NY: July, 1981.

34. Lyons, W. G., "Presentation at NRC/IDCOR Meeting on Containment Loads and Fission Product Behavior." U.S. Nuclear Regulatory Commission: May, 1984.

35. Murfin, W. B., et al. "Report of the Zion/Indian Point Study." U.S. Nuclear Regulatory Commission Report NUREG/CR-1410, Sandia National Laboratories, Albuquerque, NM: August, 1980.

36. Camp, A. L., et al. "Light Water Reactor Hydrogen Manual." U.S. Nuclear Regulatory Commission Report NUREG/CR-2726, Sandia National Laboratories, Albuquerque, NM: August, 1983.

37. Berman, M., et al. "An Uncertainty Study of PWR Steam Explosions." U.S. Nuclear Regulatory Commission Report NUREG/CR-3369, Sandia National Laboratories, Albuquerque, NM: May, 1984.

38. Niemczyk, S. J., et al. "The Consequences from Liquid Pathways After a Meltdown Accident." U.S. Nuclear Regulatory Commission Report NUREG/CR-1596, Sandia National Laboratories, Albuquerque, NM: June, 1981.

39. McClymont, A. S. and B. W. Poehlman. "Loss of Off-Site Power at Nuclear Power Plants: Data and Analysis." Electric Power Research Institute Report NP-2301 (Interim Report), Palo Alto, CA: March, 1982.

40. "Reassessment of the Technical Bases for Estimating Source Terms." U.S. Nuclear Regulatory Commission Report NUREG-0956, Washington, DC: August, 1985.

SESSION B

OPERATIONAL EXPERIENCE AND ITS RELATIONSHIP TO
CONTAINMENT PERFORMANCE DURING ACCIDENT CONDITIONS

NEW BELGIAN POSITION ON CONTAINMENT LEAKAGE TESTING

B. De Boeck

Association Vinçotte
Sureté Nucleaire
Avenue du Roi, 157
B-1060 Bruxelles, BELGIUM

ABSTRACT

The containment leakage testing requirements (up to now 10 CFR 50 App. J) have recently been revaluated in Belgium. The criterion for type A tests at half the accident pressure has been strengthened, but the periodicity has been relaxed. New overall leakage test at very low overpressure have been required after each extended cold shutdown period. A few items of the procedure for type A tests have been modified. It is felt that the new requirements improve the safety but also lower the burden of the containment leakage tests.

1. INTRODUCTION

For more than ten years, the leakage tests of the Belgian containments have been made in accordance with 10 CFR 50 appendix J. With this experience, and in view of the recent developments in France and in the USA, it seemed usefull to reassess the leakage tests methodology. Therefore, a working group with representatives from the utilities, the architect engineers and the licensed organization was set up in 1984. The final report has been published in April 1986 and shows that some aspects of the present methodology can be modified and that the result offers a better compromise, combining the safety requirements and the operational ones. This paper gives the conclusions of the report.

2. TESTS AT ACCIDENT PRESSURE

Is called "accident pressure" and abbreviated Pa, the peak pressure in the containment, following a design basis accident, like mentioned in the Safety Analysis Report (definition identical to the one from 10 CFR 50).

It is felt that leakage tests at accident pressure are not warranted. The main reason is that their operational burden is not balanced by a clear safety benefit. The main drawbacks of these tests are:

- Test duration
  The duration of such a test is clearly larger than the one of a test realised at a lower pressure (more important preparation, longer pressurization and depressurization).

- Danger
  Even if such a test does not represent a dangerous loading for the containment, it is nevertheless true that it increases the risk of fires and the difficulty to fight these, and that it increases the risk of damaging equipments in the containment.

- Representativeness
  The Pa pressure is not representative of the real pressure in the containment after a design basis accident, on the one hand because of the margins and conservative assumptions taken in the calculation of Pa, and on the other hand because of the depressurizing effect of the containment cooling systems. Some of the type A tests performed in Belgium have shown higher leakage rates at half Pa than at Pa.

Furthermore, tests realised at a lower pressure permit to meet the safety objectives.

3. TESTS AT ELEVATED PRESSURE

Is called "elevated pressure" and abbreviated Pt, any pressure between Pa/2 and Pa, Pa and Pt being expressed in relative bars.

The 1980 edition of the 10 CFR 50 App. J, permits to do leakage tests at a pressure equal to the half of the accident pressure. The leaktightness criterion is taken from the leakage rate at full pressure and the one at reduced pressure, measured during the preoperational tests. Now, these measured leakage rates are tainted with errors being bigger when the leakage rate is lower, which is generally the case. One calculates then the ratio of the two leakage rates, and depending on the result, one uses for the criterion, either the ratio itself, either the

square root of the ratio of the pressures. If the ratio of the leakage rates is used, one has seen that this ratio is not known with accuracy, but even if it were the case, then nothing indicates that it remains constant during the entire life-span of the containment. On the other hand, the square root of the ratio of the pressures does not represent the most pessimistic extrapolation law which can be obtained.

This does not imply that one should reject tests at a pressure lower than Pa, but rather that it is necessary to establish a more satisfactory criterion. The new Belgian criterion is:

$$Ltm \leq 0.75 \frac{Pt}{Pa} La$$

where - La is the leakage rate considered in the accident analysis
- 0,75 is an arbritary factor to cover the possible rise of the leakage rate in the interval between two tests
- Ltm is the 95% upper confidence limit of the measured leakage rate (appendix B of ANSI/ANS-56.8-1981 can be used to calculate this limit).

The extrapolation law of the leakage rate with the pressure, used in this criterion, is the one of the ratio of the relative pressures. This law is close to the law of the laminar flow, which gives the strongest variations of the leakage rate in function of the pressure. This law does not take into consideration the leaks with a threshold effect. Yet, the influence of such leaks is considered to be weak, as preoperational tests have shown.

To conclude, tests at elevated pressure can replace the tests at accident pressure if (1) the law of the ratio of the relative pressures is used to extrapolate the leakage rate and if (2) the test pressure is at least equal to Pa/2. There is no theoretical justification for the factor 2, but it seems desirable to test the containment at a pressure which is (1) not too different from the maximum pressure expected in the containment after accident, which (2) permits to measure the leakage rate with a reasonable accuracy, and which (3) limits the span on which the leakage rate has to be extrapolated.

4. TESTS AT REDUCED PRESSURE

4.1 Principle

In addition to the tests at elevated pressure, it is possible to perform leakage tests at a reduced pressure (i.e. lower than Pa/2), during operation. Such tests are in use in France and

have been performed experimentally in Belgium. The decision has been taken to do them periodically (see § 5). The goal of these tests is not to measure accurately the leakage rate of the containment, but to detect any gross leakage path.

In normal operation, the pressure in the reactor building has a tendency to increase owing to the leakages of the compressed air system. If one measures the flow of incoming air, the pressure, the temperature and the humidity in the building, it is possible to calculate the leakage rate. For a typical test, the pressure is allowed to go from - 20 mbar to + 60 mbar. This extends on few days and measurements are taken every hour.

Symbols:

Q : flow of incoming gas (Nm^3/h)
P : absolute pressure in reactor building (mbar)
T : absolute temperature in reactor building (°K)
X : absolute humidity in reactor building
(kg of water/kg of dry air)
Pv: partial pressure of water vapour (mbar)
V : quantity of dry air in reactor building (Nm^3)
Vr: free volume of reactor building (m^3)

One has:

$$Pv = \frac{P \cdot X}{0.622 + X}$$

and

$$V = Vr \cdot \frac{P - Pv}{1013} \cdot \frac{273}{T}$$

This computation is done at a regular interval delta t, and each time one computes delta V, the difference between V at time t and t - delta t. The leakage flow is then:

$$Qf = Q - \frac{V}{t}$$

At each time step one measures also delta P, the differential pressure between the reactor building and the outside. The values of Qf are then plotted in function of the square root of delta P (Qf is expected to be proportional to the square root of delta P). A straight line is then computed by the least squares method and translated to go thru the point Qf = 0 for delta P = 0. The value of Qf for delta P = 60 mbar (Qf60) is then compared with the criterion.

This criterion in Belgium is 17 Nm3/h, which corresponds to a circular hole of 1 cm in diameter. This value was chosen on the basis of the accuracy of the method used up to now, the goal being to minimize, on one hand the probability of not detecting an important leak, and on the other hand, the probability of starting a search for a non existent leak.

4.2 Experimental results

Tests have been performed in 1985 at Tihange 1 and 2, and Doel 3, to show the feasability of such tests. Some results are given below. Tests have been done with a normally isolated containment, like it is in operation, and also with different leakage paths. A few times, the leakage flow has been measured with a flowmeter installed on the leakage path.

It should be noted that for tests 8 and 9, there were head losses in the line in addition to the 3/4" flow restrictor.

TABLE 1

N°	UNIT	Ø opening	Qf60 Nm^3/h	Qf at delta P Nm^3/h	mbar
1	Tihange 1	/	3.1		
2	Doel 3	/	- 8.6		
3	Doel 3	/	4.3		
4	Doel 3	/	- 1.0		
5	Tihange 1	7 mm	11.0	11	60
6	Doel 3	3/8"	18.8		
7	Doel 3	3/8"	22.5	14	19
				20	38
8	Tihange 1	0→3/4"	0,7/28.1		
9	Tihange 1	3/4"	32.5	33	60
10	Doel 3	3/4"	94.7	34	9

The conclusions of these tests are:

- small holes can be detected, the detectability limit is at around 10 Nm3/h, or a hole of 7 mmm in diameter

- the accuracy of the method is good, as can be seen from the measured leakage flows (based on the square root of the ratio of the pressures, the flow extrapolated at 60 mbar is 25 Nm3/h for test 7 and 88 Nm3/h for test 10)

- it is important to accurately measure the temperature and humidity variations in the containment during the tests.

- a pressure range from - 20 mbar to 50 mbar is to be considered as a minimum to get a good accuracy, especially for small holes.

5. PERIODICITY OF THE TESTS

It is unlikely that the containment, apart from the penetrations, will change significantly on a time scale shorter than ten years. Experience from the United States shows that when a test at elevated pressure fails, it is nearly always due to one or more leaking penetrations.

If one dissociates, for the test at elevated pressure, the function which verifies the leak tightness of the containment itself from the function which detects holes left inadvertently, then a periodicity of 10 years is acceptable for the tests at elevated pressure. The second function would then be realised on the one hand by the periodic tests of the penetrations (type B and C tests), and on the other hand by the tests at reduced pressure. These should be done when a possibility exists of having a loss of leaktightness of the containment. In Belgium, a test at reduced pressure will be done after each cold shutdown of more than fifteen days.

6. MISCELLANEOUS

6.1 Use of two measuring methods in parallel

In Belgium, the overall leakage rate tests are usually performed with the absolute method and the reference vessel method. These two methods are practically independent and their results can thus be used for mutual validation. Therefore it is not always necessary nor to pursue the test for 24 hours, nor to perform the calibrated leak test to verify the accuracy of the measures.

1. End criterion.

If both methods furnish, over a period of at least 8 hours and with at least 30 measure points, a leakage rate value which meets the criterion presented in § 3, then one may end the measurement.

2. Concordance criterion.

It is not necessary to initiate a verification test (for example: calibrated leak) if at the end of the measuring period the difference between the leakage rates measured by each of the two methods over the last 8 hours is less than:

$$0.25\ Lt - 0.1\ Ltm$$

where: - $Lt = \frac{Pt}{Pa}\ La$

- Ltm is the average of the two measurements of the leakage rate.

This criterion is largely arbitrary.
The principles which have led to its establisment are the following. The fixed term (0.25 Lt) is drawn from the success criterion of the calibrated leak test of ANSI/ANS-56.8-1981 (see § 6.2). The proportional term (0.1 Ltm) forces to a better concordance when the leakage rate is close to the maximum admissible value. In that case, it is indeed more useful to be sure that the leakage rate is correctly measured than in the case where the leakage rate is well below the criterion. In total, one obtains a concordance criterion which is consistent with the expected accuracy of the measuring methods used until now and which offers a reasonable guarantee that the leakage rate is correctly measured.

6.2 Calibrated leak test

If, during a leakage rate test at elevated pressure, only one measuring method is used, or if the concordance criterion mentioned in § 6.1 is not met, it is necessary to perform the calibrated leak test (or an equivalent test). The success criterion of this test, laid down in ANSI/ANS-56.8-1981, is only applicable in case the test pressure is equal to Pa and the superimposed leak is equal to about La.

To recall, the success criterion of this test is the following:

$$|Lo + Lam - Lc| \leq 0.25\ La$$

where - Lo is the superimposed leakage rate
- Lam is the leakage rate measured before the calibrated leak is put into service
- Lc is the leakage rate measured after the calibrated leak is put into service

The following conditions have to be met to use this criterion:
- Pt = Pa
- $0.75\ La \leq Lo \leq 1.25\ Lt$

It is easy to adapt this criterion in case Pt < Pa :

$$|Lo + Ltm - Lc| \leq 0.25\ Lt$$

where $Lt = \frac{Pt}{Pa}\ La$

The conditions for application are:

- $Pa/2 \leq Pt \leq Pa$ (relative bars)
- $0.75\ Lt \leq Lo \leq 1.25\ Lt$

If one chooses to take Lo lower than 0.75 Lt, this criterion looses its sense because it becomes too easy to meet. It is therefore necessary to adapt it. The following adaptation is proposed:

$$|Lo + Ltm - Lc| \leq 0.125\ Lt + 0.125\ Lo$$

The conditions for application are:

- $Pa/2 \leq Pt \leq Pa$ (relative bars)
- max (0.75 Ltm; 0.1 Lt) $\leq Lo \leq 1.25\ Lt$

This criterion has the following advantages:

- it remains simple
- it adapts itself to the value of Lo
- it is close to the ANSI criterion when Lo is close to Lt

One can note that (1) Lo may not be lower than 0.1 Lt if one wants to have a calibrated leak which remains in the measurable range, and that (2) the factor 0.125 is chosen arbitrarily equal to half the factor 0.25 of the uncorrected criterion.

6.3 Extrapolation of the leakage rate

According to the law one chooses to characterise the leaks of the containment, one obtains different relations between the leakage rate at test conditions and the leakage rate at accident conditions. The most conservative law is that of the flow of a venturi, which results in a leakage rate after accident 1.4 times higher than in test conditions (at the same pressure).

The French use, for their plants with liners, the law of the turbulent flow in a rough pipe, which is a little less conservative and gives a factor 1.35.
In France, the criterion is thus:

$$Lam \leq \frac{0.75}{1.35} La = 0.56\ La$$

It is on the other hand useful to note that the factor 0.75 of the relation

$$Lam \leq 0.75\ La$$

of Appendix J of 10 CFR 50 is not a factor to cover an extrapolation of the leakage rate towards accident conditions, but actually a margin to cover a possible rise of the leakage rate until the next test.

Still, in Belgium, for the calculation of the radiological consequences of a LOCA, it is supposed that the leakage rate of the containment stays at its maximum value during 24 hours and is thereafter reduced to half of that for the remaining time, whereas the pressure in the containment is rapidly brought down. Consequently one disposes here of an important conservatism.

To conclude, as long as these assumptions are conserved for the calculation of the radiological consequences, it is not necessary in the criterion of § 3, to include a supplementary factor to cover the rise of the leakage rate during accident conditions.

7. CONCLUSIONS

The establisment of a working group composed of representatives from the utilities, the architect engineers and the licenced organisation, to treat a precise technical subject, has led to the proposal of a notable improvement of the strategy applied to the overall leakage rate tests of the containment.

The main improvements are:

- shorter tests (on the condition to use two independent measuring methods)

- an increased confidence in meeting the objective of leaktightness (through the use of a criterion independent of the preoperational tests and based on a conservative extrapolation law)

- an increased confidence in maintaining the leaktightness of the containment during operation, despite a lower frequency for the tests at elevated pressure (by performing tests at reduced pressure during reactor operation).

8. REFERENCES

1 ANSI/ANS-56.8-1981, Containment System Leakage Testing Requirements

2 Proposed 10 CFR 50 App. J, Working paper D5

3 Draft Regulatory Guide MS 021-5, Containment System Leakage Testing

4 NUREG/CR-3549, Evaluation of Containment Leak Rate Testing Criteria

5 ESN/85/014, Report of the Working Group on Containment Leakage Testing

6 Containment Integrity and Leak Testing Procedures Applied and Experiences Gained in European Countries, CEC, Working Group No 1 - Ad hoc subgroup on "Containment Engineering Safeguards", (To be published)

ALTERNATIVE CONTAINMENT INTEGRITY RETESTING REQUIREMENTS AND LOCAL LEAKAGE CALCULATION METHODS

J.P. Glover
Commonwealth Edison Co.
Nuclear Services Technical
P.O. Box 767
Chicago, Illinois 60690

ABSTRACT

This paper discusses two topics on containment leakage testing. First, the 'Minimum Path' method of calculating leakage from multi-valve isolation systems is examined. It will be shown that this method is overly conservative relative to its intended purpose. An upper bound upon that conservatism is found and two alternative methods are proposed.

The second topic concerns ILRT retesting requirements. Failure of two consecutive 'As Found' tests places a unit on an accelerated schedule. Using data from previous containment leak tests, it will be discussed whether 'As Found' ILRT failures are more often the results of leakage from locally tested valves, hatches, and penetrations or from the containment structure and other areas that can be found only from Type A testing. The approximate average cost of an ILRT both in terms of dollars and Man-Rem will be found. From this data, the affect upon containment integrity and cost to the utilities of accelerated Type A testing is discussed. The alternative concept of corrective action plans that address the specific sources of leakage are evaluated.

Both topics discussed here are based upon the need to correct measured Type A test results with local leak test results. The NRC currently interprets 10CFR50 Appendix J to require such corrections when repairs or adjustments are performed in the inspection period prior to the Type A test. Commonwealth Edison Co. performs the corrections because stipulations in exemption requests submitted in 1974, (and since approved) made them mandatory. Use of the local leakage corrections here is a reflection of those exemption requests and not an endorsement of the NRC's interpretation.

LOCAL LEAKAGE CALCULATION METHODS

The current Nuclear Regulatory Commission (NRC) interpretation of 10CFR50 Appendix J requires that the containment integrated leak rate test (ILRT) be performed prior to any repairs or adjustments (RAs) of containment isolation systems during the test's inspection period. The start of the inspection period has been defined[1] as the start of the outage in which the ILRT is to be performed. Due to scheduling constraints, it is often both desirable and economical to delay the leak test until the end of the refueling outage (after RAs). Reference 1 allows for performance of the ILRT after RAs only if local leak test results are used to back-correct the measured ILRT values. The intent of this procedure is to determine the ILRT leakage that would have been measured if the test had been performed prior to any RAs in that inspection period.

The NRC currently requires use of the 'Minimum Path' method for those back-corrections. The difference between the 'As Found' and the 'As Left' 'Minimum Path' leakage is the penalty that must be added to the ILRT results. The 'Minimum Path' method sets the net leakage from a dual valve isolation system, (Figure 1) equal to the leakage from/through the best of the two containment isolation valves. The 'As Found' leakage is that measured prior to any RAs on the dual valve isolation system. The 'As Left' leakage is that measured after RAs. Reference 2 gives a detailed description of the arithmetic used.

Before the 'Minimum Path' method can be used, the individual leakage from each valve in the dual valve isolation system must be determined. The leakages from and through valve 1 (Q_1) and 2 (Q_2) must be measured with full accident pressure (ΔP_a) across them. One method by which this can be accomplished is to measure the leakage from each valve independently of the other by the proper use of isolation and/or vent valves. In some cases, there is no choice but to test both valves #1 and #2 simultaneously by pressurizing through valve #3. The individual leakage from each valve can still be found. First, the initial total leakage (Q_a^i) from the two valve system is measured. One of the two valves (valve #1) is then repaired, and it is assumed that the leakage from that valve is now zero. The two valve system is then retested and a final leakage (Q_a^f) measured. The individual 'As Found' leakages can now be determined.

$$Q_a^i = Q_1^i + Q_2^i, \quad Q_a^f = Q_1^f + Q_2^f = Q_2^f = Q_2^i$$
$$Q_1^i = Q_a^i - Q_a^f, \quad Q_2^i = Q_a^f$$

Note, the assumption of zero leakage after repairs always results in conservative values of Q_1 and Q_2.

Under post accident conditions, any leakage out of containment through a duel valve isolation system would have to pass through both closed isolation valves. The 'Minimum Path' method is overly conservative because it fails to account for the restriction from the worse of the two valves. It should be noted that the order of magnitude of allowable leakage is such that the total restriction from the valves' associated piping system is usually negligible compared to the restriction of the best valve, for a passing test.

The requirement to use the 'Minimum Path' method has no regulatory basis. Currently, the NRC considers this to be a conservative method to back-correct measured Type A leakage for RAs performed prior to the ILRT. Pressurizing from containment to all three closed valves (Figure 1) is the actual condition the system would be subjected to during a Type A test. This is therefore a much more physically realistic method of measuring system leakage. Also, the unwarranted over conservatism of ignoring the worse of the two isolation valves is eliminated. The only disadvantage is that this leakage would be unsuitable for determining 'Maximum Path' leakages for satisfying the 0.6 La criteria. Additional tests would be required for that purpose.

There is still much conservatism built into the above method. The local leak tests are performed at steady state peak accident pressure. For worst case FSAR post-accident conditions, a typical PWR containment pressure versus time curve is shown in Figure 2. It can be seen that peak pressure is only attained for a short time. Thus, both the instantaneous leak rates (and therefore dose rates) and total leakage (and therefore total dose) indicated by local leak test results are always much less than would actually occur.

There are many cases where it is not physically possible or practical to test both valves in series from containment. A conservative analytical method of calculating the total system through leakage from measured individual valve leakages shall be presented here.

Leakage through the valves is assumed to be both turbulent and incompressible. The relationships between measured leakages and imposed pressure differentials for each valve are:

$$Q_1 = C_1\sqrt{\Delta P_a} \qquad (1)$$

$$Q_2 = C_2\sqrt{\Delta P_a} \qquad (2)$$

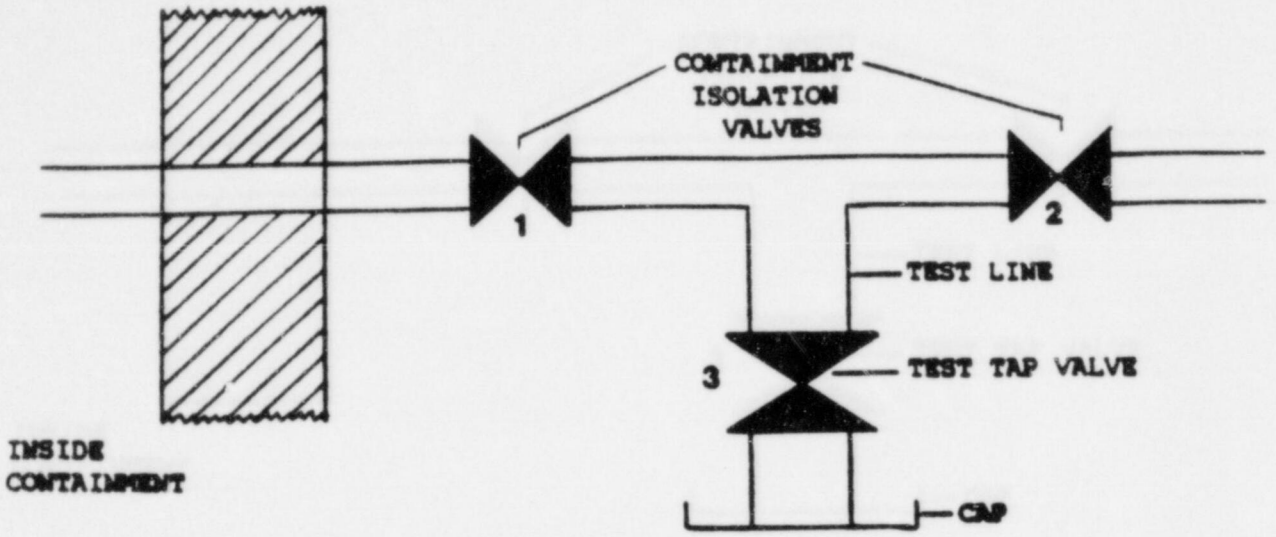


FIGURE 1. A DUAL VALVE ISOLATION SYSTEM WITH TEST TAP

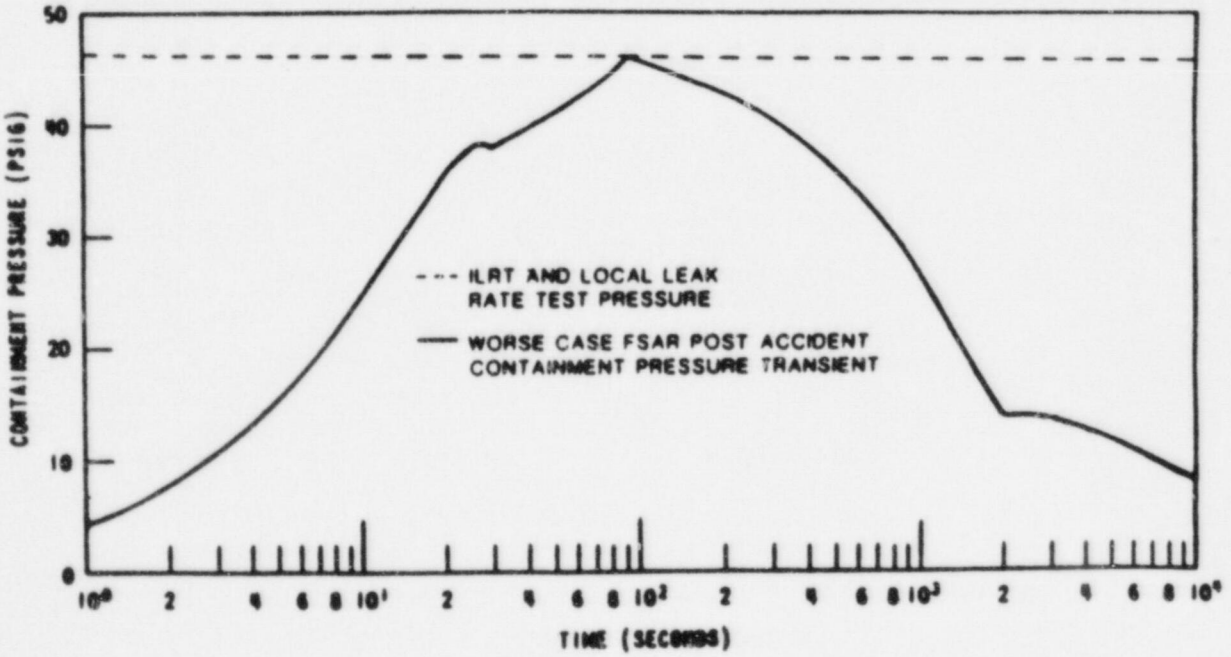


FIGURE 2. CONTAINMENT PRESSURE VERSES TIME FOR A TYPICAL PWR

In this analysis, let Q_1 be the smaller of the two leakages. For turbulent flow, C_1 and C_2 are nearly constant over a wide range of flow rates, (or range of Reynolds numbers). Actual flow (Q_a) leaving containment under post-accident conditions undergoes a pressure drop as it crosses valve #1 (ΔP_1) and valve #2 (ΔP_2). The below equations can be written.

$$Q_a = C_1 \sqrt{\Delta P_1} \qquad (3)$$

$$Q_a = C_2 \sqrt{\Delta P_2} \qquad (4)$$

Since ΔP_a must equal $\Delta P_1 + \Delta P_2$, from Equations 3 and 4:

$$\Delta P_a = \frac{Q_a^2}{C_1^2} + \frac{Q_a^2}{C_2^2} = Q_a^2 \left(\frac{1}{C_1^2} + \frac{1}{C_2^2} \right)$$

By substitution Equations (1) and (2) into the above expression:

$$Q_a^2 = \frac{\Delta P_a}{\frac{\Delta P_a}{Q_1^2} + \frac{\Delta P_a}{Q_2^2}} = \frac{1}{\frac{1}{Q_1^2} + \frac{1}{Q_2^2}}$$

or equivalently:

$$Q_a = Q_1 \left(\frac{Q_2}{\sqrt{Q_1^2 + Q_2^2}} \right) \qquad (5)$$

Where: Q_a = actual flow
Q_1 = 'Minimum Path' flow
Q_2 = 'Maximum Path' flow

When Q_2 approaches ∞, application of L' Hospital's rule to Equation (5) above indicates that Q_a becomes equal to Q_1. When valve #2 leaks badly, the 'Minimum Path' method is physically realistic and yields leakages equivalent to those given by Equation (5). The other extreme corresponds to the case when valve #2 is as good as valve #1. When $Q_1 = Q_2$, then $Q_a = 0.707\ Q_1$. Thus it is seen that up to almost 30% over-conservatism can result from using the 'Minimum Path' method.

Flow through the valves was assumed to be turbulent. There is no way to tell from the leak test results if the flow was in fact laminar. For laminar flow, Equations 1 and 2 would be replaced by the below expressions.

$$Q_1 = C_1 \Delta P_a \qquad (6)$$

$$Q_2 = C_2 \Delta P_a \qquad (7)$$

By performing an analysis similar to that done for turbulent flow, the below equation is derived in place of Equation 5.

$$Q_a = \frac{Q_1 Q_2}{Q_2 + Q_1} \qquad (8)$$

Again, let Q_1 be the smaller of the two leakages. When Q_2 approaches ∞, application of L' Hospital's rule to Equation (8) indicates that Q_a becomes equal to Q_1. When Q_1 equals Q_2, then $Q_a = Q_1/2$. This shows up to a 50% reduction is possible for laminar flow, while only a 30% reduction is possible for tubulent flow. To insure conservative results, leakage is always assumed to be turbulent.

Flow was also assumed to be incompressible. This is not a realistic assumption, since air flowing through the valves undergoes approximately a 77% pressure drop. The proper expressions for a compressible flow should include the expansion factors Y_1 and Y_2 as shown below.

$$Q_1 = Y_1 C_1 \sqrt{\Delta P_a} \qquad (9)$$

$$Q_2 = Y_2 C_2 \sqrt{\Delta P_a} \qquad (10)$$

Y is always less than 1.0. By conservatively assuming incompressible flow and setting Y equal to 1.0, Equations 9 and 10 reduce to Equations 1 and 2 from which Equation 5 was derived.

For small enough pressure differentials across a leaky valve, flow will be laminar. This flow is linearly proportional to the applied pressure differential, as shown by Equations 6 and 7. As the pressure differential increases, flow becomes turbulent and proportional to the square root of the applied differential, Equations 1 and 2. When the pressure differential becomes large enough, choked flow results. Sonic velocity occurs at the flow path's smallest cross section. Flow rate is fixed, and no longer varies with increasing pressure differential. A valve in series with a choked valve does nothing to reduce total system flowrate. Equation 5 must not be applied to a dual valve isolation system when either of the valves is choked. Prior to using Equation 5, when measuring individual valve leakages, pressures should be increased above test pressure to verify that leakage also increases. This will insure that flow is not choked.

CONTAINMENT RETESTING REQUIREMENTS

10CFR50 Appendix J, Section III.A.6(b) requires a unit that fails two consecutive ILRTs be placed upon an accelerated testing schedule. The unit would remain on that schedule until it passed two consecutive tests. While on an accelerated schedule, an ILRT must be performed every refueling outage rather than three times in every Ten Year In-Service Inspection period. For a plant that is on twelve month cycles, this requirement could result in the performance of up to five (assuming 3 month refueling outages) additional tests in the ten year period. The average costs incurred during an ILRT based upon most of the tests examined here are summarized in Table 1.

TABLE 1
ILRT COSTS

ITEM	RANGE	MEAN VALUE
Man-REM	0.3 → 6	3
Compressor Rental	7,000 → $25,000	$12,000
Personnel Overtime		~ $15,000
Instrumentation		~ $10,000
Lost Operation Time	1.7 → 11.25 days	3.9 days

Assuming a replacement power cost of $600,000 per day, the mean total cost of a single test is $2,377,000. The worst case of a plant doing five extra tests in the ten year interval corresponds to an average of $1,188,500 and 1.5 Man-REM per year per unit penalty. Actual ILRT schedules from four of the sites examined puts average costs at 56% of the above maximum values, $665,560 and 0.84 Man-REM per year per unit penalty. It should be noted that the above average costs are only estimates. They are sufficiently accurate for their intended usage here, which is to show that a significant amount of resources are spent meeting accelerated ILRT schedules.

The final test reports from 23 ILRTs were assembled. To insure representative results, tests from both BWRs and PWRs owned by a number of different utilities across the county were used. Both local and integrated leakages for each test are listed in Table 2. From this data, the effectiveness of the large expenditure of resources for accelerated testing on insuring containment integrity is evaluated. Also, this data is used to evaluate the concept of corrective action plans. Their adequacy and cost effectiveness to insure containment integrity relative to accelerated testing is discussed. The tests in Table 2 are sequentially numbered rather than identified by plant name, date, and unit number. That information is not presented because it is not the intended purpose of this paper to compare the performance of one plant to that of another.

The second column in Table 2 contains the total 'As Found Minimum Path' leakages from all Type B and C tested valve, penetration, and closure systems. This leakage is measured prior to the Type A test and prior to any repairs or adjustments (RAs) performed that outage. These numbers are intended to represent the contribution to total measured leakage out of containment from all Type B and C tested areas had the ILRT been conducted prior to any RAs on those areas. Column 3 contains the total 'As Left Minimum Path' leakages. These are intended to represent the total leakage out of containment from all Type B and C tested areas after RAs and prior to the ILRT. For the earlier test reports examined, the 'Minimum Path' leakage was not listed. In those cases, individual valve leakages were used to calculate the 'Minimum Path' leakage. Where only the leakage from simultaneously testing both valves was listed, half that value was used. Column 4 is the leakage found, measured, and repaired during the ILRT or found, isolated and then measured and repaired after the ILRT. The difference between columns 2 and 3 plus the values in column 4 are added to the 'Final Measured ILRT Leakage' in column 5 to obtain the 'Total As Found ILRT Leakage' in column 6. Note that since penalties for unvented paths (no longer required in most cases) and other causes are not listed, the arithmetic will not come out exact. It is the leakage in column 6 that is compared against the 0.75 La acceptance criteria in order to determine ILRT passage or failure. For the plants examined, 0.75 La fell between approximately 160 and 1600 SCFH.

The tests examined can be separated into four categories:

1. The total 'As Found Minimum Path' local leak test results were greater than the 0.75 La acceptance criteria. Those leaks were repaired and the total 'As Left' local leakage was well below 0.75 La. The subsequent measured Type A leakage was also less than the acceptance criteria.

TABLE 2

SUMMARY OF LOCAL AND INTEGRATED LEAK RATE TEST RESULTS

TEST	TOTAL MINIMUM PATH 'AS FOUND' B & C LEAKAGE, SCFH	TOTAL MINIMUM PATH 'AS LEFT' B & C LEAKAGE, SCFH	LEAKAGE FOUND AND REPAIRED DURING THE ILRT, AND REASON FOR THAT LEAKAGE	FINAL MEASURED ILRT LEAKAGE, SCFH	TOTAL 'AS FOUND' ILRT LEAKAGE, SCFH
1	250	154	No Repairs	215	344
2	5268 + UD*	142	1778 SCFH, Deficiency in B & C Testing Program	250	7154 + UD*
3	239	104	No Repairs	280	435
4	377	183	No Repairs	199	504
5	446 + UD*	102	No Repairs	113	525 + UD*
6	226	137	5 SCFH, Omission in B & C Testing Program	191	319
7	1913 + UD* + UD*	157	315 SCFH, Omission in B & C Testing Program	322	2422 + UD* + UD*
8	1887	135	No Repairs	133	1950
9	1550	150	50 SCFH, Now Type B or C Tested Area	168	1650
10	3200	50	~ 70 SCFH, New Modification not Previously Leak Tested	316	3600
11	1651	90	UD*, Non Type B or C Tested Area	157	1727 + UD*
12	375 + UD*	183	Less than 2 SCFH	242	434 + UD*
13	29	29	Less than 2 SCFH	14	16
14	344	44	No Repairs	222	526
15	30	30	No Repairs	107	107

*UD: Un-Defined, leakage was too large to measure.

TABLE 2 (continued)

SUMMARY OF LOCAL AND INTEGRATED LEAK RATE TEST RESULTS

TEST	TOTAL MINIMUM PATH 'AS FOUND' B & C LEAKAGE, SCFH	TOTAL MINIMUM PATH 'AS LEFT' B & C LEAKAGE, SCFH	LEAKAGE FOUND AND REPAIRED DURING THE ILRT, AND REASON FOR THAT LEAKAGE	FINAL MEASURED ILRT LEAKAGE, SCFH	TOTAL 'AS FOUND' ILRT LEAKAGE, SCFH
16	20	20	No Repairs	107	107
17	NA, PRE-OP Test	113	No Repairs	26	NA, PRE-OP Test
18	NA, PRE-OP Test	94	750 SCFH, Instrument Lines and Valve Packing	227	NA, PRE-OP Test
19	NA, PRE-OP Test	102	No Repairs	114	NA, PRE-OP Test
20	95	60	No Repairs	130	172
21	771	6	No Repairs	13	778
22	X (X - Y = 37)	Y	No Repairs	35	72
23	X (X - Y = 25)	Y	No Repairs	71	96

2. The total 'As Found Minimum Path' local leak test results were greater than the 0.75 La acceptance criteria. Those leaks were repaired and the 'As Left' total local leakage was well below 0.75 La. The subsequent measured Type A leakage was greater than the acceptance criteria, repairs were required for test passage.

3. The total 'As Found Minimum Path' local leak test results were less than the 0.75 La acceptance criteria. The subsequent measured Type A leakage was greater 0.75 La, repairs were required for test passage.

4. The total 'As Found Minimum Path' local leak test results were less than the 0.75 La acceptance criteria. The subsequent measured Type A leakage was also less than 0.75 La.

The distribution of tests between these four categories is shown in Table 3 below.

TABLE 3
LISTING OF ILRTs BY CATEGORIES

CATEGORY NUMBER	NUMBER OF TESTS	PERCENT OF TOTAL
1	6	30
2	3	15
3	0	0
4	11	55

It is significant that no test fell into category 3. If the total 'As Found' local leakage was less than the 0.75 La criteria, then the additional leakage measured during the subsequent Type A test was never enough to put the total over the acceptance criteria. This in effect says that passage or failure of the Type A tests was always determined by local leak test results performed before the Type A test began. Leakage from the structure and other parts of containment detectable only by Type A testing is almost always very low and does not change much over time. The leaks found by Type A tests were usually caused by either omissions in the local leakage testing program, or leaks in non B&C tested instrument lines and manifolds. NRC Information Notice[3] No. 86-16 also mentions cases where ILRTs found deficiencies in B&C testing programs.

There were three instances where the total 'As Left' local leakages (column 3) were low and the subsequent Type A test found large leaks. Test #18 was a Pre-Op test where most of the leakage was from instrument lines not subject to local leak testing. Another case, (test #2) the leakage was from an area that was improperly locally leak tested prior to the ILRT. The third case (test #11) was a leak from a fan cooler tube, an area that is not locally leak tested. This system was depressurized during the ILRT, but during unit operation or post accident conditions it would have been maintained at greater than accident pressure. Also, the leakage would have been found prior to start-up when the system was re-pressurized.

Type A testing has definitely been useful in finding these types of problems. Accelerated schedules in response to failures due to leaks found during the Type A test seems reasonable. In contrast, 66% of the 'As Found' failures found here were due solely to high local leakages (category #1). The performance of additional type A tests in response to these failures yields no new information. A recent NRC information notice[1] states that in some cases, a high degree of containment integrity may be better achieved through improved maintenance and testing programs for containment penetration boundaries and isolation valves rather than by performing more frequent ILRTs. To implement this, after failing two consecutive ILRTs the licensee would submit a corrective action plan as an Appendix J exemption request. If approved, the licensee may implement the plan in lieu of going on an accelerated ILRT schedule.

A corrective action plan would address correction and surveillance of the specific source(s) of leakage responsible for the test's failure. The vast majority of major leaks are from valves, closures, and penetrations. Since surveillance of these areas can be performed by local leak testing alone, implementation of corrective action plans could sharply reduce the number of unnecessary ILRTs performed. If even a small fraction of the cost per test saved is applied toward the permanent fixes of recurring problem containment isolation systems, overall containment integrity would be improved.

The above concept sounds very promising, but it has not been put into practice. The NRC has never granted a complete exemption (at least none could be found by this Author) from performing a scheduled ILRT and allowing a corrective action plan in it's place. Early talks in one specific case with a Commonwealth Edison Co. plant indicated that such an exemption would be given only if the corrective action plan included mid-cycle local leak testing. Such testing would have required unit shut down during mid-cycle operation in order to perform the local leak tests included in the plan. Since this would be almost as expensive as performing an additional ILRT and contribute nothing to plant safety, the offer was rejected.

A good corrective action plan would:

1) address the root cause(s) of leakage in such a way as to prevent any recurrence.

2) insure that the unit in question has a good Type B and C testing program.

3) insure that the local leak tests performed next outage in place of the ILRT were 'As Found' tests on the problem areas.

4) not include any additional costly requirements (such as mid-cycle testing) that add nothing to safety and there-by induce the utility to reject the plan.

CONCLUSIONS

The testing of dual valve isolation systems by pressurizing from containment with the isolation valves closed duplicates Type A test conditions. Use of the resulting measured leakages is the most reliable and accurate means of correcting Type A results for prior RAs. This method would eliminate the problems associated with testing valves in the wrong direction as discussed in Reference 3. At the same time, up to approximately a 30% reduction in the over-conservatism present in the 'Minimum Path' method can be avoided.

In many cases it is not possible or practical to simultaneous pressurize both valves from containment. Using the 'Minimum Path' and the 'Maximum Path' leakages, Equation 5 can confidently be used to calculate conservative system leakrates. Similar savings in over-conservatism to those above can be realized.

The ultimate purpose of finding the 'As Found' integrated leak rate is to insure the ability of primary reactor containment to limit the total gaseous release rate to less than 75% of the maximum allowable leakage when subjected to accident pressure. The requirement to perform more frequent ILRTs in response to 'As Found' failures can help achieve the above objective only by shortening the time between leakage discoveries, and there-by decreasing total unit operation time with diminished containment integrity. For plants with good local leak testing programs, this benefit will be realized only if the leaks found were of the kind only detectable by Type A testing, since B and C tests are performed every outage anyway.

By far, the most common cause of 'As Found' ILRT failures has been shown to be leaks in locally tested areas. The current requirement to perform additional Type A tests for those cases makes little sense. In some cases, the source of the leakage is not adequately addressed and the next test fails for the same reason. If instead, a corrective action plan that addresses permanently eliminating the specific source of leakage was implemented, probably only a small fraction of the cost of accelerated Type A testing would be required. Both cost and Man-REM would be reduced while containment integrity increased.

REFERENCES

1. Nuclear Regulatory Commission; Office of Inspection and Enforcement, Containment Integrated Leak Rate Tests, IE Information Notice, No. 85-71, August 1985.

2. Shirk, R.E. and Carey, R.M., Determination Of As Found Containment Integrated Leakage Rate, Proceedings of the Second Workshop on Containment Integrity, pp. 77-86, 1984.

3. Nuclear Regulatory Commission; Office of Inspection and Enforcement, Failures to Identify Containment Leakage Due to Inadequate Local Testing of BWR Vacuum Relief System Valves, IE Information Notice, No. 86-16, March 1986.

PRESERVICE AND INSERVICE REQUIREMENTS FOR CONTAINMENT STRUCTURES-- A STATUS REPORT

Robert F. Sammataro

General Dynamics Corporation

Electric Boat Division

Groton, Connecticut, U. S. A.

ABSTRACT

Preservice and inservice requirements for Class MC containment structures are contained in Subsection IWE, "Requirements for Class MC Components of Light-Water Cooled Power Plants," of Section XI, Rules for Inservice Inspection of Nuclear Power Plant Components, of the ASME Boiler and Pressure Vessel Code. Rules for the preservice examination, inservice inspection, repair, modification, replacement and system pressure tests for Class MC (metal) containments and steel portions of Class CC (concrete) containments not backed up by concrete and their integral attachments in PWR and BWR light-water cooled nuclear power plants are included. Rules for Class CC containments are currently being developed and will be published in Subsection IWL, "Requirements for Class CC Components of Light-Water Cooled Power Plants."

First published in the Winter, 1981 Addenda to Section XI, Subsection IWE has been adopted by a number of state jurisdictions and is presently being reviewed by the Nuclear Regulatory Commission for adoption in Title 10, Part 50 of the Code of Federal Regulations (10CFR50). In the interim, ASME Nuclear Code Case N-236, "Repair and Replacement of Class MC Vessels," may be used for the preservice examination, repair welding, acceptance standards, system pressure tests, and replacements for metal containment structures.

When approved, the requirements in Subsection IWE and Subsection IWL will provide a reasonable and systematic basis for assuring the intergity of a containment vessel during its service lifetime and will require mandatory compliance by plant owners. This paper provides an overview of these requirements with emphasis on the practical considerations that should accompany user compliance.

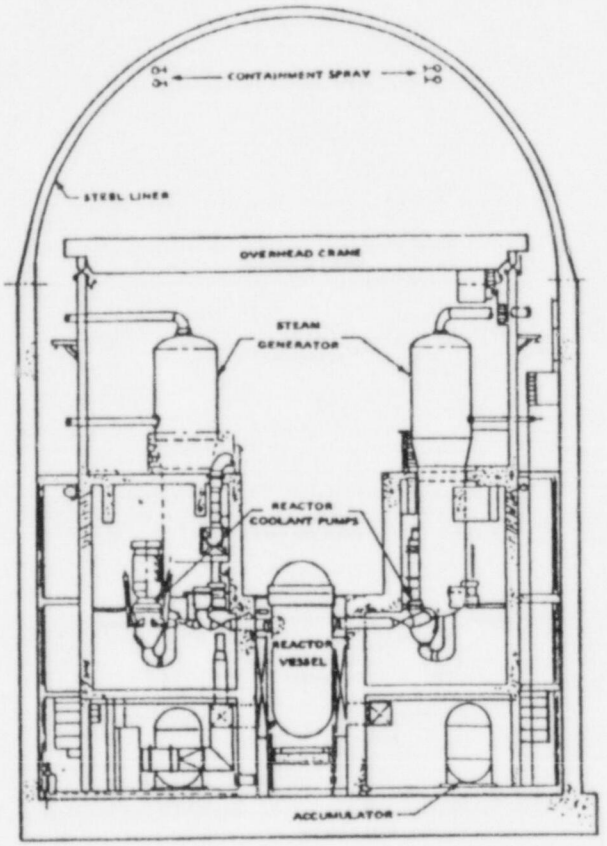
1.0 INTRODUCTION

1.1 General

The rules and requirements of Section XI, Subsection IWE, "Requirements for Class MC Components of Light-Water Cooled Power Plants," of the ASME Boiler and Pressure Vessel Code constitute a reasonable and systematic basis for assuring the continued integrity of a containment vessel during its service lifetime. Subsection IWE contains the rules and requirements for the preservice examination, inservice inspection, repair, modification, replacement and system pressure tests for Class MC (Metal Containment) pressure-retaining components and their integral attachments and steel portions of Class CC (Concrete Containment) pressure-retaining components not backed up by concrete and their integral attachments in light-water cooled nuclear power plants. The requirements are applicable to both

PWR and BWR containments as shown by the typical designs in Figures 1 and 2, respectively. Rules for concrete surfaces and other features of Class CC containment structures are presently being developed and will be published in Subsection IWL, "Requirements for Class CC Components of Light-Water Cooled Power Plants."

First published in the Winter, 1981 Addenda to Section XI of the ASME Code, Subsection IWE has been adopted by a number of state jurisdictions and is presently being reviewed by the Nuclear Regulatory Commission for adoption in Title 10, Part 50 of the Code of Federal Regulations (10CFR50). When approved, the requirements in Subsection IWE and Subsection IWL will require mandatory compliance by plant owners. In the interim, ASME Nuclear Code Case N-236, "Repair and Replacement of Class MC Vessels," may be used for preservice examination, welding, acceptance standards, system pressure tests, and replacements for metal containment structures.



TYPICAL PWR CONTAINMENT

FIGURE 1

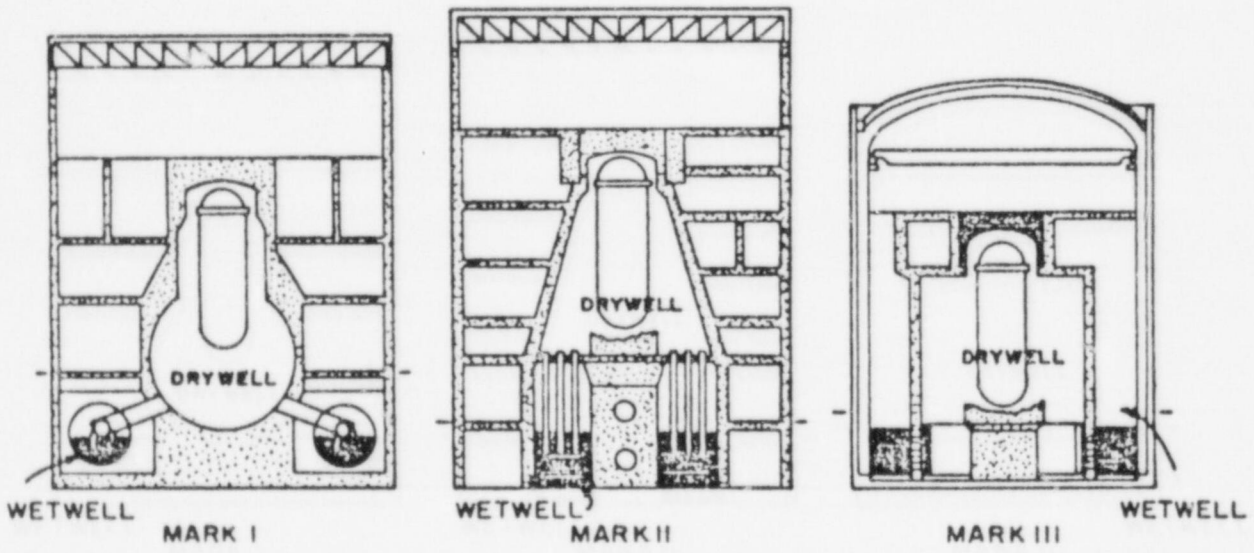
1.2 Containment Inspection Philosophy

Subsection IWE has been developed with the objective of asssuring that the critical areas of the containment--pressure-retatining welds, seals and gaskets, and pressure-retaining bolting--maintain their pressure-retaining integrity throughout the plant lifetime. To meet this objective, the preservice condition of the finished containment welds as painted or coated and the preservice condition of other pressure-retaining components must be visually examined and documented to provide a reference baseline. This baseline is then used for comparison with the exisiting condition at each inservice inspection. It is required, therefore, that the preservice

baseline records for the containment welds be restored when the existing surface treatment of the containment is altered, repaired, or replaced. Removal of paint or coatings on a wholesale basis is not required for either preservice or inservice examinations. Because of their increased sensitivity and importance, surface preservice and inservice examinations are also required for containment dissimilar metal welds. Perhaps the most misunderstood concepts for Subsection IWE are that only the containment vessel welds, not vessel surfaces, require examination and that removal of paint or coatings is not required for routine examinations of containment welds.

Subsection IWE does not require containment pressure tests other than the periodic tests specified in 10CFR50, Appendix J. This accomodation has been made within Subsection IWE to reduce the potential fatigue effects of excessive pressure testing and to recognize that the 10CFR50, Appendix J tests provide an adequate basis for assuring continued containment pressure-retaining integrity.

As for other subsections of Section XI, Subsection IWE for Class MC containment vessels has been written for new plants with considerations for older plants. Compliance with these rules is to be invoked through the regulatory process. For older plants, implementation on a plant-by-plant basis with the opportunity for justifiable waivers for individual requirements or items when granted by the Nuclear Regulatory Commission is anticipated.



TYPICAL BWR CONTAINMENTS

FIGURE 2

1.3 Interpretations

This paper represents the opinions of the author. In all cases of question, the rules and requirements that govern are those published in the edition and addenda of the ASME Boiler and Pressure Vessel Code applicable to the specific nuclear plant, system or component. Official interpretations of the ASME Code can be obtained only through the procedure established by the ASME Boiler and Pressure Vessel Committee.

2.0 SCOPE OF SUBSECTION IWE

2.1 Scope

Subsection IWE is applicable to Class MC and steel portions of Class CC pressure-retaining components and their integral attachments and to containment seals and gaskets in light-water cooled nuclear power plants. The rules in Subsection IWE do not apply to vessels, parts, and appurtenances that are outside of the boundaries of the containment vessel as defined in the Design Specification. They also do not apply to piping, pumps and valves that are part of the containment system or which penetrate or are attached to the containment vessel. These components must meet the rules of Subsection IWB or IWC of Section XI for Class 1 or Class 2 piping, pumps and valves, as applicable, as defined in the Design Specifications. Additional requirements of Section XI applicable to containment vessels as well as to other nuclear plant components are contained in Subsection IWA, "General Requirements."

2.2 Exemptions

Certain embedded or inaccessible portions of containment vessels that are within the scope of Subsection IWE may be exempted from preservice examination and inservice inspection requirements. The exemptions are limited to those portions of vessels with welds that are embedded in concrete or otherwise made inaccessible during construction of the vessel or vessel repair, modification or replacement provided (1) no openings or penetrations are embedded in the concrete, (2) all welded joints are double butt-welded and are fully radiographed and, prior to being covered, are tested for leak tightness using a gas medium test such a Halide Leak Detector Test, (3) all nozzle-to-shell welds that are not double butt-welded remain accessible for examination, and (4) the vessel is leak rate tested after completion of construction or repair to the leak rate requirements of the Design Specifications or of 10CFR50, Appendix J, as applicable.

3.0 PRESERVICE EXAMINATION

Prior to initial plant startup, containment welds, including essentially 100% of the pressure-retaining welds, must be examined using visual examination (VT) methods and must be pressure tested. Certain areas also require surface examination or other tests as defined in Table 1.

PARTS EXAMINED	EXAMINATION METHOD
Pressure-Retaining Welds in Vessels	VT-1, VT-3
Nonpressure-Retaining Welds	VT-3
Pressure-Retaining Welds in Containment Penetrations	VT-1
Pressure-Retaining Welds in Airlocks and Equipment Hatches	VT-3
Seals and Gaskets	VT-3
Integral Attachments	VT-3
Pressure-Retaining Dissimilar Metal Welds	VT-3, Surface
Pressure-Retaining Bolting	VT-1, Bolt Torque or Tension Test
All Pressure-Retaining Components	VT-2, Pressure Test

PRESERVICE EXAMINATION REQUIREMENTS

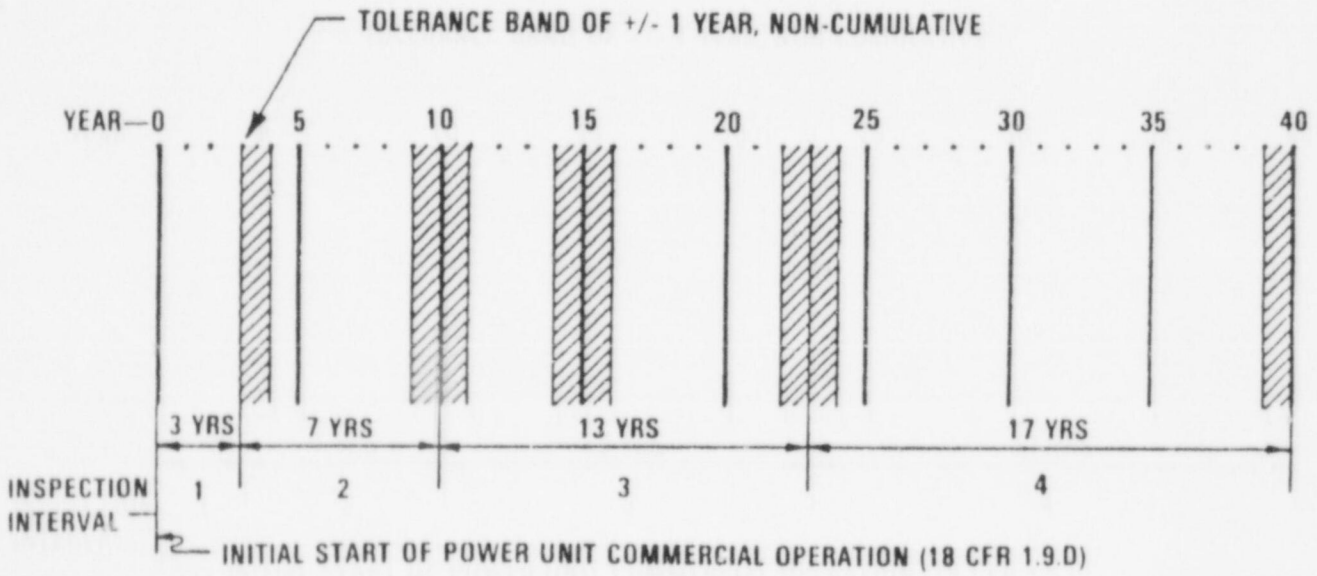
TABLE 1

Visual preservice examinations may be performed following completion of the pressure test required by the Construction Code and after applicication of paint or other protective coatings without removal of the coatings. Areas which are suspect as a result of visual examination must be cleaned by removal of paint or coatings to the base metal surface for surface examination. Exposed areas must be repaired, if required, and repainted or recoated after examination. Shop or field surface examinations performed in accordance with the Construction Code may be used in lieu of on-site preservice examinations provided the equipment and techniques are equivalent to those to be used for subsequent inservice inspections, the examination records meet Section XI requirements, and the examinations are performed after the pressure test required by the Construction Code has been completed.

4.0 INSERVICE EXAMINATIONS

4.1 Inspection Interval

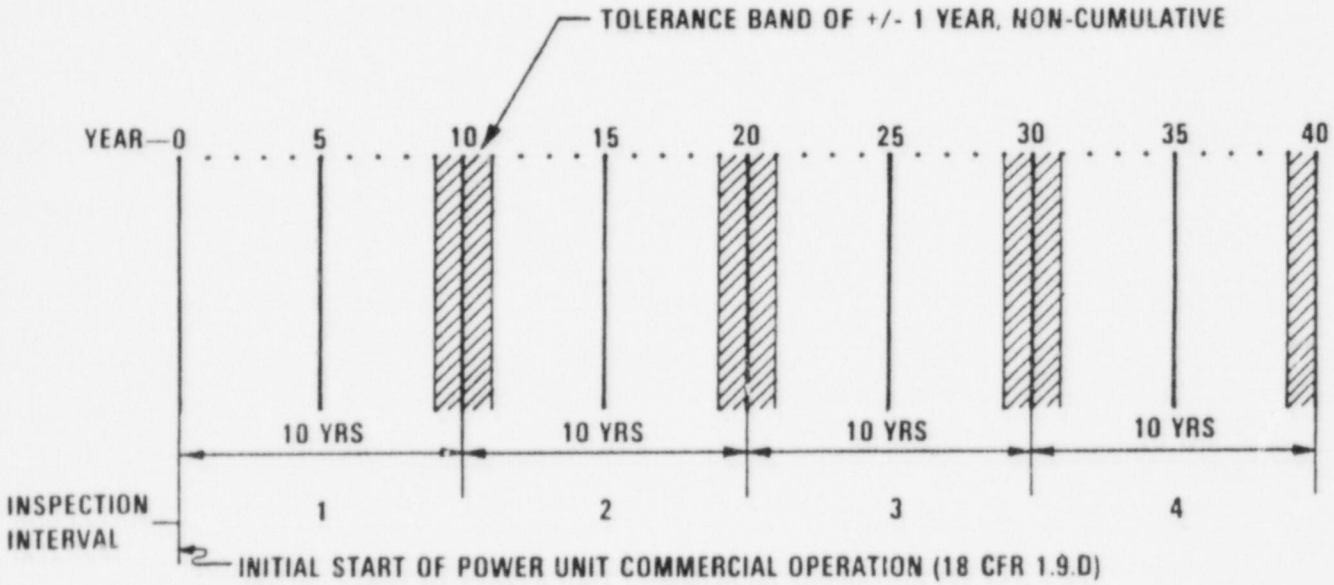
Containment vessel welds, pressure-retaining bolting, and seals and gaskets must be inspected on a scheduled basis during the normal 40 year plant lifetime. The inspections may be performed to either Inspection Program A or Inspection Program B as shown in Figures 3 and 4, respectively. Each inspection interval may be decreased or extended (but not cumulatively) by as much as one year except that the first interval for Program A may not be decreased. For power units that are out of service for 6 months or more, the inspection interval may be extended for a period equal to the outage and the original pattern of intervals extended accordingly.



INSPECTION PROGRAM A

FIGURE 3

A minimum of 25% and a maximum of 33-1/3% of the examinations must be completed in the first one-third of the inspection interval, a minimum of 50% and a maximum of 66-2/3% of the examinations must be completed in the second one-third of the inspection interval, and all examinations must be completed by the end of the interval. Examination of seals and gaskets and pressure tests may not be deferred to the end of the inspection interval. Other examinations may be deferred until the end of the interval.



INSPECTION PROGRAM B

FIGURE 4

4.2 Examination Requirements

Examination requirements for inservice inspection are the same as those for preservice examination as shown Table 1. The extent and frequency of the examinations within each inspection interval are shown in Table 2.

5.0 ACCEPTANCE REQUIREMENTS

5.1 Preservice Examination

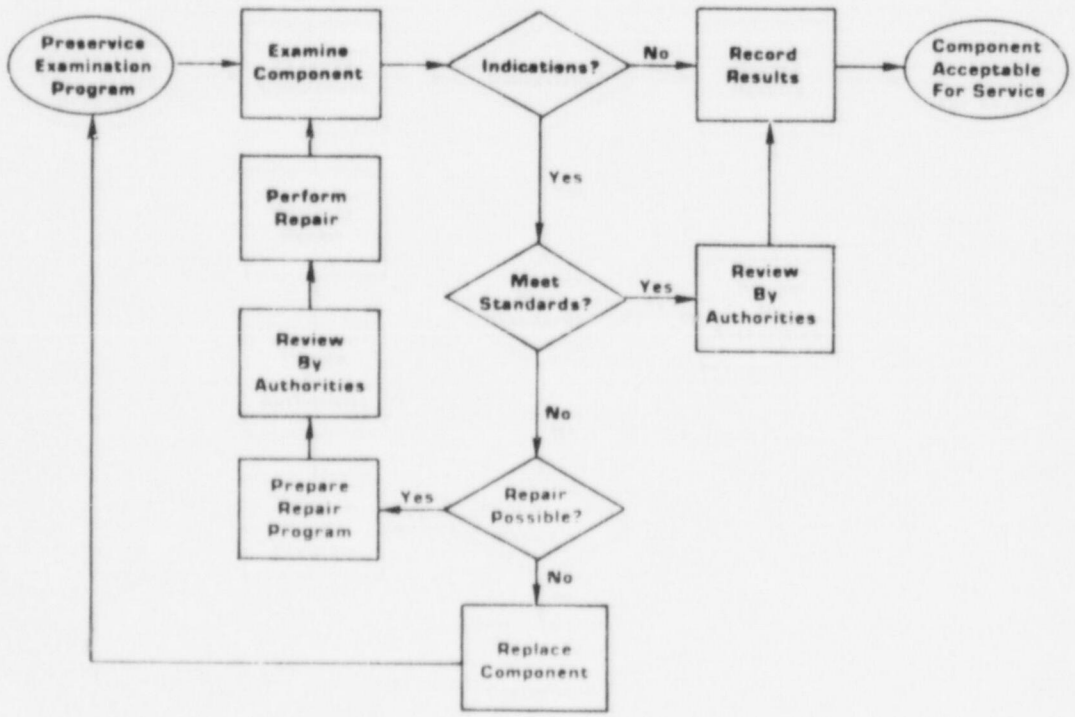
Components accepted for service as a result of a preservice examination shall either (1) have no indications from visual or surface examination that exceed the Acceptance Standards or (2) be repaired or replaced to the extent necessary to meet the Acceptance Standards prior to placement of the component into service. Visual examinations that detect surface indications must be supplemented by either surface or volumetric methods. All indications in components accepted for service that meet the Acceptance Standards shall be documented by the Owner.

Evaluation of the examination results is subject to review by the enforcement authority having jurisdiction at the plant site. Figure 5 is a flow chart that identifies the basis for acceptability of a component for service based on preservice examination requirements.

PARTS EXAMINED	EXTENT AND FREQUENCY OF EXAMINATION FOR EACH INSPECTION INTERVAL
Pressure-Retaining Welds in Vessels	25% of each Weld
Nonpressure-Retaining Welds	25% of the Total Number of Welds
Pressure-Retaining Welds in Containment Penetrations	25% of Each Weld
Pressure-Retaining Welds in Airlocks and Equipment Hatches	25% of Each Weld
Seals and Gaskets	100% of Each Item
Integral Attachments	25% of Each Weld
Pressure-Retaining Dissimilar Metal Welds	50% of Each Weld
Pressure-Retaining Bolting	100% of Bolts (Visual)
Pressure-Retaining Bolting	100 % of Each Bolted Connection (Bolt Torque or Tension Test)

EXTENT AND FREQUENCY OF INSERVICE EXAMINATIONS

TABLE 2

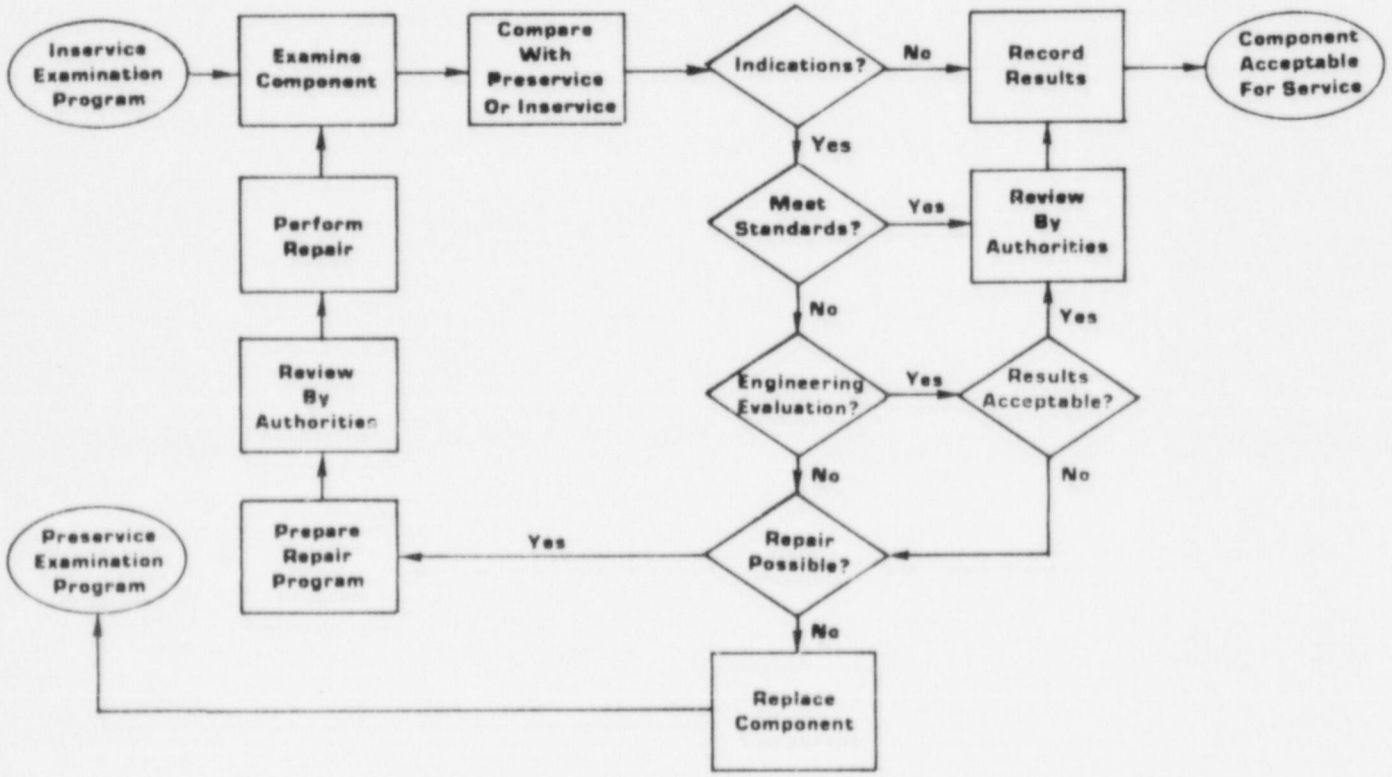


PRESERVICE EXAMINATION FLOW CHART

FIGURE 5

5.2 Inservice Inspection

Components accepted for continued service as a result of inservice examinations shall either (1) have no indications from visual or surface examination that exceed the Acceptance Standards, (2) be repaired or replaced to the extent necessary to meet the Acceptance Standards, or (3) be found acceptable for continued service by an engineering evaluation. Results of inservice examinations shall be compared with recorded results of the preservice examination and prior inservice examinations to determine acceptability for continued service. Visual examinations that detect surface indications must be supplemented by either surface or volumetric methods. When an engineering evaluation is performed, it must demonstrate that the margins required by the Design Specifications and Construction Code are maintained and is subject to review by the regulatory and enforcement authorities at the plant site. Figure 6 is a flow chart that identifies the basis for acceptability of a component for service based on inservice examination requirements.



INSERVICE EXAMINATION FLOW CHART

FIGURE 6

5.3 Acceptance Standards

Acceptance Standards for preservice and inservice examination are summarized as follows:

- Visual Examination on Painted or Coated Areas. The inspected area shall be examined for evidence of flaking, blistering, peeling, discoloration, and other signs of distress. Areas that are suspect shall be cleaned by removal of the paint or coating to the base metal or weld surface for verification by supplemental surface examination.

- Visual Examination on Uncoated Areas: The inspected area shall be examined for evidence of cracking, discoloration, wear, pitting, excessive corrosion, arc strikes, gouges, surface discontinuities, dents and other signs of surface irregularities., Areas that are suspect shall be cleaned to the base metal or weld surface for verification by supplemental surface examination.

- Visual Examination of Seals and Gaskets: The items shall be examined for wear, damage, erosion, tear, surface cracks or other defects which may violate the leak tight integrity. Defective items shall be repaired or replaced.

- Visual Examination of Bolting: The bolting materials shall be examined in accordance with the material specification for defects which may cause the bolted connection to violate either the leak tight or structural integrity. Defective items shall be replaced.

- Surface Examination: The acceptance standards applicable to Class 1 components in Section XI, Subsection IWB apply within the examination boundaries established in Subsection IWE.

- Bolt Torque or Tension Test: Either bolt torque or bolt tension shall be within the limits specified for the original design. If no limits have been specified , acceptable limits shall be determined and utilized thereafter.

- Visual Examination For Pressure Tests: For components that have been repaired or replaced, the visual examination may be limited to the repaired or replaced portion of the system but shall include any connection to the existing system.

- Leakage During Pressure Tests: Leakage shall not exceed the applicable requirements of 10CFR50, Appendix J. If the leakage requirement cannot be satisfied, corrective action shall be taken and leakage testing shall be reperformed until the leakage requirement is satisfied prior to returning the component to service.

6.0 REPAIR PROCEDURES

6.1 Repairs By Welding

Repairs by welding are permissible for containment vessels. Such repairs shall be performed and examined in accordance with the Owner's Design Specification and the original Construction Code. Later editions of the Construction Code or of Section III, either in their entirety or portions thereof, and Code Cases may be used. Preparation for repairs by welding may include either mechanical or thermal and mechanical methods. Thermal removal processes for P-1 materials, when used, may include preheating, carbon air arc gouging, plasma arc cutting, oxyfuel cutting, and other thermal processes. The preservice examination must be repeated after the repair is completed and, depending on the nature and extent of the repair, pressure tests may be required before the containment vessel is restored to service.

6.2 Alternative Welding Techniques

Two alternative welding techniques are identified in Subsection IWE and may be used when the requirements of the original Construction Code or of Section III are impractical.

- Butterbead-Temperbead Repair Technique: The butterbead- temperbead repair technique may be used when the size or configuration of the repair leads to highly restrained weld joints and when factors such as water backing make preheat and postweld heat treatment impractical. When used, the following restrictions apply:

- Limited to P-No. 1 Group 1 and P-No. 1 Group 2 pressure boundary materials.

- The Shielded Metal Arc Welding (SMAW) Process must be used.

- Specific controls apply to the use of low hydrogen electrodes.

- Controlled peening of welds is permitted with certain limitations.

- The welding procedures and welders must be qualified in accordance with Section XI and the additional requirements of Section III except that a Production Test that simulates the repair is required and specific requirements for Procedure Qualification and Performance Qualification in accordance with Subsection IWE are required.

- Examination of the completed weld must be by visual examination (VT-1) and by a magnetic particle method not less than 48 hours after the completed repair has reached ambient temperature. The acceptance criteria of Section III, Subsection NE must be met.

- Halfbead Repair Technique: The halfbead repair technique may also be used as an alternative to welding to requirements of the original Construction Code or of Section III. When used, the requirements are the same as those in Section XI, Subsection IWB for Class 1 components.

7.0 REPLACEMENTS

For installation of replacements not requiring welding, mechanical joints must meet the requirements of the original Design Specification or meet the requirements of Section III, Subsection NE for mechanical joints and penetration assemblies. For installation of replacements requiring bolted connections, the bolted connections must meet the requirements of the original Design Specification or meet the requirements of Section III, Appendix E, Bolted Connections. Requirements for the installation and examination of replacements requiring welding are the same as those for repairs by welding. Materials for replacements must comply with the requirements to which the original component or part was constructed or comply with the requirements of Section III, Subsection NE for materials.

8.0 SYSTEM PRESSURE TESTS

8.1 Pressure Test Requirements

Repair, modification or replacement of the pressure-retaining boundary of Class MC components require a Type A, Type B, or Type C pneumatic leakage test as prescribed in Title 10, Part 50 of the Code of Federal Regulations, Appendix J, Paragraph IV.A (10CFR50, J.IV.A).

- Type A Tests: "Type A Tests" means those tests intended to measure the primary reactor containment overall integrated leakage rate (1) after the containment has been completed and is ready for operation and (2) at periodic intervals thereafter.

- Type B Tests: "Type B Tests" means tests intended to detect local leaks and to measure leakage across each pressure-containing or leakage-limiting boundary for primary reactor containment penetrations.

- Type C Tests: "Type C Tests" means tests intended to measure containment isolation valve

leakage rates.

8.2 Examinations and Corrective Action

Visual examination, VT-2, is required after repair, modification or replacement and may be limited to the area of the repair, modification or replacement including any connection made to the existing system. If the applicable leakage test requirements of 10CFR50, J.IV.A cannot be satisfied, corrective action must be taken and leakage testing must be reperformed until the leakage requirement is satisfied prior to returning the component to service.

8.3 Deferral of Leakage Tests

Leakage tests following minor repairs or modifications to the pressure retaining boundary may be deferred until the next scheduled leakage test provided nondestructive examination is performed in accordance with the approved repair program. Such minor repairs or modifications are:

- Welds of attachments to the surface of the pressure-retaining boundary.
- Repair cavities, the depth of which does not penetrate the required design wall thickness by more than 10%.
- Welds attaching peneterations that are NPS 1 or smaller.

9.0 CONCRETE CONTAINMENTS

Section XI, Subsection IWE of the ASME Boiler and Pressure Vessel Code as first published in the Winter, 1981 Addenda and updated through the Winter, 1985 Addenda applies to steel portions of Class CC concrete containments not backed up by concrete. Consequently, the rules and requirements for Class MC containments as discussed in this paper are applicable.

Two actions by the Subgroup on Containment of the Section XI Subcommittee on Nuclear Inservice Inspection are currently in process to address requirements for other portions of Class CC containment vessels. First, the present Subsection IWE requirements, with only minor revisions, are being extended to apply to the metallic shell and penetration liners for Class CC containments. When the revision is published in the Winter, 1986 Section XI Code Addenda, the current rules will essentially be extended to apply to Class MC as well as the metallic shell and pentration liners of Class CC containments.

Rules for the concrete surfaces and other features of Class CC concrete containments are being prepared by the Section XI Working Group on Concrete Pressure Components and the Subgroup on Containment. It is expected that these requirements will be published as a new Subsection IWL to Section XI in a future Addenda. The rules will include requirements for the preservice examination, inservice inspection, repair, replacement, modification and pressure tests for concrete surfaces. Also to be addressed are requirements for unbonded post-tensioning systems, bonded post-tensioning systems, tendons and anchorages.

10.0 CODE CASE N-236: "REPAIR AND REPLACEMENT OF CLASS MC VESSELS"

10.1 Status and Applicability

Nuclear Code Case N-236, "Repair and Replacement of Class MC Vessels," Section XI, Division 1, was first issued on January 28, 1979 to provide interim requirements for the repair and

replacement of Class MC containment vessels. The Case was reaffirmed in 1982 and 1984 and is applicable for Section XI editions of the Code beginning with the 1974 edition, through the 1980 edition, up to and including the Winter, 1981 Addenda. A revision to the Code Case was approved by the ASME Boiler and Pressure Vessel Committee in late 1985. This revision was to show requirements for repairs by welding that are identical to those contained in Subsection IWE for use until Subsection IWE is formally approved by the U.S. Nuclear Regulatory Commission.

Code Case N-236 is addressed in USNRC Regulatory Guide 1.147, Inservice Code Case Acceptability, ASME Section XI, Division 1. The Regulatory Guide states that the Code Case is acceptable subject to certain minor conditions and clarifications.

10.2 Requirements

Code Case N-236 applies to the repair and replacement of Class MC containment vessels and to steel portions of Class CC containment vesels not backed up by concrete. The repairs and replacements must comply with the rules of Section XI, Subsection IWB for Class 1 components except as modified by the rules of the Code Case for preservice examination, repair welding, acceptance standards for flaw indications, and replacements.

11.0 APPROVAL STATUS

Rules in Section XI, Rules for Inspection of Nuclear Power Plant Components, of the ASME Boiler and Pressure Vessel Code must be approved by the U. S. Nuclear Regulatory Commission before compliance is mandated in the United States. Subsection IWE, "Requirements for Class MC Components of Light-Water Cooled Power Plants," was approved and issued by the American Society of Mechanical Engineers in the Winter, 1981 Addenda to Section XI. Although this Addenda and subsequent Addenda of Section XI, including Subsection IWE requirements, have been approved by a number of state jurisdictions, Subsection IWE has not been adopted by the U. S. Nuclear Regulatory Commission as of May, 1986.

Amendments to 10CFR50.55a define the USNRC approval of Codes and Standards for the Domestic Licensing of Production and Utilization Facilities. Current (May, 1986) requirements published in 10CFR50.55a pertaining to Section XI of the ASME Boiler and Pressure Vessel Code do not address Subsection IWE or requirements for Class MC components. Amendments to 10CFR50.55a effective on March 9, 1983 incorporated by reference the Winter, 1981 Addenda of Section XI. However, this amendment specifically excluded approval of Subsection IWE. The statement issued by the USNRC is as follows:

> "Subsection IWE, 'Requirements for Class MC Components of Light-Water Cooled Power Plants, was added to Section XI by these addenda. However, 10CFR Sec. 50.55a presently only incorporates those portions of Section XI that adddress the ISI requirements for Class 1, 2, and 3 components and their supports. The regulation does not currently address the ISI of containments. Since this amendment is only intended to update current regulatory requirements to include the latest Code addenda, the requirements for Subsection IWE are not imposed upon Commission licenses by this amendment. The applicability of Subsection IWE will be considered separately."

The regulatory process for approval of new requirements is lengthy and necessitates the issue of the document for public review and comment and the opportunity for public hearings. Consequently, the USNRC has stated that approval action on Subsection IWE may be withheld until the rules for Class CC concrete containments are approved and published by the ASME such that the approval process for the rules for both Class MC and Class CC containments may proceed simultaneously.

12.0 PRACTICAL CONSIDERATIONS

Good planning and preparation are essential to implement the rules and requirements of Subsection IWE for containment vessels in an efficient and effective manner. During vessel design, design for ease and accessibility for inspection is essential. Good planning is essential during the design and prior to the preservice examination to locate welds, identify welds, and mark welds to facilitate both the preservice and future inservice inspections. Early identification of the examination methods and tools is essential as well as the need to prepare and maintain a thorough, comprehensive preservice inspection plan and records.

Development of a comprehensive, well planned inservice inspection program, sequenced with the plant outage schedule, is essential to assure that all inservice requirements are met without interference with normal plant operation. And, a thorough knowledge of the ASME Code and related requirements is essential. With good planning and preparation, the requirements can be efficiently integrated into existing inservice inspection programs with minimum difficulty.

Finally, feedback to the ASME Code committees responsible for development of the Code requirements can assure that future revisions will reflect the needs of the utilities and others who must implement these requirements.

13.0 IN COURSE OF PREPARATION.....

The requirements of Subsection IWE for Class MC containments and Subsection IWL for Class CC containments are continually being revised, updated and expanded by the ASME Code committees. Some of the items presently "In Course of Preparation" for Subsection IWE and Subsection IWL are as follows:

- Surface Examination Through Coatings (IWE)
- Removal, Repair and Replacement of Coatings (IWE)
- Requirements for Inaccessible Welds (IWE, IWL)
- Restoration of Preservice Baseline After Alteration of Surface Condition (IWE)
- Examination of Insulated Components (IWE)
- Examination of MC/CC Interface (IWE/IWL)
- Authorized Nuclear Inspector Requirements for Concrete (IWL)
- Visual Examination Standard for Concrete (IWL)
- Repair and Replacement of Concrete (IWL).

14.0 SUMMARY

The rules and requirements of Subsection IWE, "Requirements for Class MC Components of Nuclear Power Plant Components," of Section XI of the ASME Boiler and Pressure Vessel Code constitute a reasonable and systematic basis for assuring the continued integrity of a containment vessel during its service lifetime. The rules issued to date address requirements for the preservice examination, inservice inspection, repair, modification, replacement and system pressure tests

for Class MC containment vessels and steel portions or Class CC containment vessels not backed up by concrete and their integral attachments in PWR and BWR light-water cooled nuclear power plants. Rules for metallic shell and penetration liners for Class CC containment vessels and for other features of Class CC containment structures are currently being developed.

At present, Subsection IWE has been adopted by a number of state jurisdictions and is presently being reviewed for approval by the U.S. Nuclear Regulatory Commission. When approved, the requirements in Subsection IWE will require mandatory compliance by nuclear plant owners. In the interim, ASME Nuclear Code Case N-236, "Repair and Replacement of Class MC Vessels," provides an acceptable basis for preservice examination, welding, acceptance standards, system pressure test, and replacements for Class MC metal containment vessels.

ACKNOWLEDGEMENT

Th author wishes to express appreciation to past and present colleagues on the Subcommittee on Nuclear Inservice Inspection, Subgroup on Containment, and Working Group on Concrete Pressure Components for their efforts in developing and maintaining the rules and requirements in Subsection IWE and Subsection IWL of Section XI of the ASME Boiler and Pressure Vessel Code.

REVIEW OF CONTAINMENT EXAMINATION AND TESTING REQUIREMENTS

Jeffrey F. Cook
Idaho National Engineering Laboratory
EG&G Idaho, Incorporated
Idaho Falls, Idaho, U.S.A.

ABSTRACT

At the present time, the ASME Code Section XI, Division 1, Subsection IWE, requirements for metal containment inservice inspection are not specifically referenced in the Nuclear Regulatory Commission (NRC) Regulations. A review of Subsection IWE is being performed by the Idaho National Engineering Laboratory (INEL) to assist the NRC in evaluating the acceptability of incorporating this Subsection into the NRC Regulations. The impact of Subsection IWE requirement changes compared with the present containment inservice inspection (ISI) requirements contained in Appendix J of the NRC Regulations is discussed. In addition, INEL recommendations for improvements/changes in containment ISI requirements are presented for consideration by personnel of code/standards committees and the NRC staff. For example, quantification of requirements for leak testing of localized areas in pressure boundaries is needed. Paragraph IWE-1221(b) calls out "testing for leak tightness using a gas medium test such as a Halide Detector test." The sensitivity required and acceptance criteria for this test should be specified. Both a bubble solution test and a helium mass spectrometer test are "gas medium tests", but their sensitivities could vary by a factor of 10^6. Development of training programs and qualification requirements for personnel who conduct the Appendix J containment leakage tests are also recommended.

INTRODUCTION

Subsection IWE to Section XI, Division 1 of the ASME Boiler and Pressure Vessel Code, was first published in the Winter 1981 Addenda to Section XI to provide rules for inservice inspection of MC (metal containment) structures. The NRC has not yet specifically referenced this Subsection in the Code of Federal Regulations; the INEL is assisting the NRC in evaluating the suitability of incorporating this Subsection into the NRC Regulations. Part of this review includes preparing the Regulatory Analysis which must accompany all proposed rules. As background for this Regulatory Analysis, the present MC examination practices are being compared with the IWE examinations, and input from utilities on the impact of implementing the IWE rules is being evaluated. Other documents covering containment examinations and testing were also reviewed and recommendations for improving present rules are being developed. Most domestic plants have concrete containment (CC) structures (about 90 CCs versus about 50 MCs). Since Section XI Code rules for inservice inspection of

concrete containments are now being prepared (Subsection IWL), these plants are not included in this study. This paper presents and discusses the findings to date from this review task.

IMPACT OF IWE IMPLEMENTATION

In determining the impact of implementing IWE rules, the present containment examination practices were compared with the Subsection IWE examination requirements. More information on the impact of IWE implementation is being obtained from selected utility contacts and will be available later for use in preparing the Regulatory Analysis.

In studying the impact of IWE implementation, it is first necessary to review present requirements. Appendix J of the NRC Regulations states the following:

> "V. Inspection and Reporting of Tests
>
> A. Containment inspection. A general inspection of the accessible interior and exterior surfaces of the containment structures and components shall be performed prior to any Type A test to uncover any evidence of structural deterioration which may affect either the containment structural integrity or leak-tightness. If there is evidence of structural deterioration, Type A tests shall not be performed until corrective action is taken in accordance with repair procedures, nondestructive examinations, and tests as specified in the applicable code specified in # 50.55a at the commencement of repair work. Such structural deterioration and corrective actions taken shall be reported as part of the test report submitted in accordance with V.B."

Since Appendix J indirectly references Subsection IWE repair/replacement provisions in the last part of the above quotation, they are not included here.

Subsection IWE, Table IWE-2500-1, Examination Category E-P, All Pressure Retaining Components, references and clarifies the Appendix J examination requirements. A VT-3* visual test of the pressure retaining boundary and a VT-2 visual test for leakage are specified. If leak channels are used, they are required to be unplugged and tested during the Appendix J, Type A, containment integrated leakage test or tested independently by a Type B local leakage test. A requirement of IWE, beyond Appendix J, is that the VT-2 and VT-3 visual examination personnel are required to be qualified to ANSI N45.2.6. Appendix J does not specify personnel qualification requirements.

---

*Section XI visual examination categories, as published in the Winter 1985 Addenda, are given in Appendix A to this report.

Most of the examinations specified in Subsection IWE, Table IWE-2500-1 are VT-3 visual examinations. If these examinations were documented during the Examination Category E-P VT-3 examination of the pressure retaining boundary, these examinations would meet most of the requirements of the other examination categories in Table IWE-2500-1. However, it would be necessary to verify that all welds accessible for examination met IWE requirements. Subsection IWE exempts inaccessible welds from examination provided fabrication requirements specified in IWE 1221 are met. For older plants not designed to Section III of the ASME Code, these requirements may not be met. In these cases, it would be necessary for utilities to request relief from the NRC for specific welds not meeting IWE accessibility requirements.

Another potential problem in older plants implementing Subsection IWE as part of inservice inspection plan updates is that these plants will not have the containment preservice examination results as required by IWE-2200. Instead of sampling sections of welds as is specified in Table IWE-2500-1, IWE-2200, Preservice Examination, states:

> "In addition, these preservice examinations shall be extended to include essentially 100% of the pressure retaining welds."

If the 100% examinations are required after plant operation, the impact will be greater than performing the examinations on a new plant prior to operation. The Section XI Code is not clear on how to handle preservice examination requirements implemented after plant operation.

Additional items from Subsection IWE not covered by VT-3 examinations are listed below:

(1) In Examination Category E-A, Pressure Retaining Welds in Vessels, items E1.20 (Category C Flange Welds), E1.30 (Category D Nozzle-to Shell Welds), and E1.53 (Vent System Welds Other Than Longitudinal or Circumferential Welds) all require the more stringent VT-1 visual examination.

(2) In Examination Category E-B, Pressure Retaining Welds in Containment Penetrations, item E3.10 (Containment Penetration Weld) requires VT-1 visual examination.

(3) Examination Category E-F, Pressure Retaining Dissimilar Metal Welds, requires a surface examination (magnetic particle or liquid penetrant).

(4) Examination Category E-G, Pressure Retaining Bolting, requires both a VT-1 examination and a bolt torque or tension test.

RECOMMENDED CONTAINMENT ISI REQUIREMENT CHANGES

The following recommendations are presented for for consideration by personnel of code/standard committees and the NRC staff:

(1) A widely used training program[1] prepared for nuclear power plant visual examiners does not cover the tests using gaseous test mediums that are employed for IWE or Appendix J requirements. The majority of Section XI VT-2 examinations are conducted for detection of water leakage during system pressure tests and the training reflects this. Additional training programs should therefore be developed to cover the containment leak tests.

(2) At present, neither Appendix J nor either of the ANS standards[2,3] covering containment leak testing have any personnel qualification requirements. In light of the technical complexity of setting up, conducting, and interpreting the containment leakage tests, personnel qualification requirements, such as certification to SNT-TC-1A[4], should be implemented. The containment integrated leak test should be controlled by a certified Level III Examiner.

(3) One of the conditions for exempting an inaccessible weld from examination is stated in IWE-1221(b) as: "all welded joints that are inaccessible for examination . . ., prior to being covered, are tested for leak tightness using a gas medium test, such as Halide Leak Detector Test." Specifying "leak tightness" with no acceptance criterion makes selection of the test equipment and calibration totally arbitrary. An acceptance criterion should be specified which is compatible with the Appendix J, Type B test requirements. Article 10 of Section V of the ASME Code contains rules for quantification of halogen leak detector tests. Further guidance for leak testing is contained in References 5 and 6.

(4) There is a possible conflict in ASME Section XI Code requirements in the the IWE item E6.10, Integral Attachment Welds, and the IWF support examinations. The support, except for the end attached to the containment, is covered by IWF examinations. Significant savings would result if these IWE examinations were performed and documented with the IWF support examinations; this would eliminate the need for separate examinations and records. A Code Case will be considered to resolve this potential problem.

(5) Some inaccessible welds may be accessible for indirect visual examinations using remote viewing (e.g. borescope) via leak chase channels. If this remote testing were substituted for direct visual examinations, the need for requesting relief from the NRC would be reduced.

ACKNOWLEDGMENT

Work supported by the U. S. Nuclear Regulatory Commission, Office of Research, under DOE Contract No. DE-AC07-76ID01570.

REFERENCES

1. Visual Examination Technology Training Manuals, EPRI NDE Center, 1984.

2. ANSI N45.4-1972, American National Standard Leakage-Rate Testing of Containment Structures for Nuclear Reactors.

3. ANSI/ANS-56.8-1981, Containment System Leakage Testing Requirements.

4. Recommended Practice No. SNT-TC-1A, American Society for Nondestructive Testing, 1984.

5. ASME Code Section V Standard SE-432, "Standard Recommended Practice for the Selection of a Leak Testing Method", identical with ASTM E 432-71 (1981).

6. ASME Code Section V Standard SE-479, "Recommended Guide for Preparation of a Leak Testing Specification", identical with ASTM E 479-73 (1980).

APPENDIX A
ASME CODE SECTION XI VISUAL EXAMINATION DESCRIPTIONS

IWA-2210 VISUAL EXAMINATIONS

IWA-2211 Visual Examination VT-1

A. The VT-1 visual examination shall be conducted to determine the condition of the part, component, or surface examined, including such conditions as cracks, wear, corrosion, erosion, or physical damage on the surfaces of the part or components.

B. Direct VT-1 visual examination may be conducted when access is sufficient to place the eye within 24 inches of the surface to be examined ad at an angle not less than 30 degrees to the surface. Mirrors may be used to improve the angle of vision. Lighting, natural or artificial, shall be sufficient to resolve a 1/32 in. black line on an 18% neutral gray card.

C. Remote VT-1 visual examination may be substituted for direct examination. Remote examination may use aids, such as telescopes, borescopes, fiber optics, cameras, or other suitable instruments, provided such systems have a resolution capability at least equivalent to that attainable by direct visual examination.

IWA-2212 Visual Examination VT-2

A. The VT-2 visual examination shall be conducted to locate evidence of leakage from pressure retaining components, or abnormal leakage from components with or without leakage collection systems as required during the conduct of system pressure or functional test.

B. The VT-2 visual examination shall be conducted in accordance with IWA-5240.

IWA-2213 Visual Examination VT-3

A. The VT-3 visual examination shall be conducted to determine the general mechanical and structural condition of components and their supports, such as the verification of clearances, setting, physical displacements, loose or missing parts, debris, corrosion, wear, erosion, or the loss of integrity at bolted or welded connections.

B. The VT-3 examination shall include examinations for conditions that could affect operability or functional adequacy of snubbers, and constant load and spring type supports.

C. For component support and component interiors, the visual examination may be performed remotely with or without optical aids to verify the structural integrity of the component.

PENDING REVISIONS TO ANS 56.8-81 "CONTAINMENT SYSTEMS LEAKAGE TESTING REQUIREMENTS"

Ted M. Brown
Wiss, Janney, Elstner Associates, Inc.

ABSTRACT

The U. S. Nuclear Regulatory Commission is currently processing a revision to Appendix J of Part 50, Title 10 of the Code of Federal Regulations. The revised Appendix J will not reference any ANSI standard. Processed concurrently with the revised Appendix J is a draft Regulatory Guide which does endorse ANS Standard 56.8. The draft Regulatory Guide currently takes many exceptions to the Standard. Many of the exceptions are changes the Working Group had in process and the exceptions are to bring the draft Regulatory Guide in line with the future Standard. The Working Group has completed their revisions to the Standard and its appendices. These revisions have been submitted to the Nuclear Power Plants Standards Committee (NUPPSCO). The NUPPSCO comments have recently been addressed by the Working Group and the Working Group response has been sent to the NUPPSCO commentators. This paper will discuss the revisions made to the Standard, the significance of the revisions and future tasks or Standard revisions which the ANS 56.8 Working Group may address.

1.0 INTRODUCTION

ANS 56.8 was first published in 1981 and is still effective today. In its present form, there are numerous typographical errors and inconsistencies. These are to be corrected in this Standard by a revision which is currently in process. Also in this Standard, the wording has allowed the averaging of temperatures and dew points by assigning a volume fraction to each sensor and then arithmetically averaging the results. This approach was chosen to simplify calculations. An intervener has challenged the validity of averaging the dry-bulb temperatures in this fashion.

Considering the computing capacity of today's portable computers, the Working Group has elected to revise the method of calculating average dry-bulb temperature and vapor pressure using a more academically correct method. Pertinent changes to the standard are contained in this paper. Final comments from the Nuclear Power Plant Standards Committee (NUPPSCO) should have been received and addressed by the Working Group at the time this paper is presented orally.

2.0 REVISIONS TO THE STANDARD

The foreward has been rewritten to reflect the current status of this Standard.

2.1 Chapter 1 INTRODUCTION remains unchanged.

2.2 DEFINITIONS

The following definitions have been added, deleted, or changed, to be in line with the rest of the Standard:

* Add **containment atmospheric volume weighed absolute temperature.** The temperature derived from weighing the calculated volume each sensor represents in absolute degrees.

* Delete definition of **containment isolation system functional test.** This test is not a requisite of this Standard.

* Change **leakage design basis accident (LDBA).** The accident which results in the maximum containment internal peak pressure that also results in fission product release to the containment atmosphere.

The reason is that a steam pipe rupture in a PWR could result in a higher internal containment pressure without significant radiological consequences.

* Add **minimum pathway leakage rate.** The minimum leakage rate that can be attributed to a leakage path (e.g., the smallest leakage of two valves in a series).

* Change **sensitivity.** The capacity of a measurement system to respond to changes in the measured perimeter.

* Add definitions of **should, shall, may,** in line with ANS requirements.

* Delete **definition of weighed average (air or dew point).**

2.3 LEAKAGE TESTING REQUIREMENTS

3.2.1.2 **Preoperational Tests.** The preoperational Type A test shall follow the preoperational structural integrity test. Type B and Type C test leakage not accounted for in the Type A test shall be added to UCL to estimate the overall integrated leakage rate. The leakages shall be based on minimum pathway leakage and shall include instrumentation system error.

3.2.1.3 **Periodic Tests.** Type B and C tests should be completed prior to the Type A test. Type B and C leakages not accounted for in the Type A test shall be added to UCL to estimate the overall integrated leakage rate. The leakages shall be based on minimum pathway leakage and shall include instrumentation system error.

These sections have been changed to delete reference to "a containment isolation system functional test" and to add the "minimum pathway leakage" requirement.

3.2.1.7 **Pressurizing Considerations.** Pressurized components such as tanks shall be removed, or depressurized and vented, or the pressures measured prior to and after the Type A test to demonstrate lack of leakage to the containment. All possible sources of gas leakage into the containment from any system shall be isolated from any system and vented or disconnected during the Type A test. Components not designed to withstand the test pressure, such as refueling equipment or instruments should be removed or otherwise protected.

This section has been changed for clarity.

3.2.1.8 Second paragraph deleted. The statement contained in the second paragraph is not correct.

3.2.3 **Type A Test Frequency.** Periodic Type A tests shall be conducted at the first refueling shutdown but not more than 3 years subsequent to the preoperational test and at intervals not to exceed five years thereafter. If the test interval ends while primary containment integrity is not required, the test interval may be extended provided a successful Type A test is completed prior to the plant requiring containment integrity.

This change is intended to delete testing requirements when containment integrity is not required. The test frequency contained in this section is not being endorsed by NRC.

3.2.6 **Acceptance Criteria.**

(a) The UCL, plus required local leakage rate additions, shall be less than 75 percent of the maximum allowable leakage rate, L_a.

Depending on the sensitivity of the instrumentation, the stability of the containment, and the uncertainty associated with the calculated leakage rate, the duration of a Type A test might have to be extended beyond that required in 5.4 in order to achieve reasonable assurance of acceptability. The measured containment leakage rate shall be obtained by a linear regression analysis of the test data using the method of least squares. If the leakage rate exceeds the acceptance criterion, corrective action shall be taken. If, during the performances of a Type A test, excessive leakage occurs through locally testable penetrations or isolation valves to the extent that it would interfere with the satisfactory completion of the test, these leakage paths may be isolated and the Type A test continued until completion. A local leakage test shall be performed before and

after the repair of each isolated leakage path. The sum of the post repaired local leakage rates and the UCL shall be less than 75 percent of the maximum allowable leakage rate, L_a. The leakages shall be based on minimum pathway leakage and shall include instrumentation error. Local leakage rates shall not be subtracted from the Type A test results to determine the acceptability of a test. The test results shall be reported with both the pre and post repair local leakage rates, as if two Type A tests had been conducted.

I. Pre-repair test results
II. Post-repair test results

Records of the corrective action shall be documented.

(b) Verification test shall be performed as soon as possible following each Type A test by injection or removal of a quantity of air from or into the containment. Data acquisition should not be interrupted without justification from the end of the Type A test to the start of the verification test. The verification test provides a method for assuring that systematic error or bias is given adequate consideration. During the verification test, containment pressure may decrease more than 1 psi below P_{ac}. The Type A test leakage rate to be used for comparison with the verification test is that of the last valid Type A data point.

(1) for the superimposed leak rate verification test, where a calibrated leak is imposed on the existing leaks in a containment system, acceptability is demonstrated if:

$$(L_o+L_{am}-\emptyset.25\ L_a)\leq L_c\leq(L_o+L_{am}+\emptyset.25\ L_a)$$

The superimposed leak rate (L_o) shall be between 75 and 125 percent of L_a.

(2) The mass step change verification test involves the metered removal or injection of a quantity of air from or into the containment over a short time interval. No more than 25 percent of the daily allowable leakage shall be removed or injected in any one hour period. The metered mass of air and the change of mass in containment as measured by the Type A test instrumentation shall agree within 25 percent of the metered value. The formula for mass change acceptability is:

$$\left|\frac{m-(L_{am})(t)(W_1)/2400\ -\ (W_2-W_1)}{m}\right|\ \leq\ \emptyset.25$$

where:

m = metered mass change
t = verification test duration, hours
W = mass as measured by the Type A instrumentation prior to (W_1) and following (W_2) the mass change.
L_{am} = measured leakage rate, percent/day

The metered mass change (m) shall be between 75 percent and 125 percent of the daily allowable leakage.

(c) Data Rejection. In the case where the validity of certain raw data is suspect but no strong physical reason is found, then a statistical rejection technique may be applied to the containment air mass data to lend support to a judgement. The air mass data rejection technique is used based on the assumption that the enclosed air mass change is a linear function dependent only on time. A data point may be rejected if the probability of its rejection by this criterion does not exceed a preselected probability level.

If a sensor is rejected during a test, all data points for tha test shall be calculated with that sensor's input deleted. The recalculation shall be included in the test results.

If it is decided to use a data rejection technique on a set of data gathered during a leak rate test, all of the data in the test shall be compared against the rejection criteria. The criteria shall not be applied selectively to a data set. The statistical data rejection technique may be used in any test, including preoperational and verification tests. The statistical rejection of more than five percent of the containment air mass data shall not be allowed. Data rejected, including the most probable cause of the bad data, shall be documented.

Raw data on functionally dependent parameters such as temperature, pressure and humidity shall not be rejected statistically, but may be rejected and not used in the final calculation of the air mass, provided a good physical reason (such as loss of instrument power) is found for the rejection. Data rejected, including the cause for the bad data, shall be documented. For sensors rejected or suspected of being faulty, data should be recorded if possible for the duration of the test (Type A test plus verification test).

The significant changes contained in this section are the inclusion of the minimum pathway leakage requirements and the requirement that data shall be collected after the declared end of the Type A test and prior to the verification test also that the last valid data point

shall be used for comparison with the verification test. Additional changes to this item are for clarification or editorial correction.

3.3.4 **Type B and C Test Schedule**

(a) Type B and C tests shall be performed prior to initial criticality and periodically thereafter during shutdown periods or normal plant operations, but in no case shall any individual test be constructed at intervals greater than two years. If the two-year test interval ends while primary containment integrity is not required, the test interval may be extended, provided all deferred testing is successfully completed prior to the plant requiring containment integrity.

This change suspends the test frequency requirements for B and C tests when containment integrity is not required.

2.4 INSTRUMENTATION

The changes in this chapter are primarily for clarification or correction. The following sections are of some significance.

4.2 Calibration

4.2.1 Initial calibration data provided for Type A test instrumentation shall include information concerning the accuracy. Precision pressure gage shall be checked for sensitivity also.Display-readout devices shall be verified by testing no more than six months prior to use as to instrument repeatability and resolution.

4.2.2 Instrumentation used for Type A, B, or C tests shall be individually calibrated no more than six months prior to use. Type B and C test equipment may be used outside the calibration period provided it is recalibrated within two months of use and the calibrations reviewed for adequacy. Primary test instrument calibration regarding accuracy shall be traceable to the National Bureau of Standards. Type A test instrumentation accuracy shall be certified and display/readout device repeatability and resolution shall be verified by testing no more than six months prior to use. Measurement system sensitivity shall be determined from calibration and vendor data for each measured parameter.

NOTE: Measurement system sensitivity values are used in the ISG formula since it is the change in the containment air mass, not the absolute value in mass, that is used to compute leakage. Repeatability (capability of an instrument to display the same value for identidical inputs) values are not specified for the sensors but are used for instrument display/readout devices.

2.5 TYPE A TEST PROCEDURES

The significant changes in this chapter are the requirements for volume weighing the containment atmospheric dry-bulb temperatures and vapor pressures, also a section on determining volume fractions.

5.3.1 **Temperature Stabilization.**

5.3.1.1 After the containment has been pressurized to test pressure a plot shall be made of the containment atmosphere volume weighted absolute dry-bulb temperature versus time. This plot yields a fairly smooth curve which will approach a straight line. An essentially straight line plot will be achieved sooner if pressurization air inlet temperature is matched to existing contained air temperature or the containment ventilation system fans are run to expedite air mixing, or both. A sloped straight line indicates that a heat sink or heat source (due to ventilation system operation, for example) exists inside the containment. If heat sources or heat sinks are insignificant, the plotted line will become essentially horizontal. If the status of heat sinks or sources changes during the test (starting or stopping ventilation system fans or cooling water flow, for example) the slope of the line will of course change.

5.3.1.3 The criterion for temperature stabilization shall be as follows. After reaching test pressure, the latest rate of change of the containment atmosphere volume weighted absolute dry-bulb temperature, averaged over the last hour, does not deviate by more than 0.5°F/hr (0.3°C/hr) from the average rate of change of the containment atmosphere volume weighted absolute dry-bulb temperature averaged over the last four hours.

5.3.3 **Pressure.** Containment air absolute pressure versus time should also be plotted. The pressure-time curve should follow the temperature-time curve. For example, if the current containment atmosphere volume weighted absolute dry-bulb temperature and pressure are 540°R (300°K) and 75 psia (517,125N/m^2), respectively, and the containment atmosphere volume weighted absolute dry-bulb temperature drops 0.1 R (0.06°K) in one hour, the pressure should drop about 0.014 psi (97N/m^2) or more (depending on the leakage rate) during the same hour. A single point (temperature or pressure) falling off the curve may be an indication that for example a sensor malfunction occurred, a data point was recorded incorrectly, cooling water flow was suddenly started or a fan was tripped.

5.5.1 **Dry-bulb Temperature.** Area surveys within the containment structure shall be made in advance of preoperational and the initial periodic leakage rate tests to establish any areas of regional variations in temperature for the ventilation configuration planned for each test. Fans or other means of air

circulation may be used to equalize temperatures in any region where representative temperature measurements are taken and appreciable temperature variations exist. The temperature pattern revealed by the survey shall be employed in confirming the correct location of temperature sensors for leakage-rate testing.

5.5.2 **Dewpoint Temperature.** The partial pressure of water vapor in the contained air shall be measured during the course of the leakage rate test so water pressure corrections can be made to the total absolute pressure. Psychrometric readings shall be taken throughout the containment prior to conducting the preoperational and the initial periodic leakage rate tests to determine the correct location of the sensors for the ventilation configuration planned for each test.

5.5.3 **Volume Fractions.** The temperature and humidity pretest surveys shall be used to confirm assigned volume fractions. The calculated volume fractions combined with the placement of sensors will ensure that each sensor represents the assigned volume. The sum of the volume fractions is unity. If during the conduct of a test a sensor fails or is deleted, that sensor's volume fraction shall be re-assigned to other sensors on the basis of the survey results. For subsequent tests the volume fractions shall be reviewed to determine their continued validity.

This is to provide some guidance on assigning volume fractions. There has been some discussion on closing the containment at atmospheric pressure and adjusting volume fractions to measure zero leakage. The Working Group felt this would restrict access to the containment unnecessarily.

5.6(d) Containment atmosphere volume weighted absolute dry-bulb temperature.

5.7.1 **Symbols and Subscripts.**

P_v - Containment atmosphere volume weighted vapor pressure, psia (newtons/sq meter)

T - Containment atmosphere volume weighted absolute dry-bulb temperature, °R (°K)

5.7.3 **Absolute Test Method.** For each time point (t_i), the corresponding mass of contained air (W_i) is determined directly from the application of the ideal gas law:

$$W_i = \frac{144V}{R}\left[\frac{(P_i - P_{vi})}{T_i}\right]$$

P_i - total absolute pressure in the containment at the ith interval and T_i is calculated from:

$$T_i = \frac{1}{\sum_{j=1}^{M} \frac{V_{fj}}{T_j}} \quad 12$$

T_i - containment atmosphere volume weighted absolute dry-bulb temperature at the ith interval

M - Number of temperature sensors

Vf_i - Volume fraction represented by the jth sensor

T_j - absolute temperature of the jth sensor at the ith interval

An approximation of sufficient accuracy for testing purposes for calculating the containment atmosphere volume weighted vapor pressure at the ith interval (Pv_i) is obtained from Tdp_i using the steam tables or equivalent formulations.

$$Tdp_i = \sum_{j=i}^{\ell} \left(V_{t_j}\right) \left(T_{dp_j}\right)$$

Tdp_i - Summation at the ith interval

l - Number of dewpoint sensors

Tdp_j - dewpoint temperature of the jth sensor at the ith interval

12 Reference: Containment Integrated Leak-Rate Testing Improvements, EPRI NP-2726, November 1982, Appendix Ø.

The significance of volume weighed absolute temperature is essentially that you sum the reciprocal of the volume fraction divided by temperature. The significance of containment average volume weighed vapor pressure would require temperature and dew point or humidity readings to be taken in each volume fraction converted to vapor pressure and weighed based upon the volume fraction assigned to those sensors. The standard suggests that it would be sufficiently accurate to sum the dew point temperatures based upon their volume weighing factors. The working group has looked at numerous previous tests and finds no significant difference between the methods

contained in the current edition of the standard and the practices recommended by this revision. However, this revision recommends a more academically correct approach.

2.6 TEST PROCEDURE FOR TYPE B AND TYPE C

Changes in this chapter are primarily clarification and are of little significance.

2.7 REFERENCES

Stand as they were.

2.8 APPENDICES

For the most part, changes to the appendices are corrections of typographical errors in the current edition and changes in terminology to bring the appendices in line with the body of the Standard.

Appendix B has been reformated and the alternative formulation contained in B-3 has been corrected as follows.

B3. **Alternative Formulations**

Common alternative formulations for A, B, and S are as follows:

$$A = \frac{[(t_i - \bar{t})\ (W_i - \bar{W})]}{\Sigma\,[(t_i - \bar{t})^2]}$$

where

$$\bar{t} = \frac{\Sigma\ t_i}{n} \quad ; \quad \bar{W} = \frac{\Sigma\ W_i}{n}$$

$$B = \bar{W} - A\bar{t}$$

$$S = \left\{\left(\frac{1}{n-2}\right)\left[\Sigma\,(W_i - \bar{W})^2 \quad \frac{\left[\Sigma\ (t_i - \bar{t})\ (W_i - \bar{W})\right]^2}{\Sigma\ (t_i - \bar{t})^2}\right]\right\}^{1/2}$$

These alternatives formulation can be shown to be equivalent by using the following identities.

$$\Sigma\,(t_i - \bar{t})^2 = \Sigma\, t_i^2 - (\Sigma\, t_i)^2/n$$

$$\Sigma\,(W_i - \bar{W})^2 = \Sigma\, W_i^2 - (\Sigma\, W_i)^2/n$$

$$\Sigma\,(t_i - \bar{t})\ (W_i - \bar{W}) = \Sigma\, t_i W_i - (\Sigma\, t_i)\ (\Sigma\, W_i)^2/n$$

$$\Sigma \text{ constant} = n \text{ (constant)}$$

$$\Sigma [(\Sigma t_i) t_i] = (\Sigma t_i)(\Sigma t_i) = (\Sigma t_i)^2$$

$$\Sigma [(\Sigma W_i) t_i] = (\Sigma t_i)(\Sigma W_i)$$

$$\Sigma [\text{constant } (t_i)]^2 = (\text{constant})^2 \Sigma t_i^2$$

These alternative formulations should be used when the computing facilities do not carry more than ten significant figures internally to minimize round-off errors in the data reduction.

3.Ø FUTURE ACTION

Some of the comments received from the NUPPSCO members were outside the scope of this revision. These comments will be considered as a possible future revision. Also, as the revised Standard is used, we expect to receive additional industry comments or questions. The Working Group is prepared to incorporate comments or clarifications in a future revision.

NRC has proposed an additional statistical test for the validity of short-duration test data. At the time this paper was written, the Working Group has not concurred with this statistical test. The following paper will discuss the merits of this statistical test along with alternative tests to determine the validity of short-duration test data. If the Working Group decides to recommend an approach other than the one proposed by Region 3, an appendix will be developed and published with this revision.

METHODS FOR DETERMINING INTEGRATED LEAKAGE RATE TEST DURATION
-CASE STUDIES-

by Larry R. Young, Bechtel Power Corporation

ABSTRACT

Data from sixteen Integrated Leakage Rate Tests (ILRT) are examined to determine which of the evaluated methods provides the shortest duration and reliable test results. The methods of analysis examined are: Mass Point Method; Total Time Method; Parabolic Inequality Method; Hybrid Method; and Predictor Method. The methods are examined to determine the shortest duration at which all acceptance criteria are satisfied. A method to determine ILRT duration is recommended.

1.0 INTRODUCTION

"Draft Regulatory Guide MS 021-5, Containment System Leakage Testing"[1] presents 21 positions on the use of ANSI/ANS 56.8-1981, "Containment System Leakage Testing Requirements."[2] Positions C.21.d (1) Method 1 - ANSI Extended Method (Parabolic) and (2) Method 2 - Hybrid Method (Hybrid) are evaluated in this paper. Several sets of actual test data are analyzed using Parabolic, Hybrid, Total Time Analysis[4], Mass Point Analysis[2], and the Wiss, Janney, Elstner and Associates Predictor.[3]

2.0 DISCUSSION

Mass Point[2], Parabolic[1], Hybrid[1], Total Time[4], and Predictor[3] leakage rate analytical methods have been incorporated into a version of the Bechtel ILRT Computer Program. Sixteen cases of data from actual ILRT's are analyzed and compared. Mass Point analysis is performed per reference 2. Parabolic analysis is performed per reference 1, position C.21.d.(1) Method 1 - ANSI Extended Method. Hybrid analysis is performed per reference 1, position C.21.d.(2) Method 2 - Hybrid Method, except the Hybrid 95% Upper Confidence Limit (UCL) is calculated using L_{ah} (Hybrid leakage rate at the last data point based on the slope and intercept of Mass Point leakage rates, Y_n, n=3,N, vs time) instead of Y (average of Y_n, n=3,N), where N = the last data point. Total Time analysis is performed per reference 4, except the calculated leakage rate must be positive and after 24 hours of data an alternate calculation for the 95% UCL with a smaller confidence interval is utilized. Predictor analysis is performed per reference 3. The Predictor is satisfied if the value is less than 25 percent.

Six graphs are presented for each case. Airmass plots are the dry air mass, W_i lbm X 1000 vs time, regression line and 0.75 L_a or 0.75 L_t line. Mass Point, Hybrid, and Total Time plots are leakage rates and 95% UCL vs time. Parabolic Inequality plots are the ratio of the left side divided by the right side of inequalities C.21.d.(1) a.1, a.2 and b, with values greater than 2 or less than 0 plotted as 1.85 or 0.05, 1.9 or 0.1, and 1.95 or 0.15, respectively, to provide separation and clarity, vs time. The Parabolic test is satisfied if ratio a.1 is greater than 1 and ratio a.2 is less than 1 or ratio a.1 is less than 1 and ratio a.2 is any value, and ratio b is greater than 1.

Table 1 shows when each of the five methods analyzed is first satisfied, with a 1.00 hour minimum except for the predictor, which can only be calculated after 4.00 hours minimum. Table 2 shows when each of the five methods in combination with other analyses, per the intent of the referenced document, is first satisfied. The five combinations are: Mass Point and ANS 56.8; Parabolic, Mass Point, and ANS 56.8; Hybrid, Mass Point, and ANS 56.8; Total Time and BN-TOP-1; and Predictor, Mass Point, and ANS 56.8.

TABLE 1
TIME WHEN CRITERIA FIRST SATISFIED (HOURS)

CASE	MASS POINT	PARABOLIC	HYBRID	TOTAL TIME	PREDICTOR
1	3.00	2.00	12.25	13.00	7.50
2	2.25	1.50	7.25	16.75	7.25
3	9.75	24.50	NS	NS	NS
4	1.25	1.25	2.00	10.00	6.50
5	1.00	3.00	NS	24.00	11.25
6	21.00	NS	NS	24.00	21.00
7	2.00	4.00	22.00	24.00	13.25
8	1.50	3.00	4.25	4.75	6.75
9	1.00	1.00	2.00	1.75	5.25
10	1.00	1.00	1.00	1.00	4.00
11	1.00	1.00	1.25	1.00	4.25
12	3.00	2.25	4.50	6.75	6.50
13	2.25	1.00	3.75	4.25	6.25
14	1.00	3.75	NS	24.00	20.00
15	1.00	1.00	1.25	1.50	4.00
16	8.00	3.25	NS	24.00	11.00

TABLE 2
TIME WHEN COMBINED CRITERIA FIRST SATISFIED (HOURS)

CASE	MASS POINT & ANS 56.8	PARABOLIC MASS POINT & ANS 56.8	HYBRID MASS POINT & ANS 56.8	TOTAL TIME BN-TOP-1	PREDICTOR MASS POINT & ANS 56.8
1	8.00	8.00	12.25	13.00	8.00
2	8.00	8.00	8.00	16.75	8.00
3	9.75	NS	NS	NS	NS
4	8.00	NS	8.00	10.00	8.00
5	8.00	15.00	NS	24.00	11.25
6	21.00	NS	NS	24.00	21.00
7	9.00	12.25	22.00	24.00	13.25
8	8.00	8.00	8.00	6.00	NS
9	8.00	8.00	8.00	6.00	8.00
10	8.00	8.00	8.00	6.00	8.00
11	8.00	8.00	8.00	6.00	8.00
12	8.00	8.00	8.00	6.75	8.00
13	8.00	10.00	8.00	6.00	8.00
14	8.00	12.00	NS	24.00	20.00
15	8.00	8.00	8.00	6.00	8.00
16	8.00	9.75	NS	24.00	11.00

NS = NOT SATISFIED DURING THE DATA PERIOD.

The Mass Point and ANS 56.8 combined criteria incorrectly identify 1 failure (Case 3) as a successful test, indicating that this combination of criteria is insufficient to determine the outcome of an ILRT. The Parabolic, Mass Point, and ANS 56.8 combined criteria incorrectly identify 2 successful tests (Cases 4 and 6) as failures, indicating that this combination of criteria is too conservative. The a.1 and a.2 inequalities are extremely sensitive to transients and data scatter. Case 14 demonstrates that a.1 and a.2 can be satisfied by the occurance of a single data point on the opposite side of the regression line. This erratic behavior, as exhibited in the plots of a.1 and a.2 vs time, complicates the analysis of ILRT data. Often the Parabolic method seems to indicate that less data more accurately determines the leakage rate than a larger amount of data from long duration tests. This is inconsistent with stastical analysis. The Hybrid, Mass Point and ANS 56.8 combined criteria incorrectly identify 4 successful tests (Cases 5, 6, 14 and 16) as failures, indicating that this combination of criteria is excessively conservative. (The Hybrid method has been withdrawn from consideration by the Regulators since this paper was written.) Total Time and BN-TOP-1 combined criteria correctly determine the success or failure of all sixteen cases evaluated. However, Total Time analysis is extremely sensitive to the relative magnitude of the first data point and to early less stable data. Total Time and BN-TOP-1 also have the longest average test duration. Bechtel Topical Report BN-TOP-1 is effective but excessively conservative. The Predictor, Mass Point, and ANS 56.8 incorrectly identify 1 successful test as a failure (Case 8). Because the Case 8 Mass Point leakage rate was relatively constant for the last 1.5 hours, the Predictor most likely would have been satisfied if approximately 2.5 more hours of data had been taken. Plots of the Predictor vs time reveal a smooth continuous curve useful in ILRT data analysis. Table 3 sumarizes the results of combined criteria analyses.

TABLE 3
COMBINED CRITERIA RESULTS

RESULT	MASS POINT & ANS 56.8	PARABOLIC MASS POINT & ANS 56.8	HYBRID MASS POINT & ANS 56.8	TOTAL TIME BN-TOP-1	PREDICTOR MASS POINT & ANS 56.8
CORRECTLY DETERMINED	15	14	12	16	15
FAILURE DETERMINED SUCCESS	1	0	0	0	0
SUCCESS DETERMINED FAILURE	0	2	4	0	1
AVERAGE DURATION OF CORRECT TESTS, HOURS	8.9	9.5	9.7	13.5	10.6

3.0 CONCLUSIONS

No set of criteria will always correctly determine the success or failure of an ILRT, if the test is not properly conducted. Due to the complexity of ILRT's, experienced test personnel should be utilized to ensure proper conduct of the test. One of the most critical steps in analyzing ILRT data is determining a valid start and end time for the

data set. Temperature stabilization criteria are not sufficient to determine a valid start time. Airmass stabilization and any other factors that influence the data must be considered. Other factors include leak path isolations, containment fan and cooler operation, containment coolant temperature and flow, reactor coolant temperature and flow, volume changes, and the ability of assigned volume fractions to accurately model the containment atmosphere. When temperature stabilization criteria, airmass stabilization, and other considerations warrant, a valid start time should be chosen. Airmass stabilization is defined as a time after which the airmass plot vs time exhibits a reasonably linear shape with a resonable amount of data scatter, and if Total Time or Hybrid analysis is utilized then the first airmass must be reasonably close in value to the Mass Point regression line intercept. If any leak paths are isolated, the start time should be after that isolation. Heat sources and/or sinks should be maintained at as constant a temperature as possible. Often, this is facilitated by not operating containment fans and coolers.

ILRT criteria should be easy to implement and understand, and have a technical basis. BN-TOP-1 has been criticized as too complex, resulting in improper application by test personnel not experienced in the use of BN-TOP-1. It follows that the Parabolic and Hybrid methods are also too complex. Mass Point per ANS 56.8 is said to be inadaquate for a duration less than 24 hours, as case 3 demonstrates in this study.

Based on a consensus of experienced Bechtel ILRT engineers and this study, the following recomendation is made. After a valid start time is determined, the Predictor, Mass Point and ANS 56.8 combined criteria method is preferred and sufficient to determine the success or failure and duration of an ILRT.

4.0 REFERENCES

1 "Draft Regulatory Guide MS 021-5 Containment System Leakage Testing," Draft dated May 31, 1985, Working Paper D4.

2 "American National Standard Containment System Leakage Testing Requirements," ANSI/ANS-56.8-1981

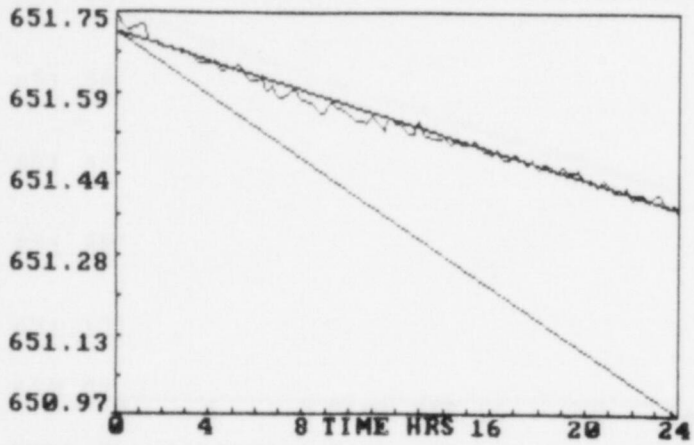
3 "Suggested Criteria for a Short Duration ILRT," Ted Brown and Louis Estenasoro, Wiss, Janney, Elstner and Associates, January 18, 1982. Presented at Reactor Operations Division, ANS, First Workshop on Containment Leakage Rate Testing.

4 "Testing Criteria for Integrated Leakage Rate Testing of Primary Containment Structures for Nuclear Power Plants," BN-TOP-1, G. V. Cranston, Bechtel Power Corporation, November 1, 1972, Revision 1.

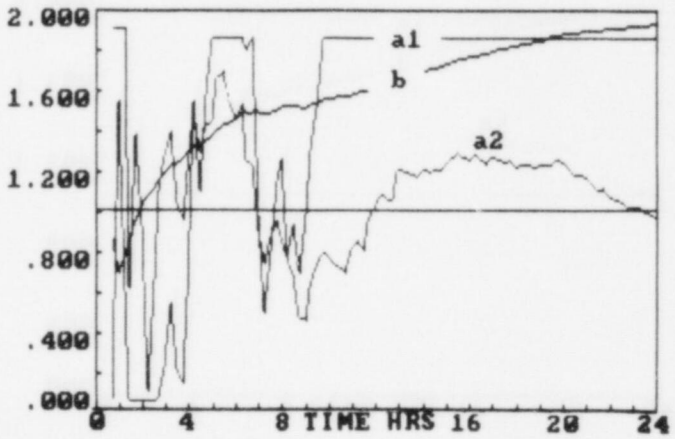
CASE 1

Case 1 is a 24 hr test, PWR, ctmt fans and coolers off, 2 x10^6 ft^3, 18 RTD's, 2 pressure gages, and 6 dewcells. The airmass plot exhibits a moderate amount of scatter and slightly parabolic shape, typical of a leakage rate slowly decreasing with time. Parabolic inequalities a.1 and a.2 are not satisfied from 4 to 7 hrs and from 12 to 23 hrs. The a.1 and a.2 inequalities seem to indicate that an 8 to 11 hr test more accurately determines the leakage rate than a 12 to 23 hr test. This is inconsistent with the data.

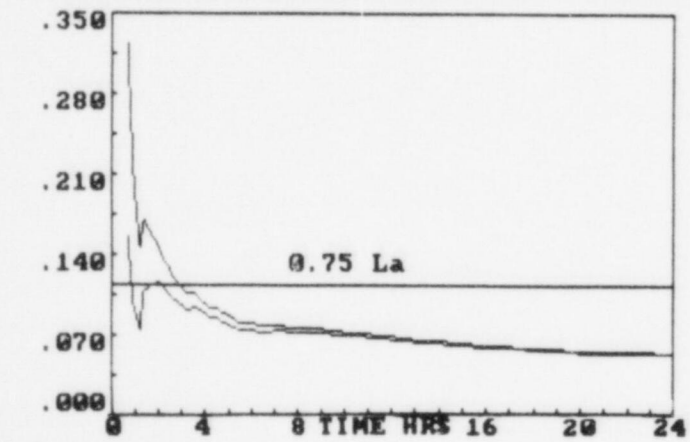
AIRMASS LBM X 1000



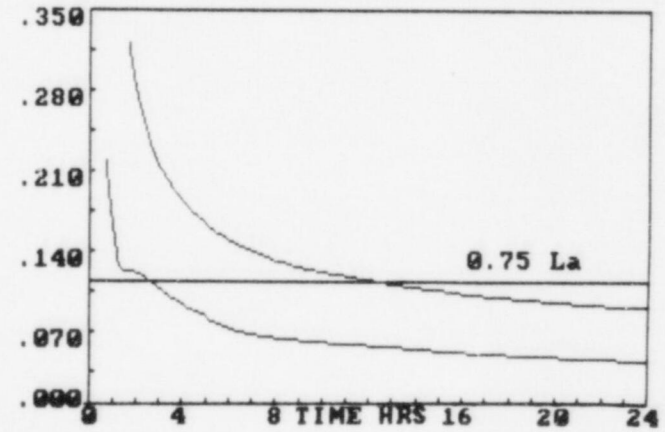
PARABOLIC INEQUALITIES a1 a2 b RATIO



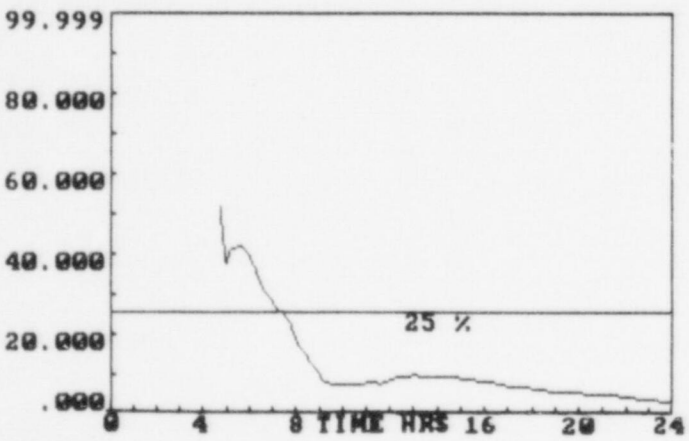
MASS POINT LEAKAGE RATE AND UCL - %/DAY



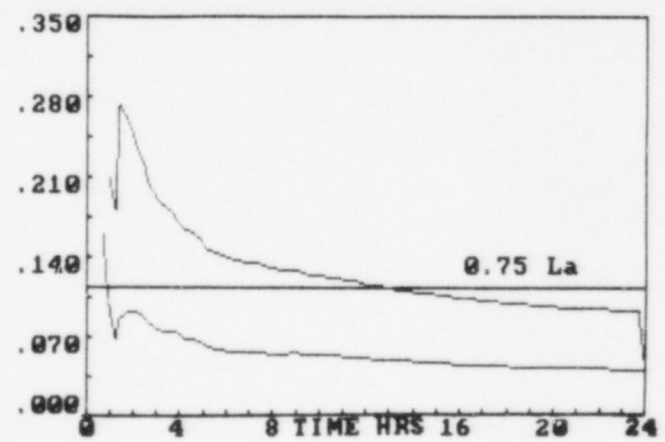
HYBRID LEAKAGE RATE AND UCL - %/DAY



PREDICTOR %



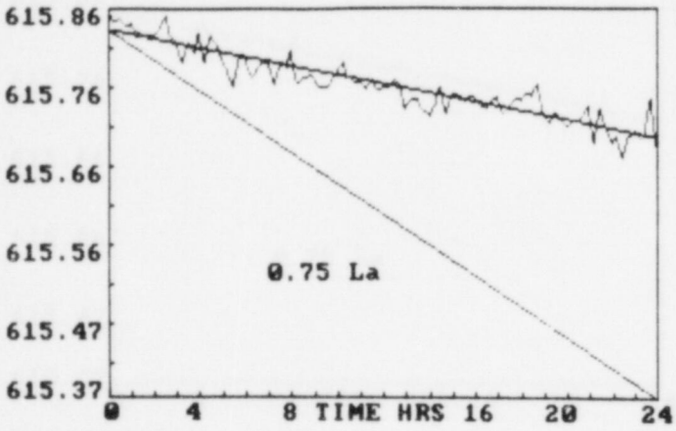
TOTAL TIME LEAKAGE RATE AND UCL - %/DAY



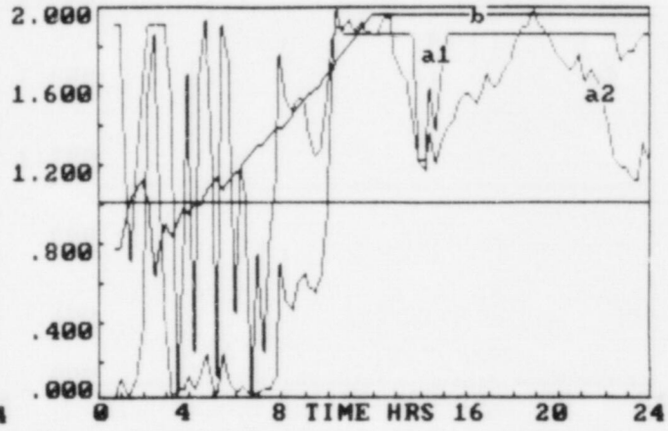
CASE 2

Case 2 is a 24 hr test, PWR, fans and coolers off, 1.7×10^6 ft^3, 18 RTD's, 2 pressure gages, and 6 dewcells. The airmass plot exhibits a larger amount of scatter and linear, slightly parabolic shape, typical of a leakage rate decreasing very slowly with time. Parabolic a.1 and a.2 are not satisfied from 2 to 4 hrs and from 10 to 24 hrs. The a.1 and a.2 inequalities seem to indicate that an 4 to 10 hr test more accurately determines the leakage rate than a 10 to 24 hr test. As in case 1, this is inconsistent with the data.

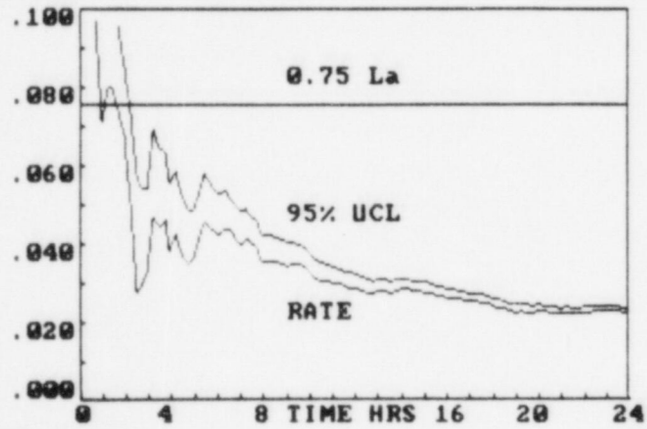
AIRMASS LBM X 1000 AND REGRESSION LINE



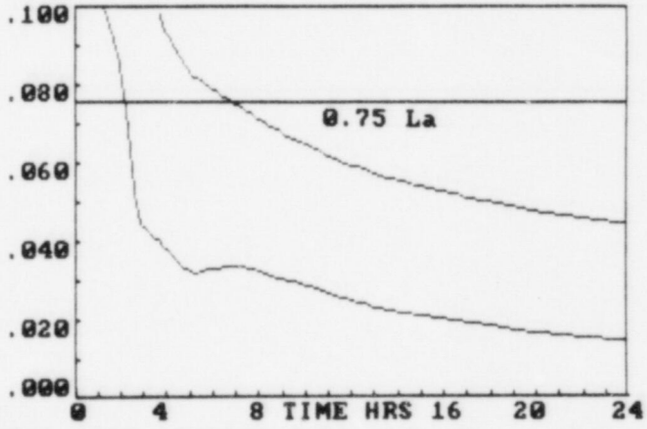
PARABOLIC INEQUALITIES a1 a2 b RATIO



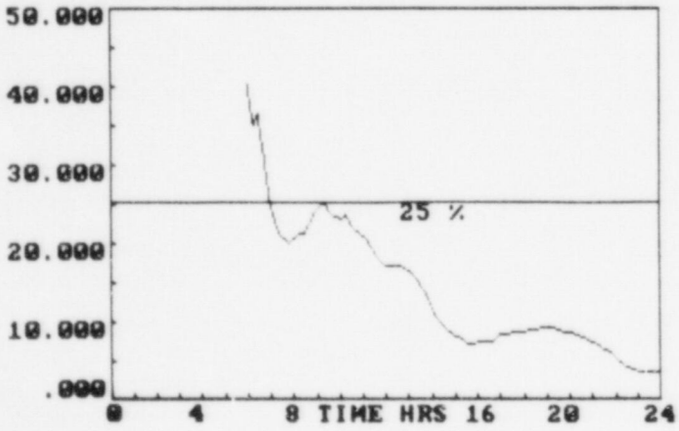
MASS POINT LEAKAGE RATE AND UCL - %/DAY



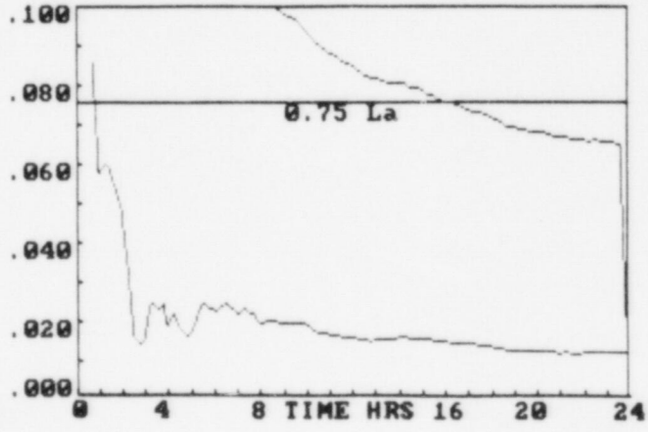
HYBRID LEAKAGE RATE AND UCL - %/DAY



PREDICTOR %



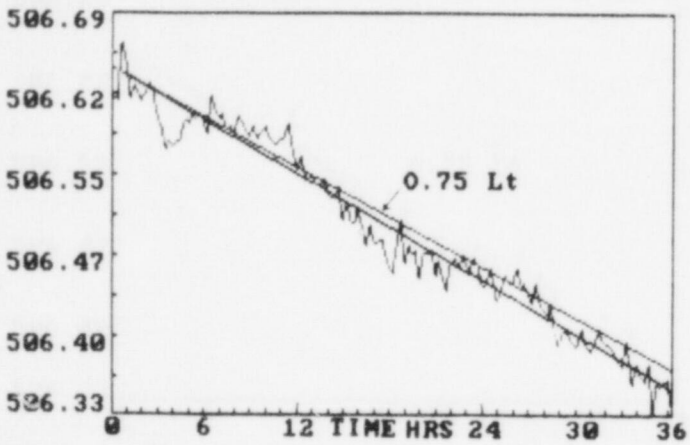
TOTAL TIME LEAKAGE RATE AND UCL - %/DAY



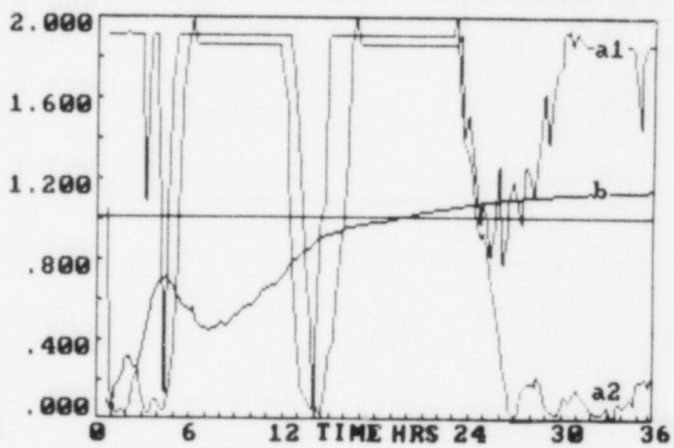
CASE 3

Case 3 is a 36 hr reduced pressure test, PWR, fans and coolers on, 2.5×10^6 ft^3, 18 RTD's, 2 pressure gages, and 6 dewcells. The airmass plot exhibits a large amount of scatter and sinusoidal shape due to the inablilty to control the amount of cooling, typical of a leakage rate that oscillates with data scatter. The Parabolic inequalities are satisfied after 24 hrs. Mass Point combined conditions are satisfied after 9.75 hrs demonstrating the failure of this method to correctly identify an unsuccesful test.

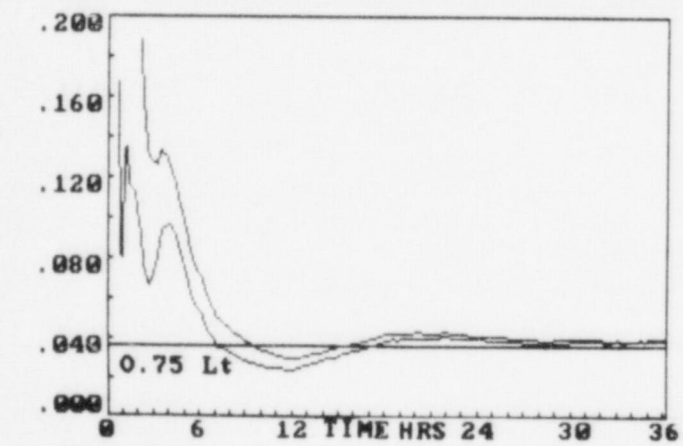
AIRMASS LBM X 1000



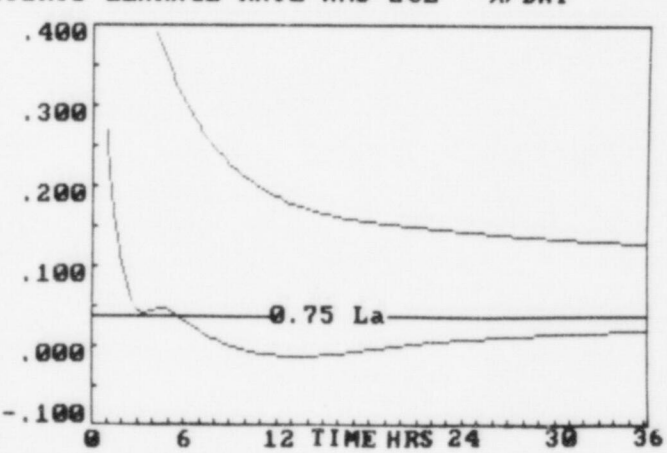
PARABOLIC INEQUALITIES a1 a2 b RATIO



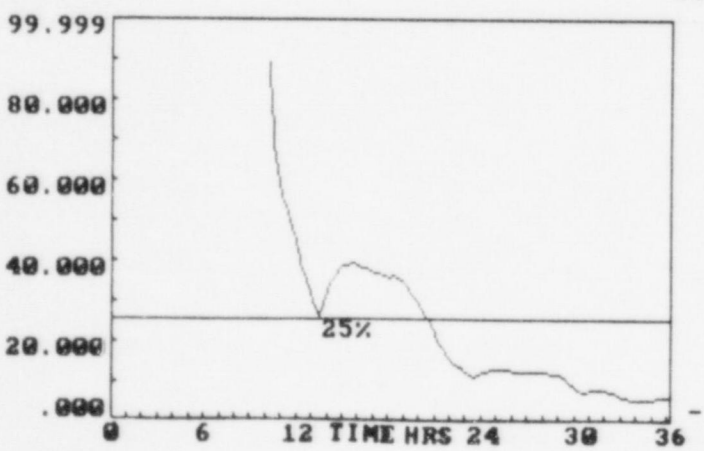
MASS POINT LEAKAGE RATE AND UCL - %/DAY



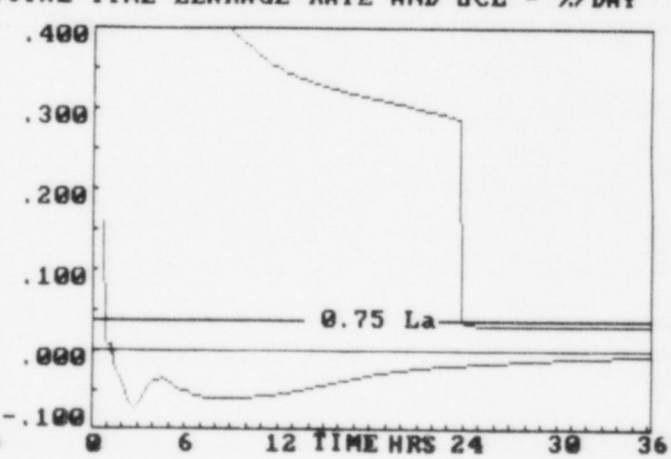
HYBRID LEAKAGE RATE AND UCL - %/DAY



PREDICTOR %



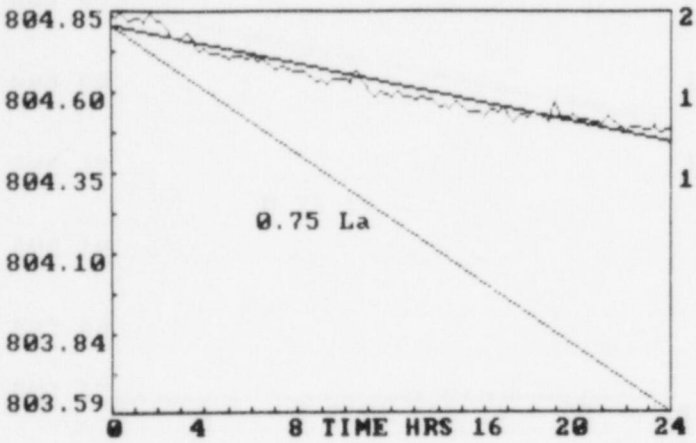
TOTAL TIME LEAKAGE RATE AND UCL - %/DAY



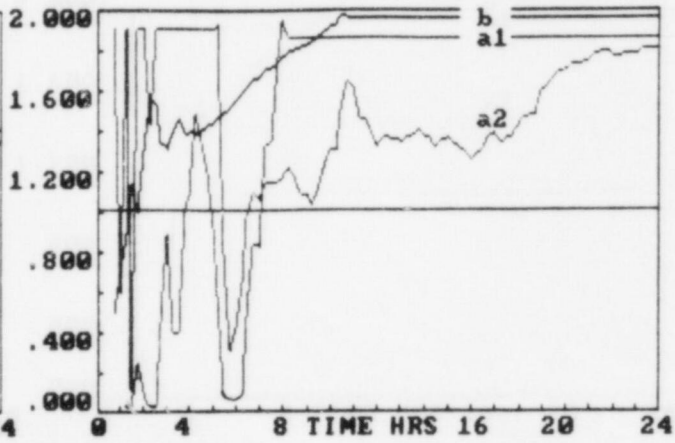
CASE 4

Case 4 a is 24 hr test, PWR, fans and coolers off, 2.5×10^6 ft^3, 24 RTD's, 2 pressure gages, and 6 dewcells. The airmass plot exhibits moderate scatter and slightly parabolic shape, typical of a leakage rate decreasing slowly with time. Parabolic inequalities a.1 and a.2 are not satisfied from 3.5 to 5 hrs and from 7 to 24 hrs. The a.1 and a.2 inequalities indicate that a 5 to 7 hr test more accurately determines the leakage rate than a 7 to 24 hr test. The parabolic combined conditions are not satisfied. This demonstrates failure of the Parabolic method to correctly identify a successful test.

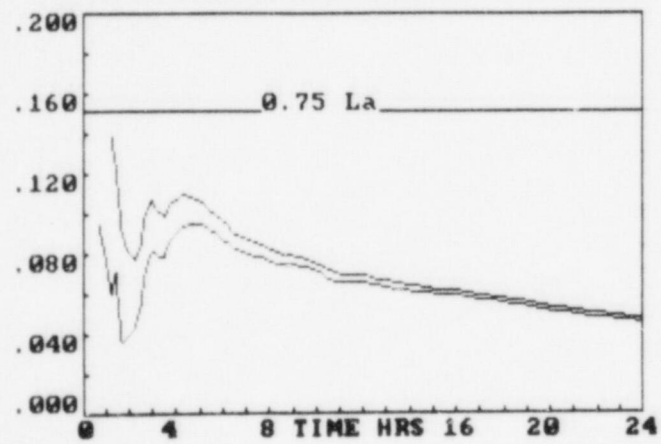
AIRMASS LBM X 1000 AND REGRESSION LINE



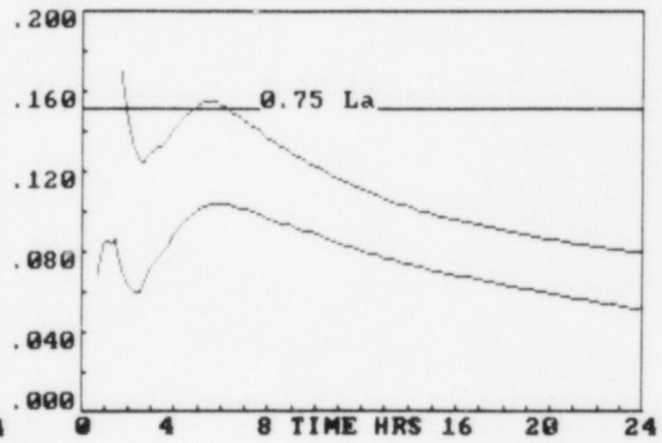
PARABOLIC INEQUALITIES a1 a2 b RATIO



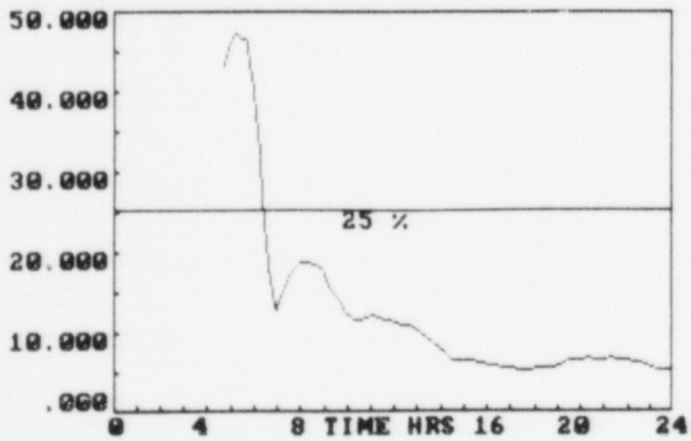
MASS POINT LEAKAGE RATE AND UCL - %/DAY



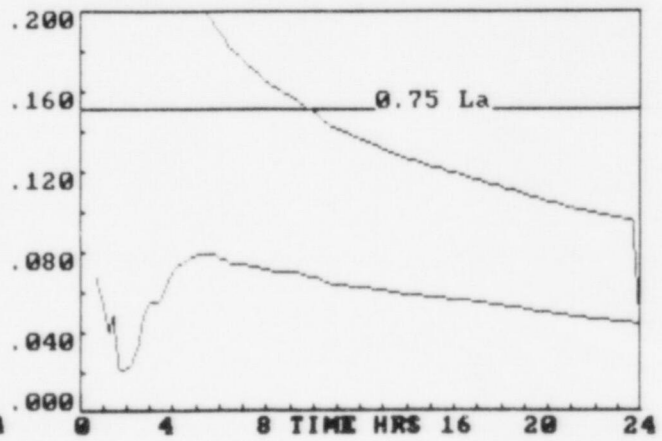
HYBRID LEAKAGE RATE AND UCL - %/DAY



PREDICTOR %



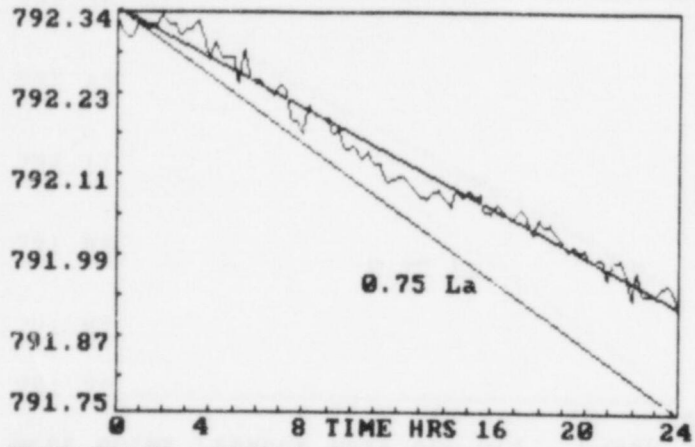
TOTAL TIME LEAKAGE RATE AND UCL - %/DAY



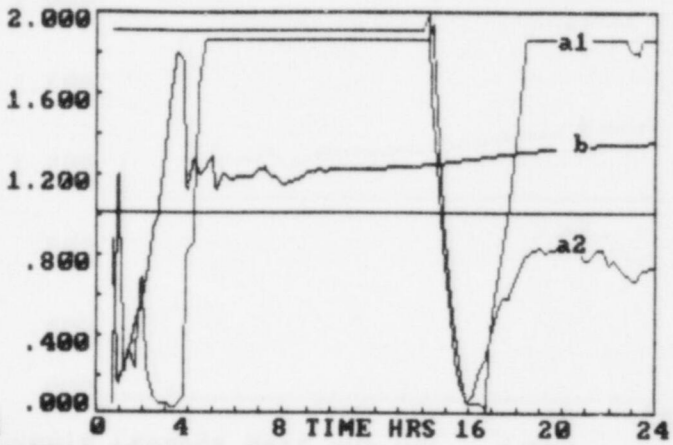
CASE 5

Case 5 is a 24 hr test, PWR, fans and coolers on, 2.5×10^6 ft^3, 18 RTD's, 2 pressure gages, and 6 dewcells. The airmass plot exhibits a large amount of scatter and sinusoidal shape, typical of a leakage rate that oscillates with temperature induced data scatter, due to the inability to regulate cooling. The Parabolic combined conditions are first satisfied after 15 hrs. The Hybrid combined conditions are never satisfied. This demonstrates the failure of the Hybrid method to correctly identify a successful test.

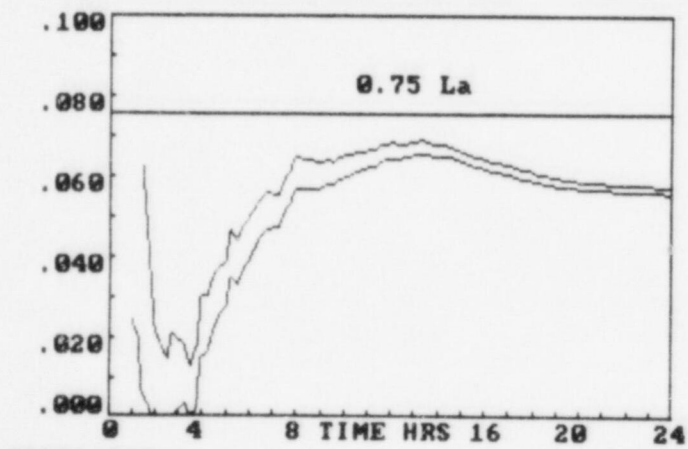
AIRMASS LBM X 1000 AND REGRESSION LINE



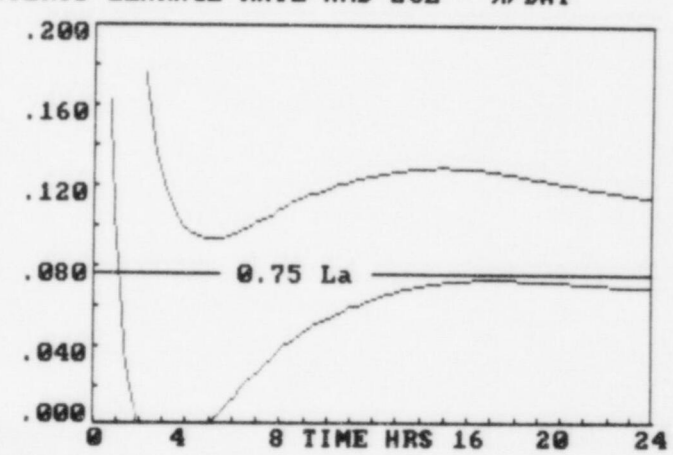
PARABOLIC INEQUALITIES a1 a2 b RATIO



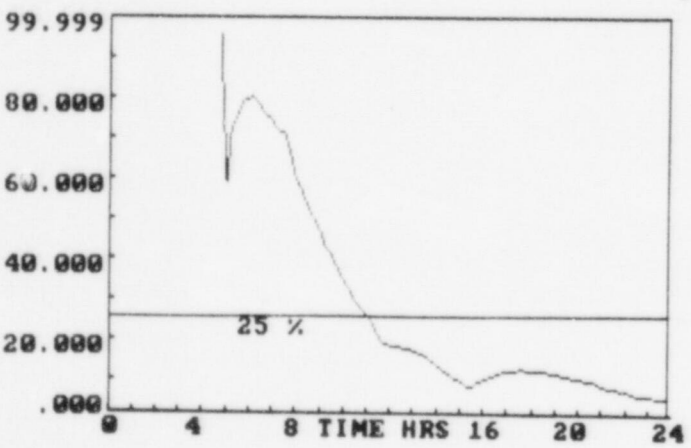
MASS POINT LEAKAGE RATE AND UCL - %/DAY



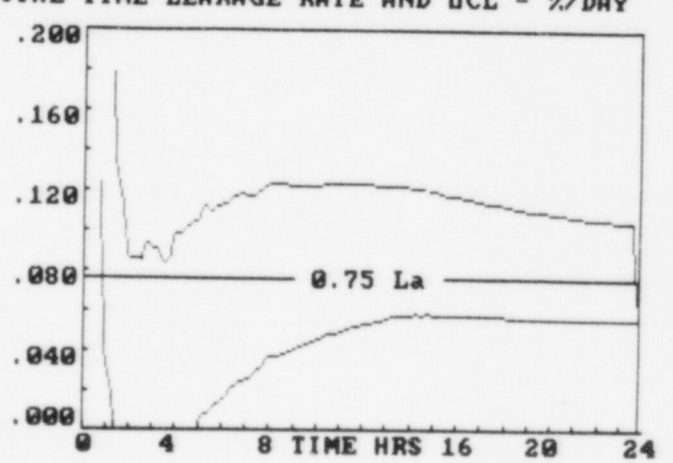
HYBRID LEAKAGE RATE AND UCL - %/DAY



PREDICTOR %

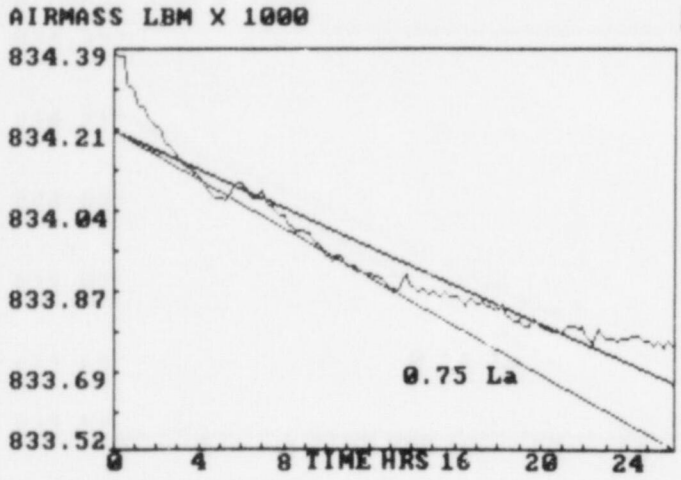


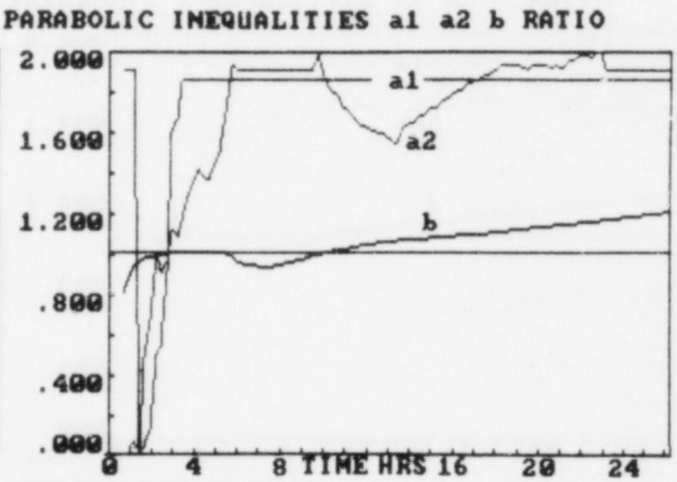
TOTAL TIME LEAKAGE RATE AND UCL - %/DAY

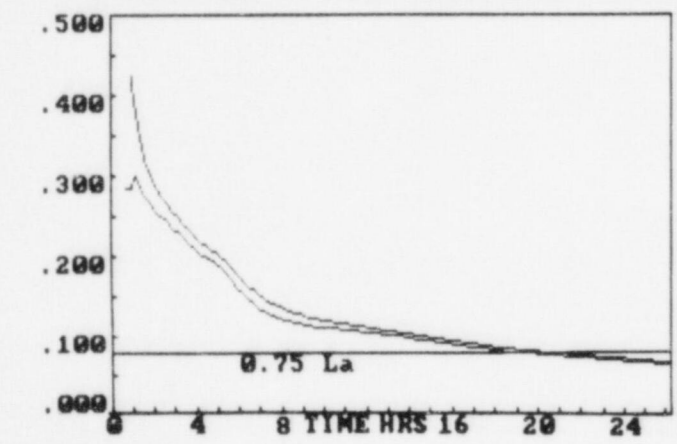


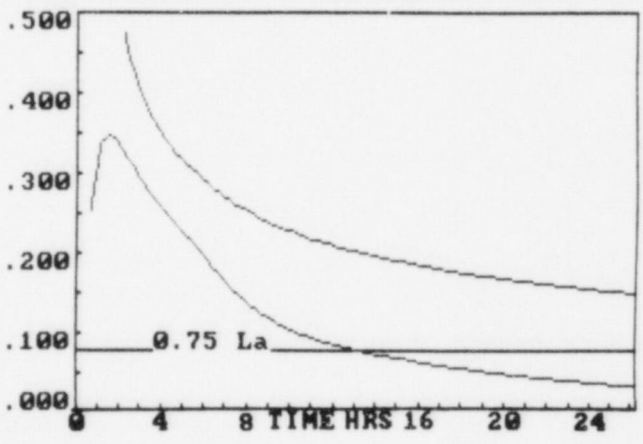
CASE 6

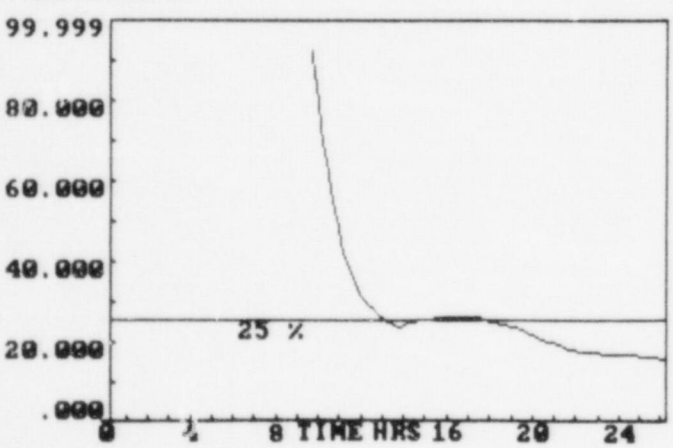
Case 6 is a 26.25 hr test, PWR, fans and coolers off, 2.3×10^6 ft^3, 18 RTD's, 2 pressure gages, and 4 dewcells. The airmass plot exhibits a moderate amount of scatter and very parabolic shape, typical of a leakage rate decreasing with time. The Parabolic combined conditions and the Hybrid combined conditions are never satisfied. This demonstrates the failure of the Parabolic and Hybrid methods to correctly identify a successful test.

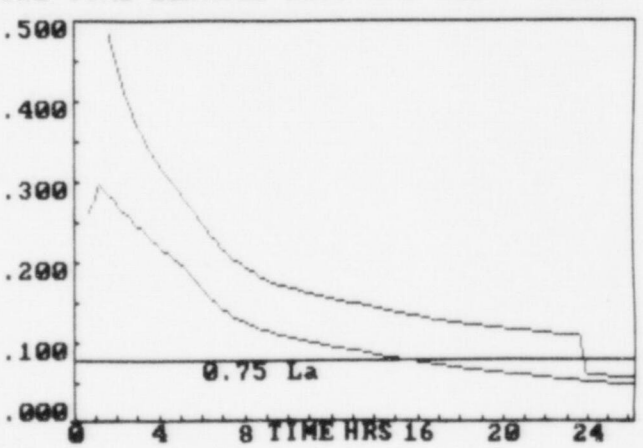








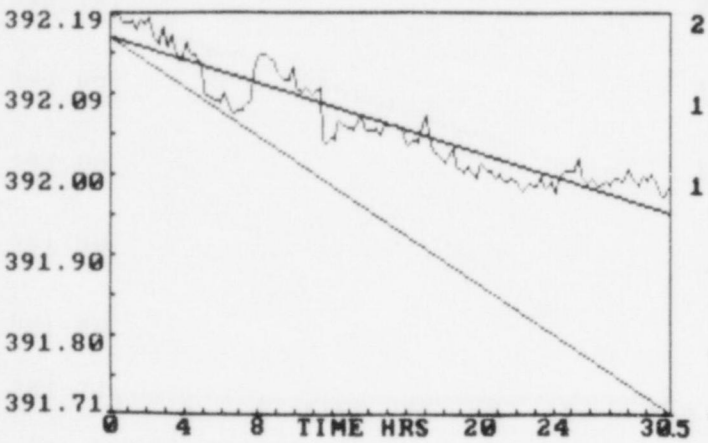




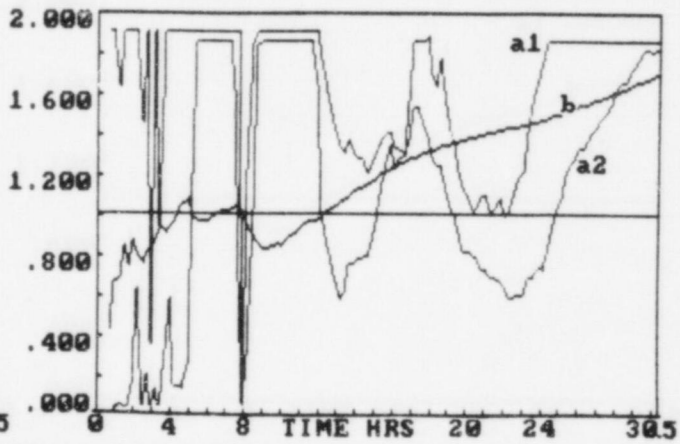
CASE 7

Case 7 is a 30.5 hr test, PWR, fans and coolers on, 1.2×10^6 ft^3, 18 RTD's, 2 pressure gages, and 4 dewcells. The airmass plot exhibits much scatter and slightly parabolic shape, typical of a leakage rate decreasing with time and oscillating due to inability to regulate cooling. Parabolic inequalities a.1 and a.2 are not satisfied from 5 to 7.5 hrs, from 8.25 to 12.25 hrs, from 15.25 to 19.25 hrs, and from 25 to 30.5 hrs of data. The a.1 and a.2 inequalities seem to be too sensitive to transients, such as the one occuring from 5 to 7 hrs, resulting in satisfied conditions during the transient.

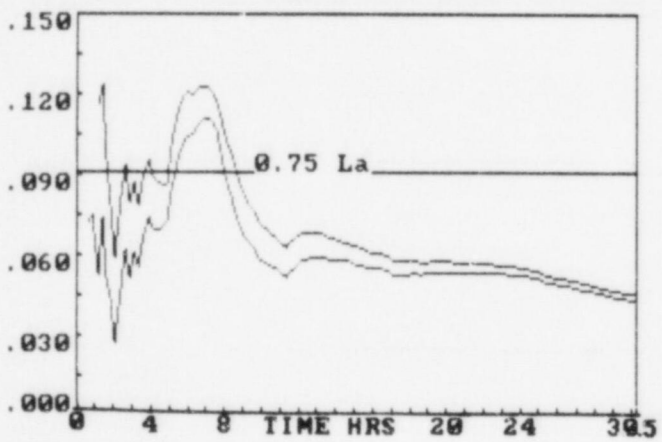
AIRMASS LBM X 1000



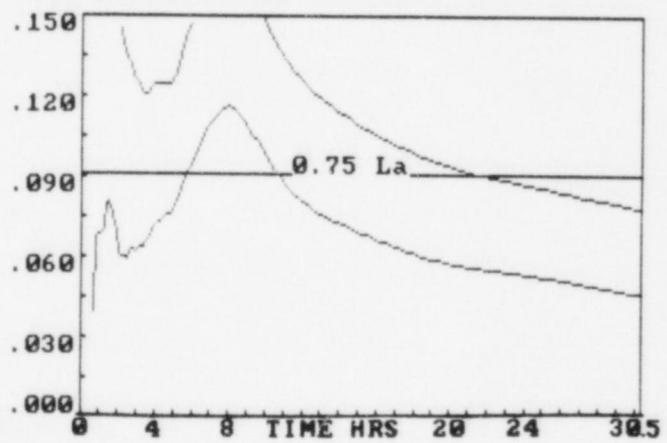
PARABOLIC INEQUALITIES a1 a2 b RATIO



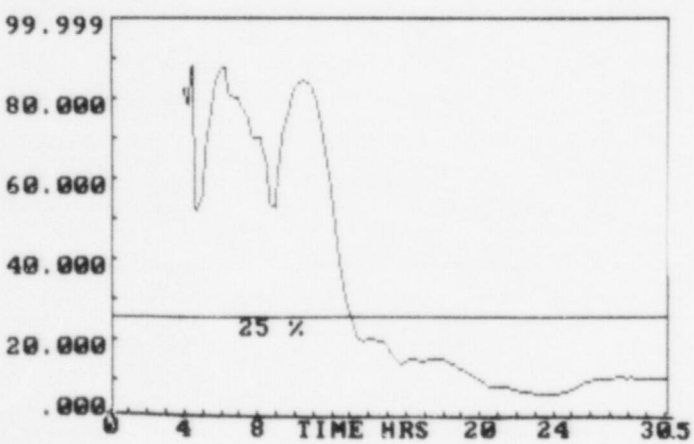
MASS POINT LEAKAGE RATE AND UCL - %/DAY



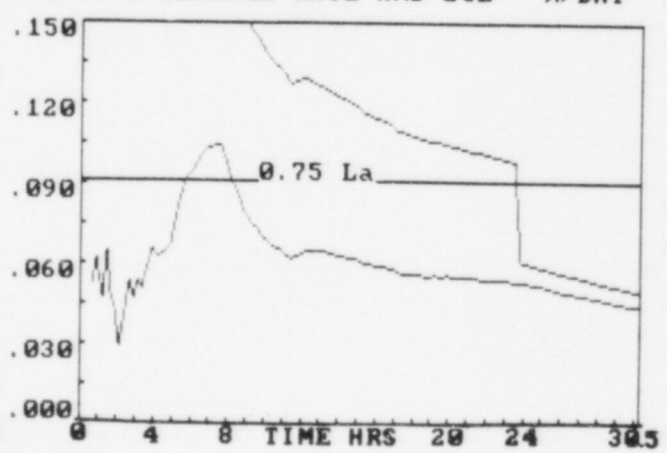
HYBRID LEAKAGE RATE AND UCL - %/DAY



PREDICTOR %



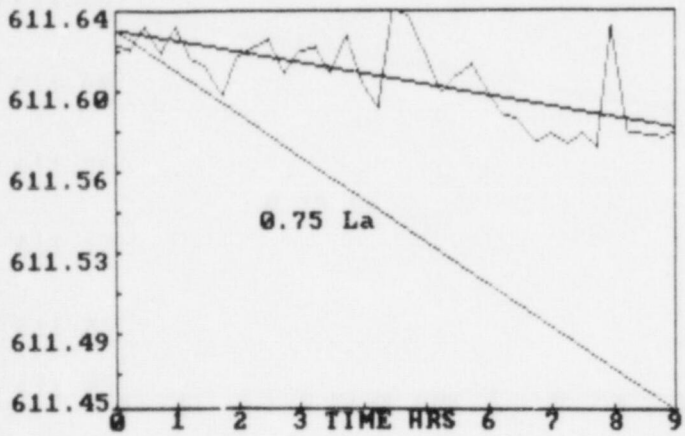
TOTAL TIME LEAKAGE RATE AND UCL - %/DAY



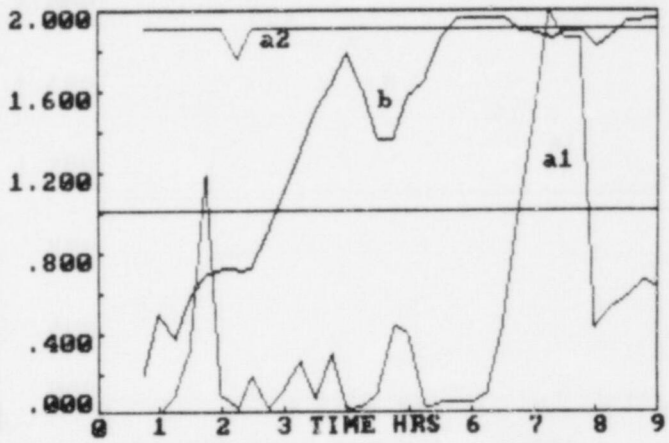
CASE 8

Case 8 is a 9 hr test, PWR, fans and coolers on, 1.7×10^6 ft^3, 18 RTD's, 2 pressure gages, and 6 dewcells. The airmass plot exhibits a large amount of scatter. The predictor is not satisfied during the 9 hr data period, demonstrating a failure to correctly identify a successful test. Extrapolation indicates that the predictor would have been satisfied after approximately 11.5 hrs of data, if the verification test had not started.

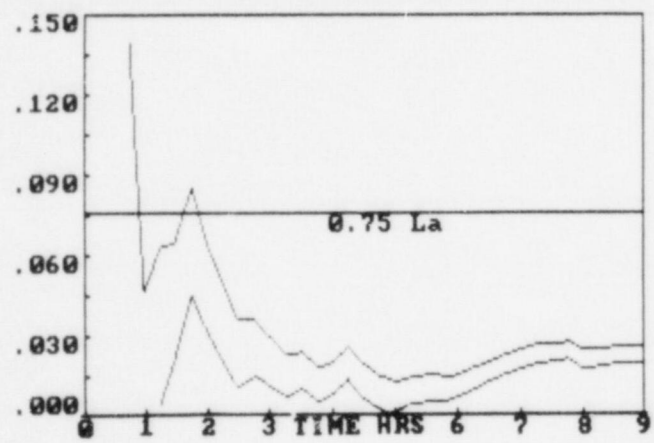
AIRMASS LBM X 1000 AND REGRESSION LINE



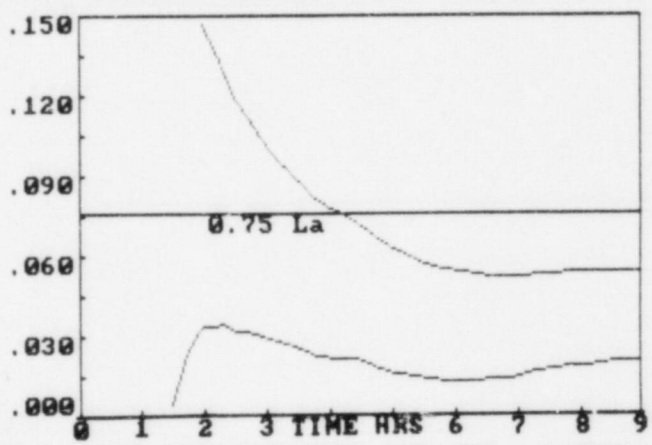
PARABOLIC INEQUALITIES a1 a2 b RATIO



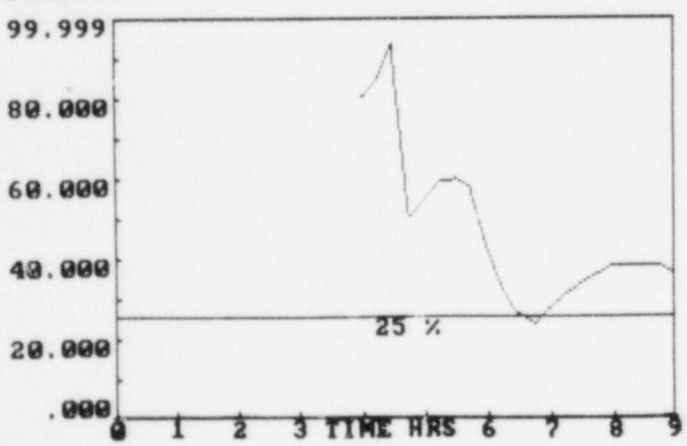
MASS POINT LEAKAGE RATE AND UCL - %/DAY



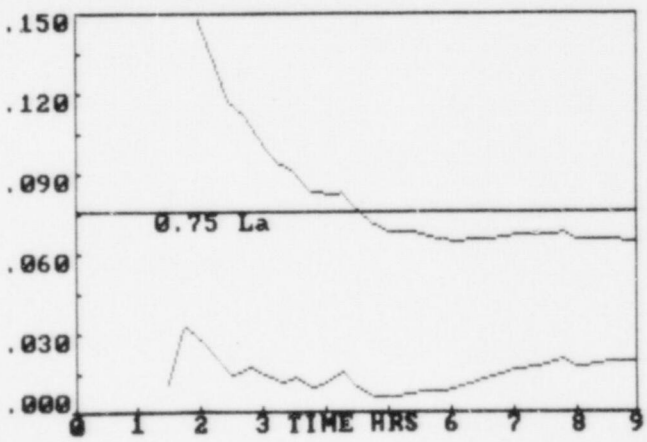
HYBRID LEAKAGE RATE AND UCL - %/DAY



PREDICTOR %



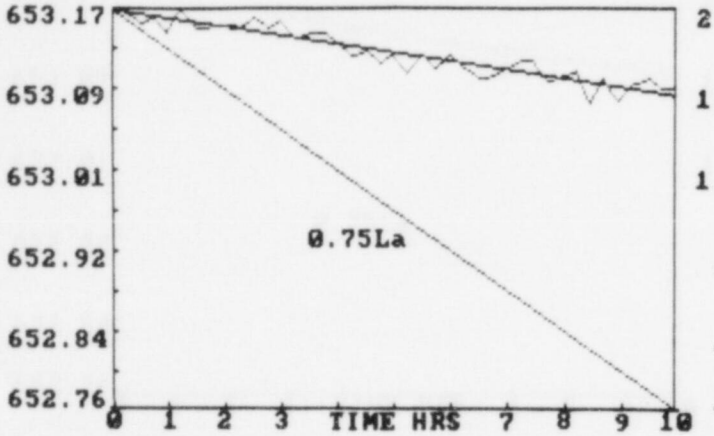
TOTAL TIME LEAKAGE RATE AND UCL - %/DAY



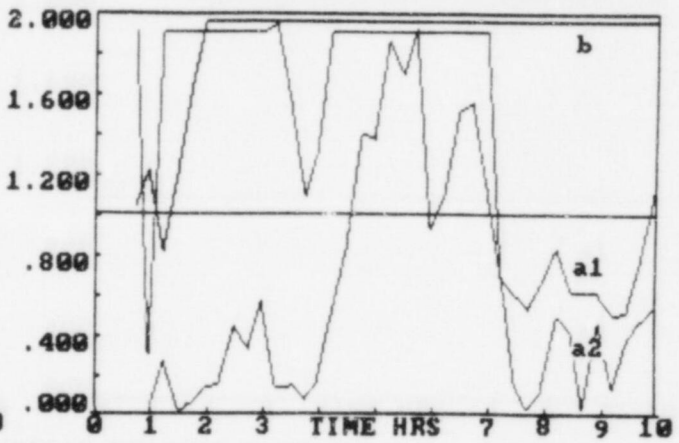
CASE 9

Case 9 is a 10 hr test, PWR, fans and coolers off, $2x10^6$ ft^3, 16 RTD's, 2 pressure gages, and 6 dewcells. The airmass plot exhibits a small amount of scatter and nearly linear shape. Parabolic inequalities a.1 and a.2 are not satisfied from 4.75 to 5.75 hrs, and from 6.25 to 7 hrs. These unsatisfied periods are inconsistent with the nearly linear data with a small amount of data scatter, demonstrating that a.1 and a.2 are excessively sensitive.

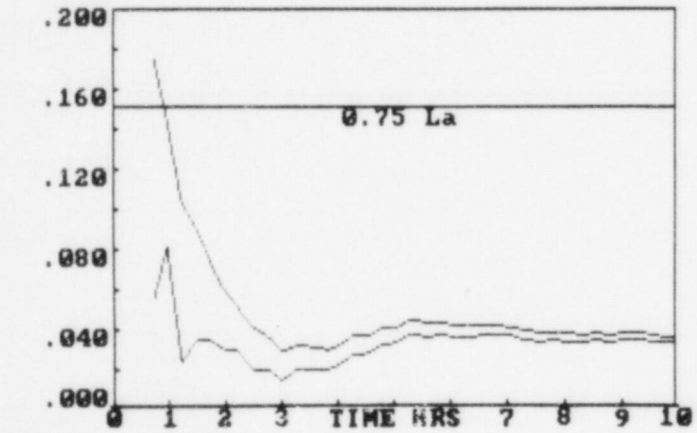
AIRMASS LBM X 1000 AND REGRESSION LINE



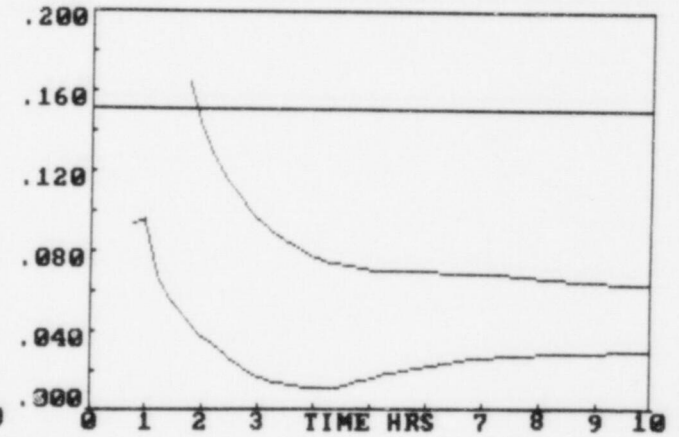
PARABOLIC INEQUALITIES a1 a2 b RATIO



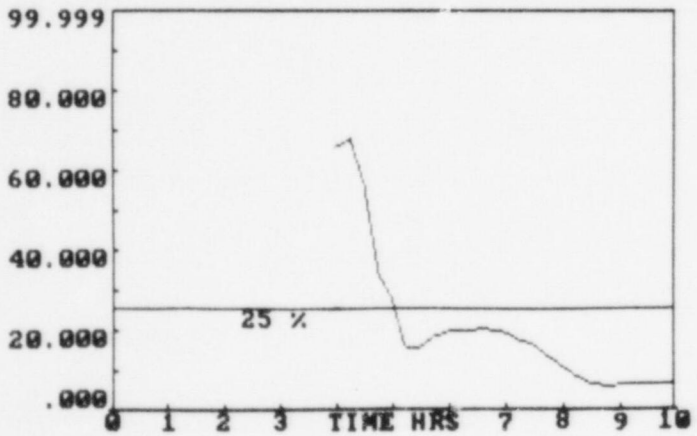
MASS POINT LEAKAGE RATE AND UCL - %/DAY



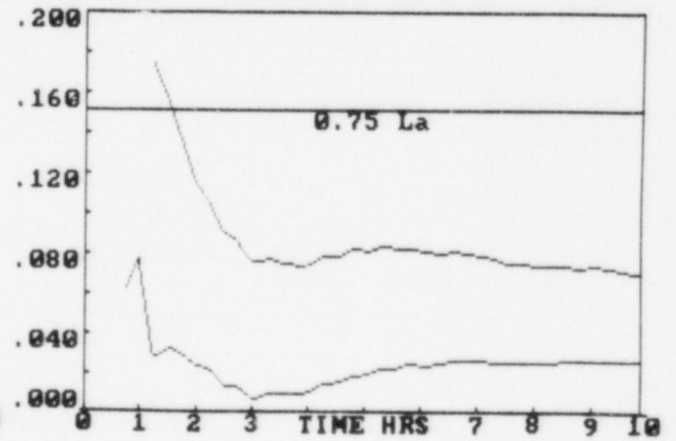
HYBRID LEAKAGE RATE AND UCL - %/DAY



PREDICTOR %



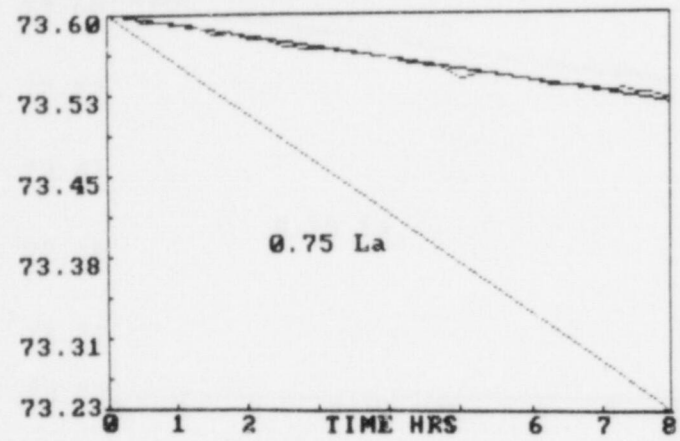
TOTAL TIME LEAKAGE RATE AND UCL - %/DAY



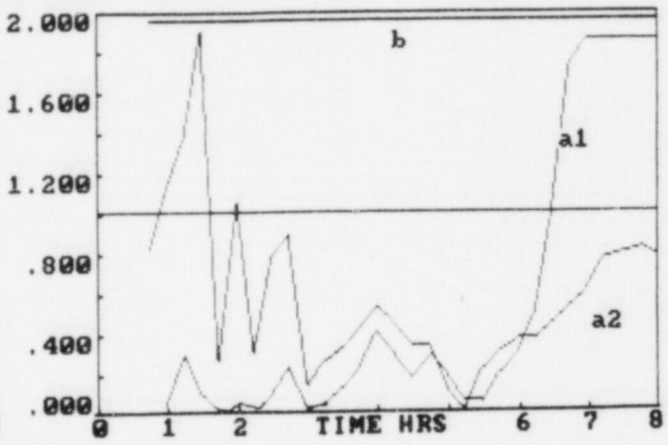
CASE 10

Case 10 is an 8 hr test, BWR, fans and coolers off, $2x10^5$ ft^3, 15 RTD's, 2 pressure gages, and 5 dewcells. The airmass plot exhibits a very small amount of scatter and very linear shape. Parabolic inequalities a.1 and a.2 are nearly not satisfied from 7.25 to 8 hrs, when the a.2 ratio is approximately 0.8 due to a small deviation from linear data. This is inconsistent with the very linear data with a small amount of data scatter, demonstrating that a.1 and a.2 are excessively sensitive.

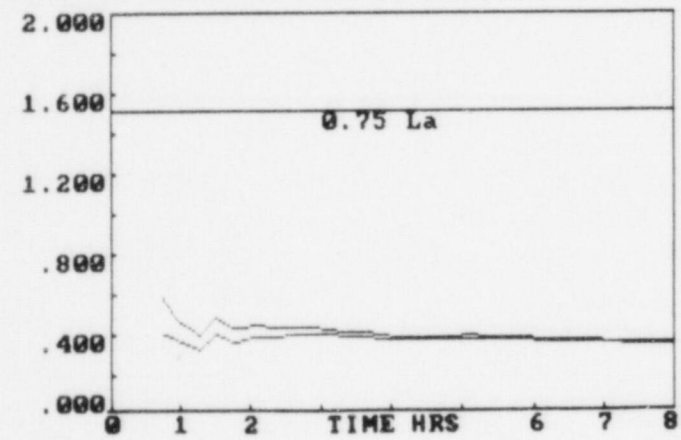
AIRMASS LBM X 1000 AND REGRESSION LINE



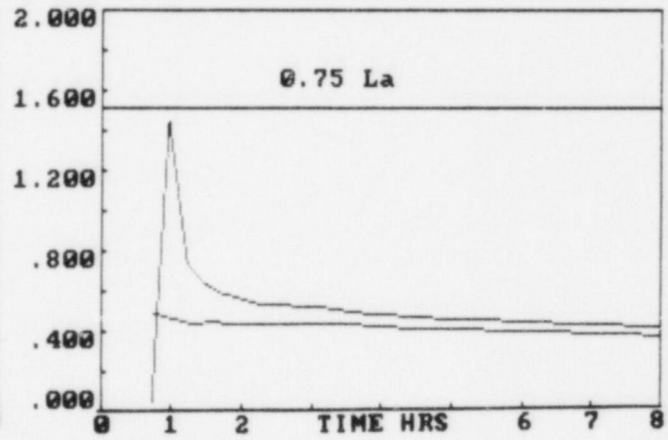
PARABOLIC INEQUALITIES a1 a2 b RATIO



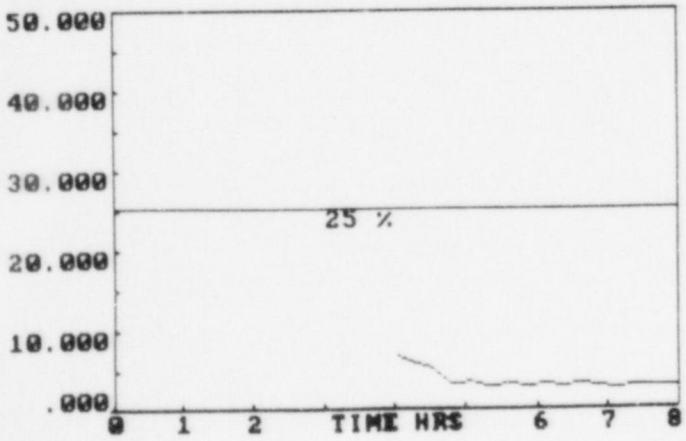
MASS POINT LEAKAGE RATE AND UCL - %/DAY



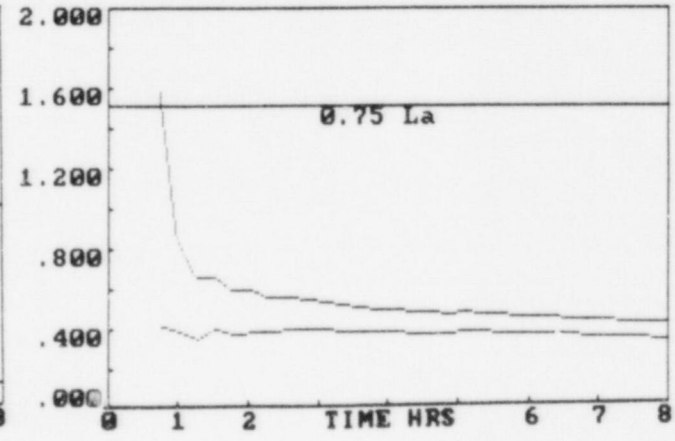
HYBRID LEAKAGE RATE AND UCL - %/DAY



PREDICTOR %



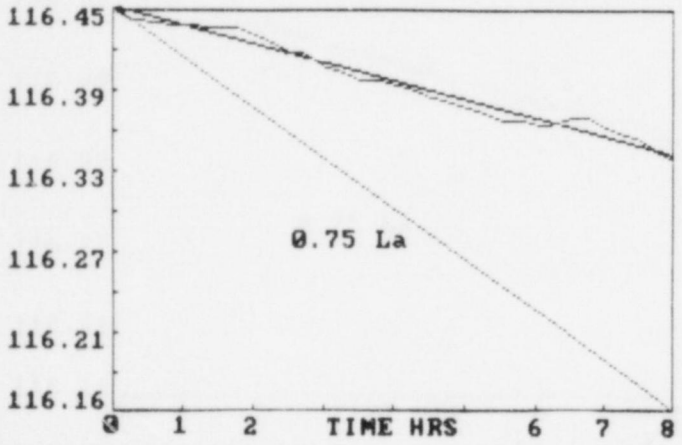
TOTAL TIME LEAKAGE RATE AND UCL - %/DAY



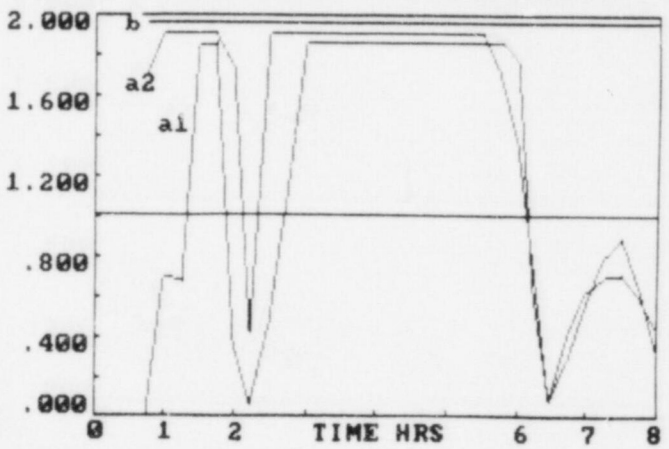
CASE 11

Case 11 is an 8 hr test, BWR,fans and coolers off, $4x10^5$ ft^3 24 RTD's, 2 pressure gages, and 9 dewcells. The airmass plot exhibits a very small amount of scatter and nearly linear shape. Parabolic inequalities a.1 and a.2 are not satisfied from 1.5 to 1.75 hrs and from 2.75 to 6 hrs. This is inconsistent with the nearly linear data with a small amount of data scatter, demonstrating that a.1 and a.2 are excessively sensitive.

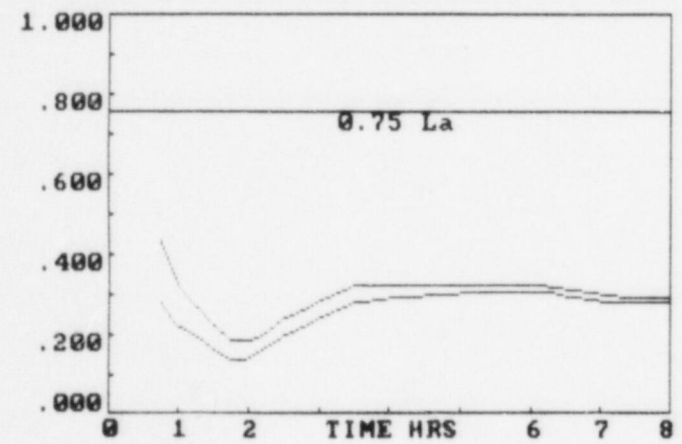
AIRMASS LBM X 1000 AND REGRESSION LINE



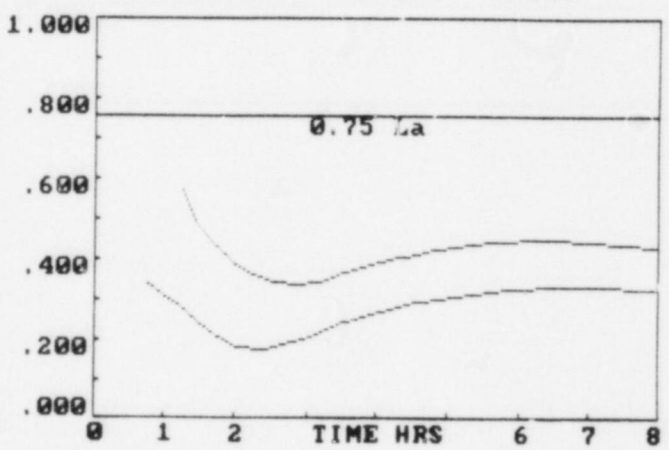
PARABOLIC INEQUALITIES a1 a2 b RATIO



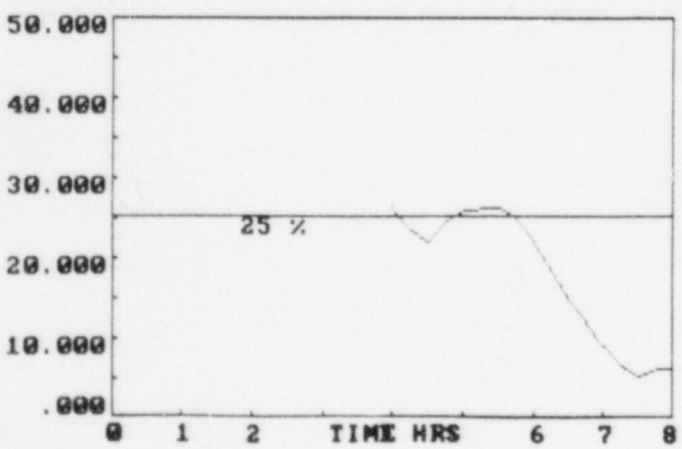
MASS POINT LEAKAGE RATE AND UCL - %/DAY



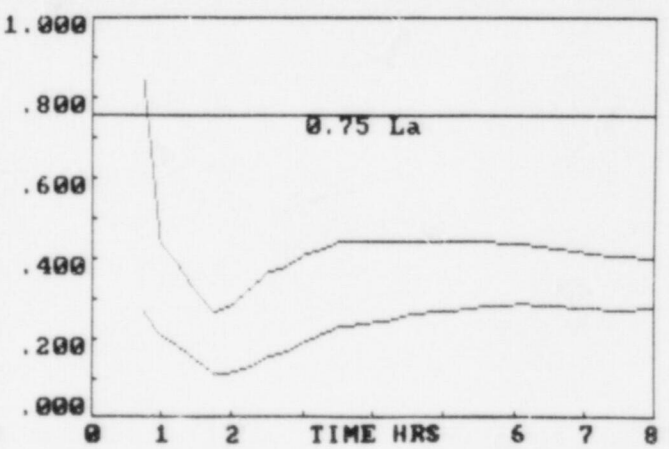
HYBRID LEAKAGE RATE AND UCL - %/DAY



PREDICTOR %



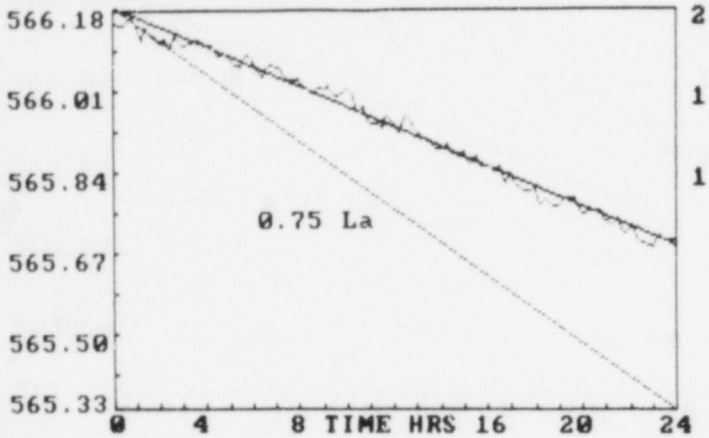
TOTAL TIME LEAKAGE RATE AND UCL - %/DAY



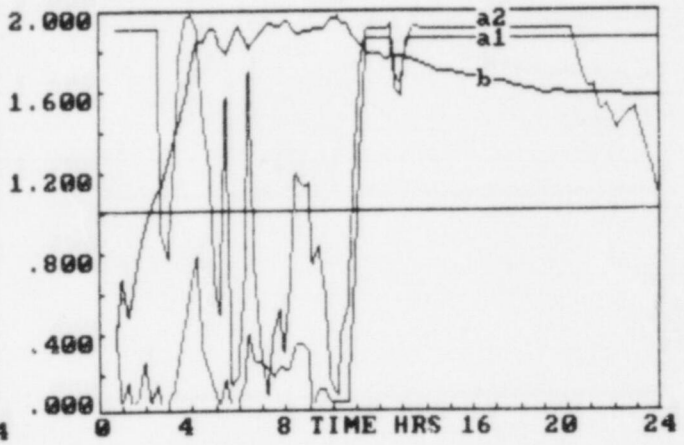
CASE 12

Case 12 is a 24 hr test, PWR, fans and coolers off, 1.8×10^6 ft^3, 24 RTD's, 2 pressure gages, and 5 dewcells. The airmass plot exhibits a moderate amount of scatter and nearly linear shape. Parabolic inequalities a.1 and a.2 are not satisfied from 11.25 to 24 hrs. The a.1 and a.2 inequalities seem to indicate that an 3 to 11 hr test more accurately determines the leakage rate than a 12 to 24 hr test. This is inconsistent with the data.

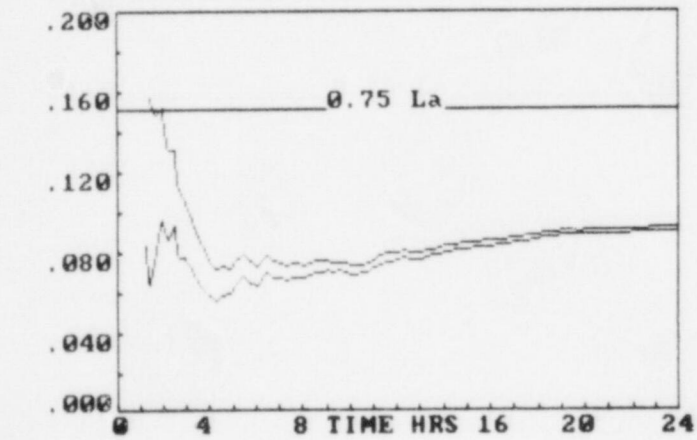
AIRMASS LBM X 1000 AND REGRESSION LINE



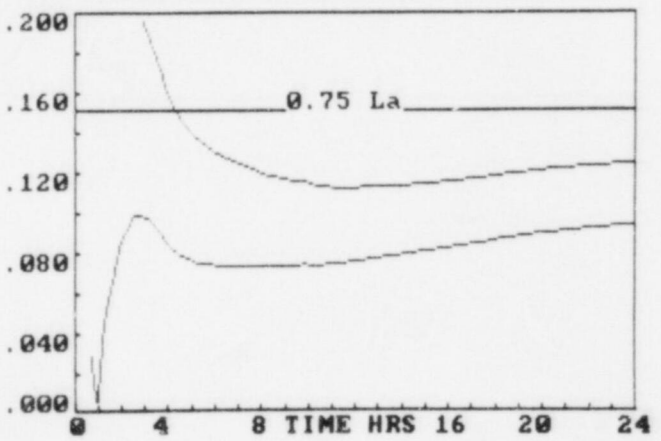
PARABOLIC INEQUALITIES a1 a2 b RATIO



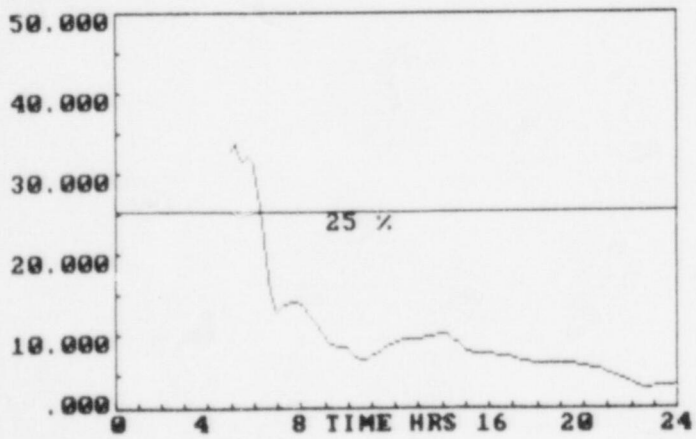
MASS POINT LEAKAGE RATE AND UCL - %/DAY



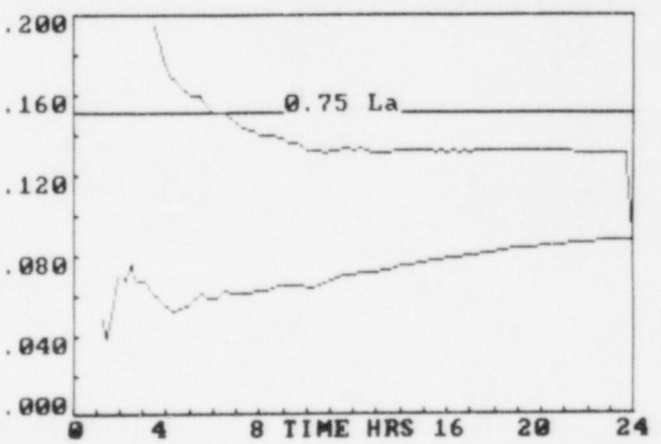
HYBRID LEAKAGE RATE AND UCL - %/DAY



PREDICTOR %

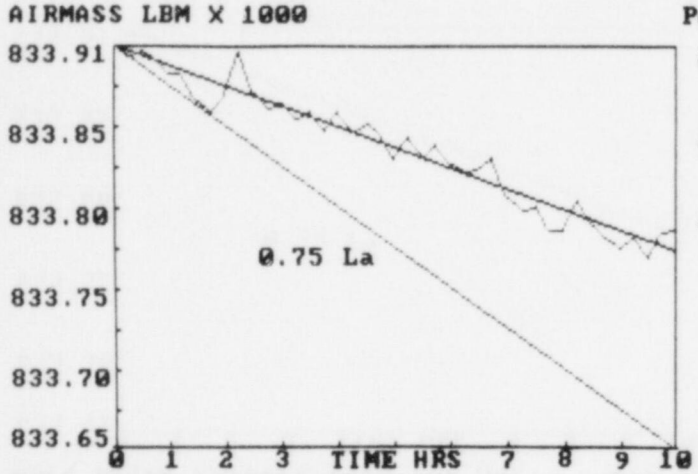


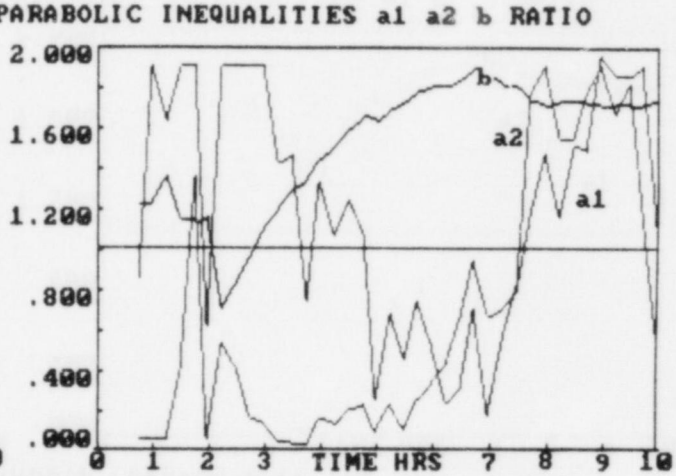
TOTAL TIME LEAKAGE RATE AND UCL - %/DAY

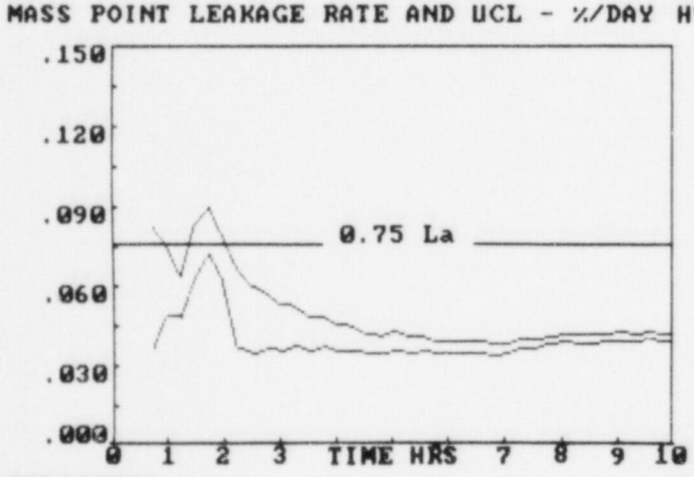


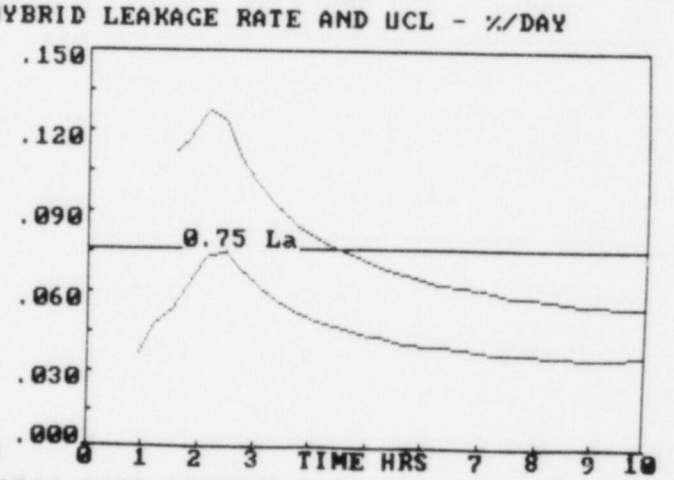
CASE 13

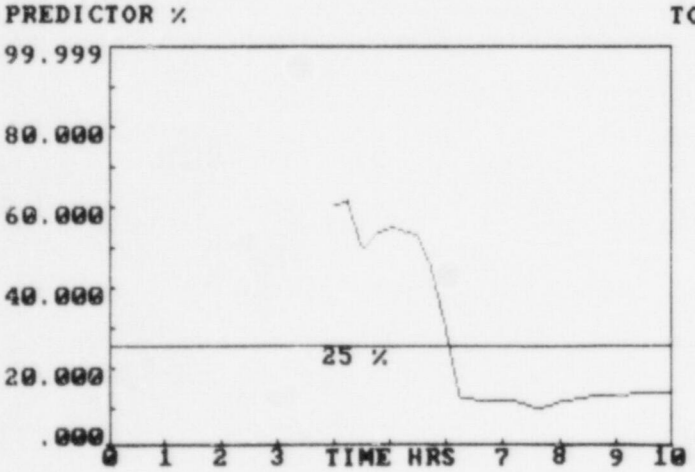
Case 13 is a 10 hr test, PWR, fans and coolers off, 2.3×10^6 ft^3, 18 RTD's, 2 pressure gages and 4 dewcells. The airmass plot exhibits a moderate amount of scatter and nearly linear shape. Parabolic inequalities a.1 and a.2 are not satisfied from 7.75 to 9.75 hrs. This unsatisfied period is inconsistent with the nearly linear data, demonstrating that a.1 and a.2 are excessively sensitive.

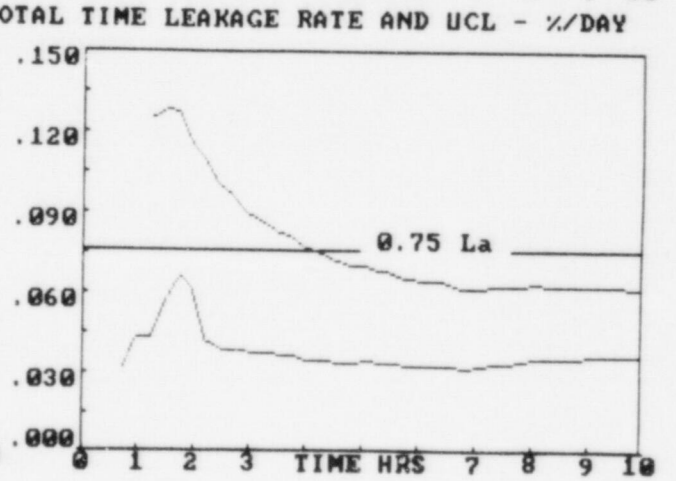






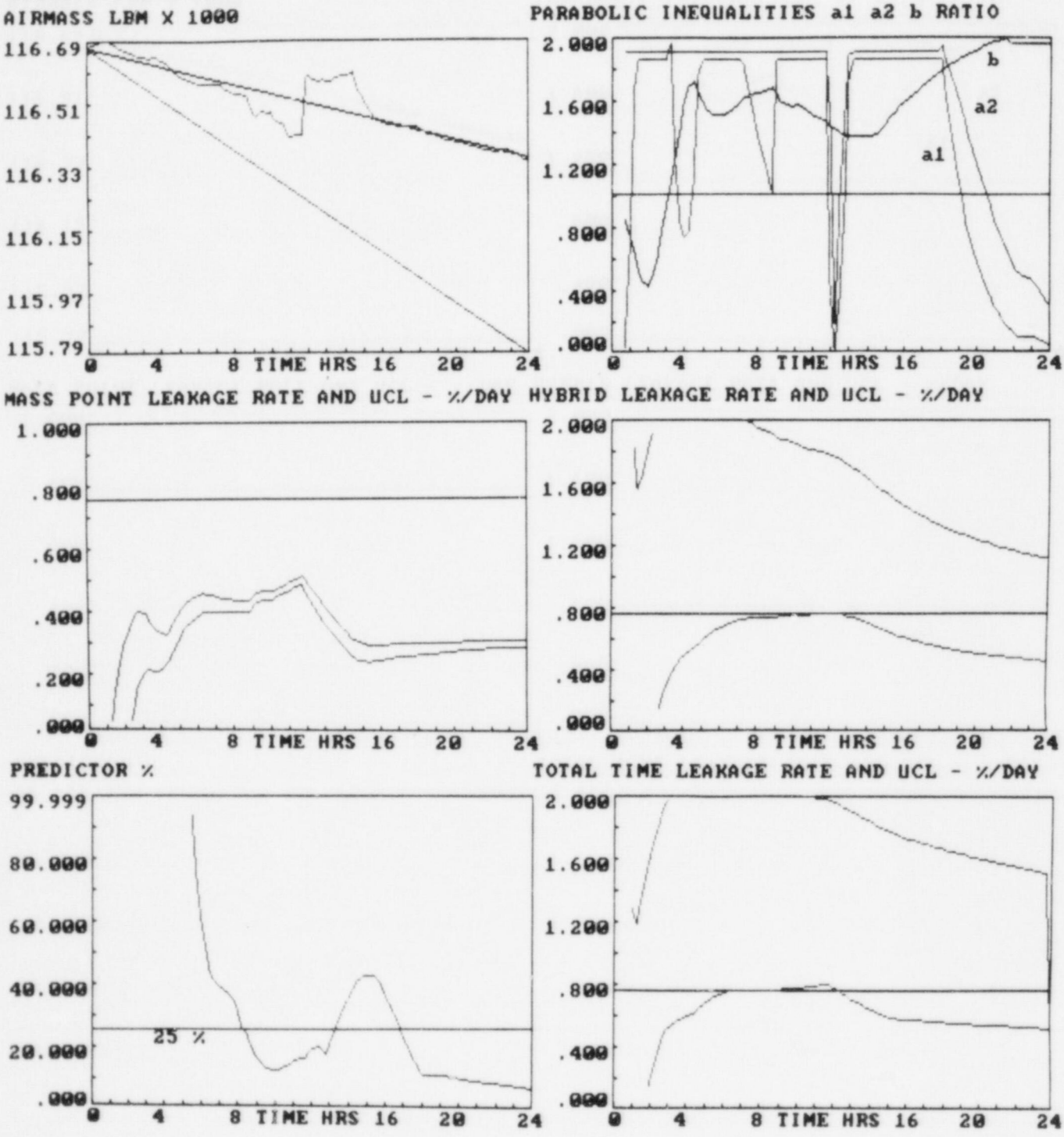






CASE 14

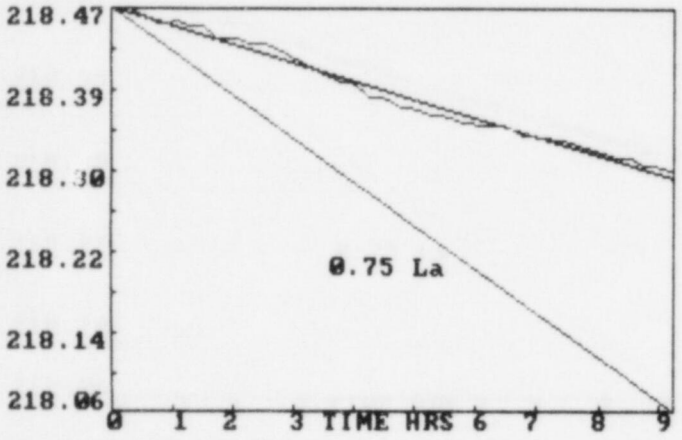
Case 14 is a 24 hr test, BWR, fans and coolers off, $4x10^5$ ft^3, 24 RTD's, 2 pressure gages, and 9 dewcells. The airmass plot exhibits a large amount of scatter and overall linear shape, with a large transient at 12 hrs. Parabolic inequalities a.1 and a.2 are satisfied from 12 to 12.75 hrs, during the transient, and from 19 to 24 hrs. This satisfied period during the transient at 12 hrs demonstrates that a.1 and a.2 are excessively sensitive to transients. The Hybrid is never satisfied.



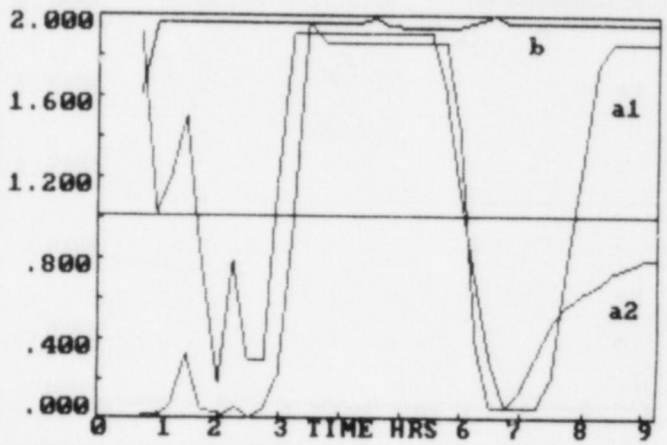
CASE 15

Case 15 is an 9.25 hr test, BWR,fans and coolers off, 1.8 x10^6 ft^3 30 RTD's, 2 pressure gages, and 9 dewcells. The airmass plot exhibits a very small amount of scatter and nearly linear shape. Parabolic inequalities a.1 and a.2 are not satisfied from 3.25 to 6 hrs caused by a very small deviation of the air mass from the regression line as shown on the air mass graph. This is inconsistent with the nearly linear data with a small amount of data scatter, demonstrating that a.1 and a.2 are excessively sensitive.

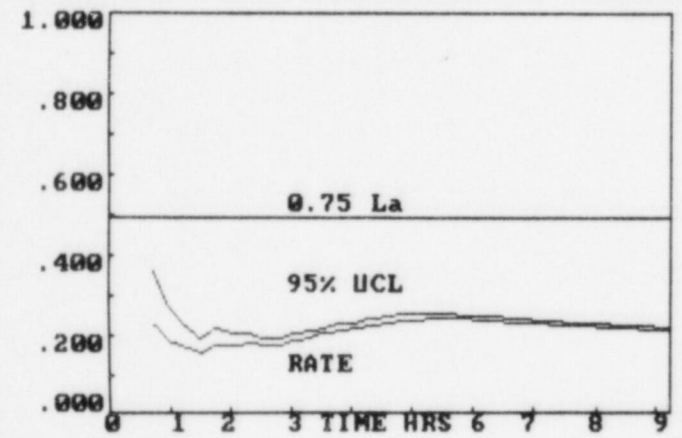
AIRMASS LBM X 1000 AND REGRESSION LINE



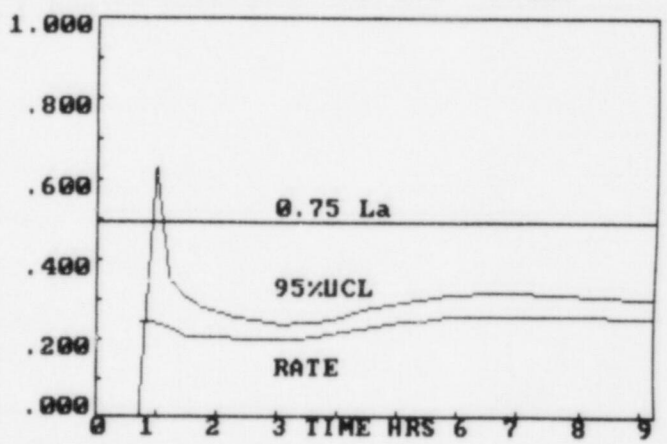
PARABOLIC INEQUALITIES a1 a2 b RATIO



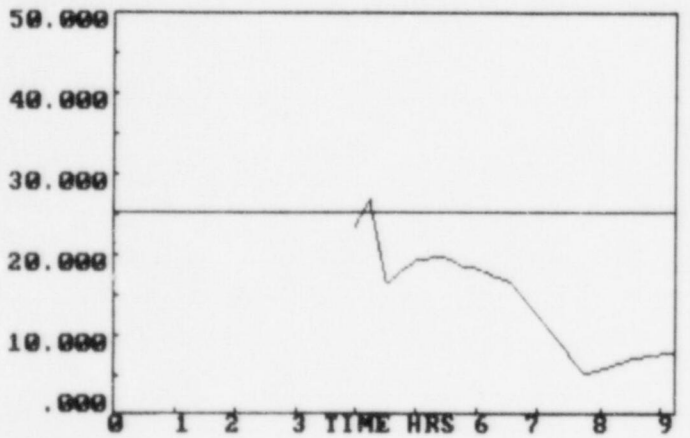
MASS POINT LEAKAGE RATE AND UCL - %/DAY



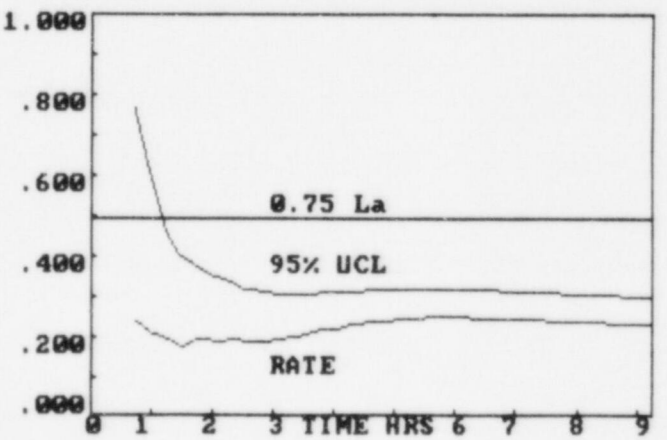
HYBRID LEAKAGE RATE AND UCL - %/DAY



PREDICTOR %



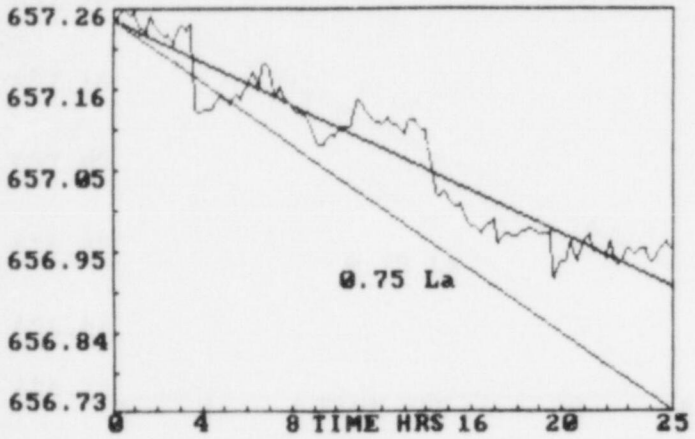
TOTAL TIME LEAKAGE RATE AND UCL - %/DAY



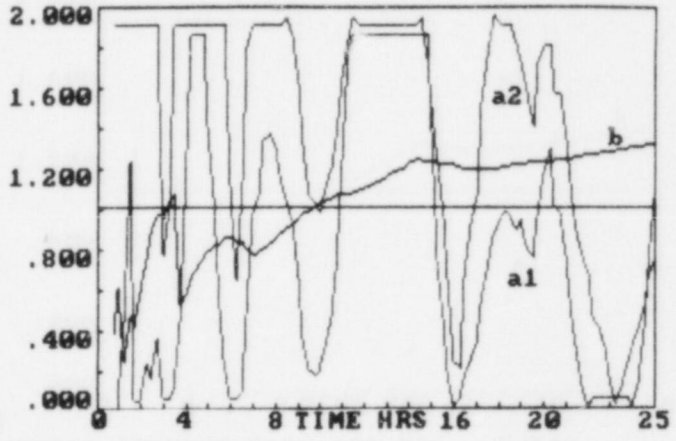
CASE 16

Case 16 is a 24 hrs test, PWR, fans and coolers off, $2x10^6$ ft^3, 24 RTD's, 2 pressure gages, and 6 dewcells. The airmass plot exhibits a large amount of scatter. Parabolic inequalities a.1 and a.2 are not satisfied from 4 to 5.25, 8 to 8.5, 10.75 to 15 and from 19.75 to 20.5 hrs. The high sensitivity of the a.1 and a.2 inequalities to data scatter is demonstrated in this case as the conditions are alternately satisfied and not satisfied five times in 25 hrs.

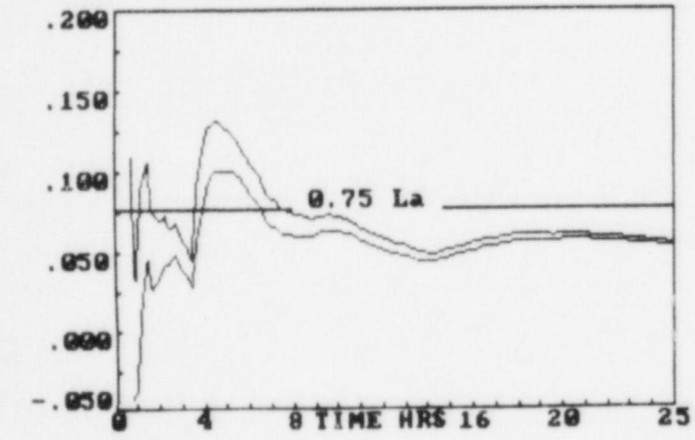
AIRMASS LBM X 1000 AND REGRESSION LINE



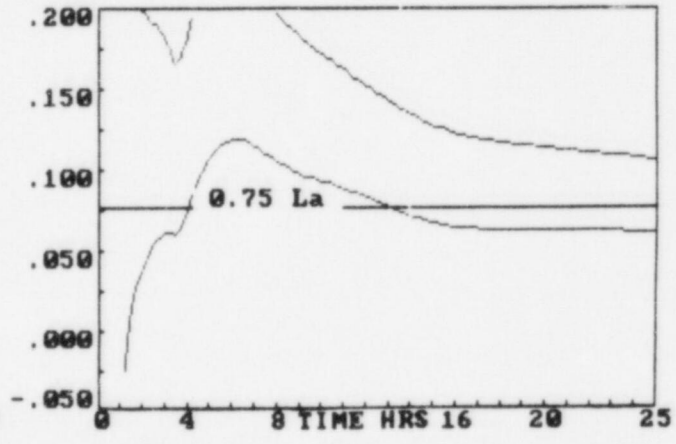
PARABOLIC INEQUALITIES a1 a2 b RATIO



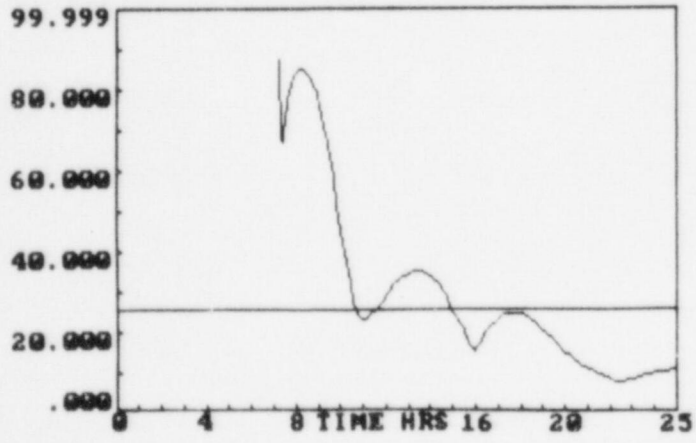
MASS POINT LEAKAGE RATE AND UCL - %/DAY



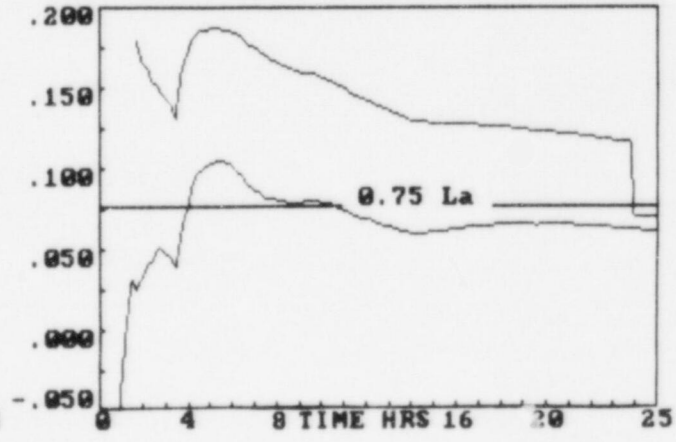
HYBRID LEAKAGE RATE AND UCL - %/DAY



PREDICTOR %



TOTAL TIME LEAKAGE RATE AND UCL - %/DAY



ALTERNATIVE CONTAINMENT INTEGRITY TEST METHODS, AN OVERVIEW OF POSSIBLE TECHNIQUES*

Barry L. Spletzer

Sandia National Laboratories
Albuquerque, NM 87185

ABSTRACT

A study is being conducted to develop and analyze alternative methods for testing of containment integrity. The study is focused on techniques for continuously monitoring containment integrity to provide rapid detection of existing leaks, thus providing greater certainty of the integrity of the containment at any time. The study is also intended to develop techniques applicable to the currently required Type A integrated leakage rate tests. A brief discussion of the range of alternative methods currently being considered is presented. The methods include applicability to all major containment types, operating and shutdown plant conditions, and quantitative and qualitative leakage measurements. The techniques are analyzed in accordance with the current state of knowledge of each method. The bulk of the techniques discussed are in the conceptual stage, have not been tested in actual plant conditions, and are presented here as a possible future direction for evaluating containment integrity.

While the results of the study are still preliminary, some observations and conclusions have been made. Of the methods considered, no single method provides optimum performance for all containment types. Several methods are limited in the types of containment for which they are applicable. Preliminary economic and plant impact considerations have shown that the cost of implementation of a technique is not necessarily related to the sensitivity of the technique. The results of the study to date indicate that techniques for continuous monitoring of containment integrity exist for many plants and may be implemented at modest cost.

---

* This work was supported by the U. S. Nuclear Regulatory Commission and performed at Sandia National Laboratories which is operated for the U. S. Department of Energy under Contract Number DE-AC04-76DP00789.

1.0 INTRODUCTION

Integrated leak rate testing (ILRT), which is required at about three-year intervals, provides an accurate and reliable assessment of containment integrity. Due to the relatively long period between these tests, undetected breaches of containment integrity (UBCI) may be present during plant operation. Methods to assess the performance of containment between ILRTs exist and are employed at some plants. Sandia National Laboratory is studying existing methods and developing new methods for the assessment of containment integrity during the time between ILRTS. To date, a wide range of methods have been conceived and assessment of the methods in terms of feasibility, sensitivity, and accuracy is underway. Several of these methods are presented briefly here along with a background discussion of the underlying principles, advantages, and limitations of containment integrity monitoring in general.

2.0 BACKGROUND

The requirements and limitations of systems designed to assess containment integrity on a continuous basis are significantly different from those of Type A testing. The following paragraphs present some of the more important issues applicable to continuous containment integrity monitoring techniques in general.

2.1 System Reliability

To be of practical importance, an alternative test method must be extremely reliable. It must reliably sense any UBCI within the range of sensitivity of the device in order to be useful in the measurement of containment integrity. Further, the method must not sense an UBCI when no such breach exists since this could result in shutdown of a plant. These two constraints leave a condition which requires extreme certainty as to the existence or absence of an UBCI. A set of approaches to these constraints has been developed. The first approach is to design methods which are inherently simple and reliable and do not rely on extremely sophisticated equipment. Where possible the methods should incorporate fail-safe attributes which would provide obviously erroneous readings in the event of most system failures. The second design approach is to develop techniques which are very sensitive but are only used to measure total integrated leakages which are much larger than the sensitivity limit. A final approach is that of redundant or verification type systems where reasonable agreement between the two systems is required before the system measurements are accepted.

2.2 Reduced Pressure Leakage Rate

An issue of general concern in any continuous monitoring technique is that of correlation of leakage rate at reduced containment pressure to the leakage rate through the same path at higher

pressures. A typical Type A test pressure is 50 psig (350 kPa), while operating pressures in containments may be 1 psig (7 kPa) or less and in no case greater than about 6 psid (40 kPa) [1]. While the reduced pressure does cause a reduction in leakage rate, the leakage, when measured in terms of per cent of enclosed mass leakage per day, is not reduced by as much as might be expected. For example, consider the leakage rate through a 50 foot (15 m) tube at various low pressures compared to the leakage through the same size tube at 50 psig (350 kPa). Figure 1 is a plot of the ratio of leakage at reduced pressure to that at 50 psig (350 kPa) versus the leakage rate in per cent of enclosed mass per day at 50 psig (350 kPa). This plot illustrates that, for leakage rates on the order of La, the mass per cent per day leakage at 1 psig (7 kPa) is 0.25 times the mass per cent leakage per day at 50 psig (350 kPa). While this comparison is not intended to cover leakage paths in general and makes no provision for pressure induced changes in leakage path geometry or leak paths which are initiated at elevated pressures, it does provide a reasonable indication that significant amounts of leakage can exist at reduced pressures [1].

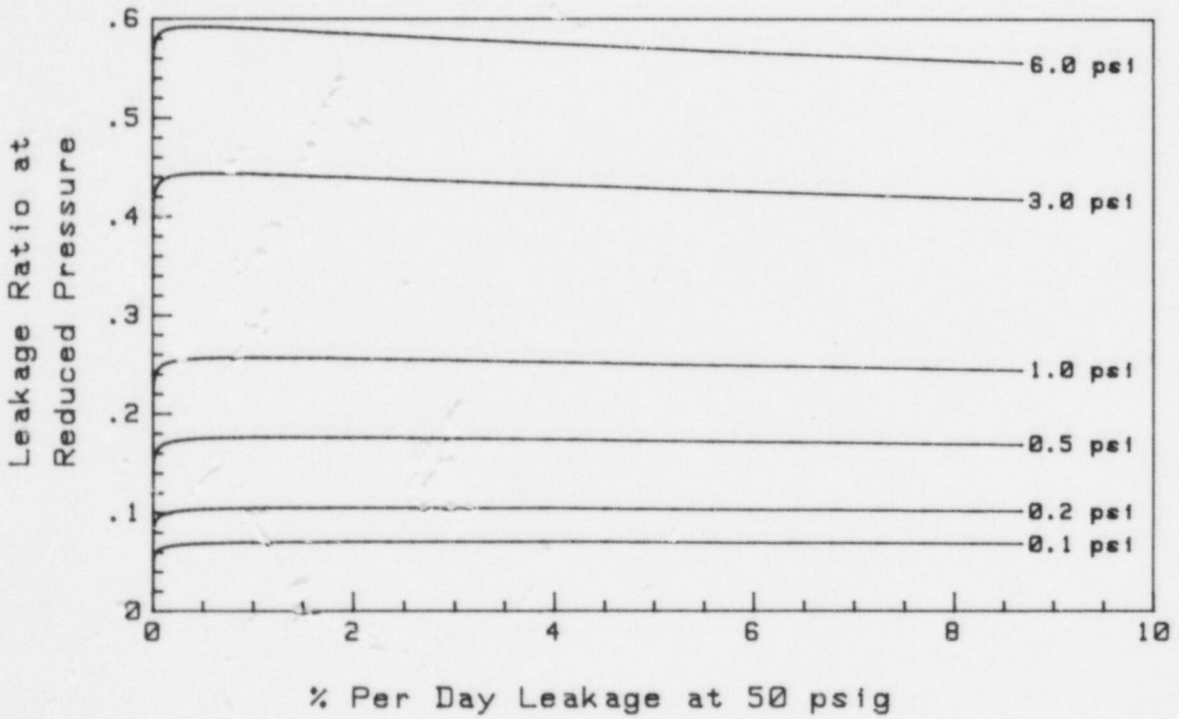


Figure 1: Leakage Ratios at Reduced Pressures Compared to Leakage at 50 psig for 50 Foot (15 m) Tubing

2.3 Leakage Rate Sensitivity

While a system capable of detecting only large UBCIs is of use, systems which can detect leakage rates on the order of the maximum allowable rate (termed La, which may be as low as 0.1% contained mass per day at test pressure) provide the most benefit by detecting the largest portion of unacceptable leaks. Detection of such small leakage rates is not usually as difficult for continuous monitoring techniques as it is for Type A testing. This is because extended time periods which are available for continuous monitoring are not available during ILRTs. There are economic advantages to restricting Type A tests to no more than 24 hours. While, for continuous monitoring, several weeks may be available. The amount of time available for a monitoring cycle in an operating plant is usually the time period between purge or vent cycles. This length of time may vary from months to a few hours depending on plant type and operating practice. The largest factor affecting the time available has been found to be the source and usage rate of instrument air. Plants with high usage of externally sourced instrument air may vent continuously or once per shift, while plants with internally sourced air or low usage rates may not vent at all during operation [1]. In plants where extended time periods are available, relatively insensitive systems may be used to measure small leakage rates by observing the total mass change over a long time period.

Most continuous monitoring techniques become more sensitive to a given leakage rate as the time of detection is increased. This is caused by the fact that most methods use a mass determination scheme somewhat like Type A testing which results in a larger signal with increasing time interval. In the methods discussed, sensitivities are usually expressed in terms of the minimum leakage rate which could be detected in the time available between upsetting influences such as containment purging. The per cent leakage per day figures will be in terms of per cent per day at test pressure, making use of the circular tubing leakage rate correlation previously presented in Figure 1 (i.e. for 1 psig (7 kPa) available, a 4 to 1 ratio exists).

2.4 Dew Point Measurements

Type A testing requires accurate dew point measurement using relatively complex instrumentation. Dew point measurement can be extremely important in elevated pressure testing since the dew point will normally be reached if undried air is used to pressurize the containment. Dew point measurements may not be necessary for some continuous monitoring methods since high pressure is not used and, in the case of many large, dry containments, humidity levels are low and reasonably invariant.

3. EXISTING TECHNIQUES

To varying degrees, three continuous monitoring techniques exist in operating plants. When discussing these techniques at operating plants, the concept of continuous monitoring has been given the broadest possible meaning such that, with the exception of the first method discussed, the methods are not used to give accurate and reliable measurements of leakage but rather only to indicate if a large UBCI exists. Three techniques are presented here.

3.1 Continuous Use of Type A Instrumentation

This method involves continuous monitoring of Type A instrumentation which is used during the periodic ILRTs. The instrumentation is left as is following a Type A test and used in the same way to continuously monitor the air mass within the containment. Venting or purging while the plant is operating is not performed. This method has been proven as being able to detect leakages of moderate size (several per cent per day) in a few hours. The sensitivity of the technique is on the order of that of the required Type A test since the same instrumentation is used. A slight reduction in accuracy could result from the pressure measurements for a pressure transducer where the minimum absolute error is larger than the specified portion of total reading error. The reduction and more controlled condition of the dew point, especially in the case of a large, dry containment, lends greater inherent accuracy to the method.

The single largest concern in the use of this method stems from the location and weighting of the temperature measurements. During shutdown, the atmosphere within containment is relatively quiet in terms of temperature gradients, convective currents and forced air velocities. While operating, more severe conditions are present due to the large amount of operating equipment and the much larger heat load in containment. For this reason, error in mass determination could result from inappropriate placement of the temperature sensors. For the method to be adequate for general use, a temperature weighting scheme for operating conditions should be conceived and tested to assure that the proper average containment temperature will be determined. Once this is done, the sensitivity of this method would be similar to that of Type A testing with an appropriate correction applied for the reduced pressure (about 4 to 1 for 1 psig (7 kPa)). Since the accuracy of the method is such that leakage rates on the order of La could be detected in a few days time, a redistribution of the temperature sensors would not necessarily be required if the error could be bounded by existing temperature data and used to determine a longer required time for leakage detection. An estimate of the sensitivity limit of the system for a large, dry containment can be made by assuming a 2 day available test cycle, yielding a detection limit of 0.2% per day leakage at test pressure.

The primary disadvantage of this method is the cost of application. Most plants do not leave the instrumentation installed during operation and, especially in the case of dewcells, extended operation of such a precision instrument within containment may not be realistic. A few plants use data multiplexing within containment during Type A testing and do not have sufficient penetrations to allow direct application. Also, in some cases, the data acquisition and computing equipment is brought to the plant for Type A testing and not available during normal operation. All these disadvantages can be overcome, if desired, resulting in a quite sensitive and effective continuous monitoring system which is applicable to all containment types.

3.2 Nitrogen Usage Monitoring

Most BWR containments are nitrogen inerted during operation using tanks of liquid nitrogen. Direct monitoring of nitrogen usage during operation can be a measure of containment leakage rates. Many BWRs do monitor nitrogen usage primarily from economic concerns of nitrogen cost. The monitoring technique frequently consists of periodic readings of liquid nitrogen tank levels. While this is not usually intended as a continuous containment integrity monitor, the practice is capable of detecting large UBCIs. With small modifications, monitoring of nitrogen usage may be applicable as a method to detect leakages on the order of L_a. These modifications would include the installation of an accurate mass flow meter in the nitrogen supply line and instrument air supply lines. Using data from these meters, coupled with approximate temperature (within 5°F (3°C)) and pressure values (within 0.01 psi (70 Pa)) within containment, leakages of about 0.5% per day could be detected between normal purge operations, with a typical purge frequency of 7 days being assumed. Without temperature and pressure data, leakage rates of about 2% enclosed mass per day may be detectable.

3.3 Continuous Exhaust

As currently employed, the exhaust of subatmospheric containments is sometimes monitored and may be used to indicate a leakage rate into containment. Leaks are assessed qualitatively by the duty cycle of the exhaust fans or the inability to maintain specified vacuum levels within containment. The capability exists to measure the exhaust flow and correlate it directly with leakage into containment or couple the integrated flow rate with basic temperature and pressure data to provide a more sensitive and rapid method of leakage rate estimation. Since the purge and vent cycle in subatmospheric containments is very long (up to several months), any alternative test method in those containments will yield an extremely small minimum detectable leakage rate. A more practical measure of system capabilities is the length of time required for detection of a leak of interest, say 1% enclosed air mass per day at test pressure. For the subatmospheric containment with no

temperature data used such a leakage rate could be detected in about 36 hours. This may be an overly optimistic estimate due to the lack of available data on dew point fluctuations during operation.

4. POTENTIAL NEW MONITORING TECHNIQUES

The methods presented here have not been applied to leak detection or measurement in the nuclear power industry. However, because they appear promising, these methods will be assessed in the near future. Generally,the methods do not measure the leakage rate directly but rely on a measurement of enclosed mass change over a given period of time to produce leakage rate estimates similar to Type A test methods. It is not expected that all the methods described will prove practical after the final analysis is complete.

4.1 Inert Tracer Concentration Monitoring

This method is primarily suited to subatmospheric containments and may provide a reliable and sensitive technique which can be implemented at low cost. The method involves release of an inert tracer gas, such as Neon, in small amounts (about 100 to 1000 ppm) in containment. After release, the mass concentration of the tracer in air is measured. As leakage into the subatmospheric containment occurs and appropriate atmosphere is exhausted, the inleakage dilutes the concentration of the tracer by an amount proportional to the total mass fraction of inleakage. A measure of mass concentration of the tracer is then used as a direct measure of total integrated leakage over the time between measurements. As small leakage continues over extended periods of time, more tracer gas must be periodically introduced as needed to maintain the levels needed for reliable concentration measurements.

While data on concentration measurement capabilities has not yet been gathered, an estimate of detection limits can be made assuming an accuracy of 1% in concentration monitoring. This technique exhibits complete insensitivity to pressure, humidity and temperature fluctuations resulting in a total error which is dependent only on the monitoring equipment. The low error limit, coupled with high available differential pressure (6 psid (40 kPa)) for subatmospherics, could allow for detection of a 1% enclosed mass per day leak at pressure in 2 days.

This technique is best suited for subatmospheric containments, but may be applied to any containment where a pressure below atmospheric is acceptable. This includes most large, dry PWRs. In the case of a large, dry containment, a maximum differential pressure of 1 psi (7 kPa) may be available. Compared to the typical value of 6 psid (40 kPa) for subatmospheric containments, the time response of the system on a large, dry containment would be approximately twice as long.

This method requires a minimum of instrumentation and, at most, a few concentration measurement sites are required. From the standpoint of implementation, it appears to have minimal impact on plant operation and procedures.

4.2 Direct Air Weighing

The weight of air within containment generates a differential pressure between the top and bottom of the building which is proportional to the product of the height and density of the enclosed air. At normal atmospheric conditions, the magnitude of this pressure is about 0.075 pounds per square foot per foot (12 Pa/m) of elevation. A system capable of accurately measuring this differential pressure would be able to give a direct indication of the total enclosed air mass within the containment. A system of this type has been devised and is illustrated in Figure 2. The system consists of two differential pressure transducers, a connecting tube, and the appropriate control and recording equipment.

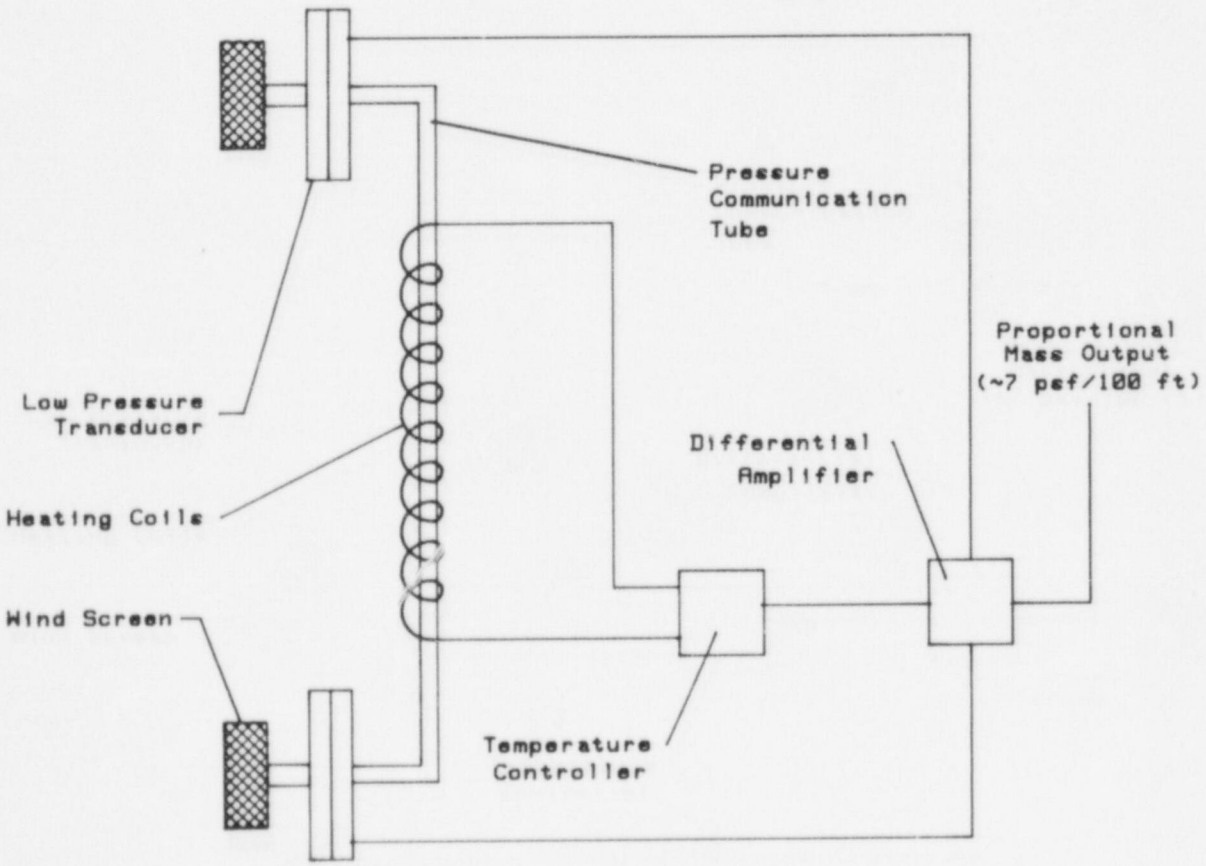


Figure 2: Schematic Representation of Direct Air Weighing Method

The system is installed with one pressure transducer near the top of the containment and the other near the bottom. The connecting tube is filled with dry air and sealed. Since the mass of air in the connecting tube is constant, the differential pressure between the tube ends is constant for any tube end elevation difference. To provide sufficient sensitivity and resolution, the pressure transducers must have a very narrow range. A typical required range for them is about 5 psf (1 inch of water, 240 Pa) for normal operation and 100 psf (5 kPa) for use in Type A testing. Transducers installed for continuous monitoring would need to be removed or isolated to prevent overpressurization during Type A testing. Since the atmospheric pressure is much larger than the range of the transducer, the temperature of the gas in the tube must be controlled to keep the differential pressure across each transducer as low as practical. This allows for the use of very low pressure range transducers. The difference in the pressure value of the two transducers is a direct measure of the weight difference of the enclosed column of air and a column of containment atmosphere of equal height. This measure can be determined by multiplying the total differential pressure by an appropriate cross-sectional area.

This method is insensitive to temperature and pressure changes in containment but does not compensate for humidity changes since the total weight of water vapor is included in the weighing process. The requirement of an effective cross-sectional area places the greatest restriction on the method in that a relatively open or constant open cross-section geometry is needed. This restricts this method to large, dry and subatmospheric containments since BWRs and ice condenser containments do not contain any large or open areas. Sensitivity of the method is limited by the resolution of the pressure transducers and the range of water vapor mass in the atmosphere. Initial work indicates that available transducers should produce a mass value that is within 1% of the actual value by total pressure reading and possibly within 0.1% if the connecting tube is used to adjust the sum of the transducer readings to zero. For large, dry containments, the range of humidity typically seen is on the order of 5 to 10% R.H. which corresponds to 0.4% of the total air mass. This results in a maximum sensitivity of 1.4% of the enclosed mass, which would give a detection of a 1% enclosed mass per day leakage rate in 6 days. With optimization of the connecting tube temperature, a detection time of 2 days could be realized. Use of dew point instrumentation could reduce the detection time to as little as 12 hours.

This method provides detection of moderately small leakage rates in time periods compatible with venting and purging operations of many large, dry containments. Instrumentation requirements are modest and a single reading yields the contained mass directly. Improvements in detection time and accuracy could be achieved through use of some humidity instrumentation. Application of the technique is limited to large, dry and subatmospheric containments.

4.3 Integrated Bulk Temperature Determination

Containment air mass determination using the ideal gas relation requires determination of both pressure and temperature. Pressure determination is straightforward since the pressure throughout containment is relatively uniform. The determination of an average temperature is somewhat more complex. Temperature values vary across containment and operating temperatures are typically less uniform than shutdown temperatures resulting in greater difficulty in accurately determining air temperatures for continuous monitoring than for Type A testing. The method discussed here provides the means for determining the average temperature of an open body of air without using the typical RTDs throughout the containment volume. Before the specific method is discussed some background in the meaning and use of average temperature values is needed.

Current Type A testing uses the ideal gas relation to determine air mass from the gathered data. According to the ideal gas relation:

$$PV = mRT$$

Where:

P = Containment pressure
V = Containment volume, constant
m = Total enclosed containment air mass
R = Ideal gas constant
T = Air temperature

Rewriting the expression, mass contained becomes:

$$m = \frac{PV}{RT}$$

For Type A testing, the total mass is considered to be the sum of a finite number of equal pressure volumes where the i subscript refers to the volume segment:

$$m = \frac{P}{R} \sum_{i=1}^{n} \frac{V_i}{T_i}$$

This may also be written in integral form using an infinite number of subvolumes:

$$m = \frac{P}{R} \int_{V} \frac{dv}{T}$$

While Type A testing uses the summation form, the integrated bulk temperature determination methods will incorporate the integral form of the mass equation. A correct representation of the enclosed mass may be determined by summing the volume to absolute temperature ratios or integrating the reciprocal absolute temperature over the volume.

A properly weighted absolute temperature can be obtained by measuring the time of transit of an acoustic or electromagnetic wave across the volume if the velocity of the wave is proportional to the absolute temperature. The time of transit is directly proportional to the reciprocal temperature integral. This assumes a constant cross section perpendicular to the direction of beam travel in the conversion from length to volume of air. The reduction of the velocity of light through a gas as compared to a vacuum is proportional to the absolute temperature of the gas. The additional time of transit of a light beam across the volume compared to the time to cross a vacuum is a direct measure of the properly weighted temperature of the gas for mass determination. The need for a reference beam to estimate the time increase does not allow for practical use of this method as described. However investigation has begun to determine the time of transit by accurately measuring the frequency required to maintain a standing radio wave across the containment. Such a system could prove sufficiently accurate, but no quantitative data are yet available.

Acoustic waves offer another approach to the problem. An acoustic wave does not give a properly weighted temperature for any temperature profile since acoustic velocity through an ideal gas is proportional to the square root of the absolute temperature. While the resulting relationship between transit time and average temperature is not exact, it does allow an error bound to be calculated. A measure of the average reciprocal temperature is the square of the time of transit. Since the function is correct if the temperature is uniform, an upper bound to the temperature error can be determined by assuming that each section of the volume is at either the maximum or minimum containment temperature. Performing the bounding calculation shows that, for a temperature range of 50°F (28°C), the error bound is 0.25% of the absolute temperature. For 100°F (56°C), it is 1%. This method does require accurate pressure determination similar to that used in Type A testing and does not compensate for humidity changes. Further, the technique is only applicable to relatively open areas of a containment. Combining the humidity variations with the error inherent to acoustic velocity measurement results in detection of a 1% leak in 6 days time in any containment and in 2 days or less for most PWRs. A system for determining the transit time of acoustic waves would most likely be based on the standing wave frequency as was the case with radio waves, but direct timing of the wave may also be possible with sufficient accuracy.

Equipment and implementation costs for this system appear relatively small, although stock equipment for standing wave and sonic transit time in such a volume may not be commercially available and multiple systems could be needed to provide sufficient data to evaluate the whole containment temperature.

4.4 Periodic Mass Injection

This method involves periodic injection of a known air mass and monitoring of the resulting pressure rise in containment. Assuming that the air is injected over a relatively short period of time such that the average containment temperature does not change during the injection, the ratio of the pressure rise to the total containment pressure before injection is equal to the ratio of injected air mass to total air mass before injection. The contained air mass can be determined this way on a periodic basis, such as following and immediately preceding each purge operation, and the leakage rate over the time period can be inferred. The method is not affected by temperature and pressure changes except those which occur during the injection and pressure measurement period. The method does not compensate for humidity changes, but the resulting error could be greatly reduced by using a single dew point measurement to determine the water vapor mass or using air with the same dew point for injection.

The method is prone to certain inaccuracies caused by the very accurate measurement of a small change in pressure imposed upon the existing atmospheric pressure. Consider the case where 1% of the total enclosed mass is added to a 2,000,000 cubic foot (57000 m^3) containment originally at 15 psia (100 kPa). This requires an air input of 2000 scfm (0.1 m^3/S) for 10 minutes, which is sufficiently short to satisfy the assumption of no temperature change during injection. If instrument accuracies as specified in ANSI/ANS 56.8 [2] are used, absolute pressure readings within 0.02% of actual can be obtained and an injected mass error of no more than 2% may be expected. For the 1% injected mass, the maximum error in pressure change will be 2% resulting in a total error in mass determination of no more than 4%. This requires a total leakage of greater than 4% before assurance of a leak is obtained which indicates, in turn, that the sensitivity of the system is limited to leaks at pressure of about 3% per day, assuming a five-day purge cycle. These error limits could be reduced by proper instrumentation, but the requirement for instrumentation with greater accuracy than that used for Type A testing is not considered practical for an operating sytem. The technique can also be done in reverse, where an air mass is removed rather than injected.

4.5 Reference Vessel Continuous Monitoring

Reference vessels consisting of a run of tubing or piping running throughout the containment have been used in ILRTs. The theory of the method is that the reference vessel is in thermal equilibrium with the local containment atmosphere, resulting in a reference vessel pressure which is a measure of the average containment temperature. Difficulties with the reference vessels led to discontinuing their use in ILRTs in favor of the absolute method. It is possible, however, that reference vessels may be used effectively in continuous monitoring techniques.

One of the methods conceived uses a run of tubing, continuous or seal welded, as the reference vessel and measures the absolute pressure of the reference vessel and the containment to determine the air mass in the containment. This method assumes that the density of air in the reference vessel is a constant and known value and the temperatures of the reference vessel and the containment are the same. The ideal gas equation for the reference vessel is:

$$P_r V_r = M_r R T$$

Where:

Pr = Reference vessel absolute pressure
Vr = Reference vessel volume, constant
Mr = Reference vessel contained mass, constant
R = Ideal gas constant
T = Reference vessel and containment absolute temperature assumed equal.

So the temperature of the reference vessel, which is the average temperature of the containment is:

$$T = \frac{P_r V_r}{M_r R}$$

Where $V_r/M_r R$ is a known constant. The mass of air in containment is then:

$$M_c = \frac{P_c V_c}{RT} = \frac{P_c V_c M_r}{P_r V_r}$$

Where:

Mc = Mass within containment
Pc = Absolute pressure of containment
Vc = Containment volume, constant

The contained air mass may be determined from the two pressure values and known constants. Greater inherent accuracy may be obtained by using one absolute pressure and the differential pressure between the two vessels. The differential pressure gage used can be a relatively narrow range gage which could achieve accuracy of 0.2% in mass leakage determination. The use of the absolute pressure of the reference vessel introduces a second 0.2% maximum error. Since this method does not account for partial pressure of water, additional errors on the order of 0.4% could result in a large, dry containment. The total expected error, and minimum detectable integrated leakage is then 0.8%, which corresponds to detection of a 1% leak in 3 days.

4.6 External Tracer Detection

Unlike the other methods presented, external tracer detection does not provide an accurate quantitative measure of the leakage rate but rather can give only an indication that a large UBCI is present. The method relies upon the use of a tracer element within containment which is detected external to the containment at an extremely reduced concentration. The scope of this concept could include detectors at all containment penetrations and the use of tracers which are detected in a liquid or solid state after leaving containment. However, to provide the widest coverage of possible leakage paths and be feasible for application, only gaseous tracers are to be seriously considered in geometries where a small number of sensors are required. The tracer most likely to be used would be ozone, which would not be introduced into containment since it occurs naturally from ionizing radiation reacting with oxygen. No data are available to adequately assess the ozone level in an operating containment. Ozone was chosen because of its existence in containment and the relative ease of sensing very low concentrations in the atmosphere. Certain radioactive isotopes which are normally present in containment may also be considered.

Primary application of the system is to BWRs where a single effluent stack is present through which all leakage from containment passes. In this case a complete system would consist of two concentration monitors, one within containment and one in the effluent stack. The ratio of concentrations would be monitored and, if a predetermined level was reached, an unacceptable leakage rate would be assumed to exist. This method could also be considered as a backup or verification technique for one of the other direct leakage measuring techniques.

Application of the method to PWRs is to be considered only in those cases where reasonable certainty exists that possible leakage

will pass by a sufficiently small number of locations. Estimation of the sensitivity of this type of system has not yet been performed.

5. CONCLUSIONS

Several methods have been presented for monitoring containment integrity during plant operation. While it appears that a single optimum method for use in all containment types does not exist, a broad range of methods is available to provide rapid detection of an UBCI at most operating plants. It must be stressed that assessment of the techniques is in the early stages and none of the methods presented should be considered to be in its final form at this time.

Methods capable of detecting leakage rates on the order of allowable containment leakage (La) have been presented along with techniques which have minimum sensitivities an order of magnitude greater than La. No definite correlation between sensitivity of a method and cost appear to exist. Methods presented cover a wide range of underlying principles and theories of operation. The existence of multiple techniques using different underlying principles affords the possibility of multiple systems which could provide independent verification of existing leakage rates.

The impact of application of these methods, when fully developed could be an improvement in the level of confidence in containment integrity accomplished at modest cost.

REFERENCES

1. A Summary of Containment Integrated Leakage Rate Testing Techniques Including Limitations and Advantages of Continuous Integrity Monitoring, B. L. Spletzer, Sandia National Laboratories, Draft report, SAND86-1115, to be published.

2. Containment System Leakage Testing Requirements, ANSI/ANS 56.8-1981, American Nuclear Society, February 1981.

SESSION C

CONTAINMENT ENVIRONMENT AND LOADING CONDITIONS
DURING SEVERE ACCIDENTS

Integrated Analysis of Core Debris Interactions and Their Effects on Containment Integrity Using the CONTAIN Computer Code*

Daniel E. Carroll, J. L. Tills**, G. D. Valdez***
K. D. Bergeron, and D. C. Williams
Sandia National Laboratories
Albuquerque, New Mexico 87185

ABSTRACT

The CONTAIN computer code includes a versatile system of phenomenological models for analyzing the physical, chemical and radiological conditions inside the containment building during severe reactor accidents. Important contributors to these conditions are the interactions which may occur between released corium and cavity concrete. The phenomena associated with interactions between ejected corium debris and the containment atmosphere (Direct Containment Heating or DCH) also pose a potential threat to containment integrity. In this paper, we describe recent enhancements of the CONTAIN code which allow an integrated analysis of these effects in the presence of other mitigating or aggravating physical processes. In particular, the recent inclusion of the CORCON and VANESA models is described and a calculational example presented. With this capability CONTAIN can model core-concrete interactions occurring simultaneously in multiple compartments and can couple the aerosols thereby generated to the mechanistic description of all atmospheric aerosol components. Also discussed are some recent results of modeling the phenomena involved in Direct Containment Heating.

* This work supported by the United States Nuclear Regulatory Commission and performed at Sandia National Laboratories which is operated for the U.S. Department of Energy under Contract Number DE-AC04-76DP00789.

** J. L. Tills and Associates,Inc., Albuquerque, New Mexico

*** Technadyne Engineering Consultants Inc., Albuquerque, New Mexico

I. INTRODUCTION

This paper discusses the use of the CONTAIN computer code to model and predict phenomena which may threaten containment integrity during and following the release of molten core debris in a severe reactor accident. CONTAIN also calculates radiological conditions inside the containment, but this aspect of the analysis will be described only briefly. We will describe recent enhancements to modeling capabilities in CONTAIN which are relevant to core debris interactions with the containment system in postulated severe reactor accidents. In particular, the incorporation of the CORCON and VANESA models for debris-concrete interactions will be described, as well as recent developments in modeling Direct Containment Heating (DCH) phenomena. Examples of the use of CONTAIN in simulations involving both debris-concrete interactions and DCH processes will be presented. These examples will demonstrate the importance of integrated system analysis for the proper understanding of the interactions of the pertinent physical mechanisms.

II. MODELING CAPABILITIES

CONTAIN offers a broad variety of models to the analyst in a system-level computational structure which allows for the complex interactions and feedback among the diverse phenomena treated. The models are activated by a keyword-driven input system which allows the user to tailor the degree of modeling complexity to the particular situation under consideration. Details of the models which may be activated in CONTAIN are presented in the CONTAIN User's Manual.[1]

Models employed in the code to account for phenomena occurring among the liquid and solid materials in a sump or cavity at the bottom of a compartment are collectively referred to as lower-cell models. A good deal of effort has recently been expended in this area, upgrading and improving the existing models and adding important new capabilities.

The lower-cell consists of layers of concrete, metals and/or oxides and coolant materials, all of which may be grouped and organized vertically as the user desires. Phenomena modeled in the lower-cell include heat transfer among the various layers, coolant pool boiling, and condensation/evaporation onto the coolant pool surface. New or improved features include radiative energy exchange between the surface of the lower-cell and the atmosphere and structures in a compartment, debris-concrete interactions using the CORCON model, and aerosol generation and radionuclide release associated with debris-concrete interactions as modeled by the VANESA code. As with other portions of the code, the user selects which models are active through the keyword-driven input.

II.1 CONTAIN-CORCON

CORCON is a widely used computer code for modeling the interactions between molten core materials and concrete. The physical models implemented in the code are explained in the CORCON Mod2 User's Manual [2] and will not be further described here. The version of

CORCON included in CONTAIN is the Mod2 version including some error corrections.

CORCON as implemented in CONTAIN runs much as it does in the stand-alone mode. It functions primarily as an effective source generator for CONTAIN, since the influence of the containment conditions on the debris layer evolution usually is not large. CORCON produces the gas sources for both the CONTAIN atmosphere and the VANESA aerosol generation calculation. It also provides an upper surface temperature (when a coolant pool is not present) that is used to compute the exchange of radiant energy with the compartment atmosphere and structures. While CORCON models a two-dimensional axisymmetric cavity, this information is not used directly by the other models in CONTAIN since the corium layer surface is the only physical interface considered. An important feature of the CONTAIN implementation of CORCON is that the user can include a debris-concrete interaction model in multiple compartments in a problem.

An important component of the physical interaction between the core debris and the rest of the containment system is the radiant energy introduced by the presence of the corium materials in the cavity. This radiant energy is coupled to the CONTAIN atmosphere and structure models by two alternative methods. In the most detailed approach, a net enclosure model is used to compute the radiant exchange between the gas, structures and the lower-cell layer. This model accounts for inter-reflections among the surfaces and represents the best estimate of the radiant energy budget. The model also requires the most detailed input definition, including structure-to-structure view factors.

A simpler model is also provided which treats the more typical case where radiation from a corium layer dominates the energy exchange. In this method, the layer exchanges energy with the gas and each structure, while structures exchange radiant energy with the gas alone. This model is approximate, but early results show good agreement with the more complete net enclosure results in those situations where the assumptions underlying the simple model are justified.

Both models make use of improved treatments of gas radiation properties which account for the presence of aerosols and optically active gas species (H_2O, CO, and CO_2). For those cases where only water vapor is present, a Cess-Lian[2] [3] correlation is used. When other species are present, a method developed by Modak [4] is employed.

II.2 CONTAIN-VANESA

The VANESA [5] code models the physical and chemical processes that result in the release of radionuclides and the production of aerosols during core debris interactions with concrete. As with CORCON, VANESA in CONTAIN runs much as the stand-alone code does, providing to CONTAIN the results of its calculations of aerosol sources and the radioisotope compositions of these aerosols. A flexible scheme has been developed in the CONTAIN implementation to allow the analyst to

choose a mechanistic treatment of the disposition of these aerosol-borne radioisotopes or to prescribe the final distribution of the radioisotopes via straightforward input structures. By such means, CONTAIN allows the determination of problem sensitivities and the evaluation of the effects of uncertainties in the modeling parameters.

There are a number of advantages to coupling VANESA directly to CONTAIN besides the obvious convenience of an integrated calculation. For example, the aerosols will affect the radiant heat exchange that takes place in the compartment, which is important to the accurate assessment of the amount of water vapor in the atmosphere. This quantity in turn has an important impact on the timing and severity of any potential hydrogen burns. Aerosol behavior also affects the location of decay heat sources. Most importantly, the radioisotope information furnished by VANESA is vital to assessment of the source term consequences of a containment failure.

III. DEBRIS-CONCRETE INTERACTIONS

That debris-concrete interactions could pose a threat to containment integrity has been a recognized issue in severe accident analysis for some time. In order to address concerns which had arisen, the Containment Loads Working Group (CLWG) was formed in July 1983 under the auspices of the NRC's Severe Accident Research Program (SARP). The group was composed of experts from the national laboratories, contracting companies, industry and government research and regulatory bodies. The goal of this group was to examine the processes and phenomena which led to containment loads (temperature and pressure excursions) and thus challenge containment integrity. Summaries of the results from the CLWG were published in NUREG-0956 [6] and NUREG-1079.[7]

The CLWG examined six "standard problems" that qualitatively represent each one of six containment designs deployed in the U.S. Analysis of the results of these problems showed that debris-concrete interactions were important for all but the large dry PWR containments. For the large dry containments the focus of attention shifted to the DCH scenario associated with the forceful expulsion of the melt from a pressurized reactor vessel and dispersion of molten corium into the containment atmosphere. This scenario is discussed in Section IV of this paper.

The CLWG identified the radiant heat loss from core debris in the cavity as an issue which had not received sufficient attention in the analysis of severe accident sequences. A parameter study done by Williams, et al., [8] examined the effects of this and other forms of heat input to the containment atmosphere for the Surry TMLB' sequence, which is the basis for the CLWG standard problem SP-2. The CONTAIN code was used in this analysis, with stand-alone CORCON generated source data and various parametric heat and steam sources introduced via table input. One conclusion of this study was that the occurrence and timing of deinerting hydrogen burns in the TMLB' sequence is quite sensitive to these steam and energy sources. In

particular, the input of a 10 MW thermal energy source to the containment atmosphere is sufficient to prevent a deinerting burn.

This accident sequence has been analyzed with the new merged version of CONTAIN-CORCON. The problem consists of a single cell nodalization with the structure heat transfer, aerosol physics, radiation exchange and water vapor condensation models activated. The primary system steam and aerosol releases are sourced into the problem via table input; at a time of 9440 seconds following scram, the CORCON model is started, including the gas generation from debris-concrete interactions and the radiant heat coupling to the atmosphere and structures.

Compartment pressure for this problem is shown in Figure 1a. Results shown in Figure 1b correspond to turning off the thermal interaction between the corium layer and the atmosphere and structures. Both runs show an initial pressure rise to about 4.7 bars due to vessel failure and steam generation when the accumulators dump onto the melt. After an initial decrease, the pressure in the full model case, Figure 1a, levels out at about 3.2 bars, then decreases to about 3.1 bars at 35000 seconds, after which a very slow pressure increase is seen. By contrast, the results shown in Figure 1b for the case of disabling radiant heat transfer from the debris show a steadily decreasing pressure, until a deinerting hydrogen burn takes place at about 21000 seconds. These results are very similar to those obtained in the Williams, et al., parameter study. Physical mechanisms responsible for this effect are discussed in detail in Reference 8 and will be briefly summarized here.

The occurrence of deinerting burns requires that the steam mole fraction in the compartment atmosphere fall below 55%. This effect is achieved through condensation of steam upon the structures. The rate of condensation is governed primarily by the rate at which heat can be conducted into the structures. Increasing the thermal load on the atmosphere-structure system results in a decreased rate of condensation because of the additional loads on the heat sinks due to either direct radiation or the larger temperature difference between the walls and the atmosphere. The latter effect is due to radiant energy absorbed directly by the atmosphere. At the high thermal loads present in this calculation (about 10 MW), the inventory of water on the structures (due to the initial condensation after vessel failure) must help absorb the thermal load. Evaporation occurs, leading to a slow increase in compartment pressure. The deinerting burn never takes place because the steam mole fraction never falls sufficiently.

These results demonstrate the advantages provided by integrated analysis, in that certain effects can easily be turned on or off to examine the impact on the system as a whole. However, these calculations are not intended as a best estimate for this plant/sequence. For example, the results of Figure 1a would certainly change with a finer nodalization of the problem. In this case, the cavity region where radiant exchange takes place would be much smaller than the compartment used in the current analysis, leading to much smaller

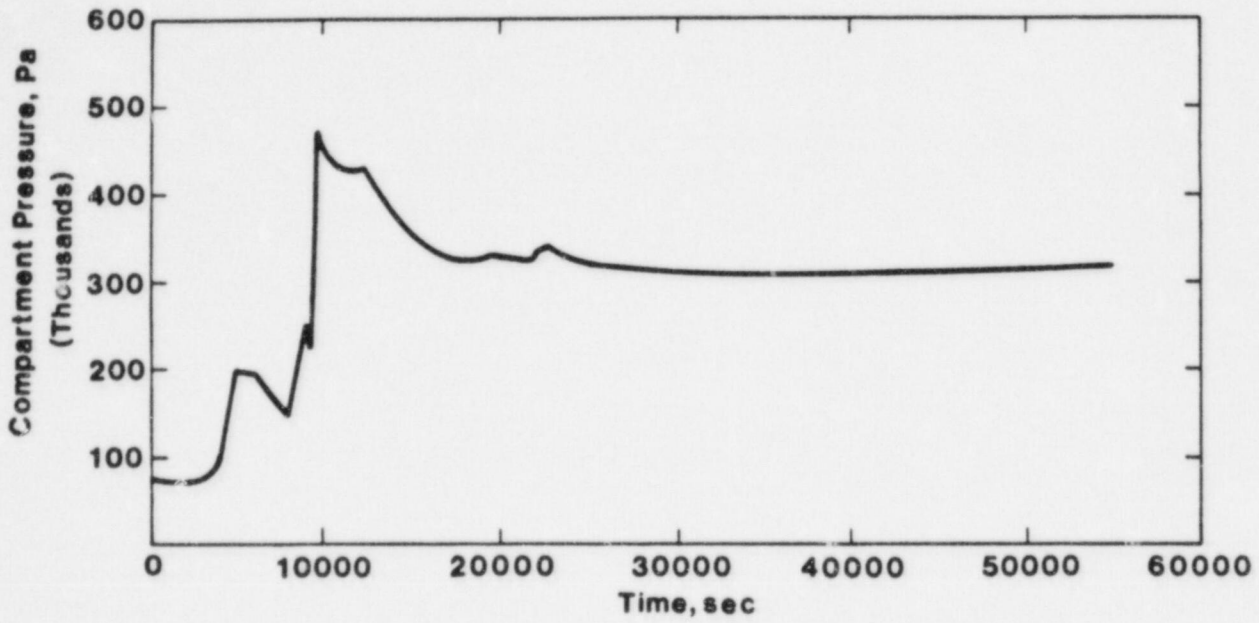


Figure 1a. Compartment pressure vs. time for the Surry TMLB' sequence with the corium layer radiation coupled to the atmosphere and structures.

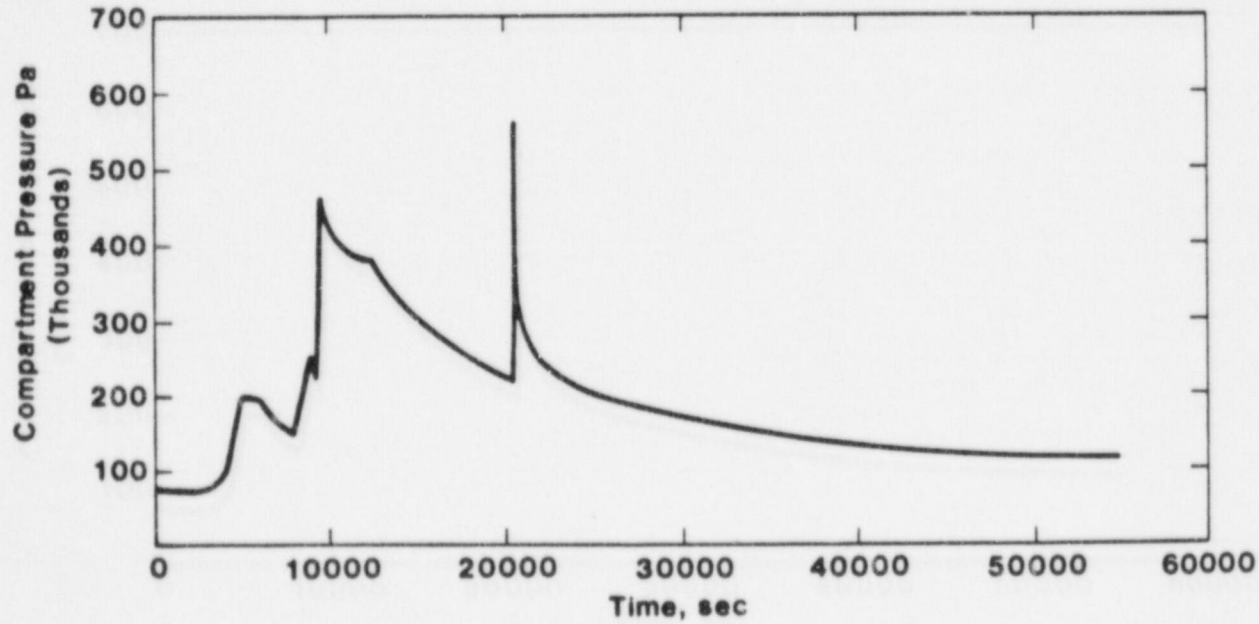


Figure 1b. Compartment pressure vs. time for the Surry TMLB' sequence with no radiative coupling between the corium layer and the atmosphere or structures. A hydrogen burn occurs around 21000 seconds.

radiation path lengths in the atmosphere and higher structure temperatures.

IV. DIRECT CONTAINMENT HEATING

As mentioned above, the issue of DCH was identified by the CLWG as requiring further analysis and study. Early methods of analysis, concurrent with the CLWG work, involved simple parameter studies. The models made simplifying and arbitrary assumptions concerning debris composition and completeness of reaction with the containment atmosphere. Reference 9 summarizes this early work.

Since then, several new modeling efforts and experimental programs have emerged. These include the work of Pilch and Tarbell, [10] Baker, [11] Pong, et al., [12] and Gonzales, et al.[13]

Recently, several aspects of these and other models have been incorporated into the CONTAIN code in order to provide the capability of assessing containment threat due to the DCH phenomenon. At present this work is in a preliminary stage and the models have not been validated against data. Much will hinge on the results of the SURTSEY experimental program at Sandia.[14] The discussion here will very briefly describe the new models provisionally added to CONTAIN and some typical results obtained to date.

A new material flow field has been added to the code, that of suspended droplets, consisting of the materials Zr, ZrO_2, Fe, FeO and UO_2. This field is allowed to have its own temperature, but the flow model used is that of homogeneous flow, allowing no slip relative to the carrier gas. The droplets are assumed to be well mixed in each control volume of gas and, within that cell, to have identical size, composition and temperature. Droplet trapping is treated parametrically by using a user-specified fractional trapping rate. Trapped drops may interact with a coolant pool if one is present or simply reside on a lower-cell layer and exchange heat with the atmosphere and the layer.

Heat transfer occurs between the droplets and the gas via convection and radiation. The convection heat transfer coefficient uses an input-specified value of the velocity of the gas relative to the droplets. Radiation is allowed to the gas and the structures in a compartment with a selectable fraction of the black body value going to each sink. In this manner the effects of aerosol opacity and atmosphere absorption on the droplet-to-gas radiation can be estimated.

Chemical reactions can take place at the surface of the droplets if they contain oxidizable material. The metal oxidation is done in a hierarchical manner, allowing first Zr, then Fe, to react with O_2 at the droplet surface, followed by allowing any available water vapor to react with Zr and then Fe. Heat produced by these reactions is added to the droplet field energy. Hydrogen generated by the metal-steam reaction is combined with any oxygen available in the bulk atmosphere and the heat so generated added to the atmosphere.

These reactions are limited by diffusion of the oxidizing gases through the gas boundary layer around each droplet. Limitations to the oxidation rate due to mass transfer within a droplet were not modeled. A lower temperature limit is included to stop any reaction when the droplet field temperature falls sufficiently. Parametric multipliers are also included for the diffusivity values to allow sensitivity analyses.

Results from a simple problem run with the modified version of CONTAIN were compared with results from a similar run with the Pilch [10] model and with the DHEAT code utilized in NUREG-1079.[7] When the assumptions of the simpler models were enforced in the CONTAIN calculation, agreement among the various methods was very good.

In order to demonstrate these new modeling capabilities, results are presented from a calculation of debris ejection in the Sequoyah ice condenser containment. Before describing these results, it must be emphasized that this exercise is not intended as a best estimate analysis of this accident sequence, but is only presented to demonstrate the importance of modeling interactions among the various phenomena.

The Sequoyah containment was coarsely nodalized (as shown in Figure 2) with three compartments. The problem was begun with the containment conditions set to those occurring at the time of vessel failure for the TMLB' sequence, as calculated by an initial CONTAIN run. Two versions of this problem will be presented. For the base case, labeled Q1, the pertinent parameters were a droplet radius of 1 mm, a velocity of the drops with respect to the gas of 5 m/s, one half of the core debris injected into the lower compartment over a period of 10 seconds with a temperature of 2550 K, with a steam injection rate of 600 kg/sec for 50 seconds. There was no trapping allowed and no in-vessel hydrogen source was included, though the Zr was assumed to be 50% oxidized at vessel failure.

The second variation of this problem, called Q7, was identical to Q1 except that a hydrogen inventory (presumed to have been generated in-vessel) of 200 kg was distributed at vessel failure time to the three cells in equal concentrations. An additional 200 kg of hydrogen was injected with the steam into the lower compartment at vessel failure. This hydrogen inventory was consistent with the 50% in-vessel oxidation assumption.

The comparison in Figure 3 of the Q1 and Q7 results for upper compartment pressure shows the occurence of a large hydrogen burn in the Q7 case. This burn, which begins in the upper cell at about 9409 seconds, takes place just before the end of the ten second source of corium into the lower cell. The burn signature can also be seen in the cell temperature values shown in Figure 4 for case Q7. The pressurization of the upper compartment forces hydrogen from the ice condenser to the lower cell, along with droplet materials. Oxygen is

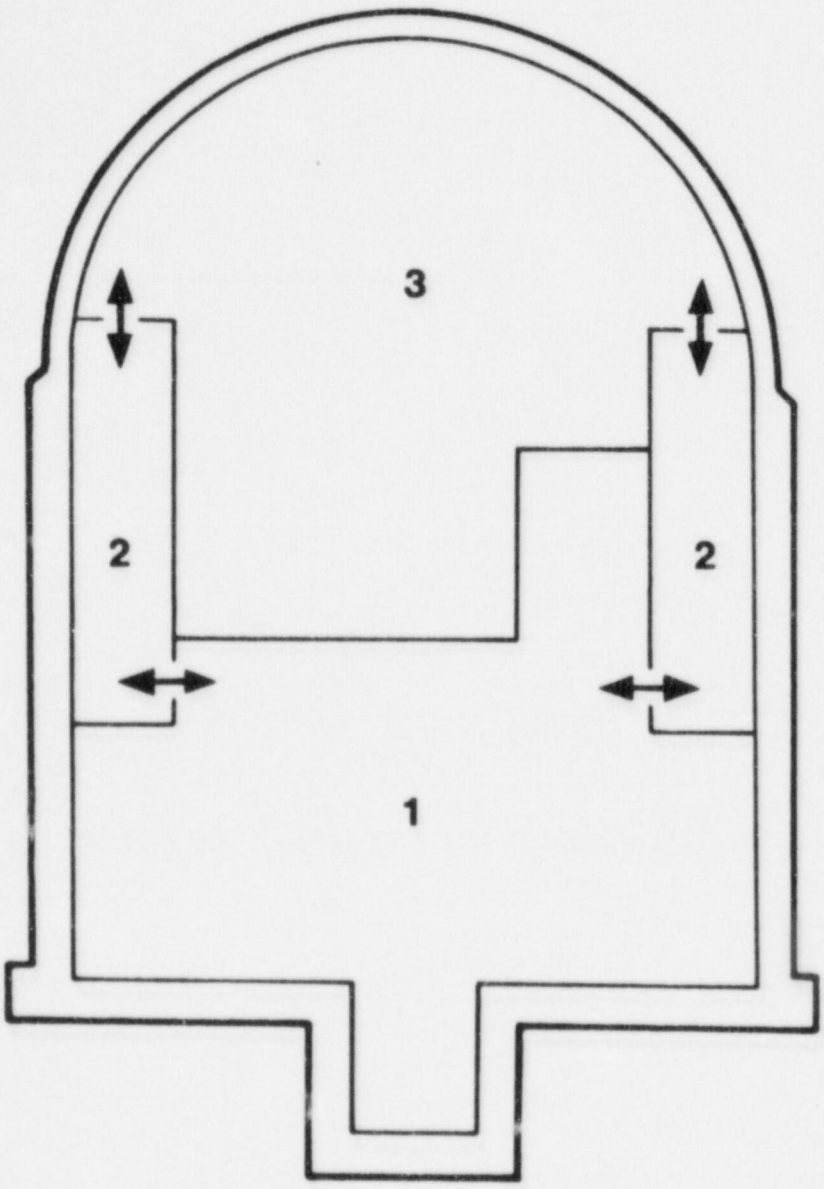


Figure 2. Schematic diagram of the three cell nodalization of the Sequoyah Ice Condenser containment used in DCH analysis. Cell 1 is the lower compartment, cell 2 is the ice compartment, and cell 3 is the upper compartment or Dome.

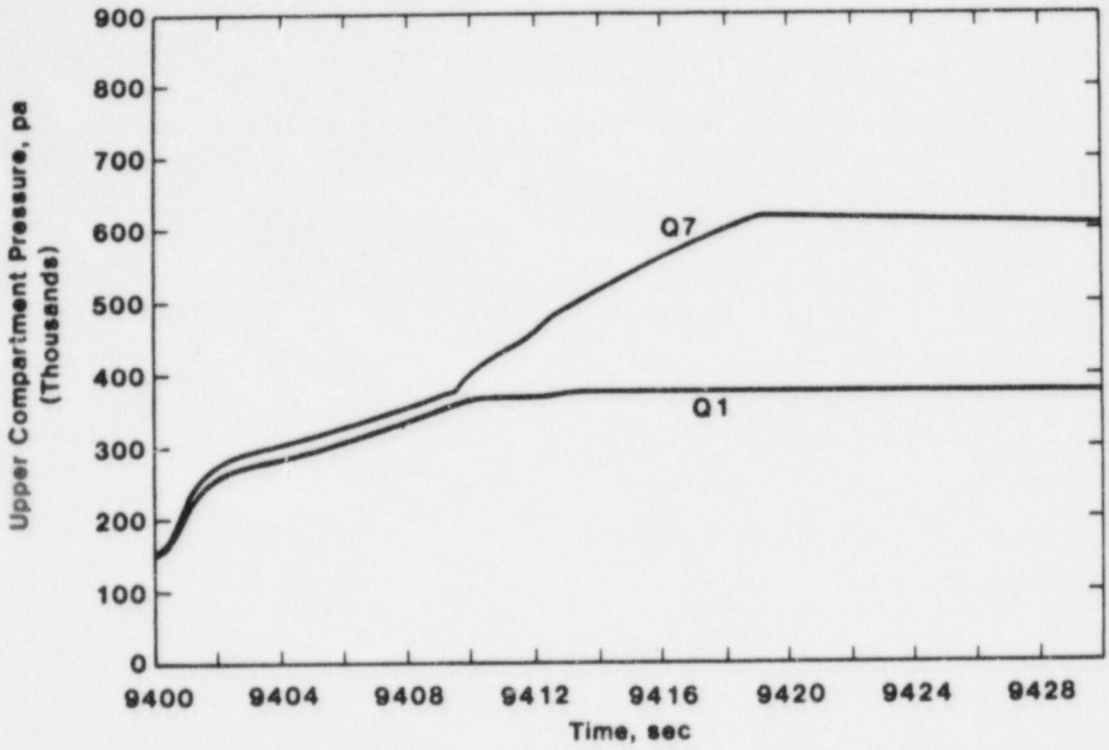


Figure 3. Comparison of the upper compartment pressures for the two DCH cases Q1 and Q7.

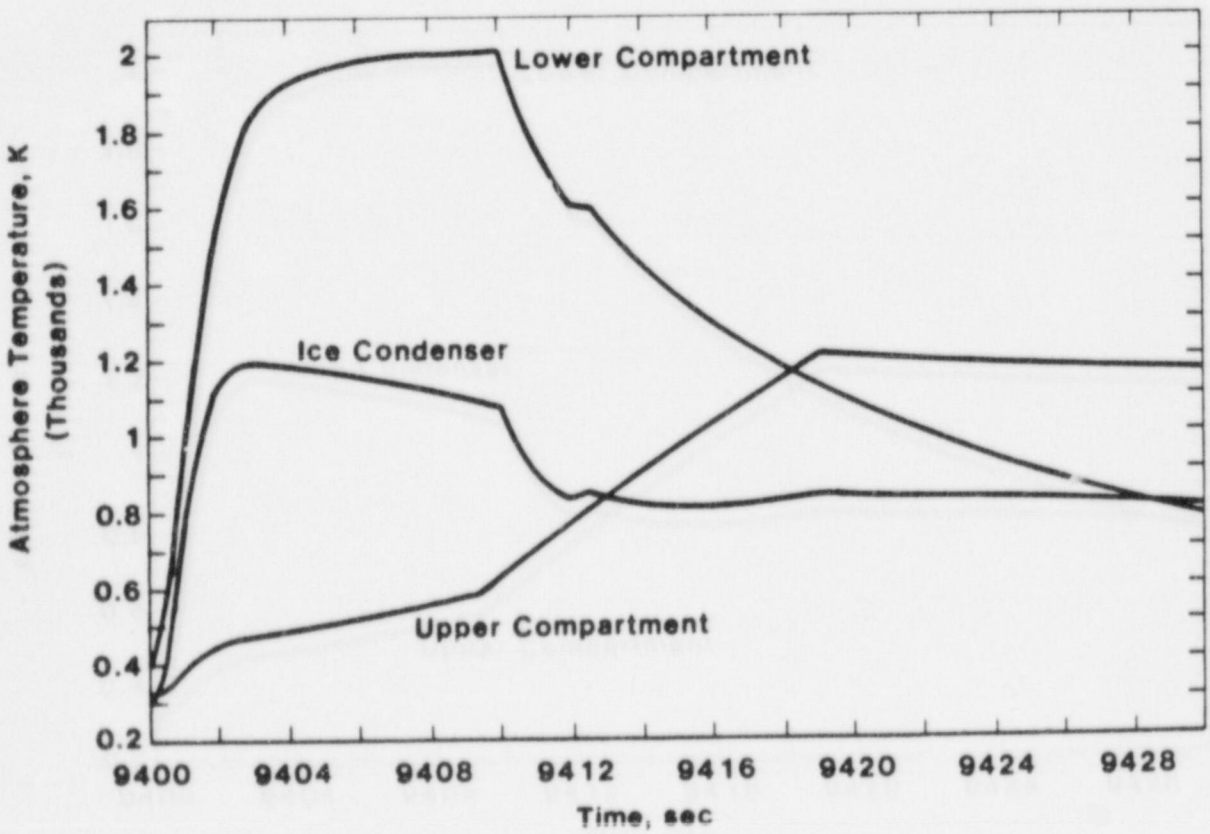


Figure 4. Values of cell atmosphere temperature vs. time for the DCH case Q7.

forced from the upper cell into the ice condensor and cavity cells, but the criteria for hydrogen burns are not met in these compartments. These backflows are possible because the ice condenser doors were modeled as remaining at least 25% open after flow reversal.

The upper compartment pressures shown in Figure 3 demonstrate that while the Q1 problem comes marginally close to the nominal failure pressure of about 400 kPa, the hydrogen burn case far exceeds this value.

The conclusion to be drawn from this comparison is the importance of the DCH phenomena as not only a direct source of thermal and chemical energy to the containment atmosphere, but also as a potentially critical source of additional hydrogen, produced by the metal-steam reactions in the debris. Not only does the hydrogen present a threat in the combustion sense, the presence of this additional non-condensible gas also inhibits vapor condensation on the ice and decreases the effectiveness of the ice condenser in removing energy from the system. This in turn allows the gases in the problem to be mixed; the hydrogen produced in the cavity cell is passed to the upper compartment, while steam is still removed in the ice condenser, resulting in the formation of flammable concentrations when combined with the in-vessel source of hydrogen.

In the course of examining this and other problems run with the DCH models in CONTAIN, the importance of the relative timing of the steam, hydrogen and corium sources has become apparent. As with all of the phenomena involved in DCH, time scales are short, and indications are that a difference of as little as a few seconds in the relative timing of the sources may be enough to make a significant difference in the accident outcome. The basic effect causing this sensitivity is the preconditioning of the upper compartment atmosphere which can occur if the steam arrives before the corium. When preceding the steam, the corium reactions heat the gas without excessive pressurization, resulting in a rapid radiation heat transfer to the structures. The result is a large temperature excursion but a relatively modest pressurization. With steam preconditioning, the energy from the thermal and chemical interactions remains in the atmosphere in the form of superheated steam. This will result in lower temperatures and lower rates of radiation heat transfer, but larger pressures in the upper compartment.

V. CONCLUSION

This paper has presented the results of recent work to improve and upgrade the CONTAIN code by adding a number of new calculational capabilities. These enhancements significantly improve CONTAIN's ability to model those situations which are postulated to threaten containment integrity due to molten debris release. The integral incorporation of the CORCON and VANESA codes into CONTAIN will allow the systematic analysis of a wide variety of such problems and the evaluation of the importance of physical and modeling uncertainties. Additionally, the source term information furnished by VANESA will allow quantitative assesment of the consequences of a failure of containment integrity. Work now being done in modeling Direct

Containment Heating phenomena will allow the use of CONTAIN to assess the importance of DCH in conjunction with NRC's ongoing experimental programs.

VI. REFERENCES

1. K. D. Bergeron, et al., User's Manual for CONTAIN 1.0, A Computer Code for Severe Nuclear Reactor Accident Containment Analysis, Sandia National Laboratories, Albuquerque, NM, May 1985, NUREG/CR-4085 (SAND84-1204).

2. R. K. Cole,Jr., D. P. Kelly, M. A. Ellis, CORCON-MOD2: A Computer Program for Analysis of Molten-Core Concrete Interactions, Sandia National Laboratories, Albuquerque, NM, August 1984, NUREG/CR-3920, (SAND84-1246).

3. R. D. Cess and M. S. Lian, "A Simple Parameterization for the Water Vapor Emissivity," Transactions, ASME Journal of Heat Transfer, 98, No. 4, pp. 676-678, 1976.

4. A. T. Modak, "Radiation from Products of Combustion," Fire Research, 1, pp. 339-361, 1979.

5. D. A. Powers, J. E. Brockmann, A. W. Shiver, VANESA: A Mechanistic Model of Radionuclide Release and Aerosol Generation During Core Debris Interactions with Concrete, NUREG/CR-4308, SAND85-1370, to be published.

6. Reassessment of the Technical Bases for Estimating Source Terms, NUREG-0956, Draft report for comment, USNRC/NRR, July 1985.

7. Estimates of Early Containment Loads from Core Melt Accidents, NUREG-1079, Draft report for comment, USNRC/NRR, Dec 1985.

8. D. C. Williams, K. D. Bergeron, P. E. Rexroth, J. L. Tills, "Integrated Phenomenological Analysis of Containment Response to Severe Core Damage Accidents", (Draft), Sandia National Laboratories, Albuquerque, NM, SAND85-0890J, to be published in Progress in Nuclear Engineering.

9. K. D. Bergeron and D. C. Williams, "CONTAIN Calculations of Containment Loading of Dry PWRs," Nuclear Engineering and Design, 90, pp 153-159, 1985.

10. M. Pilch and W. W. Tarbell, Preliminary Calculations on Direct Heating of a Containment Atmosphere by Airborne Core Debris, Sandia National Laboratories, Albuquerque, NM, April 1986, NUREG/CR-4455, SAND85-2439 to be published.

11. L. Baker, "Droplet Heat Transfer and Chemical Reactions During Direct Containment Heating," paper presented at the International ANS/ENS Topical Meeting on Thermal Reactor Safety, San Diego, California, Feb 2, 1986.

12. L. Pong, M. Corradini, G. Moses, Surry S$_2$D Severe Accident Containment Loads Calculations Using HMC, Univ. of Wisconsin Reactor Safety Research Report UWRSR-34, January 1986.

13. F. Gonzalez, I. Huhtiniemi, M. Corradini, A Transient Model for Direct Heating in a LWR Containment, Univ. of Wisconsin Reactor Safety Research Report UWRSR-35, February 1986.

14. W. Tarbell, M. Pilch, J. Brockmann, "Melt Expulsion and Direct Containment Heating in Realistic Plant Geometries," paper presented at the International ANS/ENS Topical Meeting on Thermal Reactor Safety, San Diego, CA, Feb 2, 1986.

HYDROGEN DEFLAGRATION TESTS IN HYDRO-SC FACILITY

M.Carcassi, F.Fineschi
Dipartimento di Costruzioni Meccaniche e Nucleari
Universita` di Pisa - Italy

G.Lombardi
ENEA (Comitato Nazionale per la Ricerca e per lo Sviluppo dell'Energia Nucleare e delle Energie Alternative) - Italy

ABSTRACT

In severe accidents, large amounts of hydrogen may be released in the safety containment of a nuclear plant and the gas mixture may become explosive. The University of Pisa and ENEA have undertaken an experimental program to study the physics of the flame propagation in a containment model in accidental conditions. Up to now 41 deflagration tests have been performed with HYDRO-SC facility at ambient pressure and temperature. Concentrations, water spray conditions, ignition source and gas turbulence level were varied. The vessel volume was 0.5 m^3, the ignition sources were an electrical spark discharge and an electrically heated surface (glow-plug), the hydrogen molar fractions were in the range 4-16%, the turbulence was generated by fan or spray and two different spray nozzles were utilized. The experimental data indicate that the peak pressures nearly fit the adiabatic isochoric values at the highest hydrogen concentrations and gas turbulences. Weak pressure waves were observed for H_2 molar fractions greater than 10%. A careful examination of the pressure and temperature transients gave information on the flame path and on the heat transfer process during and after the combustion. Scale effects on the peak pressures were not observed comparing the HYDRO-SC results with data obtained in other laboratories. The glow plug igniter has proved to be a reliable tool for use in deliberate ignition schemes for hydrogen control in nuclear plants.

1 INTRODUCTION

For assessing the explosion risks in Safety Containments of Nuclear Plants, the Department of Mechanical and Nuclear Constructions (DCMN) of the University of Pisa and ENEA have undertaken a research activity program on hydrogen deflagrations in closed vessels.

The objectives of the program are as follows:

1) To acquire information on the deflagration of hydrogen-air mixtures through bibliographic research, theoretical studies and experimental tests.
2) To acquire experience about reliability of measurement techniques for better evaluating the experimental results obtained by other laboratories.
3) To test equipments for hydrogen control (e.g. igniters).
4) To provide the nuclear regulatory staff with information derived from points 1), 2) and 3) for use in estimating the impact of hydrogen on the LWR safety in Italy.

A facility, HYDRO-SC (Fig.1), was set up in 1983 at university laboratories in order to perform three series of deflagration tests in a containment model at ambient temperature and pressure and at hydrogen molar fraction ranging from 4% to 16%, with or without water spray. At present, coarse sprays are being used in actual plants to reduce pressure and fission products in the containment atmosphere during loss of coolant accidents.

2 EXPERIMENTAL APPARATUS

The burns were contained in a 0.65 m diameter by 1.64 high vessel, displacing approximately 0.5 m^3, with a design pressure of 1.2 MPa. The vessel had a number of flanges with electrical feedthroughs for igniters, thermocouples and pressure transducers; other ports provided a means for transfering gas and liquid in and out of the test volume, vacuum lines and pressure measurements. A gas vent and compressed air provided purging.
In the 1st test series pre-mixing of the contents was accomplished with an electrically powered (15 W) fan of 90 mm diameter, located horizontally facing up at 3/4 of the vessel heigth. In some tests the fan was left on during the deflagration.
In the 2nd and 3rd test series gas mixing was accomplished with a water spray system utilizing in the former a Fulljet 1 H 4-2 (Spraying System Co.), producing droplets with nominal diameter of 3.2 mm at water flow rate of 0.5 Kg/s, and in the latter a Fulljet 1 1/8 G.8W (Spraying System Co.), producing smaller droplets of 1.2 mm at water flow rate of 0.07 Kg/s. The spray nozzles were located at the top of the chamber.
HYDRO-SC was equipped with two ignition sources: a spark igniter, producing a spark energy of 22 J and a glow plug igniter powered by 12 V DC source.
The spark igniter was used in four tests of the 1st series, with initial H_2 molar fractions of 4.1%, 4.3%, 7.2% and 9%. The distance between the igniters and the top of the vessel was 1.36 m.

Primary data for deflagration tests included temperature and pressure measurements and gas concentration analyses before and after the combustion event.
Pressure indications were provided by strain gage, piezoelectric and piezoresistive transducers. In the following series the instruments displaying less reliable responses were discarded: strain gage

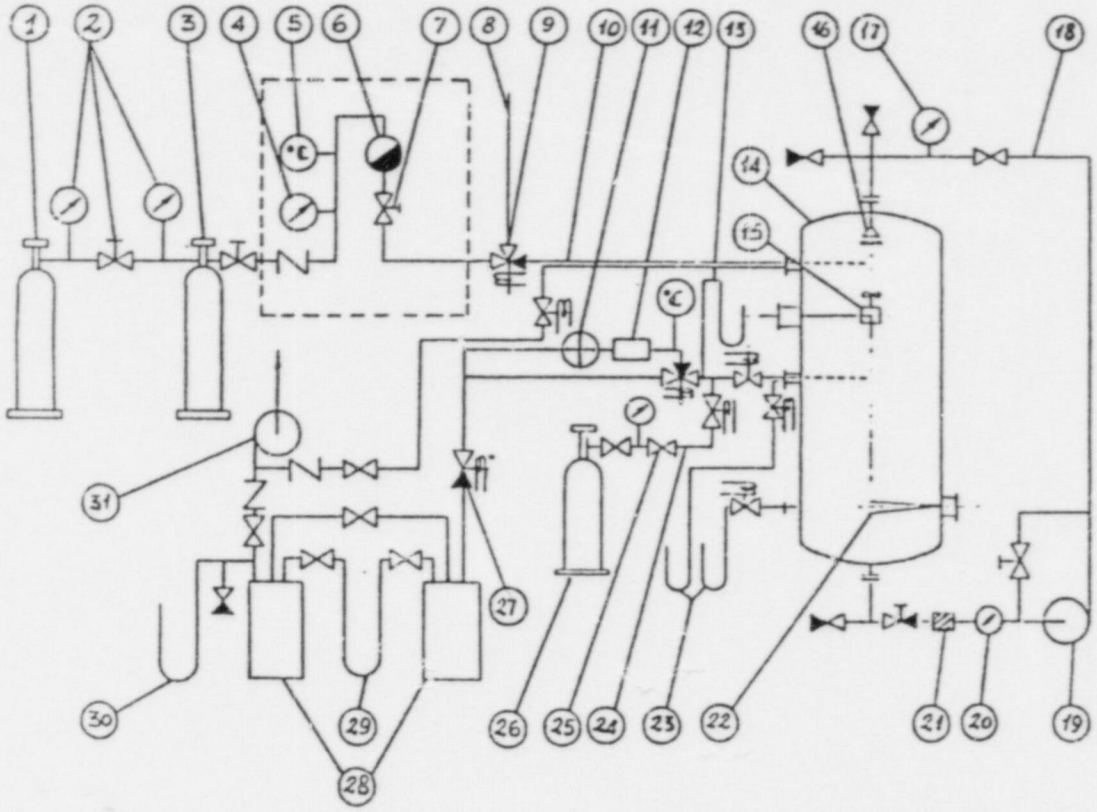


Fig.I - Flow-sheet of Hydrogen-SC Facility.

1.- H_2 Cylinder
2.- Pressure Reducing Valves
3.- Expansion Volume
4.- Pressure Gauge
5.- Thermometer
6.- Flow-meter
7.- Micrometric Valve
8.- Vent Pipe
9.- Three-Way Solenoid Valve
10.- H_2 Inlet Line
11.- Gas-chromatographic Sampling Valve
12.- Dehumidifier
13.- Hg Gauge
14.- Vessel
15.- Fan
16.- Sprayer
17.- Pressure Gauge
18.- Sprayng Circuit
19.- Motor-driven Pump
20.- Water Meter
21.- Filter
22.- Igniter
23.- Water Gauge
24.- Scavenging Line
25.- Nozzle
26.- Ar Cylinder
27.- Two-Way Solenoid Valve
28.- Vacuum Chambers
29.- Differential Pressure Gauge
30.- Hg Gauge
31.- High-Vacuum Pump

Valve

On-Off Valve

Solenoid Valve

Check Valve

pressure transducers were not utilized in the 2nd set of tests; in the 3rd set only the piezoresistive type was used.
Temperature measurements were made with chromel-alumel K-type thermocouples. Thermocouples cannot measure the actual temperature of burnt gases, because their response time is comparable to combustion development time; temperature histories at the different locations (T_{top} and T_{bottom}) inside the vessel indicated the flame front path.
Pressure and temperature measurements were recorded on Analog Tape Recorder Honeywell H 101.
Before and after the deflagration gas analyses were accomplished by a sampling system and a gas-chromatograph Carlo Erba Fractovap 2350. The concentrations were also inferred from gas law and temperature and pressure measurements.

3 TEST PROCEDURES

Performance of a test was carried out through the following steps:
- The facility systems were verified to be operational.
- The vessel atmosphere was purged, by blowing and venting air, until no residual hydrogen was detected by the gas-chromatograph.
- The vessel was evacuated to the designated air pressure and hydrogen was injected till the ambient pressure and temperature were obtained.
- The fan or spray were activated. In tests with deflagration in still air, mixing was stopped when the results of two successive gas analyses were found to be the same (uniform concentration).
- The igniter was activated, and subsequently switched off as soon as the pressure began to rise (beginning of flame propagation).
- Two post-burn gas samples were drawn and analyzed.
- The facility was prepared for the next test.

4 INITIAL CONDITIONS AND RESULTS

Three test series, for a total of 41 tests, were performed. The first series of 19 "dry" tests was carried out to determine the effects of hydrogen concentration, fan generated turbulence and igniter type on pressure transient and hydrogen fraction consumed; the other two series, each consisting of 11 tests, were performed to determine the effects of the sprays. In the second series spray flow rate was higher than in the 3rd series to better illustrate the influence of the coarse spray. In the third series the spray conditions were similar to those provided for safety containments.
For a better understanding of the phenomenon, the tape-recorded signals were translated, at first, into the following variables:
$\Delta P_M/P_0$, (peak pressure)/(initial pressure) (Fig.2),
H_{2B} , % H_2 consumed (Fig.3),
Δt , time to peak pressure,
$\Delta P_M/\Delta t$, average rate of pressure rise, which is an index of burning velocity (Fig.4).

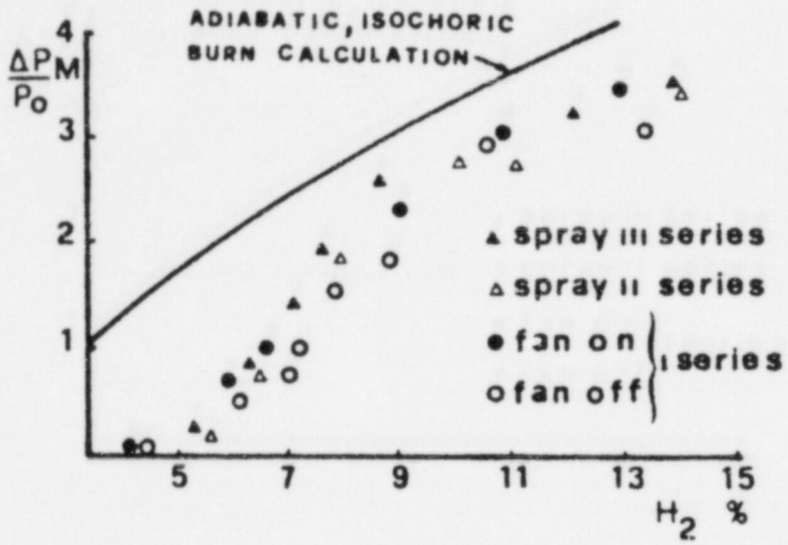


Fig.2- Normalized pressure rise as a function of Hydrogen concentration.

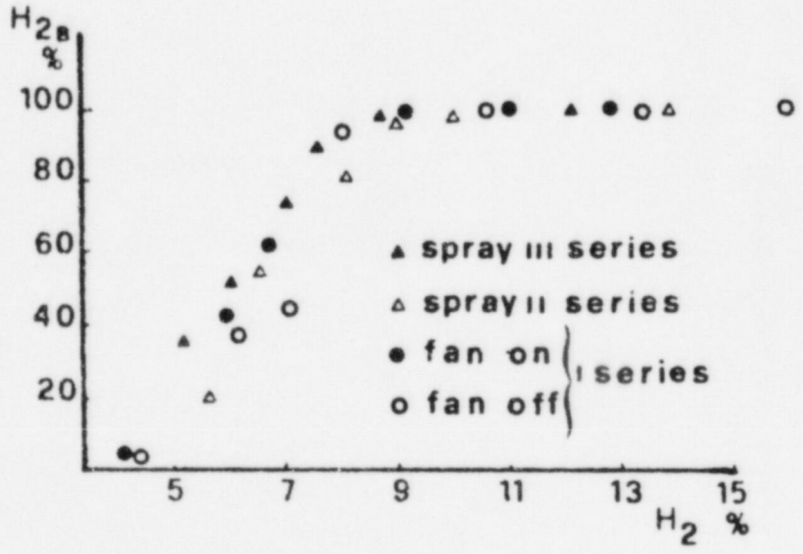


Fig.3- Hydrogen fraction burned as a function of Hydrogen concentration.

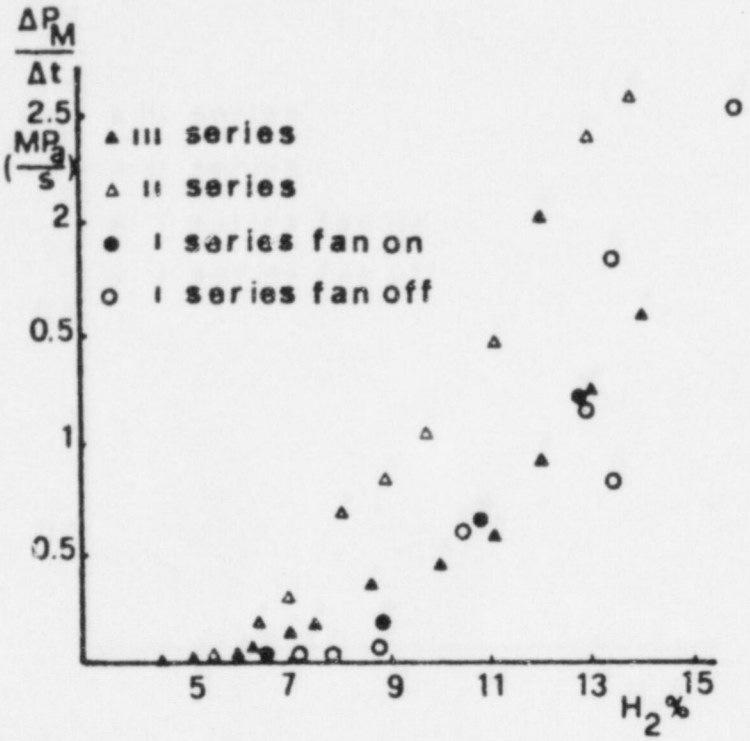


Fig.4- Rate of pressure rise as a function of hydrogen burned.

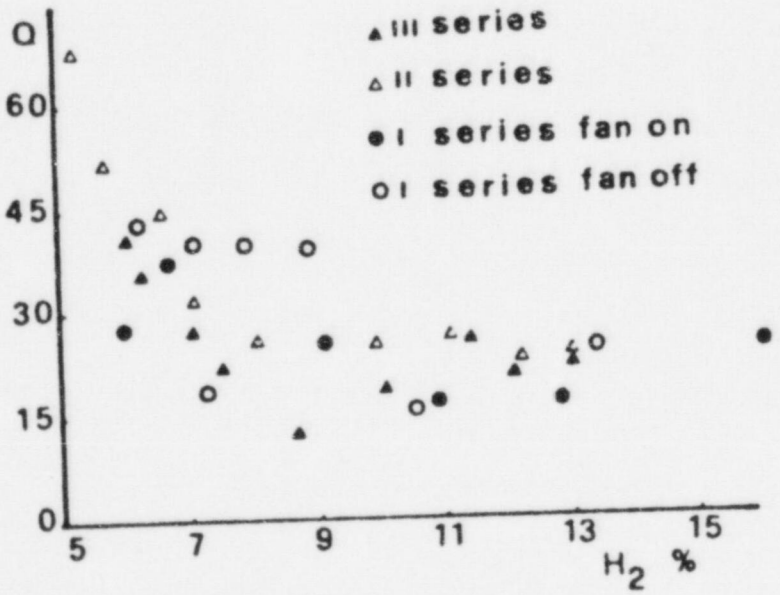


Fig.5- Chemical energy fraction lost as heat transferred to the container walls.

Adiabatic pressures were calculated for the theoretical complete burns (solid line in Fig.2) and for the measured hydrogen consumption (ΔP_B).
$Q = (\Delta P_B - \Delta P_M)/\Delta P_B$ (Fig.5) represents the fraction of released chemical energy transferred as heat to the container walls and to the water droplets, during the deflagration.

5 DISCUSSION OF RESULTS

The experimental data indicate that:

a) In the three series of tests conducted at hydrogen molar fractions > 9%, the combustion is nearly complete (Fig.3) and ΔP_M (Fig.2) and Q (Fig.5) vary only with the concentration. However pressure rises of the 2nd series are slightly lower than the others (Fig.2), consistent with a slightly higher heat transfer to washed walls and spray drops. The turbulence of this series was probably the highest, as its highest burning velocities indicate (Fig.4).

b) Pressure oscillations were observed, by an oscilloscope, in tests with initial molar fractions > 10.5%; the frequency analysis pointed out the acoustic nature of such a phenomenon, with maximum values of the pressure lower those calculated for adiabatic conditions.

c) The main differences in the three test series may be observed in the 7.5-9 % hydrogen molar fraction range. In particular, peak pressures increase (Fig.2) from the 1st series, fan-off, up to the 3rd one, in accordance with the quantity of burned hydrogen (Fig.3). Generally turbulence, generated by fan or spray, increases the hydrogen consumed (Fig.3) and the burning velocity (Fig.4). But, in the 2nd set of tests the hydrogen burned was less than in 3rd set, notwithstanding the higher turbulence, perhaps for the higher cooling rate of the spraying (Fig.5).

d) The trends observed in the 7.5-9 % H_2 molar fraction range persist up to the lower flammability limit, although less clearly.

e) In the 1st series the performances of the spark and glow plug igniters appeared to be nearly identical. The glow plug igniter, equipped with a rain shield, did not show evidence of performance degradation throughout the full series of tests with spraying.

The mechanisms of flame propagation are responsible for the different behavior of the main physical and chemical variables and are evidenced by pressure and temperature transients:

f) In the fan-off tests of the 1st series, ranging from 7.5% to 9% H_2 molar fractions, the pressure traces show a plateau, Fig.6. In the same range, temperature histories, at different locations inside the vessel, indicate an upward flame propagation, until contact is made with the top of the vessel, followed by a downward propagation, figs. 6 and 7/a. Then the flame fills the whole volume and causes the system to react more completely (Fig.3), but a high fraction of internal energy is lost (Fig.5), because during the burning, burnt gases are in contact with the containment walls for quite a long time.

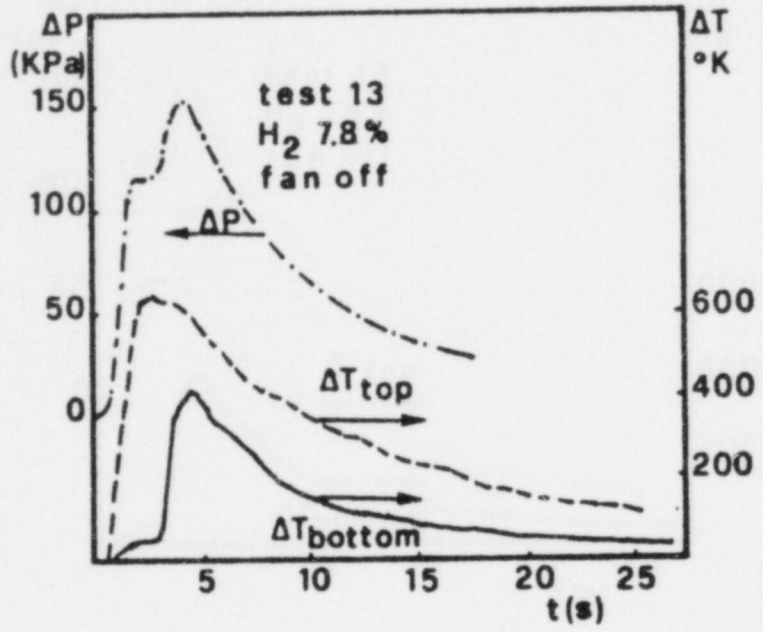


Fig.6- Transients of temperature and pressure for test I3.

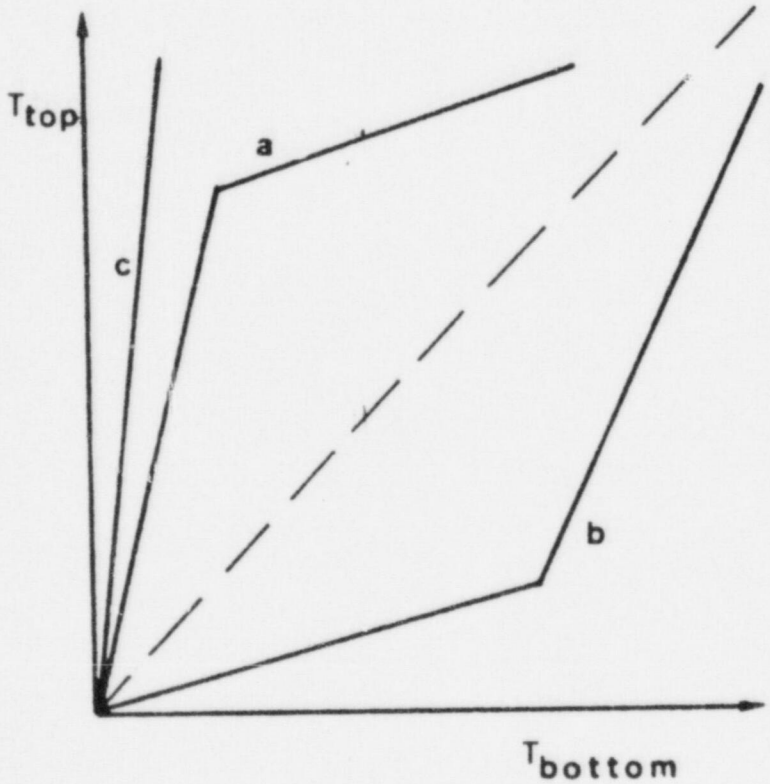


Fig.7- Thermocouple responses for different modes of flame propagation: a) upward and downward, b) isotropic, c) upward alone.

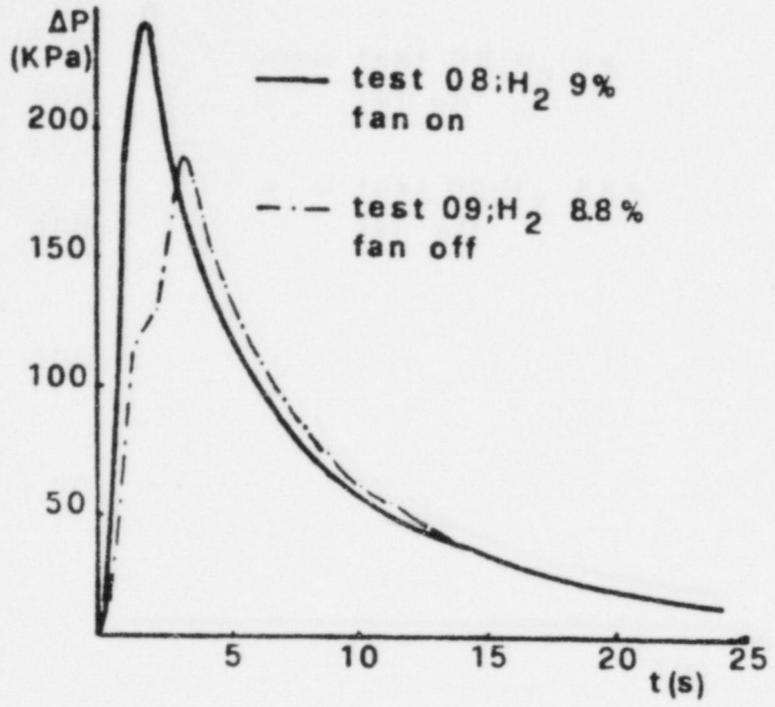


Fig.8- Pressure transients for tests 8 and 9.

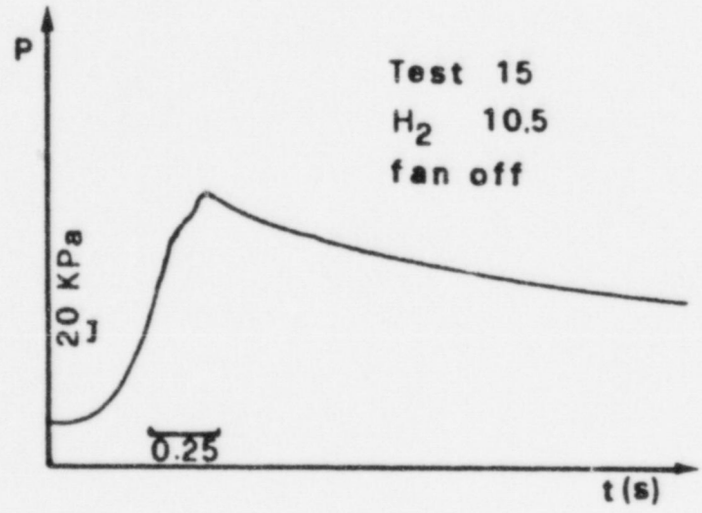


Fig.9- Pressure transients for test I5.

g) In the fan-on tests of the 1st series, in the tests of the 3rd and especially of the 2nd series, the plateau shrinks (Fig.8) and temperature histories indicate that the flame propagation is almost isotropic (Fig.7b): the turbulence is sufficient to cause an increase in flame speed large enough to reduce the buoyancy effects.

h) In all tests with hydrogen molar fractions > 9%, flame speeds are high, even without artificial turbulence. Flame propagation is isotropic around the ignition point as long as the burning develops in the lower volume, then the burnt gases touch the container walls and the flame front changes its shape and size (pressure traces inflection point). Finally, the flame propagates upward, affecting the rest of the volume (Figs. 7/b and 9).

i) For hydrogen molar fractions < 7.5%, in the 1st series, fan-off, the thermocouple signals indicate that buoyancy forces affect the flame propagation: the fireball is continually displaced upward and, when it comes in contact with the top of the vessel, heat losses cause flame quenching (Fig.7/c). With the spray and the fan on, this mechanism is limited, more or less markedly according to the turbulence level; burning efficiency increases, as well as the peak pressure increases when the heat transfer is not too high.

The heat-transfer characteristics of the system can be inferred from pressure transients after the deflagrations. For this purpose, two quantities were analyzed:

Δt_{10}, the time for pressure to decrease from the peak value to 10% of peak value.

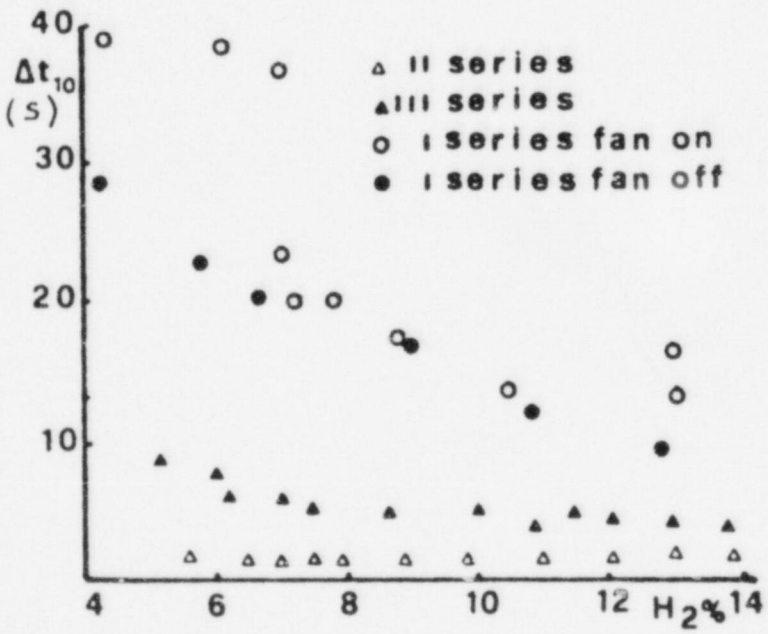


Fig.IO- Time for pressure to decrease from the peak value to IO% of peak value.

UA $\triangleq$ $-[1/(P-P_0)](dP/dt)$, which may be considered inversely proportional to the overall thermal resistances, since $-dP/dt$ is an index of the rate of internal energy variation and $(P-P_0)$ is an index representative of the temperature difference between the inside and the outside of the vessel.

In Fig.10, Δt_{10} values are shown for the three test series as a function of concentration. In Fig.11 UA is plotted versus $(P-P_0)$, which is here considered an index of natural convection. Since at a certain instant the heat transfer coefficient does not depend on the previous history of the transient, in such plots it is possible to compare values obtained from tests with different peak pressures and initial hydrogen concentrations.

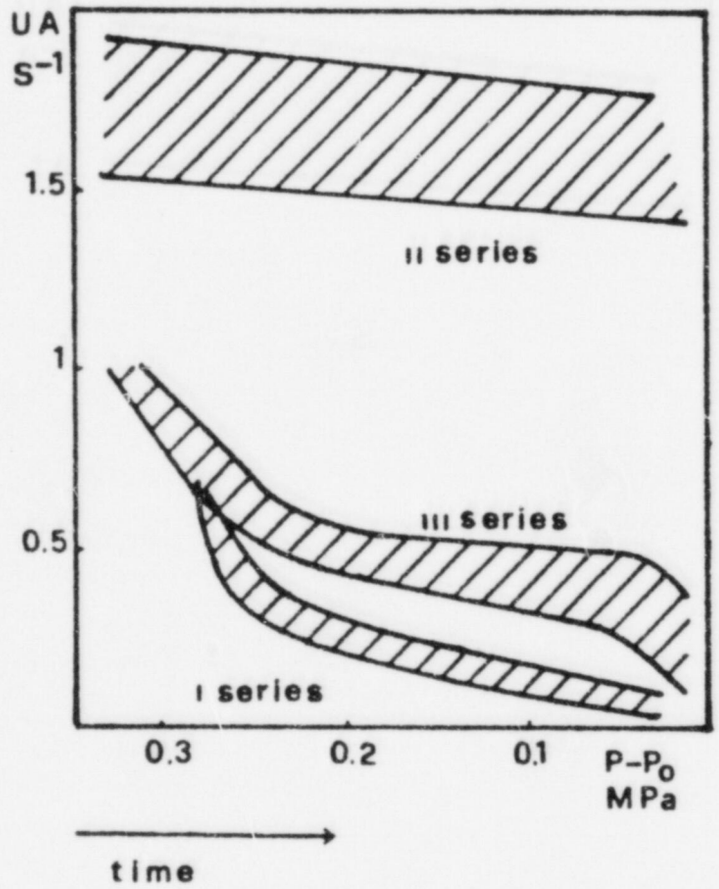


Fig.II- Comparison of heat transfer coefficients for different spray flow-rates.

j) Δt_{10} is constant in the 2nd (1-1.5 s) and 3rd (4-5 s) series; in the "dry" tests it decreases, as initial hydrogen concentration increases, although it is always higher than its values in the 2nd and 3rd series (Fig.10).

k) In the "dry" tests the heat transfer decreases as $(P-P_0)$ decreases (Fig.11), because it depends on the natural convection.

At high pressure values, that is immediately after the burn of very reactive mixtures, fan effect is quite negligible, probably because the deflagration generated turbulence is high enough; on the contrary, the effect is perceptible at lower pressure values.

l) In the 2nd series the thermal resistance values are essentially constant (Fig.11), because the strong forced convection makes buoyancy effects negligible. They are also lower than those from the "dry" tests, because heat transfer surfaces are larger and, moreover, wet (Fig.11).

m) In the 3rd series the heat transfer coefficient has intermediate values (Fig.11), due to the less severe spraying conditions.

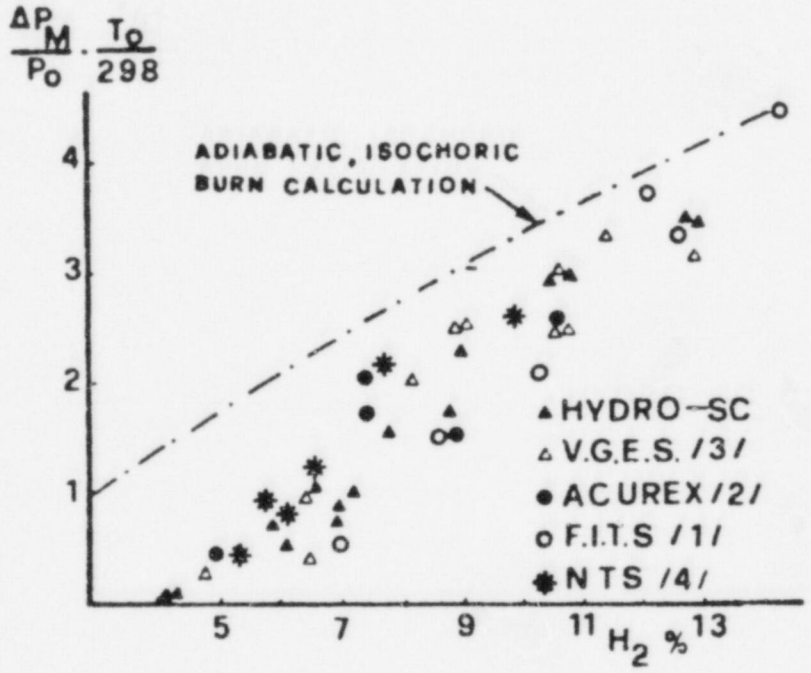


Fig.12- Comparison of normalized pressure rises for different test facilities.

6 CONCLUSIONS

The experiments on hydrogen-air deflagrations in a closed vessel, carried out with HYDRO-SC facility at University of Pisa (Italy), show that:

- The test vessel is much smaller than LWRs safety containments (8000-70000 m^3), therefore scale effects could be significant, even if the HYDRO-SC main results are in accordance with data obtained from other laboratories, Fig.12/1/2/3/4/, where also much larger (up to 2100 m^3) vessels are used. However it cannot be excluded that the same phenomena which caused the pressure oscillations in the HYDRO-SC vessel may produce pressure waves with different amplitudes and frequencies in safety containments. In fact, these phenomena are greatly affected by scale effects and by compartments and obstacles and they are one of the causes of the

deflagration-detonation transition, but, for H_2 molar fractions < 10%, this risk may be considered negligible.
- The lean flammability limit of H_2-air mixtures was confirmed and it was not influenced by the utilized water sprays.
- The glow plug igniter was effective and reliable, even with spray on.
- Burnt H_2 fraction and peak pressure are functions of gas turbulence and heat transfer, as well as of the H_2 initial concentration. In "dry" tests with the igniter located at the bottom of the vessel, at H_2 molar fractions higher than 8%, burn completeness approaches 100%, even with the fan off. In tests with spray on, the burn efficiency increases, if heat transfer is not too high, and pressure transients are faster.
- Flame development depends on buoyancy forces, mixture reactivity and forced convection.

ACKNOWLEDGMENTS

The authors would like to express their sincere thanks to F.Carnasciali, A.Cerboncini, G.B.Curti, C.Dellabiancia, G.Giusti, M.Posarelli for their active cooperation in conducting the experiments.

REFERENCES

1. Roller, S. F. and Falacy S. M.:" Proceedings of the Second International Conference on the Impact of Hydrogen on Water Reactor Safety", p.683, NUREG/CP-0038, EPRI RP 1932-35, SAND82-2456, 1982.
2. Torok, R., Siefert, K., Wachtler, W., Gay, R. R., Gloski, D. M. and Wanless, J. W.:" Hydrogen Combustion and Control Studies in Intermediate Scale", EPRI NP-2953, 1983.
3. Benedick, W. B., Cummings, J. C. and Prassinos, P. G.: "Combustion of Hydrogen:Air Mixtures in the VGES Cylindrical Tank", NUREG/CR-3273, SAND83-1022, 1984.
4. Ratzel, A. C.:" Data Analyses for Nevada Test Site (NTS) Premixed Combustion Tests", NUREG/CR-4138, SAND85-0135, 1985.

Scaling and Extrapolation of Hydrogen Distribution Experiments

H.Karwat
Techn.University Munich F.R.G.

1. Preface

The containment plays an important role in predicting the residual risk to the environment under severe accident conditions. Risk analyses show that massive fission product release from the reactor fuel can occur only if during a loss of coolant the core is severely damaged and a containment failure is anticipated. Large amounts of hydrogen inevitably, are formed during the core degradation and will be released into the containment. More combustible gases are produced later when the coremelt will contact the containment concrete.Thus a potential for an early containment failure exists if a massive hydrogen deflagration cannot be excluded. A more remote cause for early containment failure may be an energetic steam explosion which requires a number of independent conditions when the molten core material contacts residual coolant water.
The prediction of the containment loads caused by a hydrogen combustion is dependent on the prediction of the combustion mode. On the other hand the combustion mode is essentially determined by the geometry of the "combustion chamber" (the containment) and the distribution of the combustible gases, the air and water vapour released during the preceding blowdown of the initiating loss of coolant accident. Without knowledge on the pre-ignition gas distribution the predictions on loads caused by a combustion are highly unreliable and even the interpretation of combustions experiments becomes questionable. The distribution of gas concentrations throughout the containment therefore is a central problem for the prediction of the containment behaviour during severe accidents and for the interpretation and extrapolation of many combustion experiments.
Gas concentration distribution, combustion modes, resulting containment loads and possible containment failure mechanisms are predicted by a group of computer programs which have been set up to describe the course of interacting or independent physical events occurring within the containment.

This paper is based on results of a study contract with the Commission of the European Communities (Nr. ECI - B7221 - 84 - D), which will be published in total as an EUR-Report in the near future.

A previous EURATOM-sponsored investigation into the problems of scaling and extrapolation of heat transfer and fluiddynamics in the field of Design Basis Accident scenarios /1/ illuminated the continuous need for the assessment of scale effects to avoid a misinterpretation of experimental results when and wherever applied to predict the behaviour of full size prototype plants. The central role of computer codes as the indispensable analytical tool for the interpretation of experimental evidence and for the extrapolation of quantitative observations has been stressed. Fundamentally, a scale and test rig independent code system is required to achieve this task.

Code assessment is based on the comparison of experimental results with calculated parameters. Disagreement is indicative for shortcomings of the analytical simulation, if the reliability of measured data can be assured. The selection of an appropriate heat transfer option in combination with the adopted space discretisation concepts is decisive for successful predictions or posttest analyses. However, the choice of code options in combination with the applied space discretisation often varies from experiment to experiment and varies in general when comparable experiments performed in different test rigs are analyzed. Is the computer code formulation and application dependent on the test rig and its scale?

In the following paper an attempt is made to identify on basis of a dimensional analysis such areas for which particular care must be exercised when scale experimental evidence is interpreted and extrapolated with the aid of a computer code or a system of computer codes. The study is restricted to fluiddynamic phenomena of the gas distribution process within the containment atmosphere. The gas sources and the mechanical response of containment structures are considered as given boundary conditions under which the containment is to be analyzed.

2. The Distribution Equations

Natural circulation behaviour is an essential phenomenon which must be simulated to the best possible extent if hydrogen distribution within a containment is to be predicted. The basis for the following dimensional analysis has been a typical set of conservation equations on which frequently used lumped parameter codes are normally based.

The properties of air and hydrogen are assumed to follow the general gas equation in terms of their partial pressures, and the vapour pressure of water follows the usual equation of state for saturated water. Within a node thermal equilibrium between all components of the gas/vapour phase and with a liquid phase has been assumed. Gas diffusion may be neglected if compared to a natural convection process for the gas transport. The following set of equations has been considered in one - dimensional notation for the fluiddynamic state of the containment:

Air balance:

$$\frac{\partial \varrho_A}{\partial t} + \frac{\partial (\varrho_A \cdot w)}{\partial x} = 0 \qquad (1)$$

Hydrogen balance:

$$\frac{\partial \varrho_H}{\partial t} + \frac{\partial (\varrho_H \cdot w)}{\partial x} + \frac{d(\varrho_{HS} \cdot Q)}{dV_G} = 0 \qquad (2)$$

Vapour balance:

$$\frac{\partial \varrho_D}{\partial t} + \frac{\partial (\varrho_D \cdot w)}{\partial x} + \frac{d(\varrho_D \cdot Q + G_V)}{dV_G} = 0 \qquad (3)$$

Mechanical water droplet balance:

$$\frac{\partial \varrho_{WG}}{\partial t} + \frac{\partial (\varrho_{WG} \cdot w)}{\partial x} - \frac{d}{dV_G}\left(G_{W,SEP} + \frac{\varrho_{WG} \cdot V_G \cdot G_V}{M_W}\right) = 0 \qquad (4)$$

Energy balance for the gas phase:

$$\frac{\partial}{\partial t}\left[\left(\frac{w^2}{2} + h_b - \frac{P}{\varrho_b}\right)\varrho_b\right] - \frac{\partial}{\partial x}\left[\left(\frac{w^2}{2} + h_b\right)\varrho_b w\right] - q - \frac{\partial}{\partial V_b}(\varrho_S h_S Q) = 0 \qquad (5)$$

with

$$\varrho_b = \varrho_A + \varrho_H + \varrho_D + \varrho_{WG}$$

The principal source of mass and energy from the primary system is considered to be a specified volume source Q which has the specific enthalpy h_s and a mixture density ρ_s. Both must be specified from a core behaviour analysis.

The energy addition rate q may be split up into two components

$$q = q_{Vol} + q_{Struc}\frac{F_G}{V_G} \qquad q_{Vol} = \varrho_{AG} \cdot I_{Rad} \qquad (6)$$

describing the amount of heat exchanged with adjacent structures by q_{struc} and an eventual heat source distributed throughout the gas volume by q_{vol} stemming from radioactive fission products or from a uniform hydrogen burn.

The equation of motion can be expressed by

$$\frac{\partial (\varrho_b \cdot w)}{\partial t} + \frac{\partial}{\partial x}\left(\varrho_b \cdot \frac{w^2}{2}\right) - \varrho_b \cdot g \cdot \cos\alpha + \frac{\partial P}{\partial x} - R = 0 \qquad (7)$$

with cos α indicating the effect of the inclination of a flow channel from the vertical (see Fig.1).

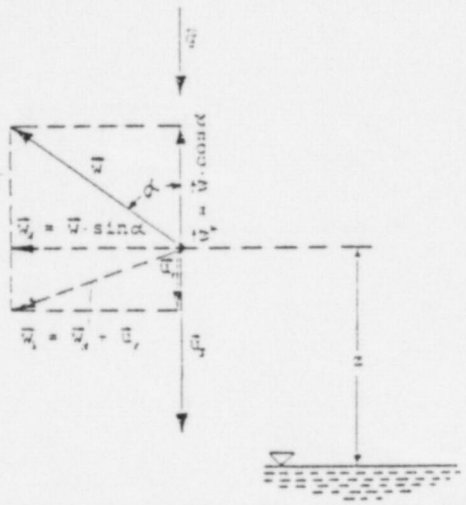


Fig.1 Velocity Diagram and Gravity Field

The flow resistance term R must be further processed in the form of an appropriate resistance law depending on the prevailing flow conditions. E.g. could it be replaced by any turbulent friction correlation.
The local overall pressure of the gas/vapour space is given by

$$P_{ges} = p_A + p_H + p_S = \frac{T}{V_G}(R_A \cdot M_A + R_H \cdot M_H) + p_s(T) \qquad (8)$$

according to Dalton`s law with the gas constants R_A for air resp. R_H for hydrogen and the absolute temperature of the mixture as the governing common variable.
The possible presence of aerosols is considered to be of influence on the overall natural convection behaviour of the containment atmosphere. Radioactive aerosols may act as volumetric heat sources and promote buoyancy effects. An estimation about the aerosol concentration within containment may be helpfull.

A typical differential equation for the <u>aerosol concentration</u> within a given space of the size dx may be

$$\frac{\partial}{\partial t}\rho_{AG} + \frac{\partial}{\partial x}(\rho_{AG} w) + \rho_{AG} Q - \left(\frac{2 g r^2}{9\eta} C(r) w \cos\alpha\right) \frac{dF_L}{dV_G} \rho_{AG} = 0 \qquad (9)$$

The last term w·cos α may be representative for the aerosol motion caused by the superficial convective field which may in general have an α-inclination from the upward vertical (opposite to gravitational effects). The aerosol density of the source ρ_{AGS} will be strongly interrelated with the source rates for vapour and hydrogen in the sense that both components serve as the carrier for aerosols and other fission products from the primary system into the containment.

<u>A liquid phase</u> must be specified for each containment subvolume for which evaporation or condensation may occur. These may take place under thermodynamic equilibrium (both exchanging phases at the same temperature) or under partial nonequilibrium to be specified empirically. For the

present study thermal equilibrium was assumed involving in particular mass exchange between droplets originating from discharging jets in the early phase of an accident, from fog formation or to a certain extent also for those droplets injected into the containment from containment spray systems. Droplets may in general be quasi homogeneously distributed within the gasphase volume while all other water masses involved (condensate films at surfaces accumulated sump water) are not. These circumstances make it extremely difficult to formulate an appropriate sump water balance in one dimensional notation, which afterwards could be treated by an available numerical solution procedure without specified precautions. For the purpose of this similarity study however, an ordinary differential equation was chosen which could be applied to an appropriate combination of specified finite differences of the gas phase or in a more easy way within a partially integrated lumped parameter concept.

$$\frac{dM_{WS}}{dt} = G_{W,SEP} - G_V\left(1 - \frac{\varrho_{WG} V_G}{M_W}\right) + S_{WS} \qquad (10)$$

with

$$G_{W,SEP} = C_{WA} G_{WG} + \frac{\sqrt{2 g H}\, M_{WG}}{H} \qquad (11)$$

Here, S_{WS} must be specified by an input function to describe the transport of liquid water, not in the constitution of airborne droplets, between corresponding compartments. It may include the condensation of the vapour at subcooled surfaces, if not determined otherwise. For thermal equilibrium the mass exchange rates between the phases may be expressed by

$$G_V = \left(-\varrho_D M_D \varepsilon_D^{-1} - \varrho_D M_W \varepsilon_W^{-1}\right) \dot{P} - F_G \frac{\varrho_D^2}{\varrho_b} \frac{\partial w}{\partial x} dx \left(1 - \frac{\varrho_{WG}}{\varrho_W}\right) \qquad (12)$$

where $M_w = \xi M_{ws} + V_G \cdot \rho_{wg}$ describes the fraction of the sump water which could be empirically specified as being in thermal equilibrium with the vapour phase. Equations (11) and (12) are also processed within the mechanical water droplet balance described in equation (4).

3. Dimensionless Parameter Groups

Similarity considerations are necessary to assess the requirements for the design and operation of scale model experiments and for the correct interpretation of test results for application in full size prototypes. The set of differential equations described in section 2 served as the basis to determine the similarity requirements for natural convection experiments. Additionally the presupposition is made that a scale geometrically similar replica of the prototype facility exists to conduct the experiment.
For all involved process parameters of the analytical description (the set of governing differential equations) dimensionless ratios

$$\frac{\Phi_{Prototype}}{\Phi_{Testing}} = \Phi^*_{Modelling} \longrightarrow \frac{\Phi}{\Phi'} = \Phi^*$$

have been defined and introduced into the set of equations. All linear dimensions of both systems are correlated by a unique geometric scaling factor and the time ratio of relevant markable events occuring in a prototype and a test rig after initiation of an experiment may eventually be correlated by

$$\frac{x_p}{x_T} = x_M^* \longrightarrow \frac{x}{x'} = x^* \qquad \frac{t_p}{t_T} = t_M^* \longrightarrow \frac{t}{t'} = t^*$$

Substituting $t = t' \cdot t^*$, $x = x' \cdot x^*$ and $\Phi_i = \Phi_i' \cdot \Phi_i^*$

within all involved field and constitutive equations correlates the differential equations of the protoptye with those of the test rig. The general form

$$\frac{\partial(\phi'\phi^*)}{\partial(t't^*)} + a'a^* \frac{\partial(\phi'\phi^*)}{\partial(x'x^*)} + b'b^*\phi'\phi^* + \cdots = y'y^* \tag{13}$$

finally results in

$$\frac{\partial\phi'}{\partial t'} + \frac{a^*t^*}{x^*} \cdot \frac{\partial\phi'}{\partial x'} + b^*t^*b'\phi' + \cdots = \frac{y^*t^*}{\phi^*} y' \tag{14}$$

The functions $\frac{\partial\Phi}{\partial t}$ and $\frac{\partial\Phi}{\partial t'}$ will describe a dynamically

similar or identical process Φ if the dimensionless parameter- group ratios π_i^* could be influenced in such a way that their values remain close to 1.0 during the time period of interest. If we are more interested to compare the local variation of the parameters
a different combination of the parameter groups will be important for similarity e.g.of a steady state process.

$$\frac{\partial\phi'}{\partial x'} + \frac{1}{\tilde{\Pi}_{i-1}^*} \cdot \frac{\partial\phi'}{\partial t'} + \frac{\tilde{\Pi}_i^*}{\tilde{\Pi}_{i-1}^*} \cdot b'\phi' + \cdots = \frac{\tilde{\Pi}_{i+1}^*}{\tilde{\Pi}_{i-1}^*} y' \tag{15}$$

The procedure has been applied to each of the conservation equations described in section 2. A modified set of one dimensional differential equations has been obtained with dimensionless parameter group ratios π_i^* linking the expected behaviour of the large size prototype to that of an experimental model (or vice versa). As example the modified balances for water vapour, hydrogen and the equation of motion are shown.

Vapour balance:

$$\frac{\partial\varrho_D'}{\partial t'} + \tilde{\Pi}_{11}^* \frac{\partial(\varrho_D' w')}{\partial x'} - \tilde{\Pi}_{12}^* \varepsilon_G' \dot{P}' + \tilde{\Pi}_{13}^* \frac{d}{dV_G'}\left(V_W' \frac{\varrho_D'}{\varrho_W'} \varepsilon_W' \dot{P}'\right) - \left(\tilde{\Pi}_{14}^* \frac{\varrho_D'}{L'} - \tilde{\Pi}_{15}^* \frac{\varrho_D'\varrho_{WG}'}{\varrho_W' L'}\right) \frac{\partial w'}{\partial x'} dx' + \tilde{\Pi}_{16}^* \frac{d(\varrho_{DG}' Q')}{dV_G'} = 0 \tag{16}$$

Hydrogen balance:

$$\frac{\partial\varrho_H'}{\partial t'} + \tilde{\Pi}_{21}^* \frac{\partial(\varrho_H' w')}{\partial x'} + \tilde{\Pi}_{22}^* \frac{d(\varrho_{HS}' Q')}{dV_G'} = 0 \tag{17}$$

Equation of motion:

$$\frac{\partial}{\partial x'}\left(\frac{w'^2}{2}\right)+\tilde{\pi}_{51}^{*}\frac{\partial w'}{\partial t'}-\tilde{\pi}_{52}^{*}\,g'\cos\alpha'-\tilde{\pi}_{53}^{*}\frac{1}{\rho_b'}\frac{\partial P'}{\partial x'}-\tilde{\pi}_{54}^{*}\frac{R'}{\rho_b'}=0 \qquad (18)$$

Tables 1 and 2 summarize the dimensionless parameter groups π_j listed according to the originating partial differential equations relevant for slow long term events. The first columns of the table give the parameter groups π_j for the time derivatives ($\partial\phi/\partial t$) while the second or third column are the parameter combinations obtained for the space derivatives ($\partial\phi/\partial x$) indicated in the tables.
The parameter groups π_j do not comprise committments with respect to an applied space discretisation concept except where the equations require a definition of the volume to which source terms or other empirical correlations may apply.

4. Discussion of Some Similarity Requirements

It is assumed that an experiment is performed within a geometrically similar test rig with the same fluid components which are expected to dominate within the containment atmosphere of the prototype plant. These are steam, water, air, hydrogen and in certain cases a typical aerosol. An attempt is made to interpret the fluiddynamic aspects of the long term behaviour of the containment and the technical boundary conditions of experiments, such as the relevant initial conditions of the containment and the determination of scaled source terms to be applied during the test (operating conditions).
The internal structures of the containment are considered as effectively determining local flow resistances and heat exchange processes with the steam-gas mixture for the entire long-term severe accident periods. They should serve as an essential orientation to select an appropriate nodalisation scheme for lumped parameter codes which together with the code form the analytical model describing the interrelated physical phenomena within the containment.
Principally, it is not possible to satisfy the basic requirement that all parameter groups π_j^* approach 1. Only to a very limited extend it may be possible to select the initial conditions and to operate an experiment in such a way that certain partial aspects of the involved physical events are optimized with respect to similarity. A carefull assessment of the involved parameter groups of each differential equation may be indicative to which extent physical similarity of the observed phenomena is to be expected.

4.1 The Initial Conditions

With a few exceptions the scenarios of severe accidents are characterized by a preceding loss of coolant accident and the associated release of large amounts of pressurized water and steam into the containment. The mass and energy release is terminated after pressure equilibrium between the

primary system and the containment has been reached. Depending on the size of the rupture the energy discharge may last for 30 seconds and more.

Some similarity considerations concerning the local and overall pressurisation of a containment have been communicated earlier in /2/. All PWR-containment pressurisation experiments have been performed so far under operating conditions preserving the overall pressure transient. The release rates for mass and energy into the containment were scaled proportional to the scaling of the free volume of the containment test rig. Although the short term local pressurisation and the pressure wave propagation process may be distorted by an unproportional local blowdown jet disintegration, this operational scaling method results in a proper energy discharge per unit of the free containment volume. The maximum total containment pressure can easily be interpreted if the increased ratio of the global surfaces to volumes F/V of the experimental test rig is known.

For the subsequent natural convection it is of primary importance to assess the energy and mass distribution within the containment atmosphere, and the energy absorption by the internal containment structures during and immediately after the blowdown. Both phenomena describe possible starting conditions of a containment long-term experiment.

For this time period the parameter groups π_{61} through π_{66} originating from the energy transport equations are of importance. Because the quasi steady starting conditions of the energy distribution will strongly influence the subsequent experimental natural convection pattern, the parameter groups which govern the local enthalpy distribution are indicative for the local distribution of the containment atmosphere temperature.

The Strouhal-number Sr, which characterizes many technical transport processes is originating from all conservation equations. It combines the ratios of the linear dimensions x* with those for the time t* and the velocity field W* during the preceding blowdown process and the natural convection established after termination of the blowdown. During the blowdown it is principally possible to influence the velocity field in the neighbourhood of the location of the coolant release by the chosen operating conditions of the high pressure energy reservoir which govern the choking properties /2/. Traditionally, LOCA experiments within containment simulators were performed heading for a time-transient conserving mode of operation resulting roughly in t*=1 as a good approximation during the blowdown.

After termination of the blowdown essentially no practicable possibility exists to influence velocity fields any longer. Therefore we have to carefully assess the physical processes for which global or local velocity fields are important.

Local energy deposition results in the generation of a temperature field via the local heat transfer and conduction capabilities of the involved structure and its surface. Clearly, this event is characterized the parameter group π_{64}, which describes the ratio storage/transport of energy. It reads

$$\tilde{\pi}_{64} = \frac{x \cdot q_{Struc} F_G}{w \rho_b \cdot h_b V_G} = \frac{\alpha_{Loc} (T_F - T_{Struc})}{w_{Loc} \rho_b \cdot h_b} \cdot \frac{x}{L}$$

if it is controlled by surface heat transfer and

$$\pi_{64} = \frac{\lambda_{Struc} \cdot \left(\frac{\partial T}{\partial x}\right)_{Struc}}{w_{Loc} \cdot \rho_b \cdot h_b} \cdot \frac{x}{L}$$

if heat soakage (or release) is controlled by the heat conduction properties of the involved structure.
For the geometrically similar test rig X* is compensated by (F/V)* reducing the parameter group π_{64}* to

$$\pi_{64}^* = \frac{\alpha_{Loc} \cdot \Delta T}{w_{Loc} \cdot \rho_b \cdot h_b}$$ (also known as the Stanton Number)

Careful measurements of the temperature distribution and the local velocities would be important elements to properly assess these conditions. As no practical possibility exists to actively influence the initial conditions of a long-term natural convection experiment, the additional necessity to couple such experiments with a preceding typical blowdown experiment is obvious. This would at least allow a minimum degree of similarity to the prototype behaviour.

4.2. Long-term Mass - Distribution Events

The assumption is made that at the end of the blowdown the typical distributions of the stored energy within adjacent structures and of the local fluid temperatures within the free containment atmosphere is known and possible distortions have been carefully assessed. At a certain prespecified time a new fluid source term consisting of a mixture of steam, hydrogen and some aerosols must be given as an "operating condition" during the subsequent test period.
Due to the nature of typical containment transients a source term has always to be specified as a localized event. It is never uniformly distributed and in analytical modelling a proper decision is required to which space discretisation element the source has to be associated. Here the parameter groups π_{22}, π_{42}, π_{66} and π_{77} are addressed. A committment to which local volume the adopted source-term has to be allocated must be made. The source term consists of a volumetric steam/gas flow rate Q and a representative information about the aerosol and/or hydrogen concentration or density (e.g. ρ_{AGS} and ρ_{HS}). For a substructured system the location of the sourceterm within the nodalized analytical model is given by the reference volume V_g which appears in the parameter groups.
For the average concentration of a component (hydrogen or aerosol) within the free space of the containment the entire volume of the containment would be the representative reference parameter. For the blowdown-related thermohydraulic experiments this concept has always been adopted leading to the time-preservation of the resulting pressure transient. If it is practical to preserve the globally averaged concentration of hydrogen or aerosols, then the source term quantification should also be scaled to the available free volume of the entire test facility, yielding a source term with an equivalent volumetric scaling ratio.

However, the combination of many parameter groups with the Strouhal Numbers $\pi_{11}=\pi_{21}=\pi_{31}=\pi_{41}=\pi_{61}$ suggests for the local distribution of observed concentrations the possibility of a distortion in one or the other direction. Again, no practicable method is available to influence the local Strouhal numbers, resp. the local velocities or the transport times.
For the lumped parameter concept the control volume V_g is a unit cell for which immediate homogenized local mixing is assumed. The Strouhal-Number Sr can be easily modified if multiplied by the specified flow-area F_b and the hydrogen (or aerosol) density. Replacing x by a characteristic length L of control volume yields

$$Sr = \frac{x}{w \cdot t} = \frac{F_b \cdot \vartheta \cdot L}{F_b \cdot \vartheta \cdot w \cdot t} = \frac{M}{G \cdot t}$$

In this form Sr may also be interpreted as a mixing or replacing intensity of the local mass flow within a specified computation cell. In combination with the local source term groups (π_{22} etc.) it gives the ratio of the source strength to the convective transport capability for the component of interest. To obtain similarity in the vicinity of the source, it may be important to preserve at least the relative size of the volume V_G to which the source should be associated. The resulting convective velocities (or mass flows) to adjacent control volumes and the resulting component densities are not amenable to active control and the associated distortions must be assessed on basis of locally measured parameters.
The generated velocity field is of utmost importance in the context as the link between the source and the resulting distribution. This leads to the interpretation of the parameter groups originating from the momentum equation. Because in long-term experiments we are primarily interested in the development of the quasi-stationary velocity field of the scaled model, the momentum equation must be discussed in the form

$$\frac{\partial\left(\frac{w'^2}{2}\right)}{\partial x'} = -\tilde{\imath}_{51}^{*} \cdot \frac{\partial w'}{\partial t'} + \tilde{\imath}_{52}^{*} g' - \tilde{\imath}_{53}^{*} \frac{1}{\vartheta_b'} \frac{\partial P'}{\partial x'} + \tilde{\imath}_{54}^{*} \frac{R'}{\vartheta_b'}$$

The term distortion may generally be defined as a partial or total suppression of physical processes (sometimes also called physical phenomena) observed by only changing the size (geometric dimensions) or the shape (arrangement of components) of the test rigs, although the same experiment with an identical goal is performed in both facilities. Such distortions may also be caused by differences in the mode of operation of the rigs considered or by the use of different materials (see also /1/).

with parameter groups π_{51}^* to π_{54}^* listed for the interpretation of velocity fields. Actually π_{51}^*, the Strouhal-Number, is of minor importance here, because the time derivatives of the velocity field may approach zero under quasi-stationary conditions. As expected, the Froude-Number and the Euler-Number are decisive. For practical application the Euler-Number

$$\tilde{\pi}_{53}^* = Eu^* = \frac{P^*}{w^{*2} \cdot \varrho_b^*} \Rightarrow \frac{\Delta P^*}{w^{*2} \cdot \varrho_b^*}$$

can be expressed by a small driving pressure difference ΔP in relation to small absolute values of W. The Eu-Number remains an important similarity parameter which must be assessed for the interpretation of an experimental result. The Froude - Number ratio

$$\tilde{\pi}_{52}^* = Fr^{*-1} = \frac{g^* \cdot x^*}{w^{*2}} = \frac{x^*}{w^{*2}}$$

correlates the buoyancy effects to the kinetic energy of the fluid and indicates the interrelation of available geodetic elevation to the achievable buoyancy driven velocity field. Only if geometric similarity is given X^* is also representative for the ratio of elevations H^*. In all other cases specific attention must be given to the geometric distortion of the test rig in vertical direction. Because of $g^*=1$ a direct relation between the kinetic energy and the available elevation is given if the velocity W is measured at many distinct locations within the containment it appears possible to assess the experiment with respect to of the important parameter groups Fr, Eu and Sr.

With respect to the local distribution of hydrogen concentrations it can be concluded, that only two possibilities exist to actively control an experiment to optimize similarity. Coupling of the experiment with a preceding volumetrically scaled blowdown may prove to yield the most similar initial conditions for the subsequent natural convection processes. Proper spatial location of the volumetrically scaled hydrogen source warrants the preservation of the globally averaged hydrogen concentration transient. An assessment of the similarity of the resulting transient concentration distribution seems only possible by a carefull analytical simulation of the experiment in combination with a sufficiently large number of local velocity measurements.

5. Code Verification and Physical Similarity

The interpretation and the extrapolation of experimental results require the committment to an appropriate simulation model. Ideally, a code should be available which has been verified by a large number of experiments performed at different scaling levels with universally valid experience in application. By "experience in application" we have in mind the choice of the code and the strategy to use it. The space discretisation concept (nodalisation of a lumped parameter approach) and the necessary degree of detailism of the heat exchange simulation with the confining structures, which together with the processed physical equations form "the simulation model" are addressed primarily. In reality, for the severe accident scenarios several codes are on hand, but little or no documented experience

in application for test rig simulation exists. The first steps of code assessment are just made.

What is the possible benefit of similarity considerations for the code assessment work?
An essential element of code assessment is the manifold comparison of measured with calculated parameter for relevant experiments. The code user describes the structures and properties of a given test rig by the chosen discretisation scheme for the fluid space and the confining structures. Both are coupled by the empirical heat transfer correlations, which also are governed by the fluiddynamic state at the surface of the structure. The code user has to specify the friction and formloss coefficients, which are very closely linked to the adopted space discretisation scheme. The properties of the source (mass and energy) have to be provided by input functions and the location of the source is again closely connected to the applied nodalisation concept. The success of the analytical simulation is decided upon the observed agreement between calculated and measured parameters, provided the measured data is a reliable decision basis. Subjective disagreement leads to the modification of the analytical model until satisfactory results are obtained and a new point of a verification matrix is produced. If perfectly done the experience in terms of recommended discretisation schemes, heat transfer correlations, friction and formloss coefficients and other hints are documented and communicated to other code users.

Similarity considerations can be helpfull to assess the general validity of the obtained empiricism in code verification, which very often varies from experiment to experiment and varies in general when comparable experiments are performed in different test rigs. Enough examples for this situation are available for code application in the field of the two-phase flow thermohydraulics of emergency core cooling. One reason for this can be seen in the fact that for such code applications the check of convergence of the calculated results with respect to the underlying space discretisation (or nodalisation) concept became impossible and is never attempted for lack of the necessary computation time.

In this context the assessment of the physical similarity of simulated events could help to identify the specific conditions under which the code was successfully applied and for which future code application would be reliable. For hydrogen distribution experiments and their gravity dominated convection flows the space discretisation, the choice of friction or formloss factors and the selected heat transfer correlations are strongly interrelated and decisive for the successfull modeling. The similarity parameter groups π_{52} to π_{54} originating from the equation of motion can be utilized to check for the similarity with respect to friction formloss and buoyancy effects caused by the flow pattern. The parameter groups π_{64} to π_{66} will give information about the similarity of the heat exchange process with the structures and the resulting influence on the density distribution, eventually in combination with a consideration of the Strouhal-number and some of those parameter groups describing mass exchange effects with the liquid phase.

The judgement of the similarity of observed physical events within a test rig with those expected to occur in a prototype plant is of course also a matter of speculation, because (fortunately) prototype experience is not available. But it could work when the behaviour of different experimental facilities is compared between each other, preferrably in case where different geometric scaling to the prototype is involved.

6. Conclusions

Scaling of hydrogen or aerosol distribution experiments is difficult to control as far as natural convection flow behaviour is concerned. A minimum requirement to obtain reasonably similar initial conditions is to perform such experiments coupled with relevant preceding primary coolant blowdown experiments. During the blowdown the characteristic distribution of energy within the free containment space and the surrounding structures is formed which later essentially controls natural convection flows. In terms of measured parameters the experimental results can be assessed in view of the similarity to other experimental evidence by means of derived parameter groups of scaling. This may be in particular important if the experimental data base is used for code verification because it offers the chance to minimize facility dependent conclusions which could jeopardize the general code applicability.

7. References

/1/ Karwat, H.;Problems of Scaling and Extrapolation of Experimental Results in the Aerea of Fluiddynamics and Associated Heat Transfer Related to Reactor Safety; CEC Research Report EUR-10028 EN; 1985

/2/ Karwat, H.; Problems Associated to the Extrapolation of Containment Experiments; Proc.Int.Meeting Thermal Nuclear Reactor Safety; 1984, KfK-Report 3380; Vol.2 p.1291-1300.

Nomenclature

A	flow area	m^2
c	constants	(locally defined)
F	heat transfer surface	m^2
g	gravity constant	m/s^2
G	mass flow rate	kg/s
h	specific enthalpy	J/kg
H	height of a compartment node	m
I	heat intensity of aerosols	W/kg
L	length between node centers	m
M	mass	kg
N	particles per volume	$1/m^3$
P	pressure	N/m^2
p	partial pressure	N/m^2
Q	source from primary system	m^3/s
q	heat source	J/m^3 s
R	gas constant	KJ/kg K
R	friction pressure loss	bar/m
r	radius	m
S	source	$kg/s \cdot m^3$
t	time	s
T	temperature	K
U_s	deposition velocity	m/s
V	volume	m^3
W	velocity	m/s
X	length coordinate	m

α	flow inclination	
ε	compressibility	kg/mN
ρ	density	kg/m^3
η	dynamic viscosity	kg/ms
ξ	part in thermal equilibrium	
π	dimensionless parameter group	

Subscripts

A_G	aerosol, gasborne
b	in motion
D	vapor phase
E	energy
G	gase phase
H	hydrogen
rad	nuclear decay
S	source related
W	water phase
WG	water droplets, gasborne
Ws	sump water
V	vaporisation

Vapour - Distribution

	transient $\frac{\delta\rho_D}{\delta t}$	stationary $\frac{\delta(\rho_D w)}{\delta x}$
Π_{11}	$\frac{w \cdot t}{x}$	$\frac{x}{w \cdot t} = Sr$
Π_{12}	$\frac{\varepsilon_D P}{\rho_D}$	$\frac{\varepsilon_D \cdot P}{\rho_D} \cdot \Pi_{11}$
Π_{13}	$\frac{\varepsilon_w P}{\rho_w} \zeta \frac{V_{ws}}{V_G}$	$\frac{\varepsilon_w P}{\rho_w} \zeta \frac{V_{ws}}{V_G} \Pi_{11}$
Π_{14}	$\Pi_{11} \cdot \frac{x}{L}$	$\frac{x}{L}$
Π_{15}	$\frac{\rho_{wG}}{\rho_w} \Pi_{14}$	$\frac{\rho_{wG}}{\rho_w} \cdot \Pi_{14}$
Π_{16}	$\frac{\rho_{DS} Q t}{V_G \rho_D}$	$\frac{\rho_{DS} Q t}{V_G \rho_D} \cdot \Pi_{11}$

Hydrogen and Air Distribution

	transient $\frac{\delta\rho_{H,A}}{\delta t}$	stationary $\frac{\delta(\rho_{H,A} \cdot w)}{\delta x}$
Π_{21}	$\frac{w \cdot t}{x}$	$\frac{x}{w \cdot t} = Sr$
Π_{22}	$\frac{\rho_{HS} Q t}{V_G \rho_H}$	$\frac{\rho_{HS} Q t}{V_G \rho_H} \cdot \Pi_{21}$

Aerosol - Density

	transient $\frac{\partial(\rho_{AG})}{\partial t}$	stationary $\frac{\partial(\rho_{AG} \cdot w)}{\partial x}$
Π_{41}	$\frac{w \cdot t}{x}$	$\frac{x}{w \cdot t} = Sr$
Π_{42}	$\frac{\rho_{AGS} Q t}{V_G \rho_{AG}}$	$\frac{\rho_{AGS} Q \cdot t}{V_G \rho_{AG}} \cdot \Pi_{41}$
Π_{43}	$\Pi_{41} \frac{x}{H} \cos\alpha$	$\frac{x}{H} \cos\alpha$
Π_{44}	$\frac{C \rho_{eff} g r_A^2 t}{\eta H}$	$\frac{C \rho_{eff} g r_A^2 t}{\eta H} \Pi_{41}$

Momentum - Equation

	Velocity Field $\frac{\partial(\frac{w^2}{2})}{\partial x}$	Pressure Field $\frac{\partial P}{\partial x}$
Π_{51}	$\frac{x}{w \cdot t}$	$\frac{\rho_b w \cdot x}{P \cdot t}$
Π_{52}	$\cos\alpha \frac{g \cdot x}{w^2} = Fr^{-1}$	$\frac{w^2 \rho_b}{P} \cos\alpha$
Π_{53}	$\frac{P}{w^2 \rho_b} = Eu$	$\frac{g \rho_b x}{P}$
Π_{54}	$\frac{R \cdot x}{w^2 \rho_b} = (Re)$	$\frac{R \cdot x}{P}$

Table 1 Dimensionless Similarity Groups for Geometrically Similar Model Experiments (Part 1)

Energy - Transport

	Enthalpy Transient $\frac{\partial(\rho_b h_b)}{\partial t}$	Pressure Transient $\frac{\partial P}{\partial t}$	Enthalpy Field $\frac{\partial(\rho_b h_b w)}{\partial x}$
Π_{61}	$\frac{w \cdot t}{x}$	$\frac{\rho_b w^2}{P}$	$\frac{x}{w \cdot t} = Sr$
Π_{62}	$\frac{w^2}{h_b}$	$\Pi_{61} \cdot \frac{w \cdot t}{x}$	$\frac{w^2}{h_b}$
Π_{63}	$\frac{P}{\rho_b h_b}$	$\frac{\rho_b h_b}{P}$	$\frac{P}{\rho_b h_b} \cdot \Pi_{61}$
Π_{64}	$\frac{q_{Struc}\, t\, F_G}{\rho_b h_b V_G}$	$\frac{q_{Struc}\, t\, F_G}{P V_G}$	$\frac{x\, q_{Struc}\, F_G}{w \rho_b h_b V_G}$
Π_{65}	$\frac{\rho_{AG} I_{rad}\, t}{\rho_b h_b}$	$\frac{\rho_{AG} I_{rad}\, t}{P}$	$\frac{x\, \rho_{AG} I_{rad}}{w \rho_b h_b}$
Π_{66}	$\frac{\rho_s h_s Q\, t}{V_G \rho_b h_b}$	$\frac{\rho_s h_s Q\, t}{P}$	$\frac{x\, \rho_s h_s Q}{w \rho_b h_b V_G}$

Liquid Phase Balance

	transient $\frac{d M_{ws}}{dt}$
Π_{71}	$C_{WA} \frac{\rho_{WG} V_G}{\rho_W V_{WS}} \frac{w \cdot t}{L}$
Π_{72}	$\sqrt{\frac{g}{H}} \frac{V_G \rho_{WG}}{V_{WS} \rho_W} t$
Π_{73}	$\frac{\varepsilon_D P}{\rho_W} \frac{V_G}{V_{WS}}$
Π_{74}	$\frac{\varepsilon_W P}{\rho_W} \cdot \zeta$
Π_{75}	$\frac{\rho_D V_G}{\rho_W V_{WS}} \frac{w \cdot t}{L}$
Π_{76}	$\Pi_{75} \cdot \frac{\rho_{WG}}{\rho_W}$
Π_{77}	$\frac{S_{WS}\, t}{V_{WS} \rho_W}$

Table 2 Dimensionless Similarity Groups for Geometrically Similar Model Experiments (Part 2)

ON TWO ASPECTS OF HYDROGEN RISK

by A. FORESTIER & S. GOLDSTEIN

D.E.M.T./S.M.T.S./T.T.M.F.

Commissariat à l'Energie Atomique - Saclay - FRANCE

I. INTRODUCTION

The hydrogen risk in nuclear reactors is an extensive problem which includes several aspects ie : the prediction of the total amount of hydrogen release, its mixing with air and possibility of overconcentration in parts of the containment, burning via deflagrations or detonations, mitigation, containment integrity etc... An extensive amount of work has already been devoted to this problem (1).

The scope of this paper is to present two subjects related to hydrogen risk which are in progress at CEA.DEMT and which to our knowledge have been unsufficiently investigated up to now. The first is the possibility of stratification of hydrogen in a large volume when injected from the bottom. The related experimental work is described in § II. The second is the computation of detonation shock waves in confined or semi-confined volumes (§ III) and the resulting impulsive load on the containments.

II. EXPERIMENTAL STUDY OF STRATIFICATION

The volume of a PWR containment can be divided into two parts : the lower compartment region and the upper dome. Most of the hydrogen accumulation experiments found in the litterature are concerned with the lower compartments. The Hanford Engineering Development Laboratory (2) performed a serie of tests in a 850 m^3 model of an ice condenser PWR containment. No hydrogen or helium concentration profiles in the dome were reported. Some fundamental tests were performed in the 80 m^3 central volume of the Battelle Frankfurt (3) facility but with an area source and a slow hydrogen injection rate.

The situation covered by the tests described below is that of a jet discharge in a large volume.

The test facility is shown fig. 1. It is made of a 6 m^3 vessel and pure helium is injected through a hole on the floor. Venting is necessary as the vessel is not designed to support internal pressure. Two vents can be used during an experiment either on the floor (vent A fig. 1) or on the top (vent B fig. 1).

The helium mass flow rate is measured with sonic venturis previously calibrated. Samples of the air-helium mixture in the vessel are taken at different heights and analysed with a mass spectrometer to get the helium concentration profile.

The parameters that can be varied are :

- the jet diameter d

- the inlet helium velocity v

Or in terms of adimensional parameters :

- the ratio = d/D of jet to vessel diameter
- the jet Reynolds number $Re = \frac{\rho_a V d}{\mu}$
- the jet Froude number $Fr = \sqrt{\frac{\rho}{g(\rho_a - \rho_h)}} \frac{V}{\sqrt{d}}$

where ρ_a, ρ_h are the air and helium densities,
μ the helium viscosity
g the gravity acceleration.

Only pure helium being injected, these three parameters are not independant. They are related by :

$$Fr = \sqrt{\frac{\mu^2}{D^3 \rho_h g(\rho_a - \rho_h)}} \frac{Re}{\alpha^{3/2}}$$

Fig. 2 shows the area investigated in these tests.

Some typical results obtained with vent B are shown in fig. 3 and 4 for d = 30 mm and d = 100 mm. The curves represent the helium concentration as a function of elevation after injection of a volume approximately equal to one half of the vessel volume. Two curves have been drawn for the highest Reynolds case due to the fact that a steady state is reached several minutes after the injection is stopped.

These results show that the stratification (c max/c) increases with the jet diameter d and with the Reynolds number.

III. COMPUTATION OF DETONATION SHOCK WAVES

Numerical models

For calculation of a blast loading, we have developped a method for fast dynamic analysis : the general formulation is the Euler equations for fluid dynamics (mass, momentum and energy equations) with an associated equation of state.

This general program uses the finite element formulation with an explicit time scheme. An A.L.E. (Arbitrary Lagrangian Eulerian) algorithm has been developped but for our case the pure lagrangian scheme is employed.

In this method, we use an upwinding and a quadratic viscosity (as Von Neumann has proposed). The finite elements are a P_o - Q_o formulation for scalar quantities and $(P_1)^n$ - $(Q_1)^n$ (n being the space dimension) for vectorial quantities.

By this algorithm, the detonation is considered as a shock front associated to a chemical reaction. Let us consider the mixture composed of perfect gases for which the reaction is :

$$2H^2 + (H_2O)_{steam} + \underbrace{(O_2 + 4N_2)}_{air} \longrightarrow 3(H_2O)_{steam} + 4N_2 + Q$$

The reaction is supposed to be adiabatic and exothermic (37 kcal produced for one mole of water created) and that the thermodynamic parameters are independent of the temperature evolution.

One-dimension calculations

Two one-dimensionnal detonation calculations have been performed in plane and axisymmetric geometry. The results of the plane case are compared to the Chapmann-Jouguet theory. The axisymmetrical case has proven the focusing effects of the shocks waves.

Definition of the test calculation :

The concentration of the components at stochiometric conditions are : hydrogen 28 %, steam 9,4 %, oxygen 13,1 % and nitrogen 49,5 %.

The initial pressure is 1.63 bar and the tube is 1 m long.

One hundred mesh points were used with initiation in the second mesh point.

The walls are supposed to be rigid (at x = 0 and x = 1 for the plane case, at x = 1 for the axisymmetrical case).

These results were presented in a paper of SMIRT-9 Brussels 1985/5. The agreement with the theoretical results of Chapmann-Jouguet theory is good.

We notice that the overpressure at the wall at the first impact of the shock wave in axisymmetric case in similar to that obtained in a plane case, while the overpressure is considerable at r = 0 when the shock wave returns to the center. This focusing effect can be encountered in reactor containments.

Two dimensional axisymmetric calculation

It has been showed (4) that focusing effects and multiple reflections can lead to important overpressures in a containment.

a) Case A - Containment filled homogenously :

The containment load is very sensitive to the location of the initiation part.

We wanted to check these conclusions by using the same calculations as these of reference (4).

The definition of the test case appears in figure 9 with the mesh used.

The results are shown in figures 5 and 6 for an initiation at mid height (35 m above the ground) and in figures 7 and 8 at the bottom.

The pressure historics at selected points in the wall (see figure 9) are shown in figure 11 for the first case and in figure 12 for the second one.

We can see that for a source located at 35 m, the effects are similar at all the points.

But if we put a source at the bottom, the pressure historics are similar except at the apex of the dome where the overpressure is 1.5 time the value obtained for the first case.

Another feature can be pointed out : the first peak is not weaker than the following ones. The secondary reflections are as damaging as the first ones in spite of the fact that they occur without chemical reaction in a completely burnt atmosphere.

b) Case B - containment stratified :

It is not realistic that the ambiant gases are all detonable. Thus it would be interesting to see the effect of the detonable mixture on the inert mixture when we suppose that temperature, pressure and energy are initially identical.

The containment is filled with stratified hydrogen and we suppose that the hydrogen is only concentred in the upper part.

The source of detonation is located at the bases of the detonable mixture and if the effect is similar in this zone to the case (a) (in particular the focusing effect at the apex), the waves are damped down in the inertial zone. The pressure histories at selected points on the wall (figure 10) are shown in figure 13 and the deformed meshes in figures 14 and 15. Figure 16 shows the isopressures at two different times.

c) Case C - Influence of aperture :

We want to see the effect of an opened window on the wave propagation in a confined volume.

We consider a cylinder of 12,5 m for the radius and 16,6 m for the elevation.

We suppose that a source of detonation is located at the base of the cylinder and that the detonable mixture has an hemispherical form with a radius of 8,6 m.

The residual gas is inert and the reflection effect in the corner is fundamental.

The mesh employed is presented in figure 17 and pressure histories obtained at different points in 18.

The effects are different for an opening located at the dome and for one at the bases of the cylinder.

As it is necessary to use an infinite domain, we use absorbant conditions which give good results. If we are interested at the same points, the effects are fundamentally different. We can see that there is no effect of the reflected waves and figure 19 gives results different of points of the wall.

In conclusion, the presence of a vent completely changes the propogation and the focusing effects of the waves (see figures 19, 21, 22, 23).

Isobars and mesh displacements are represented on figures 24, 25, 26.

IV. CONCLUSION

Two studies in progress related to hydrogen risk have been presented :

- Helium stratification in large volumes. The stratification effect increases with increasing Reynolds number and jet to vessel diameter.

- Detonation shock wave calculation in confined volumes for several actual cases.

IV. BIBLIOGRAPHY

(1) Hydrogen transport in containments : A survey of analytical tools and benchmark experiments H.W. Godbee - AM. Krichinsky - Nuclear Safety Vol 25 n° 6 Nov. Dec. 1984

(2) G.R. BLOOM and al. Second international workshop on the Impact of Hydrogen on water Reactor Safety Albuquezque Oct. 3-7 1982

(3) Federal Ministry of Research and Technology. Experimental Investigation of the Hydrogen Distribution in a Model Containment. Bonn. July 1980

(4) Calculations of hydrogen detonations in Nuclear Containments by the random choice method. M.I.T. Report (1981)

(5) Calculations of blast loading on a containment due to an internal air-hydrogen detonation. A. FORESTIER & S. GOLDSTEIN SMIRT 8/August 1985

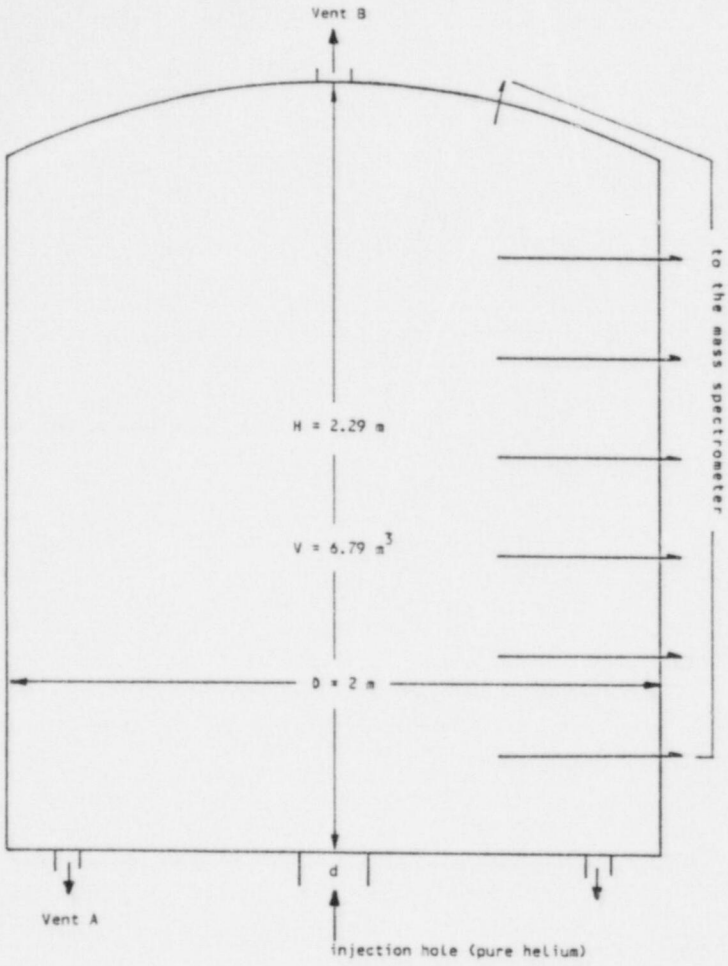


FIG. 1 Sketch of the facility

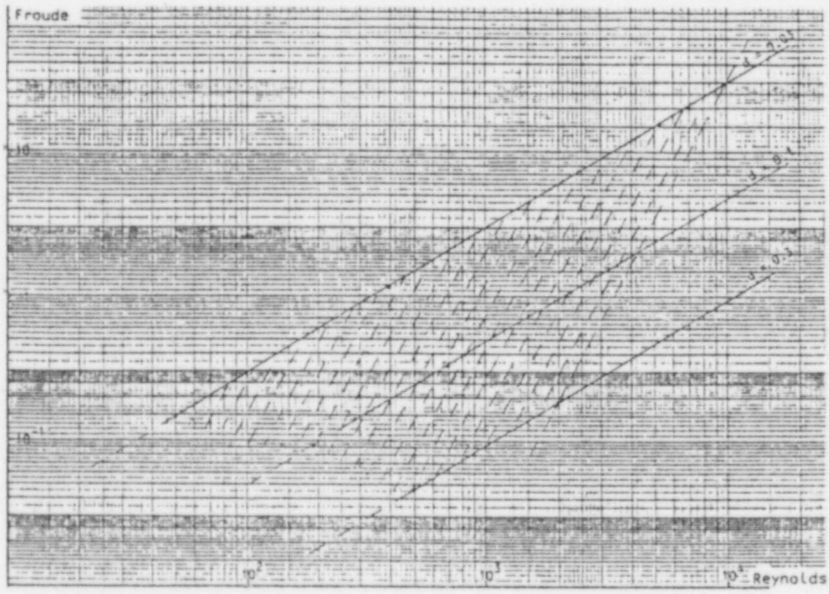


Fig. 2. Area in the Fr(Re) representation covered by the stratification tests

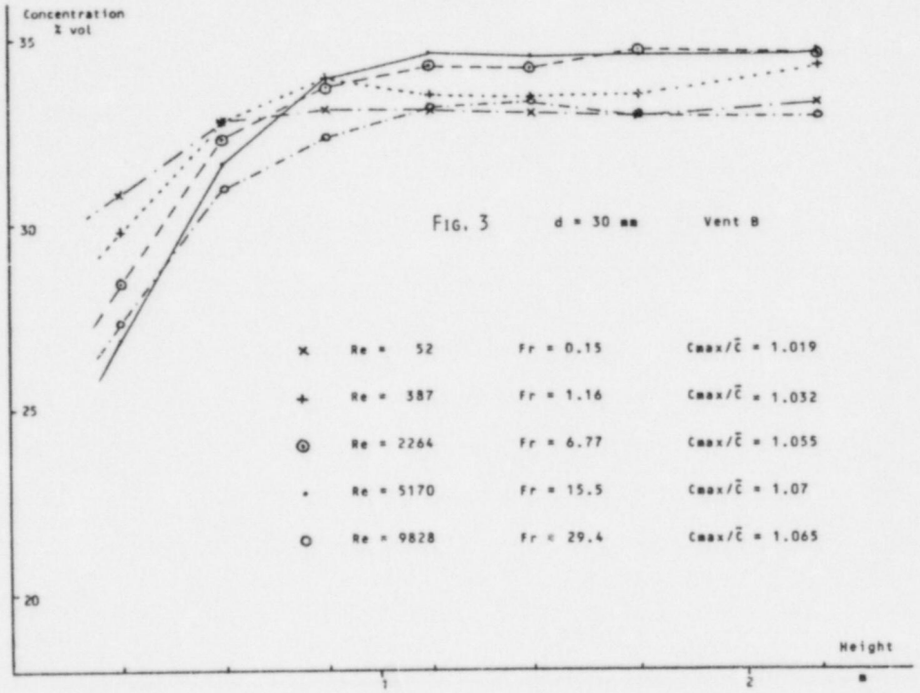


FIG. 3 d = 30 mm Vent B

×	Re = 52	Fr = 0.15	$C_{max}/\bar{C}$ = 1.019
+	Re = 387	Fr = 1.16	$C_{max}/\bar{C}$ = 1.032
⊙	Re = 2264	Fr = 6.77	$C_{max}/\bar{C}$ = 1.055
•	Re = 5170	Fr = 15.5	$C_{max}/\bar{C}$ = 1.07
○	Re = 9828	Fr = 29.4	$C_{max}/\bar{C}$ = 1.065

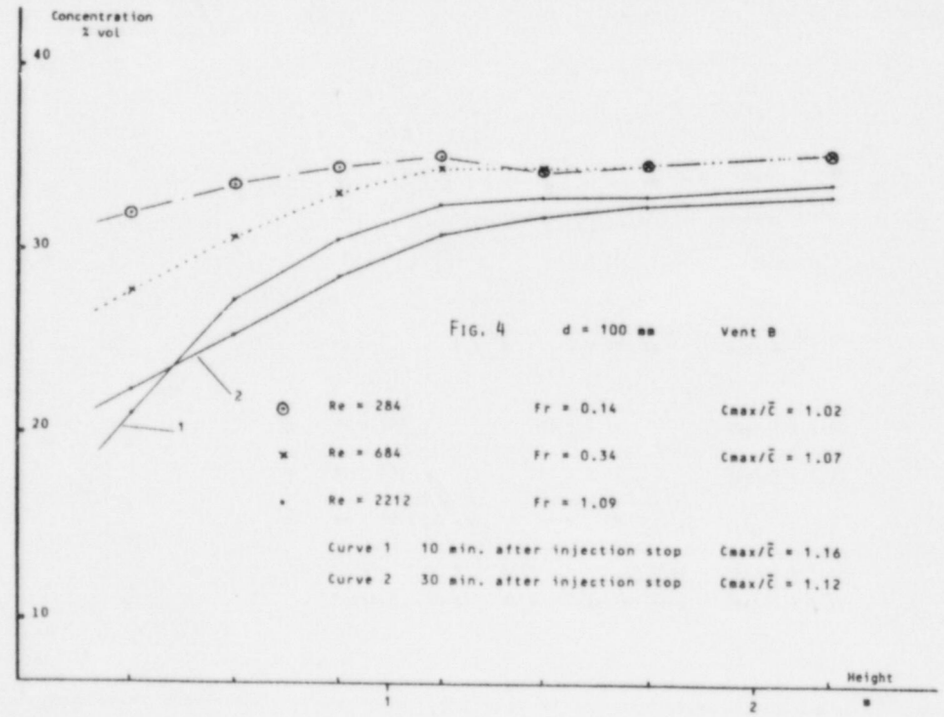


FIG. 4 d = 100 mm Vent B

⊙	Re = 284	Fr = 0.14	$C_{max}/\bar{C}$ = 1.02
×	Re = 684	Fr = 0.34	$C_{max}/\bar{C}$ = 1.07
•	Re = 2212	Fr = 1.09	
	Curve 1	10 min. after injection stop	$C_{max}/\bar{C}$ = 1.16
	Curve 2	30 min. after injection stop	$C_{max}/\bar{C}$ = 1.12

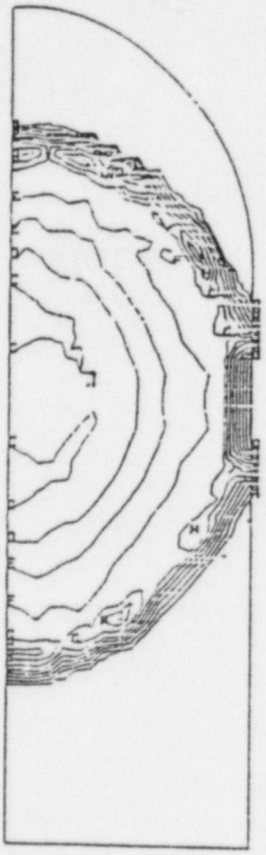


Figure 5

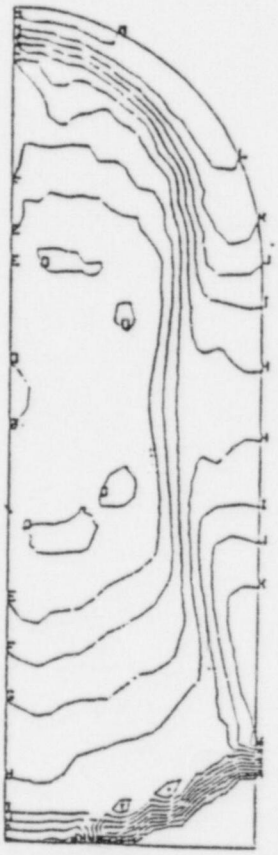


Figure 6

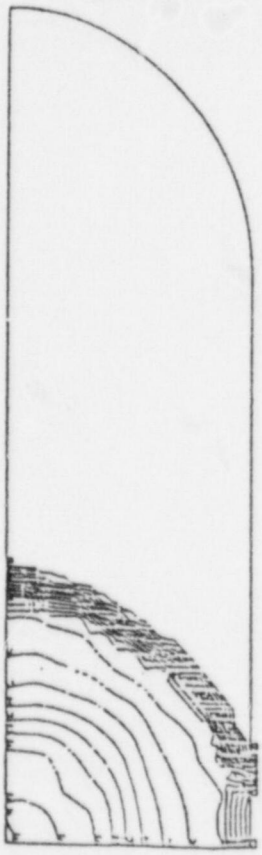


Figure 7



Figure 8

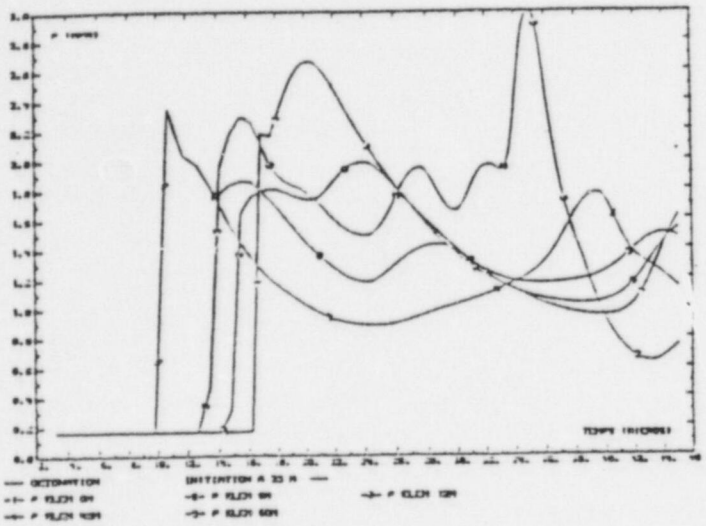


Figure 11

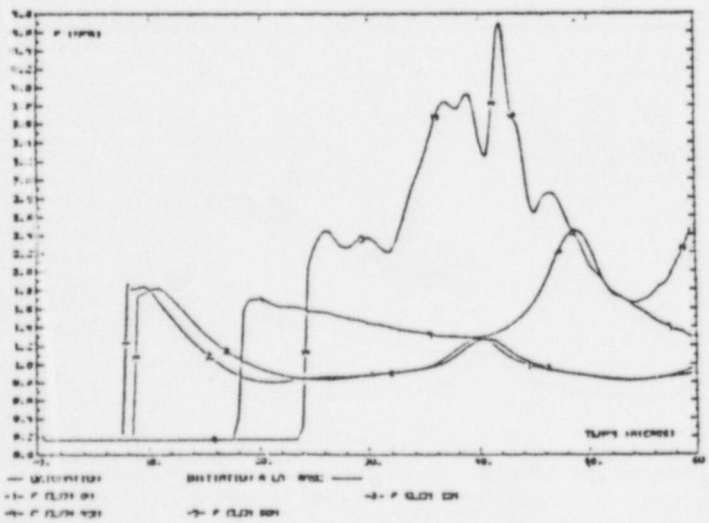


Figure 12

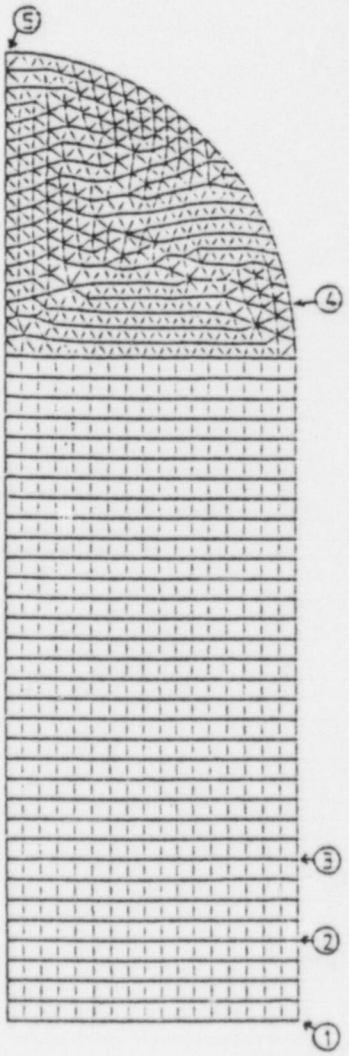


Figure 9

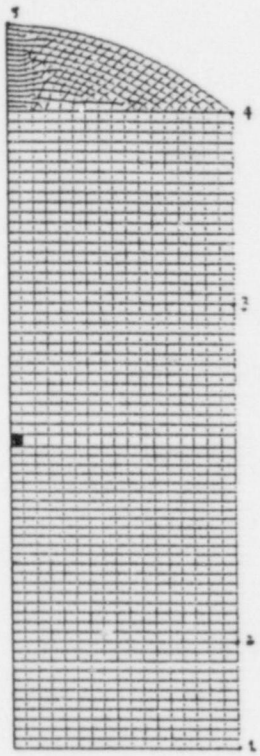


Figure 10

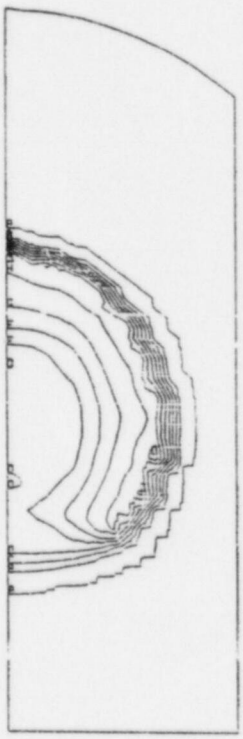


Figure 16

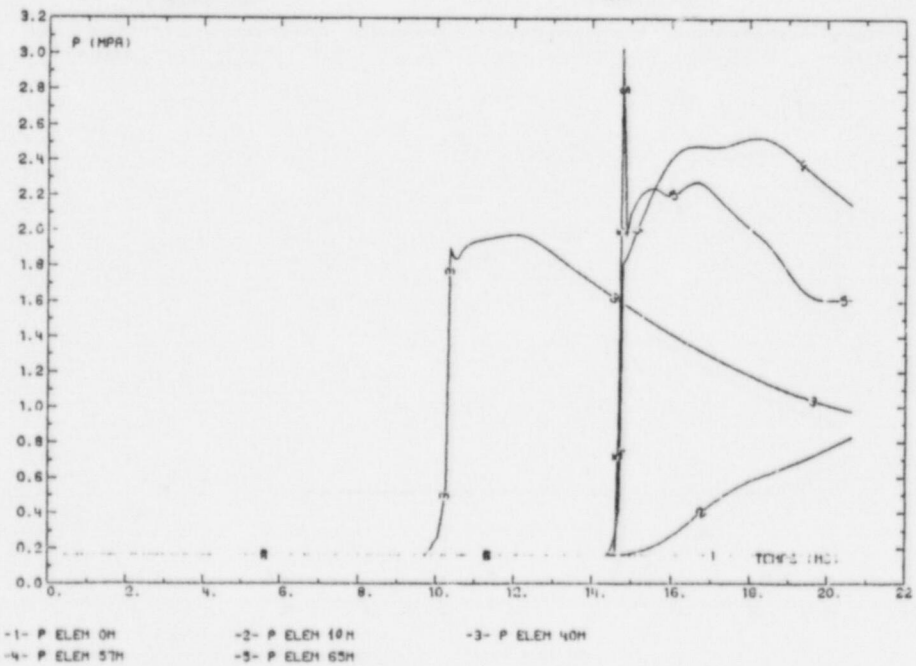


Figure 13

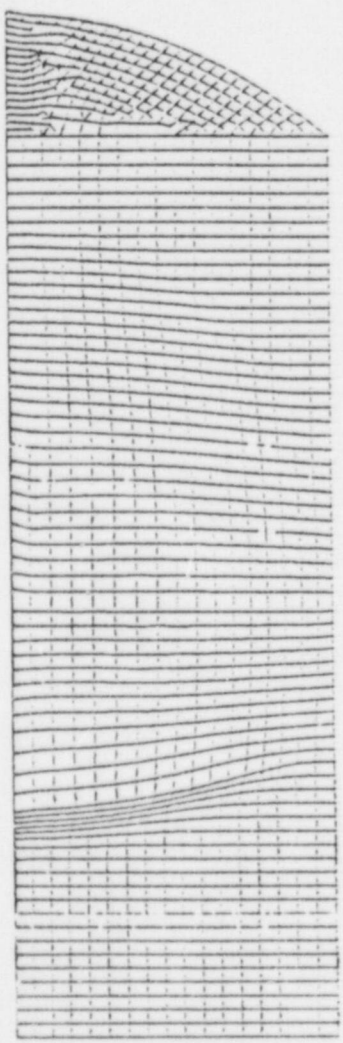


Figure 14

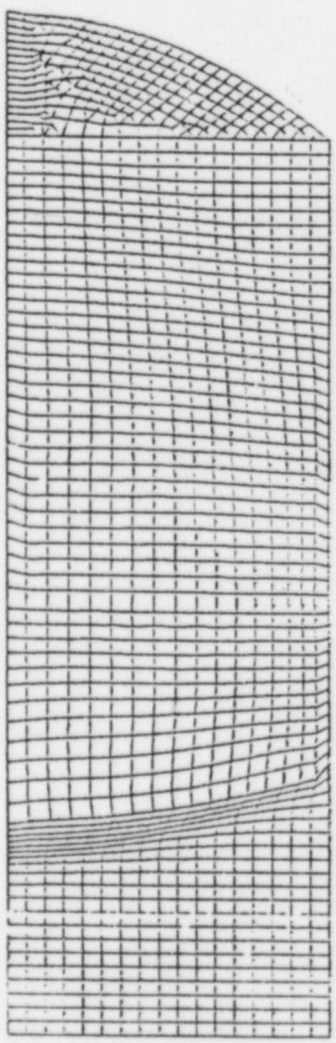


Figure 15

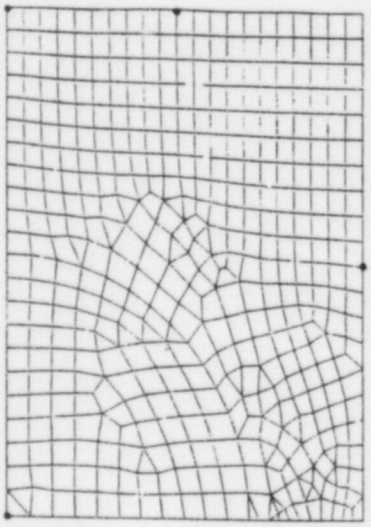


Figure 17

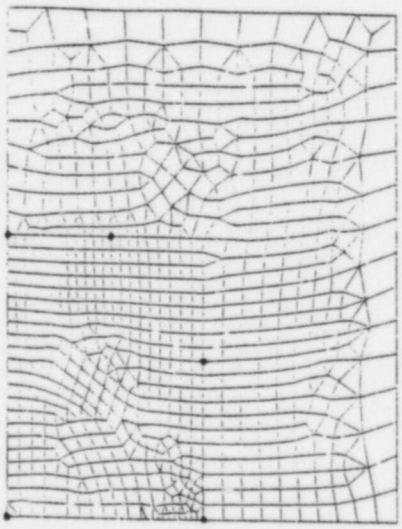


Figure 18

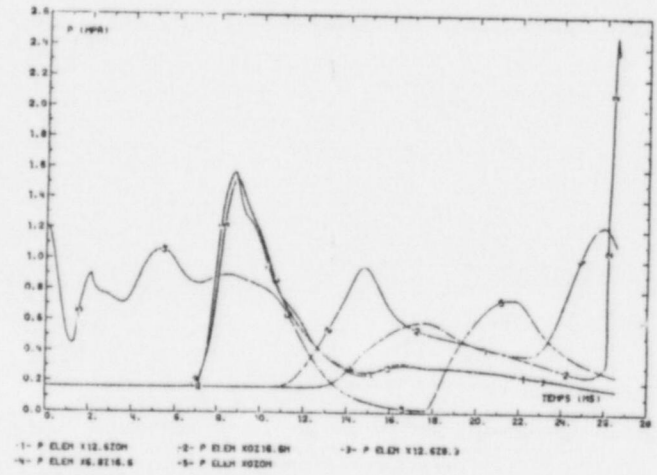


Figure 19

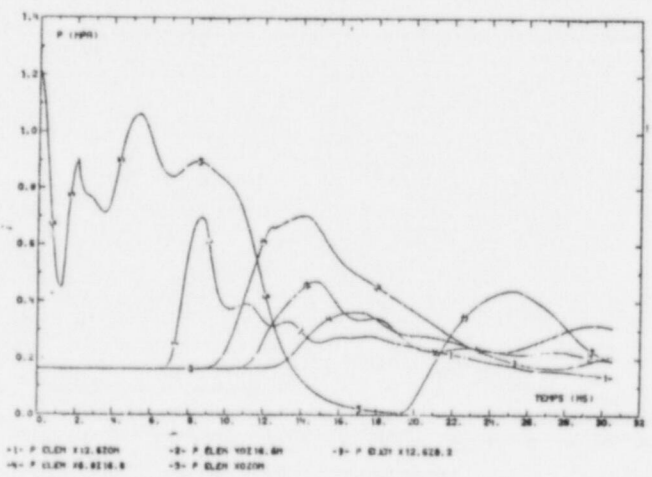




Figure 20



Figure 21

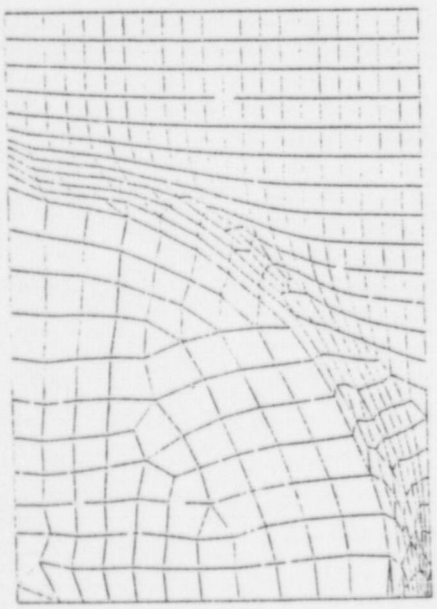


Figure 22

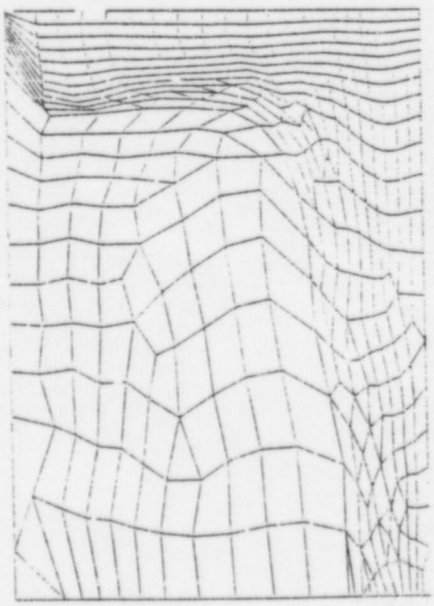


Figure 23



Figure 24



Figure 25

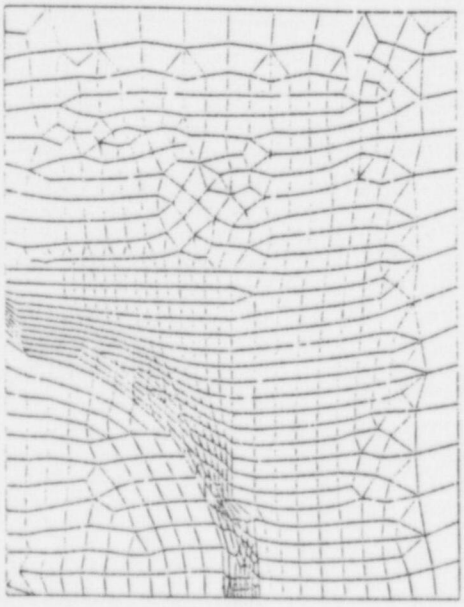


Figure 26

IMPACT OF AN HYDROGEN IGNITION SYSTEM ON DEGRADED CORE ACCIDENT IN A MARK III CONTAINMENT

Carlo CENTANARO
ANSALDO S.P.A.
Genova - ITALY

ABSTRACT

One concern during the Three Mile Island (TMI) accident arose from the generation of a large amount of hydrogen within the reactor vessel and its migration to the containment building. Though at TMI the hydrogen burning didn't jeopardize the containment safety there is a concern that other weaker containment might be vulnerable either to hydrogen combustion or to more severe accident scenarios.

Ansaldo Div. Impianti is very interested in the impact of hydrogen burning phenomena on BWR/6 plants with Mark III, free-standing steel containment.
To improve the plant capability to withstand the threat of hydrogen burning inside the containment, the need of a new tool to dispose the hydrogen release was assessed and, as an ignition system ("Sistema Bruciamento Idorgeno" or SBI) was selected, Ansaldo Div. Impianti performed a feasibility study to evaluate its requirements and performances.

As a support for this activity, some accident scenarios have been analyzed by means of a copy of HECTR code supplied on purpose by Sandia Labs.

1. INTRODUCTION

Since the accident at Three Mile Island (TMI), the phenomena of hydrogen generation and combustion in Light Water Reactors (LWRs) have been getting more and more important.

A great deal of concern has been arising as this hydrogen, if incidentally ignited inside the containment , might jeopardize both its structural and functional integrity.

Though at TMI the hydrogen burning didn't threaten the containment integrity, there is concern that other, weaker containments might be vulnerable to hydrogen combustion or that more severe pressure and temperature transients might be caused by different accident scenarios.

Ansaldo Div. Impianti is very interested in hydrogen burning phenomena which might occur in a BWR/6 plant with a MARK III containment:
a typical 218/624 BWR/6 plant with such features as a free-standing steel MARK containment, hemispherical dome and stiffeners was selected to perform a preliminary assessment on plant response.

To improve the plant capability to withstand or to eliminate the threat of hydrogen burning wild inside the containment, the need of a new tool to dispose the hydrogen release was assessed and, as an ignition system (like the one in Grand Gulf Plant) was selected, Ansaldo Div. Impianti performed a feasibility study for a "Sistema Bruciamento Idrogeno" (SBI, "Hydrogen Burning System)", to evaluate its performances.
The main task for the SBI System is to face the release of large amount of hydrogen by burning it at the lowest possible concentration, thus preventing hydrogen deflagration at high concentration or even hydrogen detonation.
As a support for the SBI System feasibility study, some analyses have been performed by a copy of HECTR code supplied on purpose by Sandia Labs

The results we are now presenting come from the analysis of three typical accident scenarios, all the release rates for both hydrogen and steam to be released inside the containment have been obtained through MARCH Code calculations.
Our analysis show that the SBI system is effective in reducing the treat posed by hydrogen generation by avoiding its concentration to reach such a high value to challenge containment integrity during the burning.

Even in the scenario with the worst hydrogen release, the peak pressure during hydrogen burning is only slightly above the design pressure of the containment and definitely lower than the allowances of ASME code Service Level C criteria.

Part of these analysis were performed under an Association Agreement between the Ansaldo Div. Impianti and the ENEA (Italian National Administration for Atomic Energy).

2. PLANT DESCRIPTION

To perform a preliminary assessment of the plant behaviour under containment environmental conditions generated by SBI System operations a BWR/6 plant with a Mark III containment was selected.
The design is that of a typical 218/624 BWR/6 plant with a free-standing steel containment, hemispherical dome and stiffeners.

The reactor building structure, shown in Fig. 2.1, may be roughly divided into Shield Building, Containment Vessel, Drywell, Suppression Pool and Upper Containment Pool.

(A) Shield Building (free volume = 357400 ft^3)÷ it is a cylindrical shell of reinforced concrete with an hemispherical roof, its functions are to further limit the nuclear radiation to the environment and to protect the containment from adverse atomospheric conditions and external missiles.

(B) Containment Vessel (1407060 ft^3) : it is a free standing, cylidrical steel pressure vessel with hemispherical head and horizontal external stiffeners and it is anchored into the reactor building foundation mat; it is a leakage barrier which prevents significant fission product releases to the shield building during an accident.

(C) Drywell (255367 ft^3) : it is a cylindrical shell of reinforced concrete with a flat roof slab which supports the upper containment pool; it contains the pressure transient for a LOCA accident and channels the blowdown to the suppression pool; in addition, it provides both protection from missiles, jet impingment and pipe wip, and more radiation shielding for the containment areas during reactor operation.

(D) Suppression Pool (126500 ft^3 at NWL) : it is an annular pool of demineralized water between the drywell and the outer containment, it maintains a water seal between these two

volumes by covering the horizontal vent openings; it provides a means to condensate any steam release into the drywell and a source of water for the Emergency Core Cooling Systems (ECCS).

(E) Upper Containment Pool (69750 ft^3 at NWL): it provides shielding for the operating floor during normal operation and refueling.

3. HYDROGEN MITIGATION SYSTEM

3.1 Overview of hydrogen mitigation devices

An overview of hydrogen mitigation devices was performed to estimate the capabilities of each hydrogen control strategy.

At first a list of the desirable features was produced to better evaluate the pros and cons of the various options.
It was assessed that an hydrogen control system should (a) be capable of handling large amount of hydrogen release (b) be quick to start to guarantee its operability even during short-term hydrogen release hystories, (c) not jeopardize normal operation activities or plant integrity in case of inadvertent actuation (d) be helpful against hydrogen pocketing and capable of burning hydrogen at low concentration. (e) minimize its impact against a pre-existing network of plant facilities.

A comparison was made among the features of several hydrogen mitigation devices.
Such system as: Gas Pre and Post-Inerting. Gas Turbine or Atmospheric burners, Ignitors. Recombiners and Fog Inerting were thoroughly examined.
At last a glow-plug ignitor system was selected as Sistema Bruciamento Idrogeno" (SBI, "Hydrogen Burning System"), for it fits very well the above requirements furthermore widely developed research programs show its effectiveness in burning the hydrogen even at low concentration (slightly above 5% v/o). near the lowest flammability limit. Fig. 3.1 produces some results from a research program on glow plug ignitors; performances performed by University of PISA (ITALY): this work was performed at the University of PISA Research Facility and supported by the ENEA (Italian National Administration for Atomic Energy) under an Association Agreement

3.2 SBI System description

The SBI system is provided to face the release of hydrogen following a degraded (but recoverable) core accident up to an extent corresponding of 75% of Metal Water Reaction in the cladding surrounding the active zone of the fuel. as stated in the latest issue of 10 CFR 50.44 (Jan. 25, 1985).
The SBI system would be manually actuated by the operator in the control room during all the event sequences which might lead to a large generation of hydrogen from Metal Water Reaction. It would be able to operate long enough to guarantee the recovery of whatever power source.

The system is designed to burn the hydrogen at low concentration thus avoiding its build-up in the containment atmosphere above the detonation limit and preventing containment overpressure failure.
A suitable distribution of ignition sources have been selected to avoid significant pocketing of hydrogen which might result in local high concentration.

The system is designed with such a redundancy that no single active component failure, including power supplies, will jeopardize the operability of the system.
The ignition units are powered from two Class IE ESF power distribution panel: each panel supplies one half of the ignition units.
As the system is supposed to be available even in the unlikely occurence of a SBO accident, provisions are available to guarantee its operability through a redundand battery system.

Ignitors location criteria suit the hints described in the following :(a) hydrogen might be released directly into the drywell atmosphere through a break: ignition units will be provided inside the drywell zone.

(b) the most probable release paths for hydrogen into the containment are the SR/V$_S$ discharge lines: ignition units will be located above the suppression pool

(c) throughout the containment a suitable location of the ignition units will be provided to guarantee an useful distribution even with only one division available: in confined areas at least one unit from each division will be located, while elsewhere a maximum distance of about 50 feet will exist between two operable units with only one division available.

Each ignition unit will include the following elements:
(1) An ignition device capable of reaching and maintaining such a high surface temperature as to ignite the hydrogen (1500 °F): glow-plugs for diesel engine have been selected on purpose.

(2) A transformer to step down the power to the required voltage necessary to achieve the ignitor operating temperature

(3) A metallic enlcosure to support the ignitor and to contain the transformer plus electrical wiring.

(4) A spray shield to protect the ignitor from the containment spray impingment.

(5) An heat shield to protect the unit components from high temperature.

(6) Accessess to the interior of the enclosure will be provided.
A final configuration for the unit and its support will be produced only after a more accurate assessment about the units location and their support components

Figure 3.2 presents the glow-plug ignitor used for the hydrogen burning tests performed by University of PISA: it is a BOSCH 12 V diesel glow-plug model 0250 200 465.

4 CONTAINMENT RESPONSE ANALYSIS

To support a feasibility study of the SBI system, some analysis to evaluate the containment response to hydrogen burning phenomena were performed.
A wide variety of cases were run using both MARCH and HECTR Codes, the former to generate steam and hydrogen release rates to the containment the latter to analyse the containment response to hydrogen burning phenomena.
Sensitivity studies were performed to examine hydrogen source terms, its dependence on ECCS recovery delay, containment compartmentalization, hydrogen migration and ESF impact on event sequence.
A particular effort was made in modelling MARK III containment internal geometry and connections between subcomparments in order to guarantee that natural recirculation loops in the containment atmosphere could be simulated during the transient

4.1 Selection of Accident Scenarios

Three typical scenarios have been selected to evaluate the hydrogen generation extent and its impact on SBI system operability and containment integrity:
these scenarios are representative of hypothetical degraded core accidents with or without recovery of ECCS systems or containment ESF.

The scenarios refer to: (a) RPV isolation transient with no water mak-up system available throught the event (this scenario was stopped at the time when the vessel breaches: a MWR of about 45% in active fuel cladding was reached); (b) RPV isolation transient with ECCS (5000.GPM) and containment ESF (Suppression Pool Cooling) recovery after an acceptable (45') delay (MWR=about 12%); (c) degraded core event arising from a Stuck Open Release Valve (SORV) with failure of ECCS systems; recovery of core cooling was assumed to occur before RPV melt-through but late enough to help hydrogen generation to reach 75% MWR in active fuel cladding.
The analysis were performed though MARCH code and the outputs were used to prepare HECTR mass and energy source term input tables.
While HECTR inputs from cases (a) and (b) came directly from MARCH runs, (c) results were modified by an arbitrary extrapolation to reach an amount of hydrogen consistent with the 75% MWR limit stated in the 10 CFR 50.44 final rule.
In (a) and (b) events, operator is supposed to depressurize the RPV once realized that both HPCS and RCIC system are unavailable.
Hydrogen release rates into containment for all the three scenarios are shown in Fig. 4.1/2/3.

4.2 Plant Model

In reproducing the containment internal geometry subcompartments configuration and heat sinks were attentively analyzed as they are of great importance in affecting the containment response to hydrogen burning phenomena.

Figure 4.4 shows the model which stands from our sensitivity studies as the most effective is reproducing natural recirculation loops that are expected to take place among the compartments throughout the transient.

The model is made-up by 6 subcompartments: numbers one to five are for containment subcompartments, while number six is the drywell, they are all connected one to another by two-way flow junctions (modelling open doors, rooms, grates or corridors) but the drywell which is connected only with compartment 3 (by a one-way junction: the Vacuum - Breaker valves) and with compartments 5 (by the vents, through the suppression pool).
Compartment 5 is the wetwell, an annular region above the suppression pool; compartments 3 and 4 model the free volume between the Hydraulic Control Unit Floor and the refueling floor, they enclose on both sides the sector-like compartment 2 which models the chimney-like, free-of-obstruction vertical volumes in the plant.
Compartment 1 is dome, above the Upper Containment Pool and the Refueling Floor, it contains no obstructions but the Polar crane.

As all the scenarios we have analyzed take place mainly in the containment, great attention was devoted in evaluating the extent and the distribution of the heat-sinks inside the containment.
For each compartment the heat-sinks model include: containment walls (steel), inside or outside drywell walls (concrete), concrete structures or slabs, sumps (if any), steel structures, gratings and equipment.

It is estimated that a BWR/6-218 Mark III free-standing containment contains about 6 Million pounds of steel (not including concrete rebars) and 30 million pound of concrete in addition the upper containment pool and the suppression pool contain at least 4.5 million pounds of water.
The total heat transfer surface areas for all the heat-sinks are estimated to be about . 5 million square feet.

These masses and surface areas provide enourmous heat transfer capabilities, so it is expected that these heat-sinks may play a decisive role in all containment response analyses.
For all the cases hydrogen ignition limit was conservatively set at 8% v/o with a combustion completeness of 100%, for atmosphere inerting and flame propagation among the compartments, the values produced in table 4.1 were selected:

4.3 Results

A complete summary of the results is shown in table 4.2 while Fig. 4.5,6 provide containment temperature and pressure transients for the case with the worst hydrogen release, (c).

As we can see, even in cases (a) and (c) where containment design pressure is exceeded, the overpressure is only slightly above the design but remains definitely beneath the ASME code Service Level A value.

Another area of major concern is that of temperature values to be reached on the containment wall and concrete structures: in all cases the design value is not even approached, while for concrete structures, A.C.I. concrete temperature limitation are completely met, nowhere in the surfaces temperature limitations for accident are reached.
In order to obtain results representative of the worst possible loadings on the containment, for all cases containment spray operation was neglected.
As containment sprays share pumps with other subsystem intended to cool the core, it appears inconsistent to assume their availability during the failure of all ECCS systems.
Another highlight from our results is that nowhere in the scenarios flammability limits were approached in the drywell, so no hydrogen burning took place there.

5. CONCLUSIONS

From our analysis it comes that even in the occurrence of a large generation of hydrogen (up to 75% MWR in active fuel cladding) and its release into the containment in a relatively short time (3000 seconds), an ignitors mitigation system enables the plant to face the event: even the loadings generated by hydrogen burning are not powerful enough to jeopardize the containment integrity.

Ansaldo Div. Impianti is now engaged in more detailed studies to improve feasibility and reliability of SBI system design and its capability to fit different plant facilities too.
A new, broadened selection of cases will be considered to ensure sufficient coverage of a representative group of degraded core scenarios which could be faced by the hydrogen ignition system operation.

6. REFERENCES

1 J.C. Cummings, et al. Review of the Grand Gulf Hydrogen Igniter System, NUREG/CR-2530, U.S. Nuclear Regulatory Commission, March 1983.

2 A.L. Camp. M.J. Webster and S.E. DIngman, HECTR Version 1.0 User's Manual, SAND84-1522, Sandia National Laboratories

3 M.J. Wester et al., Evaluation of HECTR Predictions of Hydrogen Transport, Sandia National Laboratories, Albuquerque, NM 87185

4 A.L. Camp, et al., MARCH-HECTR Analysis of Selected Accidents in an Ice-Condenser Containment, NUREG/CR-3912, Dec. 1984.

5 GESSAR II, 238 Nuclear Island
BWR/6 Standard Plant Probabilistic Risk Assessment
General Electric Company. San Jose'. Ca.

6 J.C. ELLIOT, L.B. NESBITT, et al., Assessment of Hydrogen Combustion effects in BWR/6-MARK III Standard Plant

7 D.A. HANKINS, K.W. HOLTZCLAW - Effect of Hydrogen Control on the Risk from Severe Accidents in the BWR/6-MARK III Standard Plant
General Electric Co., San Jose', CA.

8 P.F. GOU, Containment Capability Pressure for a Mark III steel containment shell, NEDE 25367
General Electric CO. San José , CA.

9 C. CENTANARO , Containment response to hydrogen burning accident in BWR/6- MARK III nuclear power plants, 42ORT3101 cl. 3 Ansaldo Div. Impianti, Genoa-Italy

10 C. CENTANARO, Valutazione Realistica del Rilascio di Idrogeno in caso di Incidente Degradato, 42ORE3102, cl. 3 Ansaldo Div. Impianti, Genoa-Italy

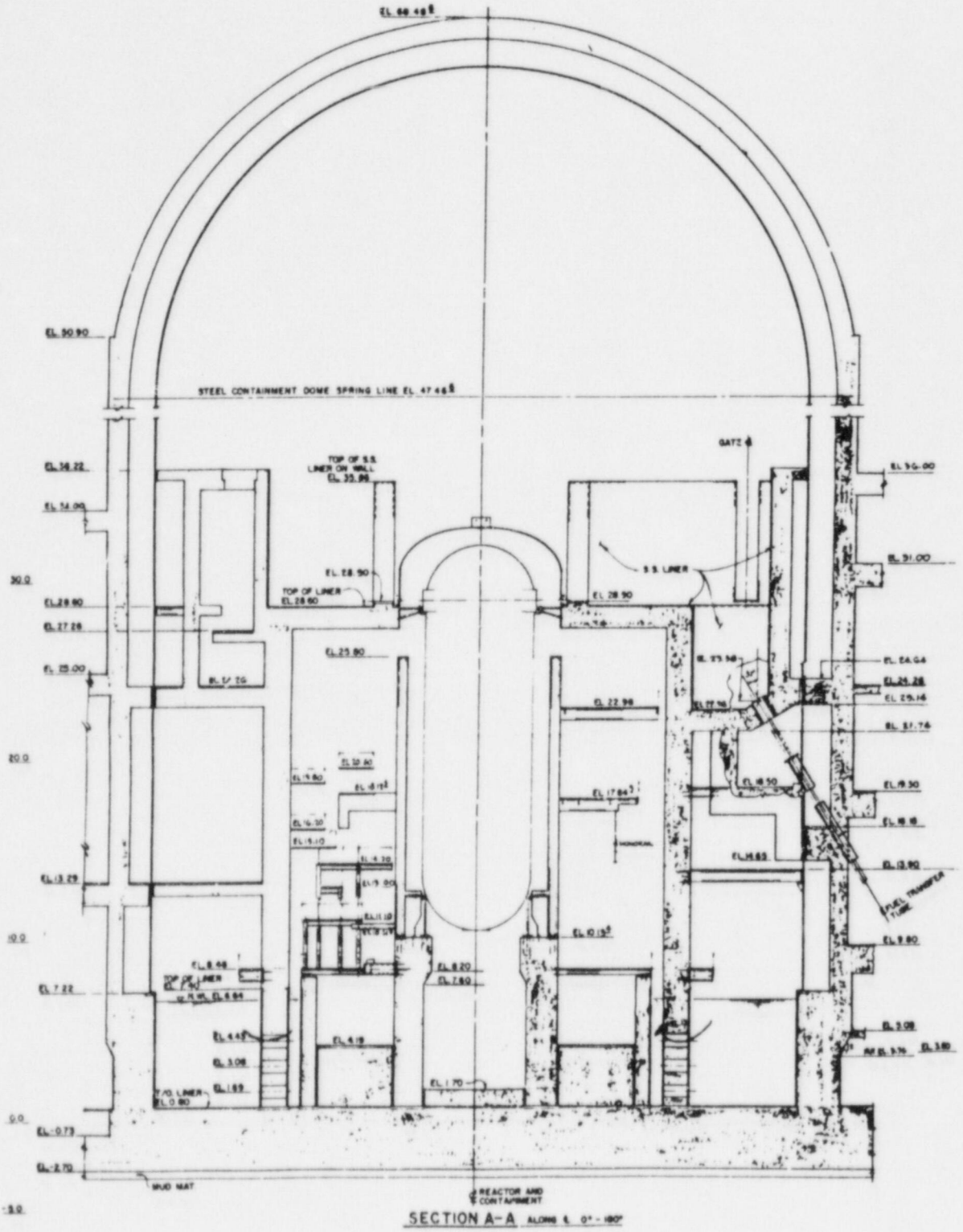


FIGURE 2.1 - BWR/6 MARK III CONTAINMENT

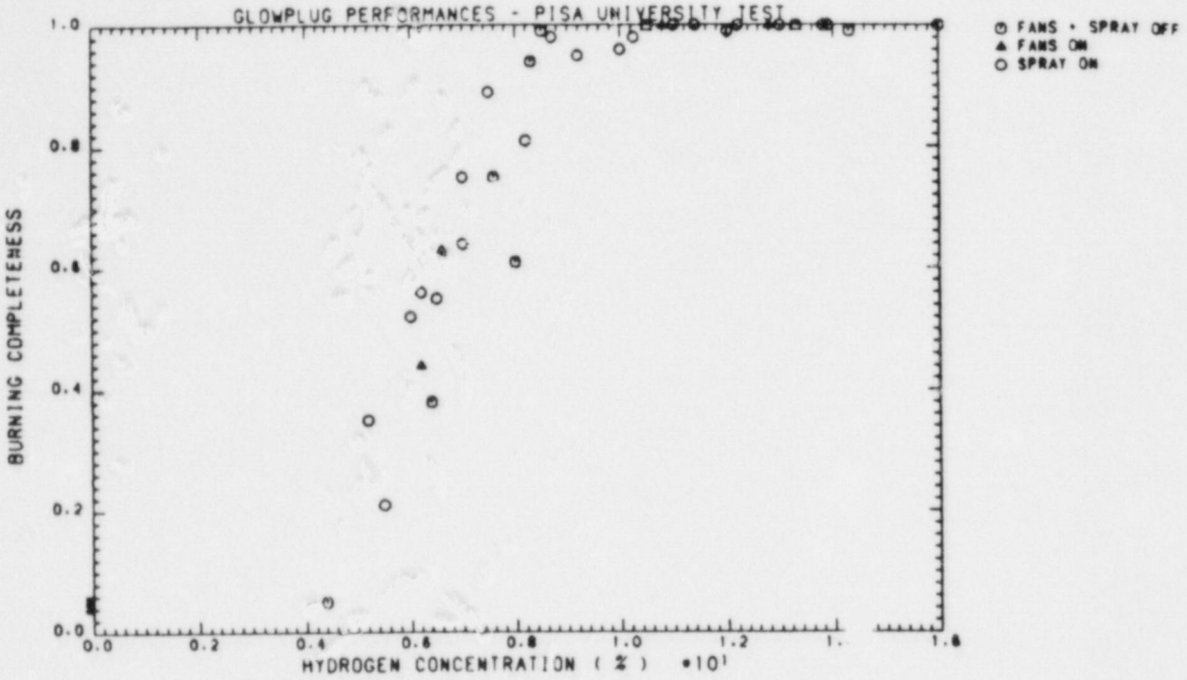


FIGURE 3.1 - GLOW-PLUG IGNITOR PERFORMANCES

UNIVERSITY OF PISA RESEARCH PROGRAM

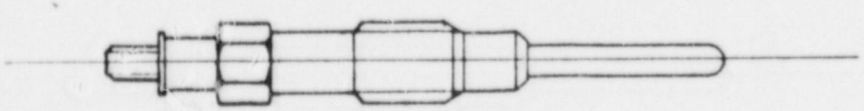


FIGURE 3.2 - DIESEL GLOW-PLUG IGNITOR

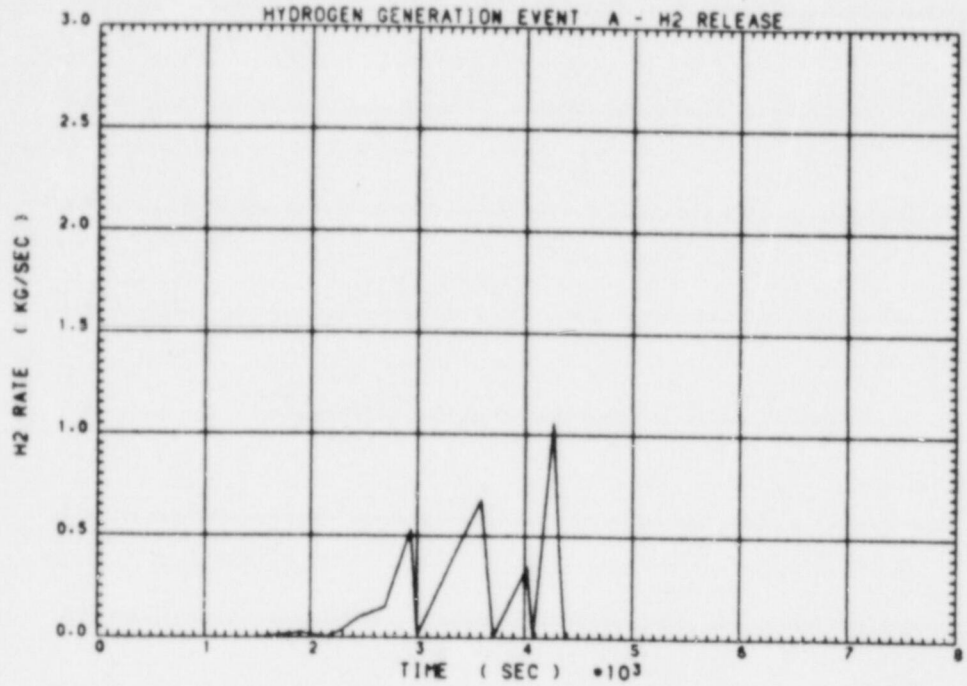


FIGURE 4.1-HYDROGEN GENERATION EVENT (a):H2 release rate

ISOLATION TRANSIENT WITH NO WATER MAKE-UP

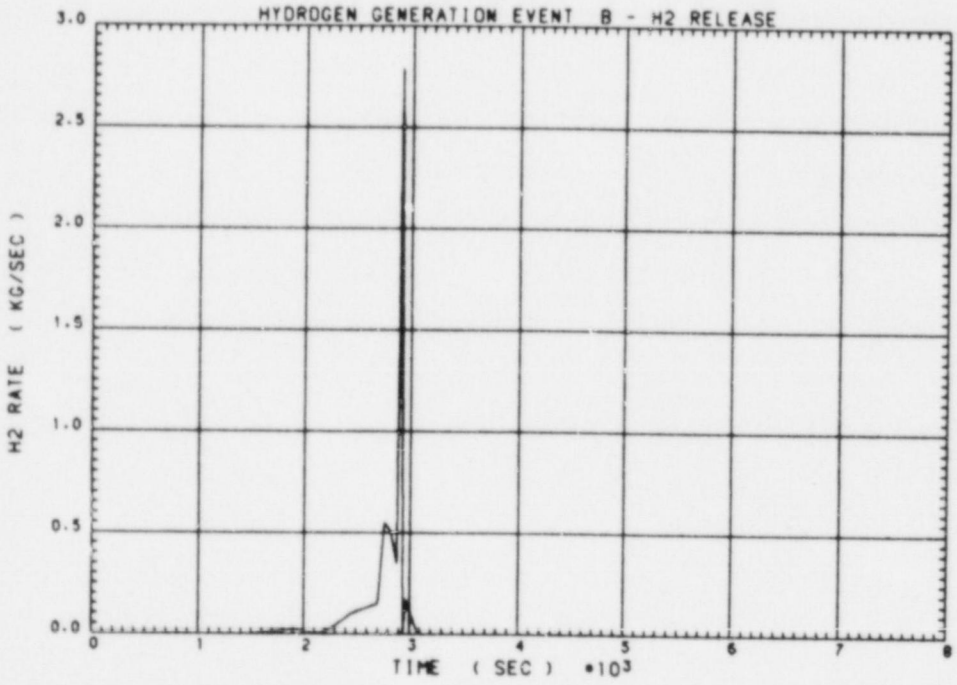


FIGURE 4.2-HYDROGEN GENERATION EVENT (b): H2 release rate

ISOLATION TRANSIENT WITH ECCS RECOVERY AT 45'

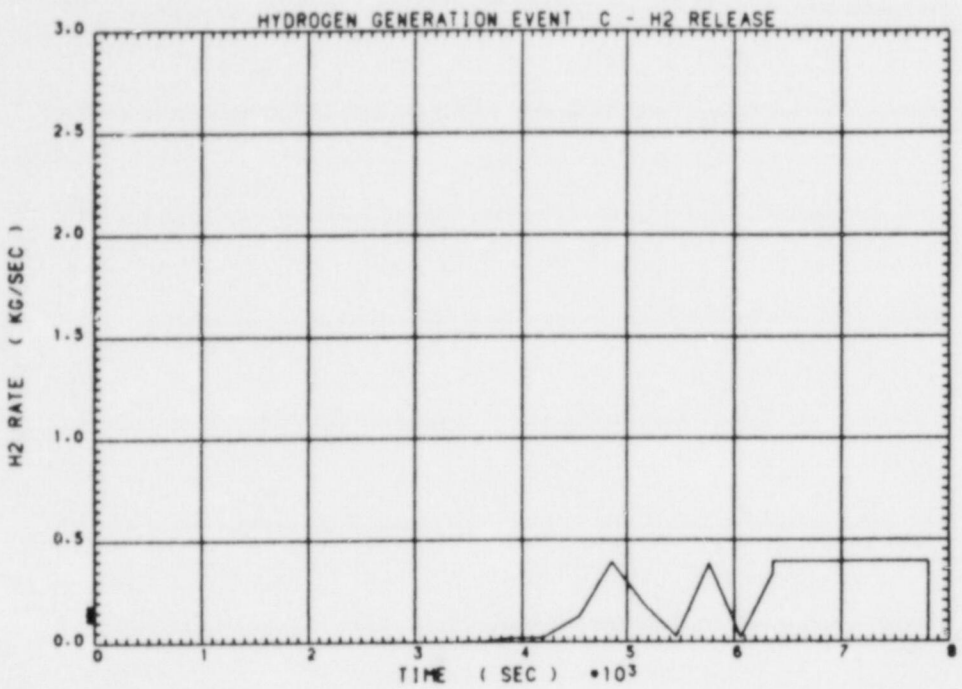


FIGURE 4.3-HYDROGEN GENERATION EVENT (c): H2 release rate

SORV EVENT WITH ECCS

RECOVERY BEFORE MELT-THROUGH

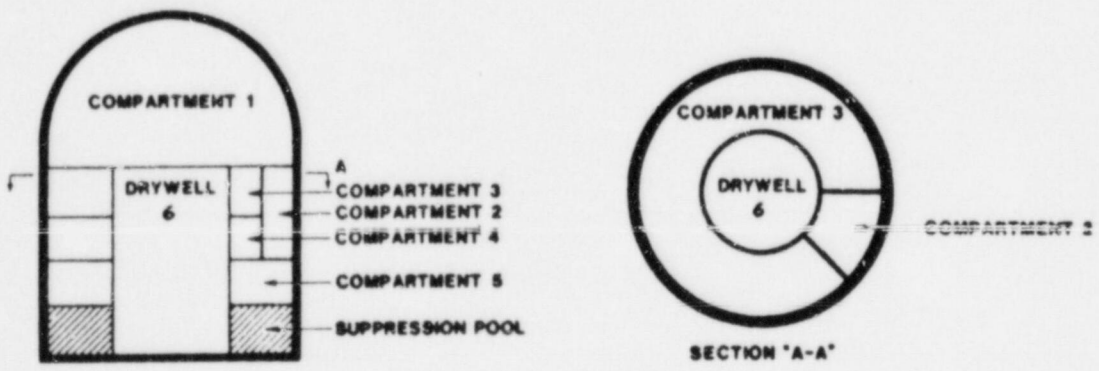


FIGURE 4.4- VOLUME COMPARTMENTALIZATION

OF MARK III CONTAINMENT

	MOLE FRACTIONS		
	H_2	O_2	H_2O
IGNITION LIMITS	$\geq$ .08	$\geq$ .05	$\leq$ .55
UPWARD PROPAGATION	$\geq$ .041	$\geq$ .05	$\leq$ .55
HORIZONTAL PROPAGATION	$\geq$ .06	$\geq$ .05	$\leq$ .55
DOWNWARD PROPAGATION	$\geq$ .09	$\geq$ .05	$\leq$ .55

TABLE 4.1 - IGNITION AND PROPAGATION LIMITS

	SCENARIO			
	(a) Transient/ no recovery	(b) Transient/ no recovery	(c) SORV/75% MWR	REFERENCE VALUES
Containment Pmax (Kpa)	224.5	164.3	260.7	206.8 design 413.7 ASME III Code S.L.A.
Containment airspace Tmax (°K)	1079.5	1140.2	1017.4	
Containment wall Tmax. (°K)	313.6	308.4	321.3	358.1 design
Containment concrete Tmax. (°K)	366.6	339.7	368.2	A.C.I. CODE: 449.8 whole surf. 616.5 local areas

TABLE 4.2 - ANALYSES RESULTS SUMMARY

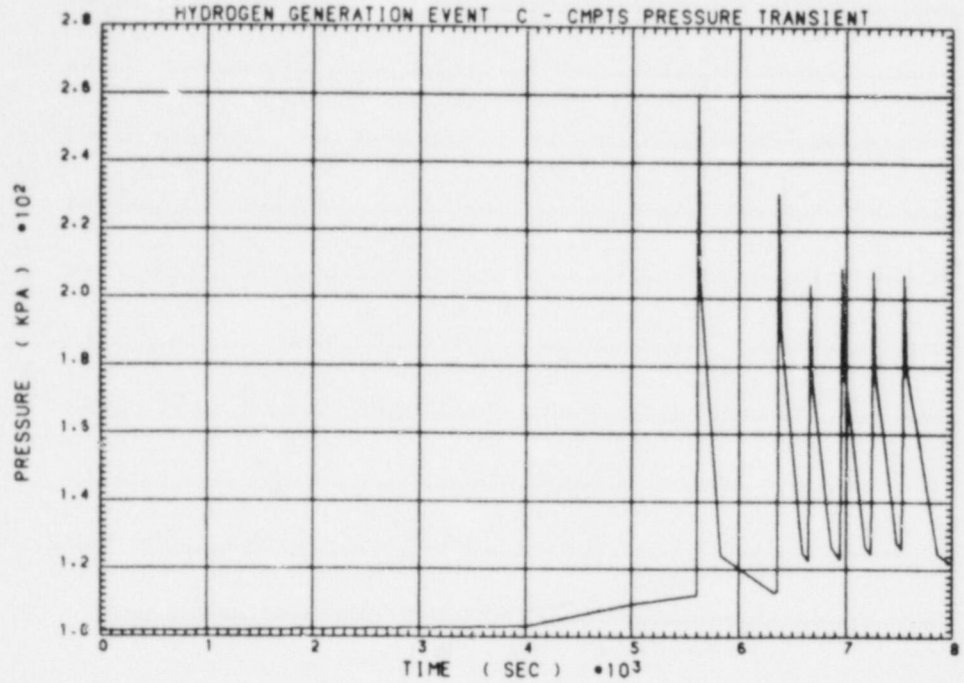


FIGURE 4.5- HYDROGEN GENERATION EVENT (c)

AVERAGE CONTAINMENT PRESSURE TRANSIENT

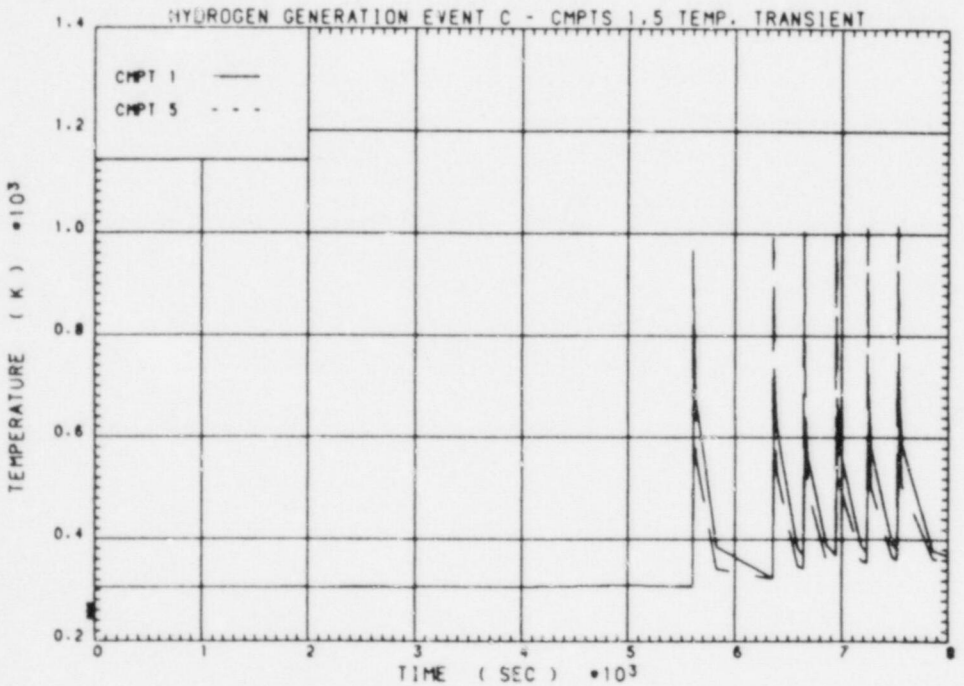


FIGURE 4.6-HYDROGEN GENERATION EVENT (c)

CONTAINMENT COMPARTMENTS TEMPERATURE TRANSIENT

Hydrogen Burn Assessment with the CONTAIN Code*

H.M. van Rij**
Netherlands Energy Research Foundation
The Netherlands

ABSTRACT

The CONTAIN computer code was developed at Sandia National Laboratories, under contract to the U.S. Nuclear Regulatory Commission (NRC). The code is intended for calculations of containment loads during severe accidents and for prediction of the radioactive source term in the event that the containment leaks or fails. A strong point of the CONTAIN code is the continuous interaction of the thermal-hydraulics phenomena, aerosol behavior and fission product behavior. The CONTAIN code can be used for Light Water Reactors as well as Liquid Metal Reactors.

In order to evaluate the CONTAIN code on its merits, comparisons between the code and experiments must be made. In this paper CONTAIN calculations for the hydrogen burn experiments, carried out at the Nevada Test Site (NTS), are presented and compared with the experimental data.

In the Large-Scale Hydrogen Combustion Facility at the NTS, 21 tests have been carried out. These tests were sponsored by the NRC and the Electric Power Research Institute (EPRI). The tests, carried out by EG&G, were performed in a spherical vessel 16 m in diameter with a design pressure of 700 kPa, substantially higher than that of most commercial nuclear containment buildings.

* This work supported by the Netherlands Energy Research Foundation and the United States Nuclear Regulatory Commission and performed at Sandia National Laboratories which is operated for the U.S. Department of Energy under Contract Number DE-AC04-76DP00789.

** On attachment to Sandia National Laboratories, Albuquerque, New Mexico.

The test matrix designed for this facility includes both premixed combustion experiments and continuous injection simulations of degraded core accidents. The initial conditions of the 21 premixed combustion experiments were chosen specifically to look at:

* Lean hydrogen burns
* Initial high-steam concentration effects
* Water spray effects
* Induced fan turbulence effects
* Igniter location effects

The hydrogen and steam concentrations ranged from 5 to 13% (by volume) and 4 to 40%, respectively. The use of sprays and/or fans enhanced the combustion rate and significantly altered the postcombustion gas cooling.

The CONTAIN code version 1.04 has been used with a few additional modifications which will be released in the next CONTAIN version. The calculations predict pressure and temperature peaks very close to the peak values obtained in the experiments. Also, the pressure and temperature decrease after reaching the maximum values is close to the experimental results. The radiative and total heat flux, as well as the radiative and total energy deposition, agree reasonably well in prediction and experiment. A significant disagreement between CONTAIN and NTS data is the hydrogen burn duration, which should be assessed by the developers of CONTAIN.

Introduction

In this paper a brief description is given about the CONTAIN code, [1] which is followed by a brief description of the NTS dewar in which the premixed combustion tests have been carried out.[2] After detailing the initial test conditions, a few characteristic parameters are defined in order to compare the experiment with the calculations. Finally, the CONTAIN calculations are compared with the experimental results and conclusions are drawn. It should be noted that calculations with the HECTR code [3] have been carried out [4] using the same NTS experimental data. Although CONTAIN uses the HECTR hydrogen burn model, it should be noted that the integrated CONTAIN code uses many other calculational models.

The CONTAIN Code

Using a mechanistic approach, the CONTAIN computer code calculates the physical, chemical, and radiological processes in the containment building during a reactor accident. The code is able to predict the source term to the atmosphere in case the containment leaks or fails.

The source into the containment building from the primary system must be supplied as input.

The CONTAIN code has a modular structure. This enables the code to incorporate models from other developed codes. One such example is the hydrogen burn models in CONTAIN which are taken from the HECTR code [3]. The CONTAIN code will not necessarily obtain the same results for hydrogen burn as HECTR because of the interaction of the hydrogen burn subroutines with the aerosol subroutines and the engineering safety equipment subroutines like sprays.

In the reactor safety field, research and experiments are an ongoing activity. As models are being improved, a user might want to use non-default values. In order to judge CONTAIN on its merits, the CONTAIN default values are used. The exceptions will be stated explicity.

NTS Dewar

The premixed and continuous-injection combustion experiments were performed in an existing facility located at test cell C, NTS. This spherical test vessel has a diameter of 15.85 m (2048 m^3 volume) and a design pressure of ~700 kPa. The dewar is comprised of two concentric stainless steel spheres, each 19 mm thick with an intermediate layer of perlite insulation ~1.0 m thick. The facility had previously been used as a hydrogen dewar and required renovation prior to commencement of the testing. In addition, the facility was modified to include the following:

* A heated-water spray system in the vessel, consisting of 16 or 17 Sprayco model 1713A hollow cone nozzled (each rated at $.946 \times 10^{-3}$ m^3/s) with the necessary control system and manifolding.

* A boiler to generate 2.1 kg/s steam at 1000 kPa for vessel and gas preheating.

* A hydrogen-steam manifold system and mixing chamber (outside the dewar) to deliver specified mixtures of combustible gas for premixed and continuous-injection combustion testing.

* Two mixing fans in the vessel, each rated at 2.4 m^3/s to be used for pretest equilibration and during some tests.

* An air compressor (rating of 0.28 m^3/s) to supply air to the mixing fans and primary spray pump air motors as well as for post-test purge and refill operations.

* A gas sampling system for pre- and posttest evaluations of the gas uniformity and combustion completeness.

In addition, hydrogen was supplied from gas cylinders in a tube trailer; after mixing with steam, it was injected into the dewar through a nozzle ~2.0 m in diameter above the bottom either as a diffuse stream or as a jet depending upon the test configuration.

The premixed combustion tests were initiated using ignition sources typical of those currently being installed in nuclear reactor containments for deliberate ignition safety systems. Six General Motors glow plugs and six Tayco coil igniters were mounted in the vessel. The ignition sources were positioned to allow for combustion initiation on the central vertical axis of the sphere at the top, bottom, or center of the dewar and also along the vessel walls. Each ignition device was a hot surface (temperatures ~1000-1400 K, depending on the input voltage) and each could be independently operated. For most of the premixed combustion testing, bottom ignition was utilized, although there are redundant tests in which the ignition site was changed to assess the effects of initiation location on combustion completeness and severity. Note that in this work, the general location of ignition (i.e., bottom, top, etc.) will be provided for each test as opposed to the particular igniter.

Premixed Combustion Initial Conditions

The EPRI/EG&G premixed combustion test program consisted of twenty-four tests using various mixtures of hydrogen (5 to 13% by volume) and steam (4 to 40%). Data were provided to SNLA for twenty-one of these tests. In two of the tests for which no data were received, there was either no combustion or the combustion completeness was so low that the tests were repeated with sprays/fans operative to affect more complete burning. For the third test for which no data were provided, the data acquisition system was inoperative necessitating a 'repeat' experiment.

Nominal precombustion data (i.e., initial conditions) for the twenty-one tests are provided in tables as obtained from [2], see Table 1. The tests have been grouped for presentation in increasing severity (i.e., increasing hydrogen concentration) according to the following:

* Tests with sprays operative are grouped together regardless of other precombustion conditions (designated as "Tests with Spray System Operative").

* Tests in which the dewar was heated, to allow for gas mixtures with steam concentrations greater than 10% (by volume), are grouped together (designated as "Steam-Laden Tests").

* Tests in which the dewar was maintained at ambient conditions so that the steam concentration was nominally 5% (by volume), are grouped together (designated as "Standard Tests").

In these tables, the tests are designated as 'NTS - P - xx', with the 'P' specifying that the test was a premixed combustion experiment and with 'xx' conforming to the EPRI/EG&G numbering system.

Prior to the tests the sprays and mixing fans were used in order to obtain saturated and premixed conditions.[5] If the fans and/or sprays were not operative during a particular experiment, they were turned off at least 10 minutes before the experiment took place.

As can be observed from Table 1 the initial hydrogen and steam molar fractions used in CONTAIN might deviate slightly from the experimental initial conditions. In case steam is present CONTAIN assumes saturated conditions at the given initial temperature and pressure and recalculates the remaining gas component molar fractions according to user-supplied ratios.

The CONTAIN Model

The NTS dewar was modeled by one control volume (or cell). The structural components were divided over a roof, wall, and floor section. Furthermore, a pool was present. The initial temperature of the structural components, the pool, and, where applicable, the spray water was set equal to the initial atmospheric temperature. All tests with sprays on had a mass flow of 16.1 kg/s except for experiment NTSP02, which had 16 sprays operative instead of 17. The calculations were carried out over a 300 s period starting at the beginning of the combustion.

CONTAIN 1.04 has been used with a few updates from the 1.05 version. Experiments [4] show the necessity of a modified combustion completeness curve as function of the initial H_2 concentration. For initial concentrations of 4% or less no burn occurs. The combustion completeness increases then linearly to 100% at an initial H_2 concentration of 8%, after which it remains 100%. Another CONTAIN 1.05 update made it possible for the user to override the H_2 concentration for the burn initiation.

It should be pointed out that in a one-cell representation such as this, it is not possible to specify the burn location precisely. Another limitation of the analysis is that CONTAIN does not treat the effect on hydrogen combustion of turbulence induced by fans.

Comparative Quantities

In order to judge the performance of CONTAIN in calculating the NTS experiments certain quantities need to be compared. The quantities this paper will focus on are:

* Combustion completeness; the molar fraction of burned hydrogen divided by the initial hydrogen molar fraction.
* Burn time; duration of the hydrogen burn.
* Dimensionless pressure peak; the ratio of the maximum pressure and the initial pressure.
* Dimensionless temperature peak; similar ratio as above.
* Temperature peak width (TPW); the time interval from the start of the burn until the decreasing temperature reaches the averaged value of peak and initial temperature.
* The maximum total heat flux and maximum radiative heat flux on the cavity boundary.
* The total energy deposition and radiative energy deposition on the cavity boundary.
* The energy deposition on the cavity boundary due to the adiabatic isochoric combustion calculation of the experiment and the CONTAIN hydrogen combustion energy.

CONTAIN vs. NTS Experiments

In Figures 1 to 9 comparisons are given from the experiment and CONTAIN calculations. The figures are divided into three categories, i.e., standard tests (Figures 1-3), steam-laden tests (Figures 4-6), and tests with sprays-on (Figures 7-9). Within each category, the dimensionless pressures, the total heat flux, and radiative heat flux is given. The experimental data figures are from Reference [2].

In Table 2 the combustion completeness is given for the NTS experiments and the CONTAIN calculations. There is close agreement between experiment and calculation given the experimental uncertainties. Comparing NTSP03 and NTSP02, both with an initial molar fraction of 5.8% hydrogen and 14.3% steam, the combustion completeness given by the experiment is 50% and 70% respectively. Hence the experimental results have significant spread.

The burn time in the experiment is defined from the time that the pressure has risen 5% up to the time the heat flux is at the maximum value. In CONTAIN the burn time is simply the time during burning.

In the calculations a non-default characteristic length of 11 m is used except for the cases where the combustion starts at the center, in which case the non-default length is set equal to the radius of the dewar. The 11 m characteristic length was taken because the ignition is not totally at the bottom of the dewar and when the flame front propagates radially from the ignition location (a burning mode which has been designated flame front propagation type 1), the remaining volume after 11 m characteristic length is quite small. Although flame front propagation type 1 is observed in other than NTS premixed combustion test, it appears that in the experiments considered here, flame front propagation type 2 is observed.[6] In type 2 the flame front propagates upward, and after reaching the roof, the flame front propagates downward along the walls. The burn time in Table 3 shows that for initial hydrogen concentrations less than 6.5% combined with initial steam concentrations less than 27% the burn time in the CONTAIN code is shorter than in the experiment. The leaner the hydrogen and steam the more CONTAIN deviates from the experiment. In NTSP01 (H_2 5.3%) the deviation was a factor of 30. With the exception of experiment NTSP12, CONTAIN has a longer burn time than observed in the experiments if the initial hydrogen concentration exceeds 6.5% combined with a steam concentration exceeding 27%. The largest discrepancy here is in experiment NTSP21 (H_2 13.2%), in which the burn time in CONTAIN is four times longer than in the experiment. It should be noted that similar results were obtained with the HECTR code [6].

Table 2 tabulates the dimensionless pressure and temperature peaks obtained by the experiments and the calculations. In addition, these peaks are computed when the adiabatic isochoric combustion (AIC) calculations are carried out using the experimental results. As also can be seen in Figure 10, CONTAIN overpredicts the experimental value, but remains under the AIC values. The AIC values are exceeded by CONTAIN if the burn is more complete than in the experiment. CONTAIN overpredicts the most when the gas mixture is lean on hydrogen and steam. This indicates that the burn time will have an influence since during slow burning, energy dissipation to the boundary of the cavity occurs while the burn is still in progress.

The TPW results are given in Table 3. In the experiment various thermocouples are used giving different results for the same experiment. Hence for each experiment the range is given for the various measurements. With CONTAIN a single value is obtained. Figure 11, which depicts this phenomenon, clearly indicates good agreement between calculation and experiment. It clearly shows the effectiveness of sprays, which have a TPW of 20 to 30 s. For high initial hydrogen concentration combustions, the TPW values are also small due to the fact that the temperature peak is very high, which causes a fast cooling off. For this reason, the TPW values in the

case of lean hydrogen combustion without sprays should increase as is observed in the table and figure.

The maximum total heat flux is given in Table 4. Experimental data was not given in [2] for the sprays on tests. The maximum radiative heat flux is presented for all tests. These types of measurements generally tend to underpredict the actual heat fluxes, [7] which make a judgement of the overprediction of CONTAIN or an underprediction of the experiment a relative and not an absolute statement. For the standard tests the maximum total heat flux is within a factor of two for the calculation and experiment, excluding test NTSP01 (5.3% hydrogen). The calculation overpredicts the maximum total heat flux, with the exception of test NTSP04 which had a 100% combustion completeness during the experiment and only 93% in the calculation. In the steam laden tests the calculations underpredict the maximum total heat flux, except where the calculations have a substantially higher combustion completeness than the experiments. For the maximum radiative heat flux it can be observed that for initial hydrogen concentrations less than 10.5%, the calculations overpredict the experimental results and for concentrations above 10.5% calculations underpredict the tests. The exceptions are the sprays-on tests NTSP02 and NTSP18, in which both cases the experimental combustion completeness exceeded the calculated ones. The experimental maximum radiative heat flux of test NTSP02 is quite a bit out of line with the steam-laden tests NTSP07-03-06 and sprays-on test NTSP22, all of which have similar hydrogen and steam initial concentrations, and similar initial temperatures and pressures. The final column in Table 4 gives the ratio of maximum radiative heat flux and maximum total heat flux. For the standard and steam laden tests it can be seen that this ratio is 0.2 higher in the calculations than in the experiments. The only exception is the initially very lean hydrogen test NTSP01 in which the ratio for the test is higher than the calculation. For the sprays-on tests no data was available.

A possibly important difference between the experiments and the way the calculations were set up was that a water film was probably present on the dewar walls at the start of the experiments, but this film was not modeled as being initially present in the CONTAIN calculations. This film may have an influence on the emissivity values for radiation as well as on the remaining heat flux to the boundary. As a consequence, the wall rise temperatures will be lower in the CONTAIN calculations than in the experiments.

Similarly, it is observed in Table 5 that the total and radiative energy deposition on the boundary of the cavity reaches larger values with the CONTAIN calculations than observed with the experiment. In CONTAIN the total energy deposition is computed from the start of the burn until 300 s later. In the experiment it is a 300 s period starting at pressure peak. The ratio of the radiative to the total energy deposition are in closer agreement in the calculation and

experiment than is observed in the similar ratio of the maximum heat fluxes. The ratio of the energy deposition in CONTAIN exceeds the experimental value.

The close agreement between the energy the hydrogen combustion released to the atmosphere in the CONTAIN calculation and the experiments is interesting. The values of the calculations exceed the experimental values slightly. The experimental values are calculated using an adiabatic isochoric combustion calculation. The values in Table 5 are per unit boundary area. Hence the numbers can be compared with the values of the previous paragraph. The values of the total energy depositon up to 300 s are 50 to 70% of the values for the hydrogen energy released per unit boundary area.

Conclusions

CONTAIN version 1.04 with the update of version 1.05 for the hydrogen combustion completeness is very capable of calculating the phenomena occuring during the premixed hydrogen burn experiments carried out in the NTS dewar. With the exception of the duration of the combustion, the quantities compared in CONTAIN and the experiments are in close agreement. The hydrogen burn duration in CONTAIN is a factor 30 too short when a combined lean hydrogen and lean steam concentration experiment is performed. The CONTAIN burn duration is a factor 4 too long when a combined rich hydrogen and rich steam concentration experiment is performed. The CONTAIN code developers need to assess this aspect of the modeling.

In order to judge CONTAIN on its merits, the phenomena should be considered in the order of importance. For containment integrity CONTAIN predicted the pressure peak very well. One reason for this is that the combustion energy was computed very well, too. As a consequence it should be expected and it is observed that the peak temperatures are predicted accurately. The next level of decreasing importance is the burn duration and the shape characteristics of the pressure and the temperature peak. Except for the burn duration CONTAIN again predicts the experimental results very well. The final and lowest level of importance is the agreement concerning heat fluxes and energy depositions. Although the agreement is reasonable, uncertainty exists in interpretation of the experimental data. The boundary wall temperature rise is predicted by CONTAIN is low, but should be considered of low-level importance.

References

[1] K. D. Bergeron et al., "User Manual for CONTAIN 1.0, A Computer Code for Severe Nuclear Reactor Accident Containment Analysis", Sandia National Laboratories, Albuquerque, NM, NUREG/CR-4085, SAND84-1204, May 1985.

[2] A. C. Ratzel, "Data Analyses for Nevada Test Site (NTS), Premixed Combustion Tests", Albuquerque, NM, NUREG/CR-4138, SAND85-0135, May 1985.

[3] A. L. Camp et al., "HECTR Version 1.0 User's Manual", Albuquerque, NM, NUREG/CR-3913, SAND84-1522, Feb 1985.

[4] C. C. Wong, "HECTR Development and Assesment", SAND85-1792C, 13th Water Reactor Safety Research Information Meeting Gaithersburg, Maryland, Oct. 22-25,1985.

[5] R. Torok, Astron, Private Communication.

[6] C. C. Wong, Sandia National Laboratories, Albuquerque, NM, Private Communication.

[7] G. D. Valdez, Sandia National Laboratories, Albuquerque, NM, Private Communication.

TABLE 1: INITIAL CONDITIONS FOR PREMIXED COMBUSTION TESTS

TEST NAME	H2/H2O[%] EXP	H2/H2O[%] CONTAIN	Po[kPa] EXP/CON	To[K] EXP/CON	IGNITION* EXP	MIXING FANS
STANDARD TESTS						
NTSP01	5.3/ 4.2	5.3/ 4.3	97.4	302.7	B	OFF
NTSP9P	6.0/ 4.6	6.0/ 4.6	89.6	302.7	B	OFF
NTSP09	6.1/ 4.2	6.1/ 4.3	91.6	301.8	B	OFF
NTSP00	6.6/ 4.5	6.6/ 4.6	91.6	303.0	B	OFF
NTSP04	7.7/ 4.8	7.7/ 4.9	97.4	305.2	B	OFF
NTSP13	7.8/ 4.4	7.8/ 4.6	97.4	303.9	B	OFF
NTSP15	9.9/ 4.2	9.9/ 3.9	109.3	304.4	B	OFF
STEAM-LADEN TESTS						
NTSP07	5.5/14.3	5.5/14.6	93.5	325.2	2E	ON
NTSP03	5.8/14.4	5.8/14.7	95.4	325.7	C	ON
NTSP06	6.0/13.7	6.0/14.0	87.6	323.0	T	ON
NTSP12	6.9/28.3	6.8/29.0	92.6	339.7	B	OFF
NTSP14	8.1/38.7	8.0/39.5	93.5	347.1	B	OFF
NTSP05	7.8/31.3	7.7/32.1	87.6	340.8	B	OFF
NTSP16	10.1/29.5	10.0/30.2	101.3	342.7	B	OFF
NTSP08	11.1/27.2	10.8/29.4	130.6	348.0	B	ON
NTSP20	12.9/27.8	12.8/28.5	104.2	342.0	B	OFF
TESTS WITH SPRAY SYSTEM OPERATIVE						
NTSP22	5.2/14.5	5.2/14.8	93.5	325.5	1E	OFF
NTSP11	5.8/ 4.9	5.8/ 4.9	93.5	304.6	T	OFF
NTSP02**	5.8/14.3	6.0/14.6	88.6	324.1	C	OFF
NTSP18	6.6/27.3	6.5/28.5	105.2	342.2	T	OFF
NTSP21	13.2/27.4	13.1/28.1	102.3	341.3	B	ON

*IGNITION AT BOTTOM (B), CENTER(C), TOP(T), OR BY 1 OR 2 IGNITERS ON THE WALL AT THE EQUATOR (1E, 2E)
**ONLY 16 SPRAYS OPERATIVE
EXP= EXPERIMENT
CON= CONTAIN

TABLE 2: PEAK GAS PRESSURE, TEMPERATURE RESULTS AND COMBUSTION COMPLETENESS

TEST NAME	H2/H2O[%] EXP	CC [%] EXP*/CON	Pmax/Po EXP/CON	Pmax/Po EXP AIC**	Tmax/To EXP/CON	Tmax/To EXP AIC**
STANDARD TESTS						
NTSP01	5.3/ 4.2	32/ 36	1.48/1.69	1.63	1.5 /1.71	1.64
NTSP9P	6.0/ 4.6	53/ 52	1.69/2.11	2.14	1.72/2.15	2.18
NTSP09	6.1/ 4.2	60/ 55	1.83/2.17	2.31	1.85/2.11	2.35
NTSP00	6.6/ 4.5	66/ 67	2.22/2.51	2.53	2.27/2.57	2.59
NTSP04	7.7/ 4.8	100/ 93	3.19/3.30	3.51	3.32/3.43	3.65
NTSP13	7.8/ 4.4	100/ 95	3.13/3.39	3.55	3.28/3.52	3.70
NTSP15	9.9/ 4.2	100/100	3.81/4.09	4.14	3.81/4.30	4.35
STEAM-LADEN TESTS						
NTSP07	5.5/14.3	45/ 40	1.66/1.71	1.82	1.69/1.73	1.84
NTSP03	5.8/14.4	50/ 47	1.78/1.87	1.94	1.81/1.90	1.97
NTSP06	6.0/13.7	54/ 52	1.84/2.00	2.06	1.87/2.03	2.10
NTSP12	6.9/28.3	58/ 72	1.85/2.31	2.18	1.90/2.38	2.23
NTSP14	8.1/38.7	94/100	2.16/2.53	2.99	2.25/2.70	3.10
NTSP05	7.8/31.3	100/ 93	2.66/2.68	3.10	2.66/2.81	3.23
NTSP16	10.1/29.5	100/100	3.2 /3.27	3.62	3.38/3.48	3.81
NTSP08	11.1/27.2	100/100	3.61/3.47	3.80	3.84/3.70	4.02
NTSP20	12.9/27.8	100/100	3.87/3.92	4.22	4.14/4.21	4.51
TESTS WITH SPRAY SYSTEM OPERATIVE						
NTSP22	5.2/14.5	31/ 33	1.36/1.52	1.48	1.35/1.52	1.44
NTSP11	5.8/ 4.9	58/ 48	1.96/1.94	2.12	1.97/1.96	2.12
NTSP02	5.8/14.3	70/ 51	2.15/1.94	2.22	2.16/1.95	2.23
NTSP18	6.6/27.3	69/ 65	2.10/1.96	2.26	2.12/1.93	2.28
NTSP21	13.2/27.4	100/100	3.91/3.90	4.25	4.12/3.99	4.47

* COMBUSTION COMPLETENESS VALUE (CC) ASSIGNED BY SANDIA [REF.2]
** RESULT FROM ADIABATIC ISOCHORIC COMBUSTION CALCULATIONS ON EXPERIMENTAL RESULTS
EXP= EXPERIMENT
CON= CONTAIN

TABLE 3: BURN DURATION AND TEMPERATURE PEAK WIDTH

TEST NAME	H2/H2O[%] EXP	BURN TIME [s] EXP/CON **	TPW[s] * EXP-EXP/CON
STANDARD TESTS ***			
NTSP01	5.3/ 4.2	86.5/ 2.7	- /127
NTSP9P	6.0/ 4.6	58.0/ 2.6	56-120/ 87
NTSP09	6.1/ 4.2	36.5/ 2.5	65-104/ 84
NTSP00	6.6/ 4.5	15.0/ 2.4	- / 65
NTSP04	7.7/ 4.8	7.0/ 2.2	- / 40
NTSP13	7.8/ 4.4	7.5/ 2.1	25- 61/ 40
NTSP15	9.9/ 4.2	6.0/ 1.7	16- 56/ 29
STEAM- LADEN TESTS ***			
NTSP07	5.5/14.3	23.5/ 4.8	- / 98
NTSP03	5.8/14.4	15.5/ 4.7	- / 84
NTSP06	6.0/13.7	18.0/ 4.4	- / 74
NTSP12	6.9/28.3	27.0/13.6	32- 74/ 61
NTSP14	8.1/38.7	19.5/34.7	30- 56/ 72
NTSP05	7.8/31.3	12.5/17.5	41- 60/ 52
NTSP16	10.1/29.5	4.5/11.7	13- 61/ 38
NTSP08	11.1/27.2	3.0/ 9.1	30- 33/ 38
NTSP20	12.9/27.8	2.0/ 6.0	23- 48/ 26
TESTS WITH SPRAY SYSTEM OPERATIVE ****			
NTSP22	5.2/14.5	8.5/ 5.1	7- 49/ 20
NTSP11	5.8/ 4.9	5.0/ 2.7	7 / 17
NTSP02	5.8/14.3	4.0/ 3.3	- / 17
NTSP18	6.6/27.3	4.5/13.4	12- 25/ 27
NTSP21	13.2/27.4	1.5/ 5.6	11- 25/ 16

* TPW: TEMPERATURE PEAK WIDTH EQUALS TIME FROM START BURN TO HALF MAX TEMP. ON THE DECREASING TEMPERATURE RANGE
** CONTAIN BURN TIME IS CALCULATED. MAX HEATFLUX IS 1.2 TIMES BURN TIME
*** IN EXPERIMENT BASED UPON MAXIMUM HEATFLUX
**** IN EXPERIMENT BASED UPON MAXIMUM PRESSURE
EXP= EXPERIMENT
CON= CONTAIN

TABLE 4: HEAT FLUXES

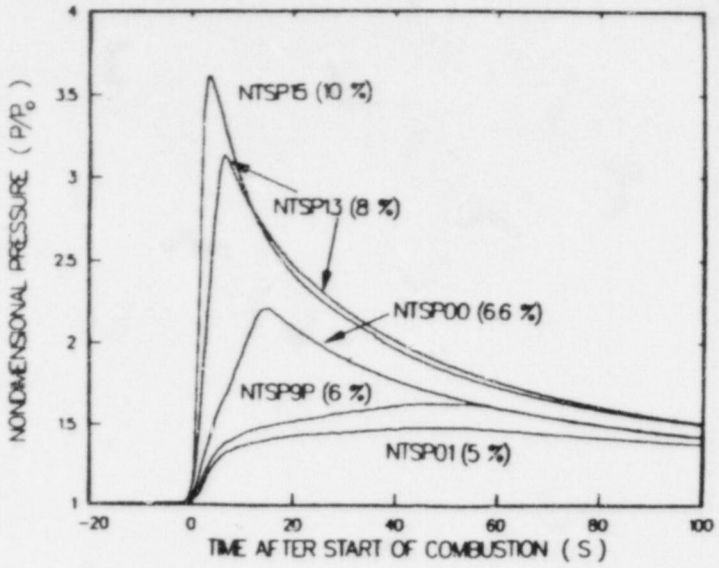
TEST NAME	H2/H2O[%] EXP	q-tot [W/CM2] EXP/CON	q-rad [W/CM2] EXP/CON	q-rad/q-tot EXP/CON
STANDARD TESTS				
NTSP01	5.3/ 4.2	16/ .38	.08/ .17	.50/.43
NTSP9P	6.0/ 4.6	.41/ .94	.14/ .50	.34/.54
NTSP09	6.1/ 4.2	.72/ 1.05	.23/ .58	.33/.55
NTSP00	6.6/ 4.5	2.03/ 1.86	.62/ 1.16	.31/.62
NTSP04	7.7/ 4.8	8.02/ 5.63	3.33/ 4.18	.42/.74
NTSP13	7.8/ 4.4	5.79/ 6.11	3.06/ 4.58	.53/.75
NTSP15	9.9/ 4.2	10.6 /12.60	5.94/10.09	.56/.80
STEAM-LADEN TESTS				
NTSP07	5.5/14.3	.72/ .60	.24/ .29	.33/.49
NTSP03	5.8/14.4	1.22/ .88	.35/ .46	.29/.52
NTSP06	6.0/13.7	1.20/ 1.06	.37/ .58	.31/.55
NTSP12	6.9/28.3	1.35/ 2.49	.55/ 1.55	.41/.62
NTSP14	8.1/38.7	2.41/ 3.82	1.31/ 2.85	.54/.74
NTSP05	7.8/31.3	6.31/ 4.35	2.61/ 3.12	.41/.72
NTSP16	10.1/29.5	9.65/ 9.18	6.75/ 7.37	.70/.80
NTSP08	11.1/27.2	21.2 /12.1	12.3 / 9.80	.58/.81
NTSP20	12.9/27.8	25.4 /17.4	15.3 /14.9	.60/.86
TESTS WITH SPRAY SYSTEM OPERATIVE				
NTSP22	5.2/14.5	/ .37	.07/ .16	/.43
NTSP11	5.8/ 4.9	/ .71	.33/ .35	/.49
NTSP02	5.8/14.3	/ .39	.77/ .17	/.43
NTSP18	6.6/27.3	/ 1.37	.97/ .64	/.46
NTSP21	13.2/27.4	/15.0	14.9 /12.14	/.81

EXP= EXPERIMENT
CON= CONTAIN

TABLE 5: ENERGY DEPOSITIONS AND ENERGY GENERATED BY H2-BURN

TEST NAME	H2/H2O[%] EXP	Q-tot [J/cm2] EXP/CON	Q-rad [J/CM2] EXP/CON	Q-rad/Q-tot EXP/CON	Q-hburn [J/cm2] EXP.AIC*/CON
STANDARD TESTS					
NTSP01	5.3/ 4.2	27/ 39	9/ 18	.33/.41	43/ 55
NTSP9P	6.0/ 4.6	35/ 65	13/ 30	.37/.46	76/ 84
NTSP09	6.1/ 4.2	49/ 70	16/ 33	.33/.47	90/ 91
NTSP00	6.6/ 4.5	72/ 95	24/ 50	.33/.53	107/120
NTSP04	7.7/ 4.8	139/165	69/103	.50/.63	203/204
NTSP13	7.8/ 4.4	144/172	71/108	.49/.63	207/212
NTSP15	9.9/ 4.2	198/258	93/178	.47/.70	296/318
STEAM-LADEN TESTS					
NTSP07	5.5/14.3	38/ 45	13/ 23	.34/.51	58/ 57
NTSP03	5.8/14.4	50/ 57	18/ 30	.36/.53	69/ 72
NTSP06	6.0/13.7	48/ 61	15/ 33	.31/.54	72/ 78
NTSP12	6.9/28.3	53/ 97	27/ 64	.51/.66	91/122
NTSP14	8.1/38.7	73/150	48/110	.66/.73	173/192
NTSP05	7.8/31.3	109/129	54/181	.49/.74	178/165
NTSP16	10.1/29.5	155/205	114/161	.70/.79	259/263
NTSP08	11.1/27.2	234/277	191/217	.81/.78	382/359
NTSP20	12.9/27.8	219/272	164/224	.75/.82	343/346
TESTS WITH SPRAY SYSTEM OPERATIVE					
NTSP22	5.2/14.5	/ 14	1/ 3	/.21	29/ 44
NTSP11	5.8/ 4.9	/ 23	5/ 6	/.26	75/ 78
NTSP02	5.8/14.3	/ 39	6/ 16	/.41	83/ 55
NTSP18	6.6/27.3	/ 46	14/ 12	/.26	108/113
NTSP21	13.2/27.4	/175	112/ 99	/.57	333/348

* BASED UPON ADIABATIC ISOCHORIC COMBUSTION CALCULATIONS USING EXPERIMENTAL DATA [REF. 2]
EXP= EXPERIMENT
CON= CONTAIN



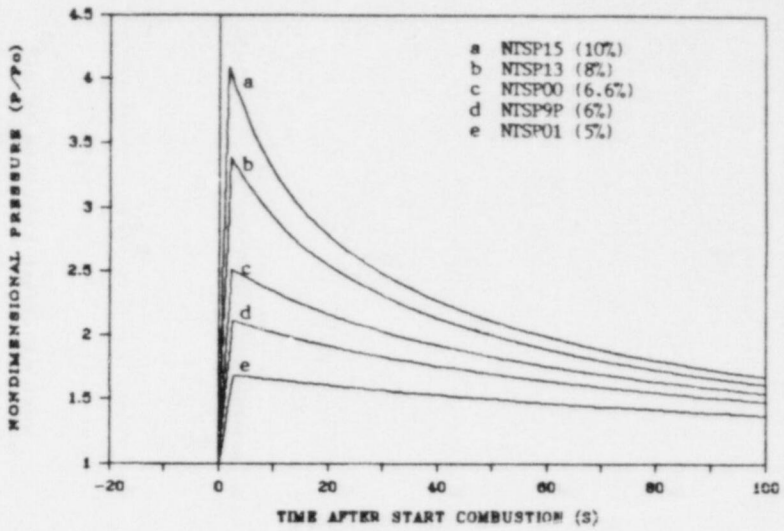
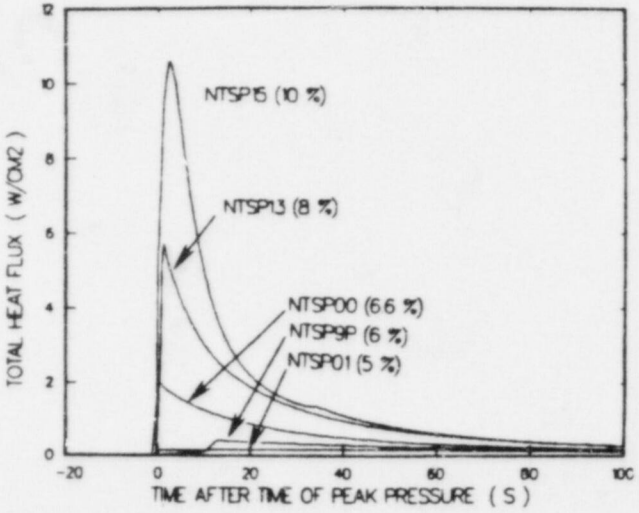


Figure 1. Gas pressure profiles for standard tests. Hydrogen concentrations are indicated. Left, NTS; right, CONTAIN



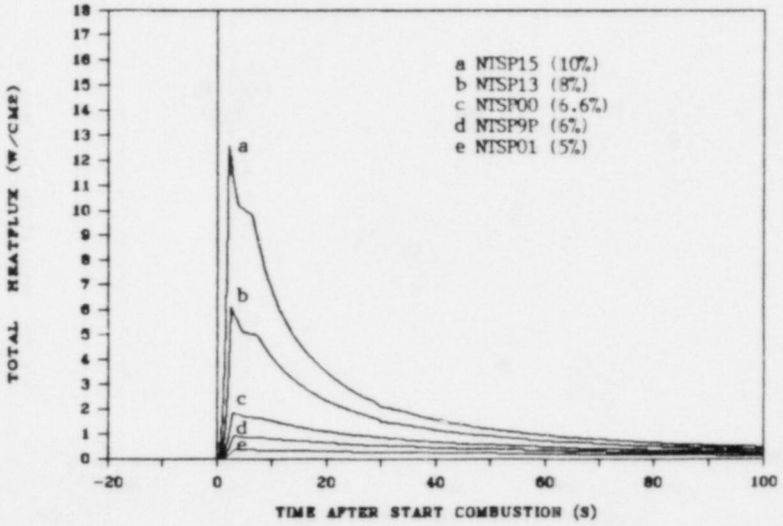


Figure 2. Total heat fluxes for standard tests from NTS pressure sensors, left; CONTAIN results, right. Hydrogen concentrations are indicated.

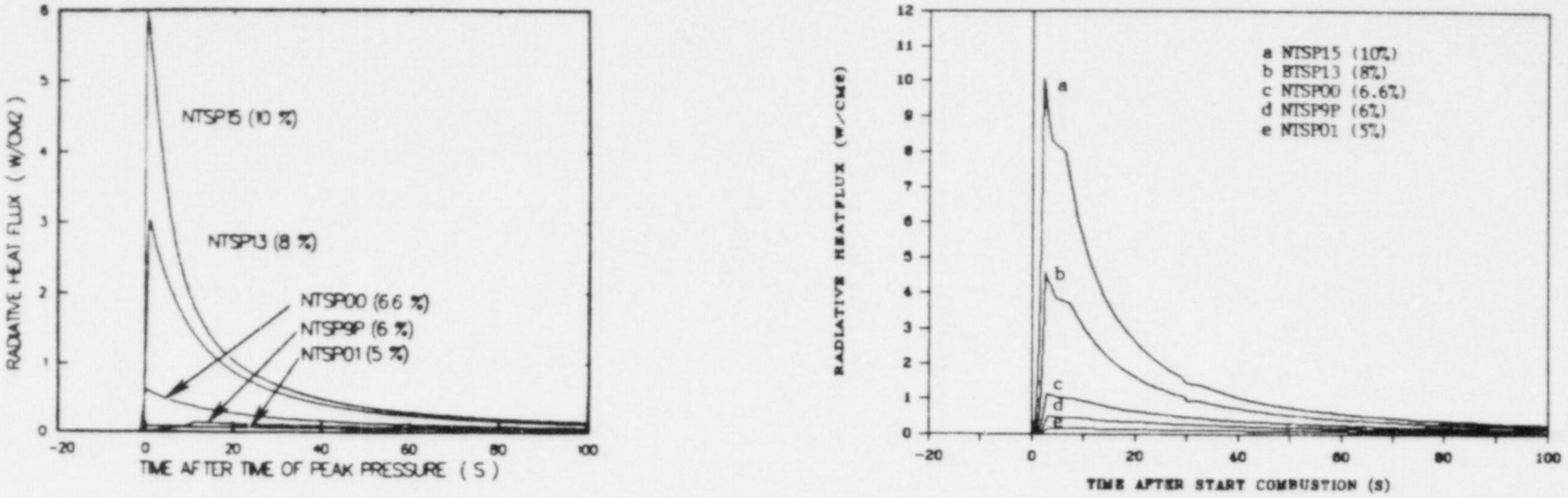


Figure 3. Radiative heat fluxes from pressure sensors for standard tests. NTS results, left; CONTAIN, right. Hydrogen concentrations are indicated.

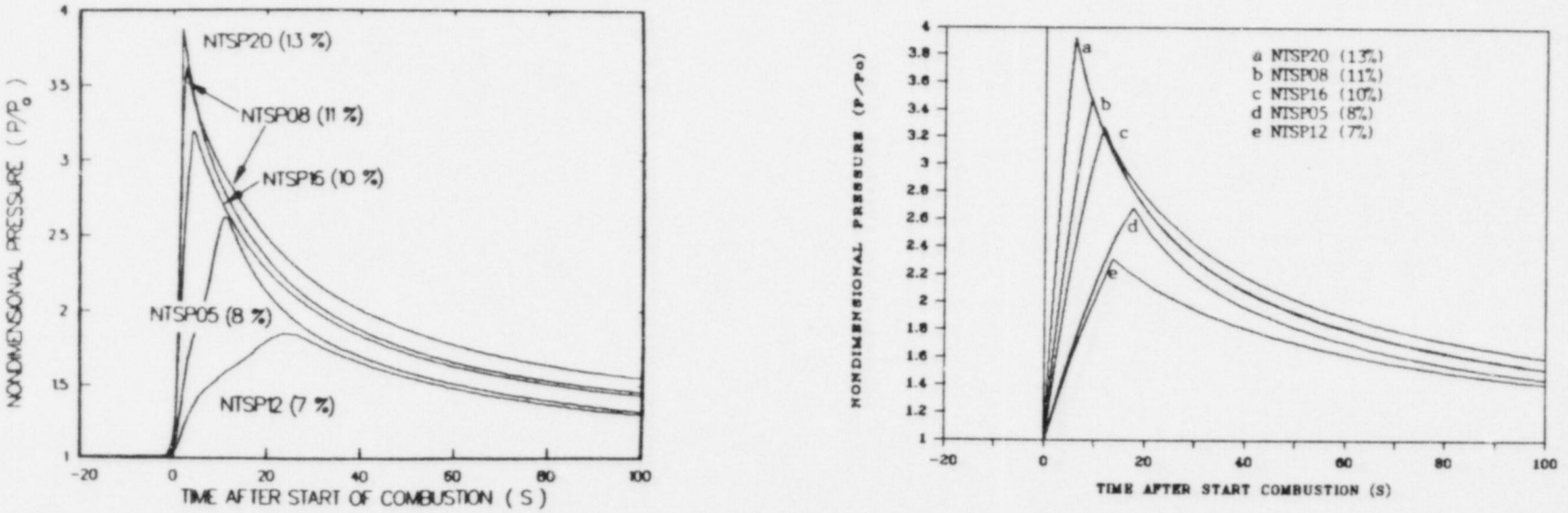


Figure 4. Gas pressure profiles for steam-laden tests. Nominal 30% steam by volume. Hydrogen concentrations as indicated. NTS, left; CONTAIN, right.

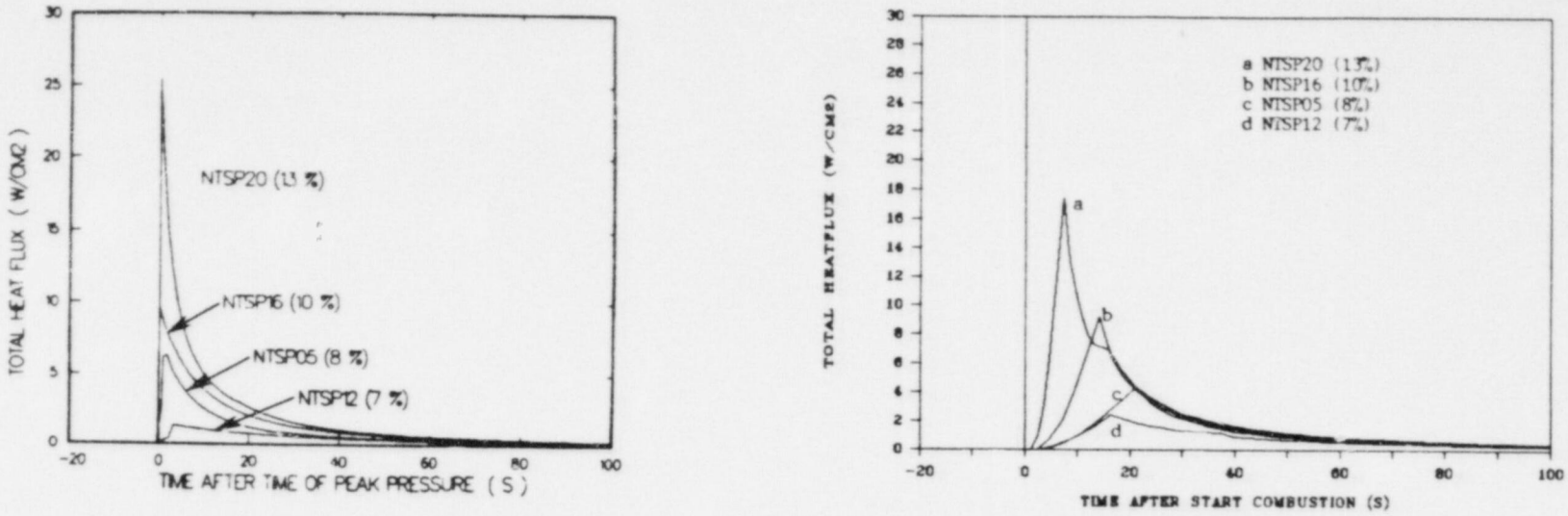


Figure 5. Total heat fluxes from NTS pressure sensors, left, for the steam-laden tests. Nominal 30% steam by volume. Hydrogen concentrations as indicated. Right, CONTAIN results.

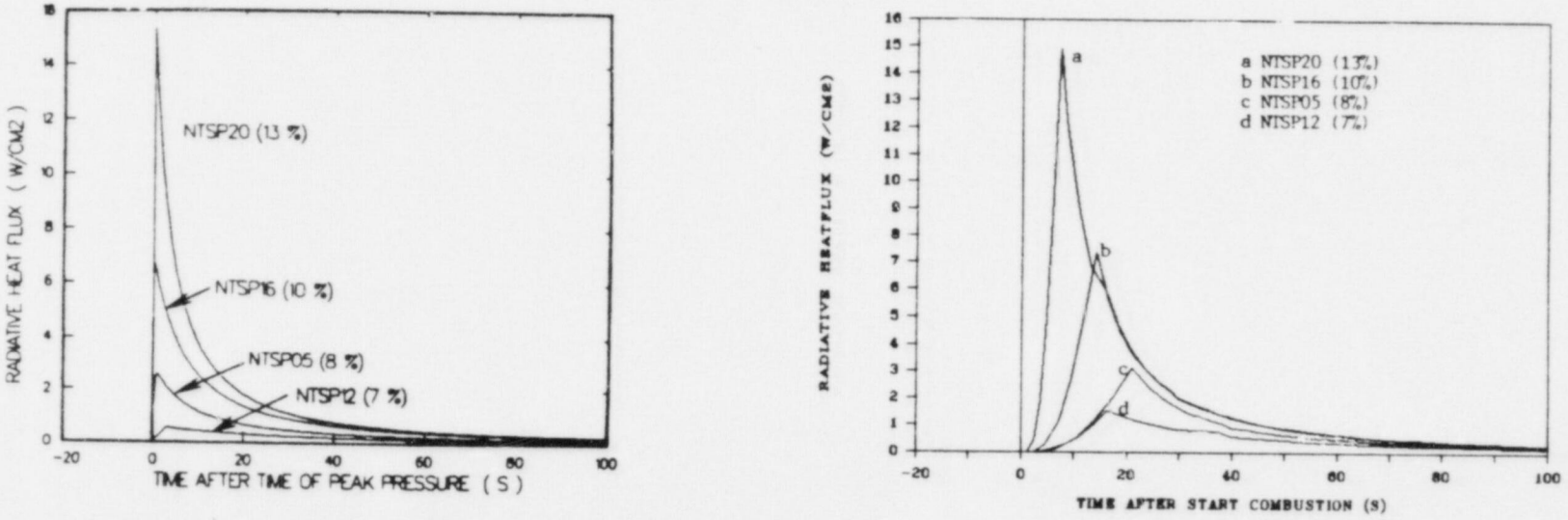


Figure 6. Radiative heat fluxes from the NTS pressure sensors, left, for the steam-laden tests. Nominal 30% steam by volume. Hydrogen concentrations as indicated. Right side, CONTAIN.

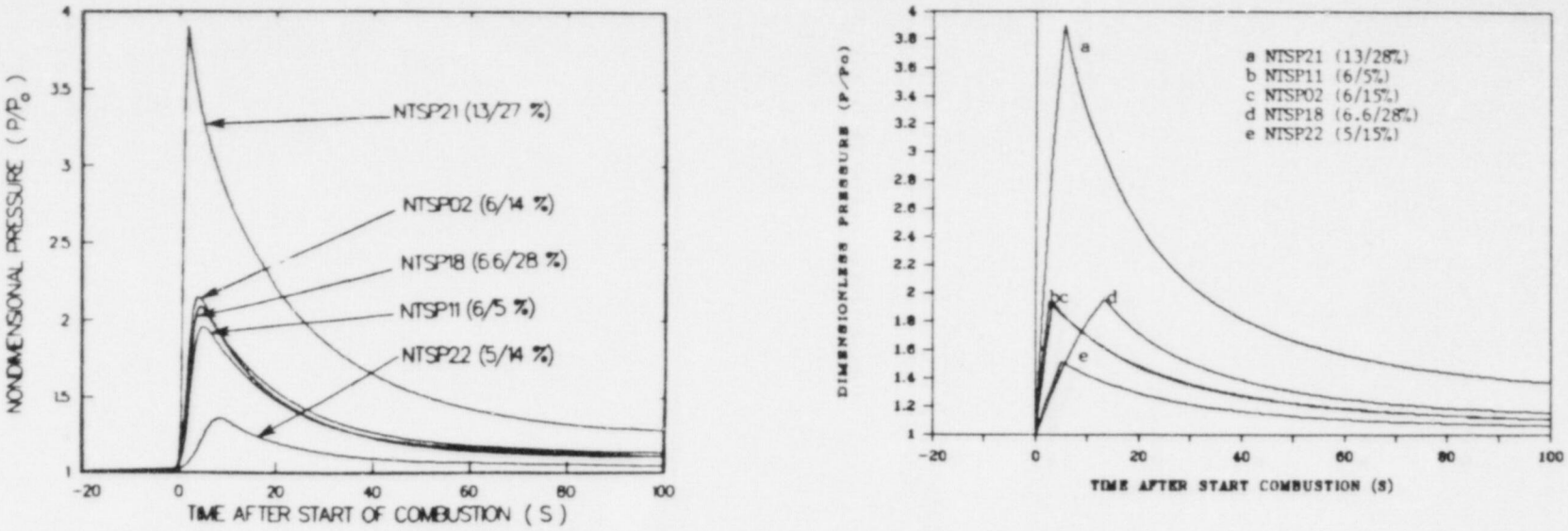


Figure 7. Gas pressure profiles for tests with sprays on. Numbers in parenthesis are initial hydrogen/steam concentrations. Left, NTS; right, CONTAIN.

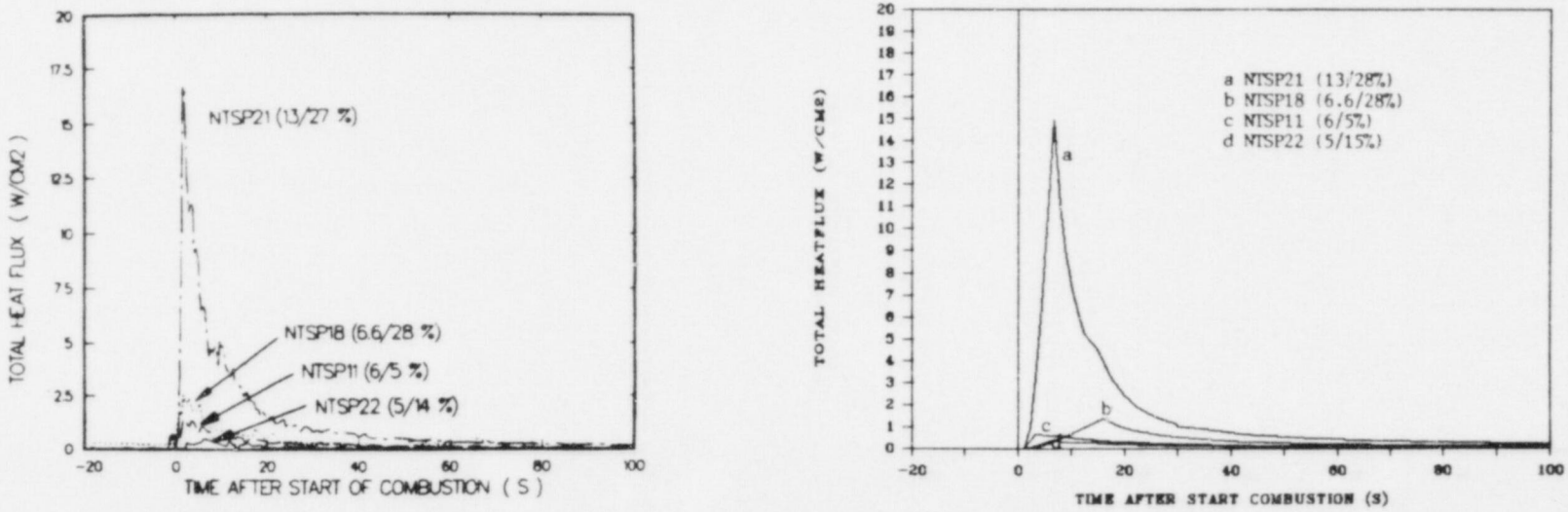


Figure 8. Total heat fluxes from NTS thin film gauge for tests with sprays-on, left. Right, CONTAIN. Numbers in parenthesis are initial hydrogen/steam concentrations.

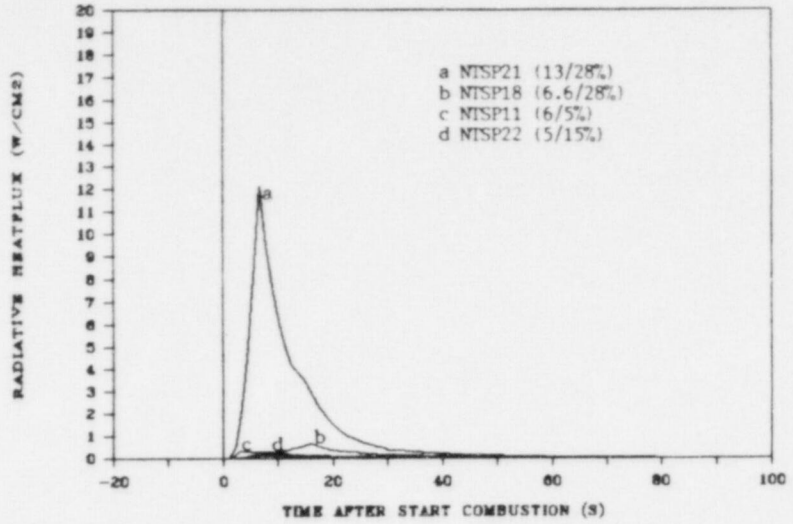


Figure 9.
Radiative heat fluxes of CONTAIN for sprays-on tests. Numbers in parenthesis are initial hydrogen/steam concentrations.

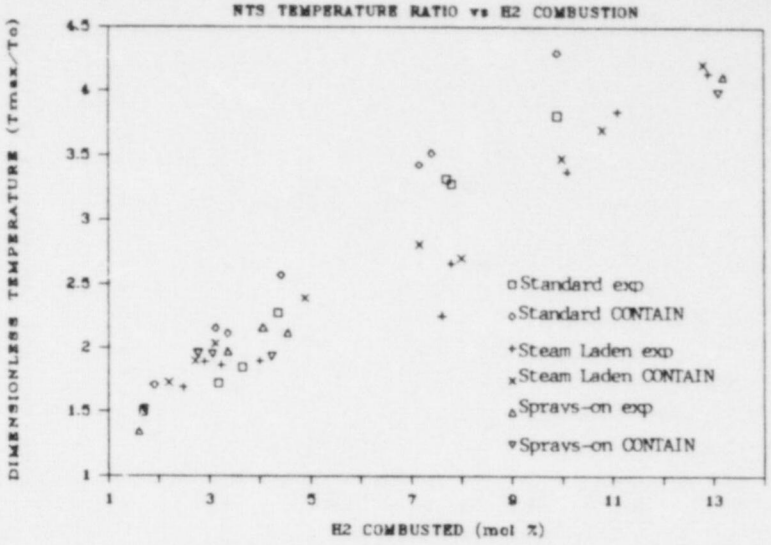


Figure 10.
The dimensionless peak pressure vs. the combusted hydrogen as obtained by NTS experiments and predicted by CONTAIN.

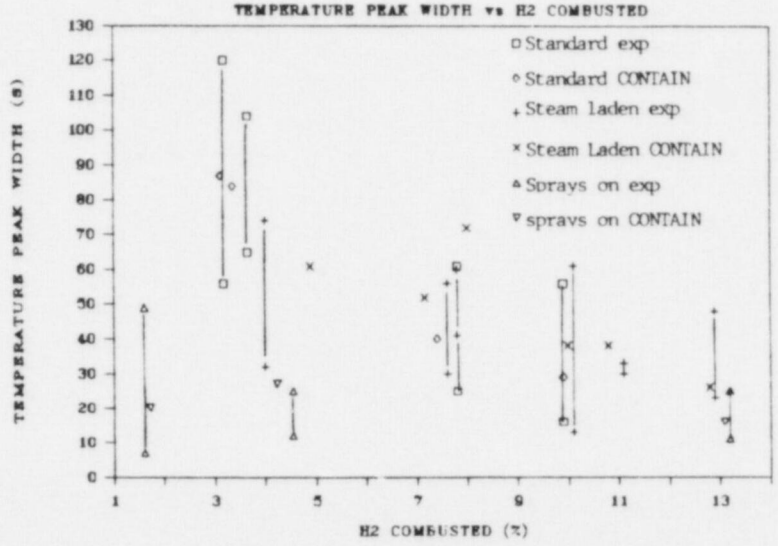


Figure 11. The temperature peak width as function of combusted hydrogen. The range is given for the NTS results. CONTAIN results are given by single points.

CONTAINMENT RESPONSE AND RADIOLOGICAL RELEASE FOR A TMLB' ACCIDENT SEQUENCE IN A LARGE DRY CONTAINMENT*

R. D. Gasser
Sandia National Laboratories

P. P. Bieniarz
Risk Management Associates

J. L. Tills
Tills and Associates

ABSTRACT

An analysis has been performed for the Bellefonte Pressurized Water Reactor (PWR) Unit 1 to determine the containment loading and the radiological releases into the environment from a station blackout accident. A number of issues have been addressed in this analysis, which include the effects of direct heating on containment loading and the effects of fission product heating and natural convection on releases from the primary system. The results indicate that direct heating which involves more than about 50% of the core can fail the Bellefonte containment, but natural convection in the Reactor Coolant System (RCS) may lead to overheating and failure of the primary system piping before core slump, thus, eliminating or mitigating direct heating. Releases from the primary system are significantly increased before vessel breach due to natural circulation and after vessel breach due to reevolution of retained fission products by fission product heating of RCS structures.

1.0 INTRODUCTION

An early attempt at an integrated "best estimate" of containment loading and radiological releases for specific accident sequences was carried out at Battelle Columbus Laboratories and disseminated in the now familiar BMI-2104 report.[1] In that study five reactors were selected in order to characterize different major reactor types, and analyses were performed for a few of the accident sequences that were thought to dominate the

*This work is supported by the United States Nuclear Regulatory Commission and performed at Sandia National Laboratories which is operated for the U.S. Department of Energy under contract number DE-AC04-76DP00789.

risk or present unique challenges to the containment. The BMI-2104 analysis employed computer codes that were run independently and in large part were in an early stage of development. A number of issues have been raised in the interim, some of which are related to phenomenology not modeled in the BMI-2104 suite of codes. It is the objective of this study to address some of these issues with a view to improving the calculated estimate of containment loading and fission product releases to the environment. The present study has been limited to large dry containments in general and to the TVA Bellefonte Unit 1 in particular. The detailed analysis will be published in a Sandia Report.[2]

An issue of considerable importance for PWRs, since it supplies a mechanism for early containment failure, is that of direct containment heating due to the high pressure ejection of molten core debris into the upper containment atmosphere. The ejected core debris, consisting of molten fuel, cladding, and structural materials, can form a dispersed aerosol capable of rapidly transferring its heat to the containment atmosphere. Because the calculated loads on the containment structure due to direct heating may challenge its integrity simultaneously with near maximum concentrations of radiological sources in the containment atmosphere, this scenario has the potential for large releases and severe effects on public health.

There are, however, a number of uncertainties attached to the direct heating question that range from the magnitude of its effect to whether it will, in fact, occur. Large uncertainties in the core meltdown phase of the accident, for example, yield a wide range of possible initial conditions for core debris at the time of vessel breach. Much of this uncertainty may be reduced when the more advanced melt-progression codes such as MELPROG and codes that mechanistically treat direct heating become available. In view of the current lack of knowledge regarding direct heating phenomenology, the present study has taken a parametric approach to the evaluation of the potential effects of direct heating.

The BMI-2104 calculations for primary system fission product transport employed a set of codes (MARCH, CORSOR, MERGE, and TRAP/MELT) that were run successively (without feedback) and which did not contain models for fission product heatup of the primary system, nor did they contain models for treatment of natural convective processes. Transport of volatile fission products through the primary system and releases of these materials into the containment are extremely sensitive to the temperature history of the primary system, so that these two processes should not be neglected. As a consequence of the absence of modeling for the aforementioned processes, the BMI-2104 calculations for the TMLB' sequence may underestimate primary system releases during the meltdown phase of the accident. Further, in that study it was not possible to calculate long-term reevolution (revaporization) subsequent to vessel

failure of those volatile fission products that had been retained on primary system surfaces during the meltdown phase. Certain containment conditions, such as a gradual depressurization due to leakage over the time period in which the volatiles are being reevolved, can supply a mechanism for moving these sources out of the primary system and ultimately into the environment.

In the present study an initial attempt has been made to treat fission product heating and natural convection in the primary system heat and mass transport calculations. An additional benefit of this modeling capability has been a somewhat improved characterization of the primary system temperature history, and as a result, the ability to gain some insight into another important issue: that of potential temperature induced failure of the hot-leg piping. Enhanced heat transfer due to natural circulation processes could generate high enough temperatures at the hot-leg nozzles or in downstream piping to weaken the structure and cause a breach. This may be particularly likely for the TMLB' Station Blackout sequence due to the high system pressure (2000-2400 psia, 138-165 MPa). If primary system failure in the hot leg occurred before core slump, the direct heating phenomenon might be effectively precluded. The potential for setsetting up a countercurrent flow regime in the pipes leading from the vessel to the pressurizer has not been established, and the present analysis probably yields heat transfer rates that are somewhat high. Multidimensional codes may be required to achieve a definitive answer regarding natural convection in the complicated geometry of the primary system.

2.0 CODES AND METHODOLOGY

The primary strategy in this analysis was to use the best calculational tools available to treat each phase of the accident. The RELAP5 code[3] was used to calculate the thermohydraulic sources during the pre-core-damage phase, and the MARCON code[4] was employed during the period from incipient core meltdown out to and including the core/concrete interaction phase (the CORCON code that treats the core/concrete interaction has been combined with the MARCH code in the MARCON code). A "hard linked" version of the MERGE, CORSOR, and TRAP/MELT codes was utilized to calculate primary system fission product releases. This code, called the MCT code,[5] contains new models for fission product heating and natural circulation. It must be noted that these models are rather simplistic and have not been extensively evaluated. The natural circulation flows are one-dimensional and driven by temperature differences between connecting volumes. Radiological releases from core/concrete interactions were calculated using the VANESA code.[6] The thermohydraulic sources due to direct heating were calculated using a small stand-alone code[7] backed up by hand calculations. Both the code and the hand calculations used an adiabatic model in which the core debris was brought into thermal equilibrium with the atmosphere. The aerosol sources

for direct heating were obtained from results of the SPITS[8] experiments conducted at Sandia National Laboratories. Heatup and degassing of the concrete floors in the containment after deposition of the debris from direct heating were also calculated using a stand-alone code.[9] The various sources, both thermohydraulic and radiological, were supplied to the CONTAIN code,[10] which calculated the containment loading, the transport and deposition of fission products in containment, and the release of radiological sources to the environment.

3.0 ACCIDENT SEQUENCES

Two basic scenarios were examined in the study. The first scenario consisted of a TMLB' sequence in which temperature induced failure of the primary system was assumed not to occur. The primary system eventually failed at instrumentation penetrations in the lower vessel head due to the thermal attack of molten core debris. Since a previous breach in the primary system boundary did not occur (except for normal operation of the Power Operated Relief Valves, PORVs), the system was at high pressure (PORV set point, about 2400 psia, 1.6 MPa) and the potential existed for direct heating. For this scenario a matrix of cases was analyzed in which selected direct heating parameters were varied. The primary system radiological releases were also varied by using MCT code predicted releases and selected combinations of the models in that code (i.e., fission product heating, natural circulation, reevolution of volatiles). Some cases were also analyzed using the RCS releases calculated in the BMI-2104 study of the Zion plant. The Zion releases were adjusted for the differences in core power between the Zion and Bellefonte plants.

The second scenario assumed a TMLB' with failure of the seals in the primary system coolant pumps (pump seal Loss of Coolant Accident, LOCA). In this scenario all four pump seals were failed at the outset of the accident, and the system was at a somewhat lower pressure at the time of vessel breach. Thus, the direct heating scenario, if it occurred, would be of a smaller magnitude. For this analysis it was assumed that a direct heating event did not occur in the pump seal LOCA scenario.

4.0 ANALYSIS AND RESULTS

4.1 DIRECT HEATING

For the accident sequences that include high pressure ejection of core debris, direct heating imposes more severe loads on the containment than occur at any other time during the course of the accident. A detailed examination of direct heating, therefore, will yield the peak loading conditions.

Uncertainties in many aspects of direct heating phenomenology required that it be treated parametrically. The assumptions used in the direct heating calculations include ejection from

the vessel of 100% of the fuel and cladding materials and about 50% (100,000 lb) of the potentially available steel. This quantity of steel is about twice the amount of steel available in the core region and accounts for partial melting of steel in the core support structures and lower plenum. The initial temperature of the debris as it exits from the vessel was taken to be the corium eutectic temperature (approx. 4130°F, 2550 K). This temperature could also have been treated parametrically, but the energy available from chemical reactions tends to dominate the thermal loads. The ejection temperature is likely to be higher than the steel melting temperature and probably not much higher than the corium eutectic.

The quantity of Zircaloy reacted in-vessel during the core meltdown phase was forced to be 50% by adjusting the core slump parameters in the MARCH code. Selection of a 50% metal/water reaction reflects the uncertainty in the degree of in-vessel clad reaction. This fraction of in-vessel oxidation was achieved by slumping the core when 65% of the core was molten. The hydrogen generated by in-vessel oxidation of Zircaloy resulted in an average H_2 concentration in containment at vessel failure of about 3 volume percent. The fraction of the remaining Zircaloy that was injected into the containment was assumed to be completely oxidized during direct heating.

The direct heating calculations were performed with a standalone code (DHEAT[7]) that calculated the end conditions assuming that direct heating was so rapid that it occurred essentially adiabatically and that the injected debris was, nevertheless, in contact with the atmosphere long enough for thermal equilibrium to be achieved. Experiments done at Sandia[8] seem to indicate that minimal holdup in the reactor cavity will occur and about 90% of the ejected core debris could be transported into the upper levels of the containment. Heat transfer and the combustion processes, as well as the aerodynamics of the direct heated process, are involved and have not yet been studied in detail analytically.

Potentially, the most important parameters that affect the magnitude of the direct heating loads on containment include the fraction of the core debris injected into containment, the degree of completion of the combustion process for the various combustible components in the debris, and the heat absorbing capacity of the containment atmosphere. The fraction of core injected into the atmosphere was varied from 0% to 90% of original core inventory. The 0% case is not discussed since it contributed no additional loading. The significant combustibles include zirconium, steel and hydrogen. At the temperatures involved it is likely that the injected zirconium will be completely burned. The steel combustion was varied by assuming no involvement or 100% involvement. Although hydrogen at a concentration of 3% is not within the normal combustion limit, it is believed that much of it may be consumed in a catalytic process

at debris particle surfaces. The hydrogen combustion contribution was assessed by calculating cases with no hydrogen combustion and complete hydrogen combustion. With regard to the heat absorbing capacity of the atmosphere, although the mass of noncondensible gases in the containment does not change significantly in the time frame of the direct heating process, the quantity of steam and water contained in the atmosphere depends largely on the accident sequence and on the timing of the direct heating event. MARCH code calculations, however, predict that about 75,000 lbs (34,000 Kg) of water will be present in the reactor cavity at vessel breach. This quantity of water, when its heat of vaporization is included, represents a large effective heat capacity. If this water is actually located in the reactor cavity, it is probable that most or all of it would be swept out with the debris and should be included in the direct heating calculation. The effect of this additional heat capacity was considered by performing the calculation both with and without the cavity water in the atmosphere. For the case in which the cavity water was assumed to be swept into containment together with the core debris, it was also assumed that the cavity water was in good thermal contact with the debris and was completely vaporized.

The results of the direct heating calculations indicate (see Table 1) that all the cases involving 90% injection resulted in containment pressure loadings that were either in or above the estimated containment failure range (144.7 to 153.7 psia).[11] The peak pressure, for example, in the case of 90% debris injection with hydrogen combustion, without steel combustion, and with complete injection of the cavity water, resulted in a peak pressure of 169 psia. Since the optimistic assumptions for the 90% injection cases resulted in loadings that exceeded the estimated failure pressure, it was not necessary to perform the cases with more conservative combinations of parameters. Note that the last column in Table 1 shows the net energy, H, transferred to the atmosphere during direct heating.

The 50% injection cases were marginally close to the containment failure criterion and quite sensitive to the assumptions regarding the oxidation of hydrogen and steel. Without the involvement of cavity water (Cases-002), it required the complete oxidation of the steel to exceed the failure pressure. Direct heating with hydrogen combustion alone produced a pressure of 139 psia, while the direct heat event with neither H_2 nor steel oxidation yielded a peak pressure of only 117 psia, well below the estimated failure range. With the involvement of the cavity water (Case-002A) only the most pessimistic assumptions regarding combustion put the peak pressures into the containment failure range.

Although there are clearly a number of uncertainties regarding the direct heating scenario, it can be generally concluded from these parametric calculations that for direct heating which

involves 90% of the core debris containment failure is essentially certain, and that for core debris involvement much in excess of about 50% containment failure is likely. The oxidation of steel appears to be the largest single factor, increasing the pressure by about 40 psi (275 kPa). Cavity water and hydrogen combustion have about equal but opposing effects, the cavity water decreasing the pressure by about 20 psi (138 kPa) and the hydrogen combustion increasing the pressure by about the same amount.

4.2 PRIMARY SYSTEM RADIOLOGICAL SOURCES

The primary system releases for Bellefonte as calculated by the MCT code package are presented here in juxtaposition with the BMI-2104 Zion plant calculations. As discussed below, the MCT type "A" calculations for Bellefonte produce releases that are comparable to those for the Zion plant. However, the BMI-2104 study also analyzed the Surry and the Sequoyah reactor plants and for those plants calculated relatively higher releases when compared to Zion results. The reason for the differences in the calculated releases between the Zion, Surry, and Sequoyah plants in the BMI-2104 study is not clear. There may be sensitivities in these calculations to differences in modeling assumptions in the code package or to the actual differences in the primary system configurations. In any case, the comparison between the present results and the BMI-2104 calculations should not be interpreted as being particularly significant. Rather, the selection of the Zion results for purposes of comparison should be viewed as an arbitrary one, and the Zion releases merely a "data base" against which the present results can be normalized.

For the high pressure cases using the MCT code with only the fission product heating model the meltdown phase releases (up to and including the releases at vessel failure, Table 2, type 'A' releases) of CsI and CsOH were slightly higher (by a factor of 1.5) than those predicted by BMI-2104 for the Zion plant. The Te releases were higher by a factor of 6, partly due to differences in the MARCH code options that affected the oxidation of zirconium in the meltdown phase and resulted in higher Te releases from the core. Although the fission product heat-up model did not produce significant changes in predicted releases during the meltdown phase, the long-term heat-up effects subsequent to vessel failure produced significant late reevolution of volatile fission products (Table 2, type 'C' releases). For the leakage cases involving a gradual containment depressurization, a mechanism existed for moving revolatilized fission products out of the breached vessel, and with these additional releases included the total releases of CsI and CsOH from the RCS exceeded the BMI-2104 estimates by a factor of 10. Implementation of the natural convection model for the meltdown phase releases (without reevolution, type 'B' releases) produced RCS releases higher than the BMI-2104 Zion results by a factor of 15 for CsI and CsOH and a factor of 4.5 for Te (approx. 30% for CsI and CsOH and 17% for Te of the original inventories of these

species). Although performance of the rather expensive computer calculations for long-term reevolution using the natural circulation models after vessel breach was beyond the scope of this analysis, the releases could be still higher than those quoted above.

There were no comparable BMI-2104 calculations against which to compare the pump seal LOCA calculated releases. Without natural convection the primary system volatile releases for this scenario were on the order of 10% of the original inventories (Table 2, type 'A' releases). With natural convection the predicted RCS releases of CsI and CsOH were very high, on the order of 80% or 90%, while Te was about 13% (type 'B' releases). However, since direct heating was not involved in this sequence, there was no early containment failure and very small containment releases.

Also of significance was the predicted primary system temperature history. The calculation of the primary system temperature history using the MCT code package indicates that the primary system temperatures are well into the regime in which failure would be expected to occur at the elevated pressures characteristic of the TMLB' sequence. This is clearly seen in Figure 1, which shows the temperatures of the structures associated with the various control volumes in the MCT model of the Bellefonte primary system. This figure indicates peak temperatures (just prior to core slump) of about 1840^{o}F (1280 K) in the upper plenum structures and in excess of 1700^{o}F (1200 K) in the hot-leg piping. Temperatures in excess of about 1300^{o}F (980 K) would be expected to induce a failure of the primary system piping under the existing RCS pressure loading. If a failure of the RCS boundary occurred of sufficient magnitude to depressurize the RCS in advance of core slump, direct heating could be eliminated or mitigated.

A preliminary evaluation of the natural circulation model has indicated that it is overpredicting the transfer of heat from the core to the downstream volumes in the RCS. The model assumes the applicability of the Bernoulli equation and substitutes a buoyancy term for the differential pressure to obtain the following equation for the natural circulation flow velocity:

$$v = [2gH(T_0/T_1-1)]^{0.5}, \qquad (1)$$

where H is the difference in elevation between two adjoining control volumes, while T_0 and T_1 are the temperatures of the control volumes. The further assumption is made that the cross sectional flow area between the volumes is divided such that half the area is engaged in upward flow and the other half in downward (return) flow. The net rate of energy exchange between volumes is then:

$$Q = [\rho_0 Avh(T_0,P_0)-\rho_1 Avh(T_1,P_1)]/2 \qquad (2)$$

In Equation 2, ρ is the gas density, A is the flow area and h is the specific enthalpy of the gases as a function of temperature and pressure (T,P). For control volumes located one above the other there is no steady flow field, and the Bernoulli equation is not strictly applicable. The result is that the average velocity and heat transfer rates (Eqns 1 & 2) are somewhat overpredicted in the model.

It is uncertain what effect a more realistic heat transfer rate would have on the primary system heatup characteristics. It is likely, however, that the RCS heatup would be somewhat retarded, delaying the time at which failure might occur and, thus, tending to limit the mitigating effect it would have on the direct heating pulse. On the other hand, the effect of natural circulation flows cooling the core, which has been neglected in this analysis, would also tend to delay core meltdown and supply some additional time for RCS failure to occur before core slump. Taken together, the results of this analysis seem to suggest a high probability for a breach in the RCS before core slump and, thus, a low probability for the direct heating sequence of events. It is uncertain whether these conclusions can be generalized to other primary system designs.

4.3 CONTAINMENT RELEASES

A general description of the containment release calculations is given in Table 3, and the releases for these cases are summarized in Table 4. The constituents of the fission product release groups shown in Table 4 are the same as those used in BMI-2104. Radiological releases from the containment are heavily dependent on the containment failure mode. Direct heating calculations indicate that for core debris involvement greater than about 50%, gross containment failure is likely in the Bellefonte containment. The 90% injection cases were, therefore, assumed to rupture the containment (7 ft^2, .65 m^2), and the releases of the volatiles, CsI and CsOH were on the order of 1.5% of the initial inventories (Table 4, Cases 001 to 011A). Since the primary system releases of these materials were a factor of 10 higher when natural convection was modeled, the releases of these materials from the containment were also proportionally higher for this case, about 15% (Case-011B). Te releases were on the order of 20% to 30%, while Ru was about 40%. Releases for the Te and Ru groups were strongly enhanced by an oxidation reaction that was assumed to occur during direct heating. Specifically, the species Te, Ru, and Mo formed volatile oxides during direct heating and were recondensed as aerosols. The oxidation fractions (the fraction of the species that was converted to the oxide) that were applied to these species were taken from the WASH-1400 report. These oxidation fractions were estimated and did not represent actual experimental results. Containment failure at the precise point of maximum fission product concentration made these cases the most severe in terms of releases to the environment.

For the 50% direct heating cases (Tables 3 & 4, Cases 002 to 112A), it was assumed that containment leakage pathways open at the time of vessel failure. Areas of 5 in^2 (.0022 m^2) and 12 in^2 (.0077 m^2) were used to estimate releases for these scenarios. For both of the leak areas used, the containment was gradually depressurized and, since much more time was available for aerosol removal, the releases were significantly lower. For the worst case (Case-112A), in which reevolution of volatiles was calculated and a 12 in^2 (.0077 m^2) leak area was used, releases of the volatiles and Ru were on the order of 2% of inventory. These releases were about a factor of 12 higher than those calculated by assuming BMI-2104 Zion-type releases from the primary system (Case-102A).

For the TMLB' scenarios without direct heating (Cases 000,100) the induced leakage area was varied between 1 in^2 (.0006 m^2) and 2.4 in^2 (.0015 m^2), and the releases for these cases were very small, on the order of 1.0E-4 of the original inventories of CsI and CsOH.

The pump seal LOCA scenarios, since they do not involve direct heating, also yielded relatively small releases, on the order of 1.0E-4 for CsI and CsOH (Tables 3 & 4, Cases 030,130). Primary system releases calculated with natural convection, however, increased the containment releases to about 0.2% for CsI and CsOH and to about 0.8% for Te (Tables 3 & 4, Cases 031,131).

5.0 CONCLUSIONS

There are several conclusions that can be drawn from this study. One of the most significant is that, if direct heating occurs in which more than about 50% of the core debris is involved, containment failure is likely. In addition, this scenario fails the containment at a time when the fission product concentration in the containment atmosphere is maximized and leads to high releases outside the containment. Introduction of simple modeling for natural convection and decay heating in the primary system fission product transport codes has significantly increased the predicted releases into the containment due to the added releases from reevolved volatiles and to natural convection heating of the primary system. However, the same modeling changes have led to a strong indication that primary system structural temperatures may be high enough to induce failure and depressurization of the primary system before core slump, thus eliminating direct heating and with it the primary mechanism for early containment failure and high containment releases for this accident sequence.

REFERENCES

1. J. A. Giesecke, et al., Radionuclide Release Under Specific LWR Accident Conditions-PWR-Large, Dry Containment Design (Zion Plant), BMI-2104, V. 6, Battelle Columbus Laboratories, July 1984.

2. R. D. Gasser, P. P. Bieniarz, J. L. Tills, Analysis of Station Blackout Accidents for the Bellefonte Pressurized Water Reactor, Sandia National Laboratories, NUREG/CR-4563, SAND86-0576, to be published.

3. C. A. Dobbe and R. Chambers, Analysis of a Station Blackout Transient for the Bellefonte Pressurized Water Reactor, EGG-NTP-6704, Idaho National Engineering Laboratories, Oct 1984.

4. C. J. Shaffer, MARCON2.OP: A Version of MARCH with State-of-the-Art Core Concrete Modeling, Sandia National Laboratories, NUREG/CR-4612, SAND86-7082, to be published.

5. P. P. Bieniarz. Source Term Analysis of Fitzpatrick Power Plant, Risk Management Associates, Albuquerque, N.M., Report Under Review, Jan 1986.

6. D. A. Powers, J. E. Brockmann, A. W. Shiver, Vanesa: A Mechanistic Model of Radionuclide and Aerosol Generation During Core Debris Interaction with Concrete, NUREG/CR-4308, SAND85-1370, Sandia National Laboratories, to be published.

7. K. D. Bergeron and D. C. Williams, "CONTAIN Calculations of Containment Loading of Dry PWR's," Sandia National Laboratories, Nuclear Science and Engineering, V. 90, pp 153-159, 1985.

8. J. E. Brockmann and W. W. Tarbell, "Aerosol Source Term in High Pressure Melt Ejection," Nuclear Science and Engineering, V. 88, pp 342-356, 1984.

9. D. K. Gabrielson, et al., ONEDIM-A Computer Code for Solving Non-Linear Heat Transfer Problems, Report No. SCL-DR-69-99, Sandia National Laboratories, Feb 1970.

10. K. D. Bergeron, et al., Users Manual for CONTAIN 1.0, A Computer Code for Severe Nucler Accident Containment Analysis, NUREG/CR-4085, SAND84-1204, Sandia National Laboratories, May 1985.

11. J. Jung, Ultimate Strength Analysis of the Watts Bar, Maine Yankee, and Bellefonte Containments, NUREG/CR-3724, SAND84-0660, Sandia National Laboratories, July 1984.

TABLE 1

RESULTS OF DIRECT HEATING CALCULATIONS

CASE	% EJECT.	%* WATER	H_2 BURN	Fe BURN	T_F (°F)	P_F (psia)	H GJ
001	90	0	NO	NO	2009	159.9	281
001	90	0	YES	NO	2288	178.0	330
001A	90	100	NO	NO	1462	148.8	305
001A	90	100	YES	NO	1719	168.8	356
002	50	0	NO	NO	1314	116.8	172
002	50	0	YES	NO	1681	138.6	226
002	50	0	NO	YES	1913	158.4	265
002	50	0	YES	YES	2223	173.8	318
002A	50	100	NO	NO	789	96.6	181
002A	50	100	YES	NO	1111	121.6	239
002A	50	100	NO	YES	1326	138.2	213
002A	50	100	YES	YES	1609	160.1	334

* % OF WATER IN REACTOR CAVITY THAT IS INJECTED INTO CONTAINMENT WITH THE CORE DEBRIS

TABLE 2

SUMMARY OF PRIMARY SYSTEM RELEASES+

MCT WITHOUT NATURAL CONVECTION

FISSION PRODUCT	BMI-2104	MELTDOWN PHASE** TYPE C	REEVOLUTION PHASE***	TOTAL	MCT W/NATURAL CONVECTION** TYPE B
(TMLB'-HPE)					
CsI	.02*	.028	.21	.24	.35
CsOH	.02*	.030	.18	.21	.28
Te	.04*	.24	---	.24	.17
(TMLB'-PSL)					
CsI	----	.084	---	.084	.93
CsOH	----	.073	---	.073	.77
Te	----	.089	---	.089	.13

+ FRACTIONS OF INITIAL INVENTORIES

* ZION STUDY

** UP TO AND INCLUDING VESSEL FAILURE

*** RELEASES SUBSEQUENT TO VESSEL FAILURE - CALCULATED USING THE DEPRESSURIZATION HISTORY FOR CONTAINMENT LEAKAGE SCENARIOS

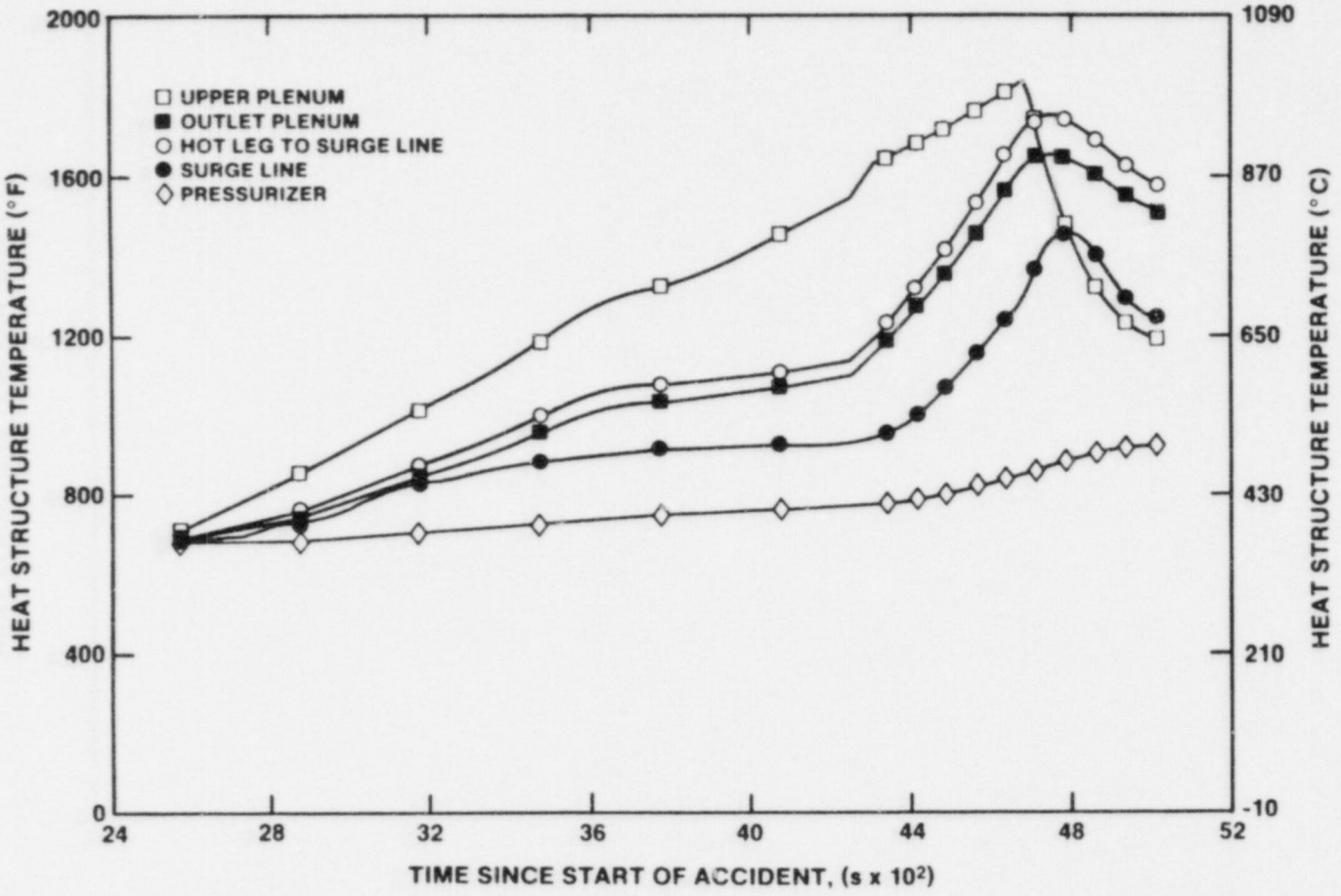


Figure 1. Primary System Structure Temperatures

TABLE 3
CASE MATRIX

CASE	% INJECT	CAVITY WATER	BREAK AREA	RCS REL.	F.P. REL.	NAT. CONV.	REEV.	CORE/CONC REL
000	0	--	$1in^2$	*	NO	NO	NO	YES
100	0	--	$2.4in^2$	*	NO	NO	NO	YES
001	90	NO	$7ft^2$	*	NO	NO	NO	NO
011	90	NO	$7ft^2$	MCT	YES	NO	NO	NO
001A	90	YES	$7ft^2$	*	NO	NO	NO	NO
011A	90	YES	$7ft^2$	MCT	YES	NO	NO	NO
011B	90	YES	$7ft^2$	MCT	YES	YES	NO	NO
002	50	NO	$5in^2$	*	NO	NO	NO	NO
102	50	NO	$12in^2$	*	NO	NO	NO	NO
012	50	NO	$5in^2$	MCT	YES	NO	YES	NO
112	50	NO	$12in^2$	MCT	YES	NO	YES	NO
002A	50	YES	$5in^2$	*	NO	NO	NO	NO
102A	50	YES	$12in^2$	*	NO	NO	NO	NO
012A	50	YES	$5in^2$	MCT	YES	NO	YES	YES
112A	50	YES	$12in^2$	MCT	YES	NO	YES	YES
030	0	---	$1in^2$	MCT	YES	NO	NO	YES
130	0	---	$2.4in^2$	MCT	YES	NO	NO	YES
031	0	---	$1in^2$	MCT	YES	YES	NO	YES
131	0	---	$2.4in^2$	MCT	YES	YES	NO	YES

*BMI-2104 ZION RELEASES

TABLE 4
CONTAINMENT RELEASES* (TO 20 HRS)

CASE	CsI	CsOH	Te	Ru	Sr	La	Xe	Kr
000	5.7E-5	9.8E-5	.018	2.1E-5	.0054	.0032	.071	.071
100	1.3E-4	2.3E-4	.043	4.9E-5	.013	.0077	.16	.16
001	.014	.014	.29	.38	.024	.0052	.77	.77
011	.015	.016	.13	.39	.0058	.0052	.77	.78
001A	.014	.014	.29	.38	.024	.0053	.78	.78
011A	.015	.016	.30	.40	.0054	.0048	.79	.79
011B	.16	.12	.21	.41	.0073	.0048	.79	.79
002	8.0E-4	8.0E-4	.0097	.012	.0012	4.0E-5	.31	.31
102	.0018	.0018	.022	.028	.0027	9.4E-5	.59	.59
012	.0061	.0056	.010	.012	8.5E-5	3.7E-5	.31	.31
112	.013	.012	.023	.028	2.0E-4	8.8E-5	.60	.60
002A	7.2E-4	7.2E-4	.0088	.011	.0011	3.8E-5	.30	.30
102A	.0017	.0017	.020	.025	.0025	8.9E-5	.57	.57
012A	.0101	.0092	.0092	.011	8.5E-5	3.5E-5	.30	.30
112A	.022	.02	.021	.025	2.3E-4	8.5E-5	.53	.53
030	6.1E-5	1.2E-4	.0032	1.1E-6	.0049	8.2E-4	.070	.070
130	1.4E-4	2.9E-4	.0078	2.6E-6	.012	.0020	.16	.16
031	8.8E-4	8.1E-4	.0034	1.9E-5	.0050	8.4E-4	.072	.072
131	.0020	.0019	.0082	8.9E-6	.012	.0020	.16	.16

*FRACTION OF INITIAL INVENTORIES

SESSION D

ANALYSIS TESTING OF CONTAINMENT SYSTEMS, PART I

PLASTIC ANALYSIS OF CONCRETE CONTAINMENT STRUCTURE

ALY HINDY AND ARI DANAY
ONTARIO HYDRO
700 UNIVERSITY AVENUE, TORONTO
ONTARIO, CANADA M5G 1X6

Overpressure capacity of a box type concrete containment structure is evaluated. Plastic analysis of the finite element model is performed using a quadrilateral plate element of homogeneous material. A special approach is used to represent nonlinear properties of reinforced concrete, such as concrete cracking and crushing and steel yielding. Those properties are represented by a set of idealized stress-strain curves of equivalent homogeneous sections.

The analysis allows for a better estimate of the overpressure capacity of the containment structure while keeping the computer cost low by avoiding the use of the more expensive reinforced concrete brick element.

1.0 INTRODUCTION

Understanding the structural behaviour of concrete containment structures under internal pressures that exceed those used in their design can lead to more realistic estimates of risk from accident conditions. The intent of this study is to obtain the maximum value of the pressure which a reinforced concrete rectangular box containment can sustain before collapse.

Several approaches may be followed to solve the problem under consideration. A simple one is the elastic analysis approach where maximum stresses are compared with material strength. This approach, while cost effective, does not utilize the ductility of reinforced concrete with its subsequent load redistribution capability. It follows that this method inherently underestimates the overpressure capacity of the containment.

On the other hand, finite element plastic analysis with a reinforced concrete brick element represent the most advanced method available to solve the problem. In this method, concrete and steel re-bars are modeled as two materials joined together as structural elements. Concrete material models account for compression plasticity and tensile cracking with post cracking tension stiffening and shear retention capabilities while reinforcement is treated as simple tension-compression members fully bonded to the concrete. This approach requires very high computer cost and still falls into the category of global effects

analysis. It lacks details for local effects calculations such as discrete cracking simulation and rebar bond model (Ref 1).

The approach being used in this study is a compromise between the two above mentioned methods. The finite element plastic analysis with a homogeneous plate element and special material properties, utilizes the concrete compressive plasticity and steel tension ductility while keeping computer cost relatively low.

2.0 CONTAINMENT STRUCTURE

As a pressure resisting mechanism, the reactor vault under consideration, acts as a stiffened rectangular box (see Figure 1). It's reinforced concrete walls and ceilings, 6 ft and 5 ft respectively, are stiffened by four frames of different sizes, two running E-W and two N-S. The total depth of the frame components, denoted 'pilasters' (vertical) and 'girders' (horizontal) is an even 14 ft for the 'shallow' frames and variable 18 ft (pilaster) to 42 ft (main girders) for the larger ones. The main girders are prestressed.

Figure 2 is a plan of the structure showing the arrangement of the boilers and pump room slabs. Boiler room slab is 5 ft thick, it has circular holes of 11 ft in diameter for boilers and one rectangular opening about 10.75 ft x 11.25 ft, in each corner of the building for the preheaters. The pump room slab is 7 ft thick with extra reinforcement steel around the openings to support the pumps.

3.0 FINITE ELEMENT MODEL

Figure 3 shows the finite element mesh used in the analysis. The model consists of a total of '444' quadrilateral plate (with some triangular ones). Only one quarter of the structure is modeled due to symmetry. The building below elevation 613 ft is composed of massive concrete which likely will not be affected by the loading and so it is excluded from the analysis.

The plate element being used in the analysis has both bending and membrane capabilities. It has six degrees of freedom at each node, with the in-plane rotational degree of freedom omitted as no torsional moments are applied.

Elements for the pressure boundary are considered to have plastic properties with the exception of the massive main girder which is assumed to act elastically due to it's large resistance. This saves considerable computing time.

4.0 METHOD OF ANALYSIS

4.1 Elastic Analysis

Elastic analysis is performed first to obtain the relation between moments and normal forces at typical sections for different loading conditions. This information is needed for stress-strain curves idealization.

In addition, elastic analysis helps to study the effect of different loading conditions, locate areas of high stress concentration and obtain a rough idea about the maximum value of pressure that can be reached.

4.2 Development of Stress-Strain Curves

In the post-cracking regime, reinforced concrete sections become asymmetric due to the shift of the neutral axis. However, that behaviour cannot be modelled by the standard plate element which is defined as symmetric. To overcome that difficulty, properties of reinforced concrete sections for different structural elements are represented by idealized stress-strain curves of equivalent sections. The idealization is achieved by replacing a 'true' reinforced concrete section with a homogeneous section of the same size and having the same moment-curvature characteristics. Standard curves are developed for typical sections of similar dimensions, reinforcements and structural behaviour. Those sections include walls, pilasters, slabs and cross girder. Moment-curvature (M-ϕ) diagram at a section is developed using the following relations.

$$N_{cr} = N_i + \alpha (P_{cr})^n \qquad (1)$$

$$M_{cr} = M_i + \beta (P_{cr})^m \qquad (2)$$

$$N_y = N_f + \alpha (P_y)^n \qquad (3)$$

$$M_y = M_f + \beta (P_y)^m \qquad (4)$$

where N, M and P are the section normal force, bending moment; and the applied internal pressure. The subscript 'cr' indicates the values as the concrete cracks and 'y' as the steel yields.

N_i and M_i are the section normal force and moment due to initial loading (dead, prestressing and thermal) assuming elastic behaviour. N_f and M_f are similar to N_i and M_i, but appear in the post-cracking regime at the onset of yield in the reinforcement. Coefficients α, β, n and m are constant.

The following assumptions are made:

(1) The section behaves elastically during initial loading (before applying the pressure). That allows the direct calculation of N_i and M_i from the elastic analysis results.

(2) In the post-cracking stage, which occurs during the pressure loading, the sectional stresses increase. However, due to it's self-limiting nature, thermal stress in the section gradually decreases as cracks develop and completely vanish as steel yields. Though the intermediate stresses are not known, this assumption allows the calculation of N_f and M_f by eliminating the thermal components of N_i and M_i in the post-yield regime.

(3) Normal force and bending moment in the section increase with internal pressure in a similar fashion (i.e., coefficients m & n are equal), which allows the ratio α/β to be taken directly from the elastic analysis results.

Using the above assumptions, the unknowns needed to develop M-ϕ diagram are reduced to six, namely N_{cr}, M_{cr}, N_y, M_y, $(P_{cr})^n$ and $(P_y)^n$. Together with equations (1) through (4), there are two more equations relating those unknowns. Those equations relate stress in concrete or steel to section forces and moments at cracking and yielding conditions. Solving the six equations, the M-ϕ diagram can be obtained for a typical section and, consequently, the equivalent stress strain curve.

The idealized stress-strain curves obtained using the above approach are shown in Figure (4) for different structural elements.

4.3 Plastic Analysis

The plastic analysis is performed using the computer program NASTRAN (Refs 2, 3). Only material nonlinearity is considered, while geometric nonlinearity is ignored as displacements are expected to be small due to the large thickness of structural elements compared to their dimensions.

Plasticity is both nonlinear and non-conservative. The nonlinear nature of the problem dictates that a number of iterations are required. The non-conservative nature of the problem dictates that the final results of the analysis are path-dependent. For that reason loads are applied in the same sequence as in the real problem. First the dead load and prestressing forces are applied, followed by the thermal loading and finally the pressure loading. Loads are applied incrementally rather than in one step, as a sharp increase in the load might cause an improper distribution of internal forces.

The plasticity model used in the analysis is based on Von-Mises yield criterion with isotropic hardening rule. The basic nonlinear

solution methods are the Quasi-Newton and modified 'Newton-Raphson' Processor. Tangent stiffness is updated automatically based on convergence rate. The maximum number of iteration per load increment is taken as 20 and increases to 30 for high values of pressure (above 40 psi). Iteration for specific load increment stops as convergency is reached based on error limits in displacements, residual forces, and plastic work.

From the results of plastic analysis, shear stresses at critical locations are checked against the resistance which, if exceeded, a shear crack is assumed. The shear carried by aggregate interlock at a crack location is calculated using the following formulae given by Walraven (Ref 4).

$$\tau = - \frac{f_{c'}}{30} + [1.8\, w^{-0.8} + (0.234\, w^{-0.707} - 0.2)\, f_{c'}]\, \Delta, \quad (\tau \geq 0) \qquad (3)$$

$$\sigma = - \frac{f_{c'}}{20} + [1.35\, w^{-0.63} + (0.191\, w^{-0.552} - 0.15)\, f_{c'}]\, \Delta, \quad (\sigma \geq 0) \qquad (4)$$

where τ, σ, W and Δ are shown in Figure (5a). The units are N/mm^2 for τ and σ and mm for W and Δ.

At a corner between two structural elements, where shear crack occurs (Fig 5b), the axial stress along the crack surface maybe written as

$$\sigma = \frac{KW}{A} - \sigma_t \qquad (5)$$

where σ_t is the tensile axial stresses caused by internal pressure, A is crack area; and K is the combined stiffness of both elements normal to crack direction. Nodes at crack location are duplicated and the stiffness 'K' is obtained by applying two sets of static forces on each side of the crack normal to it's direction. The tensile axial stresses at crack location 'σ_t' caused by internal pressure, are obtained also from plastic analysis and substituted together with the stiffness 'K' in equation (5). Subsequently, equations (3) through (5) are solved to obtain 'τ' the shear stress carried by aggregate interlock.

5.0 ANALYSIS RESULTS

The analysis is carried out to a maximum pressure of 60 psi. While up to this pressure, the structure is not showing any excessive deformations, average shear stresses along a side of N-S wall is about to exceed the average resistance. This point is chosen to terminate the analysis due to the limitation of the model to deal with progressive shear failure.

The deformed shape of the structure at maximum applied pressure of 60 psi is shown in Figure (6). Variation of maximum displacements for different structural components with pressure is shown in Figure (7). Initial displacements are due to dead, prestressing and thermal loading. It can be seen from the figure that the main girder behaves elastically, as assumed. The nonlinear behaviour of both the pump and boiler room slabs is small compared to that of the walls. Walls start to behave non-linearly at applied pressure around 25 psi. However, at the maximum pressure of 60 psi, walls still show ability to sustain more loads. Figure (8) shows the variations of effective plastic strain of the equivalent sections with pressure. The figure shows that, at the maximum applied pressure, the base section of the N-S pilaster has yielded the most. Nevertheless no complete yielding has yet occured at any location.

Figure (9) shows the variation of the maximum tensile stresses of the equivalent sections at different locations versus pressure. The sudden change in direction for any of those curves corresponds to the abrupt shift in the slope of the stress-strain curve of the equivalent section. This indicates that in the original reinforced concrete section, tensile strength of concrete is exceeded. For most locations, this occurs at about 25 psi overpressure with the exception of a localized area at the corner between the walls where cracking occurs due to thermal stresses even before pressure is applied.

Post cracking stresses obtained from the analysis are virtual stresses applicable only to equivalent homogeneous sections. In order to obtain the actual stresses in the structure, the corresponding moments and forces obtained from the analysis are applied to the original reinforced concrete sections.

Figure (10) shows the progressive development of the yielding in walls reinforcement with increasing pressure. Stresses in concrete, however, are found to be well below compressive strength.

Out of plane shear forces at different locations of the structure are checked against shear resistance calculated using ACI code formula (Ref 5). The most critical component with respect to shear is the N-S corner panel. At a pressure of about 43 psi, local

shear resistance is exceeded at a point in the middle of the corner between walls. As the pressure increases, a shear crack is expected to start at that location and propagate vertically along the edge. At the crack location, aggregate interlock is found capable of carrying shear forces up to an overpressure of about 48 psi. It is believed that factors such as aggregate interlock, dowel action of re-bars, and redistribution of tensile forces in the wall as crack develops will help to redistribute shear forces at any side to locations of higher shear resistance. Figure (11) compares the permissible resistance with the shear force acting on the four side of the N-S corner panel as pressure reaches 60 psi. This pressure (which is about four times design pressure) is chosen as the limiting one, since the average shear resistance is about to be exceeded by the average acting shear. Table (1) summarizes the observations on the structure behaviour as pressure increases from zero to the maximum value.

6.0 DISCUSSION

In the process of developing equivalent stress-strain curves, certain simplifying assumptions are made. These assumptions are examined here. The first assumption that the section behaves elastically during initial loading is satisfied for the whole structure with the exception of a localized area at the corner between the walls, where due to thermal stresses the section cracks before applying the pressure.

The second assumption that thermal stresses vanish in the section as the steel yields, is examined at different sections by comparing stress distributions obtained from plastic analysis with those obtained from elastic analysis with and without the inclusion of thermal stresses. Figure (12) shows the result of such comparison, which indicates that the actual stresses follow those values calculated with thermal effect included until cracks occur then they drop close to the values obtained ignoring thermal effect.

The third assumption that normal force and moment in a section during plastic analysis increase with pressure in a similar fashion, is examined and the values of 'm' and 'n' are found to be slightly different from unity (0.96 - 1.1). The error involved has significant effect only at high values of pressure.

7.0 CONCLUSION

A plastic finite element analysis of a reinforced concrete rectangular box containment has been performed to obtain the ultimate pressure capacity. Cracking of concrete and yielding of steel is taken into consideration via equivalent stress-strain curves for structural elements.

The analysis allows a better understanding of the structural behaviour under severe overpressure loading while keeping computer cost relatively low.

A fairly accurate assessment of the non-linear thermal effect is provided as well.

The ultimate overpressure obtained from the analysis is in the order of about four times the pressure the structure is designed for. Higher loads might be possible if an adequate shear failure model is added on to the present approach.

8.0 REFERENCES

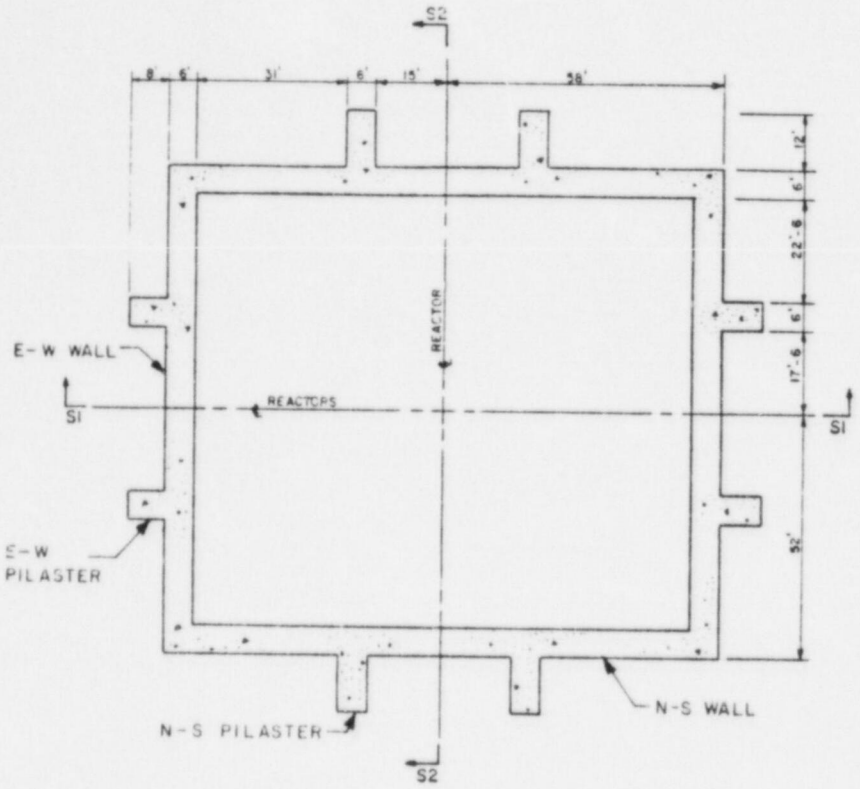
1. R.S. Dunham, et. al., "Methods for Ultimate Load Analysis of Concrete Containments", ANATECH, Interm Report to EPRI, NP-4046, June 1985.

2. McCormick, Caleb, N., 'MSC/NASTRAN User's manual Version 63'. The MacNeal-Schwendler Corporation Los Angeles, California, May 1983.

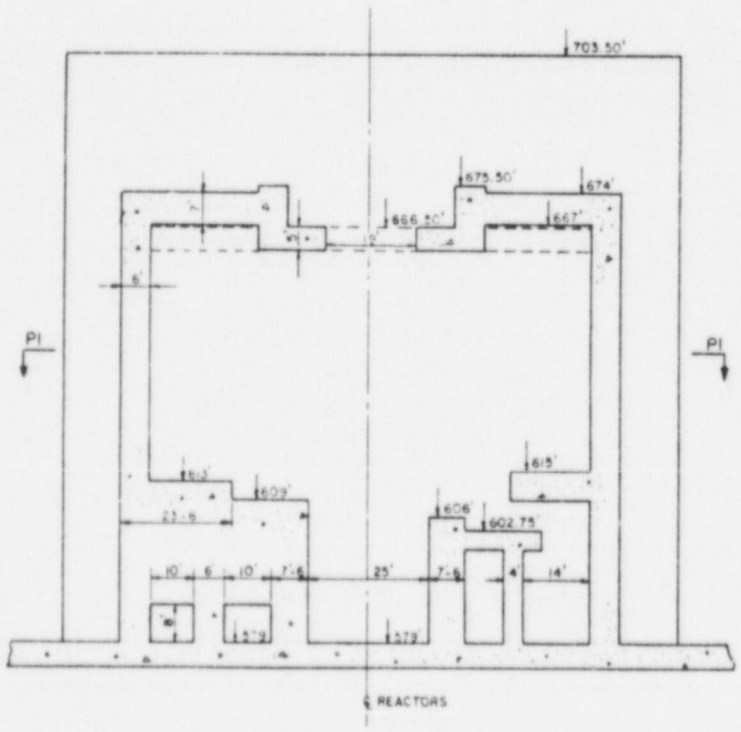
3. Jerrard A. Joseph, 'MSC/NASTRAN Application Manual', The MacNeal-Schwendler Corporation, Los Angeles, California, October 1984.

4. Walraven, J.C., 'The Behaviour of Cracks in Plain and Reinforced Concrete Subjected to Shear', IABSE Colloquium on Advanced Mechanics of Reinforced Concrete, DELFT, 1981, Vol. 34, pp. 227-245.

5. ACI 318-77 'Building Code Requirements for Reinforced Concrete', Detroit, Michigan 48219.



PLAN I



SECTION 2

FIG. 1 REACTOR BUILDING

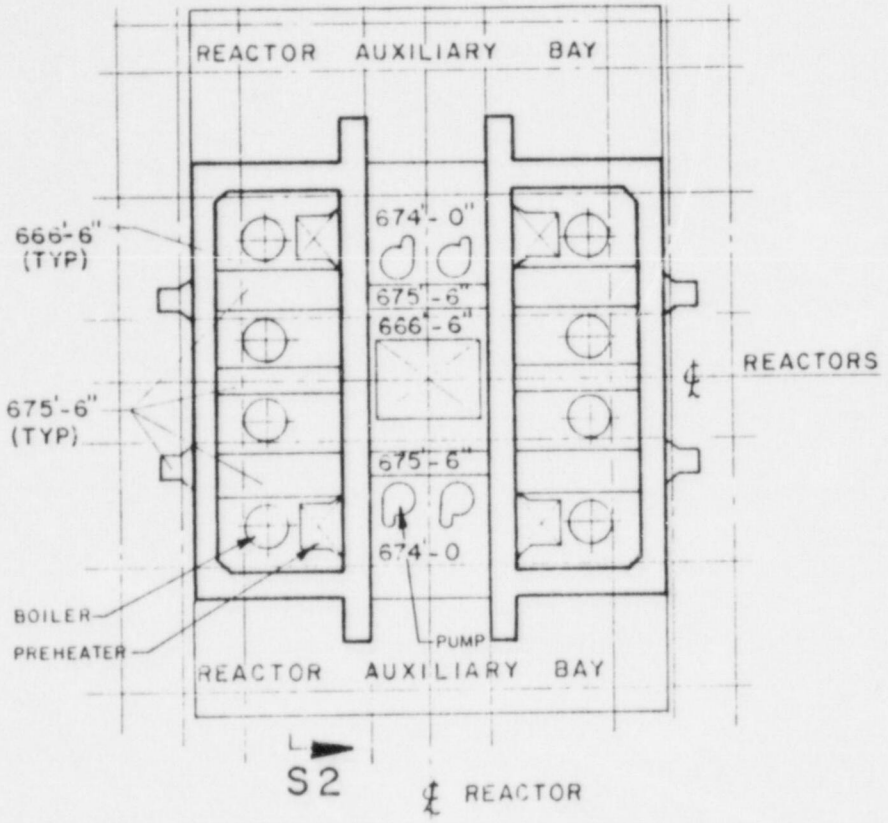


FIG. 2 BOILER AND PUMP ROOM SLABS

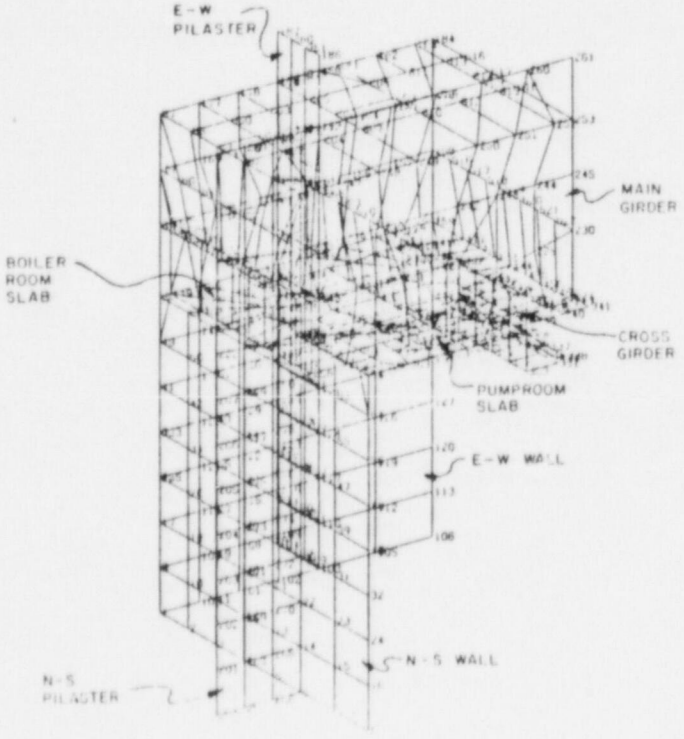


FIG. 3 FINITE ELEMENT MESH

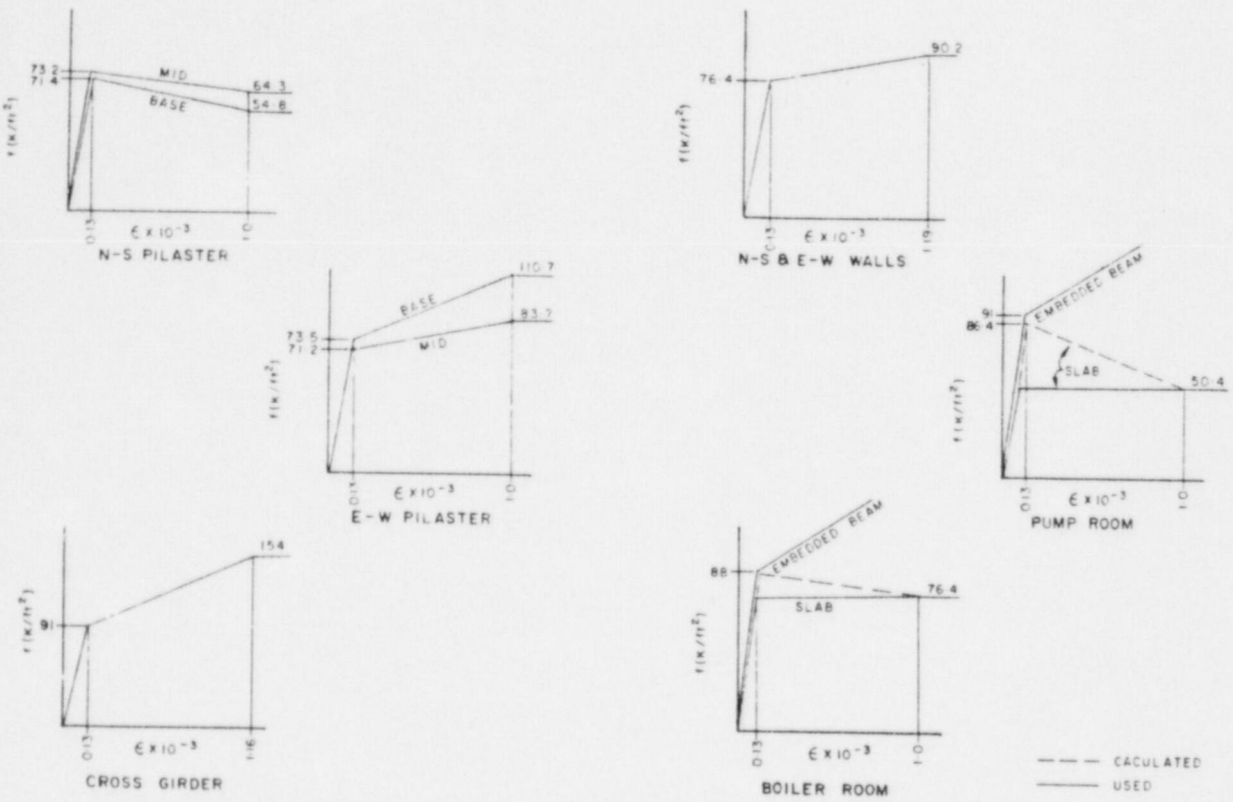


FIG. 4 IDEALIZED STRESS-STRAIN CURVES

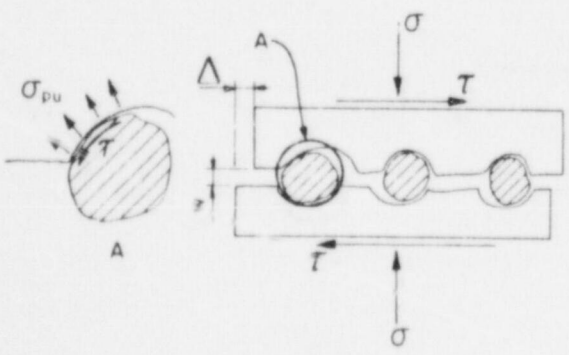


FIG. 5A REPRESENTATION OF THE AGGREGATE INTERLOCK PHENOMENON

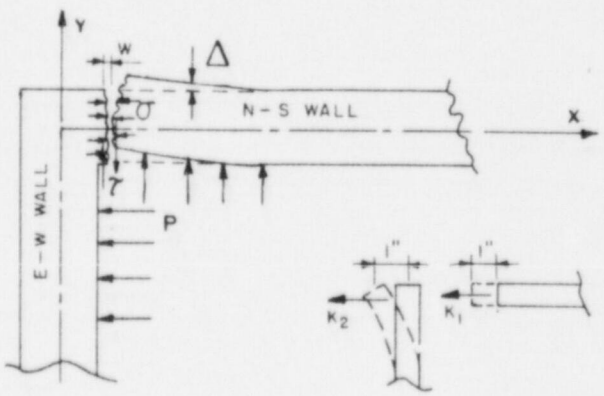
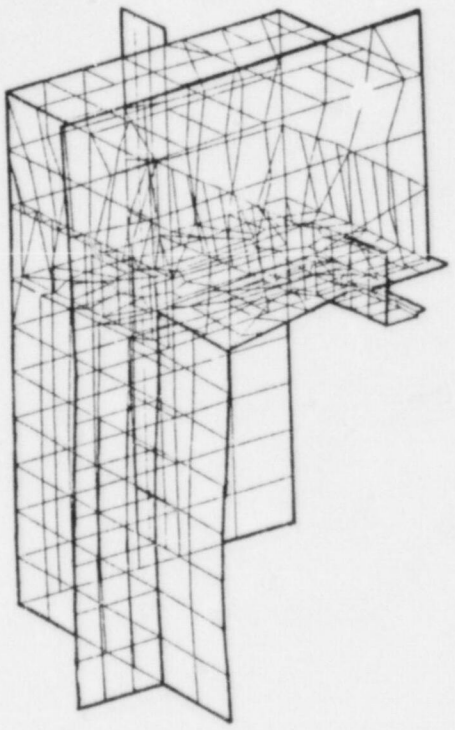


FIG. 5B CALCULATION OF SHEAR CARRIED BY AGGREGATE INTERLOCK



MAX DEFL = 0.0285 FT (NODE 127)

FIG 6 DEFORMED SHAPE AT 60 PSI PRESSURE

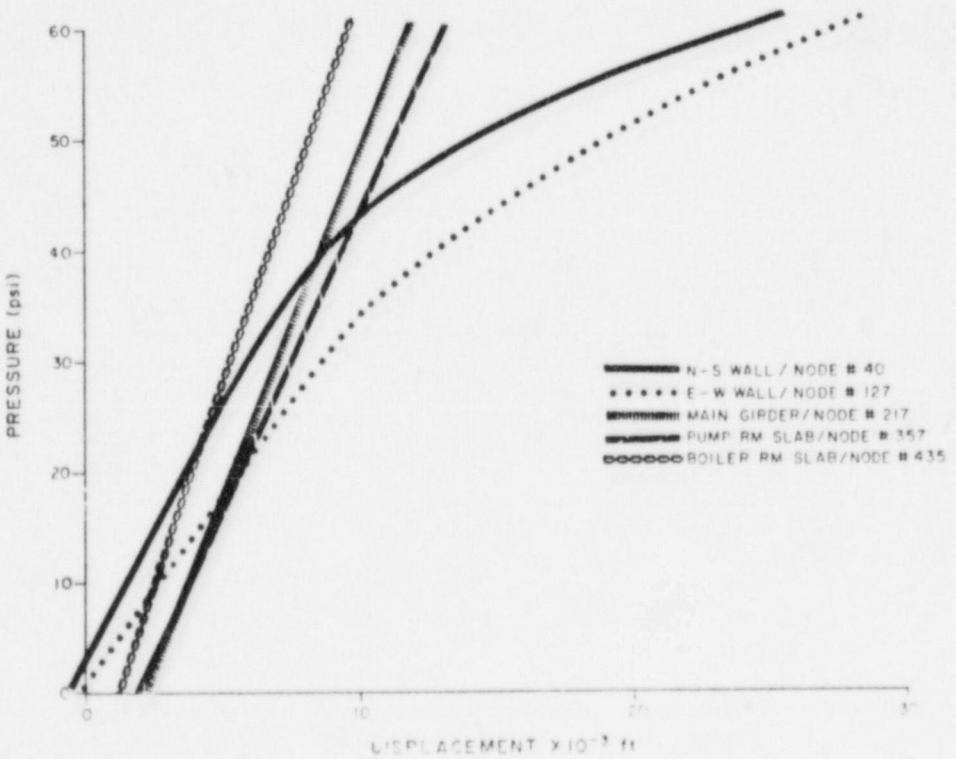


FIG. 7 MAXIMUM DISPLACEMENT VS APPLIED PRESSURE

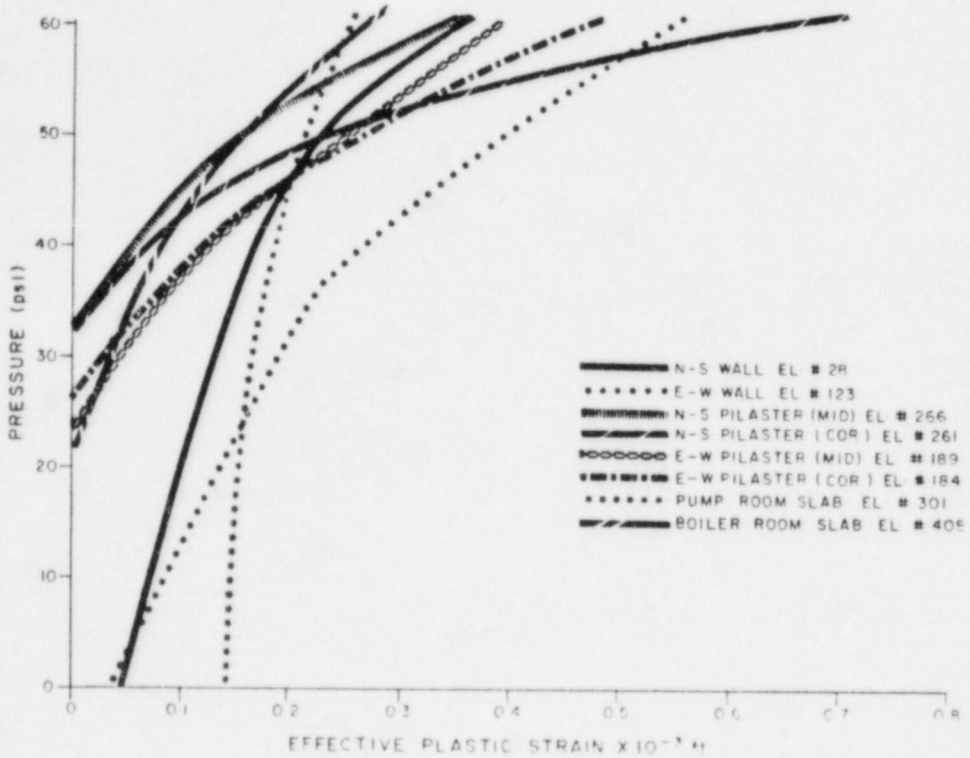


FIG. 8 EFFECTIVE PLASTIC STRAIN OF EQUIVALENT SECTIONS VS APPLIED PRESSURE

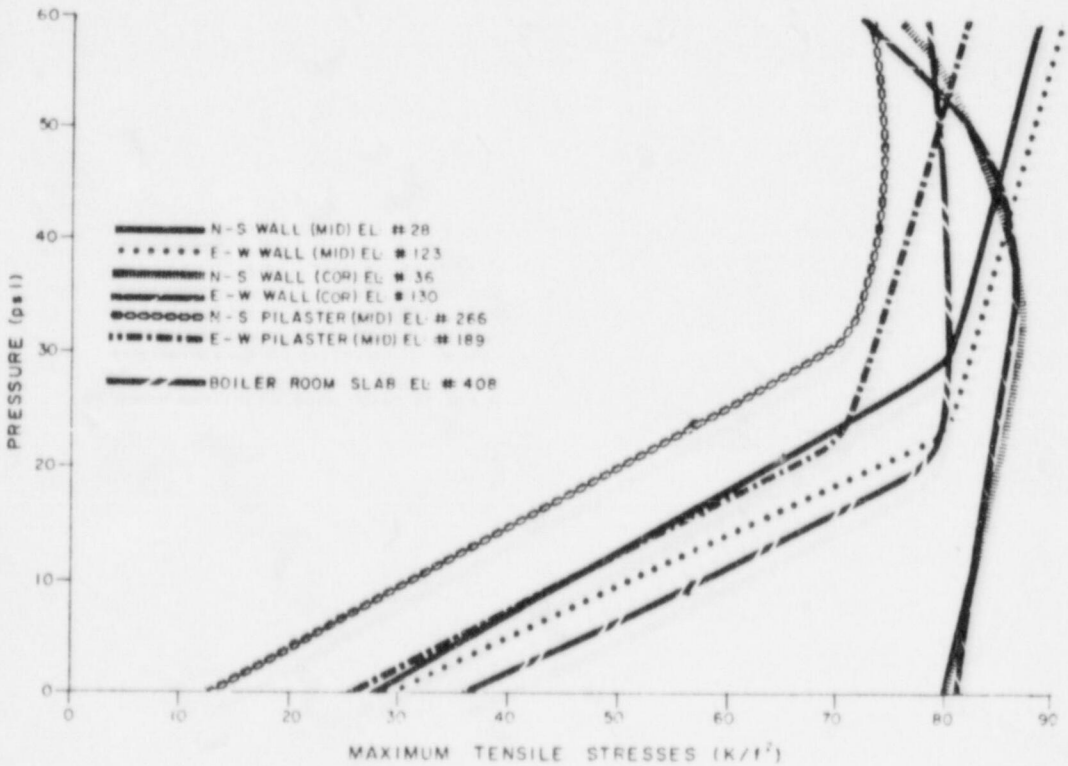
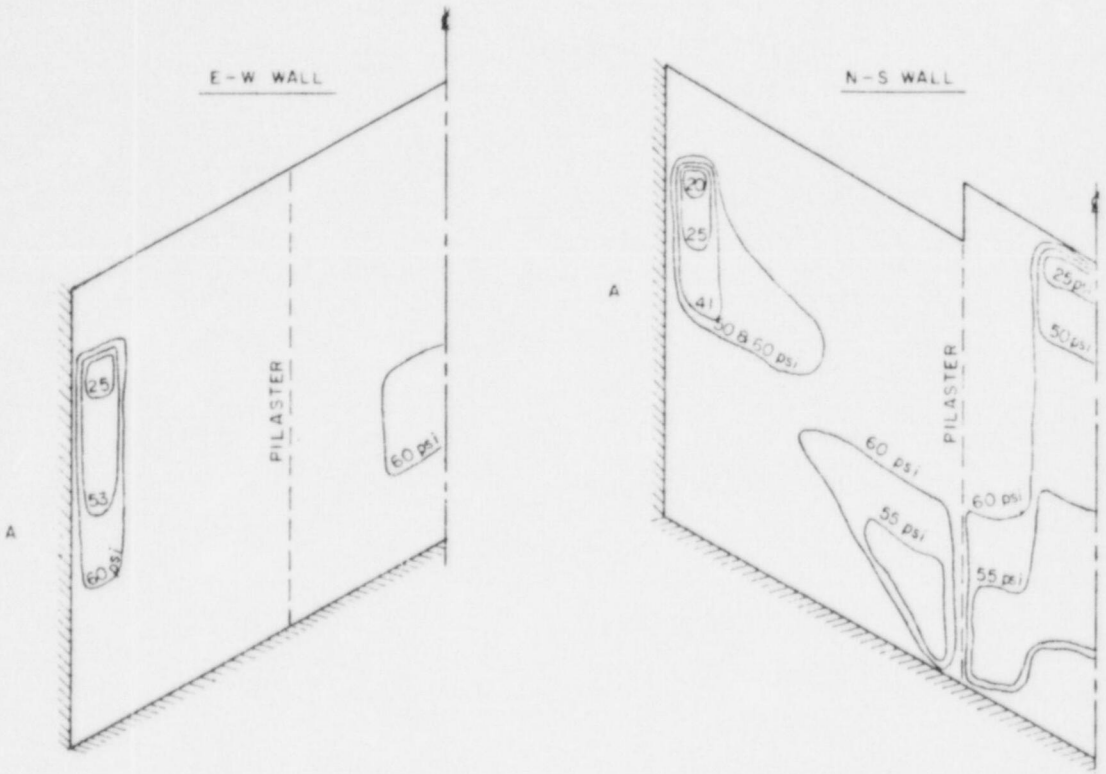
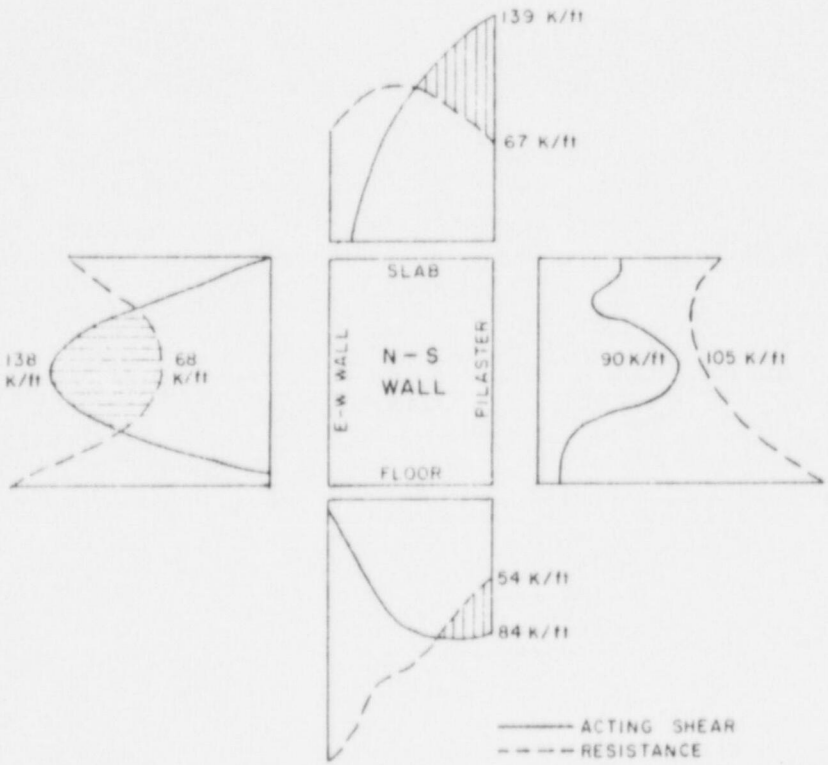


FIG. 9 MAXIMUM TENSILE STRESSES OF EQUIVALENT SECTIONS VS APPLIED PRESSURE



FIG·10 PROGRESSIVE DEVELOPMENT OF YEILDING IN REINFORCEMENT STEEL IN WALLS



FIG·11 RESISTANCE TO & ACTING "OUT OF PLANE" SHEAR FORCES FOR N-S WALL (P = 60 psi)

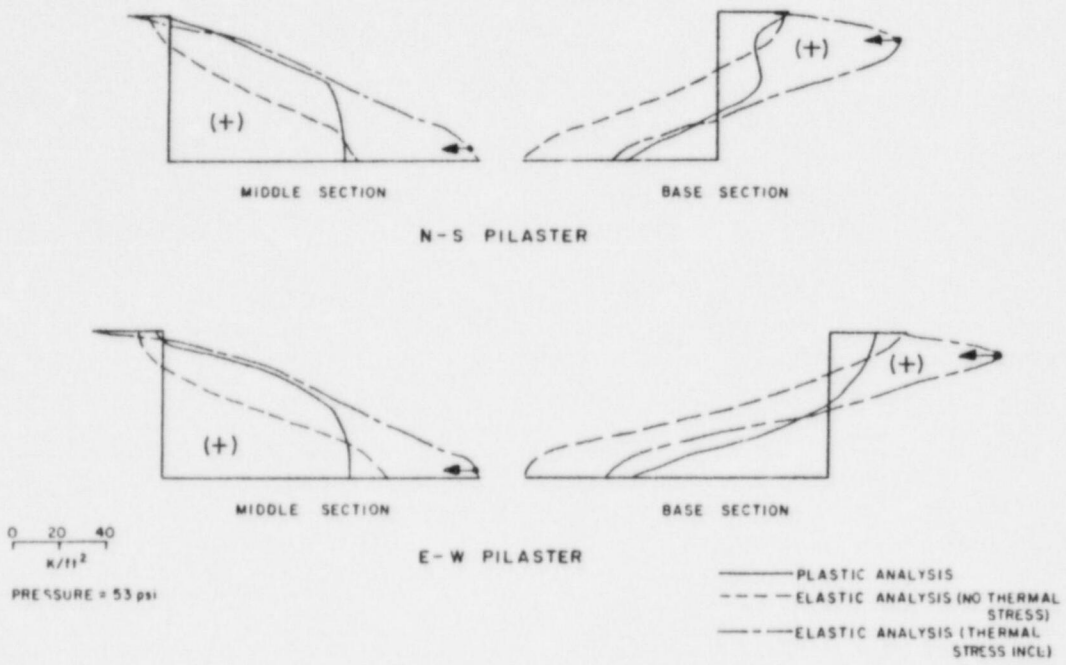


FIG 12 EFFECT OF PLASTICITY ON THERMAL STRESSES

Pressure psi	Observation
0 (End of initial loading)	Localized flexural cracking* at corner between walls
20	Yield of steel start at top of the corner of the N-S edge panel.
25	Flexural cracks start in different locations/overall nonlinear behaviour starts/yield of steel start at top of the corner of E-W edge panel.
30	Yield of steel starts in the middle section of N-S pilaster/hair cracks cover the whole structure.
43	Local shear exceeds resistance at a single point in the middle of the corner between walls.
48	Shear forces at crack location exceed aggregate interlock capacity.
50	Yield of steel starts in the base section of N-S pilaster accompanied by large strains.
55	Yield of steel start in middle of N-S centre panel/shear crack covers one third of the corner between N-S and E-W walls.
60	Yield of steel start in the E-W pilaster/yield of steel covers a large area in N-S edge panel/yield of steel starts in the middle of E-W centre panel/average shear at the top edge of N-S corner panel exceeds average shear resistance.

*Tensile stresses exceed "f_t".

TABLE I OBSERVATION OF STRUCTURE'S BEHAVIOUR WITH INCREASING PRESSURE

A Simplified Model for Concrete at Low Confining Pressures

H. D. Hibbitt
Hibbitt, Karlsson & Sorensen, Inc.
100 Medway Street
Providence
Rhode Island 02906

Abstract

The paper describes a model for the response of concrete at low confining pressures. The model uses a damaged elasticity and a "crack detection surface" in stress space to describe cracking, and a yield/flow surface to define the concrete's response in compressive states of stress. The model is simple enough that associated numerical algorithms can be implemented to allow the model to operate effectively in the context of an implicit finite element code: some modeling accuracy has been sacrificed for this purpose. Nevertheless, preliminary studies with the model indicate that it can give useful predictions.

1.0 Introduction

The paper describes a model for plain concrete which is being developed for use in the Abaqus finite element code (Abaqus, 1982). In Abaqus it is intended that reinforced concrete modeling be accomplished by combining standard elements, using this plain concrete model, with "rebars", which use a metal elastic-plastic constitutive model for the rebar material behavior. Abaqus offers very general options to model rebar as separate components for this purpose. Because of this modeling approach the paper discusses the modeling of plain concrete only.

The theory described in the paper is intended as a model of concrete behavior for relatively monotonic loadings under fairly low confining pressures (less than four to five times the largest compressive stress that can be carried by the concrete in uniaxial compression). Cracking is assumed to be the most important aspect of the behavior, and it dominates the modeling. Cracking is assumed to occur when the stresses reach a failure surface, which we call the "crack detection surface". This failure surface is taken to be a simple Coulomb line written in terms of the first and second stress invariants, $\hat{p}$ and $\hat{q}$, that are defined below. The anisotropy introduced by cracking is assumed to be important in the simulations for which the model is intended, so that the model includes consideration of this anisotropy. The model is a smeared crack model, in the sense that it does not track individual "macro" cracks: rather, constitutive calculations are performed independently at each integration point of the finite element model, and the presence of cracks enters into these calculations by the way the cracks effect the stress and material stiffness associated

with the integration point. Various objections have been raised to such smeared crack models. The principal concern is that this modeling approach inherently introduces mesh sensitivity in the solutions, in the sense that the finite element results do not converge to a unique result. For example, since cracking is associated with strain softening, finer and finer meshes will lead to narrower and narrower crack bands. Crisfield (1986) discusses this concern in detail, and concludes that Hilleborg's (1976) approach is adequate to deal with this issue for practical purposes. Hilleborg uses brittle fracture concepts to associate an energy release with cracking within the volume of material at an integration point: this energy release can be incorporated into the material model as a strain softening behavior ("tension stiffening", as shown in Figure 1) associated with the onset of cracking at the integration point. The slope of the strain softening line is chosen based on this energy release argument, using a characteristic volume associated with the integration point. In this paper "crack" is used to mean a direction in which cracking has been detected at the single constitutive calculation point in question: the closest physical concept is that there exists a continuum of micro-cracks at the point, oriented as determined by the model.

When the principal stress components are dominantly compressive the response of the concrete is modeled by an elastic-plastic theory, using a simple form of yield surface written in terms of the first two stress invariants. Associated flow and isotropic hardening are used. This model significantly simplifies the actual behavior: the associated flow assumption generally overpredicts the inelastic volume strain; the simple yield surface used does not match all data accurately (the third stress invariant would be needed to improve this aspect of the model); and, especially when the concrete is strained beyond the ultimate stress point, the assumption of constant elastic stiffness does not reproduce the observation that the unloading response is significantly weakened (the elastic response of the material appears to be damaged). In addition, when concrete is subjected to very high pressure stress it exhibits inelastic response: no attempt has been made to build this behavior into the model. These limitations are introduced for the sake of computational efficiency. In particular, assuming associated flow leads to enough symmetry in the Jacobian matrix of the constitutive model (the "material stiffness matrix") that the overall equilibrium equation solution does not require non-symmetric equation solution for this reason. All of these limitations could be removed at some sacrifice in computational cost.

The cracking and compression responses of concrete that are incorporated in the model are illustrated by the uniaxial response of a specimen shown in Figure 2. When concrete is loaded in compression it initially exhibits elastic response. As the stress is increased some non-recoverable (inelastic) straining occurs, and the response of the material softens. An ultimate stress is reached, after which the material loses strength until it can no longer carry any stress. If the load is removed at some point after inelastic straining has occurred, the unloading response is softer than the initial elastic response: this effect is ignored in the model. When a uniaxial specimen is loaded into tension it responds elastically until, at a stress that is typically 7–10% of the ultimate compressive stress, cracks form so quickly that, even on the stiffest testing machines available, it is very difficult to observe the actual behavior. As discussed above, we follow Crisfield and Hilleborg and model the cracking as strain-softening. We assume cracking causes damage, in the sense that open cracks can be represented by loss of elastic stiffness (as distinct from the non-recoverable straining that

is associated with inelastic straining, such as we are using for the compressive behavior model). The model neglects any permanent strain associated with cracking.

In multiaxial stress states these observations may be generalized through the concept of surfaces of failure and flow in stress space. These surfaces are fitted to experimental data. The surfaces used are shown in Figures 3 and 4, and are defined in Section 2.3 below.

This model makes no attempt to include prediction of cyclic response, or of the reduction in the elastic stiffness caused by inelastic straining, because the model is intended for application to relatively monotonic loading cases. Nevertheless, it is likely that, even in such cases, the stress trajectories will not be entirely radial, and the model must predict the response in such cases in a reasonable way. An isotropically hardening "compressive" yield surface forms the basis of the model for the inelastic response when the principal stresses are dominantly compressive. An independently softening "crack detection surface" is used to detect cracking. Cracking is associated with a particular direction, and, subsequent to crack detection, oriented, damaged, elasticity is used to model the existing crack. Stress components associated with an open crack are not included in the definition of the crack detection surface for detecting additional cracks at the same point and we only allow cracks to form in orthogonal directions at a point.

In a code like Abaqus the constitutive calculations must define the state and, for implicit time integration, the material stiffness, at the end of the increment, based on the state at the start of the increment and the current estimate of the kinematic solution for the response at the spatial integration point during the increment. Since, in this case, some parts of the constitutive model are defined in rate form, integration is required.

In summary, the model consists of two independent "yield" surfaces (the compression surface and the crack detection surface) and a damaged elasticity model to represent cracks that have occurred at a material calculation point. The details of this model and its integration are now presented.

2.0 Independent Surface Elastic-Plastic Model for Concrete

The model uses the classical concepts of plasticity theory: a strain (rate) decomposition into elastic and inelastic strain rates; elasticity; yield; flow; and hardening.

2.1 Strain decomposition

We begin with the standard additive strain rate decomposition of plasticity, which, by suitable definition of strain, can be integrated as:

$$\boldsymbol{\varepsilon} = \boldsymbol{\varepsilon}^{el} + \boldsymbol{\varepsilon}_c^{pl} + \boldsymbol{\varepsilon}_t^{pl}, \tag{1}$$

where $\boldsymbol{\varepsilon}$ is the total mechanical strain; $\boldsymbol{\varepsilon}^{el}$ is the elastic strain; $\boldsymbol{\varepsilon}_c^{pl}$ is the plastic strain associated with the "compression" surface; and $\boldsymbol{\varepsilon}_t^{pl}$ is the plastic strain associated with the crack detection surface. The "compression" and the crack detection yield surfaces are defined below.

2.2 Elasticity

The elasticity is written in the form:

$$\boldsymbol{\sigma} = \mathbf{D} : \boldsymbol{\varepsilon}^{el}, \tag{2}$$

where $\mathbf{D}$ is the elastic stiffness matrix for the concrete. For uncracked concrete, $\mathbf{D}$ is the usual linear, isotropic elasticity defined by Young's modulus and Poisson's ratio.

Let α represent a cracked direction, with corresponding direct stress $\sigma_{\overline{\alpha\alpha}}$ and direct elastic strain $\varepsilon^{el}_{\overline{\alpha\alpha}}$. In these expressions and in the remainder of this section, no summation is implied by repeated indices with a bar over them.

Then, in $\mathbf{D}$, $D_{\overline{\alpha\alpha}\beta\gamma}$ is undamaged if $\varepsilon_{\overline{\alpha\alpha}} \leq 0$. If $\varepsilon_{\overline{\alpha\alpha}} > 0$ we assume $D_{\overline{\alpha\alpha}\beta\gamma} = 0$ for $\beta \neq \alpha$, $\gamma \neq \alpha$, and that the elastic stiffness across the crack reduces linearly with opening strain:

$$D_{\overline{\alpha\alpha}\overline{\alpha\alpha}} = \frac{\sigma^f}{\varepsilon^f + \varepsilon^{\text{open}}_{\overline{\alpha\alpha}}},$$

where

$$\varepsilon^{\text{open}}_{\overline{\alpha\alpha}} = \max_{\text{over history}} \left(\varepsilon^{el}_{\overline{\alpha\alpha}} - \varepsilon^f \right),$$

σ^f and ε^f are the tensile stress and strain values at which cracking occurs.

The shear modulus associated with existing crack directions is ϱG, where G is the elastic shear modulus and ϱ is assumed to be a function of $\langle \varepsilon^{el}_{\overline{\alpha\alpha}} \rangle + \langle \varepsilon^{el}_{\overline{\beta\beta}} \rangle$, where α and β are the directions associated with this component of shear deformation, and $\langle f \rangle = f$ if $f > 0$, otherwise $\langle f \rangle = 0$. If $\langle \varepsilon^{el}_{\overline{\alpha\alpha}} \rangle + \langle \varepsilon^{el}_{\overline{\beta\beta}} \rangle = 0$, ϱ is assumed to be a constant that is less than 1.0.

Combining the integrated strain rate decomposition (Equation (1)) and the elasticity (Equation (2)) then gives

$$\boldsymbol{\sigma} = \mathbf{D} : \left(\boldsymbol{\varepsilon}^0 - \Delta\boldsymbol{\varepsilon}^{pl}_c - \Delta\boldsymbol{\varepsilon}^{pl}_t \right), \tag{3}$$

where, for simplicity, we define

$$\boldsymbol{\varepsilon}^0 = \boldsymbol{\varepsilon}^{el}|_t + \Delta\boldsymbol{\varepsilon}. \tag{4}$$

2.3 Yield

The model includes two independent yield surfaces. The "compression" surface is

$$f_c = \left(3q^2 - a_0 \tau_c p \right)^{\frac{1}{2}} - \tau_c = 0, \tag{5}$$

where p is the effective pressure stress and q is the Mises equivalent deviatoric stress:

$$p = -\frac{1}{3}\text{trace}(\boldsymbol{\sigma}); \quad q = \sqrt{\frac{3}{2}\mathbf{S} : \mathbf{S}},$$

where $\mathbf{S} = \boldsymbol{\sigma} + p\mathbf{I}$ are the deviatoric stress components. In Equation (5) a_0 is a constant, which is chosen from the ratio of the ultimate stress reached in biaxial compression to the ultimate stress reached in uniaxial compression, and $\tau_c(\lambda_c)$ is a hardening parameter (τ_c is the yield stress in a state of pure shear stress). The $\tau_c(\lambda_c)$ relationship is defined from uniaxial compression data.

This surface is used in the model because it provides a reasonable match to experimentally measured ultimate stress data over the range of pressure stress values of interest (see Figure 3). The particular form of the surface means that, as the hardening (λ_c) changes, the surfaces in (p–q) space are similar, so that, for example, the ratio of flow stress in biaxial loading to flow stress in uniaxial loading is the same at all flow stress levels. This does not appear to be contradicted by any experimental data, and it means that only one constant (a_0) is needed to define the shape of the surface. The value of a_0 is established from the experimentally measured ratio, r^{σ}_{bc}, of the ultimate stress magnitude in uniaxial compression, σ_c, to the magnitude of each non-zero principal stress at ultimate stress in biaxial compression, σ_{bc}: typically $r^{\sigma}_{bc} \approx 1.16$, giving $a_0 = 1.583$.

The crack detection surface is the Coulomb line

$$f_t = \hat{q} - \left(3 - b_0 \frac{\sigma_t}{\sigma^u_t}\right) \hat{p} - \left(2 - \frac{b_0}{3}\frac{\sigma_t}{\sigma^u_t}\right) \sigma_t = 0, \tag{6}$$

where σ^u_t is the failure stress in uniaxial tension, and b_0 is a constant which is defined from the value of the tensile failure stress, σ_I, in a state of biaxial stress when the other non-zero principal stress, σ_{II}, is at the uniaxial compression ultimate stress value, σ^u_c. $\sigma_t(\lambda_t)$ is a hardening parameter (σ_t is the equivalent uniaxial tensile stress). The $\sigma_t(\lambda_t)$ relationship is defined by the "tension stiffening" used to account for the smearing of cracking over the volume controlled by the integration point, as discussed in the Introduction above. The stress measures $\hat{p}$ and $\hat{q}$ are defined in the same way as p and q, except that all stress components associated with open cracks are not included in these measures.

This surface has a simple form, but matches plane stress data quite well (see Figure 3). The hardening is introduced in the particular form shown in Equation (6) so that, as $\sigma_t \to 0$, the surface becomes $q - 3p = 0$, which, in (p–q) space, is the cone containing the principal axes of stress. This means that, as the tension stiffening is exhausted in a plane stress test, the stress point will drop back onto the nearest principal stress axis.

2.4 Flow

The model currently uses the assumption of associated flow, so that

$$d\boldsymbol{\varepsilon}^{pl} = d\boldsymbol{\varepsilon}^{pl}_c + d\boldsymbol{\varepsilon}^{pl}_t,$$

where, if $f_c = 0$ and $d\lambda_c > 0$,

$$d\boldsymbol{\varepsilon}_c^{pl} = d\lambda_c \left(1 + c_0 \left(\frac{p}{\tau_c}\right)^2\right) \frac{\partial f_c}{\partial \boldsymbol{\sigma}},$$

otherwise $d\boldsymbol{\varepsilon}_c^{pl} = 0$,

and, if $f_t = 0$ and $d\lambda_t > 0$,

$$d\boldsymbol{\varepsilon}_t^{pl} = d\lambda_t \frac{\partial f_t}{\partial \boldsymbol{\sigma}},$$

otherwise $d\boldsymbol{\varepsilon}_t^{pl} = 0$.

In the definition of $d\boldsymbol{\varepsilon}_c^{pl}$, c_0 is a constant, which is chosen so that the ratio of ε_{11}^{pl} in a monotonically loaded biaxial compression test to ε_{11}^{pl} in a monotonically loaded uniaxial compression test is constant (r_{bc}^{ε}): typically $r_{bc}^{\varepsilon} \approx 1.28$. A non-zero value for c_0 is essential if the model is to match biaxial stress data with different stress trajectories. Figures 5 and 6 show examples of matching of the model to Kupfer's (1973) plane stress data. With $c_0 = 0$ the match to the biaxial experimental data, using a model calibrated from the uniaxial data, is very poor.

2.5 Cracking

As soon as the crack detection surface has been activated we assume that cracking has occurred. The crack direction, $\mathbf{n}_{\alpha}$, is taken to be the direction of that part of the maximum principal plastic strain increment conjugate to the crack detection surface, $\Delta\boldsymbol{\varepsilon}_t^{pl}$, that is orthogonal to the directions of any existing cracks at the same point. Cracking is irrevocable in the sense that, once a crack has occurred at a point, it remains throughout the rest of the calculation. Following crack detection the crack affects the calculations by damaging the elasticity, as defined in the section on Elasticity above, and, if the elastic strain across the crack is tensile, all stress components associated with the open crack direction are neglected, as described in the section above on Yield, in defining the invariants used in the crack detection surface. This implies that no more than three cracks can occur at any point (two in a plane stress case, one in a uniaxial stress case).

3.0 Integration of the model

For practical application the model must be integrated stably over finite strain increments, and the material stiffness matrix must be derived algebraically. The backward Euler method generally used with plasticity models in Abaqus meets these requirements, and is used here.

The first aspect of the integration problem is the decision about which yield surfaces are active in the increment: none, one, or two may be active. We first calculate the stresses at the end of the increment, assuming the response in the increment is purely elastic:

$$\boldsymbol{\sigma}^0 = \mathbf{D} : \boldsymbol{\varepsilon}^0, \tag{7}$$

where $\boldsymbol{\varepsilon}^0$ is defined in Equation (4) above. Note that $\mathbf{D}$ in this equation is a function of the elastic strain across any existing cracks that are open.

This solution is tested with respect to the yield surfaces:

If $f_c(\boldsymbol{\sigma}^0) \leq 0$ and $f_t(\boldsymbol{\sigma}^0) \leq 0$ the response in the increment is purely elastic, and the integration is completed by Equation (7).

If the above conditions do not hold, but $f_c(\boldsymbol{\sigma}^0) \leq 0$, the compression surface is not active in the increment, but the crack detection surface is active.

Equally, if $f_t(\boldsymbol{\sigma}^0) \leq 0$ but $f_c(\boldsymbol{\sigma}^0) > 0$, the compression surface only is active in the increment.

The remaining case is when both $f_c(\boldsymbol{\sigma}^0) > 0$ and $f_t(\boldsymbol{\sigma}^0) > 0$. In this case we first attempt a solution assuming the crack detection surface only is active. If this solution violates the compression surface (that is, $f_c > 0$ for this solution), both surfaces must be active during the increment.

In the case when the compression surface and the crack detection surface are both active, the equations of the model, integrated by the backward Euler method, are:

The elasticity, together with the integrated strain rate decomposition:

$$\boldsymbol{\sigma} = \mathbf{D} : (\boldsymbol{\varepsilon}^0 - \Delta\boldsymbol{\varepsilon}^{pl}); \tag{8}$$

The flow rule, integrated by the backward Euler method:

$$\Delta\boldsymbol{\varepsilon}^{pl} = \Delta\lambda_c\, \hat{\mathbf{n}}_c + \Delta\lambda_t\, \mathbf{n}_t, \tag{9}$$

where

$$\hat{\mathbf{n}}_c = \left(1 + c_0 \left(\frac{p}{\tau_c}\right)^2\right) \mathbf{n}_c, \quad \mathbf{n}_c = \frac{\partial f_c}{\partial \boldsymbol{\sigma}}, \quad \text{and} \quad \mathbf{n}_t = \frac{\partial f_t}{\partial \boldsymbol{\sigma}};$$

and the yield functions:

$$f_c = 0, \quad \text{and} \quad f_t = 0. \tag{10}$$

Here, and in the following development, all quantities written without a specific reference to a time point are taken at the end of the increment.

Equations (9) and (10) are a set of nonlinear algebraic equations that define the state at the end of the increment. The system of equations is solved by using Newton's method, with the unknowns taken as the plastic strain components, $\Delta\boldsymbol{\varepsilon}^{pl}$, together with $\Delta\lambda_c$ and $\Delta\lambda_t$. Once these variables have been found the solution is fully defined. If only one yield surface is active the equations are the same, with the terms associated with the inactive surface omitted.

The solution of Equations (9) and (10) is not simple, and a suitable starting "guess" for the Newton interations is usually essential. Some special cases require additional attention—for example, the case of biaxial tension in plane stress. These details are discussed in the Abaqus Theory manual.

4.0 Material stiffness

Exact definition of the "material stiffness" (the contribution of the constitutive model to the Jacobian matrix of the overall Newton scheme) is essential for efficient performance of an implicit code in highly nonlinear problems when Newton's method is used to solve the nonlinear equations (or an arc-length method is used: we use Fried's (1984) method). Indeed, one of the main motivations in this work is to have a model that is sufficiently tractable algebraically that an exact tangent material stiffness matrix can be derived. The material stiffness is obtained directly by taking variations of Equations (8), (9), and (10) with respect to all quantities at the end of the increment. We know from the solution to the integration of the increment which surfaces are active. The most complicated case is when both surfaces are active: in this case the material stiffness is:

$$\left[\mathbf{I} + \tilde{\mathbf{D}} : \mathbf{H} : \Delta\boldsymbol{\mathcal{A}}\right]^{-1} : \tilde{\mathbf{D}} : \mathbf{H},$$

where

$$\Delta\boldsymbol{\mathcal{A}} = \Delta\lambda_c \frac{\partial \hat{\mathbf{n}}_c}{\partial \boldsymbol{\sigma}} + \Delta\lambda_t \frac{\partial \mathbf{n}_t}{\partial \boldsymbol{\sigma}},$$

$$\tilde{D}_{ijkl} = D_{ijkl} + \frac{\partial D_{ijpq}}{\partial \varepsilon^{el}_{kl}} \varepsilon^{el}_{pq},$$

and

$$\mathbf{H} = \mathbf{I} - \lfloor \bar{\mathbf{n}}_c \; \bar{\mathbf{n}}_t \rfloor \begin{bmatrix} a_{cc} & a_{ct} \\ a_{tc} & a_{tt} \end{bmatrix} \begin{Bmatrix} \mathbf{m}_c \\ \mathbf{m}_t \end{Bmatrix},$$

where

$$\begin{bmatrix} a_{cc} & a_{ct} \\ a_{tc} & a_{tt} \end{bmatrix} = \begin{bmatrix} \mathbf{m}_c : \bar{\mathbf{n}}_c - \frac{\partial f_c}{\partial \tau_c} \frac{\partial \tau_c}{\partial \lambda_c} & \mathbf{m}_c : \bar{\mathbf{n}}_t \\ \mathbf{m}_t : \bar{\mathbf{n}}_c & \mathbf{m}_t : \bar{\mathbf{n}}_t - \frac{\partial f_t}{\partial \sigma_t} \frac{\partial \sigma_t}{\partial \lambda_t} \end{bmatrix}^{-1},$$

$$\bar{\mathbf{n}}_c = \hat{\mathbf{n}}_c + \Delta\lambda_c \frac{\partial \hat{\mathbf{n}}_c}{\partial \tau_c} \frac{\partial \tau_c}{\partial \lambda_c} \quad \text{and} \quad \bar{\mathbf{n}}_t = \mathbf{n}_t + \Delta\lambda_t \frac{\partial \mathbf{n}_t}{\partial \sigma_t} \frac{\partial \sigma_t}{\partial \lambda_t},$$

and

$$\mathbf{m}_c = \tilde{\mathbf{D}} : \mathbf{n}_c \quad \text{and} \quad \mathbf{m}_t = \tilde{\mathbf{D}} : \mathbf{n}_t.$$

This material stiffness is not completely symmetric. One reason is that the Jacobian of the elasticity, $\tilde{\mathbf{D}}$, may be non-symmetric (because of the dependence of shear terms on the direct strain across corresponding open cracks). Our present approach is to use the non-symmetric form if some other aspect of the model also requires a non-symmetric matrix. If not, the material stiffness is approximated by its symmetric part.

5.0 Closure

The paper has described a simple model for plain concrete under loadings where the effective pressure stress remains fairly small, and hence a parabolic Coulomb line with associated plastic flow provides a plasticity model that gives reasonable predictions. This adoption of associated plastic flow, the omission of the third stress invariant in the definitions of the compressive yield and crack detection surfaces, and the lack of damage effects in the elasticity caused by "compressive" loadings, all mark the model as only of limited accuracy. The emphasis of the effort is to provide a model that is of useful accuracy and which is computationally reliable, with priority given to the latter consideration in the context of an implicit calculation. (We assume here that such applications as quasi-static containment overpressurization are not economically amenable to explicit calculations, although this may not be correct. We have not investigated explicit methods in this context). Provided that the limitations of the model's accuracy are well documented and well understood, we believe that it does form a basis for useful predictions. It provides reasonable results in our standard test cases: we are now applying it to some containment models.

Acknowledgment

Support from the Electric Power Research Institute for part of this work is gratefully acknowledged.

References

"Abaqus manuals: User's, Theory, Example Problems, System", HKS Inc., Povidence, R. I., 1982. Also available as "Abaqus–EPGEN manuals", Electric Power Research Institute, Palo Alto, Cal.

M. A. Crisfield, "Snap-through and Snap-back Response in Concrete Structures and the Dangers of Under-integration", Int. J. Num. Meth. Eng., Vol. 22, pp 751–767, 1986.

A. Hilleborg, M. Kodeer and P. E. Petersson, "Analysis of Crack Formation and Crack Growth in Concrete by Means of Fracture Mechanics and Finite Elements", Cement Concrete Research, Vol. 6, pp 773–782, 1976.

I. Fried, "Orthogonal Trajectory Accession to the Nonlinear Equilibrium Curve", Comp. Meth. Applied Mech. and Eng., Vol. 47, pp 283–297, 1984.

H. B. Kupfer and K. H. Gerstle, "Behavior of Concrete under Biaxial Stresses", J. Eng. Mech. Div., ASCE, Vol. 99, p 853, 1973.

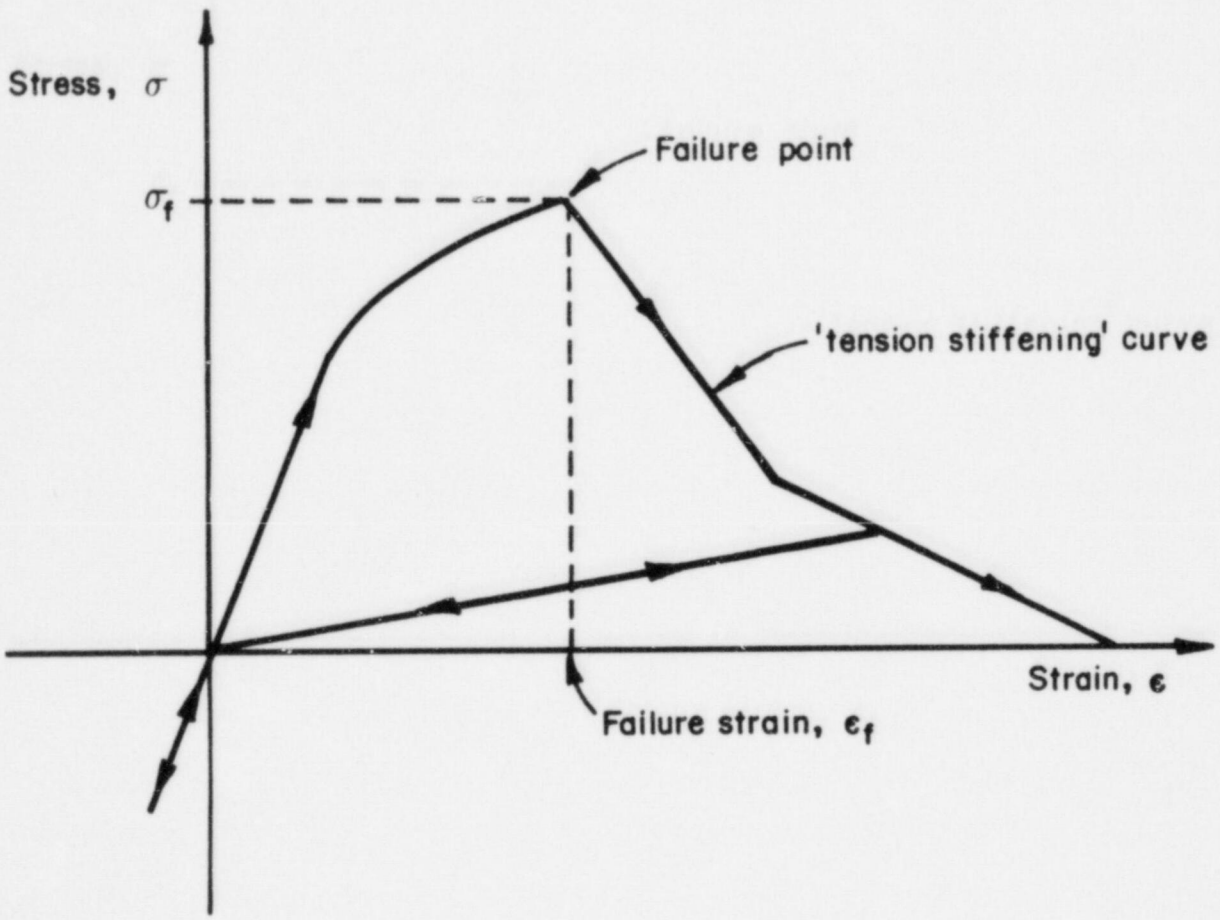


Figure 1 "Tension stiffening" model

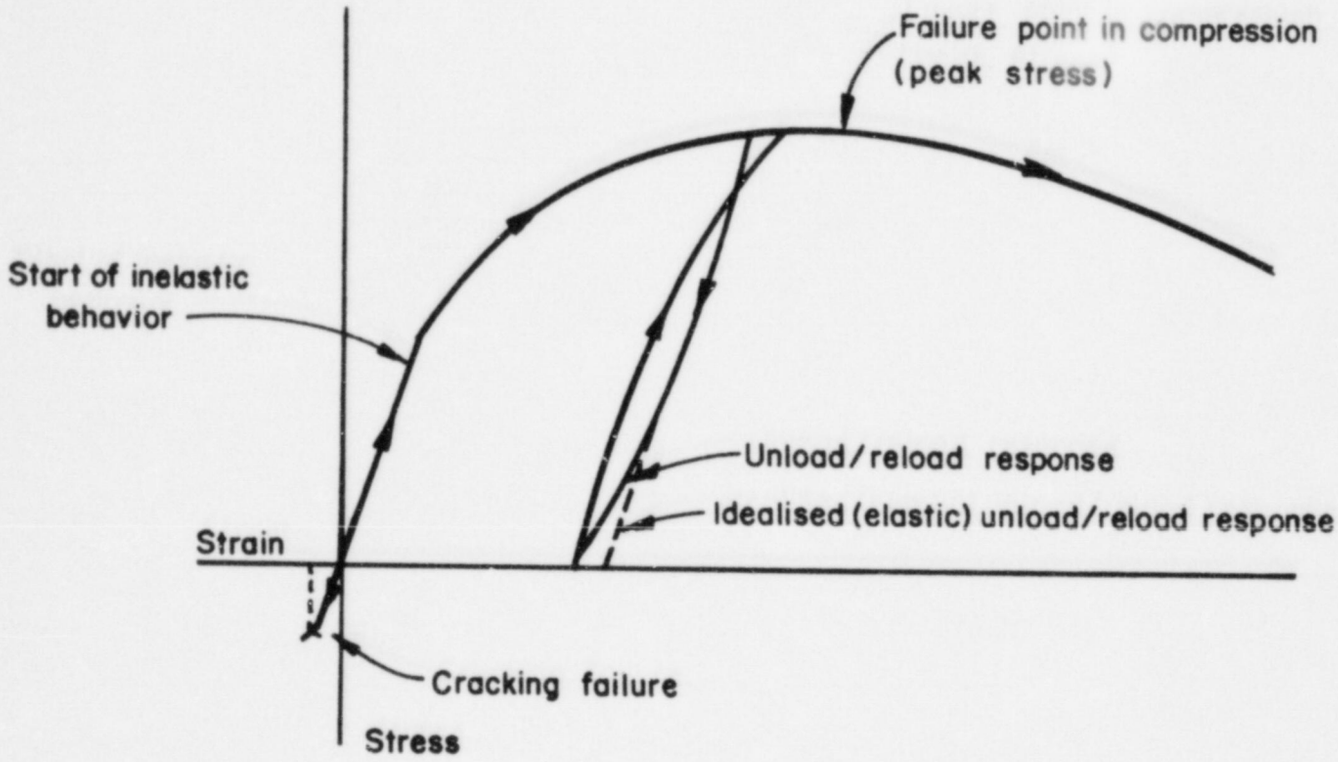


Figure 2 Uniaxial behavior of plain concrete

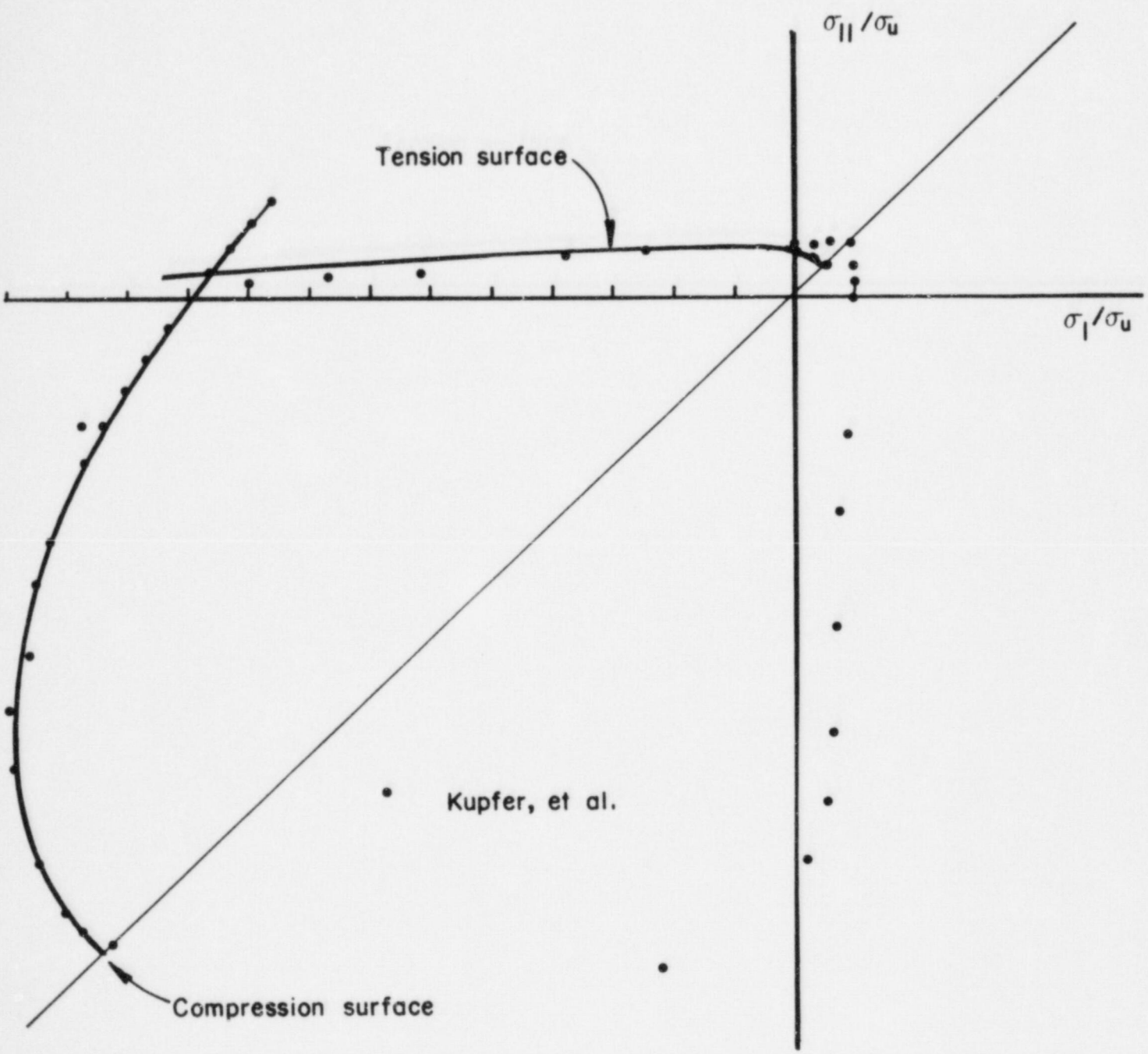


Figure 3 Concrete failure data in plane stress

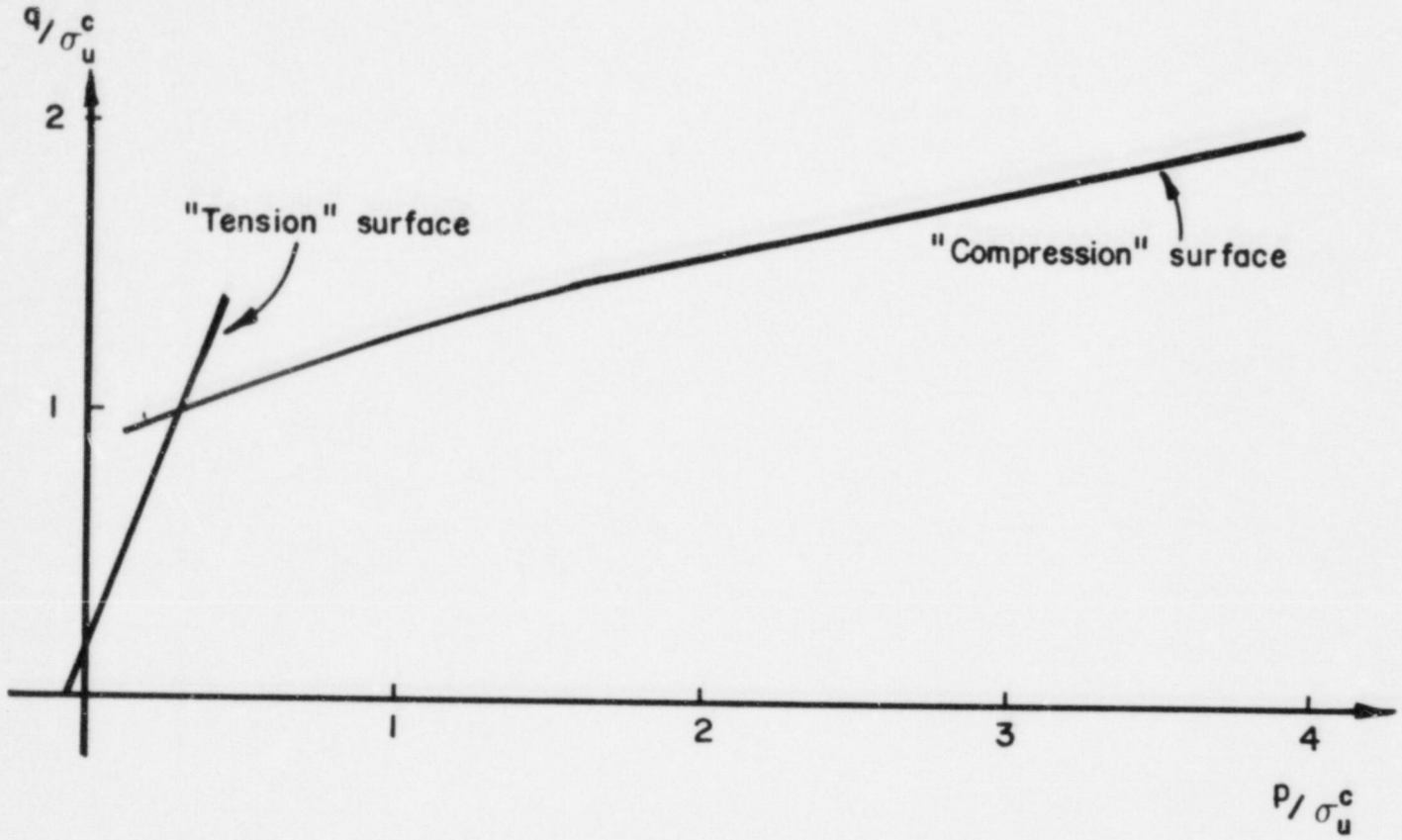


Figure 4 Concrete failure data in the $(p\text{–}q)$ plane

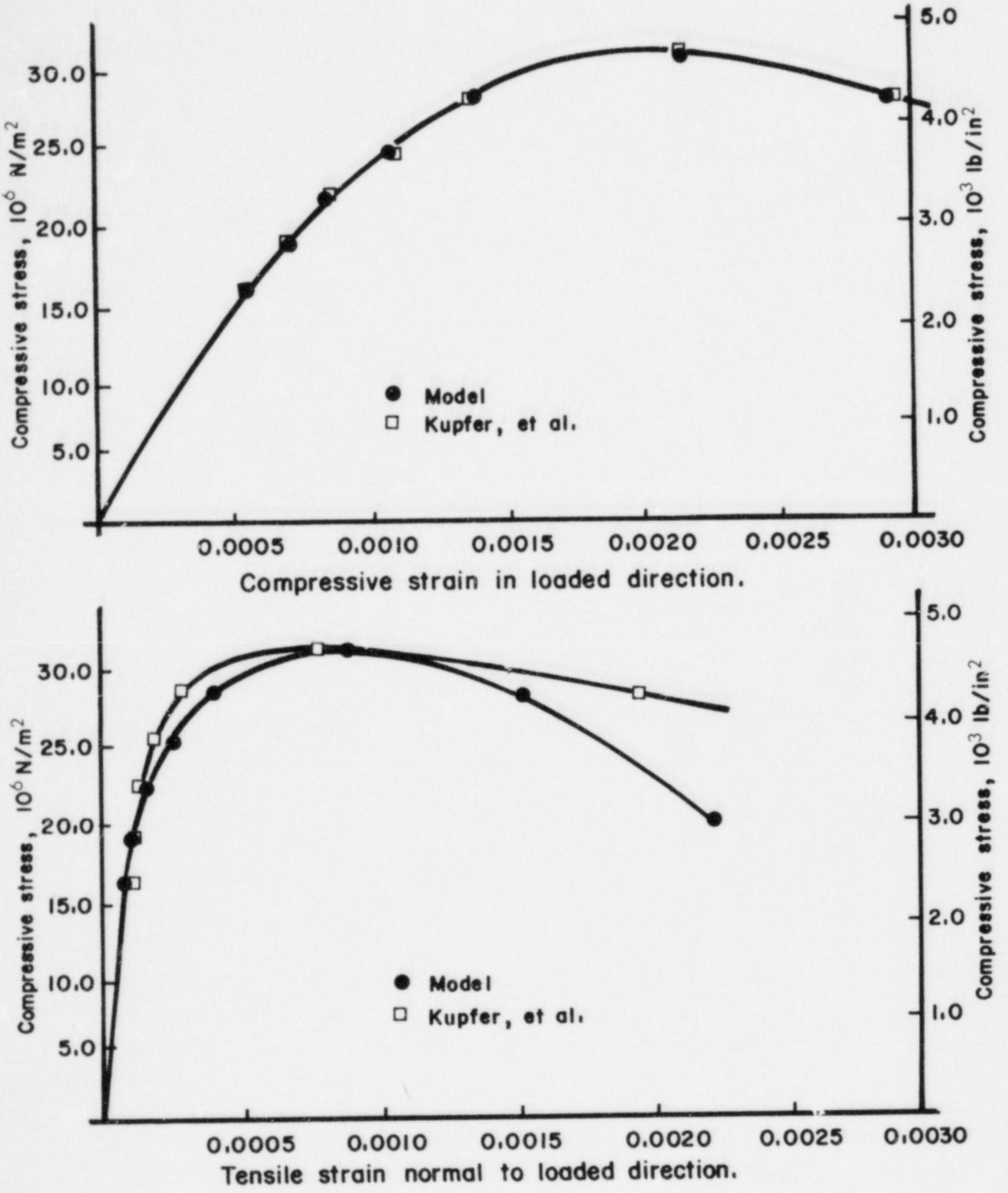


Figure 5 Comparison of model prediction and Kupfer data for uniaxial compression test

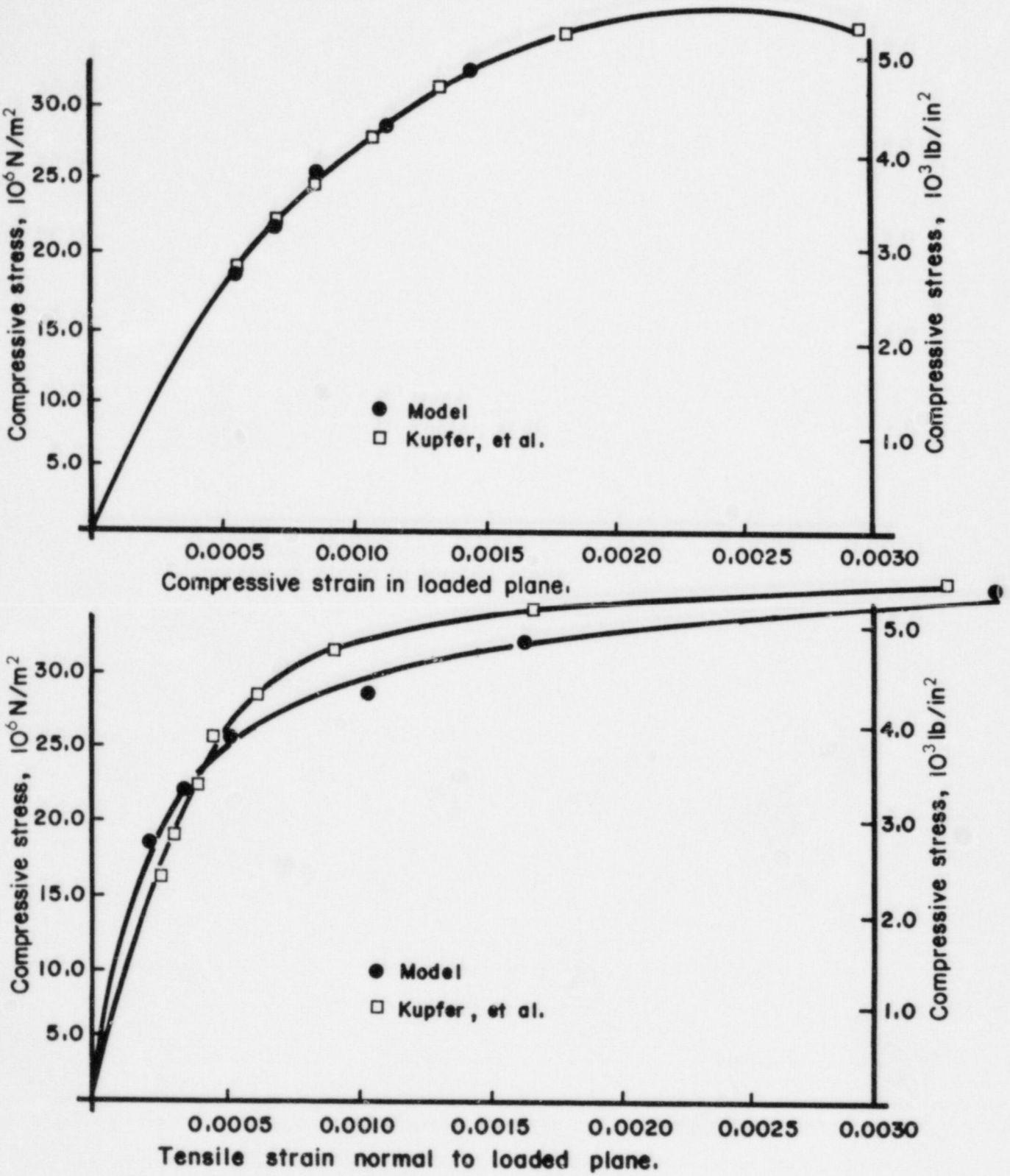


Figure 6 Comparison of model prediction and Kupfer data for biaxial compression test

EFFECT OF HIGH TEMPERATURE ON INTEGRITY OF CONCRETE CONTAINMENT STRUCTURES

P.D. Bhat
Ontario Hydro
700 University Avenue - H17
Toronto, Ontario
Canada
M5G 1X6

ABSTRACT

The effect of high temperature on concrete material properties and structural behaviour are studied in order to relate these effects to the performance of concrete containment structures. Salient data obtained from a test program undertaken to study the behaviour of a restrained concrete structure under thermal gradient loads up to its ultimate limit are described. The preliminary results indicate that concrete material properties can be considered to remain unaltered up to temperatures of 100°C. The presence of thermal gradients did not significantly affect the structures ultimate mechanical load capacity. Relaxation of restraint forces due to creep was found to be an important factor. The test findings are compared with the observations made in available literature. The effect of test findings on the integrity analysis of a containment structure are discussed.

1.0 INTRODUCTION

The high temperatures postulated inside a containment structure subsequent to a Loss of Coolant Accident (LOCA) affects the performance of reinforced concrete containments. This paper examines the effect of high temperatures on the behaviour of a concrete containment structure in the light of the results of a generic test program carried out at Ontario Hydro. The problem is studied from the viewpoint of a CANDU heavy water reactor containment. In these structures it is postulated that the maximum post LOCA temperature will be in the order of 100°C sustained for a fairly long period after the accident. The pressure inside the containment reduces quickly in a short period after the accident and hence simultaneous effect of high temperature and pressure is not addressed.

2.0 EFFECT OF HIGH TEMPERATURE ON REINFORCED CONCRETE

Reinforced concrete being the main structural barrier, is the most important component to be evaluated in examining the integrity of

containment structures. The effect of high temperature on reinforced concrete can be classified in to two categories:

(a) effect on material properties;

(b) effect on structural behaviour.

2.1 Material Properties

The important concrete material properties affected by high temperature are: compressive and tensile strengths, modulus of elasticity and coefficient of thermal expansion of concrete. These effects are the result of a combination of factors such as loss of water in concrete, changes in aggregate properties, expansion of cement paste, pore pressure and moisture migration, which are all influenced by the high temperature. A brief review of available test results from the literature is given below and compared with the findings of a test program. Implications of these findings on containment integrity analysis are indicated.

2.1.1 Compressive/Tensile Strength

Considerable research has been carried out regarding the loss of concrete strength under high temperature and reported in literature. The recent exhaustive review by Bazant and Chern (1) has shown that the strength losses up to 100^{o}C under short term conditions is insignificant. Strength changes under tension and compression are about the same. Under long term heating, up to two and a half years, a maximum strength loss of up to 15 percent could be expected. Most of the available test results pertain to small samples which are heated uniformly while the moisture in concrete may or may not have been allowed to escape. In containment structures the moisture escape is not significant.

During the thermal gradient test program carried out at Ontario Hydro (2,5) the strength properties of concrete cylinders were evaluated before and after subjecting them to more than ten cycles of thermal loads over a nine month period. The thermal cycling was done while the cylinders were immersed in water and the applied temperatures varied between room temperature and up to a maximum of about 95^{o}C. During the test period very little change in concrete strength took place. Compressive strength actually increased minimally from 42.4 MPa to 42.6 MPa. Split cylinder tensile strength rose from 3.12 MPa to 4.05 MPa.

These results further confirm that in integrity analysis of CANDU containments the strength properties of concrete can be assumed to remain unaffected under the expected high temperature.

2.1.2 Modulus of Elasticity

The available literature indicates that normal weight concrete used in containment structures experience a decrease in the elastic

modulus at temperatures above 50°C. For short term heating of three to six days at 100°C, the loss in modulus is a maximum of about 15 percent. For long term heating up to two and a half years, the loss of elastic modulus could be up to 25 percent at 100°C.

It is worth noting that the rate of loss of modulus of elasticity is faster than the loss in strength of concrete as the temperature increases. This in turn reduces the moment developed due to thermal gradients. Hence even if there is some loss in modulus it is not expected to affect the overall performance of the structure under predominantly flexural loads.

In the test program carried out the elastic modulus of concrete remained virtually unchanged at 29,000 MPa even after a number of temperature cycles.

2.1.3 Thermal Expansion

The coefficient of thermal expansion depends on a number of factors such as moisture conditions, differences in the thermal expansion of cement paste and aggregate, effect of reinforcement, temperature level and prior thermal cycling.

In the test program thermal expansion was evaluated by testing prisms and also obtained from deflection measurements of unrestrained model. The coefficient of thermal expansion in these tests varied from $7.07 \times 10^{-6}/^{o}C$ up to $8.00 \times 10^{-6}/^{o}C$.

In containment structures since only one surface gets wet and heated, for practical analysis it is adequate to use an average value in the temperature ranges considered in the CANDU containments.

2.2 Structural Behaviour

A number of structural behaviour features play a major part in the evaluation of high temperature effect and containment integrity of concrete structures. These effects are briefly reviewed below and in each case the experimental findings are given and their implications discussed.

2.2.1 Ultimate Strength

An applied temperature gradient across the thickness of the members has the effect of increasing the average temperature of the section and produce a thermal gradient. In a restrained structure this introduces compressive and flexural effects. The flexural effects cause cracking of concrete which reduces the overall stiffness of members. Since the moments developed due to thermal gradients are dependent on the stiffness, the magnitude of the moment decreases as the cracks progress. Under service conditions, the cracking is

not extensive and the post cracking tension stiffening effects contributed by the tensile concrete in between open cracks have major influence in determining the magnitude of the moments and forces developed (2). These tension stiffening effects result in increased thermal moments compared to that of a section in which tensile resistance is provided by the reinforcing bars only.

Under ultimate conditions however, the cracks become fairly extensive and the stiffness contribution from concrete in between cracks becomes negligible. Under these conditions, the thermal moments as well as the ultimate strength can be computed neglecting the tension stiffening effects.

The above discussed performance of a restrained reinforced concrete structure up to its ultimate load under the combined thermal and mechanical loads has been investigated in the experimental program (2). The objective of the test program was to derive the generic parameters which represent the above behaviour. In the test program, a reinforced concrete portal frame (Figure 1) restrained at its legs was subjected to a series of combined thermal gradient and mechanical loads. The development of moment curvature relationship was experimentally observed by measuring the restraint forces from which moments were evaluated. This observed response is shown in Figure 2. During this test the thermal gradient applied was 57^{o}C and the ultimate limit was obtained by applying mechanical loads on the legs. The measured moment-curvature relationship is essentially a bilinear curve with a well defined yield moment of 131 kN.m and a slightly ascending yield plateau beyond. Figure 2 also shows the theoretical predictions using the analytical method developed earlier (5). The method is based on an iterative, nonlinear secant stiffness approach and incorporates realistic constitutive relations. The theoretical yield moment is 138 kN.m and the yield plateau is virtually flat. The results indicate that the presence of thermal gradient does not significantly affect the structure's ulitimate load capacity.

In containment structures it is likely that the actual ultimate strength differs from the value calculated based on specified properties of rebars and concrete. This difference arises mainly due to the variation of the properties of reinforcing bars, the effect of mechanical rebar splices and the local effect mechanisms. Investigation of such effects when thermal loads are not present are available (3,4). However, influence of these factors together with thermal loads are not yet available.

2.2.2 Concrete Creep/Relaxation

Sustained high temperatures increase creep of concrete. The cause of creep and mechanism of creep depends on the temperature and load levels. Even at temperatures below 100^{o}C, under moderate stress levels creep of concrete has been found to be significant (1). Although considerable number of test results are available on creep

of concrete, most of the tests were conducted on uniformly heated small scale specimens. Test results considering temperature gradient and cracking are not available.

The test program was also useful in evaluating the relaxation effect of high temperature in restrained concrete structures considering cracking of concrete. The test program simulated a moderately stressed structure under 100°C temperature as experienced in a containment structure. The temperature load studied at present is only for short duration up to 24 hours. Even under these conditions it is observed that considerable relaxation of restraint forces takes place. Typical relaxation effects are shown in Figure 3, in which the relaxation of restraint forces are shown as a function of time after loading for a number of inside temperatures T_i and steady temperature gradient ΔT. The force relaxation indicated in these figures are expected primarily due to two factors, namely, the relaxation due to the initial slight drop in the temperature gradient while steady state levels are being achieved and relaxation due to creep.

During the test program, it was noted that the restraint forces generally peaked about 2 hours after the peak thermal loads had been reached. The force then decreased steadily over the next 24 hours. The amount of force relaxation was greater than that expected due to drop in gradient alone. For example, for the curve shown in Figure 3 with the highest temperature T_i, the force relaxation is a total of about 24 percent, whereas the change in temperature gradient is only about 12 percent. It is postulated that this additional drop in restraint force is primarily due to the creep of the concrete structure as influenced by the high temperature.

Attempts are currently being made for theoretical modelling of concrete creep/relaxation effects under the above temperature conditions. From the work carried out so far it is reasonable to say that relaxation of restraint forces due to high temperatures appears to be significant in evaluating ultimate behaviour and integrity of containments. Relaxation of restraint forces have beneficial effects in that it reduces further cracking and stress, however, deformation increases.

2.2.3 Cracking/Leakage

Thermal gradients tend to cause tension and cracking on the cold face of the structure. Although the actual crack location is dependent on the relative magnitudes of mechanical and thermal loads, nature of structure, etc. under accident conditions it is expected that most of the cracking will be on the outside face. The inside of the wall section is under compression, which prevents leakage. Hence it can be concluded that although temperature gradients will open up the cracks on the outside face, it will not adversely affect the leakage from containment. Depending on the extent of cracks prior to the application of thermal loads and the temperature drop it is possible that cracks might open up on the

inside leading to leakage, while cooling down of the structure takes place. This is not expected to occur when the maximum load the structure has experienced is below the yield limit of the rebars. For example, at on stage in the test program the structure was loaded up to 99 percent of the theoretical yield strain of rebars. Even at this high load level the structure did not show signs of significant distress or cracking of concrete. There was no leakage at this level or when the load was removed and the structure cooled down at room temperature.

A typical crack pattern in the test specimen shown earlier, at a stage when the loads were fairly high are shown in Figure 4. At this stage the peak thermal gradient had reached 75°C and the rebars were stressed to 111 percent of the specified yield strength, and 99 percent of the actual yield strength of the bars. There were extensive cracks on the outside and very few of them appeared to penetrate the inside. However, there was no leakage of water through the cracks although the load was increased well beyond the specified yielding of rebars.

3.0 SUMMARY AND CONCLUSIONS

The effect of high temperatures up to 100°C on reinforced concrete structures is studied by examining temperature effect on material properties, and ultimate behaviour under combined thermal and mechanical loads. Based on this study the following conclusions are drawn:

(a) In integrity analysis of CANDU containment structures, the important concrete material properties namely, tensile/compressive strength, elastic modulus and coefficient of thermal expansion can be assumed to remain unchanged.

(b) While analyzing ultimate limits of concrete structures considering thermal loads, the influence of tension stiffening effects become negligible. High temperatures up to 100°C cause significant relaxation of restraint forces. Even at load levels beyond the yielding of rebars the cracking is mostly confined to one face of the structure and will not result in major leakage.

4.0 REFERENCES

1. Bazant, Z.P.; Chern, J.C.; Abrams, M.S. and Gillen, M.P. "Normal and Refractory Concrete for LMFBR Applications", Volume 1, EPRI Report No. NP-2437, June 1982.

2. Bhat, P.D., "Influence of Post Cracking Behaviour on the Response of Concrete Structures Under Thermal Gradients", Paper No. H3/6, Transactions of the 8th SMIRT Conference, Brussels, Belgium, August 1985.

3. Fardis, M.N. and Nacar, A. "Static Ultimate Capacity of R/C Containment", MIT Report No. 8-22-82.

4. Dunham, R.S.; Rashid, Y.R.; Yuan, K.A. and Lu, Y.M. "Methods for Ultimate Load Analysis of Concrete Containments", EPRI Report No. NP-4046, Interim Report, June 1985.

5. Vecchio, F.J., "Modelling the Response of Reinforced Concrete Structures to Thermal Loads", Paper No. H7/4, Transactions of the 8th SMIRT Conference, Brussels, Belgium, August 1985.

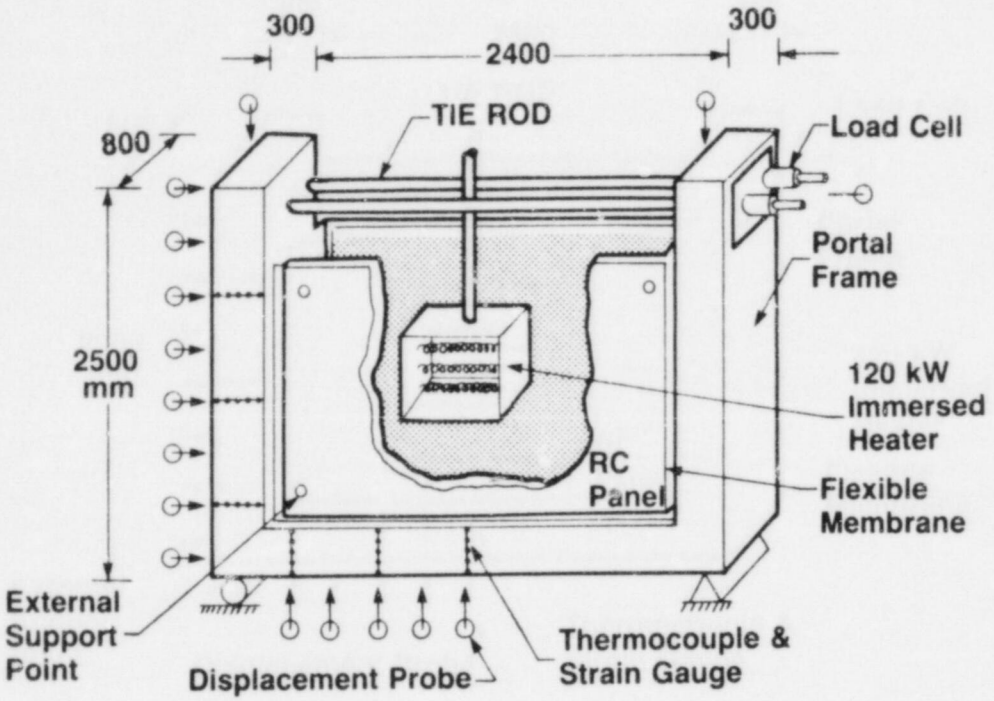


FIGURE 1: PORTAL FRAME TEST SPECIMEN

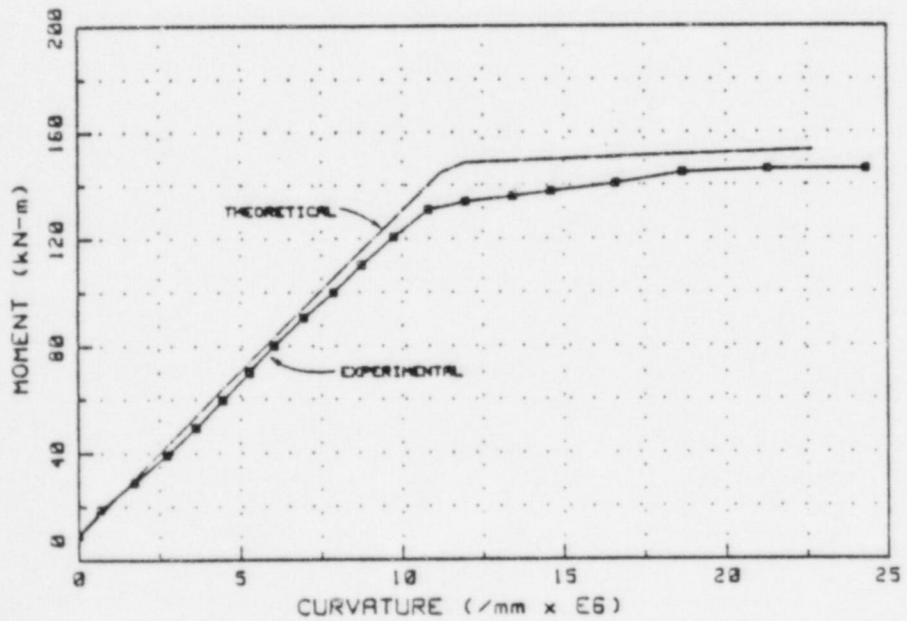


FIGURE 2: MOMENT - CURVATURE RELATIONSHIP (BEAM)

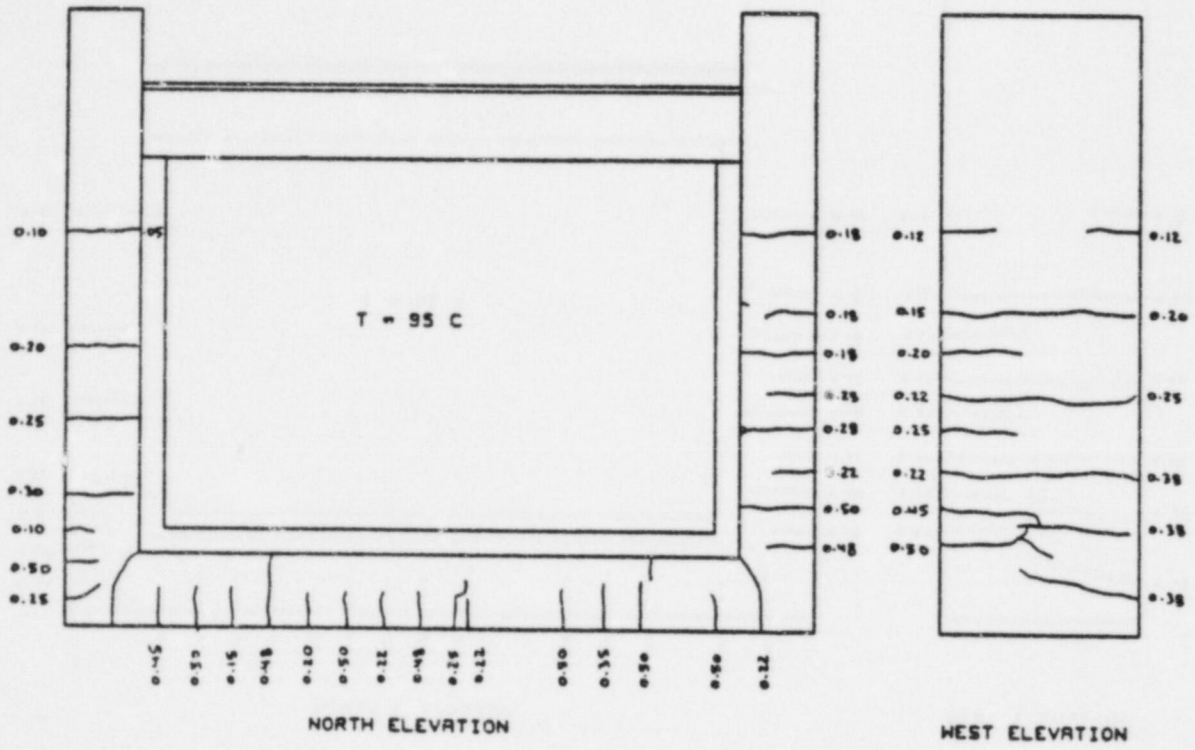


FIGURE 3: TYPICAL CRACK PATTERNS

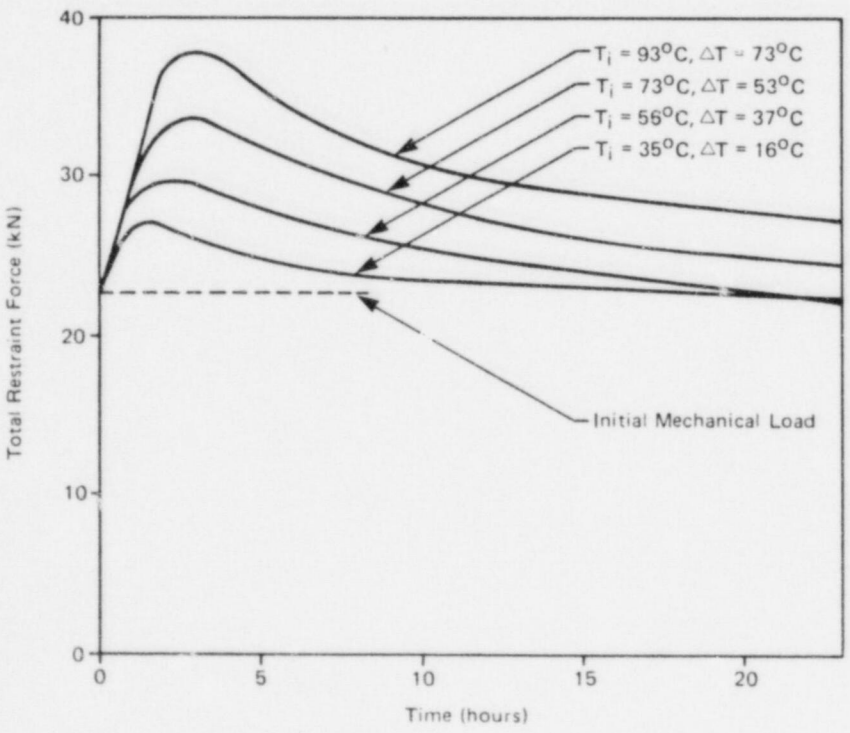


FIGURE 4: RESTRAINT FORCE RELAXATION

RESULTS OF LARGE-SCALE TEST OF DISCONTINUITY REGION IN A PRESTRESSED CONCRETE CONTAINMENT

N. W. Hanson, D. M. Schultz, and J. J. Roller
Construction Technology Laboratories
A Division of the Portland Cement Association
5420 Old Orchard Road
Skokie, Illinois 60077-4321

ABSTRACT

The test described in this paper is part of an Electric Power Research Institute (EPRI) program (Research Program RP2172-2) to provide a test-verified analytical method of estimating capacities of concrete reactor containment buildings under internal overpressurization from postulated degraded core accidents.

Phase 2 of the EPRI program, on which this paper is based, includes tests of five large-scale specimens with steel liner plates. The specimens represent structural elements of prestressed concrete containment buildings. Four full-scale square wall element specimens and one specimen representing the wall/basemat junction region were tested. This paper describes results of the wall/basemat junction region test.

Results of this experimental work indicate that highly localized strains in the steel liner plate caused by internal overpressurization or other accident conditions can result in liner tearing and subsequent containment leakage. It appears that this liner tearing occurs in a controlled manner. Extrapolating from these test results, leakage and depressurization is more likely to occur than global failure.

INTRODUCTION

To investigate the structural behavior of reactor containment buildings subjected to overpressurization, the Electric Power Research Institute (EPRI) has undertaken a comprehensive analytical and experimental program [1 through 7]. The overall objective of the EPRI program is to provide a test-verified analytical method for evaluating failure mechanisms and leak rates of reinforced and prestressed concrete reactor containment buildings under internal overpressurization from postulated degraded core accidents.

The experimental work in Phase 2 of the EPRI program included testing of both large- and full-scale concrete specimens with steel liner plates representing structural elements of containment buildings. Test specimens incorporated many details found in existing containment designs. Four square wall element specimens and one wall/basemat junction element were designed, constructed, and tested at CTL. The purpose of this paper is to discuss the results of the wall/basemat junction test.

TEST SPECIMEN

A cross-sectional view of a concrete containment building is shown in Fig. 1. Concrete containment walls are usually 3.5 to 5.5 ft (1.1 to 1.7 m) thick. In reinforced concrete containments, large diameter deformed reinforcing bars, usually No. 14 or No. 18, are placed in multiple layers in the hoop and meridional directions. In prestressed concrete containments, unbonded tendons are used in addition to several layers of reinforcing bars in each direction. A steel liner plate, usually either 1/4 or 3/8 in. (6.4 or 9.5 mm) thick is typically anchored to the inside surface of the containment building. This steel liner plate is attached to the concrete with embedded headed studs or semi-continuous light structural steel shapes.

Design and Construction

The specimen was a large-scale element representing the region where the wall and basemat intersect in a prestressed concrete containment building as illustrated in Fig. 1. The purpose of this specimen was to investigate the behavior at two possible localized failure points, the knee (wall/skirt intersection) and the basemat junction (skirt/basemat intersection). The skirt is the sloping transition region between the wall and basemat. The objective was to apply sufficient bending to yield the steel liner plate at the wall-skirt junction and at the skirt-basemat junction.

The rationale behind specimen design was that conditions of shear and bending cause high strain in the liner plate in the wall/basemat junction area. This high strain could be enhanced further due to local conditions at a crack in the concrete portion of the element. As a result, there is a potential for liner plate tearing in this specimen that might not occur in other places in the containment structure.

Two layers of No. 10 reinforcing bars were used in both the hoop and meridional directions of the wall and skirt. Reinforcement was also provided in the basemat to provide resistance to the applied loads. Shear reinforcement was included in the wall, skirt, and basemat.

The concrete was cast with a 1/4-in.-thick (6.3-mm) steel liner plate as the inner face of the wall, skirt, and basemat. Discontinuous light structural angles were welded to the liner plate to provide anchorage to the concrete. The anchorage angles were oriented in the meridional and radial directions. Interruptions in the angles occurred at the knee (wall/skirt intersection) and the basemat junction (skirt/basemat intersection). A weld running in the hoop direction joined liner plate pieces at these locations. A channel strongback, located orthogonally with respect to the angles, was included along the weld seam at the knee. A W-section, oriented similarly to the channel, was included along the weld seam at the basemat junction. Both of these details are representative of industry practice as employed in existing containments. The hoop direction of the liner plate was chosen to be coincidental with the direction of rolling of the steel stock. This represents the orientation of liner plate material in containment structures.

The tendon ducts of a prestressed unbonded containment were also modeled in the wall and skirt of this specimen. Tendon duct details were based on current

practice. No tendons were placed in the tendon ducts. Tendons were omitted since unbonded tendons behave only as external forces and therefore do not affect the location or distribution of cracks in the concrete.

Materials

All steel materials were chosen based on existing containment building designs. Reinforcement used in the test specimens conformed to minimum requirements of ASTM Designation: A615 Grade 60. The steel liner plate and weldments consisting of light structural steel shapes conformed to minimum requirements of ASTM Designation: A36. Thin walled conduit was used as tendon ducts.

Concrete was designed to have a 28-day compressive strength of 5000 psi (34.5 MPa). This design strength is representative of concrete used in prestressed containments.

TEST APPARATUS

A loading model was selected to create liner plate behavior similar to liner plate behavior in the wall/basemat junction region of a containment subject to overpressurization. This model included surface pressure on the skirt and wall in addition to stress applied to the meridional reinforcement and liner. Suitable external reactions were provided at the basemat and on the wall above the skirt. Stress was not applied to the hoop reinforcement since there is only minor hoop stress near the basemat. The specimen was tested in CTL's multi-axial test fixture.

Multi-Axial Test Fixture

The multi-axial test fixture is a large prestressed concrete structure specially designed to resist large loads applied to the test specimens.

Figure 2 illustrates the eight-sided test fixture. The fixture consists of two parallel reaction frames (top and bottom) separated by 4 ft (1.2 m) concrete spacers. The four 11x4 ft (3.4x1.2 m) openings provide access to the specimen from the outside of the test frame. Crossheads span across these openings to support hydraulic rams and react forces from load rods. Load rods are attached to liner plate load hardware or to couplers on the specimen reinforcement. Sufficient clearance is provided between the specimen and the test frame for loading hardware and for specimen elongation during testing.

Test Setup

Equipment for application of load to the wall/basemat specimen included a rubber bladder for surface pressure loading and hydraulic rams for reinforcement and liner plate loading. The arrangement of specimen, test frame, and loading equipment is shown in Fig. 3.

A rubber bladder was used in contact with the liner plate on the wall and skirt part of the specimen to apply surface pressure to the full 7-ft (2.1-m) width and 7-ft (2.1-m) length. Axial (meridional) force in the wall part of the specimen was applied by hydraulic rams connected by loading rods to the meridional wall reinforcement and liner plate. A rubber pad between the basemat and the adjacent

concrete reaction block was used as a pivot and reaction. Radial force in the basemat reinforcement was applied by hydraulic rams connected through a loading framework to reinforcing bars extending out of the basemat concrete. Roller reaction pivots were provided on the wall portion of the specimen. Dead weight of the basemat was supported from above by hydraulic rams connected to the specimen by loading rods.

Test Procedure

Three loading systems were used to control the loads. One system consisted of hydraulic jacks attached to one end of the specimen wall reinforcement and liner plate load rods to produce a meridional force. The jacks were connected to individual hydraulic pumps so that loads in the reinforcement and liner plate could be adjusted separately.

The second load system applied a uniform surface pressure over a portion of the liner plate surface of the specimen with an inflated rubber bladder.

A third load system applied a radial force to reinforcement in the basemat.

The test procedure involved incrementally increasing the meridional tension load in the wall and surface pressure on the liner plate. The axial tension load was reacted along the basemat at a known distance from the junction region, thus causing bending in the wall and skirt. The wall-skirt liner plate surface pressure also developed bending that was reacted at the two support pivots as illustrated in Fig. 3.

INSTRUMENTATION

External Gages

Load cells were used to measure loads in both the meridional reinforcement and meridional liner plate. Load cells were also used to measure the radial load applied to the basemat of the specimen. A pressure cell was used to monitor the surface pressure applied to both the wall and skirt of the specimen. Specimen displacements and localized elongations were measured by linear potentiometers.

Internal Gages

Bonded electrical strain gages were placed on four of the twelve meridional reinforcement bars. Reinforcing bar strain gages were concentrated at both the knee and the basemat junction regions of the specimen.

Strain gages were also placed on the liner plate. Two high elongated unbonded strain gages were attached by miniature studs welded to the concrete side of the liner plate at both the knee and the basemat junction. Liner plate strain gages monitored meridional or radial strains only.

TEST RESULTS

Meridional tension was applied to both the reinforcement and liner plate. A surface pressure load was applied to the liner plate over the entire skirt and part of the wall. The combination of the tension load and the surface pressure load

produced high bending moments and shear at the two potential failure locations. Selected test results are presented in Table 1. Crack patterns for the side concrete faces are shown in Fig. 4. Liner plate tear locations are shown in Fig. 5.

Table 1. Summary of Test Results

Maximum Strains:	
At Skirt/Wall Junction	
Bonded Strain Gage on Liner Plate	2.6%
High Elongation Strain Gage on Liner Plate	3.3%
Bonded Strain Gage on Reinforcing Bar	2.0%
At Basemat/Skirt Junction	
Bonded Strain Gage on Liner Plate	4.8%
Bonded Strain Gage on Reinforcing Bar	4.3%
Primary Concrete Cracking (After Unloading)	
Maximum Crack Width at Skirt/Wall Junction	0.56 in. (14.2 mm)
Maximum Crack Width at Basemat/Skirt Junction	1.25 in. (31.8 mm)

Concrete cracking on the two side faces shown in Fig. 4 shows the influence of cracking on liner behavior. At the skirt/wall junction, the concrete crack passed on both sides of the hoop direction anchor channel. With the loss of the anchorage provided by the channel at the knee, the liner pulled on the meridional angle anchors on either side of the knee. At the skirt/basemat junction, the primary flexural crack bypassed the anchorage section. With the loss of anchorage at this region, the liner was able to pull away from the concrete surface and subsequently provided only a minor contribution to the total internal forces resisting the externally applied bending moment in the junction section.

A detailed sketch in Fig. 6 of the skirt/wall region with anchorage devices and concrete cracks helps to explain the transfer of force to the ends of the anchorage angles. The highly stressed liner plate stretched across the former knee in a straight line except where held back by the anchorage angles. Local liner plate displacement occurred at each angle end as indicated in the sketch of the liner cross section in Fig. 7. Liner plate tearing such as indicated in Fig. 8 resulted from high local stress. Anchorage angle tearing was also observed as indicated in Fig. 8.

A detailed sketch of the skirt/basemat region in Fig. 9 shows the local conditions after the main corner anchorage was lost. Local liner plate displacement occurred at each angle end on the basemat side. Liner plate cracking in the form of a local circular pullout occurred at one location.

Liner plate tears occurred at both the knee and the basemat junction. Photographs of the liner plate tears, identified as A, B, C, D, or E in Fig. 6, are shown in Fig. 10.

SUMMARY AND CONCLUSIONS

To investigate the structural behavior of reactor containment buildings subjected to overpressurization, the Electric Power Research Institute (EPRI) has

undertaken a multi-phase experimental research program at Construction Technology Laboratories (CTL). Results from the test program are being used to confirm analytical models for predicting strength and deformations of containment walls. The analytical modeling is being conducted by Anatech International Corporation, La Jolla, California, in a separate parallel investigation sponsored by EPRI.

Phase 2 of the EPRI program included testing of both large- and full-scale concrete specimens with steel liner plates representing structural elements of prestressed containment buildings. Test specimens incorporated many details found in existing containment designs. Four square wall element-specimens and one wall/basemat junction element were designed, constructed, and tested at CTL. Details and results of the wall/basemat test are presented in this paper.

The objective of the wall/basemat element test was to determine if early cracking of the liner will occur at the junction region of the wall and basemat of a containment building. Large cracks in the backup concrete and high local strain in the liner are characteristic of the junction region. The test was designed to develop severe liner plate strain at the knee (junction of wall and skirt) and also at the basemat junction (junction of the skirt and basemat).

Results of the wall-basemat element test indicated that high local strains leading to liner plate fracture can develop in the junction region. Liner plate tears were detected at both the knee and basemat junction. These tears were attributed to the loss of liner plate anchorage in the junction region caused by the bending condition imposed during the test.

ACKNOWLEDGMENT

Technical discussions and assistance obtained from Drs. Y. R. Rashid and R. D. Dunham of Anatech International, who are responsible for analytical studies, as well as from Mr. R. K. Winkleblack and Dr. H. T. Tang of the Electric Power Research Institute management team are greatly appreciated.

REFERENCES

1. Tang, Y.K. and Sliter, G., "Research Activities at EPRI on Concrete Containment Integrity," Proceedings of the Workshop on Containment Integrity, Vol. 1, NUREG/CP-0033, SAND 82-1659, 1982, pp. 101-117.

2. Winkleblack, R.K. and Tang, Y.K., "Concrete Containment Integrity Program at EPRI," Proceedings of the Second Workshop on Containment Integrity, 1984, NUREG/CP-0056, SAND 84-1514, pp. 377-381.

3. Dunham, R.S., Rashid, Y.R., and Tang, Y.K., "Recent Results on Evaluation of Overpressure Response of Concrete and Steel Containments," Proceedings of the Second Workshop on Containment Integrity, 1984, NUREG/CP-0056, SAND 84-1514, pp. 533-561.

4. Julien, J.T., Schultz, D.M., and Weinmann, T.L., Concrete Containment Structural Element Tests, Volume 1: "Half-Thicknesses Element Tests - Description and Results," Electric Power Research Institute, Palo Alto, California, November 1984, 104 pp. Available through Research Reports Center, P.O. Box 50490, Palo Alto, California 94303, Document EPRI NP-3774, Volume 1.

5. Julien, J.T., Schultz, D.M., and Weinmann, T.L., Concrete Containment Structural Element Tests, Volume 2: "Half-Thicknesses Element Tests - Detailed Test Data," Electric Power Research Institute, Palo Alto, California, November 1984, 338 pp. Available through Research Reports Center, P.O. Box 50490, Palo Alto, California 94303, Document EPRI NP-3774, Volume 2.

6. Hanson, N.W., Julien, J.T., and Schultz, D.M., Concrete Containment Structural Element Tests, Volume 3: "Liner-Plate Tests," Electric Power Research Institute, Palo Alto, California, November 1984, 142 pp. Available through Research Reports Center, P.O. Box 50490, Palo Alto, California 94303, Document EPRI NP-3774, Volume 3.

7. Hanson, N.W., Schultz, D.M., Julien, J.T., Roller, J.J., and Weinmann, T.L., Concrete Containment Structural Element Tests, Phase 2 Final Report, Volume 1: "Full-Scale Wall Elements with Liner Plates - Description and Results," Electric Power Research Institute, Palo Alto, California (to be published by EPRI).

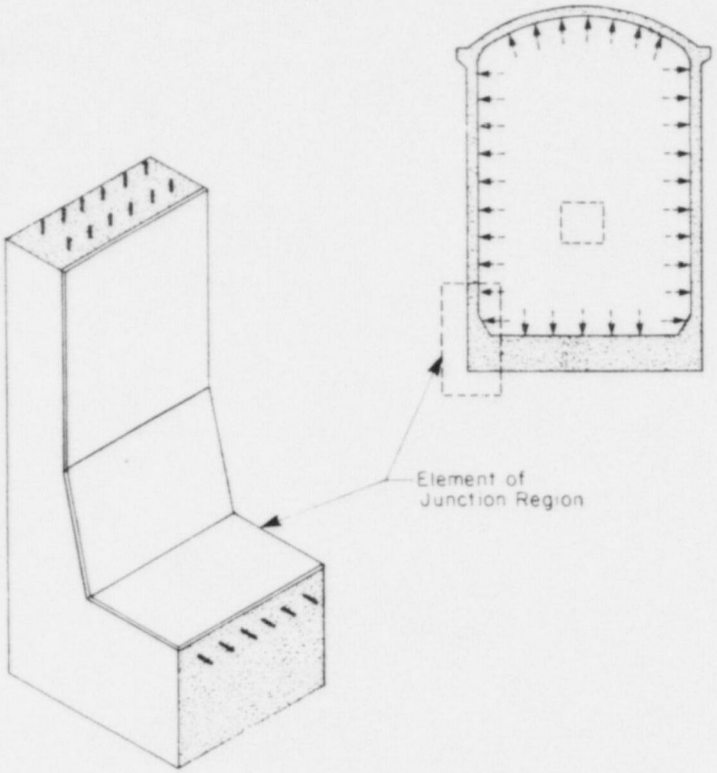
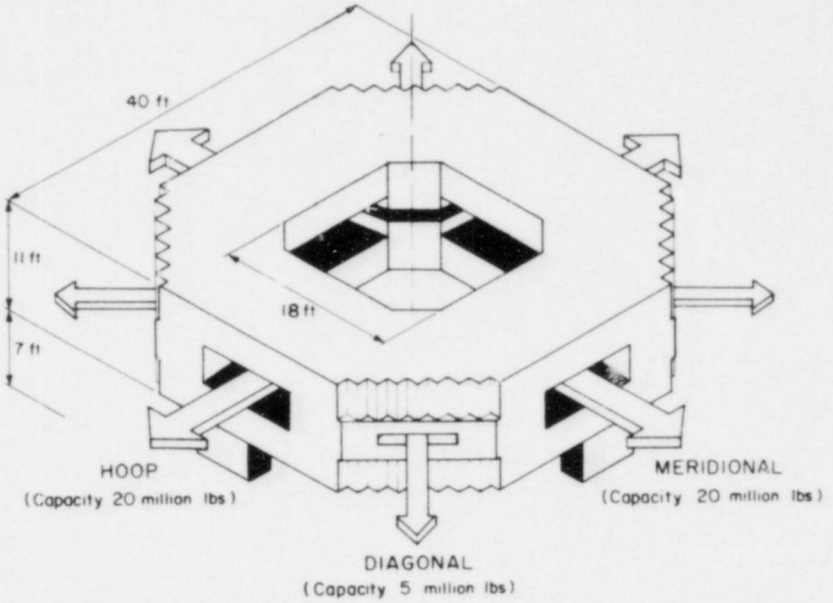


Figure 1. Element of Reactor Containment Building Wall/Basemat Intersection



Metric Equivalents
1lb = 4.448 N
1ft = 0.305 m

Figure 2. Dimensions of Multi-Axial Test Fixture

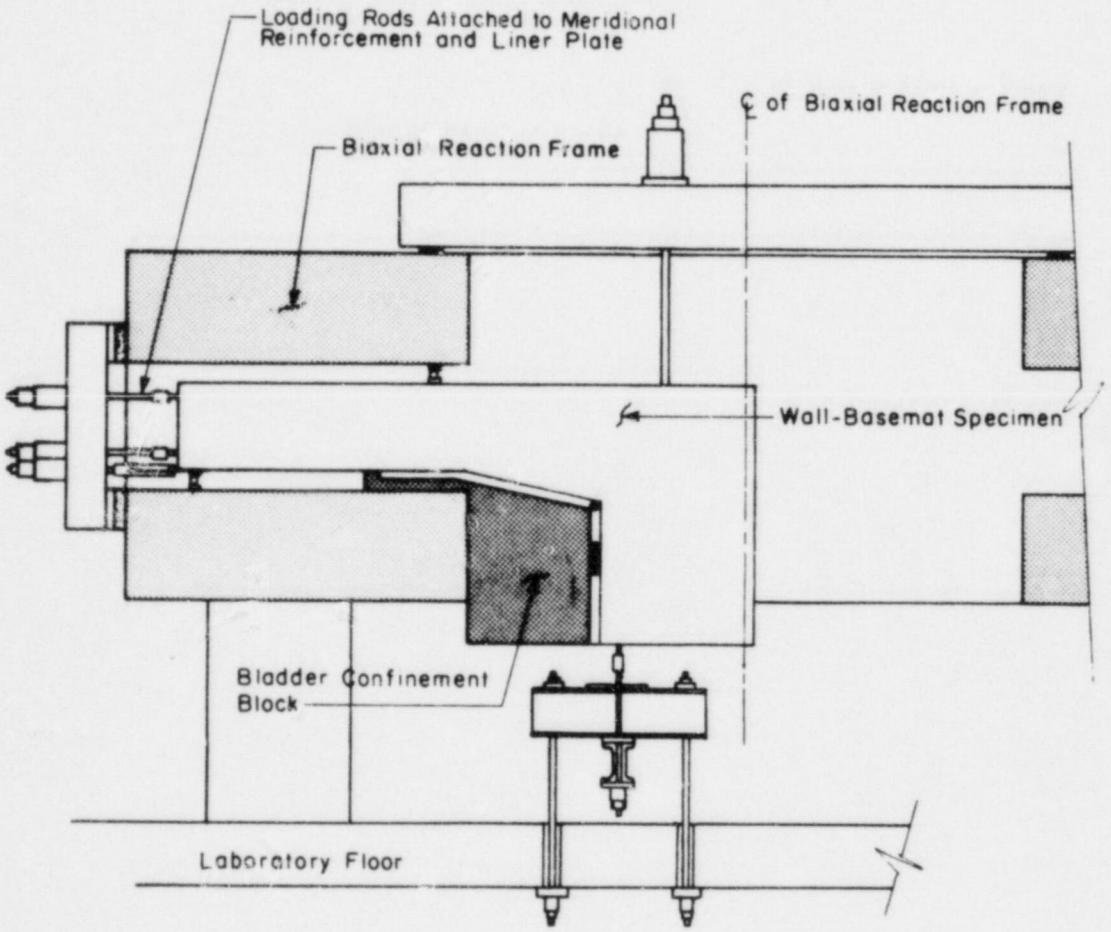


Figure 3. Test Setup for Wall/Basemat Specimen

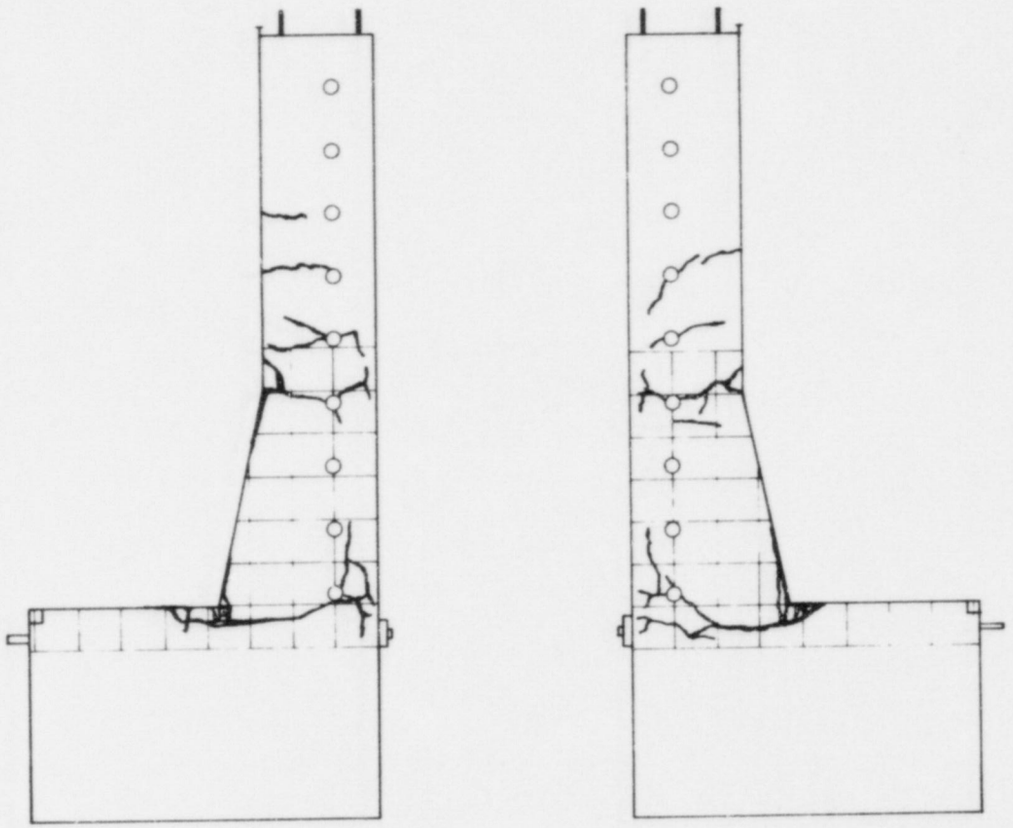


Figure 4. Cracking Patterns after Maximum Load

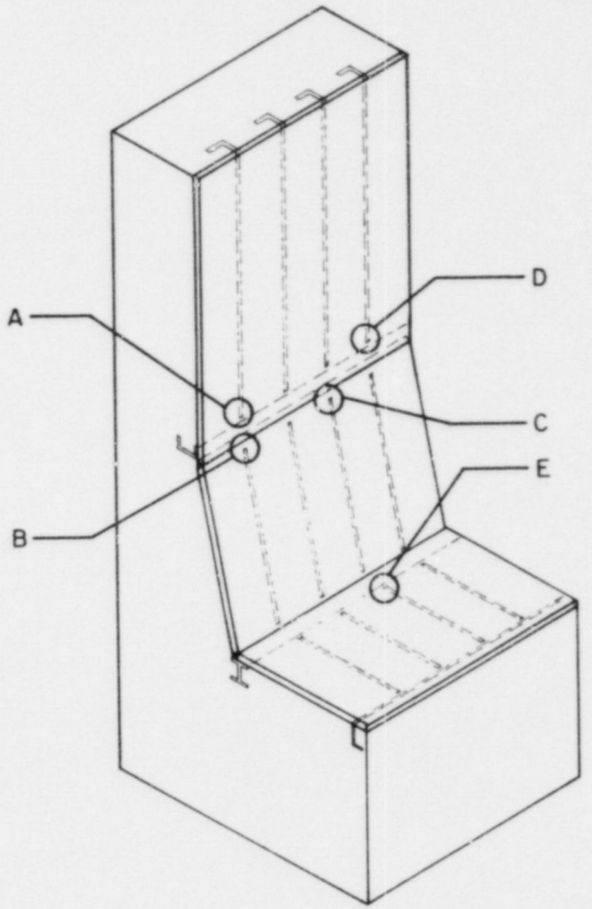
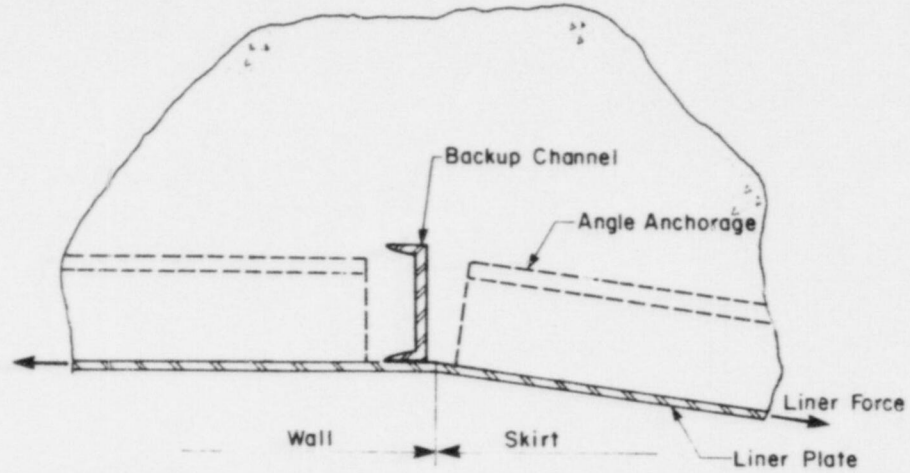
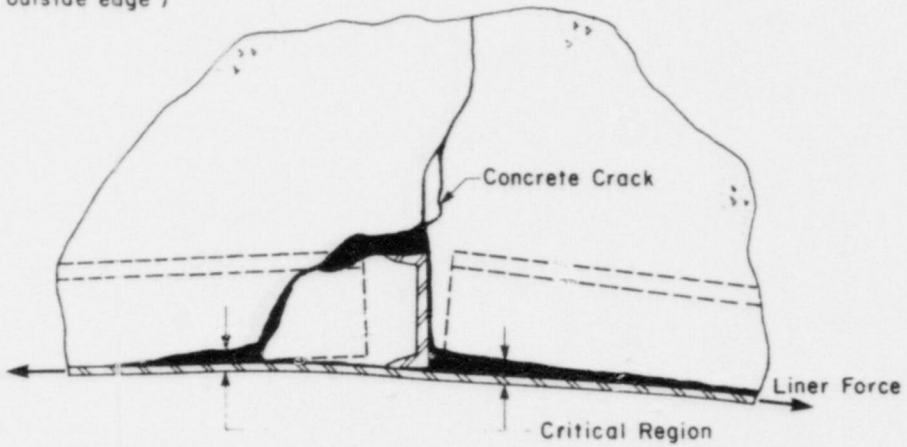


Figure 5. Liner Plate Tear Locations

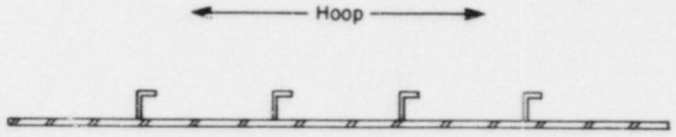


Before Testing
(at outside edge)

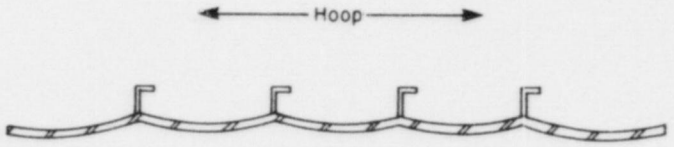


After Test
(at outside edge)

Figure 6. Detail of Skirt/Wall Region



Before Testing



After Testing

Figure 7. Liner Plate Displacement Sketch

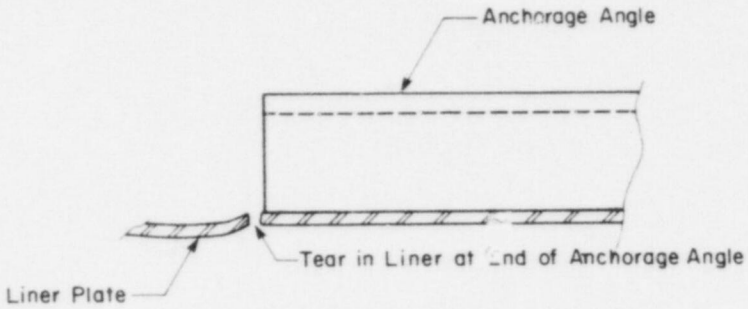


Figure 8. Tearing of Liner Plate and Anchorage Angle

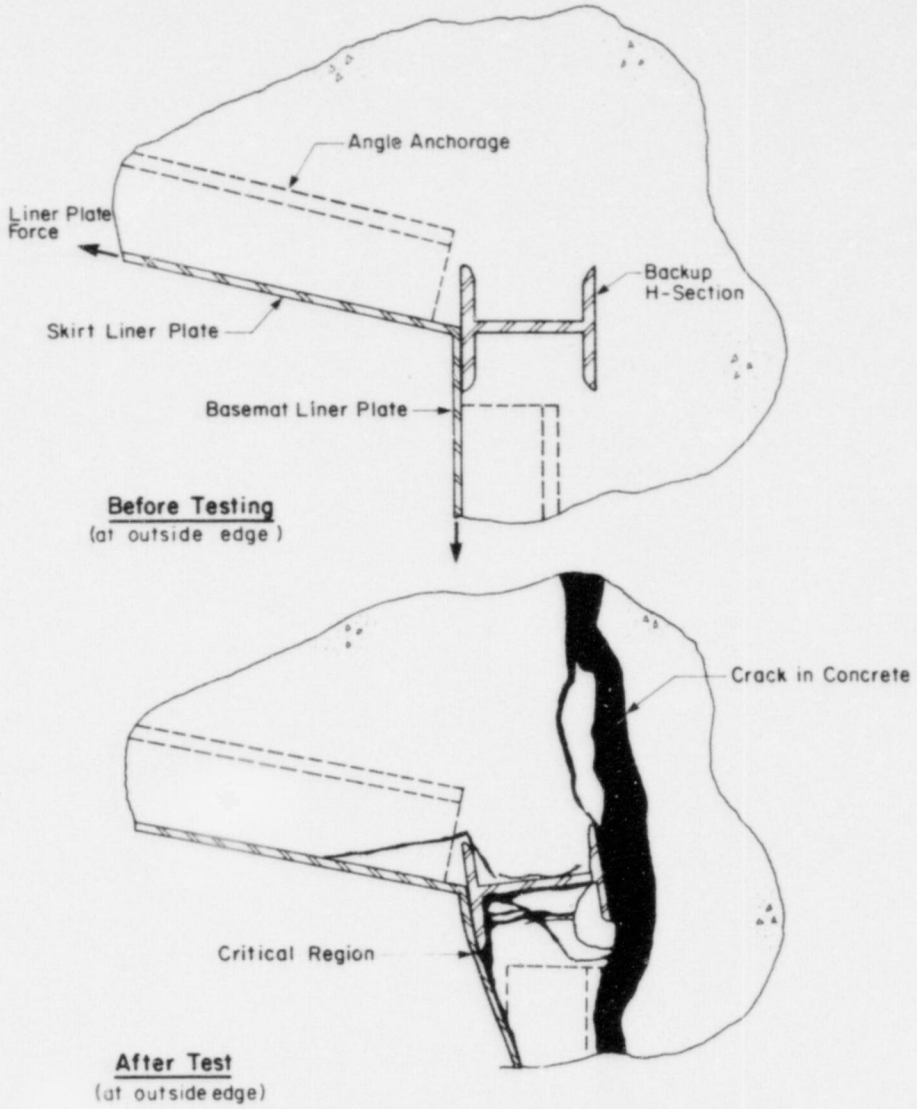
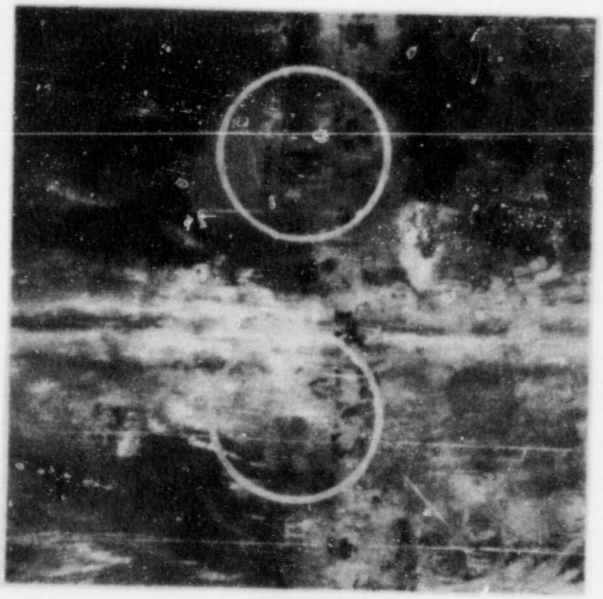


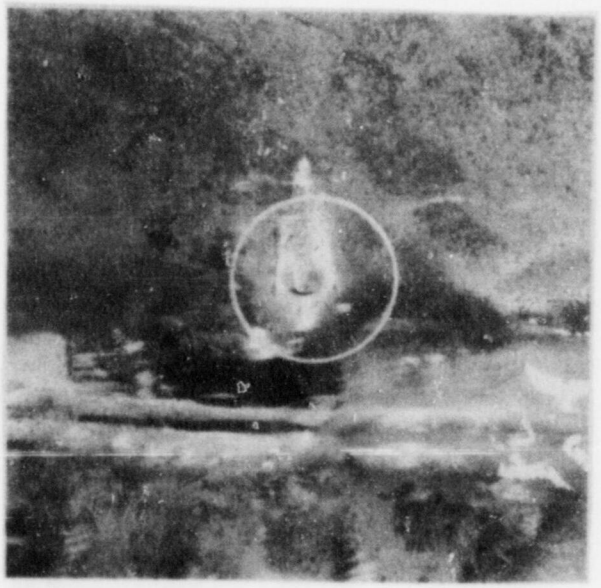
Figure 9. Detail of Skirt/Basemat Region



A and B



C



D



E

Figure 10. Liner Plate Tears

ANALYTICAL CORRELATION AND INTERPRETATION OF FULL SCALE CONTAINMENT SPECIMEN TESTS

R. A. Dameron, R. S. Dunham and Y. R. Rashid
ANATECH International Corporation
La Jolla, California

H. T. Tang
Electric Power Research Institute
Palo Alto, California

ABSTRACT

The work presented in this paper is part of an EPRI-sponsored research program to develop experimentally verified methodology for predicting failure modes and leakage characteristics of concrete containments. This paper deals specifically with recent results of the analytical correlation and interpretation of full scale specimen tests. Computational models of specimens are described, and pre-test and post-test analysis results are presented. The importance of local effects is discussed, and the role of specimen tests and analyses in failure prediction of containment structures is summarized.

1.0 INTRODUCTION

Ultimate load behavior of containment structures has been the object of considerable research in recent years by EPRI, NRC and industry groups. EPRI's program [1] is both analytical and experimental in which the major objective is to develop an experimentally-verified comprehensive methodology for realistic evaluation of the overpressure behavior of concrete containments. The experimental program includes full-scale structural specimen tests of special regions of the containment where high failure potential exists. The analytical program includes the development of appropriate concrete constitutive models which describe the nonlinear behavior of plain concrete as well as the interaction between the concrete, liner and reinforcement bars. In addition, the program addresses the development of geometric modeling techniques for concrete containment structures within the capabilities of the general purpose finite element code ABAQUS-EPGEN [2], considering global as well as local analysis requirements.

In the experimental program, which is described elsewhere in this workshop, full size specimens representing sections of prestressed and reinforced containment structures have been tested under loading conditions similar to those postulated for typical containments. The design of these specimens and the test loading simulation are optimized by analysis. Pre-test analyses are performed to calculate the expected response of the specimens and to identify possible liner

rupture locations. These analyses are also used to guide the positioning and distribution of strain gauges and to monitor the conduct of the test.

Some evidence from the experimental literature [3], supported by special local effects analyses [4], supports the postulate that leakage rather than catastrophic burst is the most likely failure mode of concrete containments. Increased understanding of this failure behavior is sought in full scale specimen tests, discussed in this paper, which include a specimen representing the skirt/wall-base mat juncture of a prestressed containment, a specimen containing a flawed liner, and a steampipe penetration specimen. In the skirt/wall-base mat specimen, the measured liner strains at the knee exceeded 4% in some gauges compared to a far-field average strain of less than yield. Liner rupture was indicated by a few of the gauges that were monitored during the test and were later verified by inspection at the conclusion of the test. The pre-test analysis of this specimen shows a similar trend with the same order of magnitude of strain concentration between the local strain at the knee and the liner average strain in the wall section. Better comparisons were obtained in the post-test analysis where the test loading history was matched and the finite element grid was refined. The data from the flawed liner specimen test, which includes crack opening displacements and crack growth data, is used in conjunction with analysis to develop liner rupture and containment depressurization criteria. The analytical/experimental correlations appear to be highly encouraging for the development of these criteria. This aspect of the experiment notwithstanding, the analytical interpretation of the test results show conclusive evidence of the constraining effects of the concrete and the reinforcement on the crack growth in the liner. The implication of these results is that liner rupture in a containment would grow in a stable manner under the action of increasing load only, thus bounding the leakage rate to the minimum rate required to depressurize the containment. The penetration specimen showed rupture under the combined effects of in-plane stretch and bending due to outward shear force. A local effects analysis of the specimen confirm these results with the added information that the bending contribution was dominant and was the primary cause of liner rupture. Another penetration test is planned with inward punch shear force, and some pre-test analysis results are presented.

2.0 MATERIAL MODELING

The present state of the art in modeling and analysis of reinforced concrete structures treats the plain concrete and steel reinforcement as two separate materials joined together as fully bonded structural elements. The plain concrete model accounts for compressive plasticity and tensile cracking (i.e., smeared over the integration points) with post-cracking tension stiffening and shear retention. Reinforcement is treated as simple tension-compression elastic-plastic structural elements. This type of modeling is suitable for design calculations and global analyses whose objective is to predict the ultimate strength of these structures. However, it is not adequate for

the treatment of important local effects, such as liner-concrete and rebar-concrete debonding and discrete cracking, which must be properly modeled in order to predict modes of failure and failure sequences of these structures.

As part of EPRI's overall research program [1], the general purpose nonlinear finite element code ABAQUS-EPGEN [2,4] has been developed with special attention given to incorporating and verifying realistic concrete constitutive models [5]. This code was used for all of the analyses presented herein. The implementation of the concrete constitutive model in ABAQUS-EPGEN was accomplished through the UMAT subroutine, which is a user-coded material model. The UMAT subroutine was also used to define the behavior of interface elements between liner and concrete and rebar and concrete.

3.0 SKIRT/WALL-BASE MAT SPECIMEN

The skirt/wall-base mat specimen, sometimes referred to as the dislocation specimen, is an L-shaped specimen designed to simulate the discontinuity in the wall/base mat juncture of a prestressed containment. As shown in Figure 3-1, it consists of three regions: a wall region, a skirt region, and a base mat region. At the wall/skirt and skirt/base mat junctures, the anchorage angles are interrupted. A channel and a wide flange section are welded to the liner in the hoop direction of the wall/skirt and skirt/base mat junctures, respectively, as stiffeners. Instrumentation of the specimen includes linear potentiometers to measure deformations and strain gages on the liner plate and on meridional rebars. The choice of the specimen geometry and discontinuity location was influenced by a previous containment global analysis (both prestressed and reinforced) [6] which showed that local shear and bending would cause high strain concentrations in the liner. The planned specimen loading was a uniform pressure (P_a) on the inner surface of the skirt and the 12" region above the knee, a uniform pressure (P_b) on the inner surface of the base mat and a tensile load (T) on the radial bars of the base mat, as illustrated in Figure 3-2. This configuration was applied in the pre-test analysis. Early test attempts showed difficulties with the P_b pressure bladder; since this was of secondary importance to P_a, P_b was replaced with two rubber reaction pads. The rebar and liner loads were adjusted during the test to develop the bending moment at the knee calculated in the pre-test analysis. This scenario was applied in the post-test analysis. A plane stress simulation of the specimen was used in the pre- and post-test analyses. The finite element grids are shown in Figure 3-3. The liner was modeled with 2-node beam elements (B21) in the pre-test analysis, but at the wall-skirt knee this was refined to 8-node continuum elements for the post-test analysis.

The remaining figures in this section show pre- and post-test analysis results. Figure 3-4 shows the deformed outline and principal strain contours from the pre-test analysis. Figure 3-5 shows the pre-test liner strain histories at the wall-skirt juncture (knee) and the skirt-base mat juncture and should be viewed with Figure 3-6

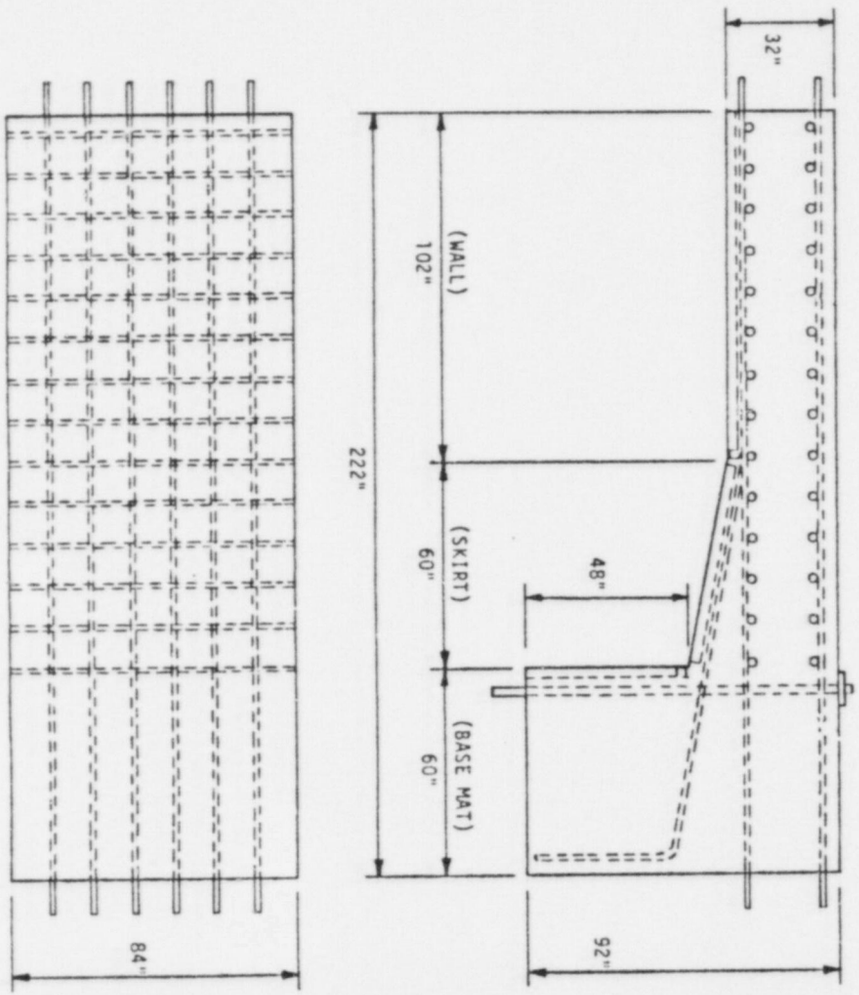


Figure 3-1
Dislocation Specimen Geometry

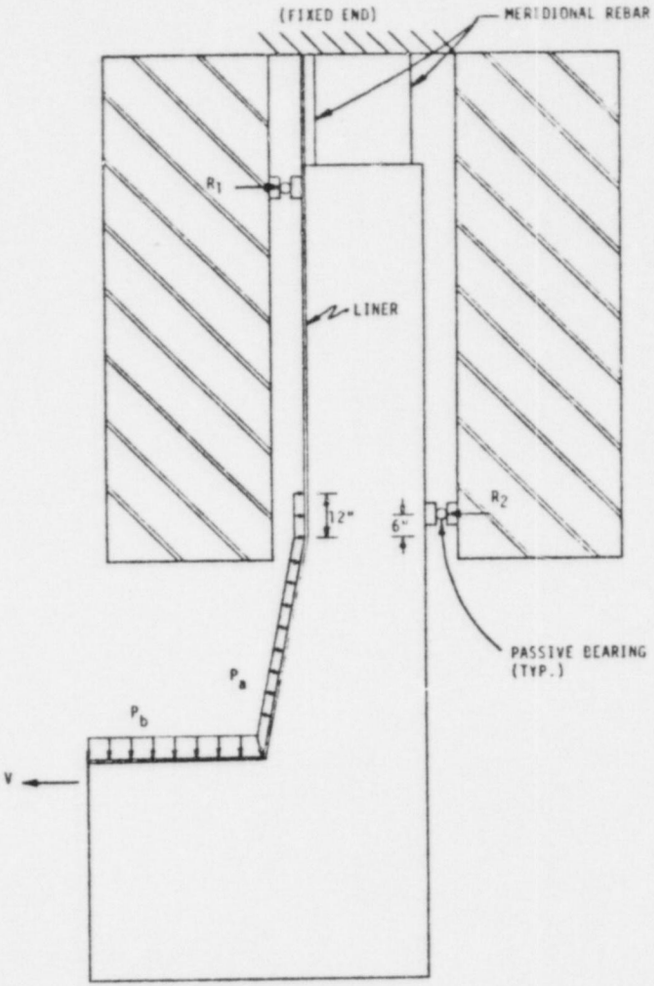


Figure 3-2
Dislocation Specimen Loading
Used in Pre-Test Analysis

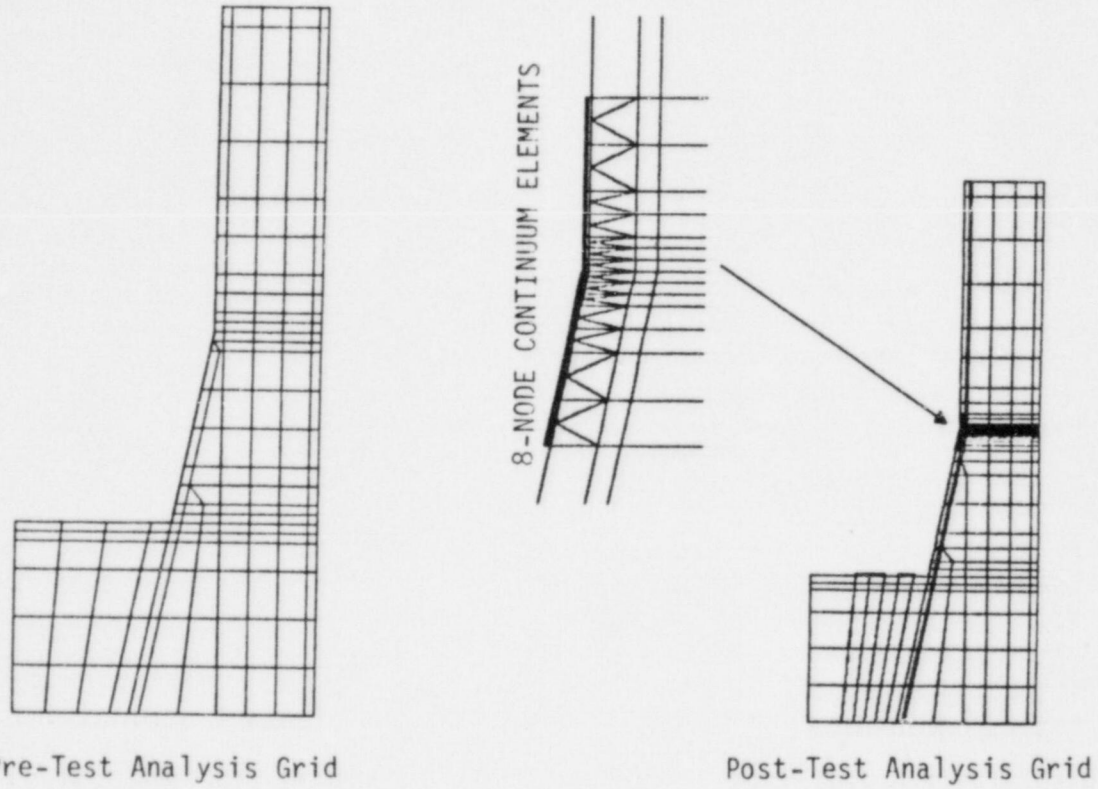


Figure 3-3. Dislocation Specimen Computational Grid

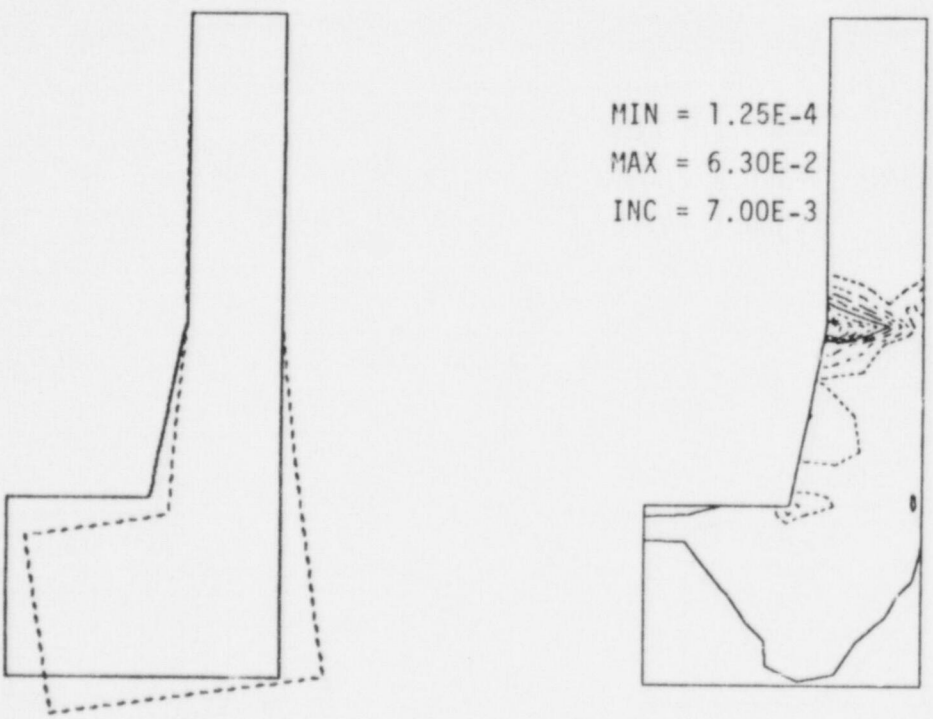


Figure 3-4. Deformed Outline and Principal Strain Contours from Pre-Test Analysis P_a=52.5 psi, P_b=310 psi

which displays similar information from the post-test analysis. As can be observed from Figures 3-5 and 3-6, the calculated liner strain in the pre-test model is significantly higher than the post-test model. This is attributed to the liner debonding which is simulated in the post-test analysis through the use of special interface elements but was not represented in the pre-test model. Nonetheless, significant strain concentration is in evidence in both analyses. Another difference between the pre-test and post-test results represented in Figures 3-5 and 3-6 is the large bending component that is present in the latter in comparison with the pre-test results shown in Figure 3-5. This could be partly due to the fact that beam elements, which are capable only of linear strain across the element, were used in the pre-test analysis versus two layers of 8-node continuum elements in the post-test analysis. As these figures demonstrate, the pre-test analysis was useful for pointing out qualitative specimen behavior and helping establish the conduct of the test.

Figure 3-7 shows the pressure side liner strain profile traversing from the left side of the base mat to the top of the specimen at the end of the post-test analysis. The skirt/base mat and wall/skirt junctures are located at approximately x=50 inches and x=110 inches, respectively. This figure clearly illustrates the strain concentration in the two juncture regions, especially at the knee. The analysis and experiment show strains at the knee of over 3%, whereas the far-field average strain is less than yield. The specimen liner was actually ruptured in places. This demonstrates the importance of the role of liner-concrete interaction. Without concrete backing and the mechanical bond of the liner to the concrete, it is clear that the liner would strain over a broader area, and strain concentrations of this magnitude would not be seen. An added benefit of the experimental results is in verifying the ABAQUS-EPGEN/UMAT analysis methodology. A strain history comparison between an analysis integration point just below the knee and a specimen high elongation strain gage located at the knee near a rupture location is shown in Figure 3-8. Other comparisons, not reported here for lack of space, show fair to good agreements [7].

4.0 LEAK RATE SPECIMEN

The purpose of the leak rate specimen was to measure the progression of leak rate through a monotonically loaded test model of a containment wall section with a flawed liner. The leak rate measurements were not sufficiently detailed to be used as a basis for analytical evaluation of pressure release through cracks. However, strains were measured near the liner flaw and the test proved to be useful in studying liner crack propagation, especially as crack growth is influenced by liner-concrete interaction. A pre-test analysis was carried out which demonstrated that strain concentrations would develop at the flaw tip and that the planned loading would be sufficient to propagate the crack.

The leak rate specimen is an 84"x84"x42" concrete slab with a 1/4" thick steel liner plate on one side of the slab. The liner plate has

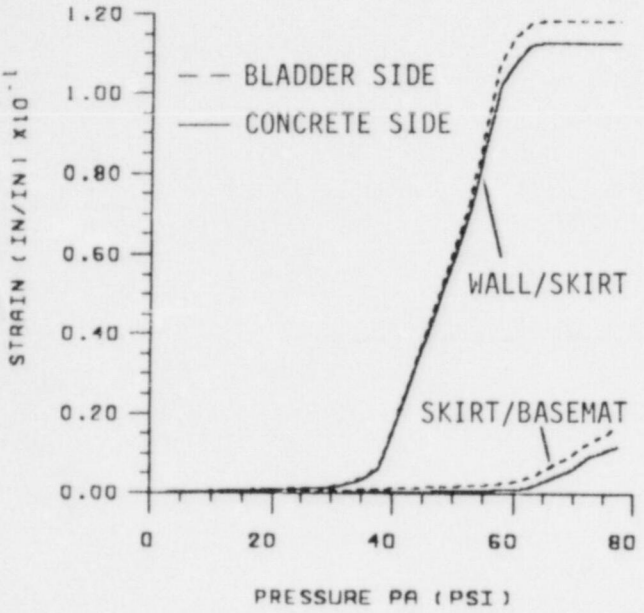


Figure 3-5
Pre-Test Liner Strains

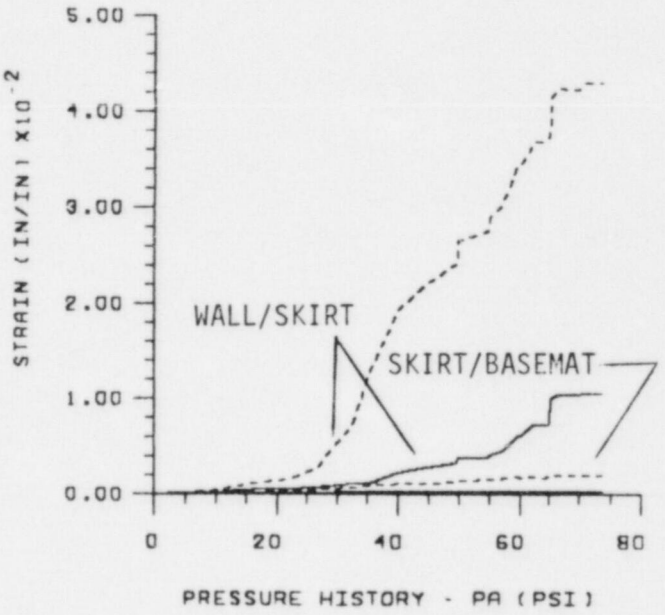


Figure 3-6
Post-Test Liner Strains

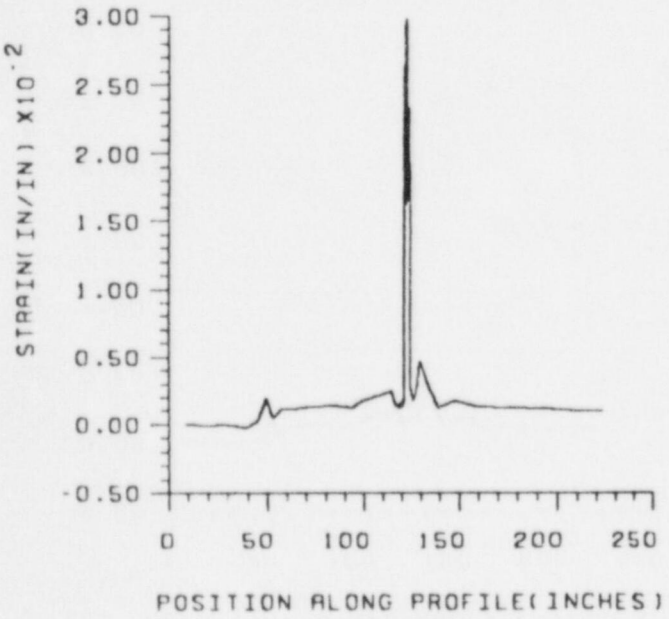


Figure 3-7
Post-Test Principal Liner Strain Profile

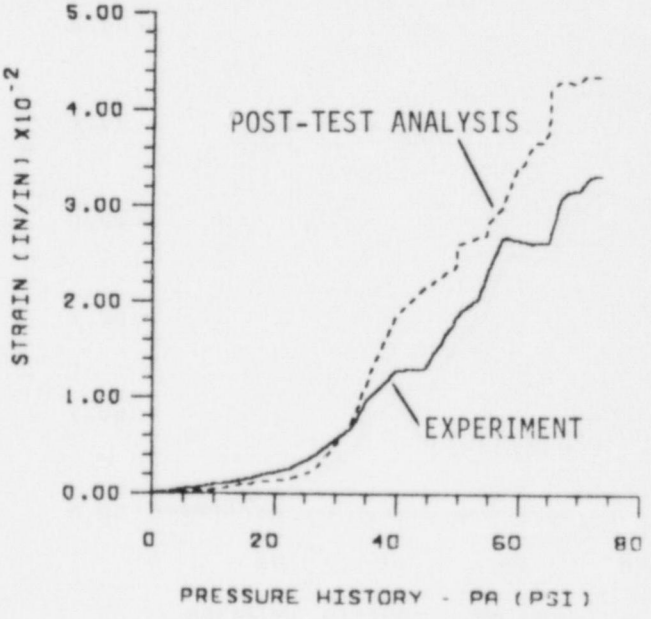


Figure 3-8
Strain History Comparison at Liner Rupture near the Knee

a welded seam oriented meridionally along the center line. To form a controlled leak path, the middle 6" was not welded. Typical reinforcement and liner anchorage details were used. Precise crack growth simulation for this test specimen was not possible because experimentally verified material property data for ductile tearing of liner material was not available. Instead, the test crack growth measurements were utilized in an analysis of the limiting case of an unsupported liner to help quantify the effect of liner-concrete interaction in the test and ultimately in containment structures in general.

A two-dimensional finite element grid with quarter-symmetry was developed to model the specimen liner plate near the flaw. Roller boundary conditions were used at the symmetry boundaries, except at the flaw. The instrumentation used in the test consisted of crack width gages across the pre-existing flaw, crack tip gages located at 0", 1", 3" and 9" from the flaw tip, rebar gages, and linear potentiometers to measure global strains across the specimen to monitor and drive the test. Test results showed that when the specimen was loaded out to large strains (global hoop strain of 1.6%) the liner crack grew in a stable manner. In fact, late in the test, the crack actually stopped growing, but it is not known when the crack arrest occurred relative to the maximum applied load.

The test global strains and measured crack widths were used to drive the post-test analysis. It was hoped that a satisfactory crack propagation scheme could be developed using a J-integral approach with the ABAQUS-EPGEN code so that the tearing of a liner plate without concrete could be compared to the tearing in the test specimen. However, attempts to correlate this technique with existing crack test literature [8] were not successful because of insufficient information on fracture data and test conditions. Consequently, an analysis approach was developed to force the tearing in a liner plate without concrete backing to match the tearing in the specimen and examine the calculated strain field to assess the effects of concrete backing. Displacement boundary conditions were applied in the analysis to reproduce the test global strain measurements. Also, using the experimental data, the roller boundary conditions at the crack tip were removed one at a time in the analysis at appropriate load levels to simulate crack growth as described below.

The experiment gages located at 0", 1" and 3" from the flaw tip are critical to the test and the analysis. The 0" gage broke at load step 15, indicating initial crack extension, and the 1" gage broke just after load step 35. Assuming that the crack tip strains at load steps 15 and 35 are equal, and assuming further that the crack extension rate is proportional to the loading rate, it is possible to carry out crack growth analysis without the use of fracture property data. Using this approach, crack propagation history analysis was carried out by releasing the boundary conditions incrementally to simulate the crack travelling 1" in 20 load steps (1/4" every 5 load steps). Figure 4-1 shows the calculated crack width history compared with the experiment. This figure shows that using this method gave very good simulation of the crack travel and width behavior.

Figures 4-2, 4-3 and 4-4 show the strain profile comparisons at three selected points in the load history. The curves marked with squares represent the analysis, and the unmarked curves represent the experiment. X=0 is at the right hand tip of the original flaw, and the experimental data points are at X=0", 1", 3" and 9", except that after load step 15 the gage at X=0 was not functioning. Figure 4-2 shows that just before the crack tip starts to move, the strain field for a liner plate without concrete interaction (analysis) and the strain field for a liner plate with concrete interaction (experiment) are of the same order of magnitude. Strain at X=0 is about 6% for the experiment and 4% for the analysis. As the crack propagates approximately 1" in 20 load steps (see remaining plots in Figures 4-3 and 4-4), the strain field without concrete interaction becomes unrealistically large, whereas the strain field with concrete interaction remains small with the strain concentration confined to a small area around the crack tip. At 1" from the original crack tip, experimental strains were 0.25%, 0.9%, and 8% at load steps 15, 20, and 35, respectively. Corresponding analytical strains without concrete interaction were 0.5%, 8%, and 85%. It is concluded that at these large strains a liner plate without concrete backing would tear much further under the same load. There was no need to continue the analysis after the crack travelled 1" because the results were already illustrative.

The calculated crack shape at selected load steps is plotted in Figure 4-5. The curve at load step 35 is compared to the experimental post-test crack shape in Figure 4-6. The experimental crack shape is a magnified portion of a photograph provided by CTL, which was taken after all loads were removed, whereas the analytical crack shape includes the elastic component of crack width. This partially accounts for the difference in magnitude in the two curves. It should be stated, however, that the value of this comparison is in demonstrating that the shape of the experimental and analytical cracks are in close agreement. Both show similar blunting up to a crack extension of 0.75" for the experiment and 1.0" for the analysis. The crack probably reached this stage at approximately load step 35, verified by the second gage located 1" from the crack tip, which broke soon after load step 35.

The results of the leak rate test and post-test analysis show that the presence of concrete backing mechanically bonded to liner plate (by means of embedded angles, or welded studs) greatly affects the behavior of a flawed liner. As the load is increased, with the presence of concrete backing, crack growth is stable and seems to be bounded. The concrete confines the strain field near the crack tip, but if the concrete interaction is removed, the strain near the crack tip is more diffused which promotes unstable crack growth. This strongly supports the "leak-before-burst" hypothesis. More specifically, in the context of this analysis, this hypothesis can be restated: a liner plate which develops local failure will tear in a stable manner under increasing load; consequently, this tear will reduce the containment pressure through leakage, and the crack will arrest without catastrophic failure.

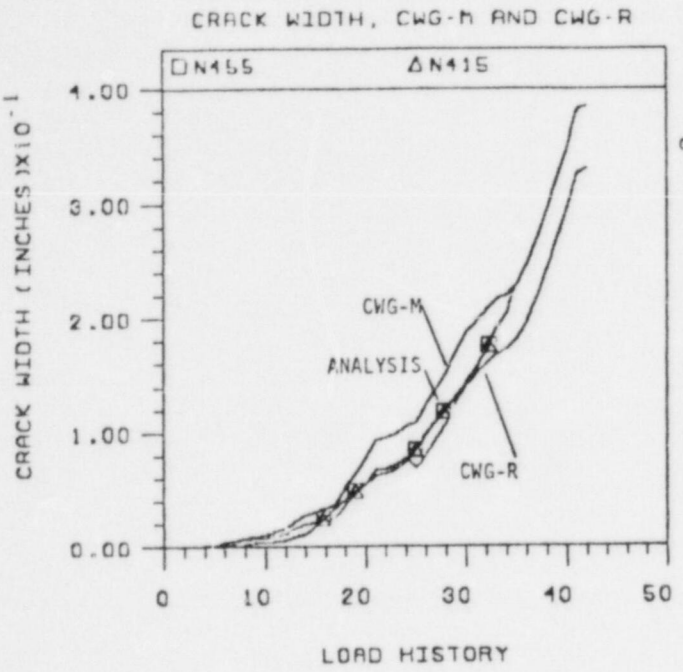


Figure 4-1
Leak Rate Test Crack Width Comparisons

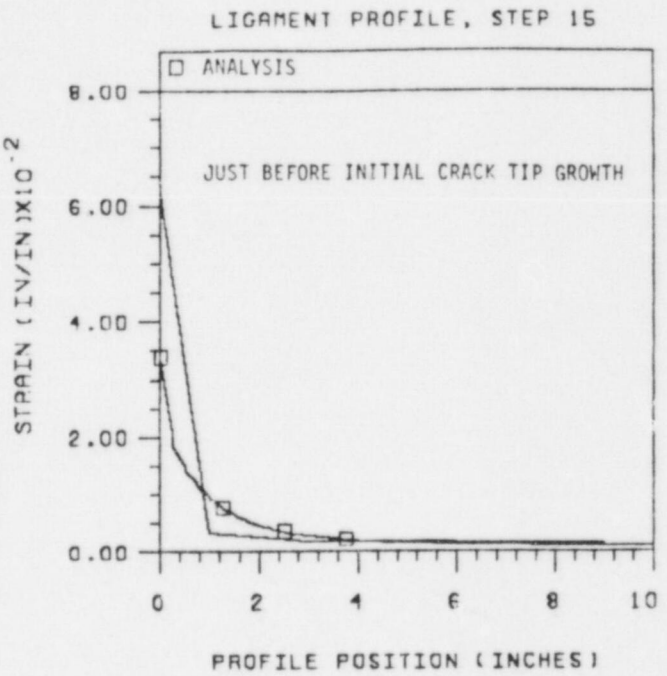


Figure 4-2
Strain Profile Comparison at Load Step 15

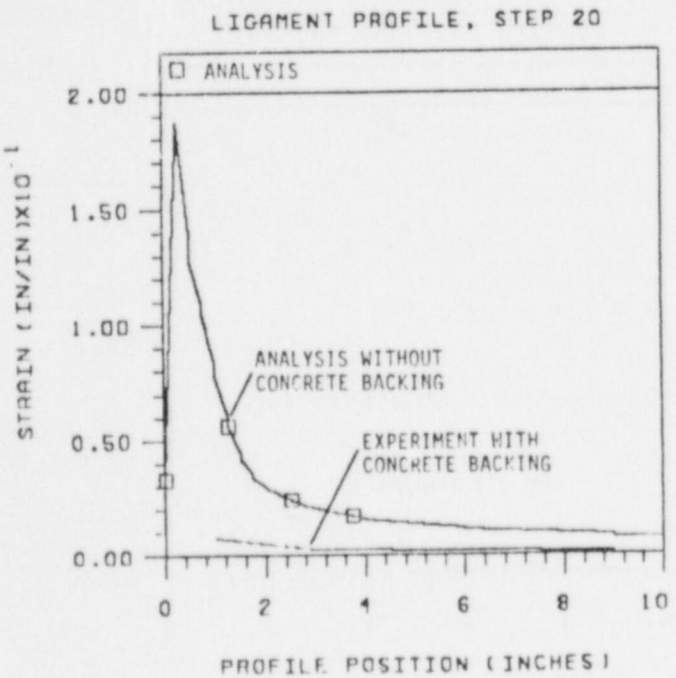


Figure 4-3
Strain Profile Comparison at Load Step 20

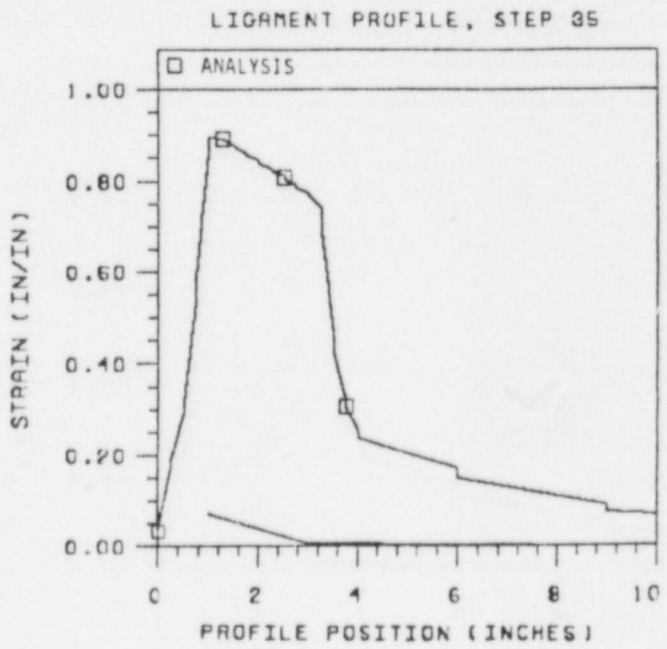


Figure 4-4
Strain Profile Comparison at Load Step 35

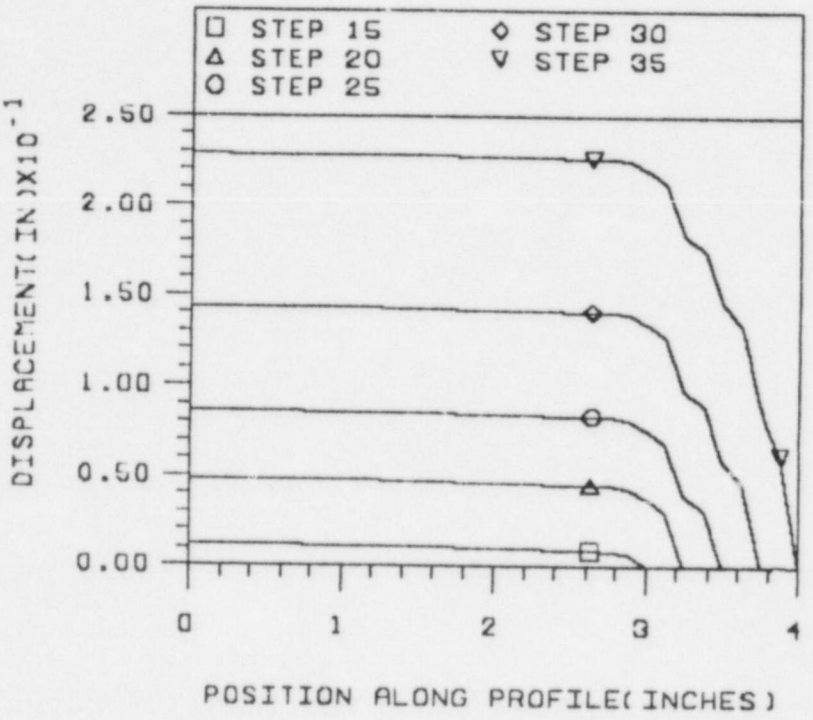


Figure 4-5. Leak Rate Test Crack Shape

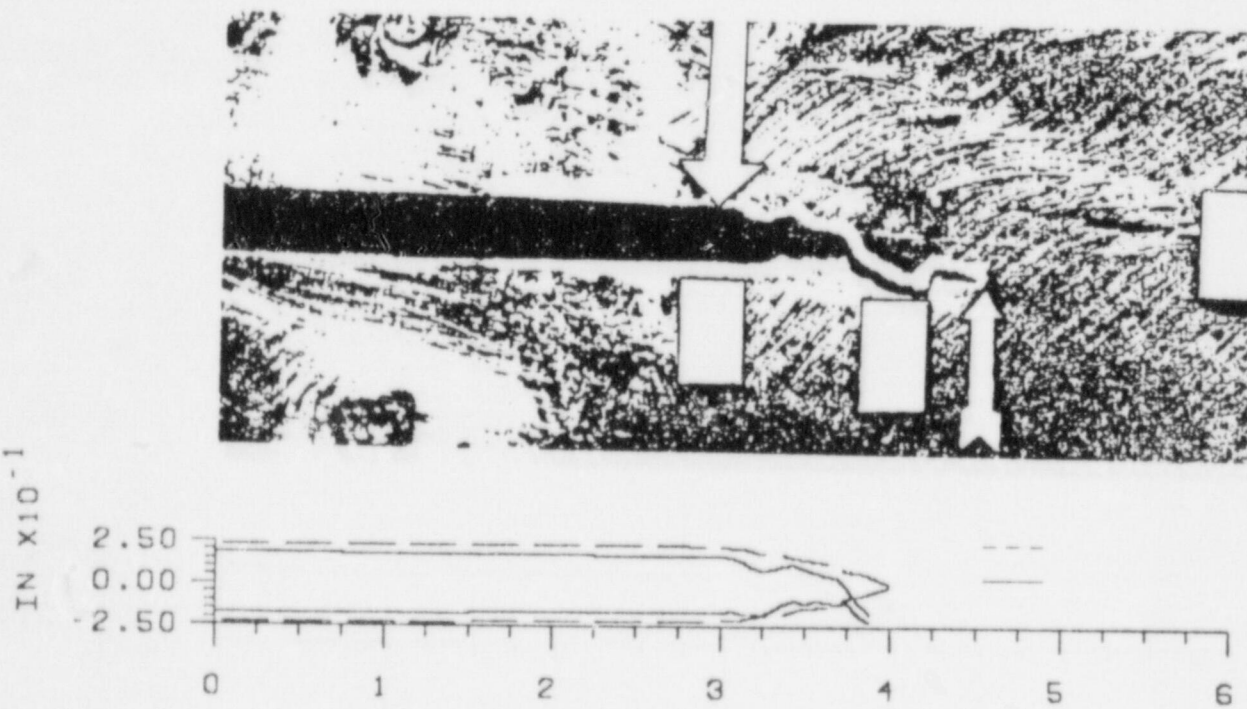


Figure 4-6. Crack Shape Comparison

5.0 PIPE PENETRATION EFFECTS

Another local region of liner stress concentration is near a containment pipe penetration, especially when the pipe is built into a nearby wall or otherwise restrained against axial motion. It is easy to find the level of stress concentration for a liner plate with an unreinforced circular hole. However, penetrations typically found in containment structures (e.g. steam pipe penetrations) consist of a thick steel cylinder welded to the liner plate and anchored to the concrete, which creates a stiff inclusion in the structure, thereby creating a complex three-dimensional stress state at the liner/cylinder juncture. An in-plane strain state due to internal pressure, which by itself may not be sufficient to cause liner rupture, could result in liner failure when combined with local bending due to radial punching load. The first penetration test specimen for a prestressed containment was tested with outward punching load, which is not the direction of expected punch shear force created by a rigidly held steam pipe. However, the test data is applicable for studying liner stretching plus bending, and it also simulates the form of shear dislocation present when a pipe penetration is allowed to expand. A reinforced containment specimen with large inward punch shear load is planned.

Detailed analyses were not carried out for the first specimen test. However, a quick post-test analysis of just the liner plate/pipe penetration juncture coupled with the test results verified that liner rupture was initiated on the concrete side at the juncture at a relatively low punch shear load. The axisymmetric grid for this analysis is shown in Figure 5-1, representing the 45° line of the specimen. Before any punch shear load was applied, the liner was stretched to 1.5% global strain. At this point the strain profile across section A-A was constant at 1.5%. After 90 kips of punch shear was applied, only 10% of the total test load, the strain profile across A-A was quite different as shown in Figure 5-2. Highly localized bending caused strain at the concrete side to reach 4.6%, while on the bottom, the net strain after the occurrence of compressive bending was around 0.5%. Many small load increments were applied in the analysis, and after a punch shear of 200 kips, the concrete side liner strain reached 60% (Figure 5-3), well over the ductility of the material. From this it is hypothesized that the crack propagated through the specimen at about 600 kips, but because the region was very tightly confined by the test apparatus, leakage was not detected until the 897 kip load step.

In preparation for the upcoming reinforced containment specimen test with inward shear loading, and as part of the overall containment research program, several two-dimensional analyses have been studied. Early results showed that the failure driving mechanism was always the interaction between the local punch shear near the pipe penetration and the global stretching of the containment shell. Analyzing the specimen alone did not provide much insight because, without the proper global stretching, the specimen was very stiff and capable of withstanding shear loads larger than the capability of the testing

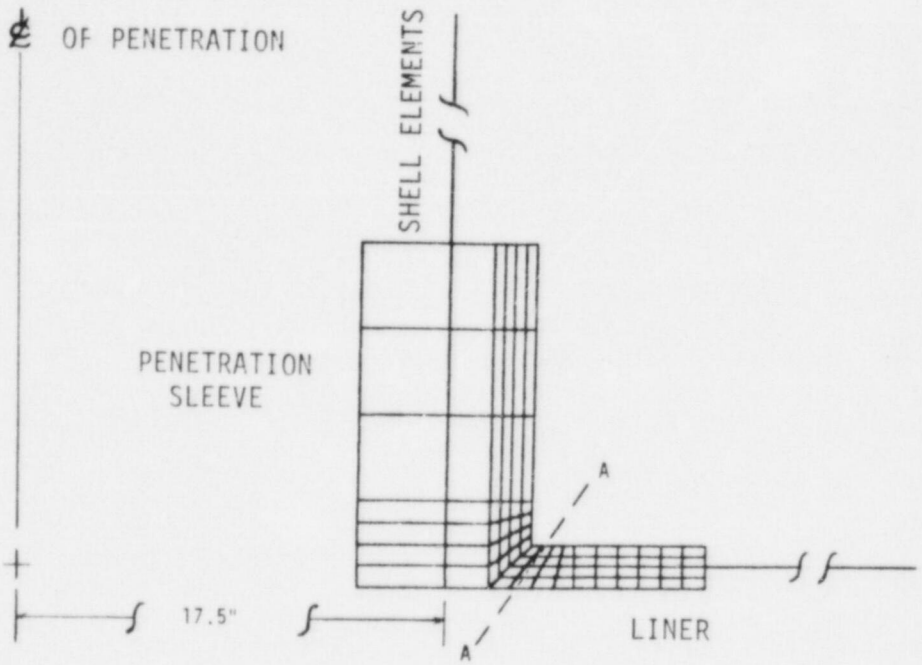


Figure 5-1
Penetration Sleeve/Liner Plate Model
for Specimen with Outward Punch Shear

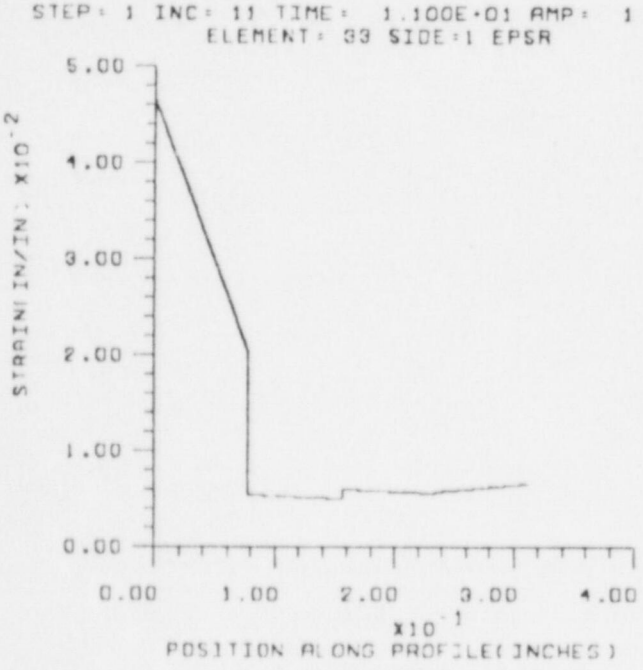


Figure 5-2
Strain Profile Across Section A-A
Shear Load = 100 kips

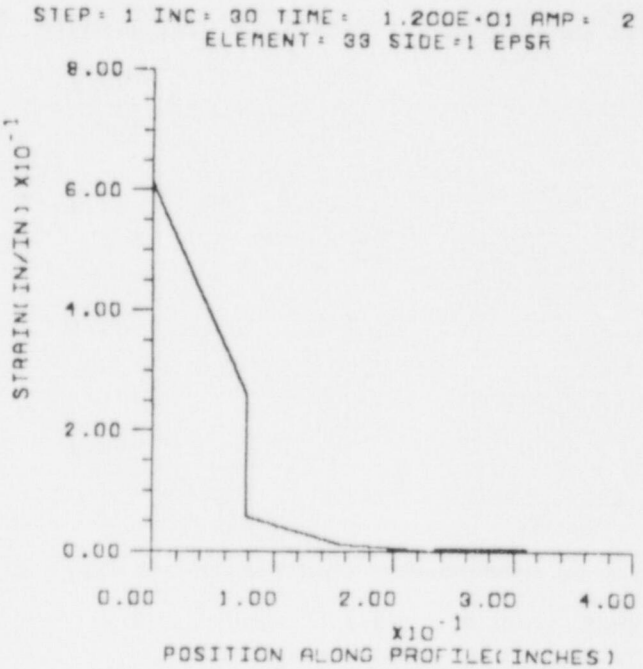


Figure 5-3
Strain Profile Across Section A-A
Shear Load = 200 kips

apparatus. Consequently, an axisymmetric 90° spherical model was developed with twice the radius of a prototypical containment on the premise that for the cylindrical portion of a containment of radius r

$$\sigma_{hoop} = \frac{pr}{t}$$

and for a sphere of radius 2r

$$\sigma_{hoop} = \sigma_{meridional} = \frac{P(2r)}{2t} = \frac{pr}{t}$$

The spherical model exhibits the same overall resistance to outward expansion as the hoop resistance in the prototype. The spherical models were run for three purposes: first, to investigate the limiting case of a containment with a rigidly constrained pipe penetration; second, to investigate the opposite limiting case of a containment without pipe constraints; and third, to develop the loading history to be used to drive the penetration experiment. The computational grids used have the same material and geometry parameters as the upcoming test specimen, except the shell thickness was increased to 54" and outer rebar layers were added to more closely approximate a prototypical containment structure.

Results of the first analysis (see Figure 5-4) for the limiting case of an unconstrained penetration showed that premature liner failure at low pressures did not occur, but because of the stiffness discontinuity due to the penetration reinforcement, the shell was forced into a more complex deformation mode. In fact at 85 psi, bending in the reverse direction was exhibited in a manner like that simulated in the first penetration specimen test with outward punch shear. Further study of this behavior is in progress. Results of the second analysis (see deformed shape in Figure 5-5) for the extreme case of a rigidly constrained penetration showed that severe liner bending occurred near the pipe, especially at the transition in thickness from the reinforced liner near the pipe to the global liner thickness. This transition is from 1/2" to 1/4" at a distance of 8" from the pipe. The liner reached a maximum of 3% strain at a pressure of about 50 psi. This represented a far-field global strain in the first 50" from the pipe of only 0.3%. Finally, the prototypical spherical model is being used to develop force histories to be applied to the upcoming specimen test. The specimen loading apparatus is capable of applying different load histories on each of the bottom two layers of rebars and the liner in conjunction with variable punch shear force of up to 3 million pounds. The displacements from the spherical analysis 50" from the pipe and the reaction force history at the pipe restraint are being used as applied displacements and punch load in an ABAQUS analysis of an axisymmetric representation of the specimen. Although results are preliminary, this analysis showed that with this combined loading the deformation behavior of the specimen is similar to the first 50" of containment around the penetration. The reaction forces at the displacement boundary conditions will in turn be used as applied loads in the specimen test, thus simulating the behavior of an actual containment.

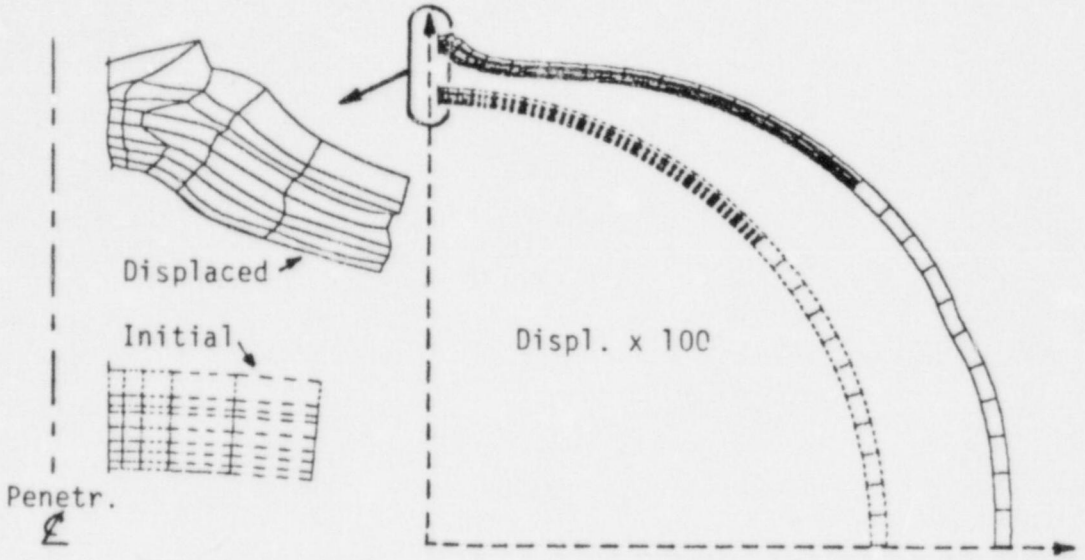


Figure 5-4. Deformed Grid-Unconstrained Case-Spherical Model

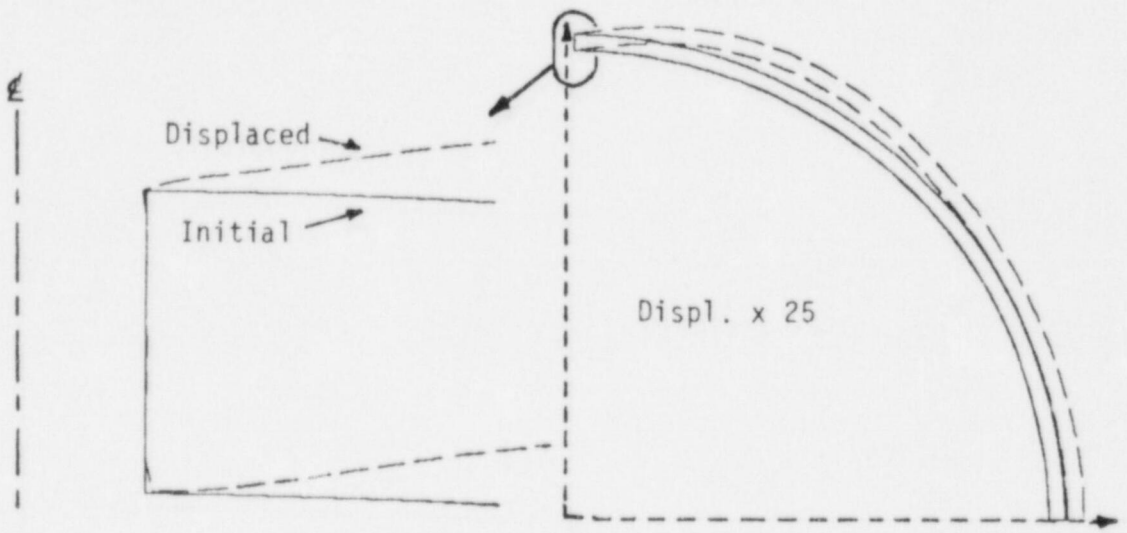


Figure 5-5. Deformed Shape-Constrained Case-Spherical Model

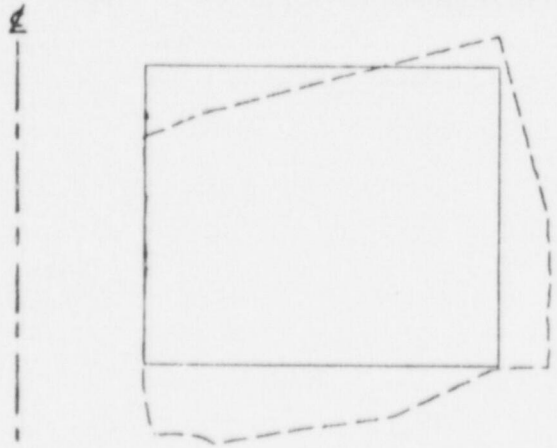


Figure 5-6. Inward Shear Specimen-Displ. x 25

6.0 REFERENCES

1. Tang, Sliter, Tang and Wall, "Overview of EPRI Research in Structural Integrity," Nuclear Engineering and Design, V77, 1984, pp. 207-227.

2. Hibbitt, "ABAQUS-EPGEN - A General Purpose Finite Element Code with Emphasis on Nonlinear Applications," Nuclear Engineering and Design, V77, 1984, pp. 271-298.

3. Conference on Prestressed Concrete Pressure Vessels at Church House, Westminster, S.W.I., March 13-17, 1967, The Institution of Civil Engineers, London, 1968.

4. Dunham, Rashid and Tang, "Recent Results on the Evaluation of the Overpressure Response of Concrete and Steel Containments," Nuclear Engineering and Design, 90, 1985, pp. 193-208.

5. Dunham, Rashid, and Yuan, "Evaluation of Calculational and Material Models for Concrete Containment Structures," Nuclear Engineering and Design, V77, 1984, pp. 393-404.

6. Dunham, Rashid, Yuan and Lu, "Methods for Ultimate Load Analysis of Concrete Containments," ANATECH Interim Report to EPRI, EPRI NP-4046, RP2172-1, June 1985.

7. Dameron, Dunham, James, Lu, Rashid, and Yuan, "Methods for Ultimate Load Analysis of Concrete Containments," ANATECH Interim Report to EPRI, RP2172-1, April 1986, to be published.

8. Zahoor and Abou-Sayed, "Prediction of Stable Crack Growth in Type 304 Stainless Steel," Computers and Structures, V13, 1981, pp. 137-144.

CONSTRUCTION AND ANALYSIS OF A 1/6th-SCALE CONCRETE CONTAINMENT MODEL*

D. S. Horschel and J. Jung
Sandia National Laboratories
Albuquerque, New Mexico 87185, U.S.A.

ABSTRACT

This paper discusses the features and preliminary analysis of a 1/6th-scale reinforced concrete containment model, which is being constructed at Sandia National Laboratories (SNL) in Albuquerque, New Mexico. The model LWR containment building was designed and is being built to the ASME code by United Engineers and Constructors Inc. The containment model will be tested to failure to determine its behavior to static overpressurization. The results from testing the heavily instrumented containment will be used to assess the capability of analytical methods.

1.0 INTRODUCTION

On behalf of the U. S. Nuclear Regulatory Commission, the Containment Integrity Division at Sandia National Laboratories (SNL) is continuing investigations into the performance of nuclear containment buildings subjected to hypothesized severe accidents. SNL has conducted static overpressurization tests on five scale models of steel containment buildings [1,2,3] and is currently preparing to test a reinforced-concrete containment building. All containment models have been tested until excessive leakage or structural failure occurs by pressurizing the models with nitrogen gas.

Light-water-reactor containment buildings, which are constructed from steel, reinforced concrete, or prestressed concrete, are the last engineered barrier to prevent the release of radioactive materials to the environment. The objective of the containment model tests is to generate data that can be used to qualify methods for reliably predicting the response of LWR containment buildings to overpressurization. The data recorded during testing include sealing surface deformations and leakage as well as strains and displacements of the containment shell.

The construction features and preliminary finite element analyses of the 1/6th-scale containment are discussed in this paper.

---

*This work is supported by the United States Nuclear Regulatory Commission and performed at Sandia National Laboratories which is operated for the U. S. Dept. of Energy under contract number DE-AC04-76DP00789.

2.0 THE CONTAINMENT MODEL

The 1/6-scale reinforced-concrete containment was designed by United Engineers and Constructors to a design pressure of 46 psig (317 kPa) in accordance to the ASME code. The diameter of the model is 22 feet (6.7 meters), with a total height of 37 feet (11.3 meters). The cylinder wall is 9-3/4-inches (25 cm) thick and the dome is 7-inches (18 cm) thick. This model has #4 (12 mm diameter) reinforcing bar for the eight layers of primary reinforcing (two layers of meridional, four layers of circumferential, and two layers of diagonal reinforcing steel). The containment also has a steel liner, which is 1/16-inch (1.6 mm) thick for the base and cylinder wall and 1/12-inch (2.1 mm) thick in the dome. Two equipment hatches, two airlocks, constrained penetrations, and several piping penetrations are also included in the containment. All materials used for constructing the model were selected such that their structural characteristics are the same or as close as possible to actual containment building materials. A schematic of the containment is shown in Fig. 1.

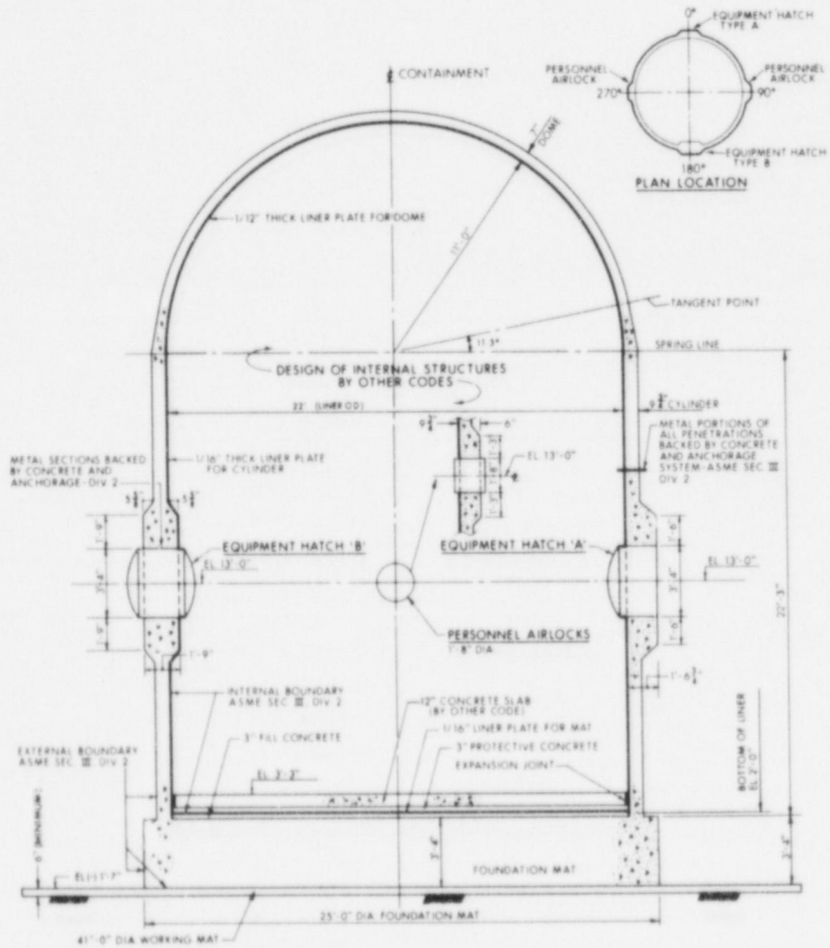


FIGURE 1: TYPICAL SECTION THROUGH 1/6-SCALE LWR REINFORCED CONCRETE MODEL SHOWING BOUNDARIES OF ASME SECTION III, DIVISION 2

2.1 Schedule for Construction and Testing

The design of the containment model began in January 1985 and was completed in June. To ensure that a high-quality model could be constructed, the design of the model and a series of preconstruction tests were conducted in parallel. Due to the containment size and schedule constraints, particular attention was paid to liner welding, splices for the reinforcing steel, concrete placement, and other construction and sequencing problems. No problems were found to preclude the containment model's construction.

Construction of the containment model began in August after comments and suggestions made by a peer review panel were incorporated into the design. The model's construction is scheduled to be completed in July 1986. During construction, over 250 strain gages were applied to the reinforcing steel. In addition, several embedment gages and thermocouples were also cast in the concrete wall. Once the model is completed, over 100 displacement transducers, 350 additional strain gages, and other instrumentation are planned to be applied to the containment model. At test time, there will be approximately 1000 channels of instrumentation. In early 1987 final checking of the data acquisition system and the overpressure testing of the containment will be performed.

2.2 Liner

The liner is the pressure boundary of U. S. containments and is located on the inside surface of the concrete. Chicago Bridge and Iron, Co. (CB&I) built the liner and the steel sections of the penetrations. As scaled from a typical containment, the liner material in the 1/6-scale containment is nominally 1/16-inch (1.6 mm) thick in the basemat and cylinder wall, with the thickness of the liner in the dome region of the containment being 1/12-inch (2.1 mm) thick. Thickened sections of the liner around penetrations are 3/16-inch (4.8-mm) thick. Standard pipe sections were used for smaller piping sections, which are made of SA 333 Grl steel.

Liners in U. S. containments are generally made using A516 Gr60 steel. Since this material was not readily available in the small quantities needed in the 1/16 and 1/12-inch (1.6 and 2.1-mm) thicknesses, it was used for only the construction of the thicker sections of the liner and the penetrations. A suitable substitute, A414 GrD, to be used in the thinner sections was located after an exhaustive search by CB&I. Table 1 shows a comparison of A516 Gr60 and A414 GrD material properties.

Table 1
Actual Material Properties of A516 Gr60 and A414 GrD

	Yield Stress ksi	Ultimate Stress ksi	Elongation %	
A516 Gr60	53.9	67.4	25.4 (in 8")	*
A516 Gr60	55.8	79.0	25 (in 2")	**
A414 GrD	51.4	71.4	24 (in 2")	

*From actual containment buildings
**From 3/16-inch (4.8-mm) thick plates used for the containment model construction (from Certified Test Reports)

The liner was constructed in sections in CB&I's Kankakee, IL, fabrication shop. Included with the liner construction was an internal support system, which supported the liner both during transportation and construction. A cylindrical section of the liner turned on edge is shown in Fig. 2. It shows both the outside surface and the internal support frame. The liner was held to the support frame by numerous threaded studs attached to the inside of the liner and then bolted to the support frame. The dome section of the liner was dished by a pressing operation before it was attached to its internal support frame. The cylinder sections were deformed elastically to their final shape when they were attached to its internal support frame. Penetrations were all added to the liner at the construction site.



Figure 2.
Section of Liner Attached to its Internal Support Frame

Over 20,000 headed studs were attached to the outside of the liner. Studs with shank lengths of 1/2 and 3/4 inch (12.7 and 19.1 mm) were attached to the model by capacitive-discharge welding. Although the prototypical stud's length would scale to about 1 inch (25.4 mm), construction sequencing and difficulty strongly discouraged their use. A 1-inch (25.4 mm) stud would penetrate the first layer of reinforcing, making placement of the reinforcing steel extremely difficult. Since final welding of the liner prevented all of the studs from being attached in the shop, several thousand studs were attached at the construction site. Field attachment of the studs on the liner is shown in Fig. 3.

At areas of discontinuity in the liner, studs were attached to the liner at the same density as in a full-size containment building--a 2 x 2 inch (51 x 51 mm) spacing on the containment model. In areas away from discontinuities the stud spacing was increased to 4 x 4 inch (100 x 100 mm) and 6 x 6 inch (150 x 150 mm) in the cylinder wall and 8 x 8 inch (200 x 200 mm) in the dome.

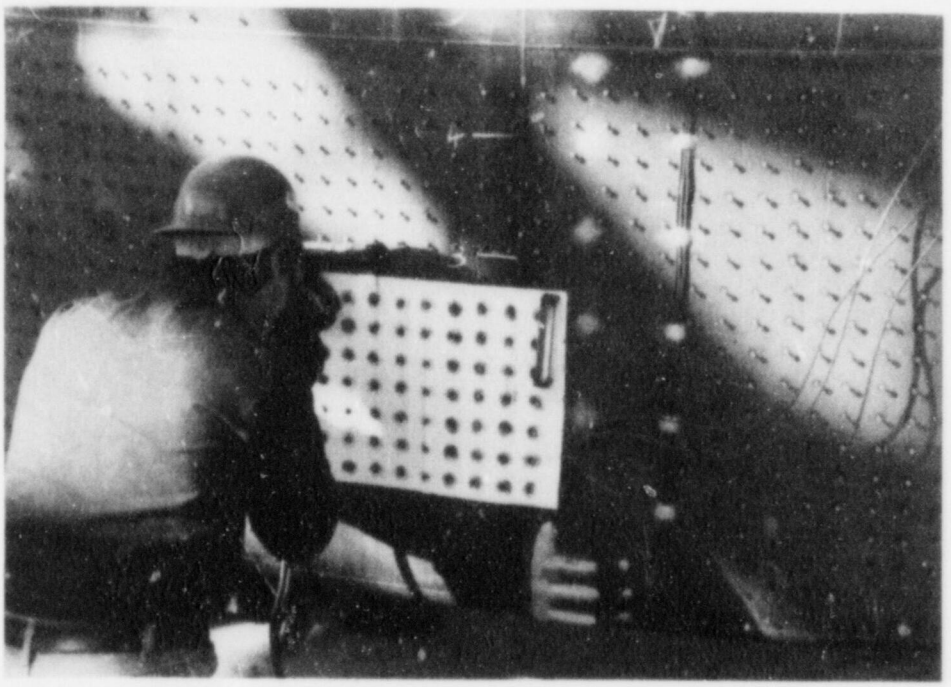


Figure 3.
Field Attachment of Headed Studs to a Liner Section

2.3 Concrete

Several trial batches of concrete were made before the proportions of the final mix were finalized. A well-rounded coarse aggregate that has a nominal maximum size of 3/8 inch (9.5 mm) that comes from an Albuquerque supplier was used. (Typical maximum aggregate size for a full-size containment is 3/4 inch (19 mm).) High range water reducers (superplasticizers) were used, along with a water/cement

ratio of 0.53. The slump required for the concrete lifts was about 8.5 inches (215 mm), except in the basemat and dome apex where the slump was reduced.

All concrete used for the model is centrally batched and hauled in trucks to the construction site. Consistency and quality of the concrete have been excellent.

Measured compressive strengths of the concrete at 28 days of age are about 5700 psi (39.3 MPa). Tensile strengths were determined by two methods: direct tension and split cylinder tests. Direct tension results are from 300 to 360 psi (2050 to 2500 kPa) and split cylinder values are higher at about 430 psi (3000 kPa).

2.4 Basemat

The 40-inch (1.0-m) thick basemat in the 1/6-scale containment is somewhat thicker than would be linearly scaled from most full-size containments. This results from the fact that when all dimensions are scaled linearly, gravitational forces in the scale model are equal to typical dead weight divided by the scale factor [4]. Since the dead weight of the model was relatively 1/6th of its full-size counterpart and no internal structures of a containment were modeled, moments at the base-wall intersection and uplift due to the bottom of the basemat bulging during pressurization were much higher than would be realized if gravitational forces scaled "properly." By scaling the moment in the basemat-cylinder wall intersection and the use of analyses, a 40-inch (1.0-m) basemat thickness was selected.

2.5 Splices

About 5000 mechanically swaged connectors were used in the splicing of the reinforcing steel. The majority of these splices were on the #4 (12 mm diameter) reinforcing steel. These splices allowed for flexible construction procedures--they could be installed using a bench mounted press or at the model itself using a hand-held press. (A picture of a splice being installed using the hand-held press is shown in Fig. 4.) The splices could be fully swaged or they could have various types of threaded ends.

All U. S. containments built to date have exclusively used a CADWELD-type splice in the reinforcing steel. During the design phase of the 1/6-scale containment, it was realized that it would be quite difficult in several regions to have proper access to allow this type of splice to be made; however, the use of CADWELDS was desired in some regions of the containment model. Since the design team had experience with mechanically swaged rebar splices, investigative efforts were begun to assess the applicability of the splices in the containment model construction.

Through this testing effort it was determined that the swaged connections for the reinforcing steel provided a very adequate splice

that was easy and quick to make that also developed the strength of the reinforcing steel as required by code.

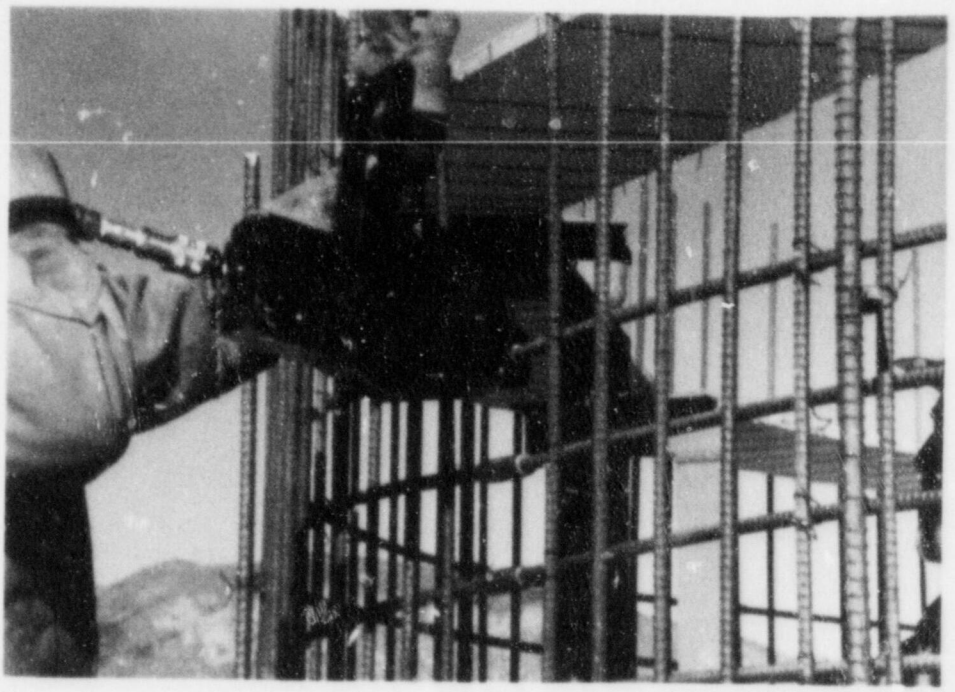


Figure 4.
Installation of a Swaged Splice Using a Hand-Held Press

CADWELDS used on a full size containment have a tendency to slip when subjected to high loads. This characteristic of splices was desirable in the containment model; however, testing determined that the smaller CADWELD splices did not exhibit this slippage. In fact, the smaller CADWELDS behaved very similarly to the swaged splices. Modifications to the smaller CADWELDS did not prove successful in duplicating the response of the larger CADWELD splices; therefore, it was decided to use only one type of splice. Since the swaged splice appeared to be somewhat easier to use, swaged splices were selected.

2.6 Penetrations

Several types of penetrations were incorporated into the containment model. The majority of the penetrations are scaled from typical penetrations found in full-size containment buildings; however, several other penetrations were included for SNL's testing purposes.

2.6.1 Personnel Airlocks

Two personnel airlocks are included in the containment, which are at the same elevation (cylinder midheight) and 180° apart. The sleeve diameter of both airlocks is about 20 inches (0.5 m) in diameter.

The reinforcing pattern around the penetrations is identical--the airlocks themselves are different.

One airlock has its sleeve dimensions scaled from a full-size personnel airlock, but uses a thick flat plate as a pressure unseating door so that it may be used for a "last man out" hatch.

The other personnel airlock, which also has its sleeve dimensions scaled from a full-size airlock, has scaled bulkheads and stiffener patterns that are typical of a full-size airlock. The inner bulkhead is a flat plate with stiffeners--no door or seals are included. The outer bulkhead has a similar stiffener pattern but no door is represented, which allows for instrumentation to be installed inside the airlock sleeve. A picture of the airlock is shown in Fig. 5 before the reinforcing steel and concrete were in place.

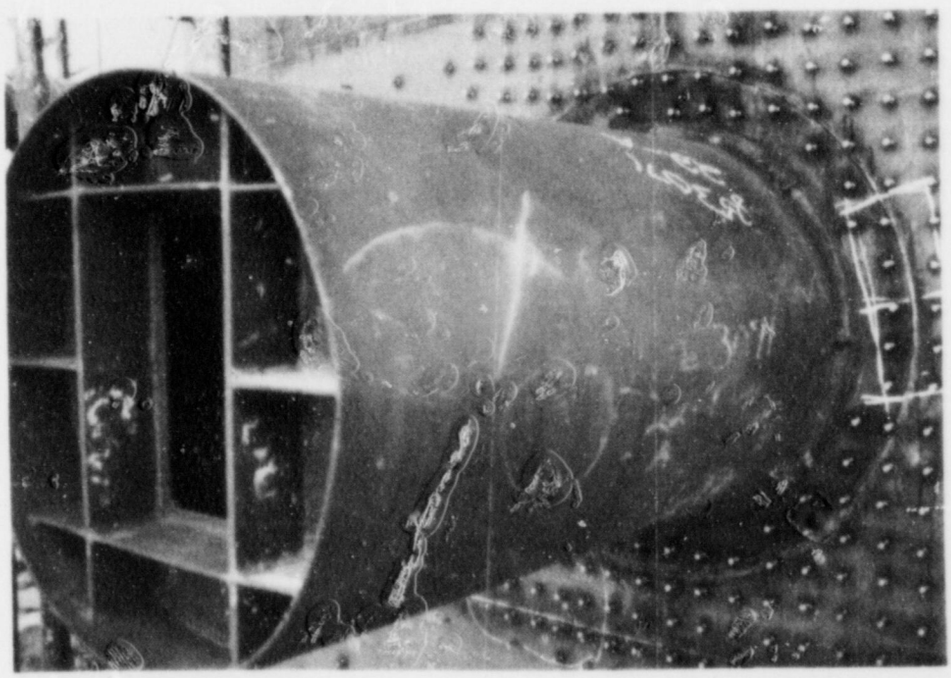


Figure 5.
Personnel Airlock and Liner Before Reinforcing Steel was in Place.

2.6.2 Equipment Hatches

Two equipment hatches are included in the containment model, which are at the same elevation (cylinder midheight) and are 180° apart from each other and 90° from the personnel airlocks. Both equipment hatches, including the sealing surfaces of the doors and sleeves, have been scaled from typical equipment hatches found in U. S. containment buildings. Both have sleeve diameters of about 40 inches (1.0 m). The major difference between the two equipment hatches is that the boss area of one projects entirely outward from the

cylinder wall (equipment hatch A) and the other boss is centered in the wall so that it projects both inward to and outward from the cylinder wall (equipment hatch B) (see Fig. 1). The primary reinforcing around each of the equipment hatches, however, is the same for both equipment hatches--only their local reinforcing is different.

Equipment hatch A has a double gumdrop seal in its 1/2-inch (12.7 mm) wide mating surface between the door and the sleeve. This is a pressure seating door; that is, as the pressure inside the containment model increases, it tends to compress the seal.

Equipment hatch B has two doors, one on the inboard end of the equipment hatch sleeve being the same design as the pressure seating door in equipment hatch A and one on the outboard end of the sleeve being a pressure unseating door. Either door can be the pressure boundary during testing by opening and closing remotely controlled valves located in the equipment hatch doors. The pressure unseating door has a double tongue-and-groove type seal arrangement in its 3/4-inch (19.1 mm) wide sealing surface.

2.6.3 Constrained Penetrations

There are two 8-inch (200 mm) diameter penetrations at the same elevation located 180° apart on the cylinder wall. They represent a major steam line penetrating the model. As a containment expands due to overpressurization during a severe accident, it is probable that the steam line will load the containment due to its inability to move freely. This loading, or constraint, was modeled in the containment by connecting the two penetrations by a small (6 mm diameter) reinforcing bar. The degree of constraint was selected by analyzing three piping systems of two full-size containments buildings. A typical stiffness was then scaled for use and selection of the constraint in the containment model.

2.6.4 Other Penetrations

Several other piping penetrations are also included in the containment model. One piping cluster, containing one 8-inch, one 4-inch, two 2-inch, and one 1-inch (one 200-mm, one 100-mm, two 51-mm, and one 25-mm) diameter penetrations is located in the containment wall.

Other penetrations included in the containment model are there to facilitate testing the containment. These penetrations include five 8-inch (200 mm) diameter penetrations that are used to pass through instrumentation wires, and a 4-inch (100 mm) diameter penetration, which will be used to connect the pressurization line to the model.

3.0 ANALYSIS OF THE CONTAINMENT

3.1 Analysis Objectives and Approach

The analyses performed to date were selected to assess the current concrete analysis capabilities and to gain an understanding of how the model will respond to static pressurization. To meet these objectives, several different finite element and constitutive models were used. Although a true assessment of which model is the "best" must wait until after the pressure test of the containment, the results of these analyses can be compared against each other and hand calculations. Some assessment of the effectiveness of each model can be obtained by doing this. For example, if the results among the analyses are not significantly different but the computational effort to obtain the results are, some very important information could be obtained.

Although this paper reports only the preliminary axisymmetric containment analyses performed to date, there are plans to conduct analyses of an equipment hatch, constrained pipe penetration, and possible liner failures. It is important to realize that the axisymmetric containment analyses performed are not adequate to detect local liner failures that may occur around studs or concrete cracks.

3.2 Description of Numerical Models

All of the containment analyses performed to date have used the ABAQUS finite element code version 4-5-171 [5]. This code was selected for the work because it has a number of features that were believed to be desirable for analyzing concrete structures. For example, it has a relatively easy method for specifying the reinforcing bar within the concrete matrix. There are no restrictions that the finite element mesh conform to the locations of the rebars, i.e., the rebar may be placed anywhere in the mesh, not just at element intersections as is required for some codes. The code also has a modified version of the Chen and Chen constitutive model for concrete [5,6] with smeared cracking at element integration points. In addition, the code's element library enables efficient modelling of a containment structure. For example, for these containment structures, the steel liner can be represented by shell elements and the concrete by continuum elements.

Two basic finite element models, an axisymmetric shell model, Fig. 6a, and an axisymmetric continuum model, Fig. 6b, have been used. The shell model is a coarse representation of the containment. The idea behind using this model was that, although it would lack the detailed refinement (particularly in the basemat and basemat-cylinder wall junction area), it would give the general containment response to internal pressure at a reduced cost from a continuum model representation. This model consisted of 2-noded axisymmetric elements for the concrete and the liner. There were 11 elements

used to represent the basemat, 20 elements for the cylinder wall, and 15 elements for the dome. As much of the steel reinforcement was included as possible. All of the main hoop, vertical, and diagonal reinforcement was incorporated. No shear reinforcement at the basemat-cylinder wall junction was included due to the modelling complexity. The liner was represented by another set of axisymmetric shell elements that overlaid the elements representing the concrete.

The axisymmetric continuum model, Fig. 6b, consisted of 947 eight-noded isoparametric elements representing the concrete and 182 axisymmetric shell elements for the liner. The liner was placed on the interior boundary of the model. As with the shell model, all major reinforcement was included except for the shear reinforcement at the basemat-cylinder wall junction. In both of these models the internal dead weight of the structure was included, and the basemat was allowed to lift off a rigid surface foundation.

The analyses reported in this paper were performed before mechanical properties tests were made on the concrete being used in the containment. Therefore, a curve based on the estimated concrete strength [7] at the time the containment will be tested was used, Fig. 7. Similarly, a tensile strength of 282 psi (1.94 MPa) for the concrete was used. Preliminary data on the reinforcing bars and liner were obtained, and these data were used to construct representative engineering stress-strain curves, Fig. 8.

One other material model was used for these analyses. In that model, the concrete was represented as a plastic material that cannot carry tension. The stress-strain curve, Fig. 7, did not allow for strain softening.

3.3 Description of Analyses and Solution Procedures

In this paper the results of three analyses are discussed, two using the axisymmetric shell model and one using the axisymmetric continuum model. The first analysis used the Chen and Chen concrete model with the shell element description of the containment, the second used the no tension plasticity model with the shell model, and the third used the Chen and Chen model with the axisymmetric continuum model. The reasons for using these different models will become clear as the results are discussed. At this point it is sufficient to say that analyzing concrete structures to failure cannot be done using "standard" procedures. There are no generally accepted procedures for the structural modelling, constitutive models, or solutions procedures. These problems are typically highly nonlinear with challenging numerical problems.

The solution technique used for these analyses was one of taking very small load steps with few, if any, subsequent iterations in that step. A typical load step was 0.1 psi (0.69 kPa) for the analyses using the shell model and 0.25 psi (1.72 kPa) for the continuum model. In addition, areas of severe cracking in the

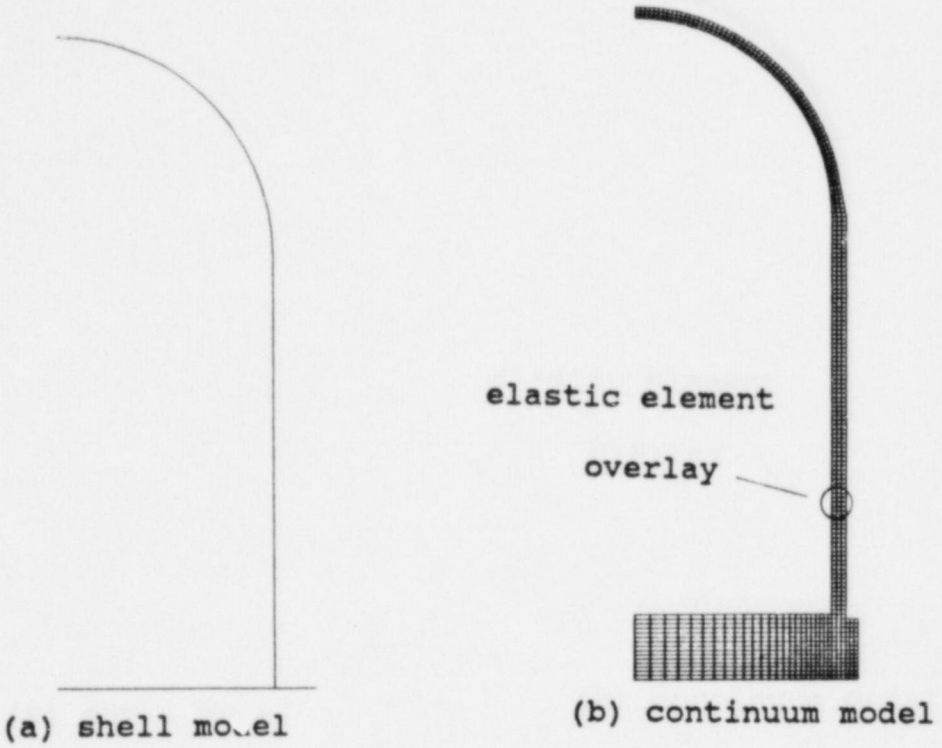


Figure 6.
Containment Models

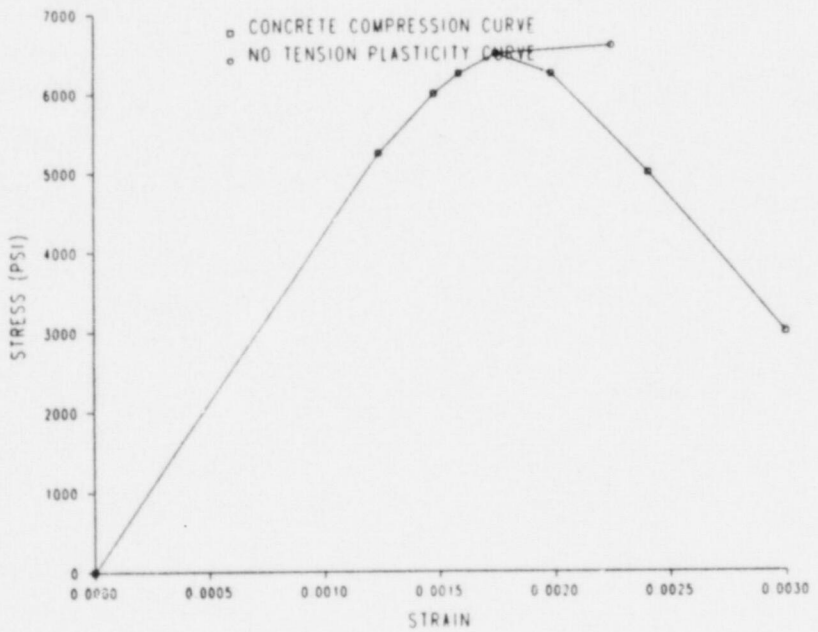


Figure 7.
Compressive Stress-Strain Curves

continuum model were overlaid with elastic elements that were assigned a Young's modulus that was three orders of magnitude lower than the initial tangent modulus of the concrete. The overlay region is shown in Fig. 6b. Also, the dome apex area of the continuum model used elastic elements to avoid severe cracking problems that occurred in earlier analyses.

In these analyses, once cracking began it was necessary to proceed through the load steps without equilibrium convergence being achieved at each step. Typically, iterations did not bring the residual forces down. Therefore, the solution strategy described above of taking small load steps with no subsequent iterations was adopted.

4.0 ANALYSIS RESULTS

4.1 General Containment Behavior

The axisymmetric shell model using the Chen and Chen constitutive model yielded the displaced shape plots shown in Fig. 9. The most dominate feature of the plots is a bulge in the cylinder that develops between 65 and 70 psi (0.44 and 0.48 MPa). Interestingly, this bulge develops at the onset of cracks whose normals are in the meridional direction (these will be called meridional cracks). Also interesting, the bulge coincides with the location where some vertical reinforcing in the cylinder wall terminates. The additional vertical reinforcing prevents the lower position of the wall from cracking so that there is a severe discontinuity in the stiffness in the bulge area. Apparently, the bulge is the result of the discontinuity. This notion is supported by the fact that no bulge developed in the shell analysis using the no-tension plasticity model, Fig. 10, to be discussed later. Hoop cracking (cracks whose normals are in the hoop direction) began at 20 psi (0.14 MPa) in the cylinder wall and spread rapidly to the dome. By 25 psi (0.17 MPa), most of the dome concrete was cracked. Meridional cracks began in the cylinder wall at 40 psi (0.28 MPa).

The basemat became severely cracked in this analysis. Both hoop and cracks in the plane of the model developed at 50 to 55 psi (0.35 to 0.38 MPa). These cracks reached the center of the basemat by 70 psi (0.48 MPa).

The liner stresses will be discussed in Section 4.4.

General yielding of the hoop cylinder wall reinforcement occurred at approximately 120 psi (0.83 MPa), which is in agreement with hand calculations.

The displaced shapes for the axisymmetric shell model with the no tension plasticity model, Fig. 10, are what would be qualitatively expected. Of course, most of the abruptness in the response associated with concrete cracking is not present; all tensile stresses must be carried by the reinforcing bars and the liner. Again,

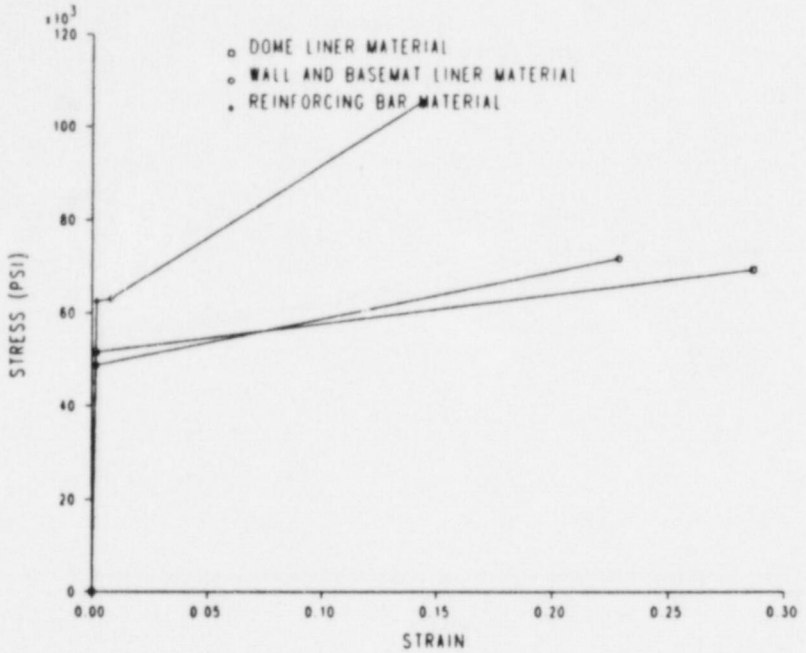


Figure 8.
Stress-Strain Curves for the Steel

Mag. Factor= 11000. Mag. Factor= 6.6 Mag. Factor= 6.1

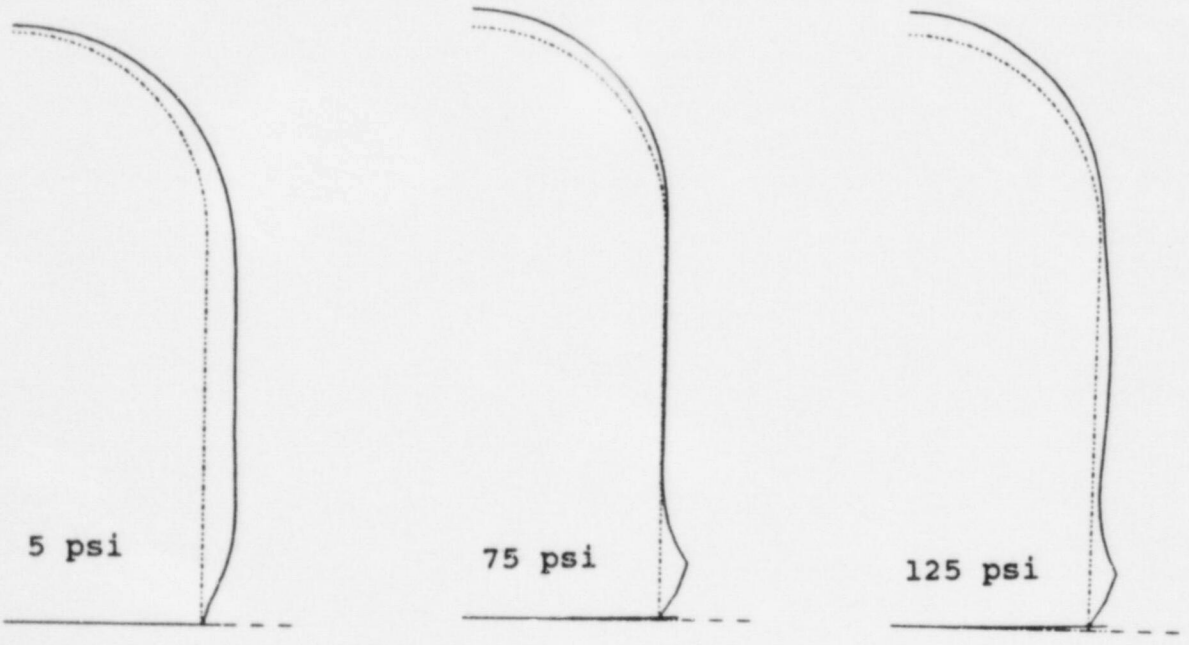


Figure 9.
Displaced Shape Plots of the Shell Model using the Concrete Model

general yielding of the hoop reinforcing bars was calculated to occur at 120 psi (0.83 MPa).

The displaced shapes for the continuum model analysis, Figs. 11, show two major characteristics that are different from the previous two analyses. First, the apex of the dome moves downward at approximately 25 psi (0.17 MPa) after initially displacing upward. Second, there is an abrupt numerical instability associated with severe damage in the basemat-cylinder wall region at 100 psi (0.69 MPa).

It is not clear at this time if the displacement of the dome apex should be down or if the downward displacement is the result of a numerical modelling detail. It is known that at least one actual containment (Washington Public Power Supply System - Unit 1) exhibited such behavior during its structural integrity test. One possible explanation for the downward displacement is that loss of stiffness of the cylinder wall supporting the dome could result in the base of the dome moving out and the apex down in an attempt to minimize the midsurface stretching. Another explanation is that because there are elastic elements at the dome apex, the change in stiffness between the cracked dome material and the uncracked dome results in a poor numerical solution.

The numerical instability at 100 psi (0.69 MPa) should not be interpreted as the pressure at which the containment will fail. Rather, this result is indicative of the severe state of stress at the basemat-cylinder wall junction and is a reflection of the material model's attempt to represent the severely damaged concrete. This type of failure has been predicted by other codes for different containments [8,9] and is a problem that most concrete containment analyses encountered. There is a low probability that the basemat-cylinder wall junction will actually fail at this pressure, but given the reliability of concrete containment analysis techniques and that the shear reinforcement in this area was not included, this would be a highly unlikely occurrence.

Hoop cracking in the cylinder wall began at 22 psi (0.15 MPa); almost the entire cylinder wall contained these cracks. These hoop cracks progressed up the dome and at 50 psi (0.34 MPa), most of the dome was cracked. Cracking in the plane of the model at the basemat-cylinder wall junction began at 45 psi (0.31 MPa). By 100 psi (0.69 MPa) this shear and bending related cracking extended 1 foot (0.3 m) down into the basemat and 3 feet (0.91 m) up into the cylinder wall. There was local cracking at an elevation of 7.5 feet (2.3 m) on the outside of the cylinder wall. This is one foot above the termination of some vertical reinforcing bars that extend up from the basemat. This cracking is probably the result of local bending in this discontinuity region.

Although hoop cracking of the cylinder wall occurred at approximately the same pressure in both the continuum and shell analyses that used the Chen and Chen model, the degree of cracking

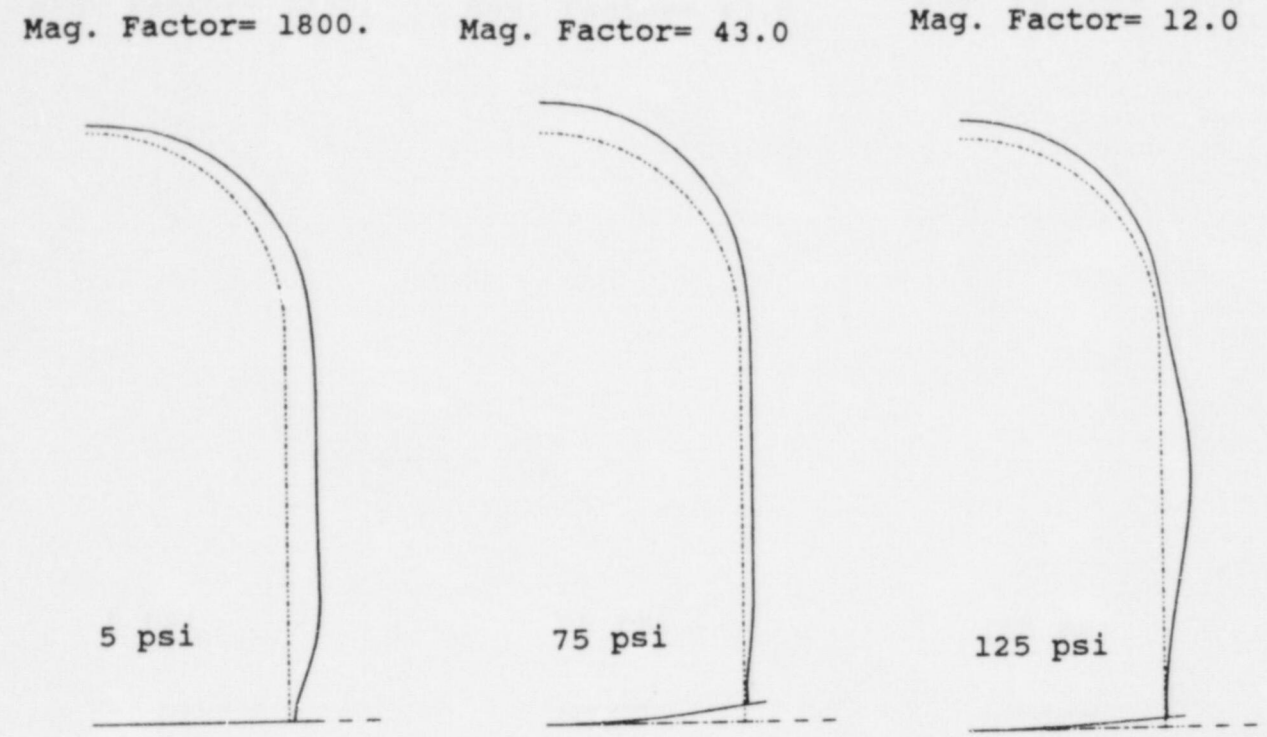


Figure 10.
Displaced Shape Plots using the No Tension Plasticity Model

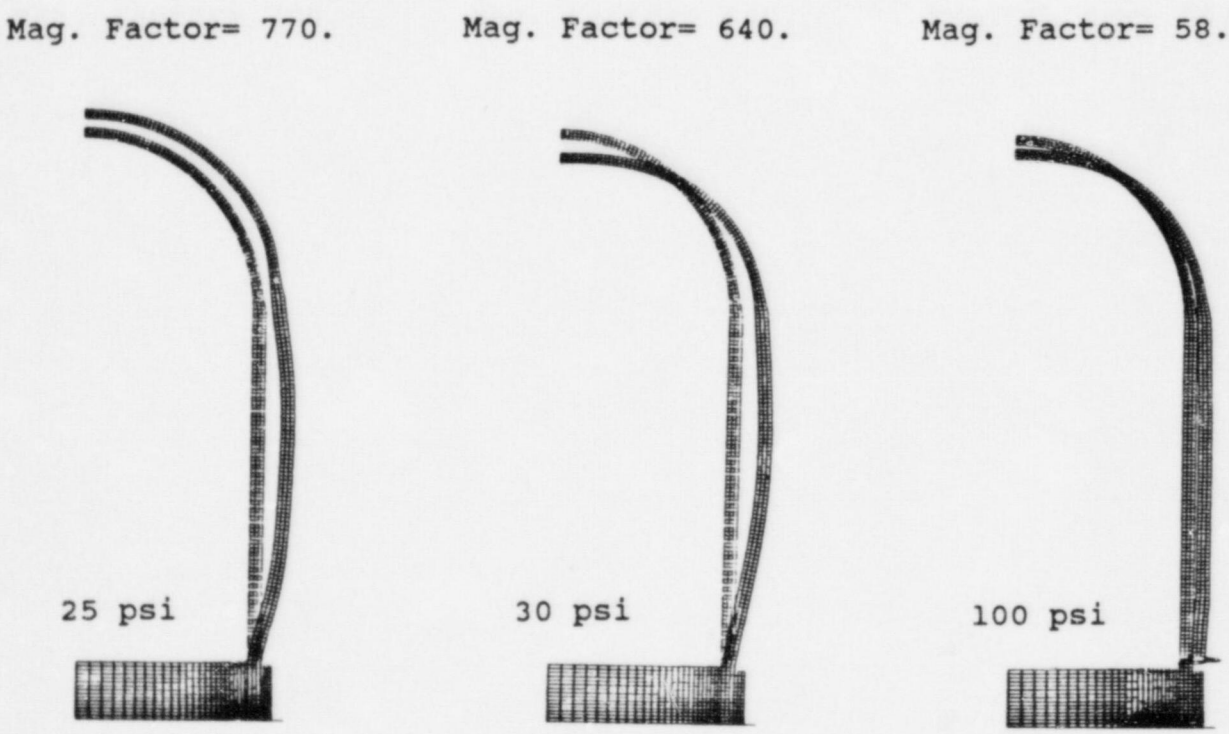


Figure 11.
Continuum Model Displaced Shape Plots

in the shell model was much more severe than in the continuum model and is probably the result of the inadequate shell model representation.

The discussion that follows will concentrate on the displacements and stresses in the reinforcing bars and liner. The stresses in the concrete are the least reliable of the stress quantities calculated and the most difficult to interpret. Therefore, a discussion of concrete stresses is not included in this paper.

4.2 Comparison of Displacements

A comparison of the cylinder wall radial deflection at midcylinder height is shown in Fig. 12. All of the analyses yielded approximately the same displacements after the effects of the initial cracking subsided. This result would be expected since the stiffness of the cylinder wall in the hoop direction is governed primarily by the stiffness of the hoop reinforcing bars.

The plot of the vertical displacements of the dome apex, Fig. 13, shows a large dome displacement for the axisymmetric shell model using the Chen and Chen model. This result can be attributed to local straining around the bulge area described earlier.

From the displacement plots, Figures 9 and 10, it is apparent that the basemat uplift is much smaller in the continuum model analysis than the shell model analysis. This is probably due to the poor representation of the basemat by the shell elements.

4.3 Comparison of Rebar Stresses

The comparison of the stresses in the hoop reinforcing bars at midcylinder height, Fig. 14, shows that the stresses are relatively close. At the lower pressures, below 25 psi (0.17 MPa), the effects of the concrete cracking are clearly shown as the load from the concrete is transferred to the reinforcing bars. Of course, this effect was not seen in the model that had no tension stress capacity. General yielding of these rebars began at about 120 psi (0.83 MPa).

From the displaced shape plots, Figs. 9 to 11, it is apparent that the shell models at midcylinder height exhibit less meridional bending than the continuum model. This effect is seen in the plot of the outer vertical rebar stresses, Fig. 15. It is not clear at this point whether this bending is a real phenomenon or if it is a result of the model not being in satisfactory equilibrium.

4.4 Comparison of Liner Stresses

The most severe loading of the liner was along the cylinder wall. The shell models show that the liner should yield at approximately 85 psi (0.55 MPa), Fig. 16. The difference between the liner hoop

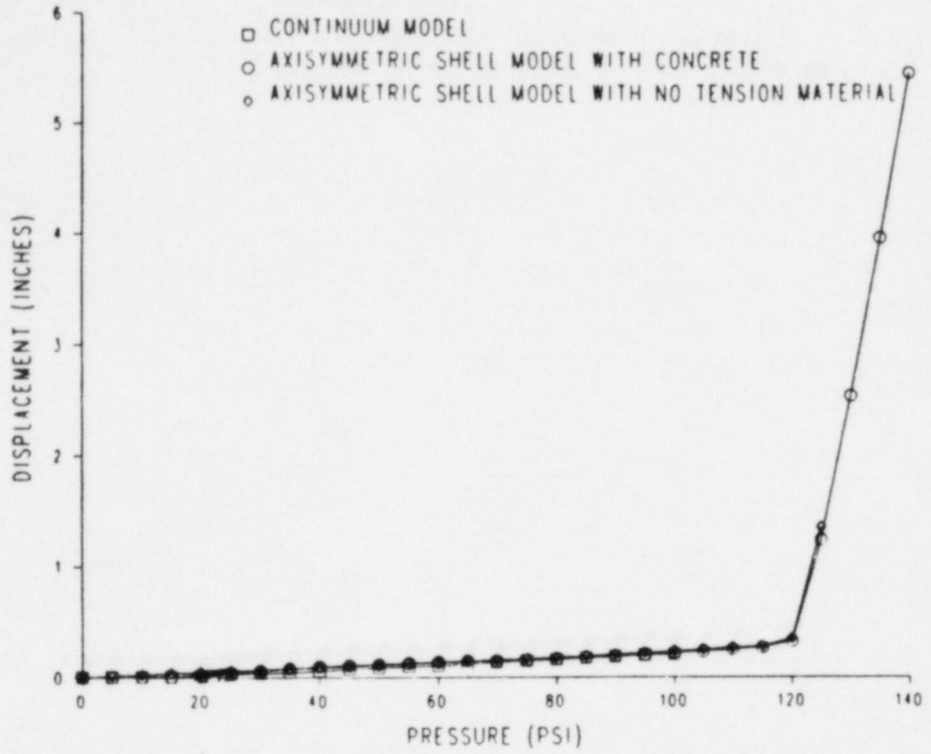


Figure 12.
Radial Displacement at Midcylinder Height

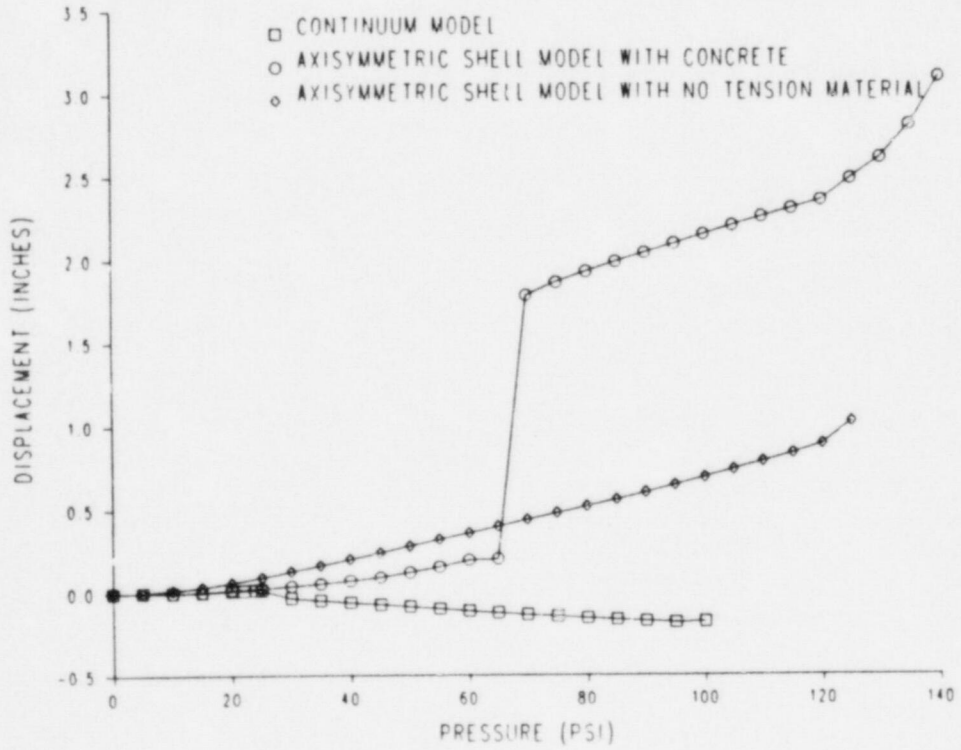


Figure 13.
Dome Vertical Displacement

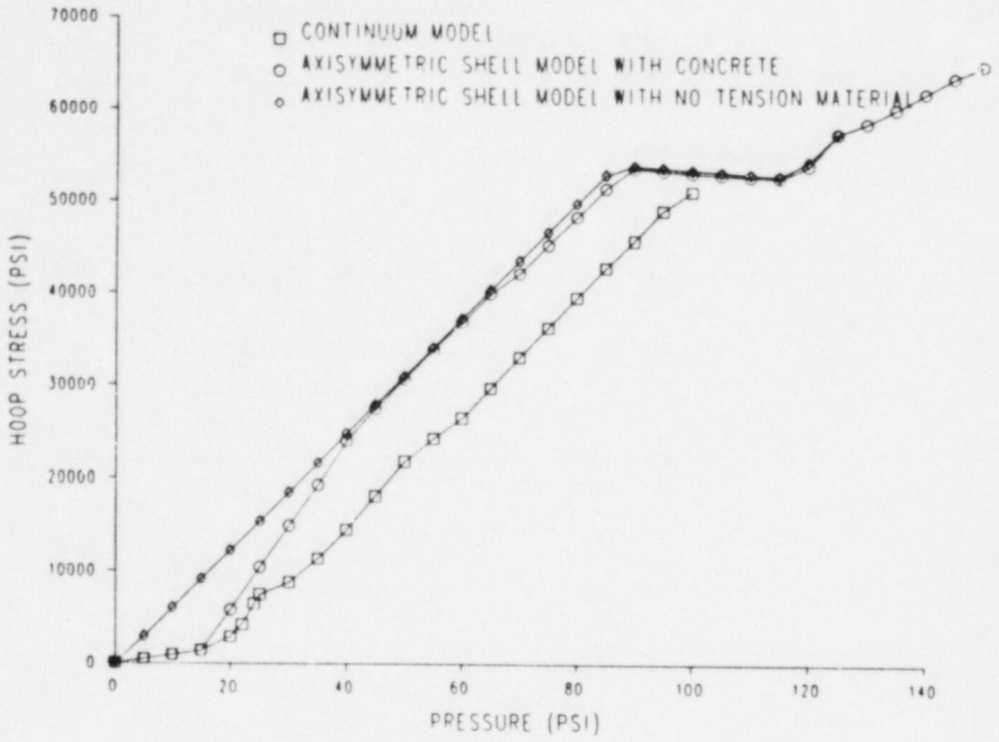


Figure 14.
Hoop Rebar Stresses at Midcylinder Height

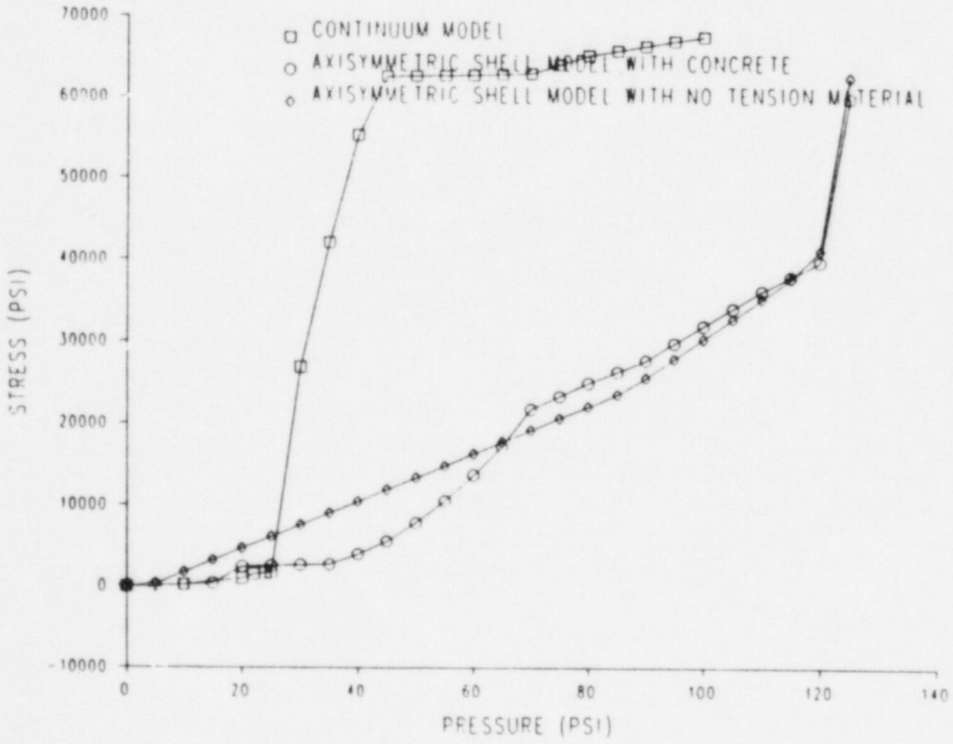


Figure 15.
Outside Vertical Rebar Stresses at Midcylinder Height

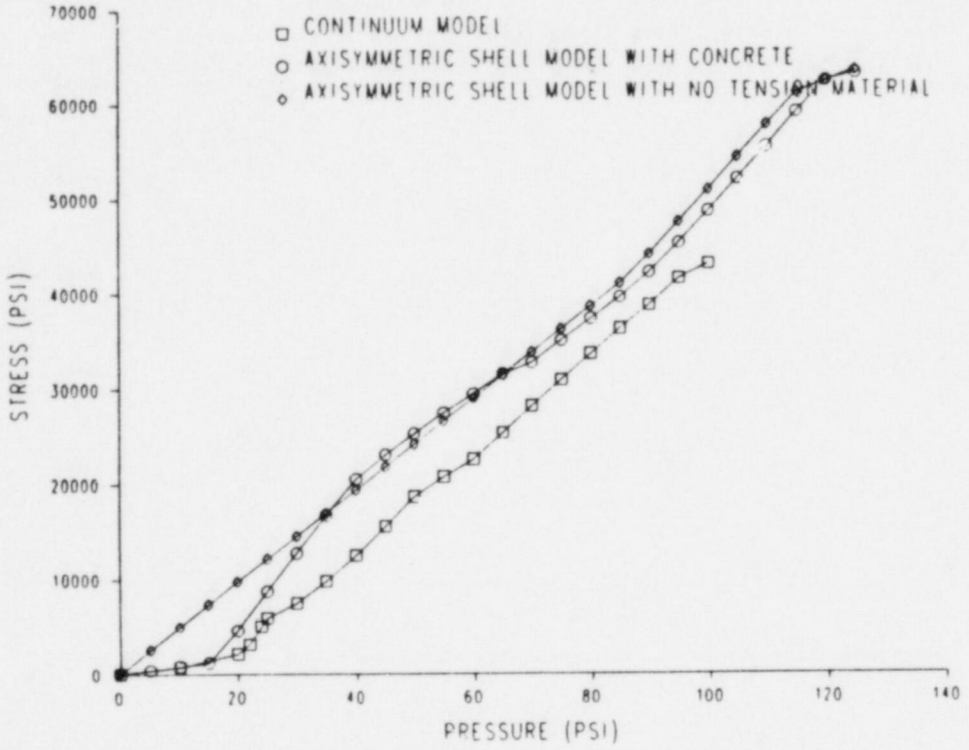


Figure 16.
Hoop Liner Stresses at Midcylinder Height

stresses from the shell models and the continuum model can be attributed to the meridional bending in the containment model since the radial deflections were very similar, Fig. 12.

5.0 SUMMARY AND CONCLUSIONS OF THE ANALYSES

At this point it is not possible to make particularly strong statements regarding the final failure pressure and failure mode(s) of the model. Aside from yielding of the hoop reinforcing bars at the midcylinder at 120 psi (0.83 MPa), the most likely failure location centers around the basemat-cylinder wall junction. The results of the analyses reported in this paper suggest that it is unlikely that there would be failures in the dome or springline region, and the basemat (away from the cylinder wall junction) appears to have adequate strength, at least to 100 psi (0.69 MPa). There are a number of interesting behaviors that merit observation during the actual containment test. First would be the displacement of the dome apex. It is fairly clear that the degree of damage in the dome and the springline will govern how the dome behaves. Second, there is a region that deserves attention at approximately elevation 7 feet (2.13 m) on the cylinder wall where some vertical reinforcing bars terminate. In two of the analyses there was a significant amount of local damage in this region. Third, the basemat-cylinder wall region should be monitored carefully. Although we cannot predict the failure pressure for this area with a high degree of confidence,

we are certain that this region will be heavily damaged at higher pressures. Finally, the penetrations are certainly complex areas that should be observed.

Although a true evaluation of the effectiveness of the finite element models used for the analyses must wait for the containment test, the simple axisymmetric shell models do have some favorable characteristics. They are simple and more numerically stable than the continuum elements when heavy cracking has occurred. In very complex regions though, such as the basemat-cylinder wall junction, the shell elements are simply not adequate to model the behavior. However, it is not clear to the authors that more complex continuum models are able to represent this behavior without encountering severe numerical problems. Most of the numerical problems appear to be related to cracking. For analyses in which the ultimate capacity of the structure is sought, there is always severe damage to the concrete. Typically, the stiffness of the concrete in the numerical model is reduced to account for the effects of the cracking. If sufficient stiffness is dropped out, that region of the model will have numerical problems. This appears to be a fundamental modelling problem that must be addressed if these types of analyses are to become reliable.

6.0 PARTICIPATION BY OTHERS

The testing of the reinforced-concrete containment model has generated much interest in organizations that see this event as a choice opportunity to qualify and verify analytical tools. Several organizations are participating in the predictive analyses of the containment model. SNL has provided construction specifications and drawings and material properties to participating analysts. With this information, a predictive analysis effort is expected from each organization.

It is anticipated that the combined participants will publish the expected response of the containment model prior to the testing of the containment in a single report.

7.0 ACKNOWLEDGMENT

The performance of United Engineers and their subcontractors in the design and construction of the containment model is evident in the quality and precision of the end product. Their understanding of the program objectives, their skills, and their attention to detail are in a very large way responsible for the success of the construction of the containment model--by no means a small feat.

8.0 REFERENCES

[1] HORSCHEL, D. S., "The Design, Fabrication, Testing and Analyses of Four 1:32-Scale Steel Containment Models," NUREG/CR-3902, SAND84-2153, Sandia National Laboratories, Albuquerque, NM, (to be published).

[2] REESE, R. T. and HORSCHEL, D. S., "Design and Fabrication of a 1/8-Scale Steel Containment Model," NUREG/CR-3647, SAND84-0048, Sandia National Laboratories, Albuquerque, NM, February 1985.

[3] CLAUSS, D. B., "Comparison of Analytical Predictions and Experimental Results for a 1:8-Scale Steel Containment Model Pressurized to Failure," NUREG/CR-4209, SAND85-0679, Sandia National Laboratories, Albuquerque, NM, July 1985.

[4] BLEJWAS, T. E., et al., "Background Study and Preliminary Plans for a Program on the Safety Margins of Containments," NUREG/CR-2549, SAND82-0324, Sandia National Laboratories, Albuquerque, NM, May 1982.

[5] HIBBITT, KARLSSON and SORENSEN, Inc., ABAQUS User's Manual, Version 4.5, July 1985.

[6] CHEN, ANDRIE C. T. and CHEN, WAI F., "Constitutive Relations for Concrete", Journal of the Engineering Mechanics Division, ASCE, Vol. 101, August, 1975, pp. 465-481.

[7] NIELSON, ARTHUR H., Design of Prestressed Concrete, John Wiley and Sons, 1978.

[8] JUNG, J., "Ultimate Strength Analyses of the Watts Bar, Maine Yankee, and Belefonte Containments," NUREG/CR-3724, SAND84-0660, Sandia National Laboratories, Albuquerque, NM, July 1984.

[9] BUTLER, T. A. and BENNETT, J. G., "Nonlinear Response of a Post-Tensioned Concrete Structure to Static and Dynamic Internal Pressure Loads," Computer and Structures, Vol. 13, pp. 647-659, 1981.

AN EVALUATION OF STRUCTURAL FAILURE MODES FOR PRESTRESSED CONCRETE CONTAINMENTS

P. Shunmugavel and O. Gurbuz
Bechtel Power Corporation, Norwalk, California

ABSTRACT

Prestressed Concrete Containment Vessels (PCCV's) have been traditionally used as secondary containments for Pressurized Water Reactors (PWR's). A typical PCCV is shown in Figure 1.

This paper presents analytically predicted ultimate pressures and seismic levels for PCCV's, considering various modes of failures. Results for six containments are presented, and correlated with the available test data.

The analytical methods use either classical techniques or finite element analyses. The ultimate capacity calculations are based upon conservative deterministic estimates of strength of the structure, under both internal pressure and earthquake loads.

1.0 INTRODUCTION

Recently, behavior of containments under internal pressure and seismic loads much greater than the design loads has become of interest. Although probability of occurrence of such extreme loads is considered very small, knowledge of behavior of the structure under such loads is essential to determining probabilities of failure as well as estimating consequences of such failures. This paper is intended to provide a better understanding of Prestressed Concrete Containment Vessels (PCCV's) for Pressurized Water Reactors (PWR's) under loads beyond design loads. The study considers six containments, designated A through F. Failure modes under increasing internal pressure and seismic loads are defined. Loads corresponding to these failure modes were determined from a review of the existing analysis results as supplemented by additional simplified calculations and, engineering judgement. Liquefaction under increasing seismic loads and possible interaction with adjacent structures are considered beyond the scope of this study.

All analyses are based on deterministic methods. Whenever necessary, conservative assumptions and approximations are made. Results are given for six containments under internal pressure and seismic loads separately. For containment D, interaction of these two extreme loads is considered and a curve is developed as a function of pressure versus seismic overload capacity.

As noted earlier, existing design calculations and reports were heavily relied upon in developing the data presented in this paper. In most cases the ultimate capacities were obtained by simple extrapolation of the elastic analyses results. It is recognized that such a method is not entirely accurate since the behavior of the structure at load levels approaching failure becomes nonlinear. Therefore, the relative magnitude of the results presented is more important than the absolute values for evaluating the adequacy of current design practices.

Review of results indicate that there is a large margin between the ultimate load capacities and design loads even though the latter are already based on rare events.

2.0 EXAMPLE CONTAINMENTS

Five of the six PCCV's included in this study have a cylindrical shell with hemispherical dome and the sixth PCCV has shallow dome. In all cases the shell and the dome are post-tensioned and the basemat is reinforced concrete.

Basic data for these containments are shown in Table 1. As can be seen from this table the diameters range from 130 to 150 feet. The wall and dome thicknesses range from 3 to 4 feet, and the basemat thicknesses range from 9 to 18 feet.

Either wire or strand system is used for prestressing. Five PCCV's utilize 1/4" liner plate and the sixth PCCV has a 3/8" thick liner. The liner plate material is either SA-285 or A-442.

Design pressures range from 47 psi to 60 psi. Prestress level is set at 1.2 to 1.5 times the design pressure. In all of the six PCCV's, there is additional orthogonal bonded reinforcement throughout the shell and the dome.

Design ground acceleration corresponding to Safe Shutdown Earthquake (SSE) ranges from a low of 0.1g to over 0.6g. The design response spectra are compatible with the R.G. 1.60 spectra in four out of the six PCCV's; site specific spectra have been utilized in the design of remaining two.

Finally, the allowable soil bearing capacities indicate that all the plants are founded on competent soil or rock.

3.0 INTERNAL PRESSURE CAPACITIES

3.1 General

The general approach to calculating the ultimate pressure capacity was as follows: First, the internal force distribution corresponding to the design pressure was determined from the finite element analyses. In cases where no finite element analysis was available or in situations where the forces can be readily computed using the classical methods, simplified analyses were carried out.

The next step was to determine the capacities of the sections or structural elements using the data on strengths of concrete, reinforcement, prestressing and liner. Then, the capacities were calculated. This approach is similar to those given in References 1 and 2. It is to be noted that specified minimum material strengths were used in all cases except one where the as-built material strengths were available.

3.2 Failure Modes

One obvious failure mode of a PCCV under increasing internal pressure is related to the hoop membrane forces at about the mid-height of the PCCV, away from the discontinuities. The maximum hoop capacity is reached when the last steel element, which is usually the prestressing tendons, starts yielding.

Similarly, the ultimate pressure capacity considering the meridional and dome membrane forces are calculated.

Another potential failure mode involves bending plus membrane stress condition at the wall-basemat junction. A plastic hinge forms at this point under about twice the design internal pressure. Then the containment acts as a cylinder with hinged end condition and the section rotates under increasing pressure. Failure is reached when available rotational capacity corresponding to a maximum extreme fiber concrete strain of 0.003 is used up. The corresponding reinforcement ductility is about only four which is not the limiting factor.

In the case of radial shear at the wall-basemat junction, shear capacities of both concrete and radial steel reinforcement are relied on. Shear capacity is based on the ASME, Section III, Div. 2 Code (Reference 3) which results in a conservative estimate of ultimate pressure capacity. Alternatively, the radial shear capacity can be determined as the compression force due to flexure times the coefficient of friction at the interface. This method usually results in a higher capacity and is used only in one case.

Failure modes involving the basemat are considered to be of two types: shear near the edge and flexure. The latter can take place at two locations: near the edge (negative moment) and midway between the edge and reactor cavity. It is to be noted that existence of the reactor cavity strengthens the basemat significantly. For containment B with a flat basemat, the maximum positive moment occurs at the center and the magnitude is much greater. For that reason, this containment has a much thicker basemat. The basemat forces are determined from the existing computer analyses.

It has been stated in the past that the ultimate internal pressure capacity of a PCCV may be governed by penetrations. It can be readily demonstrated that the penetrations themselves, such as flue heads or sleeves, do not govern the design. Review of the penetration areas indicate that the wall section surrounding the penetration is provided with additional reinforcement and, in larger penetrations, with a thickened section. The design in these areas usually require that the section be stronger than the concrete it replaces. Nevertheless, the equipment hatch area was assumed to be representative of large penetrations and calculations were performed to determine its capacity. The failure mode involved is the punch-out shear which was calculated based on Reference 4.

The above failure modes under internal pressure are considered to be the only credible ones. It is believed that the PCCV leak tight integrity will be maintained without significant degradation, thus assuring that the ultimate internal pressures given in this study will be realized. This assumption is reasonable since the liner plate is a ductile material and under internal pressure it will be compressed against the concrete.

3.3 Numerical Results

Results of the ultimate internal pressure calculations for the six PCCV's are shown in Table 2. The governing failure mode for each containment, which is simply the smallest number in each column, is indicated by underlining the numerical value.

A review of this table indicates the following:

* The PCCV's studied had an ultimate internal pressure ranging from 2.3 to 2.9 times the design pressure. These results indicate uniformity of design performed by different engineers and by different entities.

* The governing failure mode in most cases is the hoop membrane failure.

* In the case of containment C the ultimate pressure capacity is governed by the wall-basemat junction.

* In containment B, the capacity is governed by shear in the basemat. However, the pressure for the hoop failure mode is a close second.

* Equipment hatch area failure pressure is at least 30% greater than the governing case, thus supporting the statement that the penetrations are designed to be stronger than the sections they replace.

It is recognized that the capacity calculations are based on simplified methods. In reality, numerous nonlinearities will come into play as the pressure is increased. Also, large deformations, severe concrete cracking, and steel yielding will probably cause some redistribution of stresses. However, all these effects will be local in nature and will not significantly impact the overall behavior. Therefore, the ultimate pressure capacities listed are considered to be accurate measures of minimum deterministic values.

4.0 SEISMIC CAPACITIES

4.1 General

For determining the seismic capacities, the analytical approach is similar to that for internal pressure. Results from three different types of analyses were utilized. The majority of calculations are based on results from a lumped-mass model analysis of the PCCV, involving both time- history and response spectrum techniques. Soil structure interaction is accounted by the impedance method. The second type of analysis used a finite element model of the containment and the soil medium. Results in terms of seismic design forces from these analyses were already available.

The third method of analysis,which was performed during the course of this study, involved the use of energy balance method. This method is applicable for determining the seismic margins against sliding and overturning of the structure (References 5 and 6).

4.2 Failure Modes

The governing structural failure mode under seismic loads is considered to be tangential shear failure preceded by membrane tension yielding at the heel near the wall-basemat junction. It is well known that maximum membrane forces occur, say, at azimuths 0 and 180 degrees while the maximum tangential shear occurs at

azimuths 90 and 270 degrees. Near the ultimate load the shell would yield, say, at azimuth 0 degrees and the yielding would propogate towards azimuths 90 and 270 degrees. As the seismic input is increased, the shell is predicted to shear off (slide) near the shell basemat junction. The seismic level that would cause such a failure was calculated based on Reference 7. It has been shown that the failure is accompanied by general yielding of the orthogonal reinforcement. The above ductile failure mode can be termed as the "combined membrane tension and tangential shear failure mode".

Other structural failure modes under seismic loads have been advanced in the past. Included among these are the flexural and shear failure of the basemat and the junction area. However, such structural failure modes will be preceded by other types of failure. This conclusion is supported by the probabilistic risk assessment study performed for the Zion plant (Reference 8).

The soil failure mode is considered next. Data regarding the ultimate bearing capacity of soil for the PCCV's are available in the existing documentation. In order to determine the soil pressure corresponding to an earthquake considering soil structure separation, the energy balance method was used. The input earthquake energy based on spectral acceleration is equated to the energy absorbed by the total system. The seismic level corresponding to the ultimate soil pressure capacity is then determined.

Two stability related failure modes, namely, sliding and overturning are also considered in this study. It should be realized that physical overturning of the PCCV during an earthquake is nearly impossible. However, large seismic displacements can lead to failure of safety related systems and components. For the purposes of this study, overturning failure was defined as reaching a displacement of six inches due to rocking of the structure. Most containments can deflect that much without a significant impact on adjacent structures. The systems that penetrate the containment are considered to be sufficiently flexible and ductile to permit such a displacement without the loss of a safety related function.

In the case of sliding stability, the actual sliding distance as a function of the ground velocity and friction between the structure and soil was calculated. Again considering the functional requirements, a maximum permissible translation of three inches was assumed.

4.3 Numerical Results

The results of the study are presented in Table 3. A review of this table indicates the following:

* As expected, there is a wide variation in the seismic margins for each type of failure mode.

* In the structural failure mode, the margin factor (seismic level at failure divided by SSE) ranges from 3.1 for plant F to 9.4 for plant B. Not surprisingly, plant F has the highest SSE and plant B has the lowest.

* Even though the seismic margins presented are based on conservative deterministic methods, there is significant margin beyond the SSE.

* Soil bearing failure is not in general the governing failure mode as shown in Table 3 and the corresponding seismic margin is at least 3.3.

* Overturning stability criterion leads to seismic margin ranging from 1.9 to 7.9. Four out of the six containments are governed by this criterion.

* Sliding stability criterion gives seismic margin from 2.0 to 15.2. None of the six containments is governed by this stability. Only for Containment F, this sliding stability gives a margin close to the governing overturning stability.

4.4 Additional Conservatism

In addition to the conservatism associated with the broad-band response spectra and SSE acceleration level, there is more conservatism associated with the seismic margins presented in this study.

First of all, the actual material strengths will increase the seismic margins.

Secondly, the seismic margins will be increased by the ductility of the structures. It can be stated that the PCCV's can absorb 2 to 4 times more energy than implied by the margin calculations presented in this paper (Reference 11).

Thirdly, the seismic analysis results which formed the basis of this study were all performed using low damping values. As the structure approaches failure levels the structural damping values will be greatly increased thus decreasing the structural response (Reference 9). In addition, some of the seismic analysis for the PCCV's included in this study had an artificial limit on soil radiation damping that was imposed during the early stages of criteria development for the nuclear power plants.

Consideration of these factors seems to indicate that the conservative deterministic seismic margin factors presented in Table 3 can be increased by a factor of 3 or more in order to arrive at a more realistic estimate of available seismic margin.

5.0 SEISMIC CAPACITY UNDER DIFFERENT INTERNAL PRESSURE LEVELS

Figure 2 show the seismic margin (seismic capacity divided by SSE) of Containment D under different internal pressure loads. Seismic capacity of this containment is governed by the overturning criterion up to about 1.25 times the design pressure load. The corresponding seismic margin is 2.4. As the pressure load increases, the seismic capacity decreases and it is governed by the "combined membrane tension and tangential shear failure." Because of the as-built arrangement of orthogonal bonded reinforcement in this PCCV, the elevation of tangential shear failure plane shifts from near the base of the cylindrical shell to about midheight as the pressure load increases.

6.0 REVIEW OF AVAILABLE TEST RESULTS

Reference 10 reports the results of internal pressure test to failure on a 1:14 scale model PCCV. The failure was by rupturing of hoop tendons at about midheight away from the discontinuities. Results of the present study shown on Table 2 compare well with the test. Four out of the six containments are governed by the hoop failure mode. Also, hoop failure for the remaining two containments gives a pressure capacity only about 4% and 18% above the governing failure modes.

Reference 7 summarizes the results from thirteen scale model containment tests to failure under cyclic lateral loads simulating horizontal seismic excitations. These tests were conducted in Japan. The first seven tests were on PCCV models. Four out of the seven PCCV models had a constant internal pressure load of about 60 psig. The distribution of shear force and bending moments along the height of the test specimens from the externally applied cyclic lateral loads was similar to that on an actual PCCV during an earthquake. Since the basemat of the test specimens were restrained from overturning and sliding, the test results are applicable only to the seismic behavior of containment shell. The test results showed the governing failure mode to be the "combined membrane tension and tangential shear failure" near the base. The seismic capacities corresponding to this failure mode for the six PCCV's in the present study correlate with the general yield condition of the scale model test specimens.

7.0 SUMMARY AND CONCLUSIONS

Analytical methods to predict the internal pressure and seismic capacities of a Prestressed Concrete Containment Vessel (PCCV) corresponding to various failure modes are discussed. The methods requires the extrapolation of the results of original design calculations and some simple additional calculations. All the calculations are based on deterministic methods with conservative assumptions and approximations.

Internal pressure capacities and seismic capacities were calculated separately for six PCCV's. For one of the six PCCV's, the seismic capacities were calculated under various internal pressure conditions. The available scale model test results were discussed with reference to the analytical results for the six PCCV's.

Based on the evaluation of the six PCCV's, the following conclusions can be reached:

1. Internal pressure capacity of a PCCV designed and built in the U.S. is about 2.5 times the design pressure.

2. Hoop tension failure at about midheight of a PCCV away from the discontinuities is the most likely mode of failure under pressure load. However, the other seven failure modes (Table 2) should also be evaluated for a specific PCCV.

3. Simple analytical methods are adequate to predict the pressure capacities.

4. Seismic capacity of a PCCV is at least two times the Safe Shutdown Earthquake (SSE) for PCCV's in the U.S.

5. Seismic capacity varies widely among PCCV's depending on the SSE level and the foundation characteristics.

6. Structural design details of a PCCV dictates the location of "combined membrane tension and tangential shear failure". Available scale model test results can be used to predict the corresponding seismic capacity.

7. Foundation characteristics govern the seismic capacity of a PCCV leading to either soil bearing or stability failure. The stability failure corresponds to large displacements either from rocking (overturning) or from sliding mode of behavior.

8. Seismic capacity of a PCCV decreases with internal pressure.

9. Conservatisms in the analytical methods presented for seismic capacity calculations can be reduced based on a study of PCCV's involving: nonlinear time history analyses, strain dependent material damping, as-built material strengths, separation of basement from soil, sliding, etc.

10. Based on the conservative deterministic seismic margins presented in Table 3, a containment structure is expected to contribute very little to the overall seismic risk of a nuclear power plant.

8.0 REFERENCES

1. Shunmugavel, P. and Johnson, T. E., "Internal Pressure Capacity of Prestressed Concrete Containments For Nuclear Power Plants", pp. 37-66, NUREG/CP-0033, Volume II, U. S. Nuclear Regulatory Commission, 1982.

2. Walser, A., "Primary Containment Ultimate Capacity of Zion Nuclear Power Plant For Internal Pressure Load", pp. 67-108, NUREG/CP-0033, Volume II, U. S. Nuclear Regulatory Commission, 1982.

3. "Code for Concrete Reactor Vessels and Containments", ASME, Section III, Division 2, 1983.

4. White, R. N. and Gergely, "Punching and Radial Shear Problems in Reinforced Concrete Containments", pp. 109-122, NUREG/CP-0033, Volume II, U. S. Nuclear Regulatory Commission, 1982.

5. Tseng, W. S. and Liou, D. D., "Simplified Methods for Predicting Seismic Basemat Uplift of Nuclear Power Plant Structures", K 3/6, 6th SMiRT Conference, 1981.

6. Newmark, N. M., "Effects of Earthquake on Dams and Embankments", Geotechnique, Volume XV, No. 2, pp. 139-159, June 1965.

7. Shunmugavel, P., "Analysis and Design of Concrete Containments for Tangential Shear Loads", J 5/2, 7th SMiRT Conference, 1983.

8. "Zion Probabilistic Safety Study", Commonwealth Edison Company, 1983.

9. Newmark, N. M. and Hall, W. J., "Development of Criteria for Seismic Review of Selected Nuclear Power Plants", NUREG/CR-0098, U. S. Nuclear Regulatory Commission, 1978.

10. Rizkalla, S., Simmonds, S. H. and MacGregor, J. G., "A Test of a Model of a Thin-Walled Prestressed Concrete Secondary Containment Structure", J 4/2, 5th SMiRT Conference, 1979.

11. Proceedings, EPRI/NRC Workshop on Nuclear Power Plant Reevaluation to Quantify Seismic Margins, Appendix A, August 1985.

TABLE 1

BASIC DATA ON THE EXAMPLE CONTAINMENTS

No.	Data Description	Data for Various Containments A	B	C	D	E	F
I	Geometry						
	Internal Diameter	140'	150'	140'	146'	130'	150'
	Wall Thickness	3'-6"	4'-0"	3'-9"	4'	4'	4'
	Dome Type	Shallow	Hemi-spherical	Hemi-spherical	Hemi-spherical	Hemi-spherical	Hemi-spherical
	Dome Thickness	2'-8"	3'-0",	3'-9"	3'-6"	3'-0"	3'-6"
	Basemat Thickness	9'-0"	18'-0", 12'-6"	10'-6"	10'-6"	10'-0"	9'-0"
	Basemat Diameter	157'	166'	154'-6"	161'	146'	184'
II	Material						
	Concrete - Shell	5500 psi	5500 psi	6000 psi	6000 psi	6000 psi	6000 psi
	- Basemat	5000 psi	4000 psi	5000 psi	5000 psi	5000 psi	6000 psi
	Liner	1/4", A-442	3/8", SA-285	1/4", SA-285	1/4", SA-285	1/4", SA-285	1/4", SA-285
	Prestress Type	90, 1/4" wire	186, 1/4" wire	55, 1/2" strand	186, 1/4" wire	55, 1/2" strand	55, 1/2" strand
	Ultimate Bearing Capacity	40 ksf	54 ksf	62 ksf	36 ksf	200 ksf	60 ksf
III	Design Parameters						
	Internal Pressure P_d	47 psig	56.5 psig	52 psig	60 psig	60 psig	60 psig
	Prestress Level	1.5 P_d	1.5 P_d	1.5 P_d	1.2 P_d	1.2 P_d	1.3 P_d

TABLE 2

PRESSURE CAPACITIES OF EXAMPLE CONTAINMENTS

No.	Failure Modes	Pressure Capacity/Design Pressure					
		A*	B	C	D	E	F
1.	Hoop	<u>2.9</u>	2.5	3.3	<u>2.5</u>	<u>2.3</u>	<u>2.4</u>
2.	Meridional	3.4	3.2	4.7	2.9	3.7	3.2
3.	Dome	3.3	3.2	3.4	2.9	3.3	2.9
Wall-Basemat Junction							
4.	Shear	3.7	3.3	--	3.5	3.8	5.2
5.	Flexural	16.7	3.2	<u>2.8</u>	2.9	2.6	2.6
Basemat							
6.	Shear	3.8	<u>2.4</u>	--	3.2	2.8	2.5
7.	Flexural	11.0	2.8	--	3.8	--	2.8
8.	Equipment Hatch Area	3.7	6.8	4.1	3.8	4.7	3.2

* Based on as-built actual material strengths. All other containments are based on minimum specified material strengths.

Notes:

1. Underlined numbers indicate the governing (minimum) pressure capacity.
2. Where no numerical value is provided, pressure capacity is greater than the minimum valve presented.

TABLE 3

SEISMIC CAPACITIES OF EXAMPLE CONTAINMENTS

No.	Failure Modes	Seismic Capacity/SSE Prestressed Concrete Containment Vessel					
		A	B	C	D	E	F
1.	Tangential shear	5.3	9.4	4.1	3.8	5.1	3.1
2.	Soil bearing pressure	3.7	6.9*	5.2	3.3	7.9*	3.7*
3.	Overturning stability	4.3	5.9	3.5	2.4	7.9*	1.9
4.	Sliding stability	7.1	15.2	5.5	5.9	6.4	2.0

* Seismic capacity is at least this value based on the simple analysis.

Notes:

1. Tangential shear failure mode provides the smallest seismic margin of structural failure modes.
2. Overturning stability criterion is based on 6 inches of displacement.
3. Sliding stability criterion is based on 3 inches of displacement.

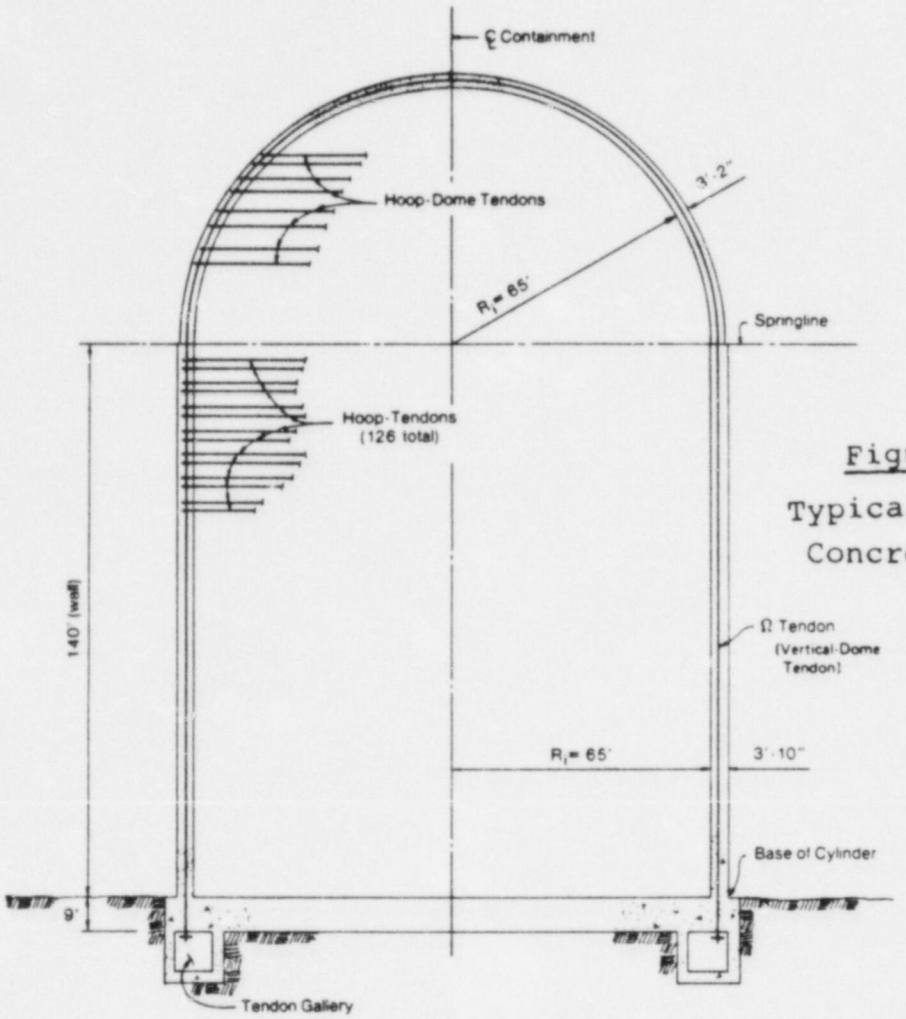
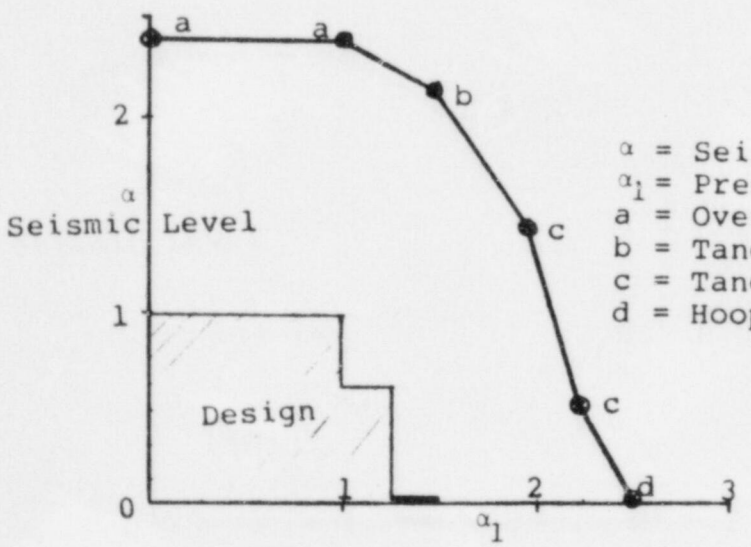


Figure 1
Typical Prestressed
Concrete Containment



α = Seismic Capacity/SSE
α_1 = Pressure/Design Pressure
a = Overturning
b = Tangential Shear at Base
c = Tangential Shear at Midheight
d = Hoop Tension at Midheight

Figure 2 Seismic Capacity Under Various Pressure Load

THE INFLUENCE OF NON-LINEARITY AND FOUNDATION BEHAVIOUR ON CONTAINMENT INTEGRITY

J J B Evans
Ove Arup & Partners
13 Fitzroy Street
London W1P 6BQ

P M Keogh
Ove Arup & Partners
13 Fitzroy Street
London W1P 6BQ

ABSTRACT

A series of analyses have been carried out to examine the structural behaviour of a PWR containment subjected to internal pressure. The containment examined was of the type proposed for Sizewell 'B' in England.

The analyses considered variations and non-linear behaviour in the soil properties, the influence of the reactor pit and the effect of non-linear behaviour of the prestressed concrete walls. The philosophy adopted throughout this work was to use simplified engineering methods to assess the significant aspects of the response of the containment and establish areas for particular attention in the design.

The paper records the results obtained and identifies the benefit of increasing shear strength at the wall base interface to a level that ensures it is not a dominant failure mechanism.

INTRODUCTION

A series of studies of a PWR containment structure of the type proposed for Sizewell B in England has been carried out on behalf of HM Nuclear Installations Inspectorate. This paper reports some of the work done on the base slab and containment wall when subjected to internal pressure taking account of soil response and concrete non-linear behaviour. The work falls into three logical sections, these being:

a) study of the sensitivity of the structural response to variations in soil stiffness properties under a factored design basis pressure.

b) analysis of the base slab, acting under factored design basis pressure, to determine the influence of the reactor pit.

c) analysis of the containment under extreme pressure allowing for non-linear behaviour of the prestressed concrete wall.

The paper will follow these sections.

As far as possible simple methods have been used in preference to detailed finite element models in order that results may be obtained rapidly allowing areas for subsequent research and attention to be identified at an early stage.

The views expressed in this paper are not necessarily those of HM Nuclear Installations Inspectorate.

SENSITIVITY TO SOIL PROPERTIES

The sensitivity of the structural response to variations in soil properties is of interest since there is always some uncertainty in the soil properties. A parametric study of the soil stiffness variations also allowed extrapolation of the results to other sites.

The containment was modelled using 3 noded axisymmetric, linear elastic, shell elements. The soil was modelled as a series of independent springs. The stiffness of each spring was calculated to take account of the semi-infinite nature of the supporting soil and the non-linear variation of the soil stiffness with the average achieved strain at each depth through the soil. The details of the method are described below.

The soil profile at the Sizewell site is shown in figure 1.

Five stiffness profiles were evaluated to allow for a full range of possible foundation types. These are indicated in figure 2. The stiffness profile "C" was taken as the stiffness evaluated at each level using in-situ pressuremeter results from site investigation reports. This stiffness profile was used in other analyses and enabled the method to be compared with more rigorous modelling techniques.

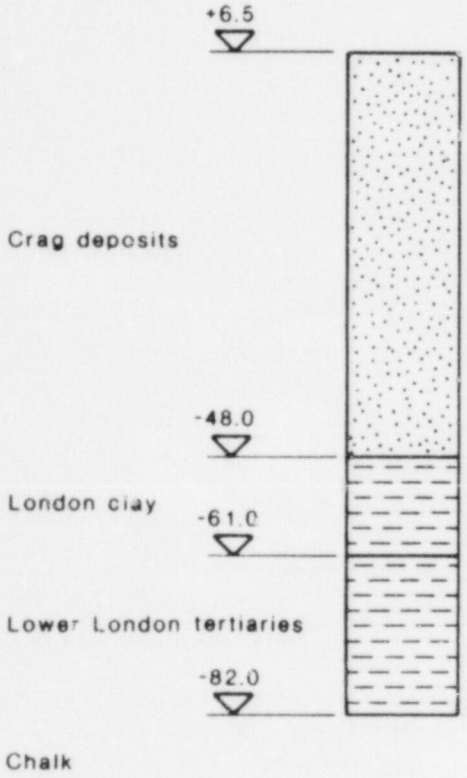


Fig.1 SOIL PROFILE

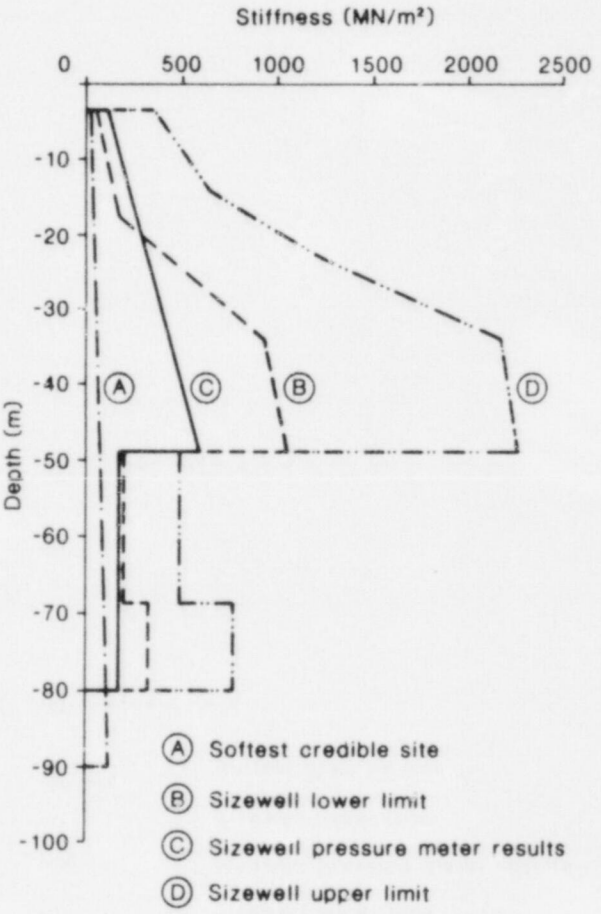


Fig.2 SOIL STIFFNESS PROFILES

The solution of the Boussinesq equations with the Steinbrenner approximation for layered soils was incorporated in a computer program VDISP [1]. The surface profile under a uniformly distributed load, to simulate the containment building, was calculated neglecting the stiffness of the building. The reciprocal of the displacement achieved at each location was used

to calculate the spring stiffnesses to be used in the finite element model.

The soil stiffness profiles "B" and "D" were developed from consideration of the lower and upper ranges of low strain stiffness which enveloped the uncertainty given by the test results.

For the Crag layer, the low strain stiffness was then converted to a secant stiffness which took account of the expected average strain over the plan area of the containment within each layer of soil. The actual strain computed was used to recalculate the soil stiffness and the process was repeated until convergence was achieved. The variation of secant shear modulus with shear strain was developed under a separate study [2] and used work reported in [4]. This latter reference drew the important conclusion that at each level of strain, the ratio of secant modulus to the low strain secant modulus is virtually constant for granular materials.

For the clay layers, a similar procedure was used but taking the ratio of secant shear modulus to undrained shear strength as a constant at each level of shear strain amplitude. The appropriate curve was developed from the site results and took into account the work done in [4] and [5] for clay materials.

The resulting stiffness profiles shown in figure 2 were then used to calculate spring stiffnesses for use in the axisymmetric model of the containment building.

The stiffness profile "A" was based on a softest credible clay material. An undrained shear strength of 150 kN/m² was assumed since it was considered that softer soil would not support the containment building adequately even under static loads. The results indicated that the precise value chosen was not critical since the containment structural response was found to be insensitive to soil variations when the soil was very soft. The spring stiffnesses were calculated as before.

The foundation "E" was assumed to be infinitely rigid and base "lift-off" was allowed for.

The results obtained from consideration of an internal pressure of 1.5 times the design pressure and using the five soil profiles are shown in figures 3, 4, 5 and 6. The horizontal axis in each case has been taken as the equivalent spring stiffness of the soil at the centre of the base slab. This is an arbitrary choice since the stiffness will vary with base vertical pressure and base radius but it does allow some comparison of the results by stiffness.

The results show a step function between analyses D and E. If the results are plotted against flexibility rather than stiffness, a smooth curve is obtained but most of the results are compressed into one end and become less useful.

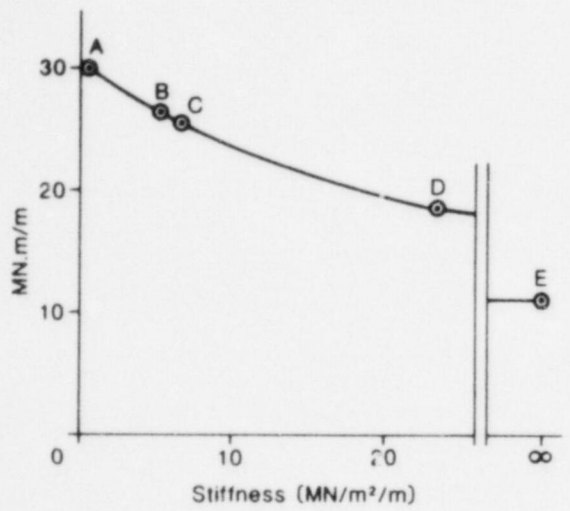


Fig.3 BASE MAXIMUM BENDING MOMENT

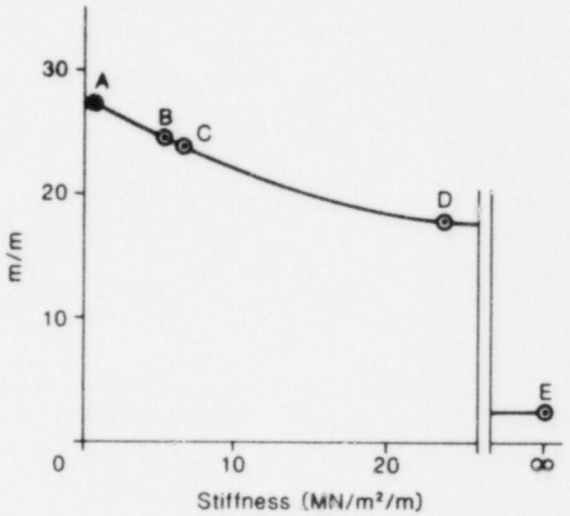


Fig.4 BASE DEFLECTION (EDGE TO CENTRE)

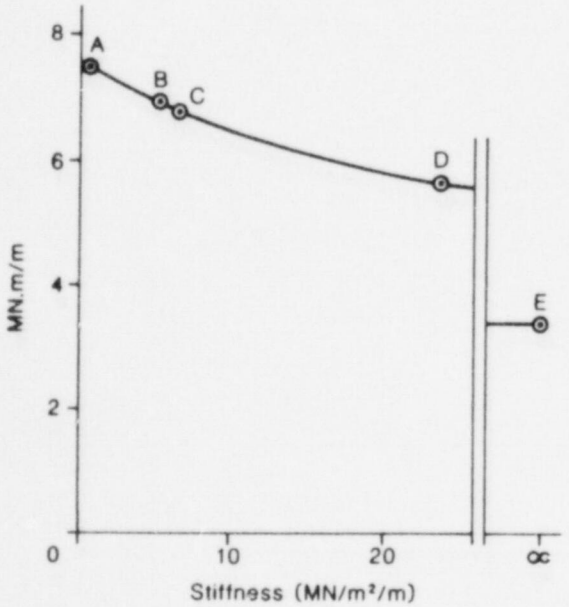


Fig.5 WALL / BASE BENDING MOMENT

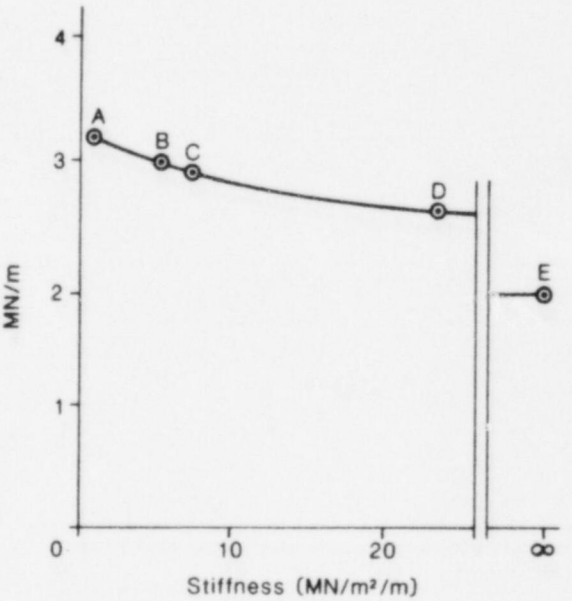


Fig.6 WALL / BASE SHEAR

ANALYSIS OF BASE SLAB ALLOWING FOR THE REACTOR PIT

The containment structure, acting under design basis accident pressure factored by 1.5, was analysed. Three separate computations were executed and their results compared.

They were:

a) using a specialised program for foundation slab analysis, including the reactor pit;

b) using a finite element program with the soil represented by independent springs, and including the reactor pit;

c) a repeat of b) above with a flat base slab, that is, without a reactor pit.

The complex internal structures were simplified to line loads from the main walls. The stiffness contribution of the internal structures was not included. The loads from plant were allowed for.

The structure was initially analysed as a symmetric half model using 4 noded isoparametric elements. The soil stiffness profile was taken to be that indicated by pressuremeter results (soil stiffness profile C, described earlier). The model was analysed using the program RAFT [3]. This program models the soil as a substructured super element. To achieve this, the soil surface is subjected to a unit load at each contact node position and the deflection at each of the nodes is calculated. This gives a flexibility matrix which is then inverted to give a stiffness matrix.

The results of the RAFT analysis gave deflection behaviour in line with that expected and in particular, gave a surface stiffness comparable with that calculated by VDISP. This was an important observation, supporting the validity of the use of VDISP and independent nodal soil springs in this series of analyses.

The model was recreated using 8 noded semi-loof elements, which are a feature of the finite element program PAFEC used for the analysis. The soil was modelled as a series of discrete springs attached to each node. The spring stiffnesses were calculated using the program VDISP in the manner already described. The model used and the deflected shape are shown in Figure 7.

The bending moments achieved about a tangential axis are shown in Figure 8.

The analysis was repeated with the reactor pit removed, that is using a flat base slab. The bending moment diagram was smooth with a maximum value of 26MNm/m compared with the maximum of 35MNm/m (peak) value found before.

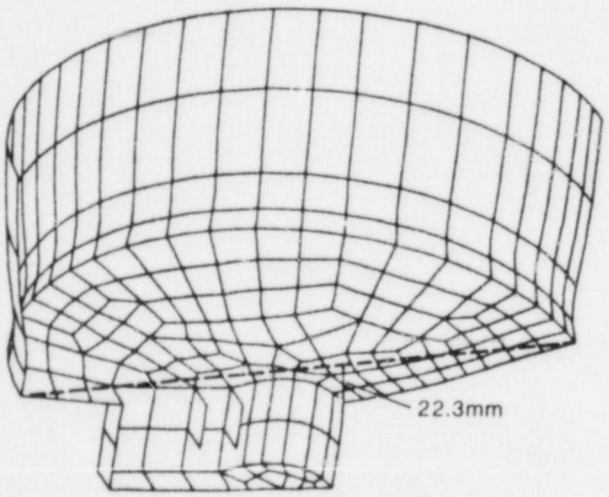


Fig.7 MODEL AND DISPLACED SHAPE FOR BASE SLAB ANALYSIS

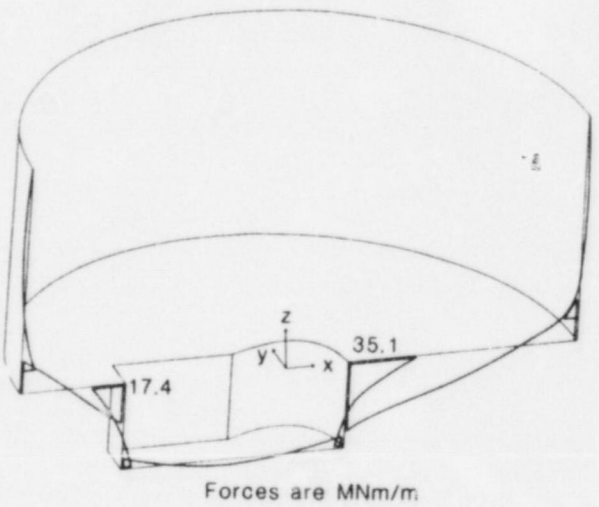


Fig.8 BASE BENDING MOMENTS ON TANGENTIAL AXIS

The results show a significant stress concentration at the rounded end of the reactor pit. The highest values occur within the wall thickness of the pit and will clearly be modified if the region was modelled more accurately using brick elements for example.

The asymmetry of the pit was also reflected in the bending moments achieved in the wall. A variation from 5.67MNm/m to 7.32MNm/m was found at locations remote from and on the line of the model symmetry respectively.

The presence of the pit also caused concentrations of the base slab membrane forces. The tension forces were greatest at the rounded end of the reactor pit and would affect the reinforcement required.

The deflections of the base slab did not differ greatly with or without the pit.

THE EFFECTS OF EXTREME PRESSURE ON THE CONTAINMENT

The purpose of this part of the assessment was to estimate the ultimate capacity and mode of failure caused by an extreme internal pressure load. Conventional linear elastic analysis is not adequate to deal with the complex composite of structural materials present in a prestressed concrete containment structure at the high levels of strain caused by this type of loading condition.

Usually, in these circumstances either simple non-linear manual calculations are performed to examine particular failure mechanisms or large scale non-linear finite element analyses are carried out. The latter option was not pursued in this work as the objective was to gain an initial appreciation of the non linear behaviour using relatively simple methods.

Therefore, for this work, an iterative approach was adopted with repeated use of the linear elastic finite element program PAFEC. A piecewise linear method was used to account for the softening constitutive behaviour of the prestressed reinforced concrete and thereby to identify the extent of stress relief and stress re-distribution within the containment. The structure was treated axisymmetrically. Failures initiated by local effects such as prestressing buttresses and access hatches were treated separately and are not reported here.

The failure mode was anticipated to be either by failure of the wall/base connection due to locally high bending moments and shear forces or by failure at the mid-height of the cylinder wall due to high membrane tensions ('barrel-bursting'). The latter effect was evaluated by manual calculation of the non-linear response which indicated the various stages of containment deformation. At each stage the overall behaviour of the containment structure was evaluated using the non-linear technique described until failure was reached at some point in the containment structure.

Loading Conditions and Material Properties

The loads acting on the containment were taken to be those during normal operation (gravity and prestress) in addition to the extreme temperatures and pressures particular to a loss of coolant accident.

The operating differential temperature at early life produces stresses opposite in sign to the pressure load. In the late life condition these stresses reduce to zero because of creep of the concrete. Therefore, to obtain a conservative estimate of the ultimate pressure capacity, the late life condition was examined and the differential temperature stresses neglected. This also had the effect of reducing the effective prestressing loads because of creep and shrinkage of the concrete.

The prestress effects were applied as equivalent pressures and non-axisymmetric effects due to the particular pattern of the prestressing tendons in the dome were neglected.

A thermal shock of 160°C was applied to the liner, which was assumed to be fully bonded throughout. The pressure was considered to be a quasi-static load.

The material properties used were generic for the various materials since the design was still at the scheme stage. For example the reinforcement was taken to be high yield with average properties from manufacturers literature and the concrete had an assumed rectangular/parabolic stress block in bending. The properties used in the analysis were determined for an equivalent homogeneous section. That is, the containment wall which has various structural components (concrete, reinforcement, liner, prestress) was treated as an equivalent single material with pseudo-thickness and elastic modulus.

The soil was modelled using discrete springs by the methods described earlier using a soil stiffness profile based on the pressuremeter results. It was anticipated that the springs would be progressively released as uplift occurred, but because of the softness of the soil this was not necessary.

Manual Calculation of Barrel Bursting

As a pre-cursor to the main axisymmetric analysis, membrane failures of the containment were examined at the critical mid-height of the containment wall. In 'membrane' zones such as this, the behaviour is defined by simple equilibrium considerations so a high level of detail in the calculations is possible. An analysis was carried out to estimate the levels of internal pressure corresponding to the various stages of containment deformation using the following assumptions:-

(i) the concrete and liner are isotropic.

(ii) the reinforcement in the two directions is substantially independent but interacts through Poisson's ratio effects in the concrete.

(iii) the prestressing steel is un-bonded and does not respond to local concrete strains.

(iv) creep and shrinkage in the concrete are uniform and can be represented in the initial stress state by a reduced (long term) modulus. A short term elastic modulus was used in the calculation of the pressure effects.

(v) the thermal shock load causes a uniform pre-strain in the liner, but does not have time to affect the concrete. This resulted in an initial pre-stress in the liner such that it was in a state of compressive yield.

(vi) differential creep effects had occurred due to the operating temperature.

(vii) the concrete is pre-cracked.

The results of these calculations showing the internal pressure versus radial displacement are shown in Figure 9.

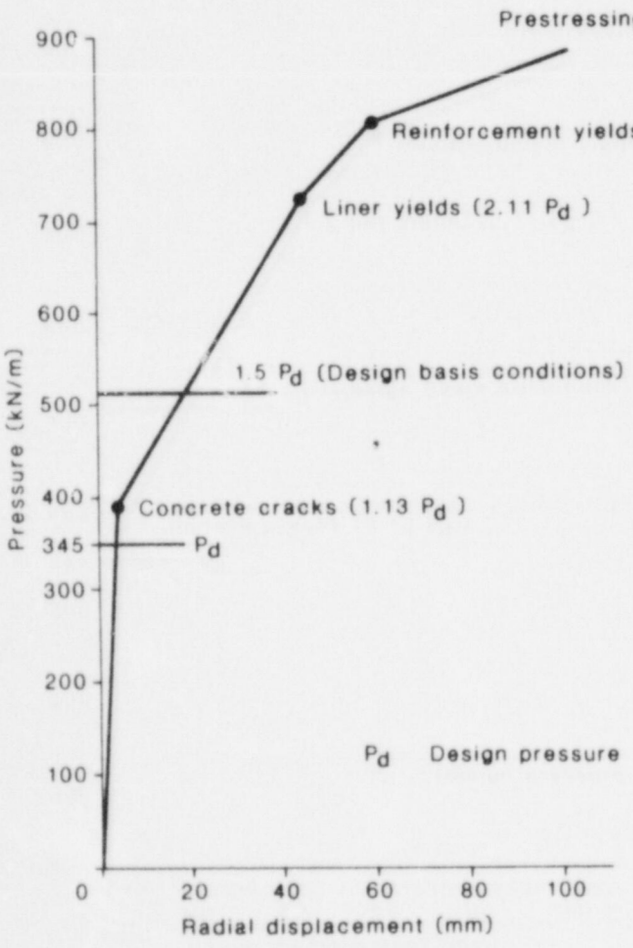


Fig.9 INTERNAL PRESSURE DISPLACEMENT RELATION OF THE MEMBRANE ZONE OF THE CYLINDER

Axisymmetric Non Linear Finite Element Analysis

For this analysis the structure was assumed axisymmetric and the finite element program PAFEC was used. The element selected was a three-noded thin isotropic shell of revolution. The behaviour of the steel/concrete composite section was defined using standard reinforced concrete theory based on a linear strain diagram. The moment/curvature relations, and shear and axial force to displacement relations were calculated at the various transition stages of pressurisation: cracking of concrete, yielding of liner etc. This is shown in figure 10 which also shows the effects of an unbonded liner and bonded tendons. These relationships were used to define an equivalent homogeneous section with pseudo-thickness and elastic modulus. Non-linearity was accounted for using a 'secant modulus' approach based on the meridional moment/curvature relations and the hoop axial force/displacement relations. This technique is iterative and is based on the repeated solution of linear systems until convergence is achieved (refer figure 11).

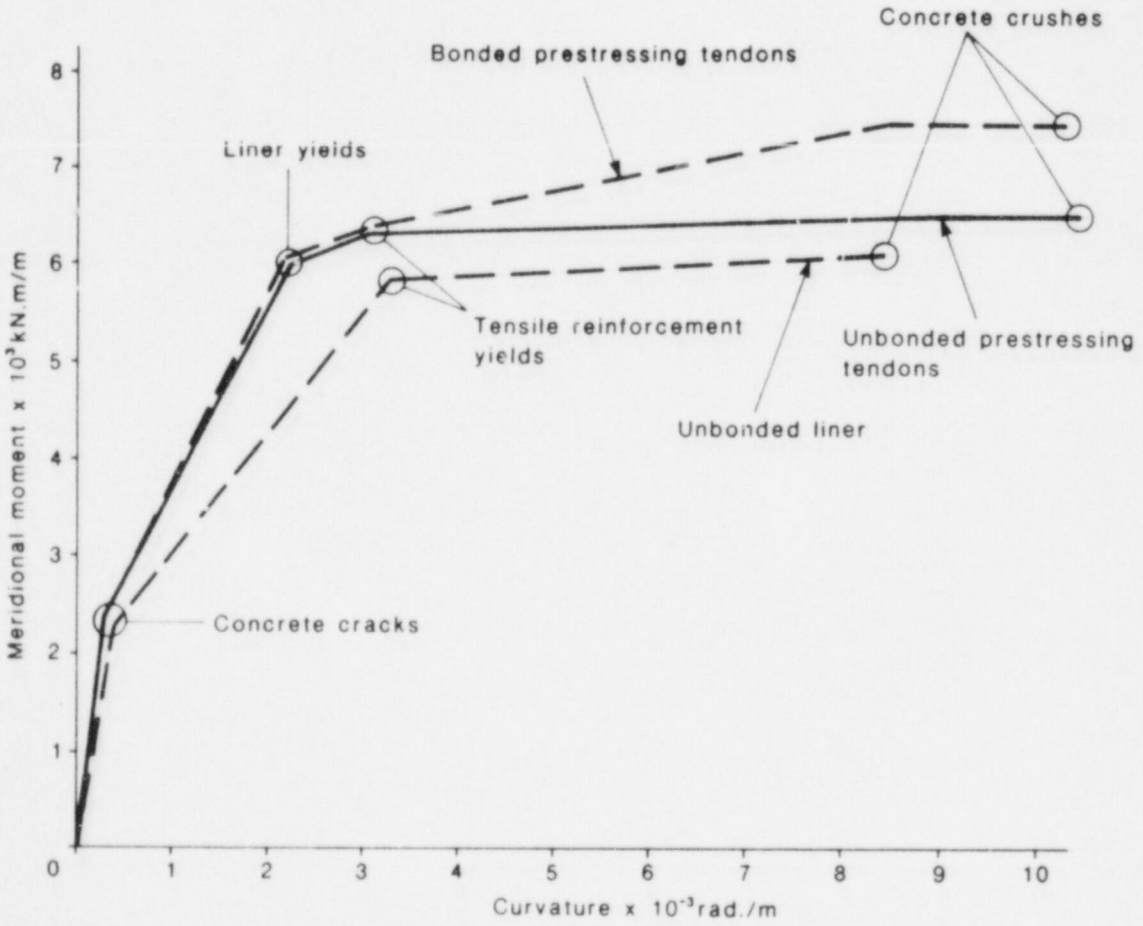


Fig. 10 MOMENT CURVATURE RELATION - CYLINDER WALL BASE

The finite element stress results do not have direct physical significance but, when converted into stress resultants (axial forces and bending moments) using the equivalent section properties, they can be interpreted directly using reinforced concrete theory. The converged solution at each pressure level was interpreted in terms of stresses and strains in the concrete, reinforcement, liner and prestressing steel. The failure criterion used to assess the potential for shear failures that the wall-base connection was based on the equations developed for BS8110 [9] described in an unpublished paper. The criterion used related failure to meridional bending, shear and axial tension.

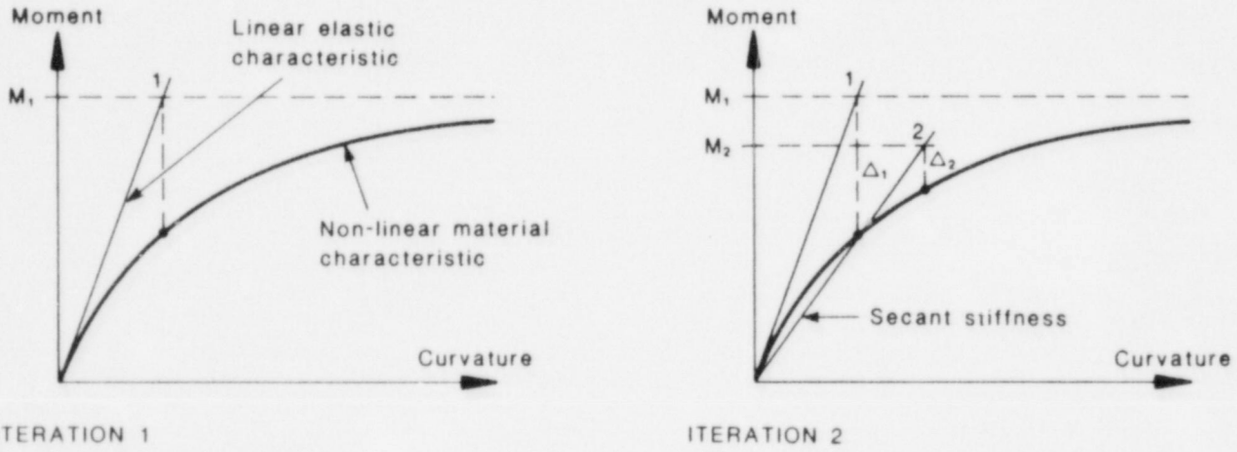


Fig.11 NON-LINEAR ANALYSIS

The results indicated that the ultimate pressure load for the proposed Sizewell "B" Containment was about 2.3 times the design pressure. The failure mode was expected to be radial shear failure at the wall/base connection despite significant redistribution of the discontinuity forces at this location.

The ultimate failure pressure at which 'barrel-bursting' was calculated to occur was about 3.6 times the design pressure.

DISCUSSION OF RESULTS

The results of the soil sensitivity study show a significant variation of the containment structural response with soil stiffness and that the softest soil profile is the most onerous for internal pressure loads. The results also show that the soil stiffness profile based on pressuremeter results at Sizewell gives results similar to those for the lower design limit suggested for the site. Whether the use of this profile would satisfy any probabilistic design requirements when used with factored Design Basis Accident pressure was beyond the scope of this study.

The variation of the structural response with variation of the soil properties is in line with the results reported in [6] for Maine Yankee containment building. In that report, basement lift off was inhibited then released and this changed the mode of failure from barrel bursting (117 psig) to wall/base interface failure (96 psig).

The results reported here indicate that analyses based on a rigid base, or an assumption of rigid foundation material, will underestimate the forces applied to the structure under internal pressurisation, unless, of course, the containment is actually sited on hard rock.

The results of the base slab analysis allowing for the reactor pit show the significant variation of forces in the base slab, and in the wall, in comparison to those forces calculated assuming a flat base. It should be noted however, that the variation in wall forces will be mitigated to some extent by the influence of non linear behaviour as extreme pressures are applied to the containment.

The results of the non linear analysis reported here indicates that it is possible for the present Sizewell design to be justified as meeting its design criteria, particularly in respect of the need to satisfy an ultimate failure level of 2.0 times the design basis accident pressure. This could not be done using linear analysis.

The pressure at which shear failure occurs is subject to significant uncertainties particularly as the design equations do not closely model the relatively short shear span generated in the wall. The behaviour and its complexity is discussed at some length in [7]. In the elastic condition, the shear span is approximately 2.0 times the effective depth. As non linear behaviour begins to dominate, the wall/base interface bending moment is reduced and the point of contraflexure, that is zero bending moment, moves down the wall. In this condition the shear span is reduced.

The uncertainty is increased by the nature of shear failure itself. A statistical study [8] showed that the coefficient of variation of shear strength is significant. For a section with nominal shear steel, a coefficient of variation (standard deviation/mean strength) would be about 15%.

The figure of 15% did not include variations in shear resistance due to effects such as longitudinal bar diameter used, bond variations of bars, variations of quality around a containment circumference, workmanship generally on site and detailing standards.

Results from Monte Carlo methods lead to lower bound estimates of variability, generally, and it is clear that shear failure is subject to large variability and hence uncertainty.

Shear failure is also potentially brittle. That is, failure can occur rapidly with little or no sign of initial distress. This is dependent on the level of shear reinforcement used.

Shear strength, at the wall base, interface, can be increased relatively easily by the addition of shear links and this represents a simple way in which the overall reliability of a containment structure can be enhanced.

In view of the uncertain nature of shear failure, raising the shear resistance level to a pressure significantly above that associated with barrel bursting pressure appears desirable.

It should be noted that the conclusions drawn in this paper depend on specific structural arrangements and would not necessarily apply to all containments.

ACKNOWLEDGEMENT

The assistance and support of HM Nuclear Installations Inspectorate in preparing and presenting this paper is gratefully acknowledged.

REFERENCES

1) Ove Arup and Partners VDISP, A computer program for settlement calculations.

2) Ove Arup and Partners, Sizewell B PWR, Soil Structure Interaction Study, phase 1. March 1985.

3) Hooper J.A. Raft analysis and design, some practical examples. The Structural Engineer. V62A/No. 8. August 1984.

4) Seed H.B., Idriss I.M. Soil Modulus and damping factors for dynamic response analysis. Earthquake Eng. Research Centre Report No. EERC 70-10. December 1970.

5) Koutsoftas D.C., Fisher J.A., Dynamic properties of two marine clays. Journal Geo. Eng. Div. ASCE. Vol 106, No. GT6. June 1980.

6) Blejwas T.E., Horschel D.S., Jung J., Reese R.T. Containment Integrity Program, Quarterly Report, January - March 1980. NUREG/CR-3412. January 1984.

7) Rogowski, MacGregor. Shear strength of deep reinforced concrete continuous beams. Structural Engineering Report No. 110. Dept. of Civil Engineering. University of Alberta. November 1983.

8) Mirza, MacGregor. Statistical Study of Shear Strength of Reinforced Concrete Slender Beams. ACI Journal. November 1979.

9) British Standards Institute.
BS8110, The Structural Use of Concrete, Part 1. 1985.

SESSION E

ANALYSIS/TESTING OF CONTAINMENT SYSTEMS, PART II

Structural Analysis of a Japanese BWR MARK-I Containment under Internal Pressure Loading

T. Isozaki, K. Soda, S. Miyazono

Japan Atomic Energy Research Institute
Tokai Research Establishment
Tokai-mura, Ibaraki-ken 319-11, Japan

Abstract

This paper describes the elastic-plastic analysis of the Japanese BWR MARK-I steel containment vessel under pressure loadings by general purpose Finite Element Method code ADINA. The present study is focused on an entire deformation of the vessel rather than the stress or strain concentrations around the structural singularities such as penetrations. Elastic deformation limit, displacement, equivalent stress and strain distributions are discussed.

1. Introduction

One of the important roles of a containment vessel of a light water reactor is to prevent fission products release to the environments as the last physical barrier. There arises a question as to whether the containment integrity can be maintained or not under extreme conditions which are anticipated during a severe accident, and it has become important issues among nuclear communities /1/ .

The containment integrity is especially critical for a risk assessment of a nuclear reactor, since prediction of when and where a containment loses its integrity has a significant impact on an amount of fission products which would be released to the environments.

In order to obtain quantitative information on a containment integrity under severe accident conditions, an elastic-plastic analysis was conducted by using the ADINA code /2/,/3/ for a Japanese BWR MARK-I containment.

Objectives of the analysis are to investigate an overall deformation, to clarify stress and strain distributions and the limit of linear deformation of the vessel under internal pressure loading, and to identify the locations and the pressure at which the containment vessel may yield. In this report, stress and strain concentrations around the penetrations in a strict sense were not included to simplify the analysis. It should be mentioned that the present analysis considered an internal pressure loading only and temperature effect was not taken into account to save the computing time.

2. Modelling of the Containment Vessel

2.1 Configuration of the Japanese BWR MARK-I Containment

The Japanese BWR MARK-I containment has a larger volume in a drywell than the original MARK-I containment, with the design pressure

of 0.524 MPa and the design temperature of 171 °C /4/ . The existing Japanese BWR MARK-I steel containment vessel is shown in Fig. 1. Inner diameter and inner height are 23.9 m and 38.25 m, respectively. The vessel is made of JIS type SGV 49 and SPV 50 which are equivalent to SA 516 Grade 70 and SA 537 Class 1. By using SA 537 which has higher yield strength than SA 516, the thickness at the bottom part of the drywell can be reduced to 38 mm, and therefore no post weld heat treatment (PWHT) is needed /4/ . The vessel is equipped with hatches, locks, penetrations and a suppression chamber. Moreover, the vessel is surrounded by a biological shield wall with a distance about 35 mm between the vessel and the wall.

2.2 Finite Element Model

The containment vessel was represented by the finite element model as shown in Fig. 2, where a number of penetrations of the vessel were reduced to only three, namely an equipment hatch with inner diameter of 3.66 m, a personnel airlock with inner diameter of 2.6 m and a safety relief valve hatch with inner diameter of 2.0 m. Suppression chamber was not considered in the present analysis. The equipment hatch and the personnel airlock were rotated circumferentially from the original position without changing the elevation so that only one half of the vessel is analyzed.

The finite elements used in the present analysis were 6- node and/or 8-node shell element, shell transition element and solid element. Transition elements and solid elements were applied to the intersections of the vessel, a cylinder and a cover at each penetration. Figure 3 illustrates, as an example, how the three different elements were employed at the shell intersections of a personnel airlock where the black dots represent the nodes.

Covers of the three penetrations were modelled with a circular flat plate for a personnel airlock, an inwards concave plate for an equipment hatch and a convex plate for a safety relief valve hatch. All of the covers were assumed to have a constant thickness without any stiffners.

Total numbers of the elements and the nodes in this modelling were 344 and 1069, respectively.

2.3 Material Model

The stress-strain diagram of SA 516 Grade 70 and SA 537 Class 1 is shown in Fig. 4. Bilinear model was used for the ADINA shell elements. It can be seen from this figure that SA 537 has superior material strength to SA 516. The ADINA code requires Young's modulus E, Poisson's ratio ν, yield strength σ_y and strain hardening modulus E_T as input data. The values used in the present analysis were summarized in Fig. 4. In ADINA, von Mises yield criteria, and isotropic work hardening are assumed in the shell element to describe the material nonlinearity.

3. Results and Discussion

3.1 Overall Deformation of the Vessel

Overall deformation of the containment vessel under internal pressure of 0.39, 1.08, 1.57 and 2.06 MPa is shown in Fig. 5. Deformations are exaggerated by a factor of ten. It can be seen from this figure that a large deformation occurred at the cylindrical part of the vessel and the knuckle. Figure 6 shows front, side and top views of the deformation of the vessel at 2.06 MPa. The large deformation at the vessel cylinder and the knuckle can be easily recognized from the front and side views in this figure.

As was mentioned previously, there exists the initial gap between the containment vessel and the biological shield wall. However, this gap might be closed by an excessive deformation of the vessel due to increasing internal pressure. The geometrical relations between the gap and deformation are shown in Figs. 7 and 8. At 1.57 MPa, there was no contact of the vessel with the biological shield wall. However, when the pressure increased to 2.06 MPa, the gap was already closed both at the cylinder and the knuckle. It is shown later in section 3.4 that the closure of the gaps could occur at the internal pressure exceeding 1.98 MPa.

In addition, it should be noted that if the thermal expansion of the vessel in the radial direction is taken into account, this gap would be closed earlier before the pressure reaches 1.98 MPa. If we take temperature increase to 171 ^{o}C of the design temperature, free thermal expansion at the cylindrical part of the vessel would be 20 mm. Therefore, the gap will be closed earlier at 1.05 MPa since the remaining gap at that temperature is 15 mm .

3.2 Displacements along Horizontal and Vertical Reference Lines

Displacements were calculated in the radial direction (parallel to X-Y plane) as well as in the axial (Z axis) directions along the two horizontal lines indicated by HB and HT in Fig. 9 and the three vertical lines indicated by VC, VL and VR in Fig. 10. These lines were selected in such a way that the lines intersect the three penetrations. Radial displacements along the lines HB , VC and VRR are shown in Figs. 9, 10 and 11, respectively. The line VRR is the one where the effect of stress or strain concentrations around the hatches is negligible. Figure 10 shows that two positive peak displacements occurred at points M and D, corresponding to middle section of the cylindrical part of the vessel and the knuckle, and that the negative displacements occurred at the location E corresponding to the upper head of the vessel. It can be seen from Figs. 9 , 10 and 11 that the maximum radial displacement occurred at point M.

3.3 Equivalent Stress and Strain along the Reference Lines

In order to estimate at what part of the containment yield occur, equivalent stress and strain were calculated along the reference lines. The present analysis employed the 3x3x4 Gauss integration point stations for one shell element. In ADINA-PLOT only the integral points at the corners of each element are available to figure the

element stress or strain output. Therefore, equivalent stress and equivalent total strain were obtained and plotted at these integral points. The equivalent stress and equivalent total strain along the lines HB and VC are shown in Figs. 12 through 15. Equivalent stress and strain are given by the following equations /5/ where $\sigma_t = 0$.

$$\bar{\sigma} = \frac{1}{\sqrt{2}} \sqrt{(\sigma_r - \sigma_s)^2 + (\sigma_s - \sigma_t)^2 + (\sigma_t - \sigma_r)^2 + 6(\tau_{rs}^2 + \tau_{st}^2 + \tau_{tr}^2)}$$

$$\bar{\varepsilon} = \frac{\sqrt{2}}{3} \sqrt{(\varepsilon_r - \varepsilon_s)^2 + (\varepsilon_s - \varepsilon_t)^2 + (\varepsilon_t - \varepsilon_r)^2 + \frac{3}{2}(\gamma_{rs}^2 + \gamma_{st}^2 + \gamma_{tr}^2)}$$

It can be recognized also in Figs. 12 and 13 that the reinforcement plates work effectively to lower the stress around the penetrations. Figure 12 shows that yield has already occurred at 2.06 MPa along the line HB except at the reinforcement plate, since equivalent stress exceeded the yield strength of SA 537. Figure 13 illustrates the boundary where SA 516 and SA 537 were used, also yield strength of them are shown. It can be seen in Figs. 12 and 13 that no yield occurred in the containment vessel itself when the pressure was below 1.57 MPa, while yield would occur in the vicinity of the points M and D when the pressure reached 2.06 MPa. Points M and D correspond to the cylindrical part of the vessel and the knuckle, respectively, where displacements are large as shown in Fig. 10.

By using SA 537 as a substitute for SA 516 for a higher quality at the bottom part of the vessel, stresses in this part can be maintained below the yield strength of SA 537 even at 1.57 MPa, which achieves no contact between the vessel and shield wall. If the entire containment vessel had been constructed with SA 516, it could be easily imagined that the yield occurred at the bottom part of the vessel at the pressure of 1.57 MPa. This is more clearly explained by Fig. 15 where 1.17 % of equivalent strain is observed at point D at 2.06 MPa where SA 516 was used while at point M it is only 0.3 %, which is definitely attributed to proper selection of SA 537.

3.4 Elastic Limit

Elastic limit on the vessel can be obtained by examining the influence of inner pressure upon the displacement. In section 3.3 it was clarified that until 1.57 MPa the vessel itself remains in an elastic deformation as a whole , however at 2.06 Mpa yielding was observed both at the cylinder and at the knuckle.

Figures 16 and 17 show relations between radial and axial displacement and inner pressure. It can be concluded from these figures that the deformation was proportional to the applied pressure up to 1.67 MPa at the point D where SA 516 was used. On the other hand, the point M on the line VC where SA 537 was used deformed linearly up to 1.76 MPa. Elastic limit pressure of the vessel was then determined as 1.67 MPa. The closure of the gap between the vessel and biological shield wall was expected to occur when the pressure was 1.98 MPa.

4. Conclusions

Elastic-plastic analysis was done concerning the Japanese BWR MARK-I steel containment by using ADINA code. The present study was focused on an entire deformation of the vessel rather than the stress or strain concentrations around the structural singularities such as penetrations. The main conclusions drawn from the analytical results are summarized in the following.

(1) The containment deforms elastically as a whole up to 1.67 MPa.
(2) Initial gap between the containment vessel and the biological shield wall is closed at 1.98 MPa at the cylindrical part of the vessel. If the thermal expansion of the vessel is taken into account , this gap will be closed earlier.
(3) It is proved to be an appropriate choice of structural material that SA 537 is used at the bottom part of the containment.

References

/1/ Toni Molina and Ruby Cochrell, editors,Proceedings of the Second Workshop on Containment Integrity, NUREG/CP-0056, 1984.
/2/ ADINA users manual, REPORT AE-81-1, ADINA Engineering, 1981.
/3/ ADINA-PLOT users manual, REPORT AE83-3, ADINA Engineering, 1983.
/4/ Atsumi Okamoto and Kiyoharu Nakamura, Ishikawajima- Harima Engineering Review, vol. 25 No. 3, p 199-200 (in Japanese) 1985.
/5/ R.Hill, The Mathematical Theory of Plasticity (translated into Japanese) BAIFUKAN Japan, 1950.

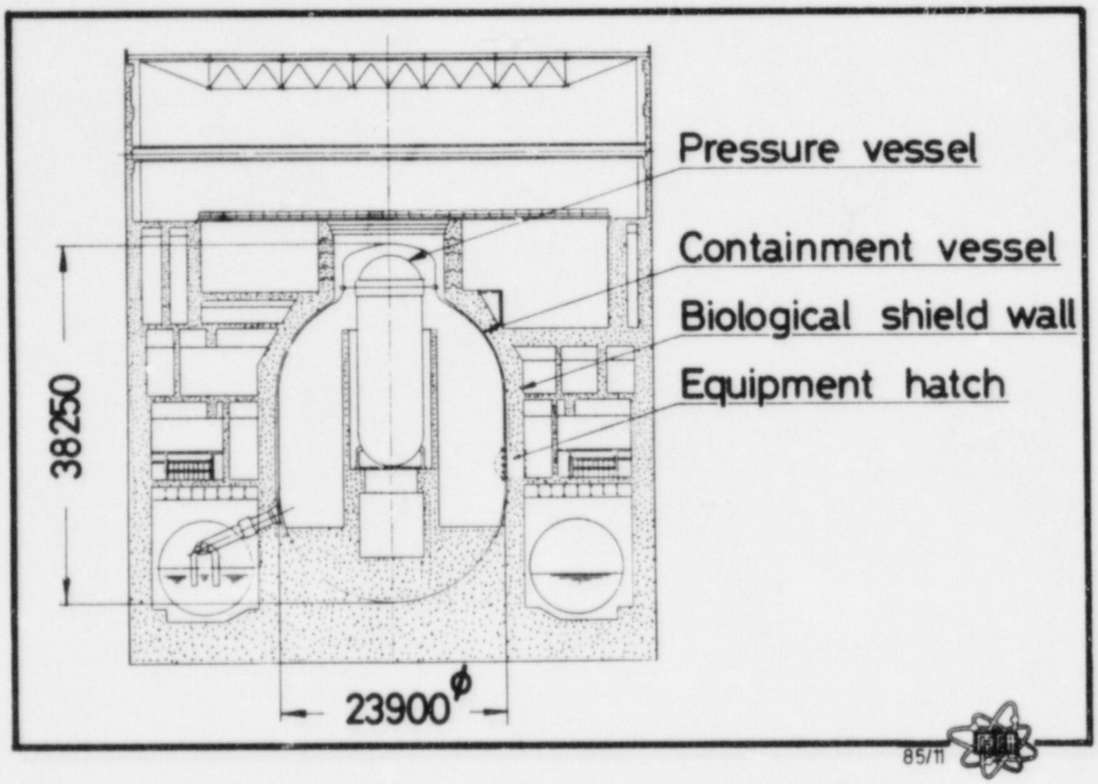


Fig. 1 Japanese BWR MARK-I steel containment

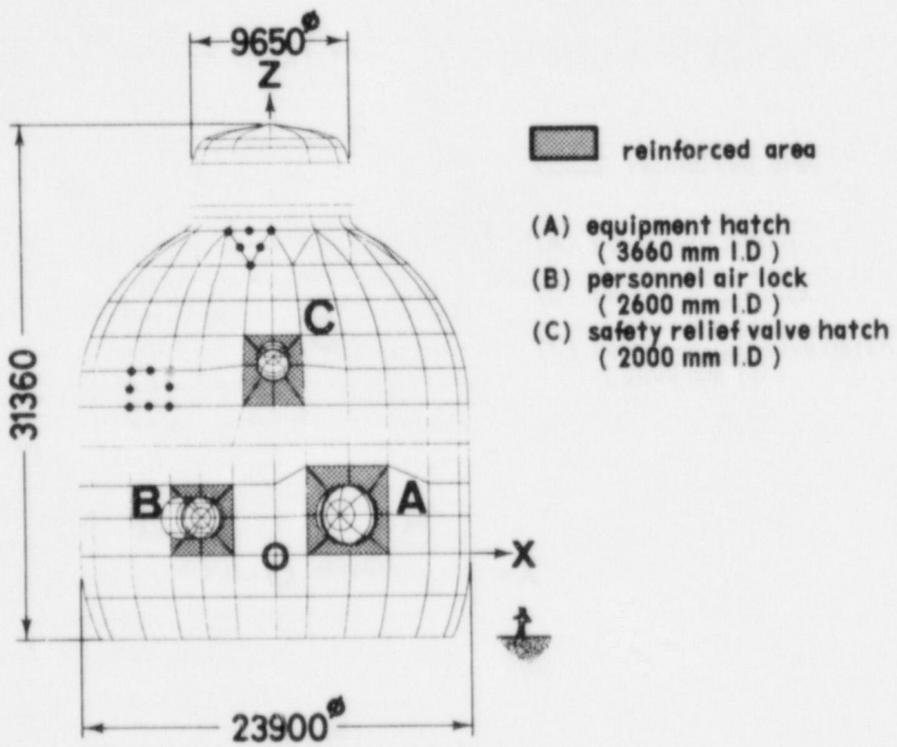


Fig. 2 Finite element model

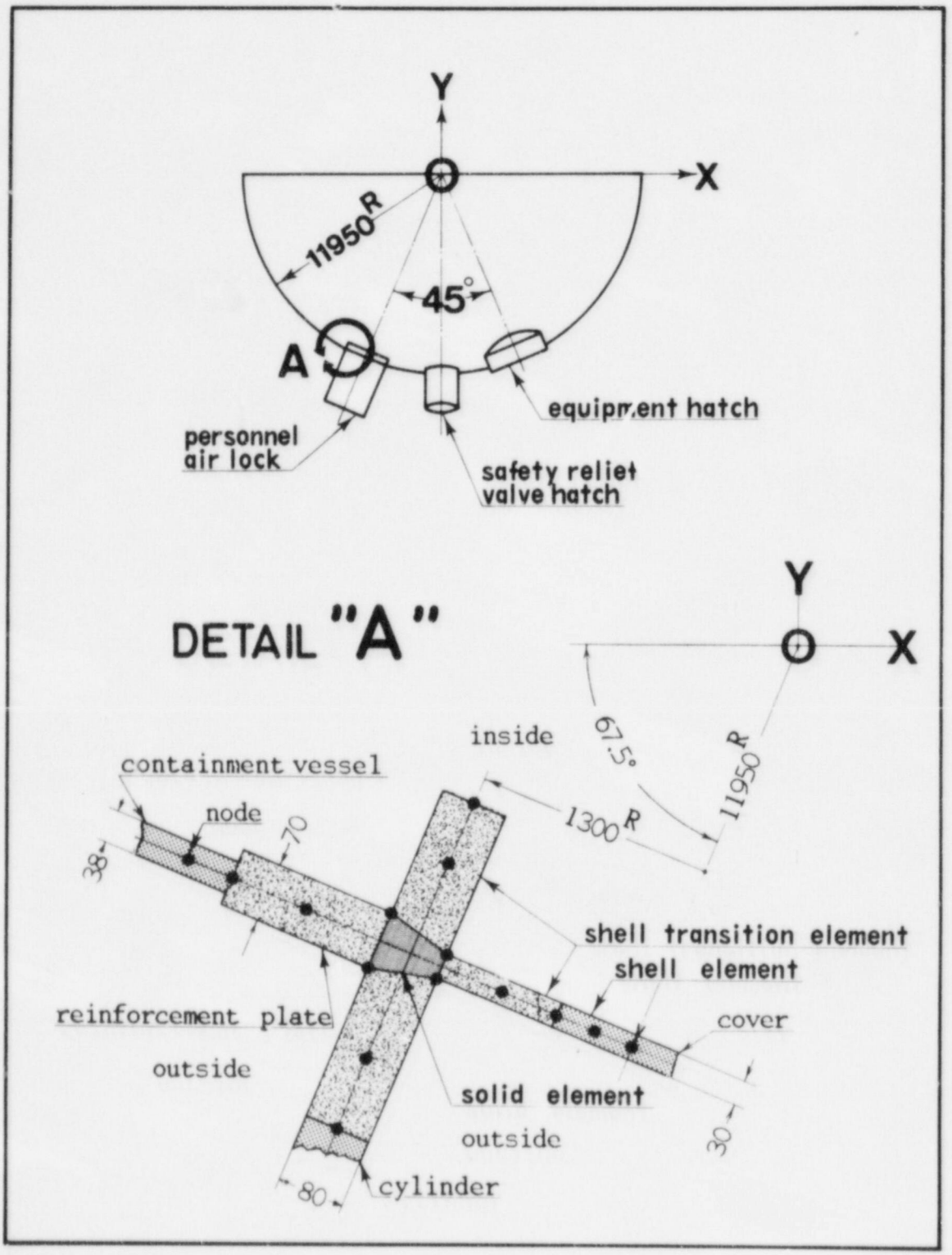
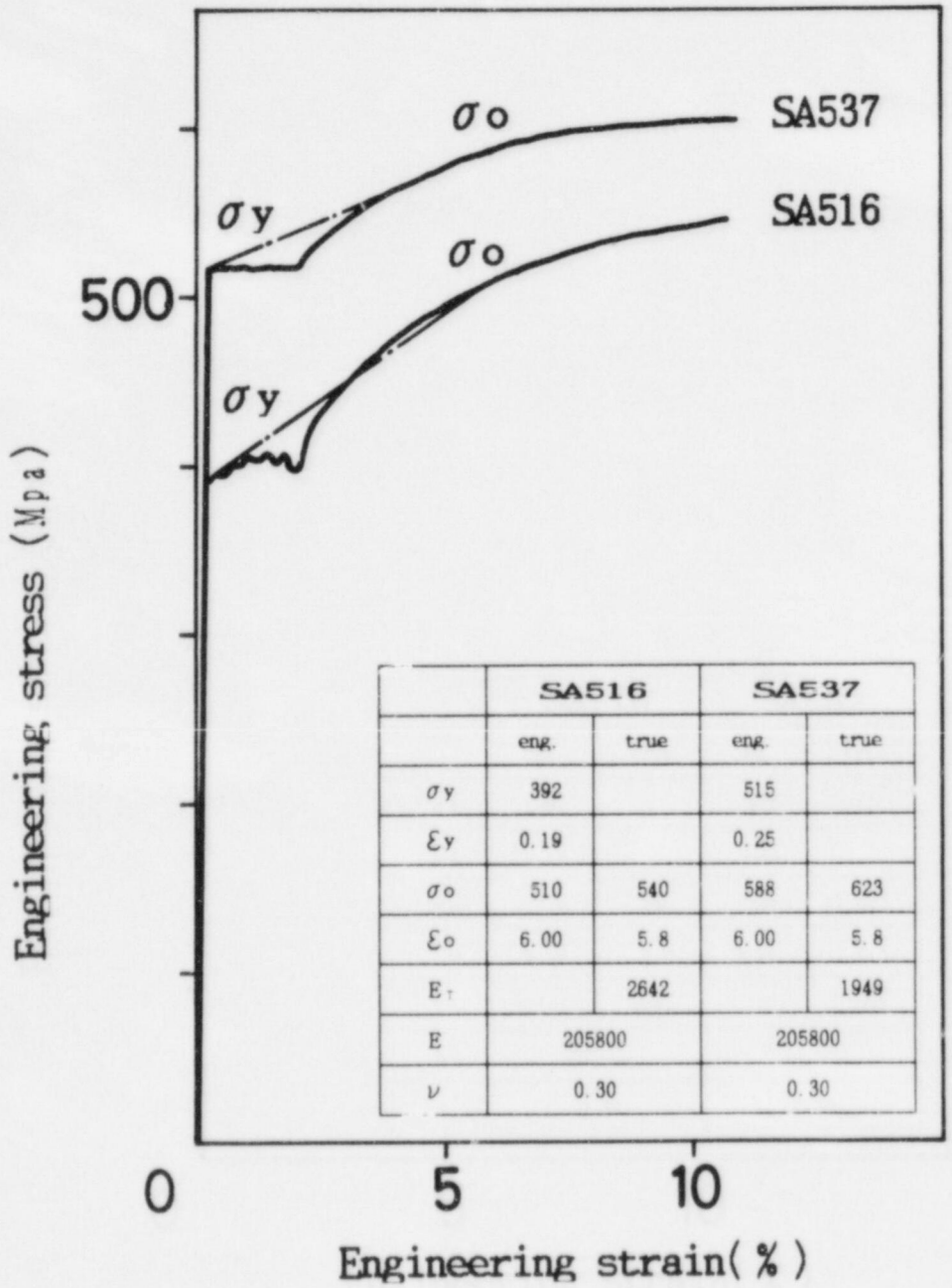


Fig. 3 Finite element model at shell intersections



	SA516		SA537	
	eng.	true	eng.	true
σ_y	392		515	
ε_y	0.19		0.25	
σ_o	510	540	588	623
ε_o	6.00	5.8	6.00	5.8
E_T		2642		1949
E	205800		205800	
ν	0.30		0.30	

Fig. 4 Stress-strain diagram of SA 516 and SA 537

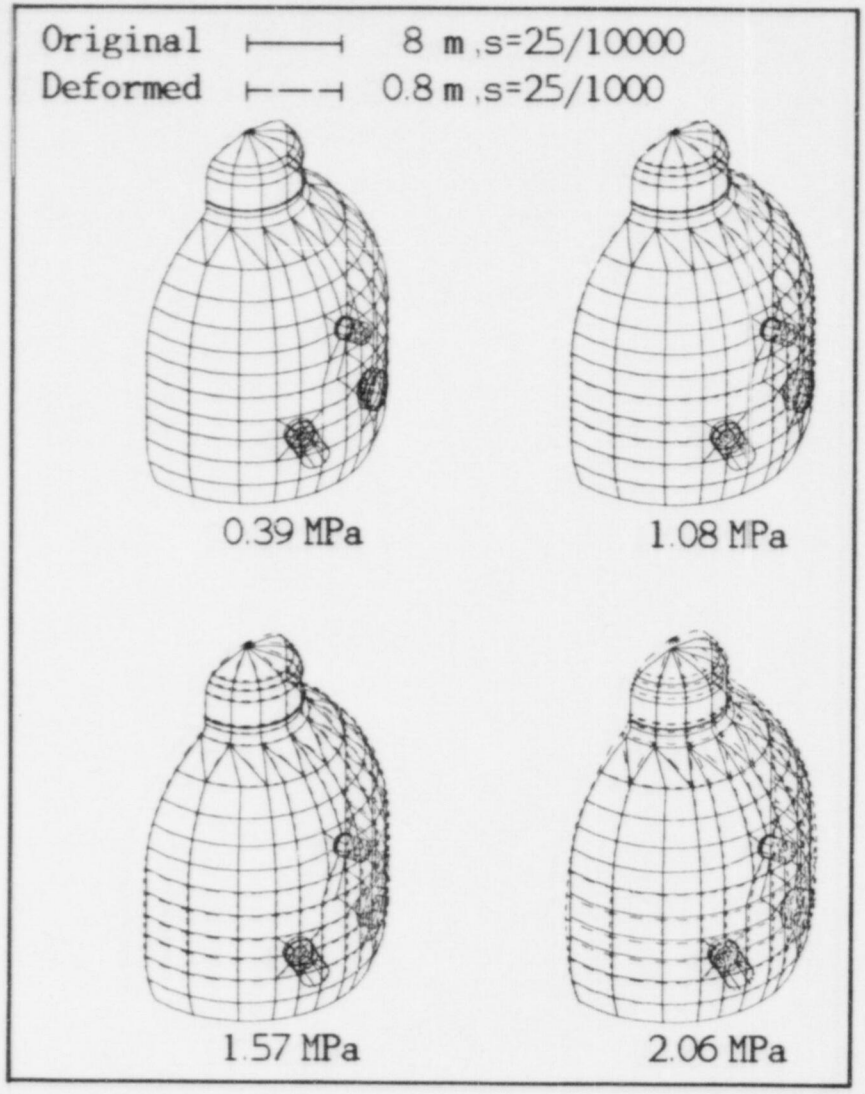


Fig. 5 Overall deformation
(deformation exaggrated by a factor of ten)

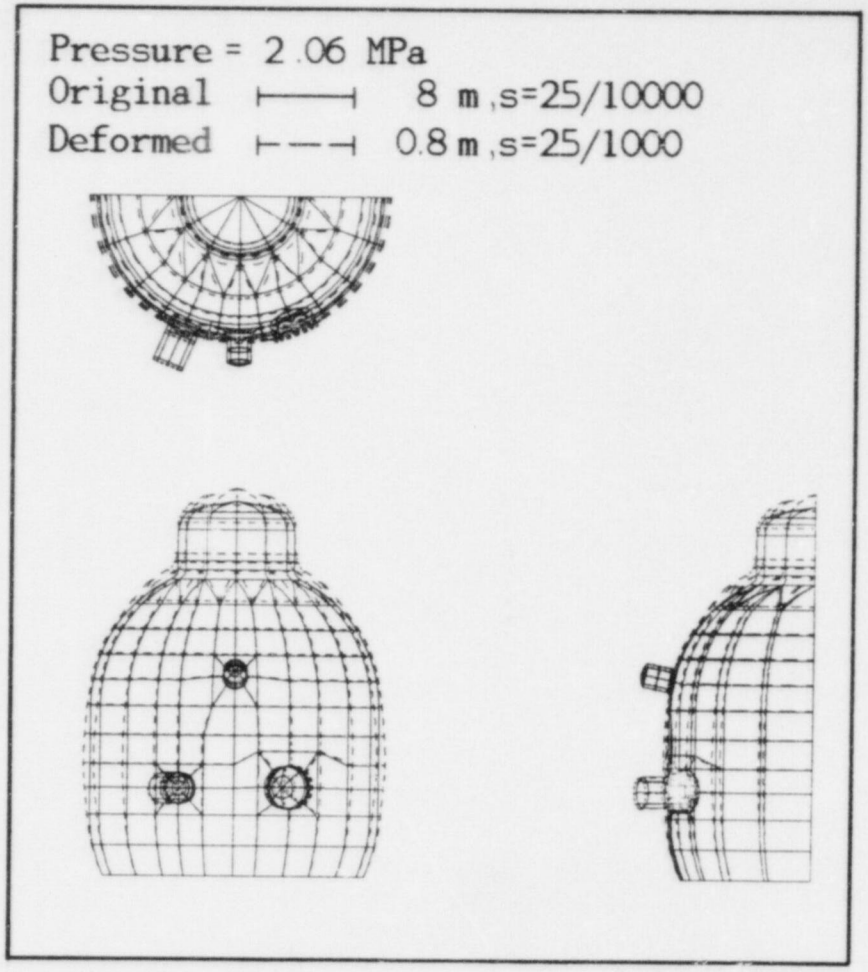


Fig. 6 Deformation diagram at 2.06 MPa
(deformation exaggrated by a factor of ten)

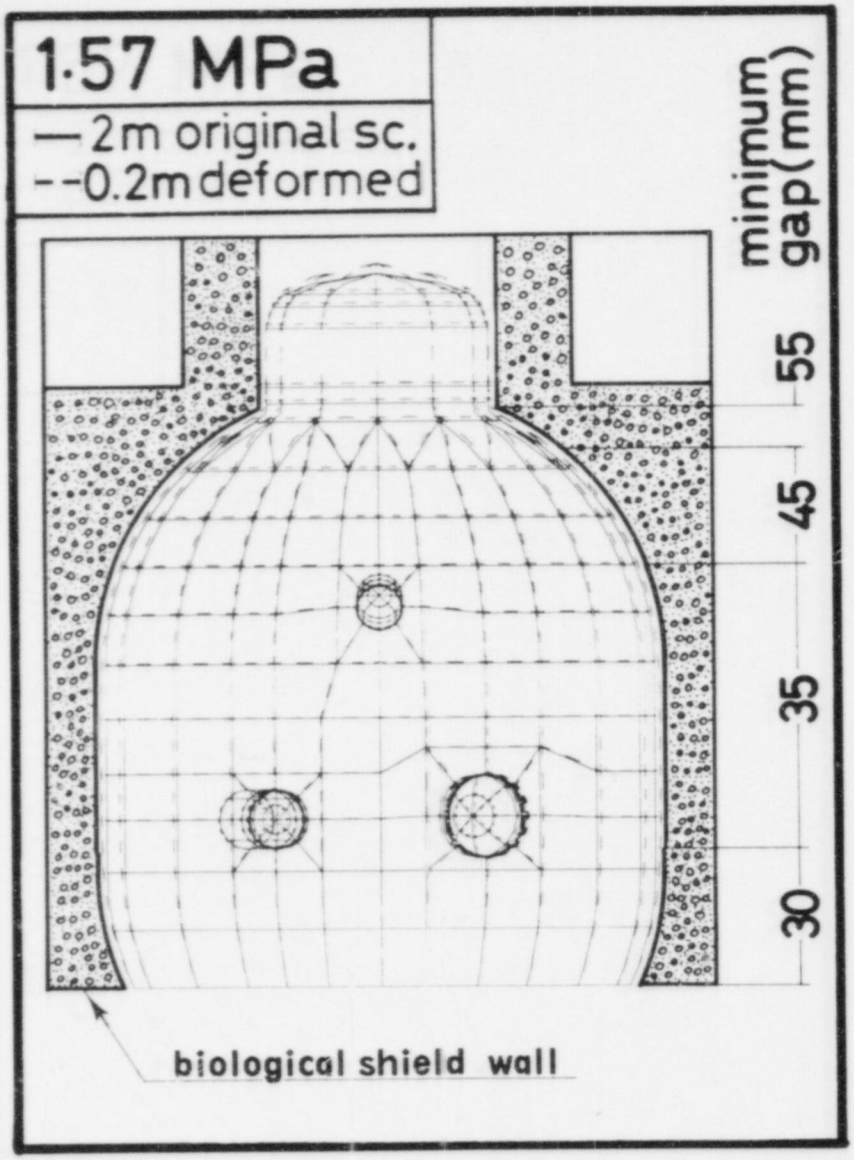


Fig. 7 Relation between deformed containment at 1.57 MPa and initial gap

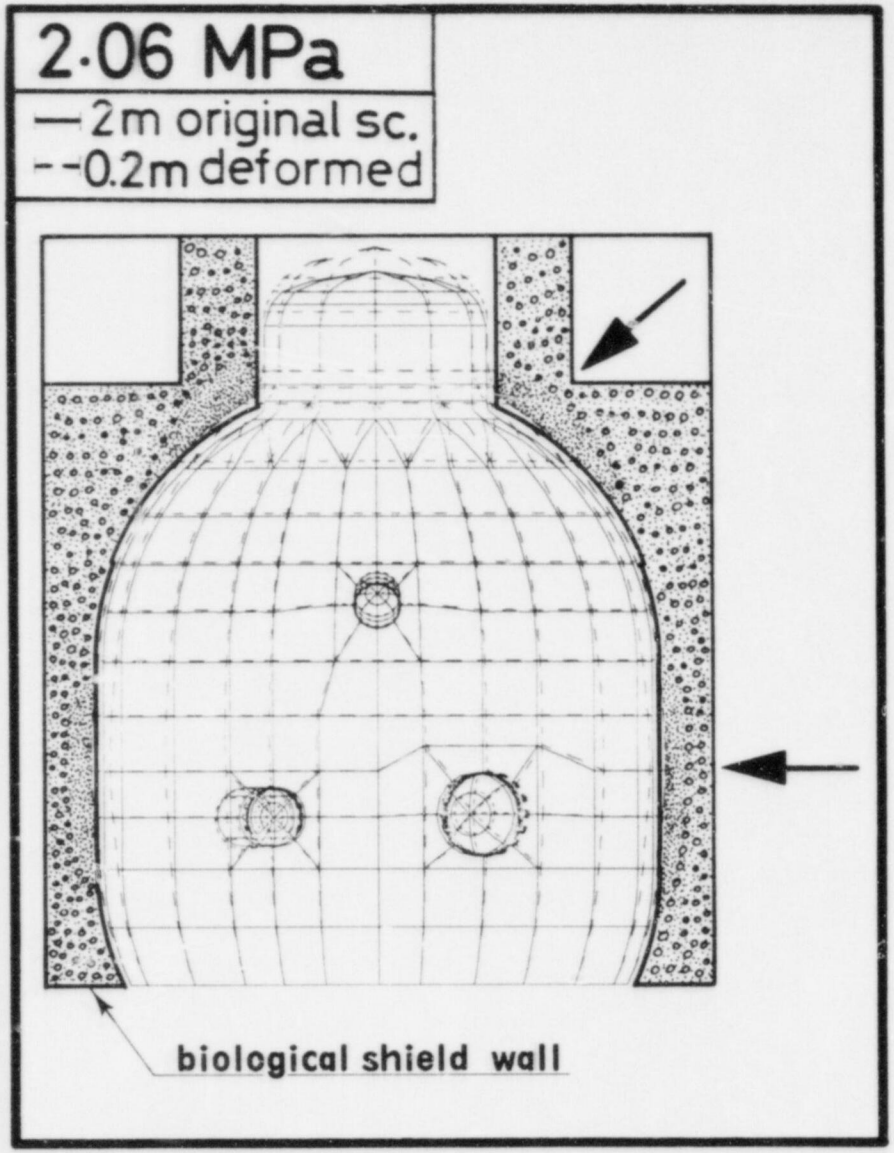


Fig. 8 Relation between deformed containment at 2.06 MPa and initial gap

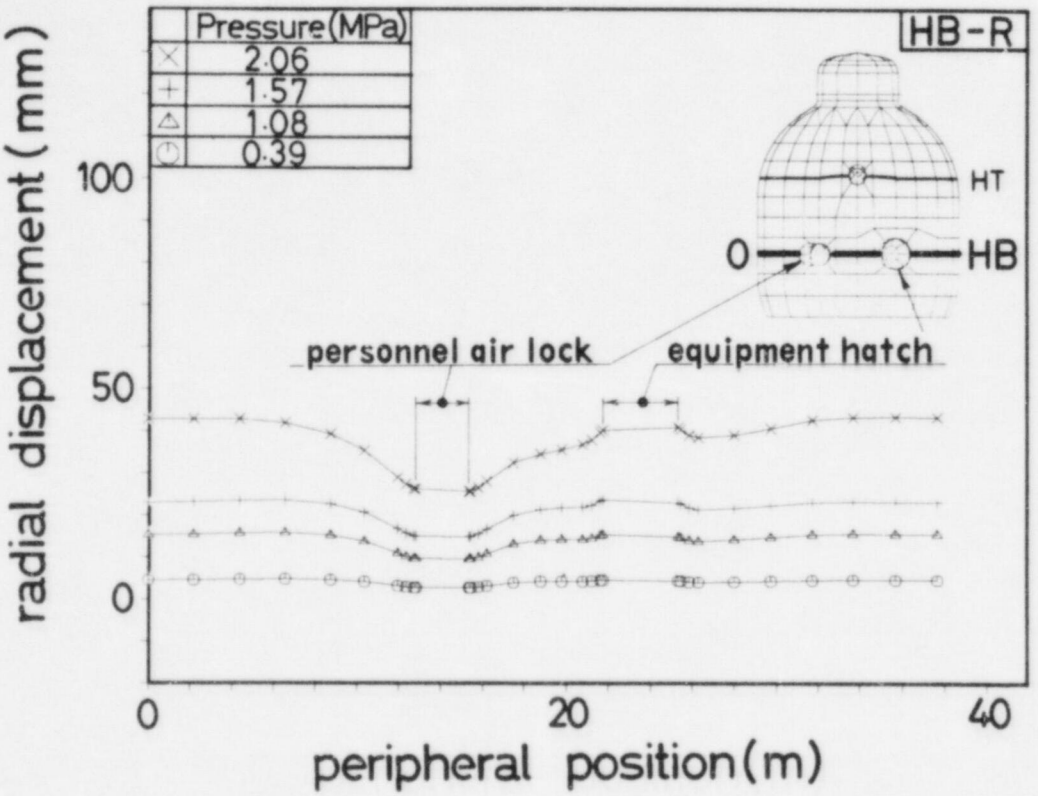


Fig. 9 Distribution of radial displacement along Horizontal Bottom line

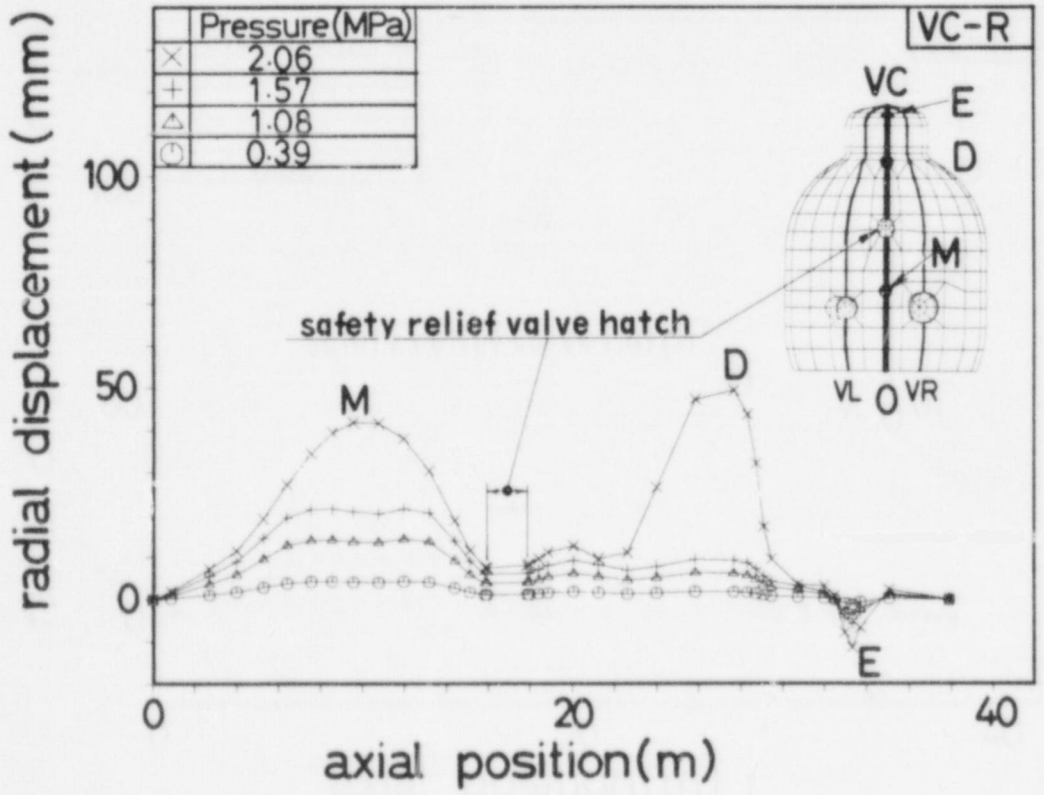


Fig. 10 Distribution of radial displacement along Vertical Center line

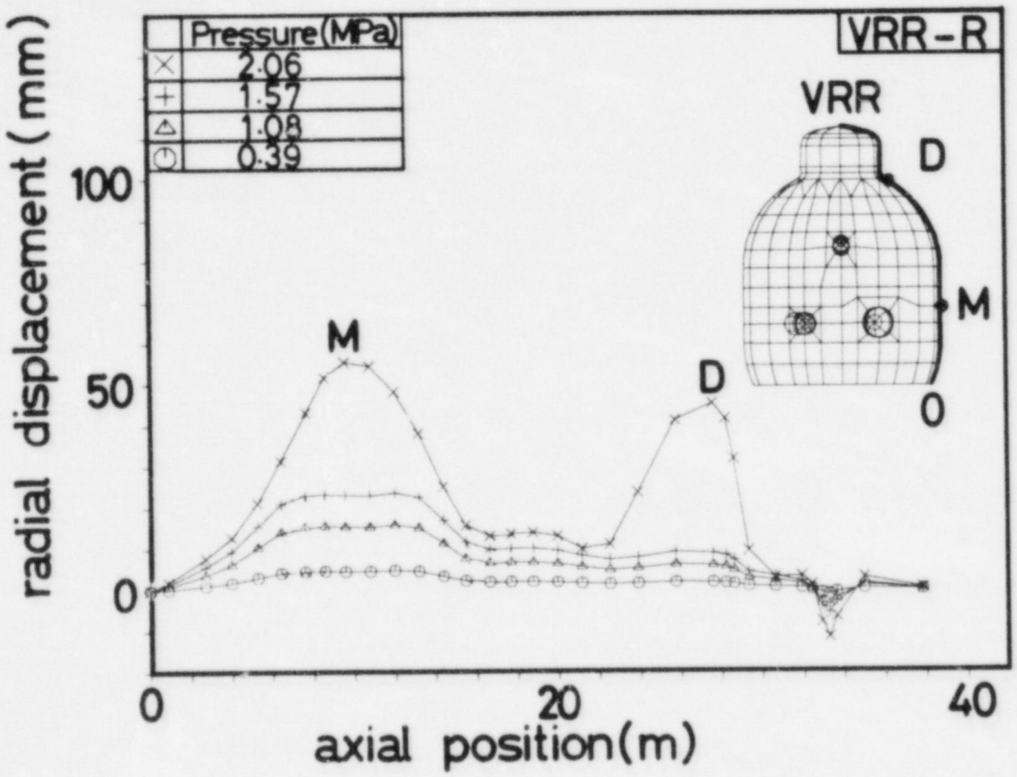


Fig. 11 Distribution of radial displacement along Vertical most Right line

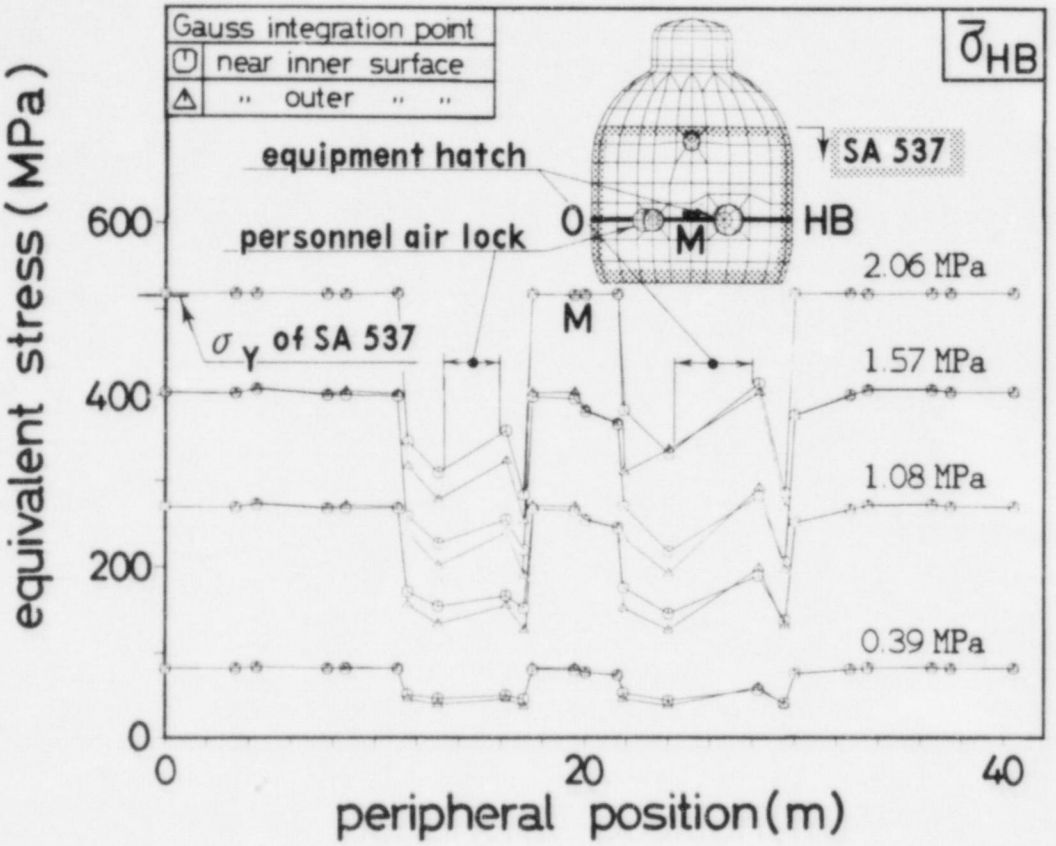


Fig. 12 Distribution of equivalent stress along Horizontal Bottom line

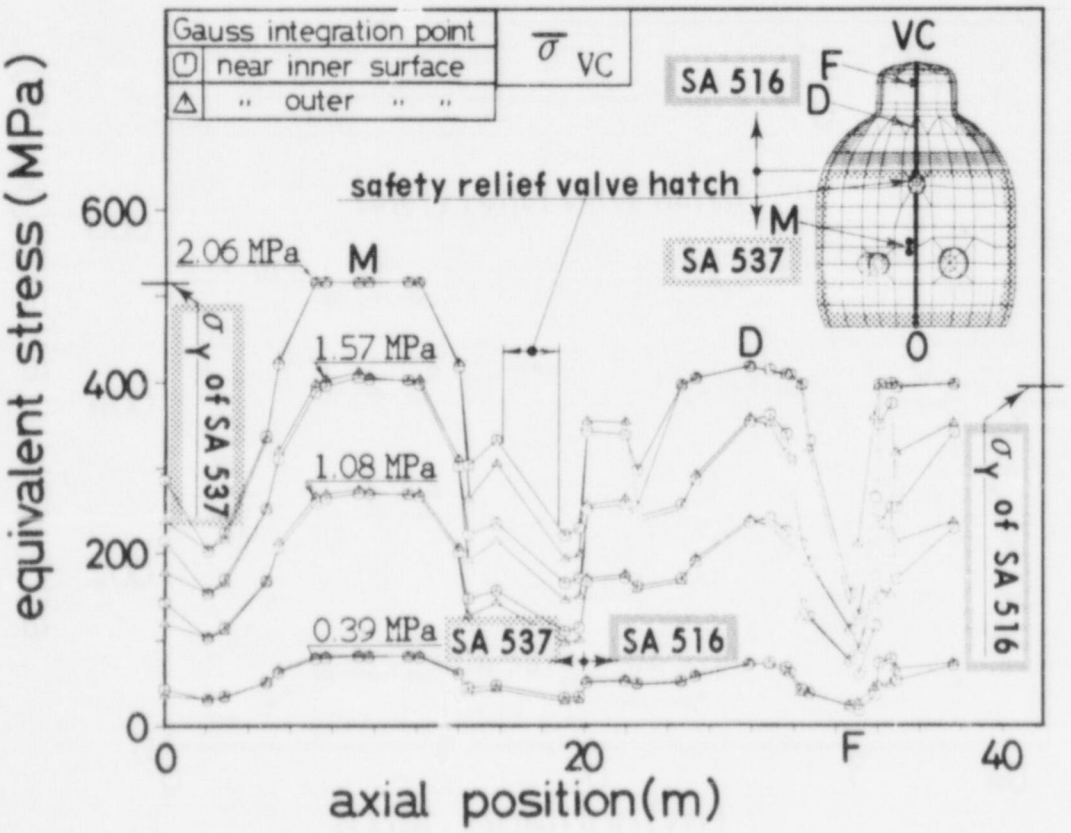


Fig. 13 Distribution of equivalent stress along Vertical Center line

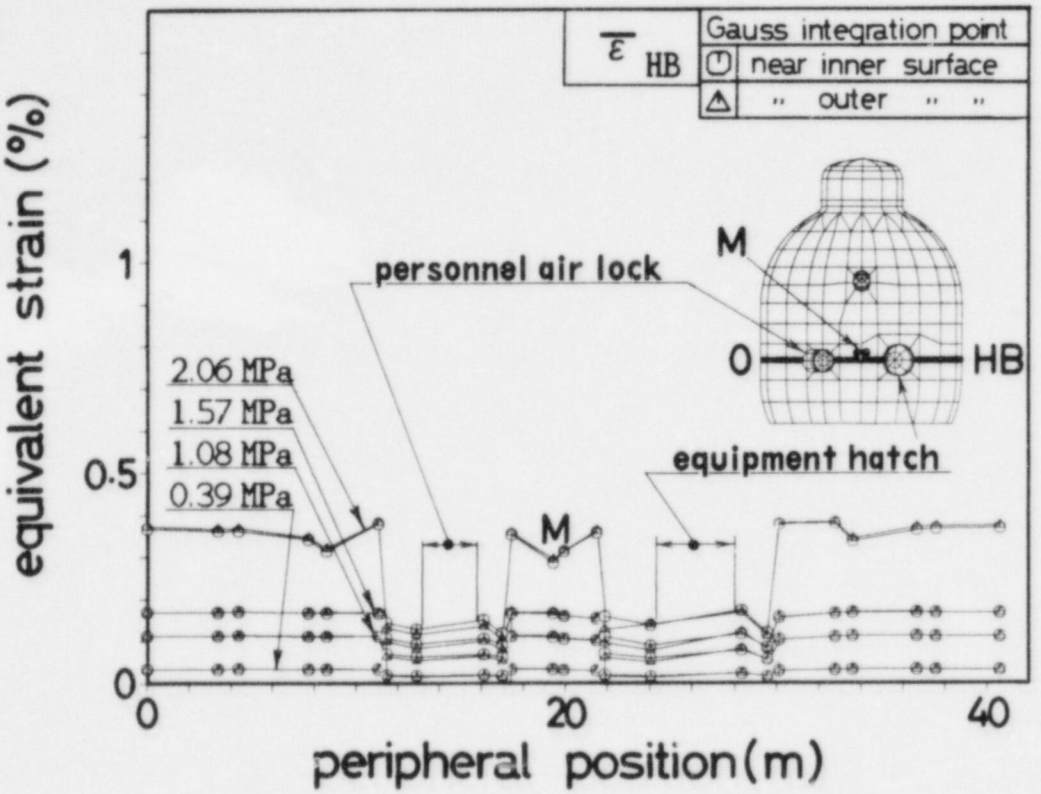


Fig. 14 Distribution of equivalent strain along Horizontal Bottom line

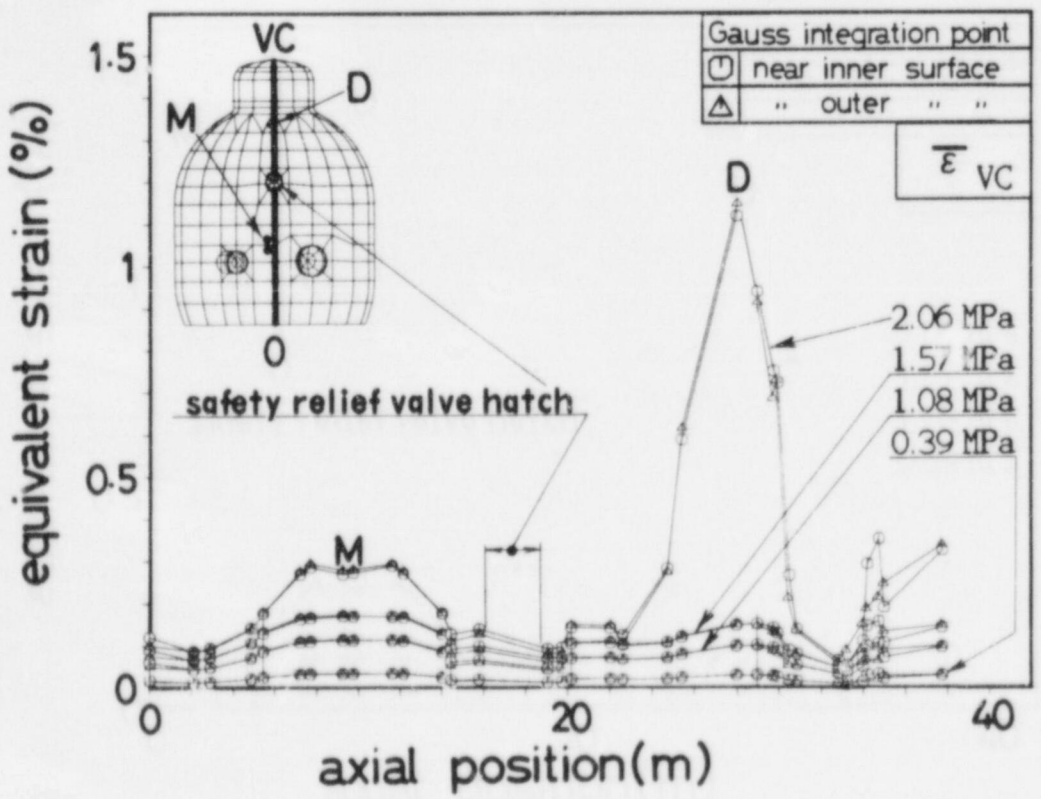


Fig. 15 Distribution of equivalent strain along Vertical Center line

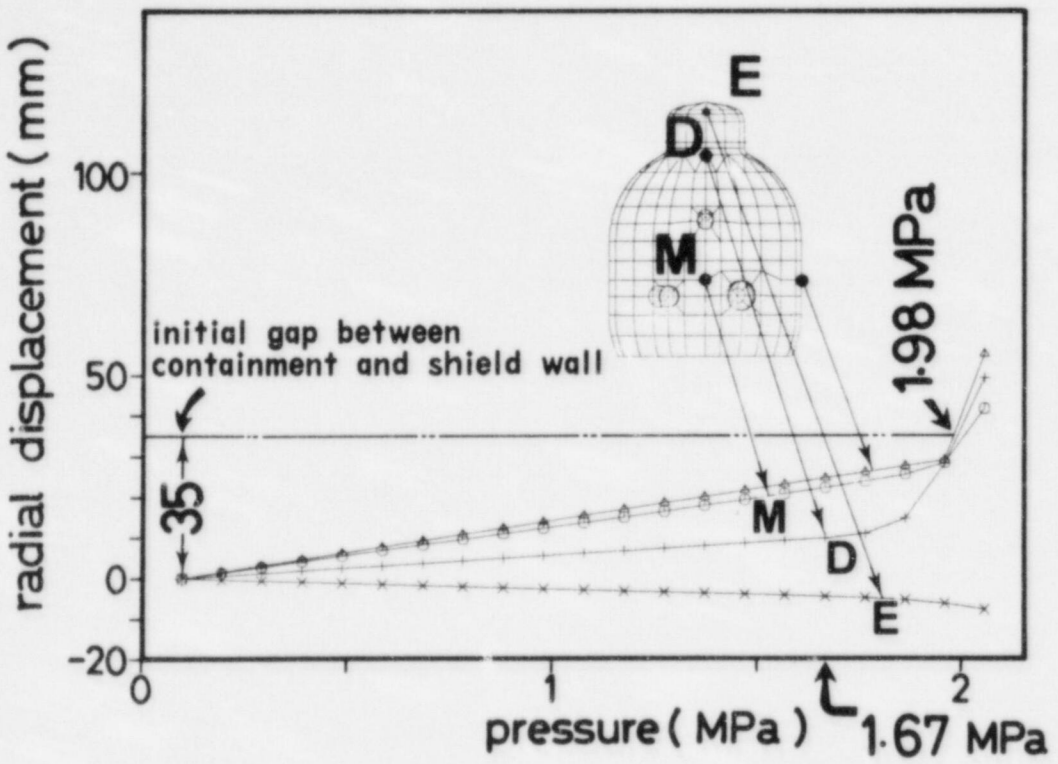


Fig. 16 Radial displacement and applied pressure loading

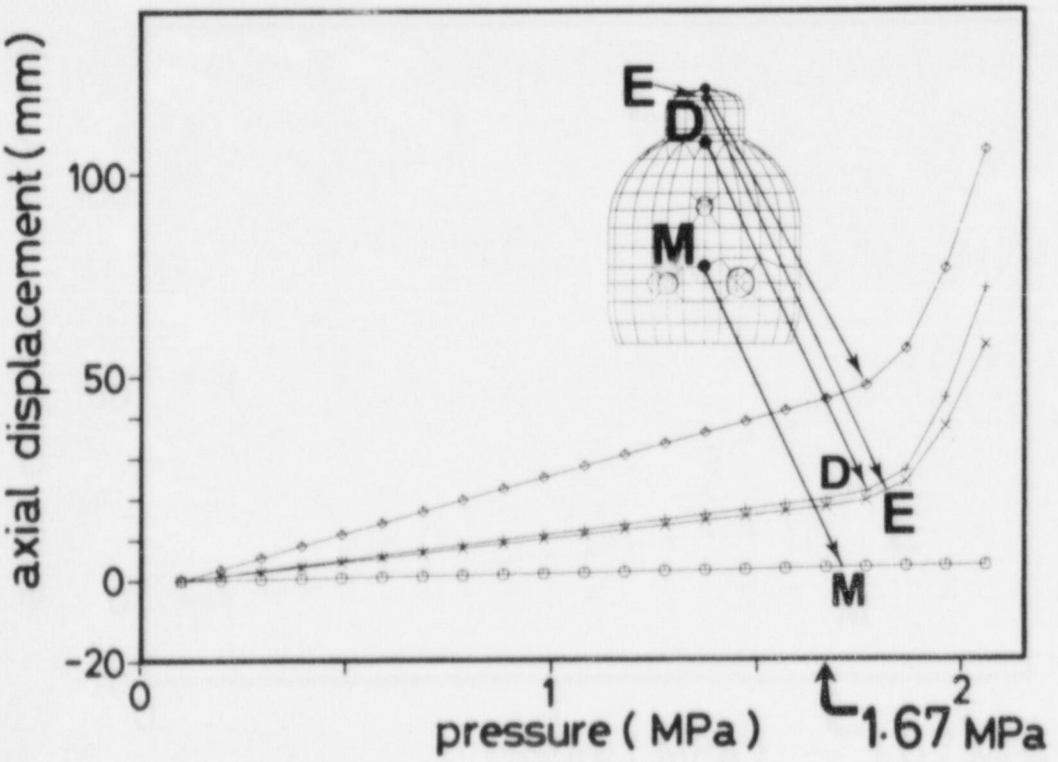


Fig. 17 Axial displacement and applied pressure loading

Crack Propagation in High Strain Regions of a Steel Containment

Fouad Fanous** and Lowell Greimann**

Ames Laboratory*
Iowa State University
Ames, Iowa 50011

ABSTRACT

During a severe accident, a containment may develop a controlled relatively small leak before the pressure reaches the point where general rupture of the shell occurs. Another hypothesis states that an overall failure will occur with total release of the vessel contents. This work represents a preliminary study to predict crack propagation from an initially small defect in a high strain location in a typical steel containment. The J integral approach is used. A virtual crack extension method for calculating J is developed for use with general finite element programs. Two through cracks with different lengths were found to be unstable at the pressure which caused a surface crack to propagate through the containment thickness. In other words, the resulting through crack will not be stable and general failure will occur with the almost instantaneous release of the vessel contents.

1.0 INTRODUCTION

During a severe accident, a containment may develop a controlled, relatively small, leak before the pressure reaches the point where a general rupture of the shell occurs. On the other hand, overall failure may occur with total instantaneous release of the vessel contents. Either possibility may occur, depending primarily upon local geometry, material details and the applied pressure [1]. Reference [2] summarizes a study of several models of containment leakage such as pre-existing leakage, hatch seals, general rupture and flange opening.

Consider the portion of a steel containment shown in Fig. (1). If a through crack develops at any high strain location in the containment shell, leakage will begin. The amount of leakage will depend

---

*Operated for the U.S. Department of Energy under Contract W-7405-Eng-82

**Department of Civil Engineering, Iowa State University

upon how far the crack extends. For example, a crack in the 1/2-inch containment plate, Fig. 1, may be arrested by an adjacent stiffener or the adjacent thicker plate; or, it may propagate through both of these. The objective of this work is to predict the extent of crack propagation which will occur from a postulated small crack in the high strain regions of a steel containment.

2.0 CRACK GROWTH CRITERIA

2.1 Crack Growth Criteria

For the nuclear containment leakage considered here, the crack will be assumed to begin as a partially-through surface crack of approximately elliptical shape (Fig. 2a). Figure 2b shows such a crack in a flat plate subjected to a uniaxial stress, σ. As the stress is increased, the crack is visualized as first propagating through the thickness B (Fig. 2c). Leakage begins when the crack reaches the opposite surface. The extent of leakage is controlled by how far the through crack (Fig. 2d) propagates across the plate.

There are no crack growth criteria for ductile materials which are generally accepted by the fracture mechanics community. No single parameter or combination of parameters has been found which satisfactorily characterizes the growth of cracks through regions of high strain of highly ductile materials. Currently, the state-of-the-art in fracture mechanics permits the reliable prediction of small crack growths in regions of limited plasticity. It is beyond the scope of this work to review completely the state-of-the-art in elastic-plastic fracture mechanics (EPFM). Briefly:

J Integral. The J integral is a measure of the energy release rate as a crack extends. This approach has become popular in the United States for nuclear reactor vessels [3, 4, 5, 6].

Crack Tip Opening Displacement (CTOD). The CTOD hypothesis states that a crack will grow when the opening near the crack tip reaches a critical value [5, 6].

Modified R-6 Assessment Diagram. This approach, which is popular in the United Kingdom, presents an interaction type equation between the extreme limits of crack extension in a perfectly elastic material (brittle fracture) and plastic collapse governed by a limit load [7, 8].

Crack Tip Energy Release Rate. Probably related to the J integral approach, the crack tip energy release rate criterion considers the amount of plastic energy in the immediate vicinity of the crack tip [9].

Strain Energy Density. In the strain energy density criterion, the crack is assumed to grow when the strain energy density immediately ahead of the crack reaches a critical value which can be obtained from a uniaxial tensile test [10, 11].

Each of these criteria has its proponents. They have been reviewed by experts in the fracture mechanics field and compared [8, 12, 13]. Each has an area of application and, yet, none is completely satisfactory for the complete description of ductile crack growth. If the number of proponents can be used as a legitimate measure of the validity of the criterion, the J integral and CTOD approaches are more accepted [8, 13]. The J integral criteria will be adopted herein.

The J integral has been defined in a number of ways but perhaps the most physically appealing way is to define J as the generalized force associated with an increment of crack growth. The energy balance equations for an increment of crack area δA is

$$J\,\delta A + \delta U + \delta V = 0 \tag{2.1}$$

where

$$\delta U = \delta \int_V W dv; \quad W = \int_0^{\varepsilon} \sigma d\varepsilon; \quad \text{and} \quad \delta V = -F\,\delta u \tag{2.2}$$

δU is the increment in internal strain energy for the increment in strain $\delta\varepsilon$ which is associated with the δA growth. The quantity W is the strain energy density and the quantity δV is the increment in external energy for the increment in displacement δu associated with δA. The first term in Eq. 2.1 is the energy required to form the new crack with a surface area of δA. The applied J integral can be calculated in a number of ways, as summarized in Ref. [14]. Crack growth is presumed to occur when J reaches some critical value J_R, usually considered to be a material property. Hence, crack growth occurs if

$$J \geq J_R \tag{2.3}$$

The amount of growth is controlled by the J_R curve. The J criteria applies to a limited amount of growth [3, 6]:

$$C >> \begin{cases} J_R/\sigma_y \\ J_R/\left(\dfrac{dJ_R}{da}\right) \end{cases} \tag{2.4}$$

where C is the remaining ligament, i.e., the remaining portion of the material ahead of the crack tip (Fig. 3).

2.2 J - Applied

2.2.1 Crack Idealization and Elastic Solutions

As shown in Fig. 2, two crack shapes are envisioned as the crack grows--an initial surface crack and a through crack. The surface crack can probably best be idealized as an elliptic crack. However, there are limited plastic solutions for this crack shape. If the

crack is long (a<<c), the conditions at the base of the crack are approximated by a single edge cracked plate under tension (ECPT) in plane strain. After the crack has propagated through the plate, the conditions approximate a center cracked plate (CCP) in plane stress. For these conditions, the elastic solution for J can be written as [15]

$$J_e = \frac{Y^2 \pi \sigma^2 a}{E} \tag{2.5}$$

in which

$$Y = \begin{cases} 1.12 & 1 - \nu^2 \quad \text{ECPT} \\ \sec \frac{\pi a}{w} & \text{CCP} \end{cases} \tag{2.6}$$

The above solution for the ECPT case is limited to shallow cracks (a<<B).

2.2.2 Analytic Elastic-Plastic Solutions

The application of J in the nonlinear range depends upon the calculation of J and this has been the subject of many studies--both analytical and numerical (finite element). The following summarizes a few solutions which seem to attract the most attention. Most of these solutions use a Ramberg-Osgood approximation to the true stress-true strain curve from a uniaxial tensile test of the material:

$$\frac{\varepsilon}{\varepsilon_y} = \frac{\sigma}{\sigma_y} + \alpha \left(\frac{\sigma}{\sigma_y}\right)^n \tag{2.7}$$

in which σ_y and ε_y are the material true yield stress and strain, respectively, and α and n are material constants which are selected to provide a good fit to the experimental curve [16]. For purposes of presentation, a yield value of J will be defined by

$$J_y = \frac{Y^2 \pi \sigma_y^2 a}{E} \quad . \tag{2.8}$$

Turner [12, 17] gives, perhaps, the simplest approximation to J as

$$\frac{J}{J_y} = \begin{cases} \left(\frac{\varepsilon}{\varepsilon_y}\right)^2 \left[1 + 0.5 \left(\frac{\varepsilon}{\varepsilon_y}\right)^2\right] & \frac{\varepsilon}{\varepsilon_y} \leq 1.2 \\ 2.5 \left(\frac{\varepsilon}{\varepsilon_y} - 0.2\right) & \frac{\varepsilon}{\varepsilon_y} \geq 1.2 \end{cases} \tag{2.9}$$

This approximation is intended to be an upper bound to most practical cases, including surface and through cracks. The above equation

does not include a correction for deep notches which Turner has suggested.

Paris [3] has presented an equation for surface and through cracks in A533 steel for the ductile range as

$$\frac{J}{J_y} = \frac{1}{\pi}\begin{cases} 3.3\left(\frac{\sigma}{\sigma_y}\right)^2 + 3.14\ \alpha\ \left(\frac{\sigma}{\sigma_y}\right)^{n+1} & \text{Surface} \\ 4.3\left(\frac{\sigma}{\sigma_y}\right)^2 + 10.6\ \alpha\ \left(\frac{\sigma}{\sigma_y}\right)^{n+1} & \text{Through} \end{cases} \qquad (2.10)$$

After several years of study, the EPRI [4, 5, 6,] presents J solutions as the sum of the elastic and fully-plastic cases

$$\frac{J}{J_y} = \left(\frac{\sigma}{\sigma_y}\right)^2 + \frac{\alpha\ h_1\ c}{\pi\ b\ Y^2}\left(\frac{P}{P_y}\right)^{n+1} \qquad (2.11)$$

in which the notation is as follows:

		ECPT	CCP
c (net width)	=	b - a	W/2 - a
b (total width)	=	B	W/2
P (load)	=	σB	σW
P_y (limit load)	=	$1.46\ \sigma_y\ [(c^2+a^2)^{1/2} - a]$	σ_y(W-2a)
$h_1(\frac{a}{b} = \frac{1}{8})$	=	21.7	4.62
$h_1(\frac{a}{b} = \frac{1}{4})$	=	3.02	2.86
Y	=	$P_y/(\sigma_y\ B)$	$P_y/(\sigma_y\ W)$

In this equation, h_1 is dependent upon the specimen shape, crack size, and material shape parameter n. It has been obtained for several cases by EPRI using numerical methods for the fully plastic solutions. The values tabulated above are for a shape factor n = 10. The solution for the plane strain ECPT case are from [18] (not [6]) and for the plane stress CCP are from [6]. The EPRI correction for effective crack length in the elastic portion has not been included.

A modified form of the R-6 assessment diagram has been suggested by Chell and Milne [8] and is given by a parametric equation as

$$\frac{J}{J_y} = \frac{8}{\pi^2 \gamma} \ln \sec \frac{\pi}{2}\rho \qquad (2.12)$$

$$\frac{P}{P_y} = \left[\rho + \left(1 - \sqrt[4]{\frac{J_y \rho^2}{J}}\right)\left(\frac{\sigma_u}{\sigma_y} - 1\right)\right] \frac{(1 + \sigma_u/\sigma_y)}{2} \qquad (2.13)$$

in which the parameter ρ ranges as

$$0 \leq \rho < 1$$

and σ_u is the ultimate tensile stress. The term on the extreme right follows their suggestion to use a flow stress (arithmetic mean of the yield and ultimate) in the evaluation of the limit load.

2.2.3 Finite Element Elastic-Plastic Solutions

Most numerical solutions for the J integral are by one of two methods. In one method, the contour integral formulation of J is used directly [3, 4, 5, 6, 15, 19] by integrating along several paths around the crack tip. The virtual crack extension (VCE) method is a second popular method [19, 20, 22, 23, 24]. The VCE method, which will be adopted here, basically uses the J definition in Eq. 2.1. The crack is given a virtual area growth δA. The virtual change in internal and external energy caused by this growth can be calculated. This is equal to the amount of surface energy released during the growth. The generalized force J can then be calculated directly by Eq. 2.1.

The virtual crack extension is usually accomplished by a series of stress-free nodal shifts and releases as the crack propagates [4, 5, 22, 25, 26] and is not the same as a virtual displacement. Hence, in Fig. 4 node C is given a virtual stress-free coordinate shift of δa to C'. The nodes on the boundary are not permitted to move during this virtual change. The virtual coordinate changes between C' and the boundary are usually taken to vary linearly [5].

To accomplish the virtual coordinate shift in an existing general purpose finite element program with a minimum of change, phantom elements are introduced. In the region depicted in Fig. 4, the phantom elements duplicate the real elements except they are connected to the node C'. The phantom elements are given a very small thickness, say 0.0001 times the real thickness. Hence, as the structure is loaded, these elements accumulate stress and strain, i.e., strain energy density. However, the strain energy is insignificant since their volume is very small. Suppose the structure with the real and phantom elements has been loaded to same load level at which the J calculation is desired. At this point, the crack is given a virtual crack extension, δa, that is, the phantom elements became real elements and vice versa. Since the boundary does not move, the change in external potential energy is zero and, using Eq. 2.1,

$$J = -\frac{1}{\delta A} \delta U \qquad (2.14)$$

or, using Eq. 2.2,

$$J = -\frac{1}{\delta A}\left(\int_V \delta W \, dV + \int_{\delta V} W dV\right) \qquad (2.15)$$

To check this approach and compare it to the analytical methods, it was applied to the CCP specimen in Fig. 5. The finite element idealization was analyzed with ANSYS [27]. (Note the crude mesh of constant strain triangles.) The virtual crack extension was 0.6 inch. Phantom elements duplicated the real elements in the lightly shaded area except node C was shifted up 0.6 inch.

To reach a converged solution using a reasonable number of iterations, the slow dynamic analysis procedure suggested in Ref. [27] was used. The applied edge stress was increased in steps. For each step, the applied stress was first increased over a rise time of one second, which is larger than several times the structure fundamental period. Next, the applied stress was held constant for several seconds. In each step a very small integration step size, Δt, was used (0.001 sec.). During the solution, Δt does not remain constant but changes automatically as optimized by the ANSYS program based on the third derivative of the displacement with respect to time.

The finite element results were used in conjunction with Eq. 2.15 to calculate J at different applied stress levels. The calculated J for the CCP specimen in Fig. 5 are plotted in Fig. 6 along with the results obtained using EPRI, Paris, Turner and Modified R-6 approaches. For the elastic case (Linear Elastic Fracture Mechanics), the exact J for an applied nominal stress of 10 ksi is

$$J_e = 0.0636 \quad k \text{ in/in}^2$$

The finite element procedure using phantom elements give

$$J_e = 0.0643 \quad k \text{ in/in}^2$$

which is certainly a favorable comparison considering the coarse mesh. As can be seen from Fig. 6, the proposed analysis gives results below the results predicted by Paris, EPRI and Turner in the high strain region (several times yield). This discrepancy is mostly caused by the coarse mesh around the crack.

3.0 TYPICAL CONTAINMENT VESSEL

3.1 Surface Crack to Through Crack Propagation

Three regions have been selected in the containment as locations at which through cracks could develop and leakage occur: containment shell, near springline (Fig. 1); a typical penetration; and the equipment hatch sleeve. Each of these regions has been analyzed by the finite element method.

Following Sec. 2.1 and Fig. 2, an initial surface crack is postulated in each of these regions. For this study, the crack is assumed to be long and shallow, i.e., ECPT case in Sec. 2.2.1. With

reference to ASME acceptance standards for radiographed welds in containment vessels [28], this is a linear indication with length limits, ℓ, as listed in Fig. 7. Since ℓ/a is greater than 3 for linear indications, the maximum crack depth, a, is also listed.

The maximum depth surface crack listed in Fig. 7 is postulated to occur in each of the three high strain regions. (The value for the crack in Fig. 1 is listed in Table 1.) As described in Sec. 2.2.1, this case is approximated by a flat plate in plane strain with an edge crack (ECPT). Using the analytic solutions summarized in Sec. 2.2.2 for this case, the calculated value of the applied J can be obtained for various levels of nominal true strain. The Turner values are representative and easier to calculate and, hence, will be used in the following.

The J resistance of the material is probably the most uncertain quatity in this analysis. No J_R values were available for the containment material (A516 Gr. 60 steel) when this study was conducted. The bounds listed in Table 1 are appropriate for the 1/2-inch thickness. For use in both the analytical and finite element analyses to follow, the stress-strain curve for the steel is idealized as in Fig. 8 and Table 1. The true stress-true strain curve approximates that found for the steel in much thinner plate [29].

Upon setting the applied J values (Eqs. 2.9) equal to the material resistance J_R, the nominal strain ε_R for surface crack propagation is found and listed in Table 1.

Using the strain results from each of the three finite element analyses, the calculated strains will reach ε_R and the postulated surface crack will propagate to a through crack at some pressure beyond 65 psi. (The finite element analyses were extended only far enough to permit determination of this lower bound.)

3.2 Propagation of Through Crack

One area, the 1/2-inch plate at the springline, was selected for further study--both to extend the finite element analyses into the high strain regime and to estimate the extent to which the through crack will propagate. In this regard, the finite element model illustrated in Fig. 9 was formulated. The model includes the 1/2-inch plate near the containment springline and extends into the hemispherical head and into the 5/8-inch plate below. Stringers and rings are included in the model and the actual material properties of Table 1 and Fig. 8 are used. Symmetry boundary conditions are imposed on both vertical boundaries. The top boundary is constrained in the tangent plane of the hemisphere, but permitted free motion perpendicular to this plane. The meridional forces induced by pressure loading are applied to the lower boundary, which is constrained to move uniformly in the vertical direction. Internal pressure loading is applied to the shell elements which represent the containment shell. A total of 308 elements and 158 nodes are included in the model.

As illustrated in Fig. 9, the finite element model has provisions for a 12-inch and 72-inch crack. Phantom elements, as described in Sec. 2.2.3, are associated with each of these cracks.

During the first phases of loading, there is no crack in the model. The pressure is increased from zero in increments. At a pressure of 78 psi, the maximum membrane strain in the entire model was 6.5 percent. This occurred in the 1/2-inch plate at Elev. 783' 5/8".

At a membrane strain of 6.5 percent, the postulated surface crack was assumed to propagate through the 1/2-inch plate forming a crack with a length of 12 inches. (This is within the ε_R range in Table 1.) The node at the center of this crack was released and the solution was continued at a pressure level of 78 psi until a converged solution was reached. Using the VCE method as described in Sec. 2.2.3, the value of the applied J was calculated to be about 120 k in/in^2. This is much larger than any conceivable J-resistance of the material. One must conclude, therefore, that at a pressure of 78 psi, a through crack of 12 inches will continue to propagate in the meridional direction in the 1/2-inch plate.

The solution was continued to investigate whether this crack would be arrested at the 5/8-inch plate below and the ring above at Elev. 788' 5/8". A 72-inch crack was simulated by releasing all nodes along the left vertical edge in the 1/2-inch plate between these elevations. The solution was continued until convergence. The VCE method was implemented and an applied J of 3860 k in/in^2 was calculated. Again, this unrealistically high value of J indicates the crack will continue to propagate through the ring stiffeners at the top and the 5/8-inch plate at the bottom, i.e., there will be an overall failure.

Note that only one cracking sequence has been studied in this work. If, for example, the postulated surface crack was assumed to propagate through the 1/2-inch plate at a membrane strain of, say, one percent (about 60 psi), the resulting through crack could possibly have been arrested.

4.0 SUMMARY AND CONCLUSION

The rate of release of radioactive materials from a containment during a severe accident has a significant impact on the consequences of the accident. One hypothesis for a containment leakage model states that the containment will develop a controlled, relatively small leak before the pressure reaches the point where a general rupture of the shell occurs. Another hypothesis states that an overall failure will occur with total release of the vessel contents almost instantaneously. In this work three critical high strain locations in a typical steel containment were studied to predict crack propagation from an initially small defect.

Several crack growth criteria are presented in the literature for predicting crack growth in highly ductile materials such as containment steels. The J integral approach is adopted herein and a vir-

tual crack extension method for calculating J has been developed for use with a general purpose finite element programs.

An initially small surface flaw is first postulated in each of the critical high strain regions. The most critical region was selected for further study. Using the virtual crack extension method, two through cracks with different lengths were found to be unstable at the pressure which caused a surface crack to propagate through the thickness. In other words, the resulting through crack will not be stable and general failure will occur with the almost instantaneous release of the vessel contents. This study should be considered very preliminary. Elastic-plastic fracture mechanics has clearly been pushed beyond the acknowledged state-of-the-art. However, the above conclusion for this application will, most likely, not change.

5.0 REFERENCES

1. Kussmaul, K., et. al, "Crack Arrest Behavior in Pressure Vessels," Paper B/F 4/10, SMIRT, August 1983, pp. 337-346.

2. Containment Performance Working Group, "Containment Leak Rate Estimates,", NUREG/1037, March 1984.

3. Paris, P.C. and Johnson, R.E.," A Method of Application of Elastic-Plastic Fracture Mechanics to Nuclear Vessel Analysis," Elastic-Plastic Fracture: Second Symposium, Volume II - Fracture Resistance Curves and Engineering Applications, ASTM Special Technical Publication 803, October 1981, pp. II-5 to II-40.

4. Shih, C.F., Kumar, V. and German, M.D., "Studies of the Failure Assessment Diagram using the Estimation Method and J-Controlled Crack Growth Approach," Elastic-Plastic Fracture: Second Symposium, Volume II - Fracture Resistance Curves and Engineering Applications, ASTM Special Technical Publication 803, October 1981, pp. II-239 to II-261.

5. Kumar, V., et. al, Advances in Elastic-Plastic Fracture Analysis, Electric Power Research Institute, EPRI NP-3607, August 1984.

6. Kumar, V., German, M.D. and Shih, C.F., An Engineering Approach for Elastic-Plastic Fracture Analysis, Electric Power Research Institute, EPRI NP-1931, July 1981.

7. Milne, I., "Calculating the Load Bearing Capacity of a Structure Failing by Ductile Crack Growth," Advances in Fracture Research, Proceedings of 5th International Conference on Fracture, Cannes, France, March 29-April 3, 1981, pp. 1751-1757.

8. Chell, G.G. and Milne, I., "Ductile Tearing Instability Analysis: A Comparison of Available Techniques," Elastic-Plastic Fracture: Second Symposium, Volume II - Fracture Resistance Curves and Engineering Applications, ASTM Special Technical Publication 803, October 1981, pp. II-179 to II-205.

9. Saka, M., et. al, "A Criterion Based on Crack-Tip Energy Dissipation in Plane-Strain Crack Growth Under Large-Scale Yielding," Elastic-Plastic Fracture: Second Symposium, Volume I - Inelastic Crack Analysis, ASTM Special Technical Publication 803, October 1981, pp. I-130 to I-158.

10. Sih, G.C., "Mechanics of Subcritical Crack Growth," Fracture Mechanics Technology Applied to Material Evaluation and Structure Design, The Hague: Marinus Nijhoff, 1983, pp. 3-18.

11. Sih, G.C. and Tzou, D.Y., "Mechanics of Nonlinear Crack Growth: Effects of Specimen Size and Loading Rate," Modeling Problems in Crack Tip Mechanics, University of Waterloo, Ontario, Canada, August 1983, pp. 155-169.

12. Turner, C.E., "Further Developments on a J-Based Design Curve and its Relationship to Other Procedures," Elastic-Plastic Fracture: Second Symposium, Volume II - Fracture Resistance Curves and Engineering Applications, ASTM Special Technical Publication 803, October 1981, pp. II-80 to II-102.

13. Marston, T.V., Et. al, "Development of a Plastic Fracture Methodology for Nuclear Systems," Elastic-Plastic Fracture: Second Symposium, Volume II - Fracture Resistance Curves and Engineering Applications, ASTM Special Technical Publication 803, October 1981, pp. II-115 to II-132.

14. Greimann, L.F., Fanous, F. and Bluhm D., "Crack Propagation In High Strain Regions Of Sequoyah Containment", Draft of final report to USNRC, NUREG/CR 4273, July 1985.

15. Broek, D., Elementary Engineering Fracture Mechanics, Third Edition, Boston: Martinus Nijhoff, 1982.

16. Hodulak, L. and Blavel, J.G.," Application of Two Approximate Methods for Ductile Failure Assessment," Elastic-Plastic Fracture: Second Symposium, Volume II - Fracture Resistance Curves and Engineering Applications, ASTM Special Technical Publication 803, October 1981, pp. II-103 to II-114.

17. Turner, C.E., "A Review of Elastic-Plastic Fracture Design Methods and Suggestions for a Related Hierarchy of Procedures to Suit Various Structural Uses," Analytical and Experimental Fracture Mechanics," Sijthoff and Noordhoff, Alphen aan den Rijn, The Netherlands, 1981, pp. 39-58.

18. Shih, C.F. and Needleman, A., "Fully Plastic Crack Problems, Part I: Solutions by a Penalty Method and Part II: Application of Consistency Checks," Journal of Applied Mechanics, Vol. 106, ASME, March 1984, pp. 48-64.

19. de Lorenzi, H.G., "Elastic-Plastic Analysis of the Maximum Postulated Flaw in the Beltline Region of a Reactor Vessel," Aspects of Fracture Mechanics in Pressure Vessels and Piping, PVP-Vol. 58, ASME, July 1982, pp. 71-90.

20. Yong, C.F. and Palusamy, S.S., "VCE Method of J Determination for a Pressurized Pipe Under Bending," Aspects of Fracture Mechanics in Pressure Vessels and Piping, PVP-Vol. 58, ASME, July 1982, pp. 143-157.

21. Schmitt, W., "Three-Dimensional Finite Element Simulation of Post-Yield Fracture Experiments," Computational Fracture Mechanics - Nonlinear and 3-D Problems, PVP-Vol. 85, ASME, June 1984, pp. 119-131.

22. Bakker, A., "On the Numerical Evaluation of the J-Integral," Paper G/F 2/4, SMIRT, August 1983, pp. 181-189.

23. Cells, A., Squillani, A. and Milella, P.P., "Experimental and Numerical Evaluation of J Integral on Tubes," Paper G/F 4/2, SMIRT, August 1983, pp. 275-281.

24. Beliczey, S. and Hofler, A., "Calculations to Experimental Results of Crack Growth," Paper G/F 4/9, SMIRT, August 1983, pp. 329-335.

25. de Lorenzi, H.G., "3-D Elastic-Plastic Fracture Mechanics with ADINA," Computer and Structures, Vol. 13, 1981, pp. 613-621.

26. de Lorenzi, H.G., "On the Energy Release Rate and the J-Integral for the 3-D Crack Configuration," International Journal of Fracture, Vol. 19, 1982, pp. 183-193.

27. ANSYS Engineering Analysis System User's Manual, Swanson Analysis System, Inc., Houston, PA, (Version 4.1c) 1984.

28. ASME Boiler and Pressure Vessel Code, ASME, Section III, Subsection NE, Class MC Components, Paragraph NE 5320.

29. Blejwas, T.E., Woodfin, R.L., Dennis, A.W. and Horschel, D.S., "Containment Integrity Program," NUREG/CR-3131/1, SAND83-0417, March 1983.

Table 1. Steel Properties and Postulated Initial Crack Depth

Plate Thickness	σ_y(ksi)	σ_u(ksi)	Crack Depth	J_R k in/in^2	ε_R
1/2"	47.3	66.6	0.083"	3.0 ± 1.0	9 ± 3%
5/8"	49.2	68.3	0.083"		

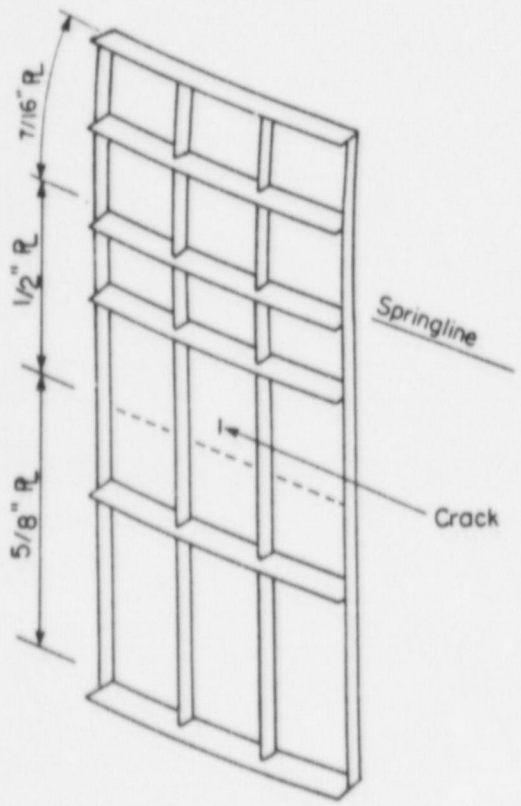


Figure 1. Crack in 1/2-inch Plate Near Springline of Sequoyah Containment

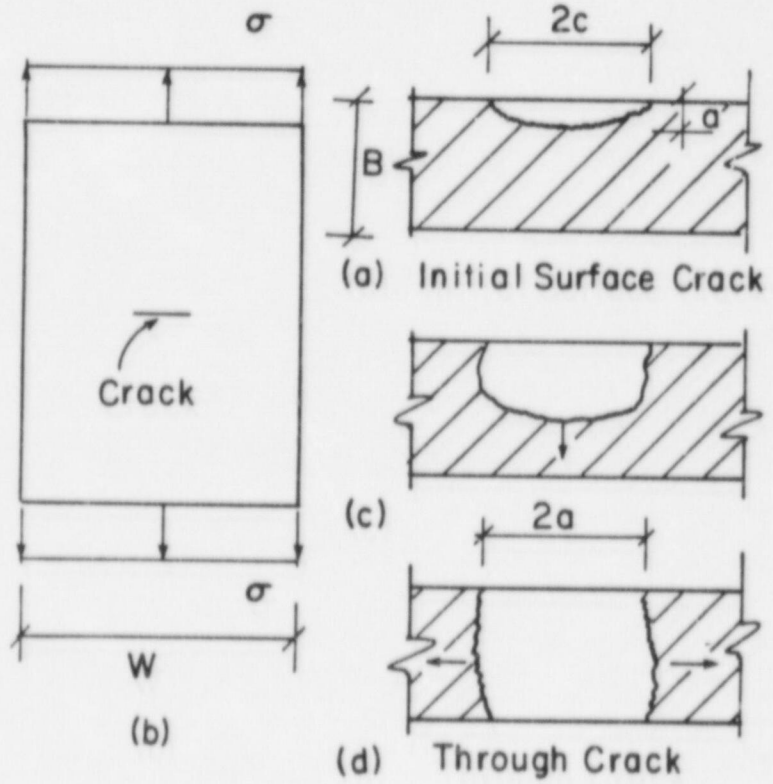


Figure 2. Idealized Crack Growth Process

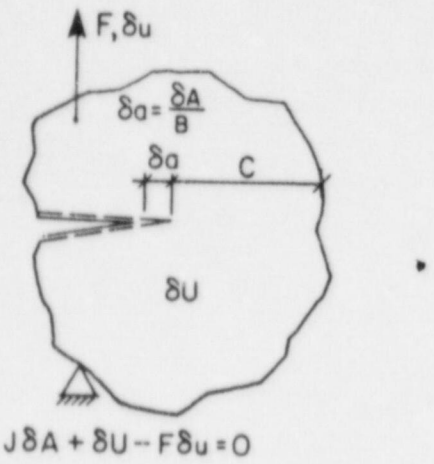


Figure 3. Definition of J as Generalized Force for Crack Movement

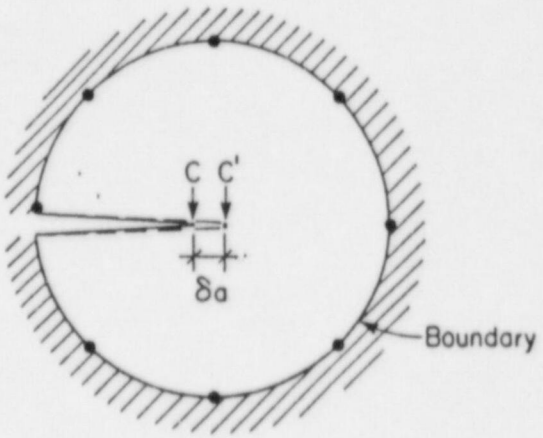


Figure 4. Virtual Crack Extension Pattern

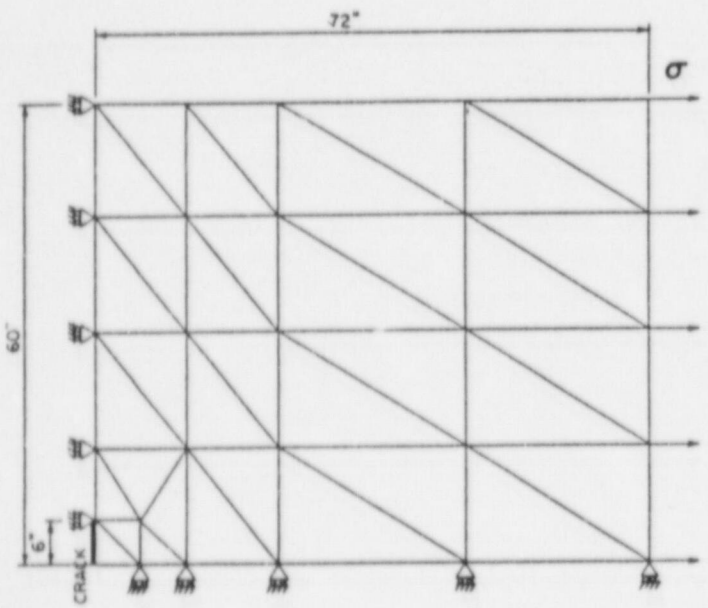


Figure 5. One-quarter of Center Cracked Plate Finite Element Mesh (1/2 in. Plate, a/b = 0.1 α = 1, n = 10)

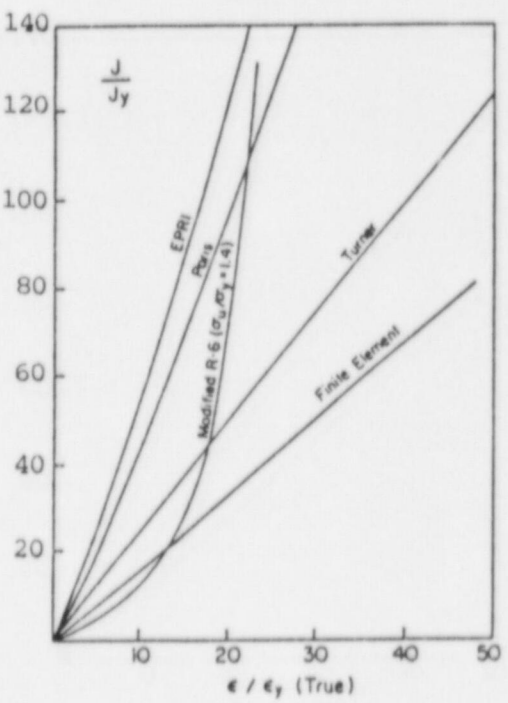
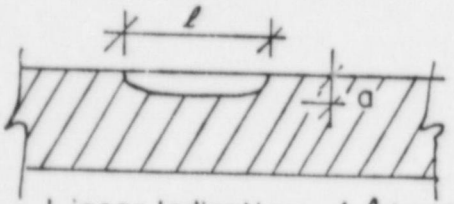
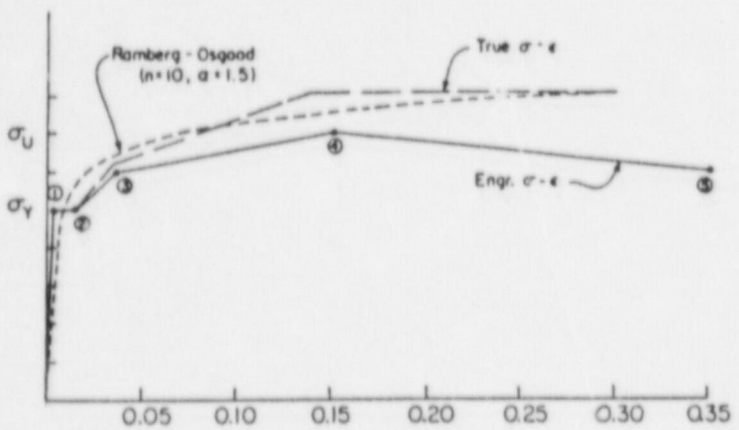


Figure 6. Comparison of J Calculations, Center Cracked Plate (CCP) (a/b = 0.1, α = 1, n = 10)



Thickness	Maximum ℓ	Maximum a
less than 3/4"	1/4"	1/12"
3/4" to 2 1/4"	t/4	t/9
greater than 2 1/4"	3/4"	1/4"

Figure 7. ASME Acceptance Standards for Radiograph Welds (Section III, Subsection NE, Class MC Components, Paragraph NE 5320)



ENGINEERING

Point	ε	σ
1	ϵ_Y	σ_Y
2	0.015	σ_Y
3	0.035	$(\sigma_Y+\sigma_U)/2$
4	0.15	σ_U
5	0.35	$(\sigma_Y+\sigma_U)/2$

Figure 8. Idealized Stress-Strain Curve for A516, Gr. 60

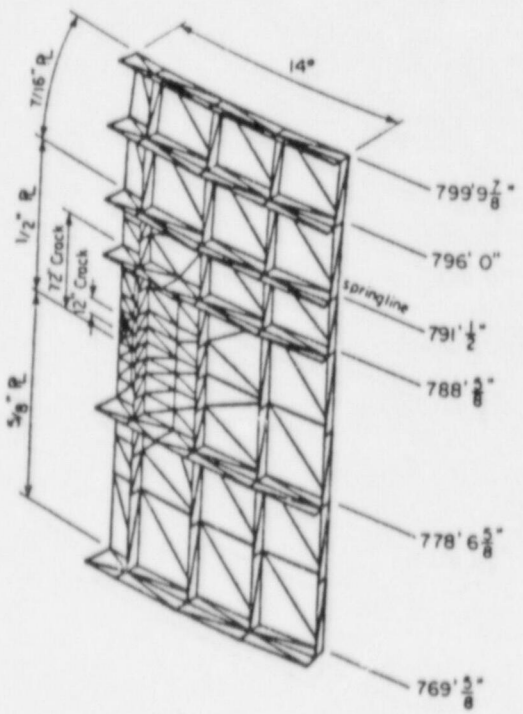


Figure 9. Finite Element Model of a Section of the Containment Near the Springline

Failure Mechanisms of LWR Steel Containment Buildings Subject to Severe Accident Loadings*

David B. Clauss
Containment Integrity Division
Sandia National Laboratories
Albuquerque, New Mexico 87185

ABSTRACT

The potential failure mechanisms in LWR steel containment buildings subject to quasi-static pressurization and elevated temperature are identified. For each failure mechanism, the relevant structural response measures are discussed. For mechanisms involving leakage, the importance of seal performance is also discussed. Criteria that can be used to evaluate threshold environments are presented for several failure mechanisms. Results of tests on scale models and seal tests that support the criteria are referenced.

1. INTRODUCTION

During a severe (degraded core) accident, containment buildings may be subject to loads that significantly exceed their design basis loads. The performance of the containment building, which represents the last engineered barrier to release of radioactive material, affects the consequences of a severe accident. A partial list of the containment performance parameters that affect severe accident consequences follows:

Capacity (Are the severe accident loads sufficient to cause a failure, i.e., a significant release of radioactive material?)

Timing (In general, risk from an early failure is greater than that from a late failure, because early in an accident sequence aerosols and other radioactive particles are more likely to be airborne.)

Location of failure (Is a release directly to the environment or filtered through other structures, for example, the reactor auxiliary building?)

Leakage rate or "hole size" (Is the leakage rate sufficient to preclude further pressurization of the containment building? Consequences are proportional to leakage rate, at least over some intermediate range of values. Rupture could result in resuspension of radioactive aerosols.)

It should be evident that the predicted failure mechanism will have

* This work supported by the U.S. Nuclear Regulatory Commission and performed at Sandia National Laboratories, which is operated by the U.S. Department of Energy under contract number DE-AC04-76DP00789.

a significant effect on risk estimates. In fact, failure mechanisms are containment specific as well as scenario dependent -- for instance, for a given containment, the failure mode due to a hydrogen detonation could be much different than that due to quasi-static pressurization.

This paper will focus on the potential failure mechanisms in a steel LWR containment building subject to quasi-static pressurization and elevated temperature. The failure mechanisms considered in this paper are:

- Failure of the Containment Shell
- Leakage Past Sealing Surfaces (Operable Penetrations)
  - Equipment Hatch Sleeve Ovalization
  - Pressure Unseating Equipment Hatches and Drywell Heads
  - Personnel Airlocks
- Leakage from Electrical Penetration Assemblies
- Leakage Through Purge and Vent Valves
- Leakage Due to Failure of a Bellows (Expansion Joint)

For each potential failure mechanism, the important structural response measures and seal performance parameters are discussed. Preliminary criteria are presented for evaluating rupture of the shell and leakage from equipment hatches and drywell heads.

The discussion is limited to the range of response wherein the containment building behaves like a freestanding steel shell. Most steel containment buildings are enclosed by a concrete shield wall. If large membrane plastic strains are developed in the containment shell before failure occurs, the containment and shield wall will come into contact. In BWR Mk I containment buildings, the gap between the steel shell and the shield wall corresponds to approximately 0.5% membrane strain; in other types of plants with freestanding steel containments the gap typically corresponds to 5% membrane strain. If contact occurs, the performance of the containment building will be affected. Different failure modes may come into play, or the shield wall may strengthen the containment building, or both. The effect of contact with concrete shield walls on the failure mechanisms of LWR containments are not considered in this paper.

2. FAILURE OF THE CONTAINMENT SHELL

The containment shell is defined as the pressure boundary of the containment, exclusive of those parts of the boundary made up of penetrations, including equipment hatches, personnel airlocks, piping, and electrical penetrations assemblies. A loss of integrity associated with the containment shell must involve a cohesive material failure, i.e., a through-wall crack or tear in the pressure boundary. If a through-wall crack or tear is developed, it is highly likely that rupture (unstable crack growth) will rapidly ensue.

Based on results of tests on scale models of steel containment buildings that were pressurized to failure [1,2], a simple strain criterion appears to be adequate for estimating the point at which a

through-wall crack or tear will develop. The steel most commonly used in U.S. containments, A516 Gr 70, has exceptional ductility, and very large plastic strains may be developed prior to failure.

The following criterion for evaluating rupture is proposed:

- Rupture will occur if, at any point on the pressure boundary, the equivalent strain exceeds the material's ultimate strain (the strain at maximum load as determined from a uniaxial tensile test). If the strain is due primarily to bending, somewhat higher strain may be allowable (to account for crack growth through the thickness).

The above criterion should be used only with detailed three-dimensional finite element analyses, which would need to include at least major penetrations and stiffeners. Results can be very sensitive to design details, such as stiffener patterns around penetrations [2,3]. Any failure criterion must be consistent with the analysis used to calculate the response measures used in the criterion. If axisymmetric analyses are used to predict rupture, the limiting value of strain used to predict rupture must be decreased to account for the effects of penetrations and stiffeners.

Many of the discontinuities in the containment shell, such as the springline and the base embedment, result in self-limiting states of stress, and consequently, a cohesive material failure is not likely to initiate in these areas. On the other hand, large penetrations cause local strain concentrations in the shell that reduce the capacity relative to an undisturbed shell. Stiffeners tend to increase the general yield pressure, but they do not necessarily increase the ultimate strength by a like amount.

There is a large body of evidence that indicates that if a through-wall crack or tear is developed a steel containment shell will rupture catastrophically. Kiefner [4] developed empirical equations based on a large number of tests on pressurized cylinders that show that rupture will occur unless the initial through-wall crack is the result of a deep surface flaw (depth of the surface flaw must be at least one-half the wall thickness). Four of the five steel containment models tested at Sandia ruptured; in the one exception, leakage from a through-wall crack was sufficient to depressurize the model. However, in that particular model, the cylindrical wall had been severely thinned by excessive grinding adjacent to a repaired weld, which was equivalent to a deep surface flaw [3]. At least qualitatively, the formulas developed by Kiefner explain why rupture did not occur in that model. A final example is the J-integral analysis of the Sequoyah containment conducted by Griemann [5]. Griemann's analysis showed that a through-wall crack originating in the thinner wall sections near the springline would not be arrested at the thicker wall sections used at lower elevations, and he concluded that unstable crack growth (rupture) would occur.

Although exceptions are possible, it seems clear that steel containments are highly likely to rupture if a through-wall crack is developed at any point in the containment shell. (It is assumed that initial surface flaws do not exceed 20% of the shell thickness.)

3. LEAKAGE FROM OPERABLE PENETRATIONS

Any penetration that is intended to be used for access to the containment is categorized as an operable penetration. In U.S. steel containments, this would include equipment hatches, personnel airlocks, escape hatches, and BWR Mk I and Mk II drywell heads. The potential for leakage between the sealing surfaces of these types of penetrations is considered in this section.

In general, leakage from operable penetrations depends on both displacement and performance of the seal. Tests have shown that if metal to metal contact is maintained between the sealing surfaces, significant leakage does not occur regardless of the condition of the seal material [6]. On the other hand, because the seals are compressed typically one-quarter inch, large separations of the sealing surfaces can arise without significant leakage if the performance of the seal is not compromised.

Relative displacements of the sealing surfaces can be categorized as either separation (relative motion perpendicular to the sealing surfaces) or sliding (relative motion in the plane of the surfaces). Tests on seal and gasket materials [6] suggest that there are at least two ways in which performance of the seal can be compromised: (1) radiation or thermal aging can result in a loss of resiliency, and (2) high temperatures (500 F to 650 F, depending on the type of material) degrade the seal materials, that is, the materials outgas, then become dry and powdery).

In special cases, leakage may be a function of performance of the seal only, or sealing surface deformation only. In personnel airlocks with inflatable seals, the door and bulkhead are not designed to be in intimate contact, and therefore, leakage will arise if the performance of the seal is compromised, irrespective of structural deformations. The performance of the seal may also be the only factor preventing leakage if there is significant out-of-flatness between the sealing surfaces. This is a condition that would not be detected by Integrated Leak Rate Tests; at design levels, seal performance prevents leakage. However, in BWR Mk I and Mk II plants, severe accident temperatures are expected to be sufficient to degrade seals and out-of-flatness could result in leakage without additional separation or sliding of the sealing surfaces. In cases where sliding or separation of the sealing surfaces is very large, leakage can result even if the performance of the seal is not compromised.

3.1 Equipment Hatch Sleeve Ovalization

Typical details of equipment hatches used in U.S. steel containments are shown in Figures 1 and 2. In a cylindrical containment shell, an equipment hatch sleeve will deform into an oval shape due to interaction with the containment shell. The horizontal diameter of the sleeve increases while the vertical diameter decreases by a like amount; the deformations can become quite large (on the order of the sleeve wall thickness) after general yielding of the cylindrical

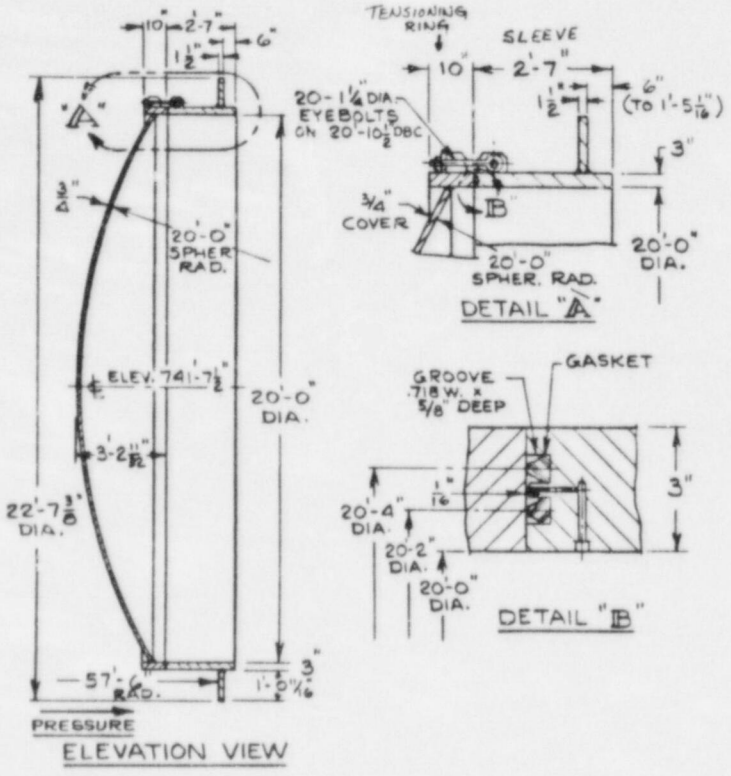


Figure 1 - Details of a Pressure Seating Equipment Hatch

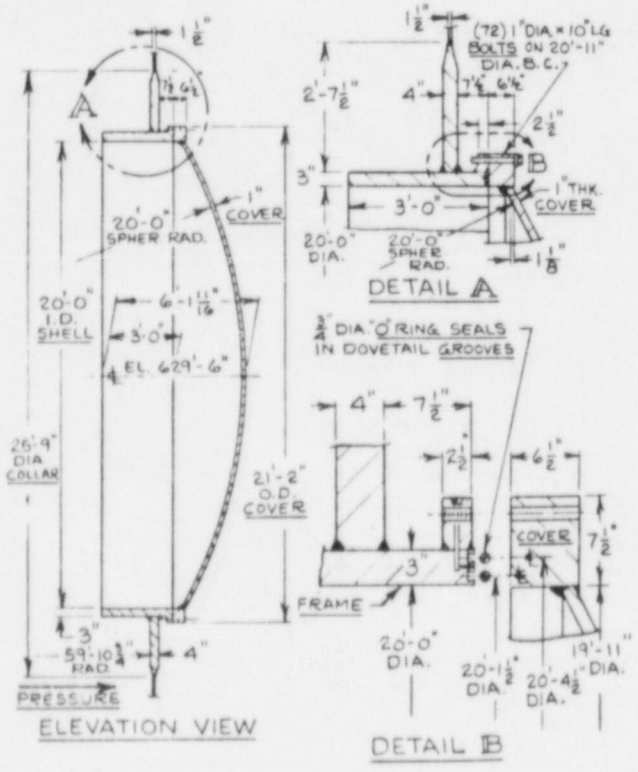
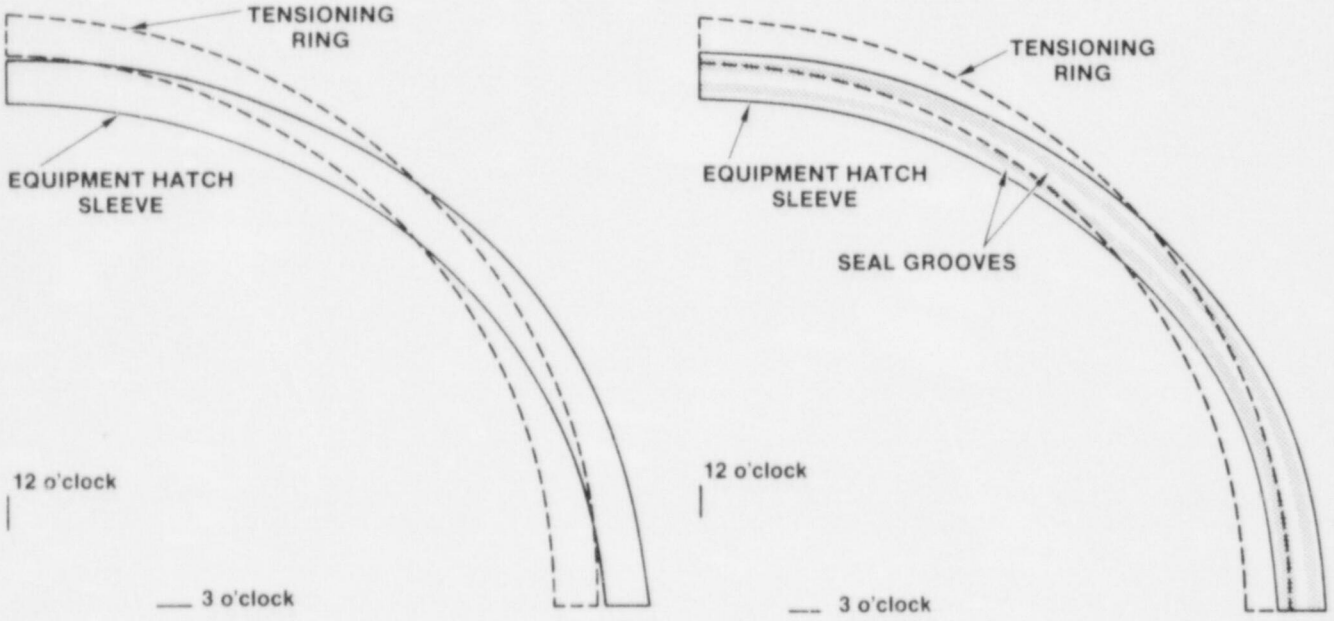


Figure 2 - Details of a Pressure Unseating Equipment Hatch

containment shell. The equipment hatch cover and tensioning ring deform axisymmetrically, i.e., they retain their circular shape. Changes in the diameter of the tensioning ring are expected to be quite small (except possibly for pressure seating hatches that are susceptible to buckling). The mismatch caused by the sleeve sliding relative to the tensioning ring is greatest along the horizontal and vertical centerlines; as indicated in Figure 3a, eventually the sleeve and tensioning ring will lose contact at these points, resulting in leakage. Under these conditions, the performance of the seal material does not affect the leakage potential.



(a) Without seal degradation (b) With Seal Degradation

Figure 3 - Leakage Path Created by Ovalization of Sleeve

The deformation of the equipment hatch sleeve can be related to the average membrane strain in the containment shell in an approximate way. Ovalization of the equipment hatch sleeve is primarily an inextensional (no stretching of the midsurface) deformation, and consequently it is a relatively flexible mode of deformation. Thus, the equipment hatch sleeve basically conforms to the membrane displacements of the containment shell at their intersection. As illustrated in Figure 4, the increase in the horizontal radius of the sleeve, Δr_H, can be approximated as

$$\Delta r_H = \epsilon r \qquad (1)$$

where ϵ is the average membrane circumferential strain in the shell at the elevation of the equipment hatch centerline, and r is the original sleeve radius. Assuming the cover and tensioning ring do not deform significantly, leakage due to ovalization is assured for

$$\Delta r > t \qquad (2)$$

where Δr is the change in the sleeve radius and t is the sleeve wall

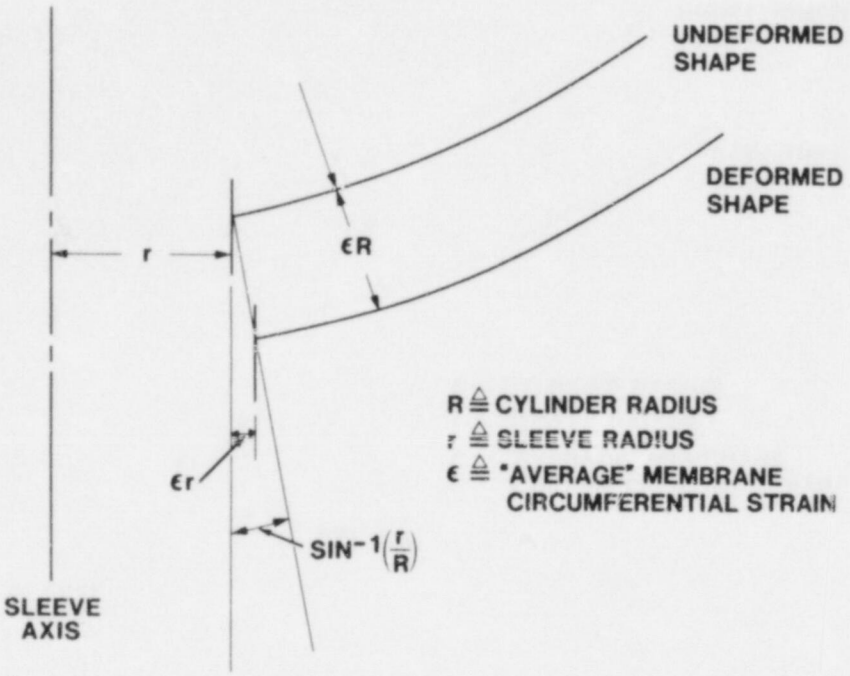


Figure 4 - Equipment Hatch Sleeve and Containment Shell Interaction

thickness at the sealing surface. Combining Eqs. 1 and 2, the approximate leakage criterion is

$$\epsilon r/t > 1 \ . \qquad (3)$$

The average membrane strain in the shell at the elevation of an equipment hatch corresponding to leakage from ovalization, ϵ', can be calculated from Eq. 3. For equipment hatches used in steel containments identified in a survey conducted by Argonne National Laboratory [7,8], ϵ' ranged from 2.5% to 7.3%, as indicated in Table 1. Clearly, significant plastic membrane strains must be developed in the containment shell before ovalization of an equipment hatch sleeves will cause leakage.

Unit	t	r	$\epsilon'^{(1)}$	$\epsilon'^{(2)}$	Seal Type
1	5-1/4"	72"	7.3%	4.5%	gumdrop
2	4-1/2"	72"	6.3%	4.2%	gumdrop
3	4-1/2"	84"	5.4%	3.9%	gumdrop
4	4-1/2"	84"	5.4%	3.6%	gumdrop
5	4-1/2"	126"	3.6%	2.3%	gasket
6	4-1/2"	126"	3.6%	2.3%	gasket
7	4-1/2"	126"	3.6%	2.3%	gasket
10	3"	120"	2.5%	1.7%	gumdrop

Note: (1) Assuming seal degradation has not occurred
(2) Assuming seal has been severely degraded and ejected

Table 1 - Critical Strain for Equipment Hatch Leakage (by Ovalization) In Steel Containments

Under certain conditions, leakage caused by ovalization may occur at lower values of average membrane strain. If the seal material is severely degraded, the grooves that hold the seals could act as a leakage path, as suggested by Figure 3b. For a pressure seating hatch, the grooves would be exposed to the inside of the containment at 3 and 9 o'clock and to the outside at 6 and 12 o'clock, yielding critical strains (') from 1.7 to 4.5%, as indicated in Table 1. However, in order for this leakage path to be realized, a substantial amount of the seal would probably have to be degraded and ejected from the seal grooves.

The approximate method outlined above did prove accurate for the equipment hatches in the 1:8-scale model [2,3]. In particular, the change in the horizontal diameter calculated from Eq. (1) was within 10% of the measured displacement. However, it is unknown how accurate this approximate method would be for different reinforcement designs and stiffener patterns.

3.2 Separation of Pressure Unseating Hatches

Schematics of a pressure-unseating equipment hatch and a BWR Mk I drywell head are depicted in Figures 2 and 5, respectively. In both cases the bolts are preloaded to maintain leak tightness during internal pressurization of the containment. Typically the bolts are tightened until metal to metal contact is achieved, and then a specified level of torque or load is applied. Internal pressure

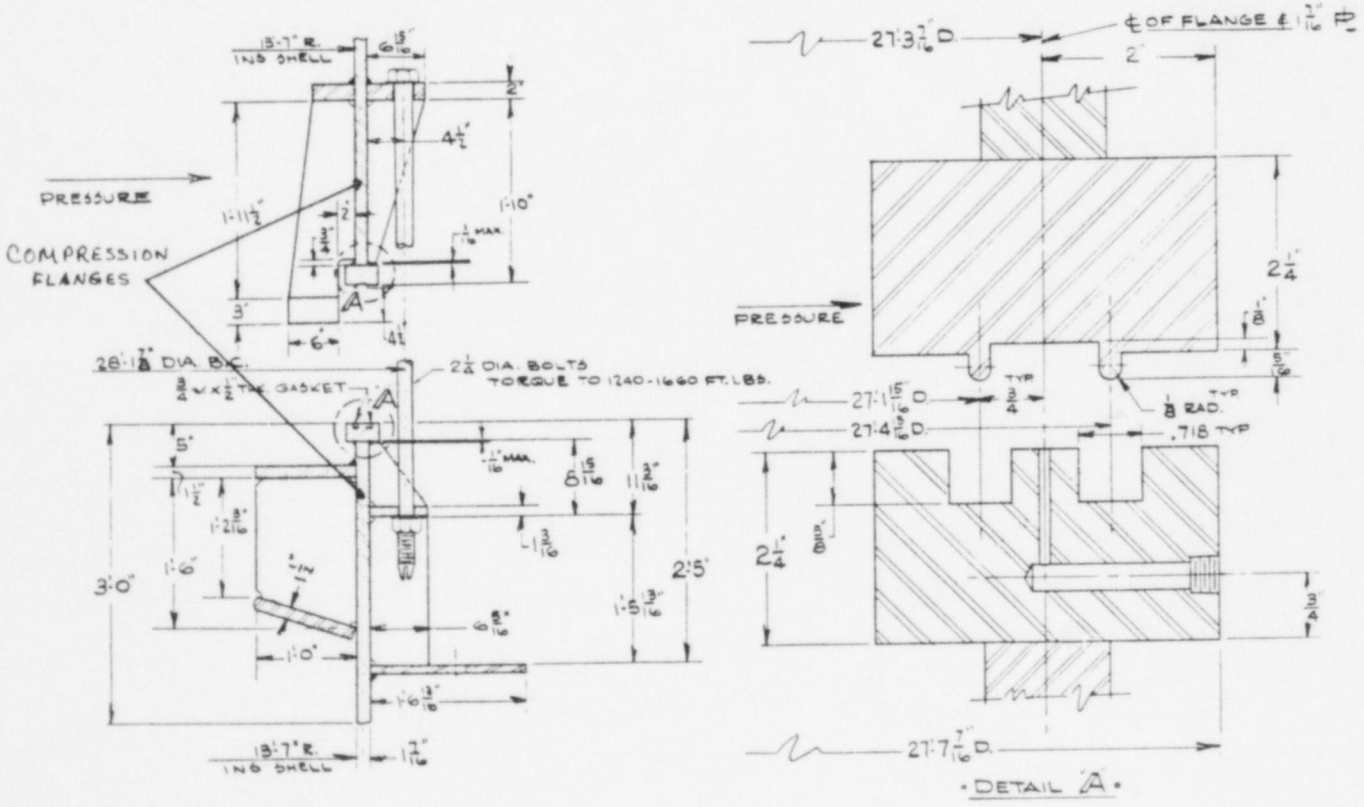


Figure 5 - Details of a BWR Mk I Drywell Head

acts in the opposite direction of the bolt preload and tends to separate the sealing surfaces. The effects of temperature must also be considered; from a heat transfer viewpoint, the bolts, if they are exposed to air, will act as convective fins. Thus, in many designs, the average temperature of the bolts will be less than that of the compression flanges. Differential thermal expansion (when the bolts expand less the compression flanges) tends to maintain contact between the sealing surfaces, that is, it acts in the opposite sense of internal pressurization.

The following criterion are proposed for evaluating the onset of leakage from pressure unseating hatches and heads:

- If the seals are exposed to temperatures high enough to cause degradation (500 F to 650 F, depending on the material), leakage will occur when the internal pressure is sufficient to cause separation of the sealing surfaces.
- If the seals are not degraded, but at some time into the accident aging causes a loss of resiliency, a subsequent increase in separation will cause leakage.
- If the seals are not degraded and do not lose resiliency, leakage will occur when the seal squeeze becomes equal to zero (when the separation is equal to the initial seal compression).

Recent tests on silicon 'O' rings suggest that even degraded seals may prevent leakage through small gaps, up to about five or six mils. If this is substantiated, the above criteria would have to be modified so that leakage for separations less than 5 or 6 mils is not allowed regardless of the condition of the seal.

Assuming linear elastic behavior of the bolts and compression flanges, the internal pressure at which separation begins for pressure unseating hatches and heads, p_s, can be calculated as:

$$p_s = [(k_b+k_f)F_i/k_f + k_b(\epsilon_{Tf}-\epsilon_{Tb})L]/(1+2\nu k_b/k_f)\pi r^2 \quad . \qquad (4)$$

The subscripts f and b denote the compression flanges and bolts, respectively. F_i is the bolt preload, k is the axial stiffness, ϵ_T is the thermal strain, L is the bolt grip, ν is Poisson's ratio, and r is the average radius of the equipment hatch sleeve or drywell head. Eq. 4 was determined by introducing terms representing the axial thermal expansion of the bolts and the compression flanges and the axial deflection of the compression flanges due to hoop stress to expressions in [9]. The resulting equation for the force in the compression flanges was set to zero and solved for p_s. Additional pressure is carried entirely by the bolts, so that the separation between the sealing surfaces, s, is given by

$$s = \pi r^2(p - p_s)/k_b \quad \text{for } p > p_s \quad . \qquad (5)$$

The separation pressure for drywell heads and pressure unseating equipment hatches used in steel containments that were identified in the ANL survey of containment penetrations [7,8] is tabulated in Table 2. The mean temperature of the compression flanges was taken

	Unit	p_s (psig)	k_b (10^6 lb/in)	s @ p_s + 10 psi (mils)	
Drywell Heads					
BWR Mk I :	1	135	199	4.2	
	2-5	127	410	3.3	
	6	119	278	4.3	
Equipment Hatches					
BWR Mk I :	1	171	91	1.8	
	6	?	140	1.2	Note 1
BWR Mk III :	8-9	34	194	2.3	Note 2

Note: (1) Specified torque not known.
(2) Mean temperature of bolts and compression flanges taken to be 350 F and 400 F, respectively.

Table 2 - Separation Pressure for BWR Mk I Drywell Heads

to be 700 F and that in the bolts was taken to be 550 F (these temperatures are based on heat transfer calculations made for the drywell head region of a given containment). The results are very sensitive to the bolt preload, which is difficult to know accurately. Generally, preload is specified in terms of torque, and the axial load developed in the bolt depends on friction, which is difficult to characterize. The axial preload was calculated using the following expression from [9]:

$$T = 0.2F_i d \ , \tag{6}$$

where T is the specified bolt torque and d is the bolt diameter. The coefficient of 0.2 in Eq. 6 corresponds to a friction coefficient of 0.15; lubricants may substantially reduce the friction coefficient, resulting in higher axial preloads for the same specified torque. On the other hand, relaxation, which reduces the axial load in the bolts and is also difficult to characterize, occurs with time. A survey of axial preload in bolts of pressure unseating hatches and heads actually obtained in the field would help quantify leakage potential for these types of penetrations.

3.3 Personnel airlocks

A personnel airlock with double dog-ear seals is shown in Figure 6. The inner door and bulkhead are the primary pressure boundary, however, if leakage were to occur past the inner door, there is a redundant outer door. The doors and bulkheads are essentially flat plates that are stiffened by webs and flanges. Internal pressurization is resisted primarily by bending action, and therefore, rather large out-of-plane deformations may arise for beyond design basis loads.

Although the door is pressure seating, separation may still be possible at certain points. For instance, in a simply supported rectangular plate subject to uniform pressure, significant reaction

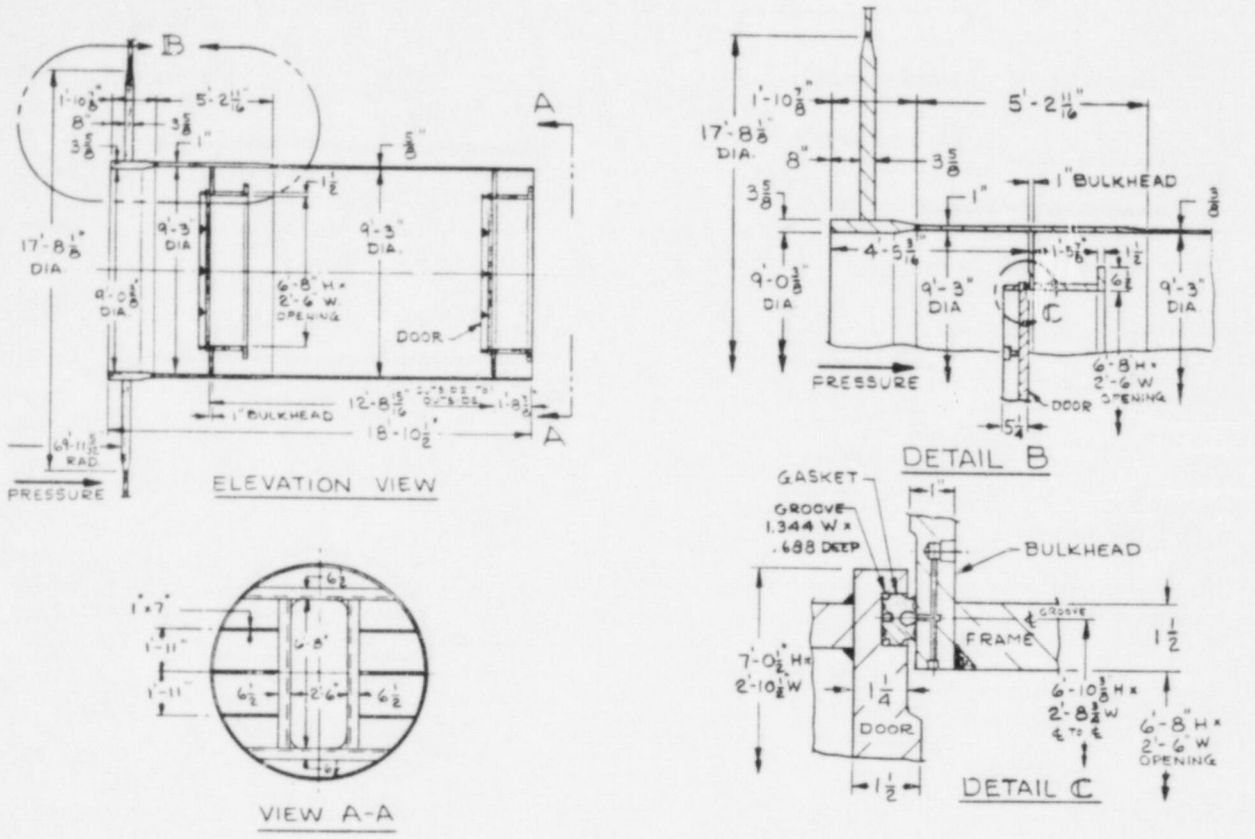


Figure 6 - Details of a Personnel Airlock with Double Dog-ear Seals

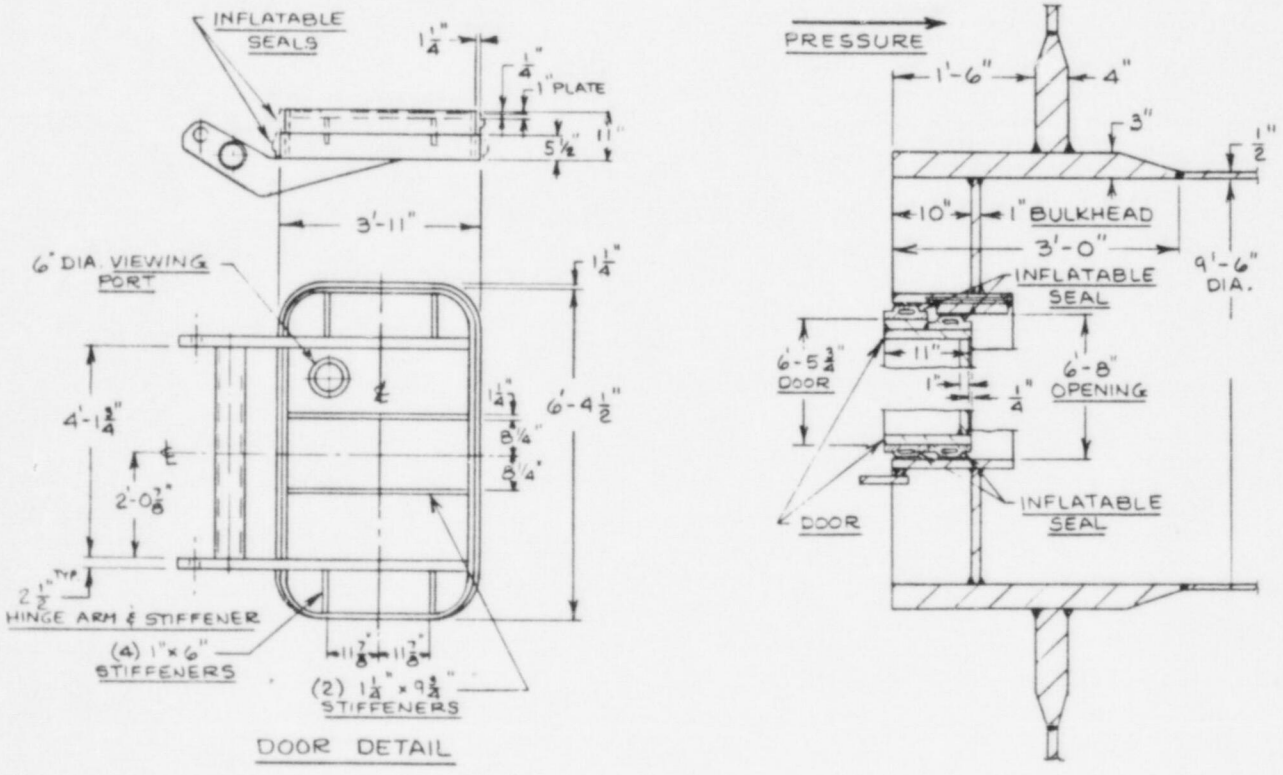


Figure 7 - Details of a Personnel Airlock With Inflatable Seals

forces must occur at the corners; if the corners are not held down, the corners will lift off. The door could be thought of as a plate that is simply supported by the bulkhead; separation of the sealing surfaces at the door corners may be possible. Also, if the stiffness of the door and bulkhead are not matched, their out-of-plane bending displacements may differ, especially near the horizontal stiffeners, resulting in separation of the sealing surfaces. If the performance of the seal material is compromised, small separations may result in leakage.

Plans for testing a personnel airlock similar to that shown in Figure 6 are being formulated, as described in [6]. The personnel airlock will be subject to elevated temperature (700 F) and internal pressure; deformation of the sealing surfaces and leakage will be closely monitored. Finite element analyses will be conducted in support of this test. When the tests and analyses of this personnel airlock are completed, much more definitive statements about the leakage potential of personnel airlocks should be possible.

Personnel airlocks with inflatable seals are used in a number of steel containments. As shown in Figure 7, there is a large gap between the door and the bulkhead that is blocked by the inflatable seals. The seals are pressurized and expand against the sealing surface; only seal performance prevents leakage. Inflatable seals are subject to degradation at elevated temperatures similar to other organic seals that have already been tested. In addition, high temperatures could reduce the material strength, and the seal could rupture due to its own internal pressure. In the absence of elevated temperature, it is suspected that inflatable seals would begin to leak when the internal pressure in the containment is approximately the same as the seal pressure. Since the seal pressure has a significant effect on leakage past inflatable seals, typical industry practice for pressurizing these types of seals will be surveyed. Tests are planned in the next year to determine the conditions under which the performance of inflatable seals is compromised.

Viewports (sometimes called sightglasses) are located in the bulkheads of some personnel airlocks, as shown in Figure 7. By treating a viewport as a circular plate with either simply supported or clamped edges and assuming that brittle fracture occurs when the maximum stress equals the glass tensile strength, estimates for the pressure capacity of a viewport can be made. Typical Pyrex glass has a tensile strength of two ksi and a Poisson's ratio of 0.22. For a viewport six inches in diameter and three-quarters inch thick, the calculated failure pressure for a simply supported plate is 104 psig, and for a clamped plate it is 167 psig. Details of viewports used in U. S. containments should be obtained, so that analysis of actual viewports can be conducted.

4. MISCELLANEOUS

Tests have been conducted on D. G. O'Brien and Westinghouse electrical penetration assemblies (EPAs) to determine their leakage characteristics during severe accidents [10]. Leakage was not detected during the testing of either EPA, although there was a small leak (0.13cc/sec) from the D. G. O'Brien EPA during cooldown. The D. G. O'Brien and Westinghouse EPAs were tested to PWR and BWR Mk III severe accident environments, respectively. Both these environments have maximum temperatures below that required to degrade the elastomer seals. A Conax EPA will be tested in the more severe BWR Mk I and Mk II environment (maximum temperature of 700 F) in July 1986.

Idaho National Engineering Laboratory conducted leak integrity tests on purge and vent valves subject to severe accident loads up to 350 F and 120 psig [11]. INEL's results seem to indicate that leakage during cooldown was possible under these conditions due to permanent set of the elastomer seal. Again there has not been testing in severe accident environments that have maximum temperatures capable of degrading the elastomer seals.

There are also numerous mechanical and "dummy" penetrations that have flat plate covers. Although flat plates carry internal pressurization by primary bending, these covers generally appear to be designed for higher loads than the containment shell, and failure or leakage is unlikely to initiate at these points.

The capacities of bellows (expansion joints) have not yet been documented in the open literature. Bellows are considered to be most susceptible to torsional and shear loads. Long range plans call for testing a bellows in severe accident environments to investigate failure modes and capacity.

5.0 CONCLUSIONS

If a through-wall crack or tear is developed in a steel containment shell during a severe accident, it is likely that rupture will rapidly ensue. However, there are a number of potential leakage paths in steel containment shells from which significant leakage could occur before a through-wall crack is developed. Leakage could be sufficient to depressurize the containment, thus precluding rupture. The leakage potential of penetrations and capacity of the containment shell are design dependent (containment specific), and need to be evaluated on a case by case basis.

The leakage potential of mechanical and electrical penetrations does not appear to be significant. Operable penetrations appear to have the most likely source of significant leakage during a severe accident. Methods for evaluating the leakage potential of equipment hatches and drywell heads were presented in this paper. NRC plans for testing a personnel airlock, inflatable seals, and a bellows will resolve many unanswered questions.

Characterization of leakage from containment penetrations subject to severe accident conditions could be improved by undertaking the following efforts:

In-field survey of operable containment penetrations to measure (i) out-of-flatness of sealing surfaces, (ii) any decrease in the performance of seal materials (i.e., loss of resiliency) during normal operation, and (iii) actual bolt preloads in pressure unseating hatches and heads.

Quantification of leakage rates for irregular path geometries and also taking into account the effects of aerosols.

Experiments on seal and gasket materials to study the time dependence of performance degradation.

The response and potential failure modes of steel containments subject to dynamic pressurization may also need to be studied more carefully. As mentioned in the Introduction to this paper, it is quite likely that, for a given containment, the failure mode due to a detonation is altogether different than that due to slow pressurization. Estimates of a containment's pressure capability used to assess risk are based on static analysis for both dynamic and quasi-static pressurization. Improvements to these risk estimates can be obtained by an analytical or experimental investigation, or a combined approach, to study the response of containment buildings to dynamic loading.

6.0 ACKNOWLEDGMENT

The hypotheses and conclusions presented in this paper are based largely on experiment studies directed by L. N. Koenig, D. S. Horschel, and J. D. Keck from Sandia National Laboratories. Their efforts are gratefully acknowledged.

7.0 REFERENCES

[1] HORSCHEL, D. S., "The Design, Fabrication, Testing and Analyses of Four 1:32-Scale Steel Containment Models", NUREG/CR-3902, SAND84-2153, Sandia National Laboratories, Albuquerque, NM (to be published).

[2] CLAUSS, D. B., "Comparison of Analytical Predictions and Experimental Results for a 1:8-Scale Steel Containment Model Pressurized to Failure", NUREG/CR-4209, SAND85-0679, Sandia National Laboratories, Albuquerque, NM, July 1985.

[3] CLAUSS, D. B., HORSCHEL, D. S., and BLEJWAS, T. E., "Insights Into the Behavior of LWR Steel Containments Buildings During Severe Accidents", proposed for publication in Nuclear Engineering and Design, Sandia National Laboratories, Albuquerque, NM.

[4] KIEFNER, J. F., et al., "Failure Stress Levels of Flaws in Pressurized Cylinders", Progress in Flaw Growth and Fracture Toughness Testing, ASTM STP536, American Society for Testing and Materials, 1973, pp 461-481.

[5] GRIEMANN, L., FANOUS, F., and BLUHM, D., "Crack Propagation in High Strain Regions of Sequoyah Containment", NUREG/CR-4273, Ames Laboratory, Ames, Iowa, July 1985.

[6] KOENIG, L. N., "Leakage Potential Through Mechanical Penetrations in a Severe Accident Environment", to be presented at the Third Workshop on Containment Integrity, Washington D. C., May 21-23, 1986.

[7] BUMP, T. R., et al., "Characterization of Nuclear Reactor Containment Penetrations - Preliminary Report", NUREG/CR-3855, SAND84-7139, Sandia National Laboratories, Albuquerque, NM, June 1984.

[8] SHACKELFORD, M. H., et al., "Characterization of Nuclear Reactor Containment Penetrations - Final Report", NUREG/CR-3855, SAND84-7180, Sandia National Laboratories, Albuquerque, NM, February 1985.

[9] SHIGLEY, J. E., Mechanical Engineering Design, McGraw-Hill, New York, 1977, pp 240-250.

[10] KECK, J. D., and THOME, F. V., "Leak Behavior Through EPAs Under Severe Accident Conditions", to be presented at the Third Workshop on Containment Integrity, Washington D. C., May 21-23, 1986.

[11] STEELE, R., JR., and WATKINS, J. C., "Containment Purge and Vent Valve Test Program Final Report", NUREG/CR-4141, EG&G Idaho, Inc., Idaho Falls, Idaho, September 1985.

FAILURE PRESSURE AND FAILURE MODE OF THE LATEST TYPE OF GERMAN PWR CONTAINMENTS

R. Krieg, B. Göller, G. Messemer, E. Wolf
Kernforschungszentrum Karlsruhe GmbH
Institut für Reaktorentwicklung
Projekt Nukleare Sicherheit
Postfach 3640, D-7500 Karlsruhe

ABSTRACT

For the pressurized water reactor Philippsburg (KKP II) a slowly increasing containment pressure typical for a core melt accident is assumed. The failure pressure and failure mode of the containment are determined. It turns out that the sealing box covering the bolted connection at the equipment hatch will fail at a containment overpressure between 12.9 and 13.7 bar. Then the leakage through the bolted connection is sufficient to prevent further pressure increase. However, if the sealing box failed at a somewhat higher pressure, a global containment failure with extreme mechanical damage would have to be expected.

1. INTRODUCTION

The latest type of German pressurized water reactor containments consists of a free standing spherical steel shell with a diameter of 56 m and a wall thickness of 38 mm (Fig. 1). It is clamped into the concrete basement at an angle of 40° below the equator. The containment shell is made of approximately 500 curved sheets which are welded together. The material is the ferritic steel 15MnNi63. Further design details refer to the pressurized water reactor built in Philippsburg (KKP II).

During a hypothetical core melt accident the pressure inside the containment is expected to grow beyond the design limit, leading to large plastic deformations and finally to failure of the containment shell /1, 2/. In order to assess the consequences of such an accident the failure pressure and failure mode have been investigated. Of special interest is whether a moderate leakage occurs preventing a further pressure increase or whether a global failure must be expected causing considerable mechanical damage.

At the Sandia National Laboratories the same questions are being asked for the US-types of containments. Because of their difficult geometries the most adequate way to get reliable answers was to carry out several tests with complete containment mock-ups, the largest having a height of about 6.6 m and a diameter of 4.3 m /3, 4/.

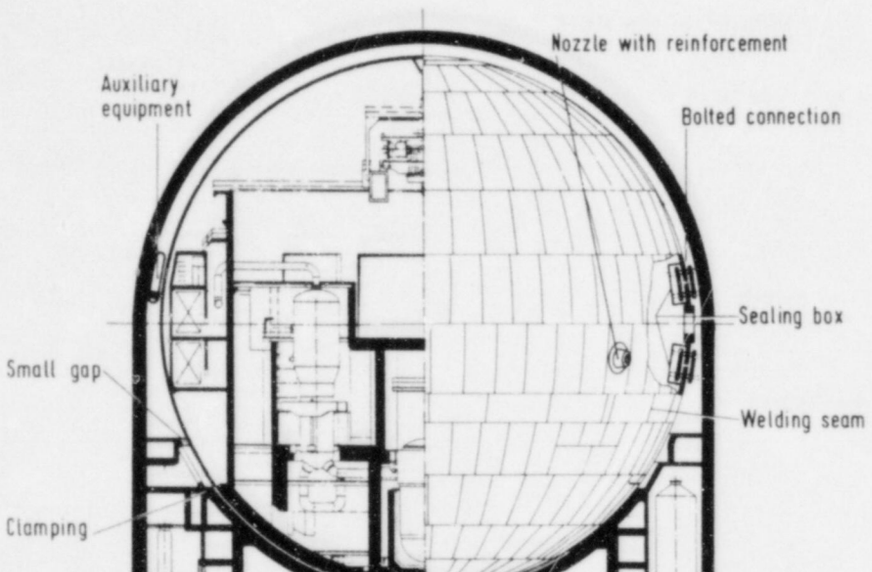


Fig. 1:
Containment of a pressurized water reactor including the weak parts

In Germany, the spherical geometry of the containments is somewhat simpler. Therefore it turned out that the ultimate load carrying capacity of many parts of the containment could be described reliably by a theoretical model, the computer code ROTMEM, especially developed and thoroughly checked for these problems. Only a few parts of the containment had to be investigated by testing of detailed mock-ups. In comparison to using complete containment mock-ups, this way of investigation is cheaper and allows more insight in active mechanisms. In some cases also questions about the influence of certain parameter variations, which must be considered for technical problems, can be answered. The investigation program and parts of the results have been described in more detail in /5, 6, 7/.

2. DETERMINATION OF FAILURE

The ferritic steel 15MnNi63 used for the containments is very ductile. In tensile tests the maximum (logarithmic) strain in the necking region before failure was about 150 %. In membrane tests (two-axial loading) the maximum equivalent strain was about 50 % /7/.

For many structures these local ultimate strains are reached after the loading has attained its maximum value. On the other hand in many cases including the containment problem the loading is prescribed and hence stable structural conditions exist only before the loading has attained its maximum. This means instead of the local ultimate strain the structural conditions where the load reaches its maximum value, or in other words the maximum load carrying capacity, represents the point of failure. Having in mind that in such problems plastic deformations play an important role, the above fact is often expressed by the statement that plastic instability determines failure /8/.

This finding is of essential advantage. The local ultimate strain is

very sensitive to complex details of the material properties and also to details of the way of loading. Therefore determination of this strain suffers under large uncertainties. However, the structural conditions where the load reaches its maximum value is well defined by the (true) stress-strain-relation of the material and the geometry-relations of the structure.

Consequently, if the problem is solved by experiments, the inevitable uncertainties of the different parameters will cause only slight variations of the results. (Only in singular cases large variations are conceivable.) If the problem is solved by computation the only difficulty - but often a serious difficulty - is the mathematical solution of the given equations.

It should be mentioned, however, if the solution can be obtained, in general only the failure loading is known. Additional measures are necessary to determine also the failure mode. But this is very important since the type of failure propagation has a strong influence on the consequences of the postulated core melt accident.

3. THEORETICAL MODEL AND ITS VERIFICATION

The maximum load carrying capacity of the structure is the result of two opposite effects. For growing strains the true stresses increase according to the stress-strain-relation of the material, but the load carrying cross-sections decrease due to the lateral contractions, for instance. Therefore a reliable determination of the maximum load carrying capacity, which for prescribed loading is identical with the determination of the point of failure, requires a detailed description of both effects, the material nonlinearity and the geometry nonlinearity.

If the load approaches the point of failure, the mathematical problem approaches instability. Furthermore, in order to find the solution the mathematical description must be approximated by numerical procedures which have an additional tendency to instability. As a consequence, the approximate solution of the problem may become instable long before the point of failure has been reached. Therefore the approximations must be such that aditional non-physical instability effects do not have essential influence.

For any structures commercially available computer codes are not yet able to meet all these requirements. This may be understood if one considers that the strains occurring for the maximum load carrying capacity are usually in order of more than 10 %. This is more than 100 times the amount of the elastic strains.

However, for axisymmetric thin shells the computer program ROTMEM has been written which yields adequate results. It includes both the material nonlinearity and the geometry nonlinearity, but it neglects all kinds of bending effects /9/. In order to check the program several membrane tests have been compared with computations /5, 7/. The membranes having a diameter of 0.8 m and a thickness of 2 mm were

machined from sheets of the containment material. During the tests the membranes were pressurized from one side, and the resulting deformations were measured at several pressure levels. Based on this, the stresses acting in the membrane could be determined. Although membrane tests of that type are very sensitive to parameter variations and model simplifications, it turned out that the deviations between the measured and calculated failure pressure are in the order of 5 % only. Higher accuracies may hardly be achieved since the deviations between the measured maximum loads of tensile tests carried out for the same material are also in the order of 5 %.

In order to reach such accuracies also for membranes with varying thickness, the three-dimensional stress conditions had to be considered. That means, in ROTMEM an approximation of the stresses perpendicular to the shell surface had to be included.

Now with ROTMEM many weak parts of the containment can be investigated. Their failure pressures and in some cases even their failure modes can be determined.

4. INVESTIGATION OF THE WEAK PARTS OF THE CONTAINMENT

As already mentioned the investigation concept followed here is to determine the failure pressure and failure mode of all essential weak parts separately. This is advantageous since many problems occurring at the spherical containment can be investigated theoretically with the computer program ROTMEM. Only for a few cases direct experimental simulations are necessary.

A survey over most of the weak parts discussed in the following paragraphs is provided in Fig. 1. The results obtained will be presented in Tab. I.

4.1 Welding Seams

As indicated in Fig. 1 during manufacturing the containment shell some kilometers of welding seams are necessary. However, tensile tests carried out with plates having weldings of real size showed that these weldings do not reduce the strength and ductility significantly. Rather strain components of about 20 % occured prior to rupture /10/. From additional tensile tests with especially prepared specimens one knows that also small cracks having a depth of 20 % of the wall thickness do not influence the maximum load carrying capacity in a detectable way /11/. So the conclusion is that welding seams and cracks possibly caused during the welding do not represent weak parts of the containment shell.

4.2 Clamping Region of the Containment

This part of the containment could be investigated using ROTMEM. The results show that the equivalent strains in the clamping region at the meridional angle between 120° and 130° are considerably lower than in other parts of the containment shell (Fig. 2).

4.3 Shell Regions Near Circular Reinforcements

Nozzles penetrating the containment are surrounded by circular reinforcements. These regions could be investigated by ROTMEM, assuming that the nozzle is located at the north pole of the containment. Stresses and strains in the circular reinforcements are smaller than in the containment, such that a failure of the reinforcement or at the connection to the nozzle can be excluded (Fig. 2, meridional angle $\varphi < 2.6^{\circ}$). Instead the shell region near the reinforcement represents the weak part /7/. Here the equivalent strains are significantly higher than far away from the reinforcements (Fig. 2, meridional angle $\varphi > 2.6^{\circ}$).

Nevertheless, according to calculations with ROTMEM the failure pressures of containments without reinforcements and with typical reinforcements are almost the same. They assume values between 15.4 and 15.5 bar*. Taking into account the achievable accuracy of such computations discussed in the paragraph before, failure can be expected to occur between 14.5 and 15.5 bar. However, the maximum equivalent strains occurring just before failure depend strongly on the type of reinforcement (Fig. 3, cases P1 to P4).



Fig. 2: Equivalent strains in the containment. Reinforcement for $\varphi < 2.6^{\circ}$

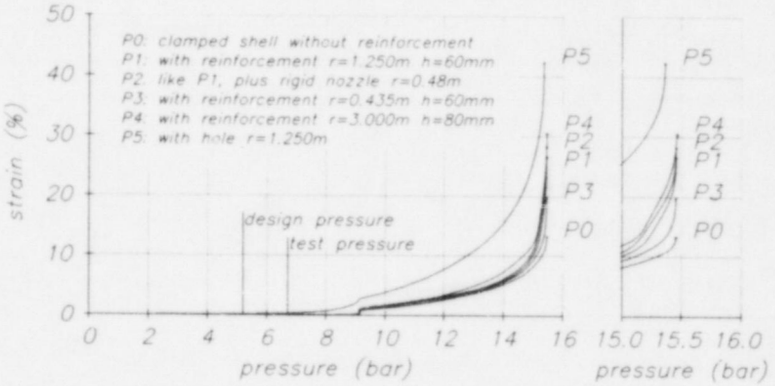


Fig. 3: Equivalent strains and failure points in the containment for different reinforcements

Based on ROTMEM calculations, also the failure mode, can be predicted. From the strain distributions obtained it is evident that during failure first a crack will propagate around the reinforcement creating a big hole in the containment. This has been confirmed by several membrane tests (Fig. 4). During this process the pressure acting at the containment will not be reduced significantly because of the large amount of compressible gas in the containment. On the other hand, the failure pressure for a containment with hole is slightly smaller and the maximum strains are considerably higher than for a containment without hole (Fig. 3, case P5). As a consequence large cracks will propagate in radial direction from the hole leading to global failure of the containment.

---

* Pressures mentioned in this paper denotes internal overpressure

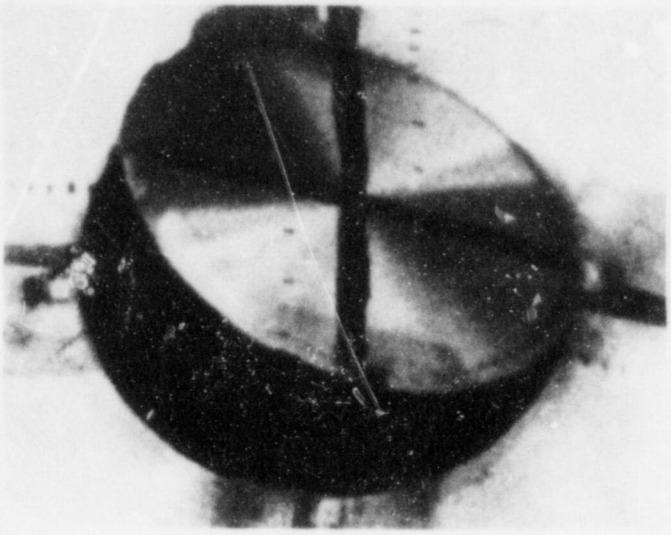


Fig. 4: Membrane with circular reinforcement after failure

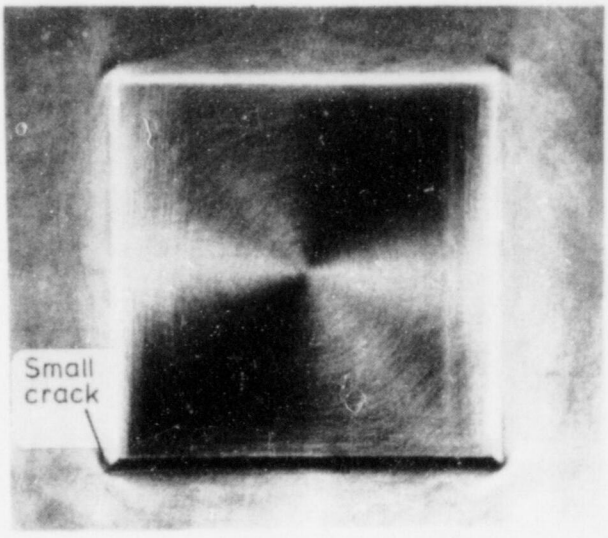


Fig. 5: Membrane with rectang. reinforcement after failure

4.4 Shell Regions Near Rectangular Reinforcements

At some locations the containment has rectangular reinforcements. From comparisons between membrane tests with that kind of reinforcements and ROTMEM calculations it turned out that also in this case failure can be expected to occur between 14.5 and 15.5 bar.

However, a unique determination of the failure mode is not possible. During the membrane tests failure occured in form of a limited crack at a corner of the reinforcement (Fig. 5). But after sealing this leakage, only a slight pressure increase caused global failure.

4.5 Nozzles with Restricted Radial Movement

For some of the largest nozzles (diameter of 0.8 m) the radial movement is restricted to 0.1 m. Assuming that the radial support will not fail, considerable contact forces will be transmitted from the nozzle to the containment shell. Calculations with ROTMEM showed that in this case the strains in the reinforcement near the nozzle are somewhat higher than the strains in the containment shell near the reinforcement. As a consequence failure will occur in the reinforcement. The failure pressure was calculated to 15.1 bar. Taking into account the different uncertainties again failure can be expected to occur between 14.5 and 15.5 bar.

Since during failure the contact forces vanish, the failure mode should be restricted to the reinforcement only. However, due to the high loading conditions in the close neighborhood a definitive statement about the failure mode cannot be made.

4.6 Containment Contacting the Concrete Encasing

Contact between the deforming containment shell and the concrete

encasing before containment failure is expected only in a circular region a few meters above the containment clamping. Here the gap width is only 0.2 m. Calculations with ROTMEM showed that such a contact causes certain reductions of the stresses and strains in the shell. Consequently, the contact region is not a weak part.

4.7 Containment Contacting Auxiliary Equipment Inside the Concrete Encasing

Some auxiliary equipment is built into the gap between the containment shell and the concrete encasing. Due to the increasing containment pressure the containment shell may contact this equipment. The most critical components are some double-T girders having almost radial orientation to the containment shell. The height of such a girder is 0.2 m, its length is 1.4 m, and its distance from the containment shell is 0.2 m.

First calculations were done with ROTMEM approximating the girder by a circular rod. The results show that after contact between the girder and the containment, the girder fails while the containment is not seriously affected.

Since the above simplifications may be questionable, a direct experimental simulation was carried out, scaled down by a factor of 19. The models for the containment shell and for the double-T girder were made from the same material as used in reality. The experiment confirmed the above finding (Fig. 6). The double-T girders do not endanger the integrity of the containment shell.

4.8 Variation of the Material Properties

All computations were performed with material data measured at a temperature of 170 ^{o}C and a strain rate of 10^{-6}/s. These parameters are typical for a core melt accident. It is interesting to note that under these conditions the true stresses versus the true strains are somewhat higher than the measured values for a temperature of 20 ^{o}C and the standard strain rate. However, it is more important that the data are significantly higher than the data guaranteed for the material (Fig. 7).

Of course, if the whole containment had been fabricated from a steel which just reaches the guaranteed values, the failure pressure calculated with ROTMEM would be reduced considerably, namely from 15.4 to 11.7 bar (Fig. 8, cases P0 and P8).

In reality, the majority of the sheets used to fabricate the containment will meet the measured data. Only a few outliers may just reach the lower guaranteed values. In order to simulate this, a calculation has been done with ROTMEM where in a small area of 3 m radius the guaranteed material data were used. The results show that the failure pressure is not significantly reduced while the failure strain is considerably higher than obtained for uniform material material properties (Fig. 8, case P7). Since the ductility of the material

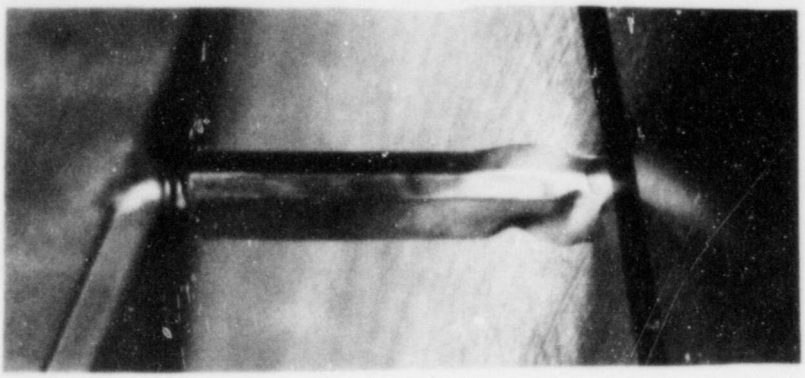


Fig. 6:
Experimental simulation of the containment being pressed against a double-T girder

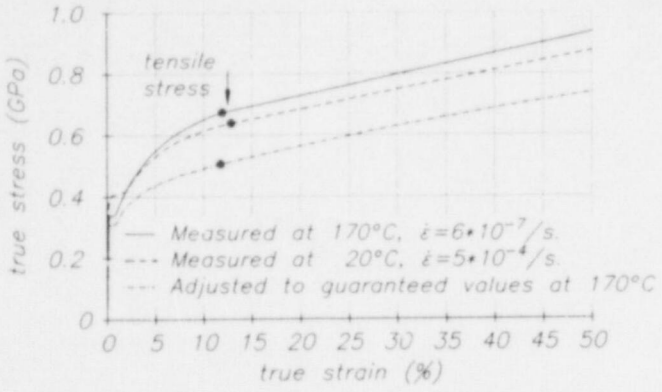


Fig. 7: Properties of the containment steel 15MnNi63

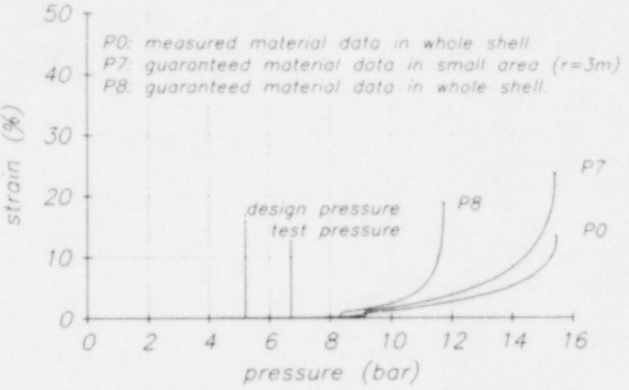


Fig. 8: Equivalent strains and failure points in containments composed of diff. materials

allows relative high strains, it can be concluded that also for usual variations of the material data the containment can be expected to fail between 14.5 and 15.5 bar.

As discussed in 4.3, also in this case the failure mode will be such that the whole containment shell will undergo severe cracking.

4.9 Bolted Connection Between Equipment Hatch and Containment Shell

The construction of the bolted connection is shown in Fig. 9. It is important to note that the containment shell is not reinforced in this area. The screws connecting the shells with the cover plates are prestressed such that sliding is expected for a containment pressure of about 7 bar. For higher pressure the screws will be loaded additionally by shear forces.

As discussed in /7/, a purely theoretical investigation of the bolted connection up to its failure would not be able to yield adequate results. Therefore an experimental simulation has been carried out. In order to keep the costs within reasonable limits, the test section included only a part of the bolted connection with about 160 screws (Fig. 10). The complete connection includes more than 1500 screws. Furthermore the test section was scaled down by a factor of 3.75. Therefore the diameter of the screws was reduced from 30 mm to 8 mm and the shell thickness from 38 mm to 10.1 mm. Of course, the test

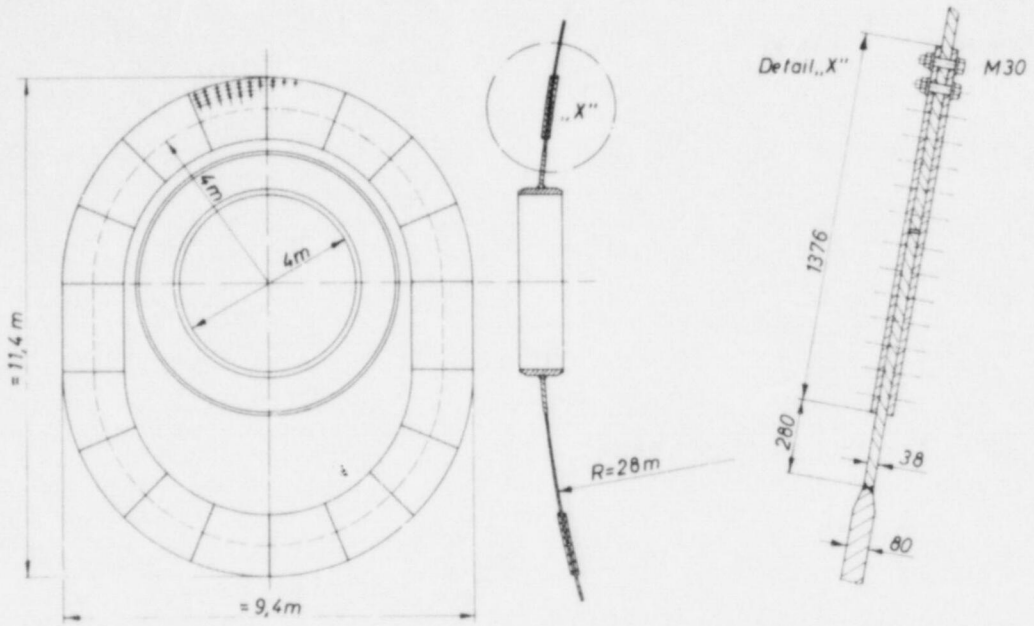


Fig. 9: Multiple-row bolted connection between equipment hatch and containment shell

section was machined from a sheet of the same material and of the same thickness as used in reality. In order to apply realistic two-axial loadings a special device was manufactured consisting of a heavy ring with 16 hydraulic cylinders each of them allowing for a tension force up to 1.4 x 10^6 N (Figs. 10 and 11). A special problem was to transfer these forces to the test section. This required strong tension rods and heavy clamping jaws.

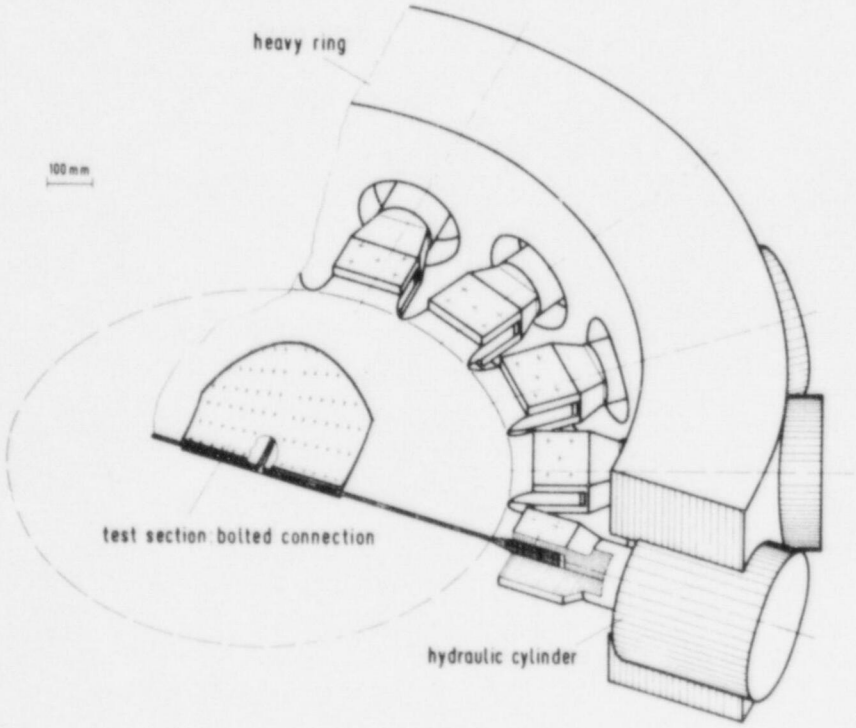


Fig. 10:
A part of the bolted connection loaded in the two-axial test device

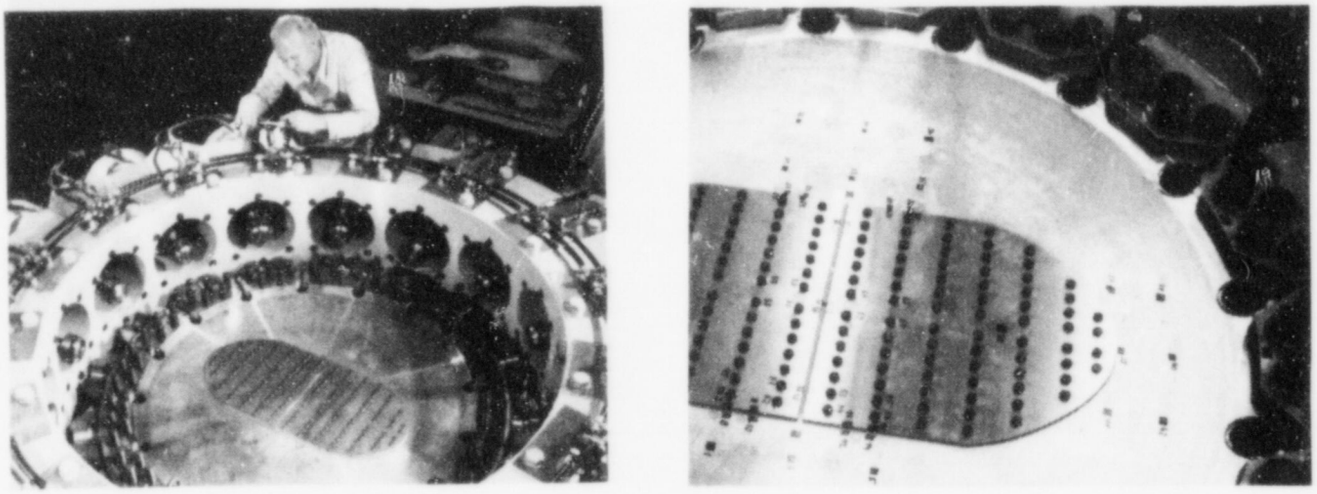


Fig. 11: Details of the two-axial test device

During the experiment the forces transmitted from the hydraulic cylinders were increased step by step. In order to obtain a similar deformation pattern as in the containment close to the equipment hatch, the forces acting along the bolted connection had been reduced in comparison to those across the bolted connection. For each pressure step the deformations of the test section were determined by measuring the coordinates of certain marking points (Fig. 12). In this way, the strains of the membrane outside of the bolted connection and, using the stress-strain-relation of the material, the stresses in the membrane outside of the bolted connection could be found. In addition, for each pressure step also the leakage of the connection was determined by blowing air through the bolted connection and measuring the pressure drop and the resulting volume flow.

The highest loading which could be applied caused an equivalent stress of 530 MPa and an equivalent strain of 4.9 % outside of the

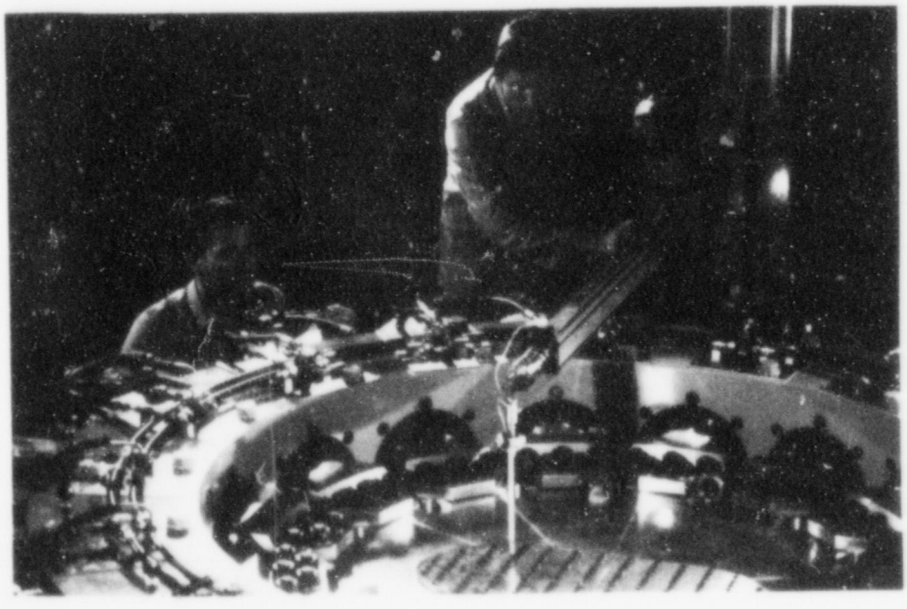


Fig. 12:
Measuring the locations of marking points using a three coordinate measuring machine

bolted connection. These conditions led to an average strain of 3 % across and 1.3 % along the bolten connection (Fig. 13). No cracks were observed. The bolts showed almost no deformations. The total leak area was 340 cm^2 (crossing gaps about 130 cm^2, screws about 210 cm^2). In the unloaded condition the total leak area was 2.3 cm^2. All these leak areas are already converted to the real containment dimensions using standard relations for an ideal gas. By the way, the leak area necessary to prevent additional pressure increases was estimated to about 15 cm^2.

The next load step caused failure at one of the clamping jaws. That means, the failure of the bolted connection could not be reached.

From uniaxial tensile tests with bolted connections carried out in different scales it turned out that scaling has only little influence on the resulting stresses and strains /7/. Therefore it can be concluded that the bolted connection of the containment will not fail up to an equivalent membrane stress in the containment shell close to the connection of 530 MPa, corresponding to an equivalent strain of 4.9 %. Using the computer code ROTMEM the corresponding containment pressure was found to be 14.0 bar. In this calculation the deviation from the axial symmetry shown in Fig. 9 was neglected. Furthermore, a rough simulation of the nonlinear behavior measured for the bolted connection had to be considered. It is interesting to note that this simulation had only little influence on the results (change of the containment pressure up to 0.2 bar). Finally the results had been converted from a temperature of 20 °C to the actual temperature of 170 °C according to Fig. 7.

Since in the experiment rupture of the bolted connection did not occur, no definite statement about the failure mode can be made. However, a failure of the whole bolted connection probably resulting in a global failure of the containment should be expected.

4.10 Sealing Box Covering the Bolted Connection

As mentioned in the preceding paragraph, the bolted connection does not allow for complete tightness, even in the unloaded condition. Therefore the sealing box shown in Fig. 14 is covering the bolted connection.

Pressurization of the containment causes considerable movements of the connection points between the containment and the feet of the sealing box. However, as a result of the particular stiffnesses, this causes only small movements of the cover of the sealing box. Therefore the feet of the sealing box undergo large deformations. The question is, for which containment pressure the feet will fail such that the box looses its tightness and the leakage through the bolted connection prevents any further pressure increase.

Since the stiffness of the sealing box has a certain influence on the deformations of the containment, the program ROTMEM has been extended in order to describe the coupled problem consisting of both structu-

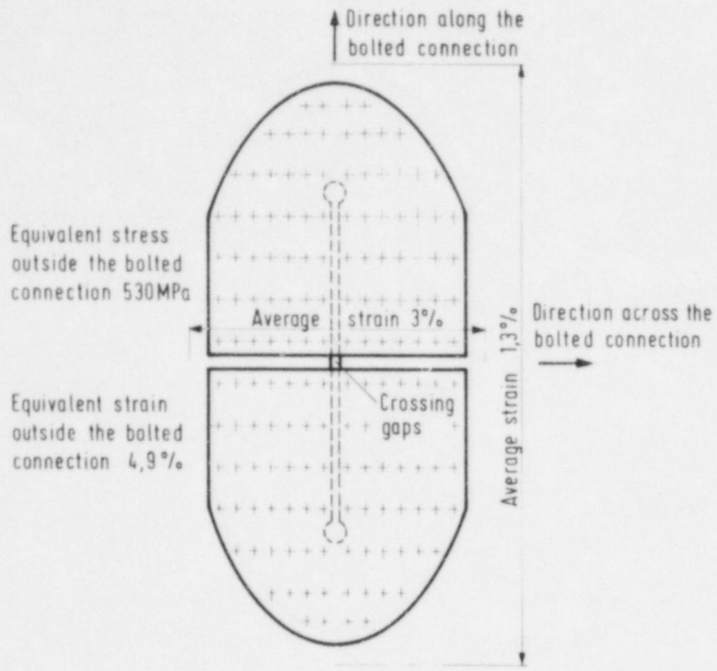


Fig. 13: Highest stresses and strains reached with the two-axial test device



Fig. 14: Sealing box covering the bolted connection

ral elements. In this computational model the stiffness and the failure point of the feet of the sealing box are input.

These data have been provided by tension tests with strips of the sealing box. Since the weldings at the feet of the sealing box play an important role, full size mock-ups have been used. The effect of scattering of the failure points due to slightly varying welding conditions has been considered by referring to a total of six tests.

In some tests first an inside welding and then the outside welding failed (Fig. 15). Consequently, in the diagrams showing the measured force in the containment shell versus the displacement of the foot of the sealing box two maxima occurred (Fig. 16). In a few tests the sequence of failure was inverse. In both cases reliable opening of the sealing box occured after failure of the second welding. The displacements of the foot of the sealing box, measured for this case, varied between 29 and 42 mm. The failure pressures of the containment, calculated for this case with ROTMEM, varied between 12.9 and 13.7 bar.

That means, immediately after failure of the sealing box the bolted connection is still intact. Thus it was correct to omit the load carrying effect of the sealing box during the determination of the containment pressure from the measured state in the preceding paragraph.

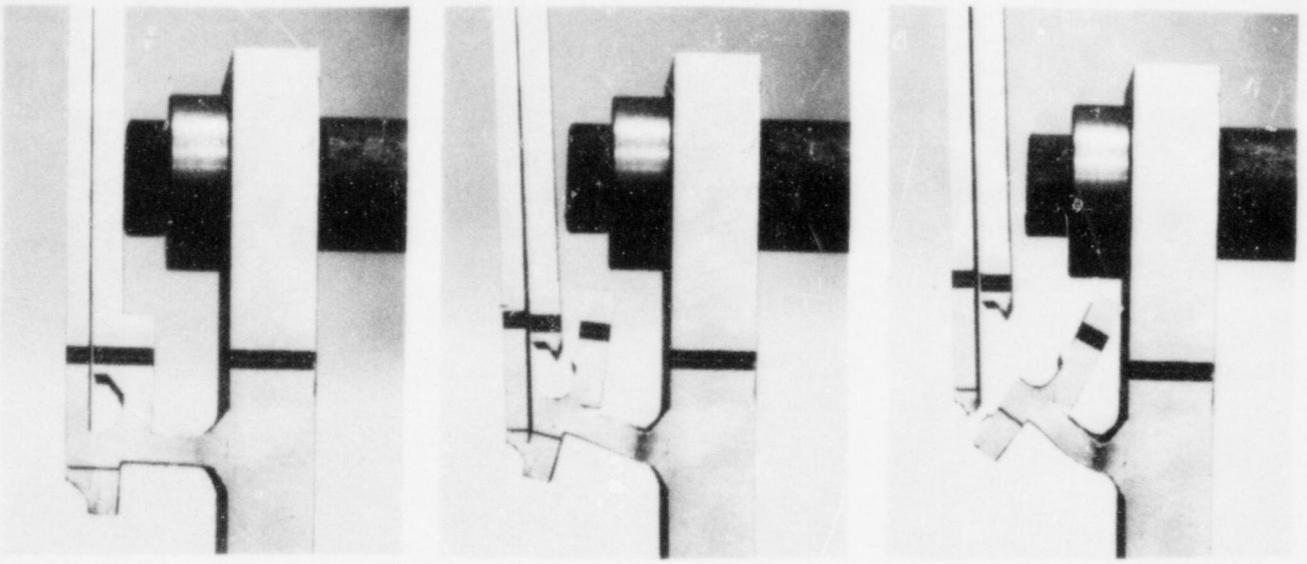


Fig. 15: Test with a strip of the foot section of the sealing box

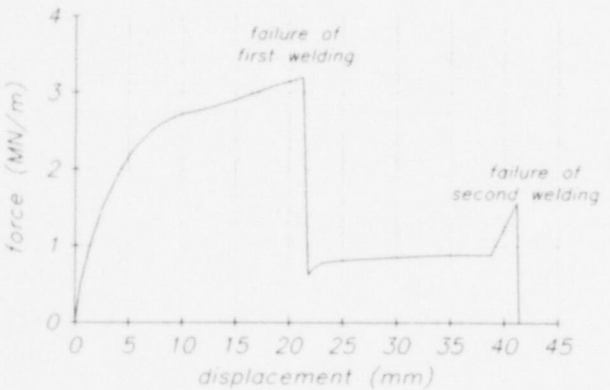


Fig. 16:
Force in the containment shell due to the displacement of the foot of the sealing box

5. CONCLUSIONS

The weak parts described in the preceding paragraphs and listed in Tab. I include all mechanisms which may lead to a global containment failure. They include also all mechanisms which may lead to local failure, provided a reliable failure pressure can be given. Therefore such items as gaskets, cable penetrations, bellows etc., where the failure is unable to propagate and a reasonable upper limit of the failure pressure cannot be determined, have not been considered.

It is self-evident that failure of the whole containment including all the weak parts discussed will occur at that part with the lowest failure pressure. This answers also the question for the failure mode. Reviewing Tab. I yields:

> If the overpressure in the containment increases slowly, the sealing box covering the bolted connection fails between 12.9 and 13.7 bar. Then the leakage area at the bolted connection becomes effective. It has a value between 150 and 300 cm^2, which is essentially higher than the value of about 15 cm^2 for which

the pressure increase caused by the postulated core melt accident and the pressure drop caused by the leakage are just balanced. As a consequence the overpressure in the containment drops slowly. Other weak parts in the containment are not addressed.

Tab. I: Weak Parts of Containment

weak part	*investigation method*	*failure pressure*	*failure mode*
welding seams		*no weak part*	
clamping region	*ROTMEM*	*no weak part*	
shell regions near circular reinforcements	*ROTMEM*	*14.5 – 15.5 bar*	*global*
shell regions near rectangular reinforcements	*experiments, ROTMEM*	*14.5 – 15.5 bar*	*local, global*
nozzles with restricted radial movement	*ROTMEM*	*14.5 – 15.5 bar*	*local, global*
containment contacting the concrete encasing	*ROTMEM*	*no weak part*	
containment contacting auxiliary equipment	*experiment, (ROTMEM)*	*no weak part*	
variation of the material properties	*ROTMEM*	*14.5 – 15.5 bar*	*global*
bolted connection	*experiment, ROTMEM*	*leakage area increasing from 2.3cm² to 340cm² at 14 bar*	
		>14 bar	*global*
sealing box	*experiments, ROTMEM*	*12.9 – 13.7 bar*	*local **
**after failure of the sealing box the leakage area of the bolted connection is sufficient to prevent further pressure increase.*			

One should, however, have in mind that only a small delay of the failure of the sealing box (delay > 0.3 - 1.1 bar) would result in an additional failure of the bolted connection. Then a propagation to a rapid failure of the whole containment shell including strong dynamic processes and extreme damage at the reactor site and its close environment would be likely.

Of course, there is a small probability that this may happen. However, for risk studies where the initiating event has already a very small probability, such extreme assumptions are not reasonable. Consequently the global containment failure and its severe consequences are ruled out here.

On the other hand, small design changes which may not be felt worth mentioning, can also cause dramatic changes of the consequences as discussed above. Therefore, it should be emphasized again that the conclusions drawn in this paper are only valid for the pressurized water reactor Philippsburg (KKP II).

REFERENCES

/1/ Gesellschaft für Reaktorsicherheit: Deutsche Risikostudie Kernkraftwerke - Fachband 5, TÜV Rheinland GmbH, 1980

/2/ J.P. Hosemann, H.H. Hennies, K. Hassmann: German results on consequences of LWR severe accidents. ANS/ENS Int. Conf., Nov. 11-16, 1984, Washington D.C.

/3/ T.E. Blejwas and W.A. von Riesemann: Pneumatic pressure test of steel containment models - recent developments. Nucl. Engng. Des. 79 (1984) 203-209

/4/ D.B. Clauss: Comparison of analytical predictions and experimental results for a 1:8-scale steel containment model pressurized to failure

/5/ B. Göller, R. Krieg, G. Messemer: Behavior of spherical PWR-containments close to reinforced sections under excessive internal pressure. Proc. of the Second Workshop on Containment Integrity, NUREG/CP-0056, SAND 84-1514 (1984)

/6/ R. Krieg et al.: Spherical steel containments of pressurized water reactors under accident conditions. Nucl. Engng. Des. 82 (1984) 77-87

/7/ B. Göller, R. Krieg, G. Messemer, E. Wolf: On the failure of spherical steel containments under excessive internal pressure. to be published in Nucl. Engng. Des.

/8/ N.A. Weil, N.M. Newmark: Large plastic deformations of circular membranes. Journ. of Appl. Mech. 77 (1955) 533-538

/9/ B. Göller: Zum Verhalten eines DWR-Containments unter hohem, quasi-statischem Innendruck - Grundlagen des Programms ROTMEM. Kernforschungszentrum Karlsruhe, Internal Report

/10/ Zugversuche mit geschweißten Großplatten aus dem Werkstoff 15MnNi63, Staatliche Materialprüfungsanstalt an der Universität Stuttgart, Internal Report

/11/ S. Müller, D. Munz: Untersuchungen zum Versagen der Sicherheitshülle eines Druckwasserreaktors bei Überdruckbelastung, Kernforschungszentrum Karlsruhe, Internal Report

/12/ Ergänzende Untersuchungen zum Containmentverhalten bei BIBLIS-B bei hypothetischen Störfällen, Kraftwerk Union, Internal Report

ANALYSIS OF SEVERE ACCIDENTS AND ESTIMATES OF ULTIMATE LOADING CAPACITY OF THE STEEL CONTAINMENT

F.W. Heuser (Project Manager German Risk Study Phase B)
A. Hoefler (Section Manager Fracture Mechanics)
H. Schulz (Head, Structural Mechanics Department)
Gesellschaft fuer Reaktorsicherheit (GRS mbH),
Schwertnergasse 1, D-5000 Koeln 1, Germany

Abstract

Referring to a German PWR on overview on the analysis of severe accidents is given, performed within the German Risk Study, Phase B. The course of hypothetical core melt accidents, potential containment failure modes and sequences leading to radioactive release are discussed briefly. Then the ultimate loading capacity and the potential for limited leakage of the spherical steel containment of the reference plant are analyzed, based on pressure and temperature loading according to core melt accidents and H_2-deflagration. Most analyses have been performed by elastic-plastic FE-calculations including shell disturbances caused by nozzles and locks as well as constraints. By assessment of strains and stresses against different failure criteria scatter bands of the ultimate pressures could be investigated.

I. Analysis of Severe Accidents

1. Introduction

In Phase A of the German Risk Study /1/ which was mainly along the methods used in WASH 1400 /2/ main parts of the analysis were based on simplifying assumptions thus leading to an over-estimate of risk. Therefore, in order to come up with a more realistic description in Phase B of the study methods and models have been refined taking into account the present status and progress of safety research. As before, the plant studies of Phase B refer to the reference of Biblis B, a 1300 MWel PWR plant of KWU design.

In what follows some main results of the accident analysis of Phase B are discussed briefly.

2. System and Event Tree Analysis

In Phase A the overall core melt frequency was calculated to 9 x 10^{-5} per reactor year (mean value) with the 90 % confidence interval ranging from 1 x 10^{-5} to 3 x 10^{-4} per reactor year. Moreover the dominant contribution to the core melt frequency was due to an uncoped "Small LOCA", because operator action required to cool down the plant significantly reduce the availability of the safety system functions. The second largest contribution was due to transients, e.g. "Loss of Preferred Power".

Although the analysis of Phase A mainly confirmed the validity and effectiveness of the safety design several weak points have been identified which gave the loading terms to the core melt frequency. Thus, in order to reduce risk, some system modifications have been performed, e.g.

- automatic control for the cooling down procedure in the case of a "Small LOCA",
- instrumentation of the main feedwater system adequate to LOCA conditions,
- electric power supply, modifications for return to normal power in case the emergency diesel generators fail.

The analysis including these system modifications show that the contributions of both, the uncoped "Small LOCA" as well as the "Loss of Preferred Power" are well below 1 x 10^{-5} per reactor year.

Furtheron additional accident initiating events and undetected sequences are analyzed quantitatively, e.g.

- leaks in the secondary system, e.g. leak in a main steamline,
- leakages in steam generator heating tubes,
- a loss at coolant via a leak in a connecting line of the reactor coolant system (V-sequence).

V-sequences only give a negligible contribution to the core melt frequency since a leak within a connecting line can be separated immediately by sequential blocking valves.

Compared to the improved level of safety, however, leaks in the secondary system as well as leakages of steam generator heating tubes may constitute major contributions to the core melt frequency. Thus, for instance, the contribution to core melt frequency, which is due to an uncoped break of a main steam line amounts about 1 x 10^{-5} per reactor year.

3. Analysis of Core Melt Accidents

Within Phase B of the German Risk Study substantial progress has been made in the analysis of core melt accidents. This mainly is based on recent results obtained within the Reactor Safety Research Program of the Federal Minister of Research and Technology during the last years.

Mostly all conceivable pathes of core melt accidents can be covered by two boundary cases, the low pressure path (LP-path) and the high pressure path (HP-path). Accident sequences of the LP-path are initiated by a large LOCA thus leading to core melt under low pressure conditions. Sequences related to the HP-path are due to uncoped transients leading to core melt unter high pressure.

Fig. 1 shows the long term pressure time history in the containment for both the LP- und the HP-path. Apart from the initial phase of core melt and melt-concrete interaction in the long timed phase both curves are nearly identical. Due to the evaporation of the sump water internal pressure increases steadily until failure pressure of the containment in reached at about 4 days after the accident initiating event.

Fig. 2 shows the pressure time history considering the initial phase of the core melt accident. In addition to the LP- und HP-path Fig. 2 includes a plot referring to an uncoped small leak in the RCS. The pressure peak due to failure of the reactor pressure vessel (at about 2 hours) is below the maximum value of the HP-case.

Details of the containment failure mode analysis are discussed in the second part of this paper. In general the following failure modes have to be considered

- containment leakage, e.g. due to a failure of welds or a failure of the containment isolation system,

- containment failure due to dynamic loads, e.g. a hydrogen combustion which is strong enough to threaten the containment steel shell,

- late containment failure due to overpressurization (not until four days after the accident initiating event).

Final results on the calculation of the source terms correlated to the various containment failure modes are not yet available. Preliminary results however show, that compared to the figures of Phase A, the source term for late radioactive release as well as for early containmment failure will be reduced considerably.

II. Ultimate Loading Capacity of Steel Containment

1. Introduction

Because the steel containment is the final barrier to avoid a release of radioactivity to the atmosphere its integrity and leaktightness has always been the dominant design goal. Until now for light water reactors the principle design basis against internal events is the maximum pressure- and temperature-build-up due to a sudden release of the reactor coolant.

In the course of risk studies loading conditions beyond design accidents have been investigated with respect to the topics "ultimate loading capacity" and "defined leakage area".

In the German Risk Study, Phase A /1/, the ultimate pressure was estimated for the undisturbed global shell structure of the 1200 MWe PWR reference plant Biblis B, under uniform static pressure and temperature loading conditions (see Fig. 3). For the failure criteria "flow stress" and "linear elastic fracture mechanics" (LEFM) ultimate absolute pressures of 0.95 MPa and 0.85 MPa respectively have been calculated.

In the present work (Phase B of the German Risk Study) more detailed analyses are performed to investigate the ultimate pressures of the global shell structure as well as the penetration areas (shell disturbances) under different loading conditions /3/. Especially the questions of leak before break and local or global failure of the shell with disturbances and restrained radial displacements are to be clarified for the hypothetical core melt accident which includes the potential for global or local H_2-deflagration pressure loading.

2. Loading Conditions and Material Characterization

The calculations are based on the following loading conditions:

- static pressure-build-up due to core-meltdown (global),
- dynamic pressure-build-up due to H_2-deflagration (global and local),
- loadings of the shell due to constraint of radial displacements,
- calculated maximum shell reference temperature of 135 °C assumed for each case.

A typical quasi-static pressure-build-up due to the low pressure core melt accident is shown in the upper part of Fig. 4. The lower part shows one of the possible load functions of a global/local

H_2-deflagration. For the cases of H_2-deflagrations or even the faster-detonations parametric studies have been performed to analyze the structural response.

The spherical shell is made of the fine grain high strength steel FG 47 WS. For caracterization of the elastic-plastic behaviour of the material the true stress-strain-curves have been adopted, based on the median and minimum values from the probability density functions of the yield stress ($R_{p0,2}$) and the ultimate stress (R_m) at reference temperature (see Fig. 5).

3. Structural Models

For the reference plant an in-situ design review was performed before the structure has been modeled. In view of the large deformations to be expected for the steel shell (nearly one order higher than the approximately 40 mm radial displacement of the elastic layout) special attention has to be given not only to the as-built penetrations but also to the surrounding restraining structures. Although all the PWR containments of the Kraftwerk Union design seem to be very similar, minor differences in design or as-built conditions may change the results quite drastically with respect to the leakage path.

Fig. 6 shows schematically the important representative areas of the reference plant to be analyzed for probable failure and also their figures of deformation in principle after being restrained by interfering external structures. Some details of the constructions of the steam line penetration (protection pipe, containment nozzle, bellows, fixed point) and the concrete embedding of the spherical shell (graduated steps of styrene foam) are shown in Fig. 7 and 8.

The finite-element idealization of the shell structure with rotational symmetric isoparametric continuum elements is shown in Fig. 9. In the areas with dominant membrane stresses only one layer of elements across the wall thickness is chosen wheras at the discontinuties an apropriate narrow mesh is modeled to cover the additional bending stresses. Because of the rotational symmetry the shell disturbances A (penetration) and E (cantilever) have to be transferred to the pole. This can be done without losing accuracy because the influence of bending disappears after a short length compared to the length between the discontinuities themselves. The geometrical nonlinear contact problems between shell and external structures (points A, B, E) are idealized by springs with bilinear stiffness characteristic (gap trusses /4/) and the concrete embedding (point E) with multilinear truss characteristics modelling the elastic-plastic foam behaviour as well as that of the concrete.

The bolted connection of the material hatch to the spherical shell has been analyzed with a separate analytical model (point D, Fig. 6

and Fig. 10) with respect to the distribution of the bolt shear forces and the integrity and leakage potential of the joint and the covering as-welded sealing plates.

In case of dynamic loadings the structural response has been calculated using the dynamic elastic-plastic finite-element model as well as an analytical approach which is described in /5/ in detail. For spherical symmetry the solution results in an ordinary differential equation for the radial displacement, derived from the equilibrium of membrane forces and for an elastic-plastic bilinear stress-strain relation. In the special case of elastic-ideal plastic material and impulsive loading a simple formula for the maximum strain as a function of the initial shell impulse results, which is approximately valid for local pressure loads, too.

The nonlinear calculated structural responses as radial displacements, strains and stresses are compared to several failure criteria. This assessment leads to deterministically calculated failure pressures for each investigated area, the band width can be valued probabilistically, if necessary.

4. Failure Criteria

For the evaluation of the range of possible failure pressures of each area commonly used stress criteria, advanced strain criteria and fracture mechanical methods, shown in Table 1, have been applied. The strain limit criteria used is based on a method including defects as shown in /6/ and using a triaxiality factor similar to /7/. This criteria regards the reduction of the minimum uniform elongation derived from the uniaxial tension test by measure of the stress triaxiality in the structure as well as the reduction by an assumed reference flaw and also size and weld influences.

The criteria "major principle stress" is only adopted within areas of high internal constraint (approximately hydrostatic stress state).

A probabilistic approach to assess the penetration areas against LEFM-criteria has been done in /8/.

The possibilities of calculating a certain amount of stable crack growth and a leak cross section by EPFM-methods, i.e. the J_R-curve, are under investigation.

5. Results

As a result of one of the static FE-analyses the restrained deformation (enlarged) of the containment is shown in Fig. 11, including the investigated areas A, B, C and F at an internal pressure of 1.2

MPa and Fig. 12 the real deformation of the embedding point C at 0.98 MPa for material 2. Representative for all investigated areas Fig. 13 shows the real deformation of the steam line nozzle (A) after blocking of the bellows. Because of the large difference of stiffnesses a strain concentration area in the shell close to the welds has built up, with strains three times as high as in the undisturbed shell. On the right Fig. 13 shows the isolines of the effective v. Mises-stresses with plastic zones and bending stress concentrations prior to the weld regions.

The dynamic behaviour of the shell is characterized by the mode shapes and frequencies of Fig. 14, calculated with 3D and 2D FE-models. The results of the assumed H_2-deflagration in the annular channel are shown in Fig. 15 and 16 in form of deformation or displacement time histories respectively for several structural points.

Although the shell shows a relatively large annular bulge only the embedded part undergoes considerably plastic deformation and damping (see Fig. 16).

All results of the calculations for the ultimate loading capacity are summarized in Table 2 and 3 as bar charts.

In addition to the failure pressure differences (Δp = 10 bar = 1 MPa) the equivalent stress, the radial displacement and the begin of yielding of the shell using minimum and median material mechanical properties are indicated.

The large penetration, point A, shows the lowest failure pressure for the static pressure case because of very high stress conditions.

In the dynamic loading case the failure pressure of the shell would be lower if no increase of material properties due to strain rate effects are assumed. The final dynamic loading case has not been specified yet but first calculations with the high-peaked test function show only very small reductions.

The analyses of possible leakage paths have been concentrated first on the bolted connection of the material hatch. Depending on the design of the area early leakage can be calculated for one case, i.e. the convoi type of containment, but not for the older Biblis-type.

6. Conclusions

In addition to previous studies which concentrated more on the undisturbed shell structure, present investigations include also penetration areas and local restraints by the surrounding structures.

Preliminary conclusion can be summarized as follows:

o ultimate loading capacity
  - present design requirements have provided a large margin of safety, so considerable loads beyond design basis can be taken,
  - detailed elasto-plastic calculations yielded results similar to previous estimates /1/ and studies in /7/, /8/,
  - failure criteria should be selected according to the local state of stress (strain),
  - the overall deformation behaviour can be influenced by local heatup for certain geometries.

o defined leakage path
  - the most probable leakage path is largely affected by local conditions of the structure under investigation,
  - significant problems arise in the calculation of limited leak cross sections because of the high amount of stored energy in the shell at overpressure failure level.

7. References

/1/ Deutsche Risikostudie Kernkraftwerke, Fachband 5
Gesellschaft für Reaktorsicherheit (GRS) mbH, Verlag TÜV Rheinland, Köln, 1980

/2/ Rasmussen, N.C.
Reactor Safety Study - An Assessment of Accident Risks in US Commercial Nuclear Power Plants
NUREG-75/014, Oc. 1975 (WASH 1400)

/3/ Höfler, A., Eisert, P.
Untersuchungen zum Versagensverhalten des DWR-Sicherheitsbehälters im Rahmen der Risikostudie
Beitrag 9.1, Jahresbericht 1984, Gesellschaft für Reaktorsicherheit (GRS) mbH, Köln, Mai 1985

/4/ Bathe, K.-J.
ADINA: A Finite Element Program for Automatic Dynamic Incremental Nonlinear Analysis
MIT-Report 82-558-1, 1978

/5/ Klassmann, W.
Dynamische und elastoplastische Beanspruchung einer Kugelschale unter lokaler und globaler Innendruckbelastung
Ein Beitrag zur Risikostudie (Phase B), GRS-A-910, Gesellschaft für Reaktorsicherheit (GRS) mbH, Köln, Dez. 1980

/6/ Schulz, H., Glahn, M.
Requirements on the Mechanical Design of Reactor Systems Operating at Elevated Temperatures
SMIRT 5, L 6/4, Berlin 1979

/7/ Ju, F.D., Butler, T.A.
Review of Proposed Failure Criteria for Ductile Materials
NUREG/CR-3644, April 1984

/8/ R. Wellein, G. Weckesser, R. Wölk, G. Reinheimer
Untersuchungen zum Gebäudeabschluß, Freisetzungspfade im Rahmen der DRS, Phase B
Abschlußbericht Förderungsvorhaben BMFT 1500576, April 1985

/9/ Jeschke, J.
Limit Load Analysis of Actual Spherical Containments Subjected to Static Internal Pressure and Temperature
NUREG/CP-0056, Aug. 1984

Table 1. Failure Criteria

- Strain limit

  $\varepsilon_{sl} = \varepsilon_u \times f_1 \times f_2/TF \qquad TF = (\sigma_1 + \sigma_2 + \sigma_3)\ /\sigma_v$

  ε_{sl} = strain limit
  ε_u = minimum uniform elongation
  f_1 = size effect (plate thickness and weld)
  f_2 = crack influence (determined for a reference defect)

- engineering flow-stress

  $\sigma_v \leqq \sigma_F \qquad \sigma_F = (R_{p\,0,2} + R_m) / (2 \ldots 2.4)$

- equivalent stress "v. Mises"

  $\sigma_v \leqq R_m \cdot f_1 \cdot f_2$

- major principle stress

  $\sigma_i \leqq R_m \cdot f_1 \cdot f_2$

- linear elastic fracture mechanics

  $K_I \leqq K_{IC}$

- elastoplastic fracture mechanics
  - J-Integral
  - plastic-collapse

Table 2. Bandwidth of the Ultimate Pressures ΔP of Steel Containment Biblis B

TEMPERATURE: 135°C MATERIAL CHARACTERISTICS: MEDIAN VALUES: III, MINIMUM VALUES: II, $R_{p0,2}$ = 400 N/MM²: I

ANALYSED PARTS	FAILURE CRITERIA	ULT. PRESS. DIFF. ΔP(BAR)	f_1	Mat.
UNDISTURBED SPHERICAL SHELL	$\varepsilon_{eff} \leq \varepsilon_{ult.}$ (TF, f_i)	>12.0	.7	III
		>10.7	.7	II
		11.8	.5	III
		10.6	.5	II
FE – ANALYSIS (QUASI-STAT.)	$\sigma_{eff} \leq \sigma_{ult.} \cdot f_2$	12.0		III
		>10.7		II
	$\sigma^{M}_{eff} \leq \sigma_{Flow} \cdot f_2$	10.8		III
		9.6		II
	$\sigma_i \leq \sigma_{ult.} \cdot f_2$	11.7 TF=2		III
		10.6		
NOZZLE OF STEAM LINE PENETRATION CONSTRAINT: U_r>300 MM (MAT. III: ΔP = 11.1 BAR) FE – ANALYSIS (QUASI-STAT.)	$\varepsilon_{eff} \leq \varepsilon_{ult.}$ (TF	11.6	.7	III
		9.9	.7	II
		11.0	.5	III
		9.8	.5	II
	$\sigma^{M,B}_{eff} \leq \sigma_{Flow} \cdot f_2$	9.4		III
		8.4		II
	$\sigma_i \leq \sigma_{ult.} \cdot f_2$	10.6 TF > 5		III
		9.5		II
	$K_I \leq K_{IC}$	(>7.5 : KWU)		
	$J_I \leq J_{Iin}$	–		
RISK STUDY PHASE A UNDISTURBED SPHERICAL SHELL	$\sigma^{M}_{eff} \leq \sigma_{Flow} \cdot f_2$	8.5 MAT. LOWER BOUND	f_2 .9	I
	$K_I \leq K_{IC}$	7.5 CRITICAL FLAW		I

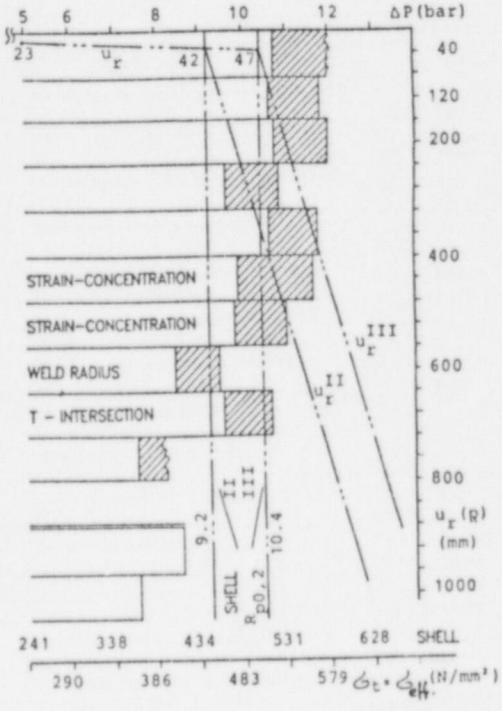
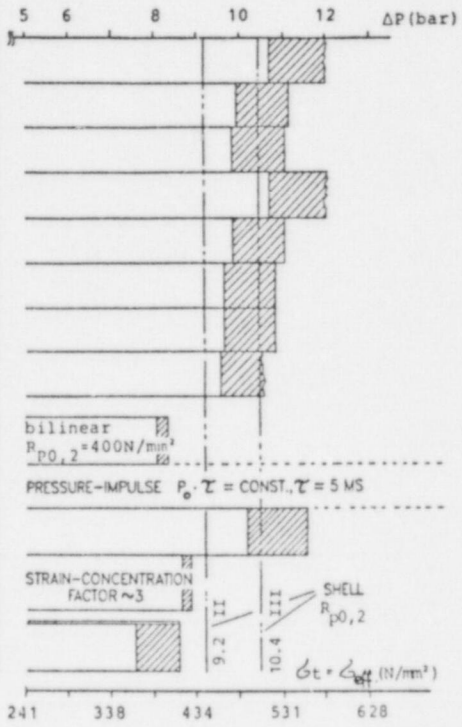


Table 3. Bandwidth of the Ultimate Pressures ΔP of Steel Containment Biblis B

TEMPERATURE: 135°C MATERIAL CHARACTERISTICS: MEDIAN VALUES: III, MINIMUM VALUES: II, $R_{p0,2}$ = 400 N/MM²: I

ANALYSED PARTS	FAILURE CRITERIA	ULT. PRESS. DIFF. ΔP(BAR)	f_1	Mat.
CONCRETE ANNULAR CONSOLE	$\varepsilon_{eff.} \leq \varepsilon_{ult.}$ (TF)	≥12.0 ≥10.7	.5 .5	III II
CONSTRAINT: U_r > 200 MM (MAT. III: ΔP = 11.0 BAR)	$\sigma_1^{M\cdot B} \leq \sigma_{ult.} \cdot f_2$	11.1 9.9 TF = 3		III II
FE – ANALYSIS (QUASI–STAT.)	$\sigma_{eff}^{M} \leq \sigma_{Flow} \cdot f_2$	11.0 9.8		III II
CONCRETE EMBEDDING	$\varepsilon_{eff} \leq \varepsilon_{ult.}$ (TF)	≥12.0 ≥10.7		III II
FE – ANALYSIS (QUASI–STAT.)	$\sigma_{eff}^{M\cdot B} \leq \sigma_{Flow} \cdot f_2$	11.0 9.8		III II
SINGLE STEEL CANTILEVER	$\varepsilon_{eff} \leq \varepsilon_{ult.}$ (TF)	10.6 9.6		III II
CONSTRAINT: U_r > 120 MM FE – ANALYSIS(QUASI–STAT.)	$\sigma_{eff} \leq \sigma_{Flow} \cdot f_2$	10.8 9.6		III II
BOLTED JOINT MATERIAL HATCH	ELASTIC APPROXIMATION NO LEAKAGE	≥9.5 9.5 (T=150°C)		III II
H_2–DYNAMIC (ANALYTIC)	$\varepsilon_{eff} \geq 2\varepsilon_t \leq \varepsilon_{ult.}$	≥8.3 ≥8.0	.7 .5	I
	$\varepsilon_{eff} \leq \varepsilon_{ult.}$ (TF) $P_0 \cdot \tau$ = .02 " = .01	≈40 ≈20		I
FE–DYNAMIC 360 BAR/S	DLF=1.6	(11.5) (10.1)		I
FE–DYN.,EL–PL. 36 BAR/S SHELL REINFORCEMENT	elast.-plast. DLF=1.05 STRAIN–CONCENTR. $\varepsilon_{eff} \leq \varepsilon_{ult.}$ (TF) $R_{p0,2}$=400	8.8 8.6	.7 .5	I
RISK STUDY PHASE A	$\sigma_{eff} \leq \sigma_{Flow}$ $K_I \leq K_{IC}$	8.5 7.5		I I



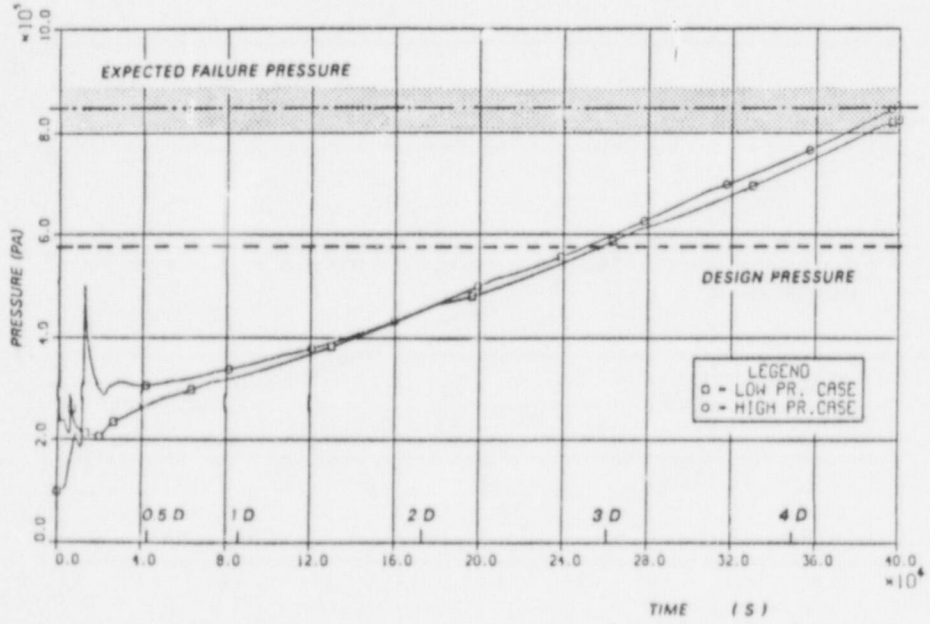


Figure 1. Pressure-Time History Due to Core Meltdown Accidents

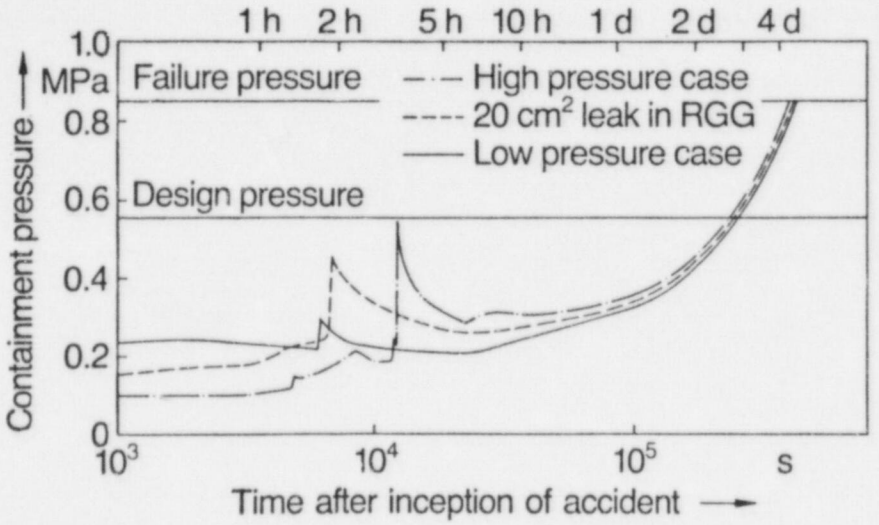
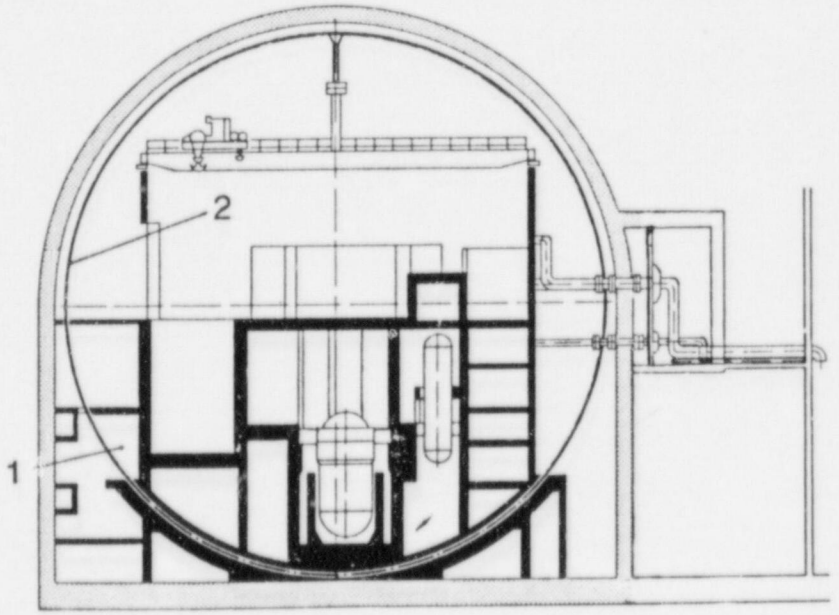
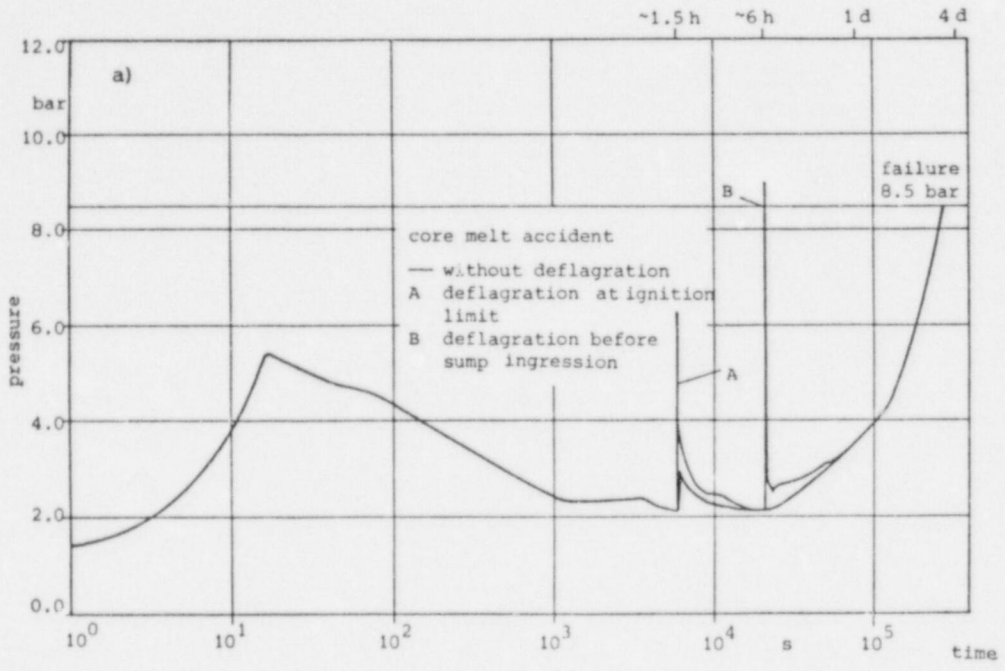


Figure 2. Containment Pressure Time History Low Pressure Case



1: annular compartment, Local H_2- Loading
2: containment steel shell

Figure 3. Nuclear Power Plant Biblis B



Containment Pressure with H_2-Deflagration Assumptions
Reference Plant Biblis B, Low Pressure Case (GRS-A-906)

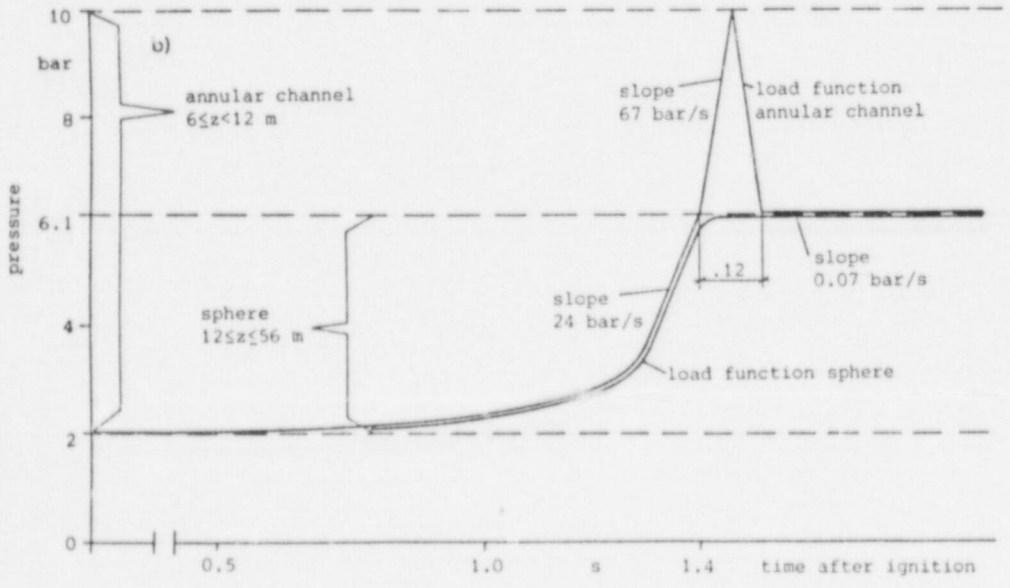


Figure 4. Load Functions, Core Meltdown Accident

(a) Long Term, Steam
(b) Short Term, H_2-Deflagration (assumed)

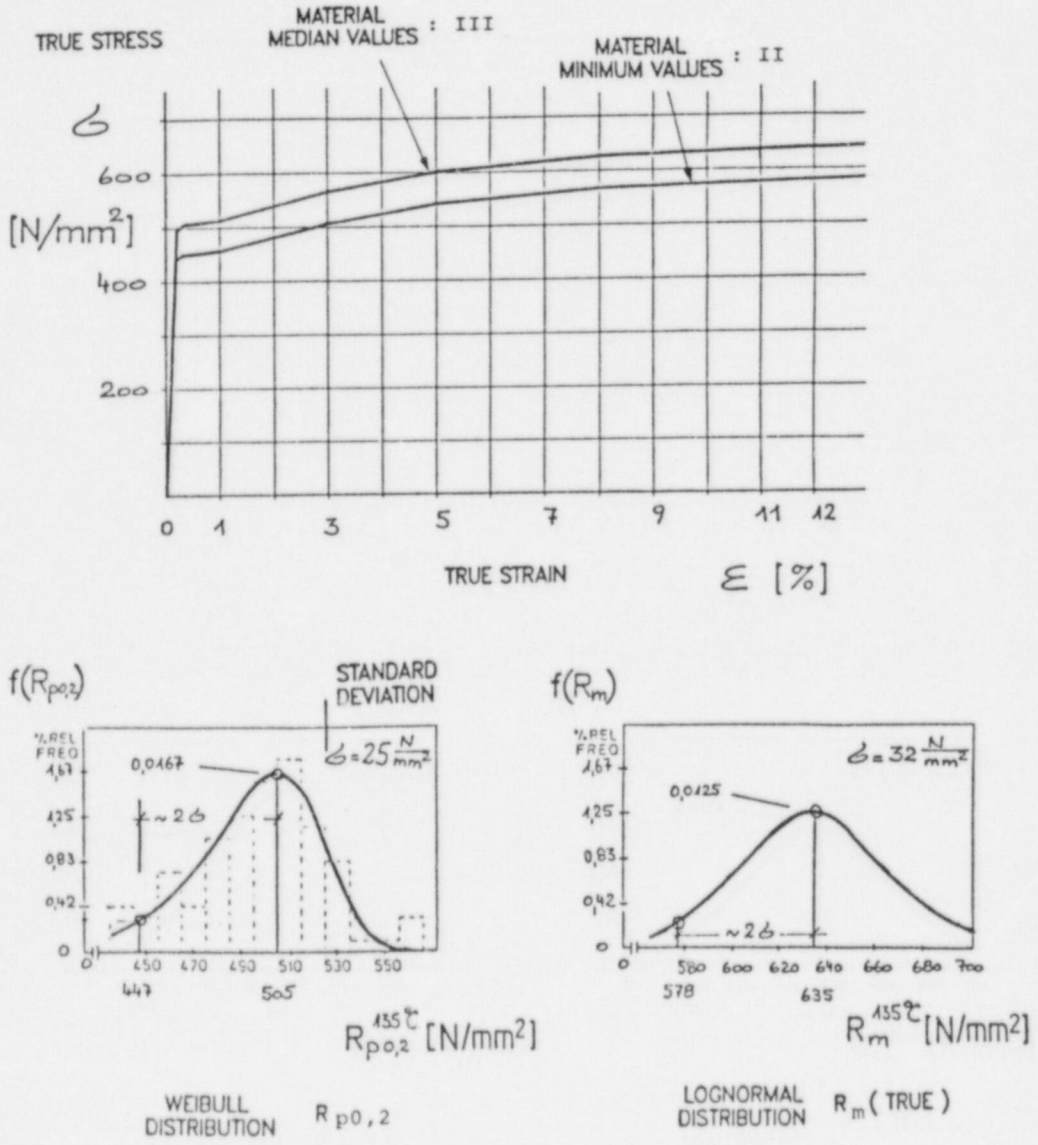


Figure 5. Stress-Stain-Input for Steel FG 47 WS (T=135°C)
Probability Density Functions for σ_F^T and σ_{ult}^T

DISTURBANCES OF STEEL CONTAINMENT

A: Nozzle for Steam Line Penetration
(Stress Concentration)
B: Annular Concrete Console(Gap ≈ 200 mm)
C: Embedding of Steel(Additional Bending)
D: Bolted Joint to Material Hatch(Distribution of Forces)
E: Single Steel Cantilever
(Gap ≈ 120 mm ; Concentrated Force)

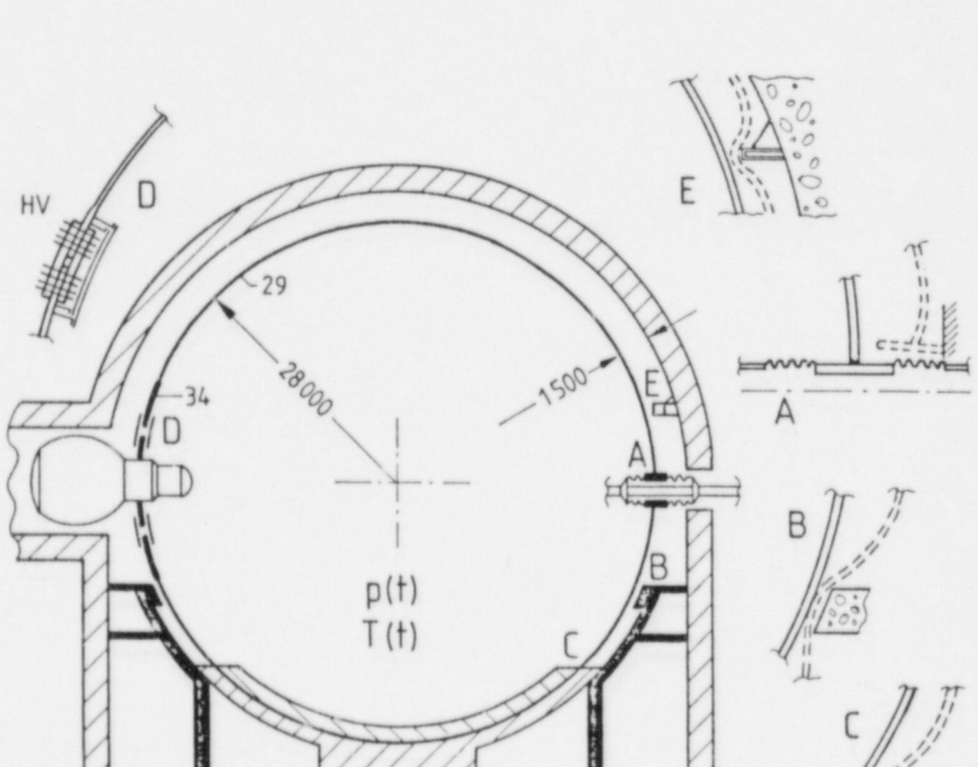


Figure 6. DRS Phase B, Shell Disturbances Investigated

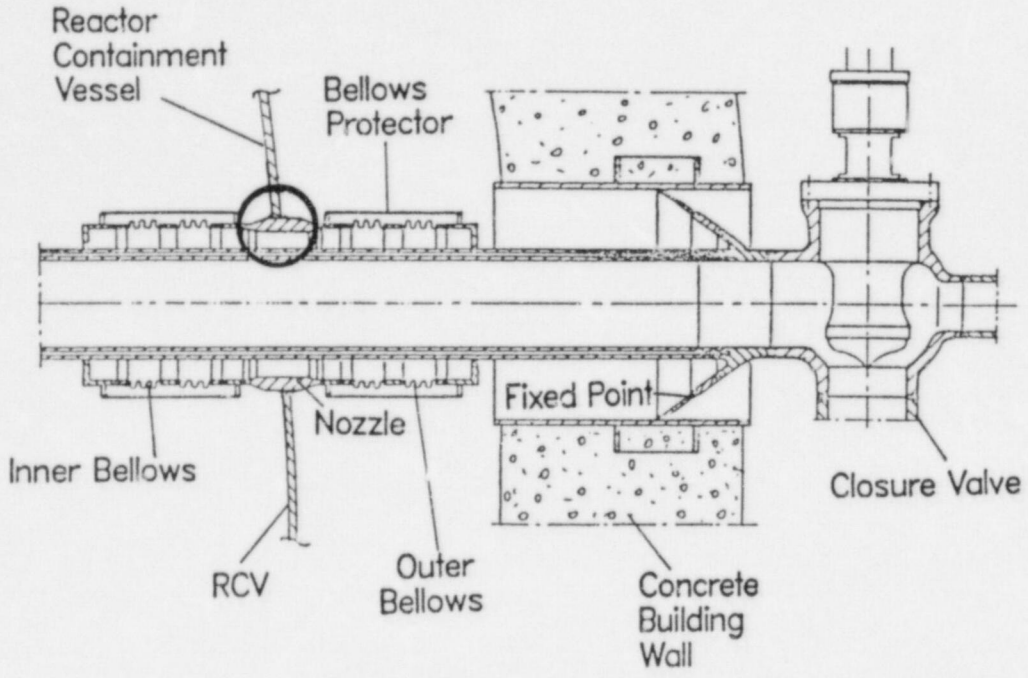


Figure 7. Penetration of Steam Line (PWR)

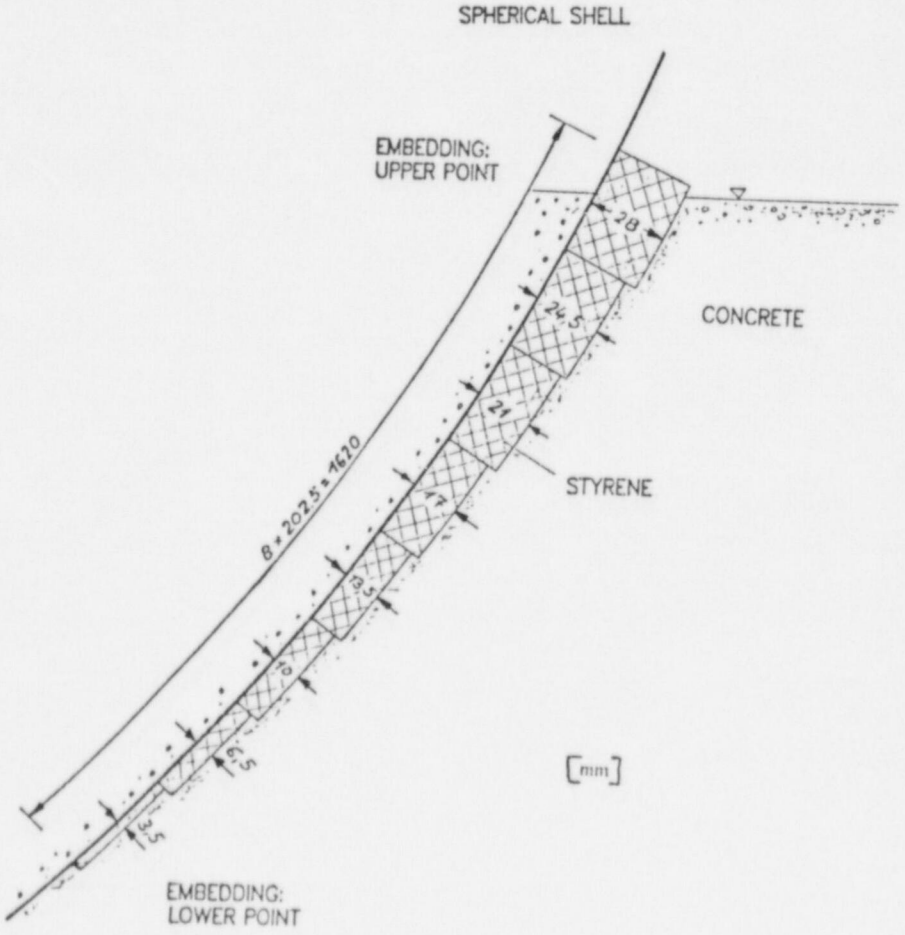


Figure 8. Concrete-Embedding of Sperical Shell

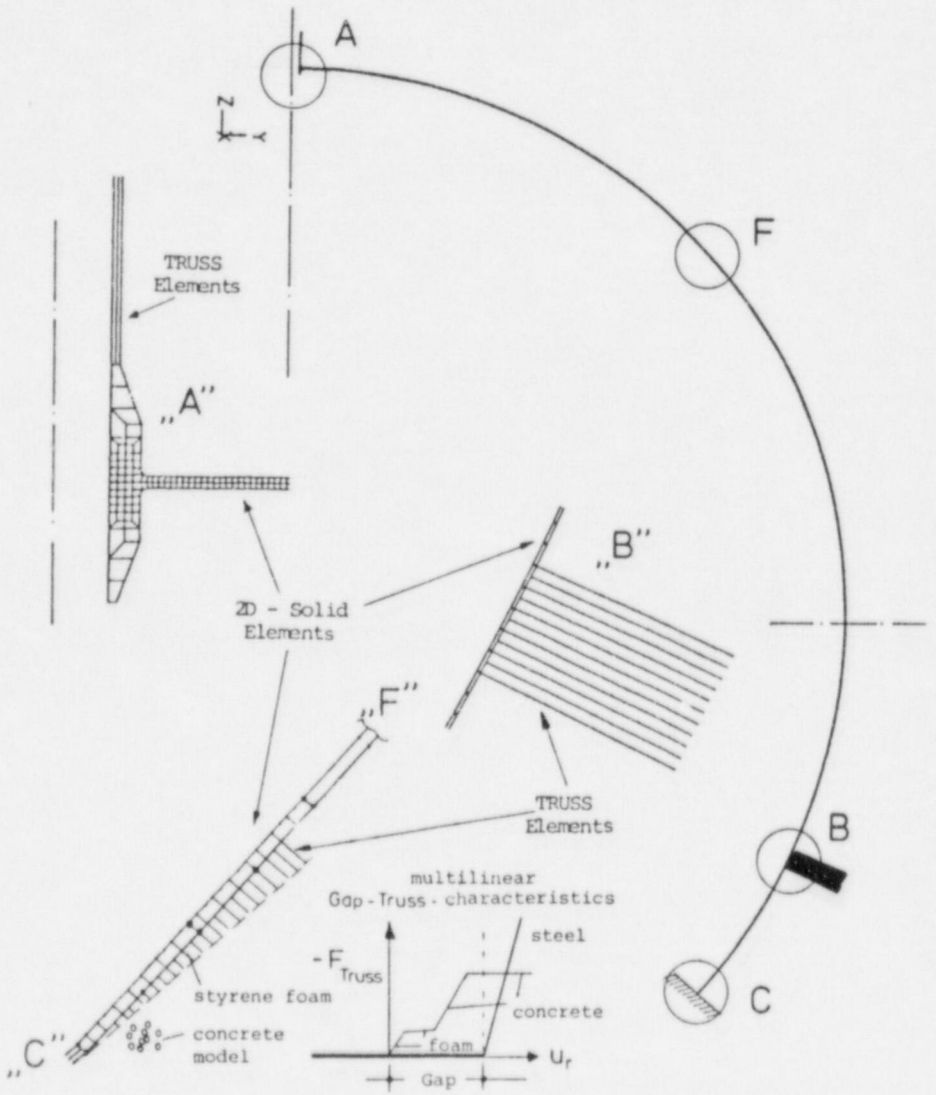


Figure 9. FE-Model for Investigation of Following Areas:

(A) Nozzle of Steam Line Penetration
(B) Annular Concrete Console
(C) Concrete Embedding
(F) Undisturbed Shell

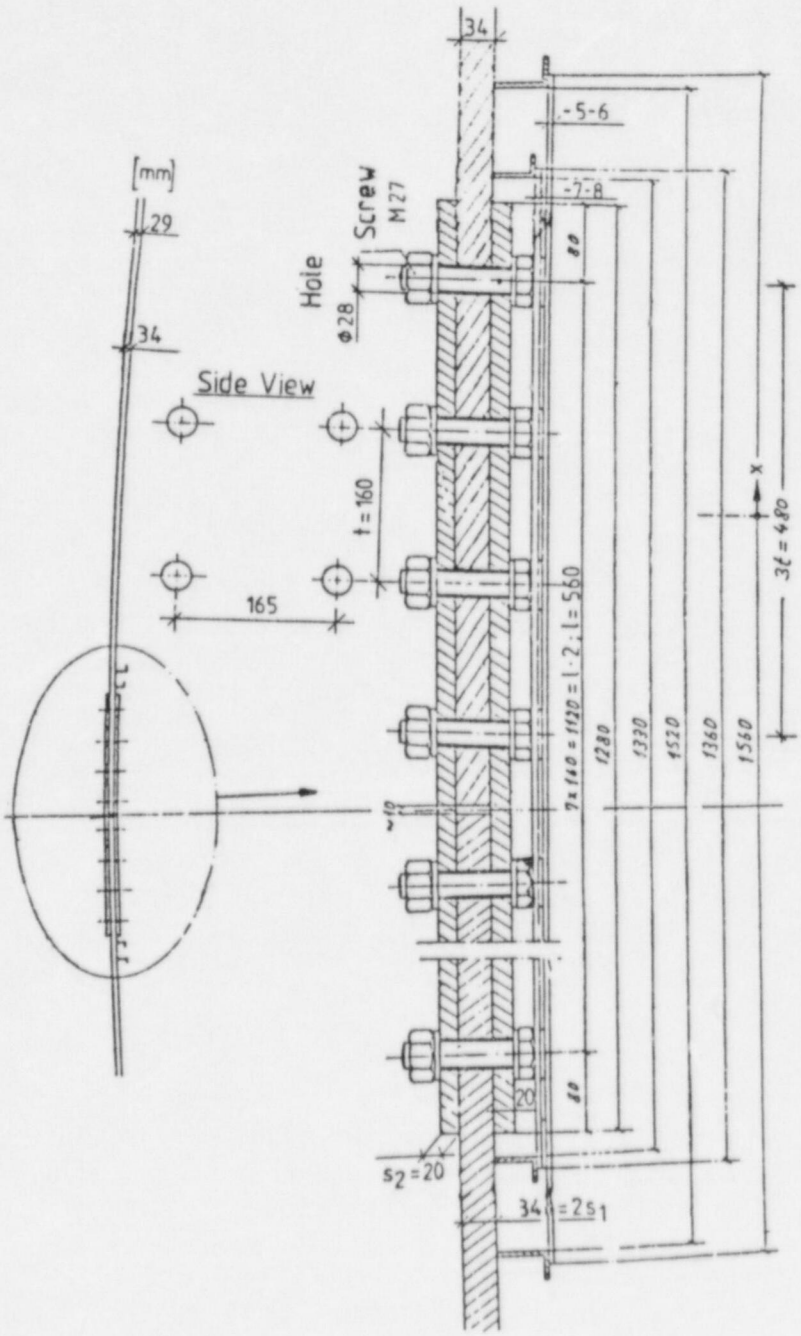


Figure 10. Bolted Joint to Material Match (Biblis B)

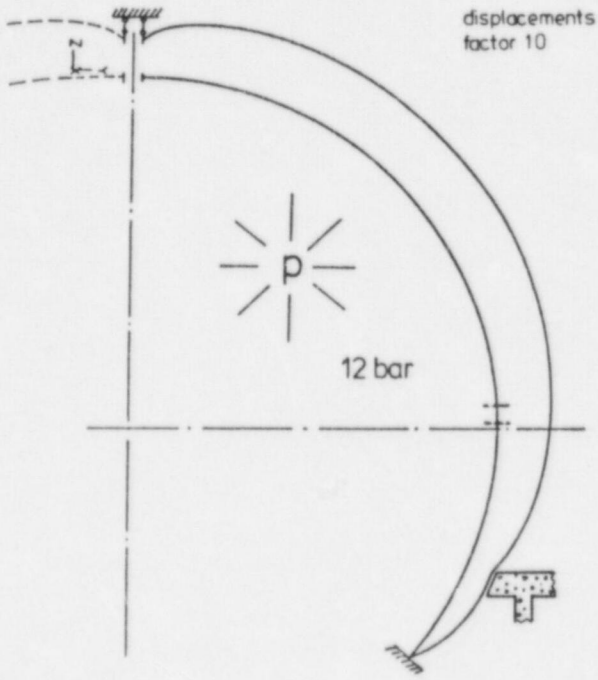


Figure 11. Model of Spherical Shell, Rotational Symmetric Shell Deformation, Constraints, Mat. III

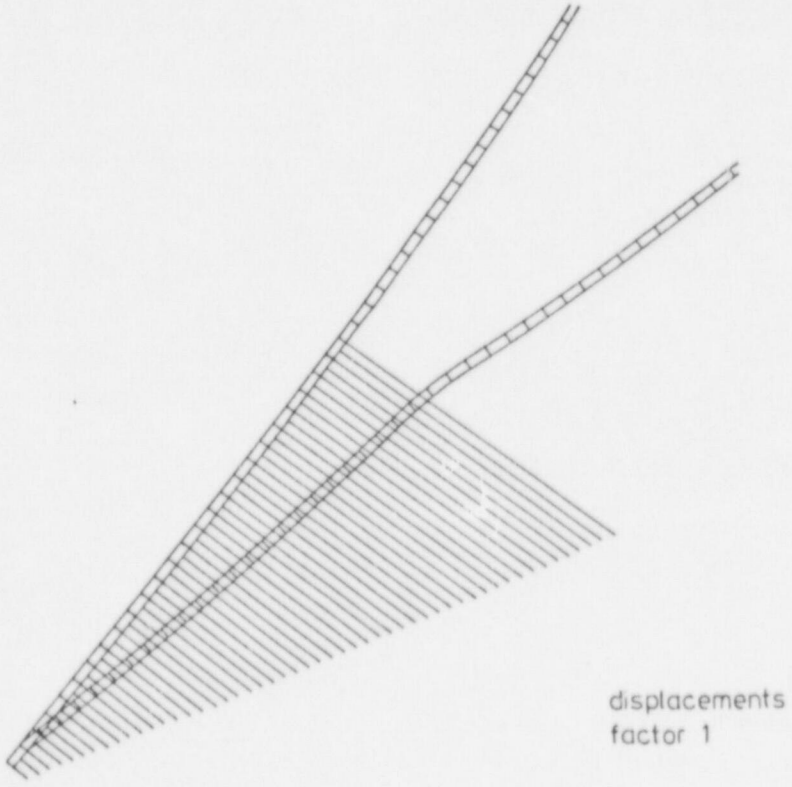
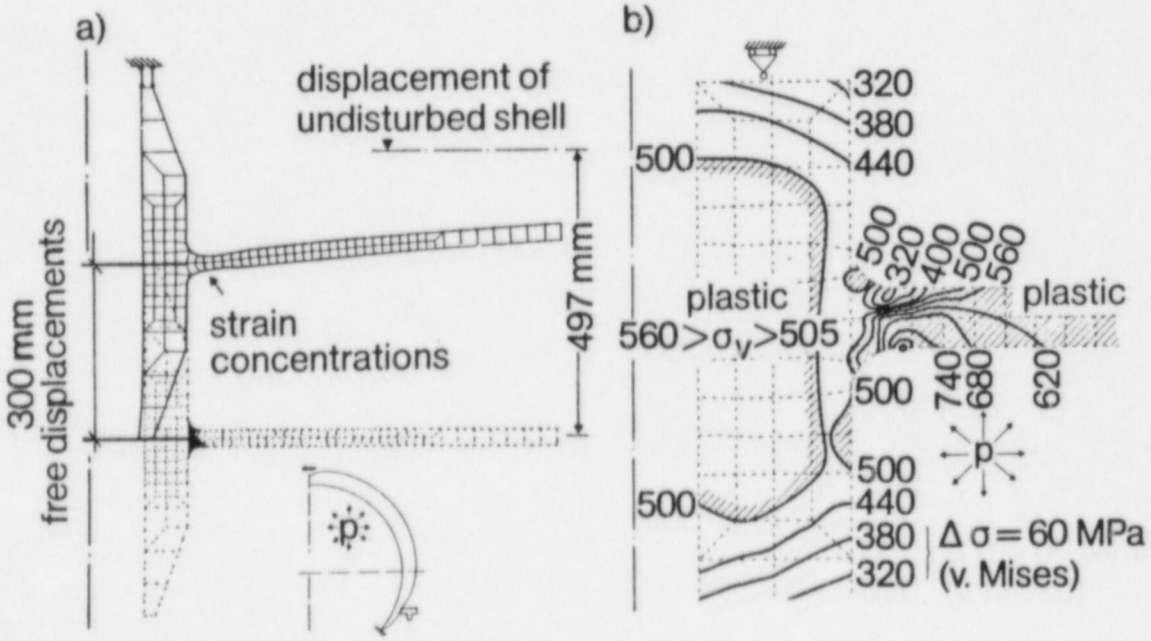


Figure 12. Containment Embedding, Deformation at 9.8 bar, Mat. II



a) Deformation and Strain Concentration
b) Isolines of Effective Stresses
Material Median Values

Figure 13. Nozzle of Steam Line Penetration,
12 bar = (Constraint 11 bar)

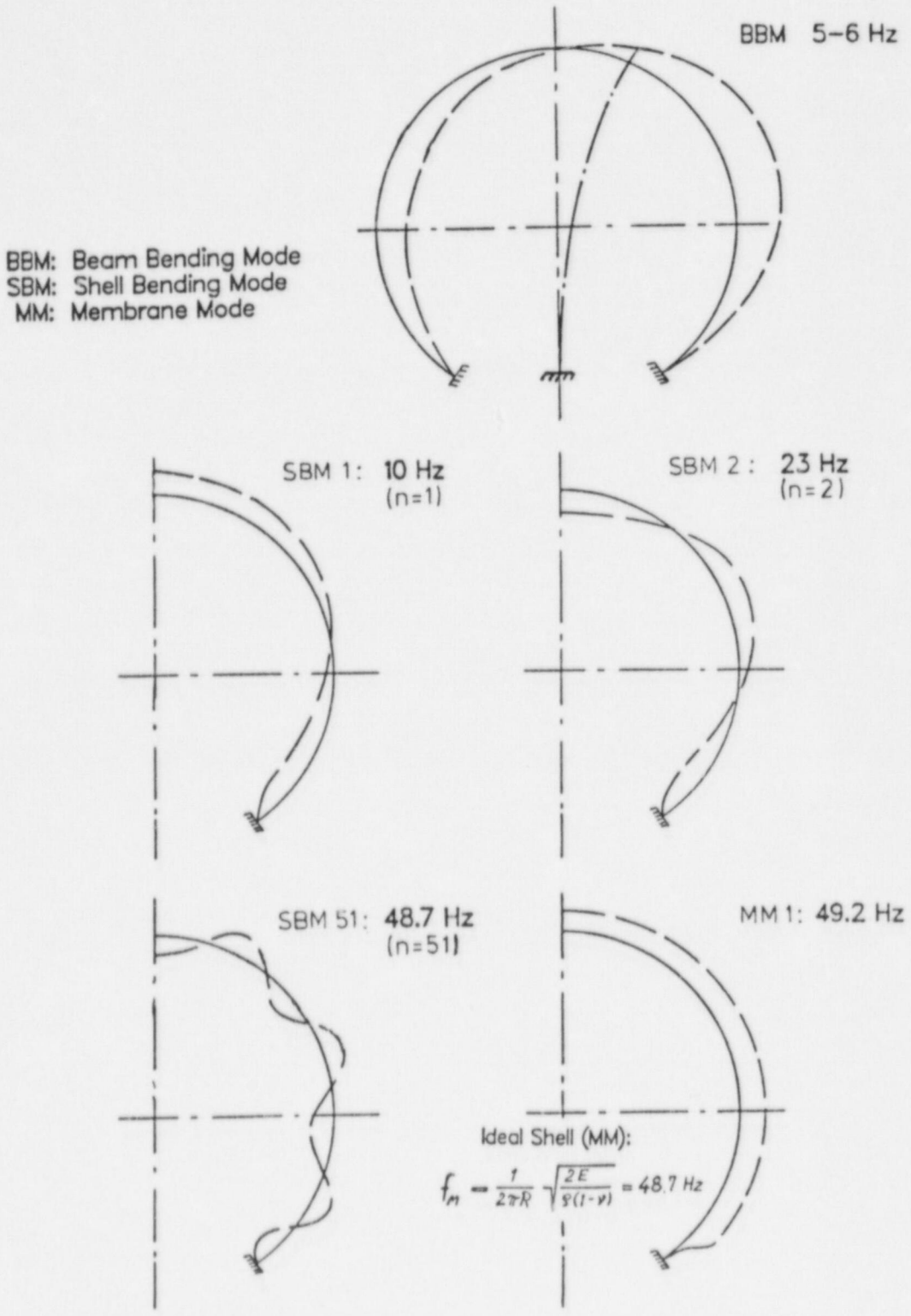


Figure 14. Eigenvalues and Mode Shapes

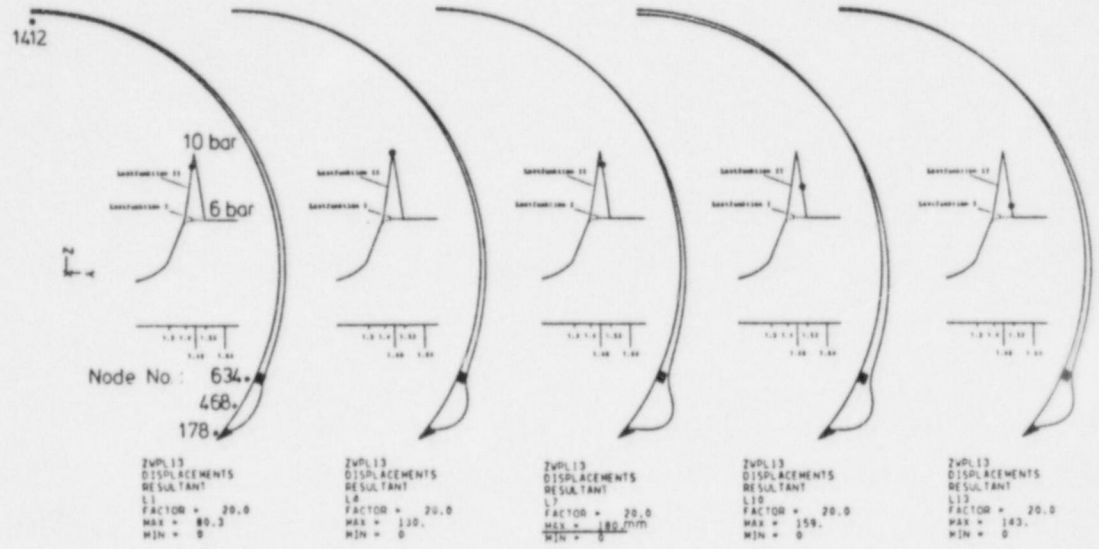


Figure 15. Dynamic Displacements Due to H_2-Loading at Annular Channel

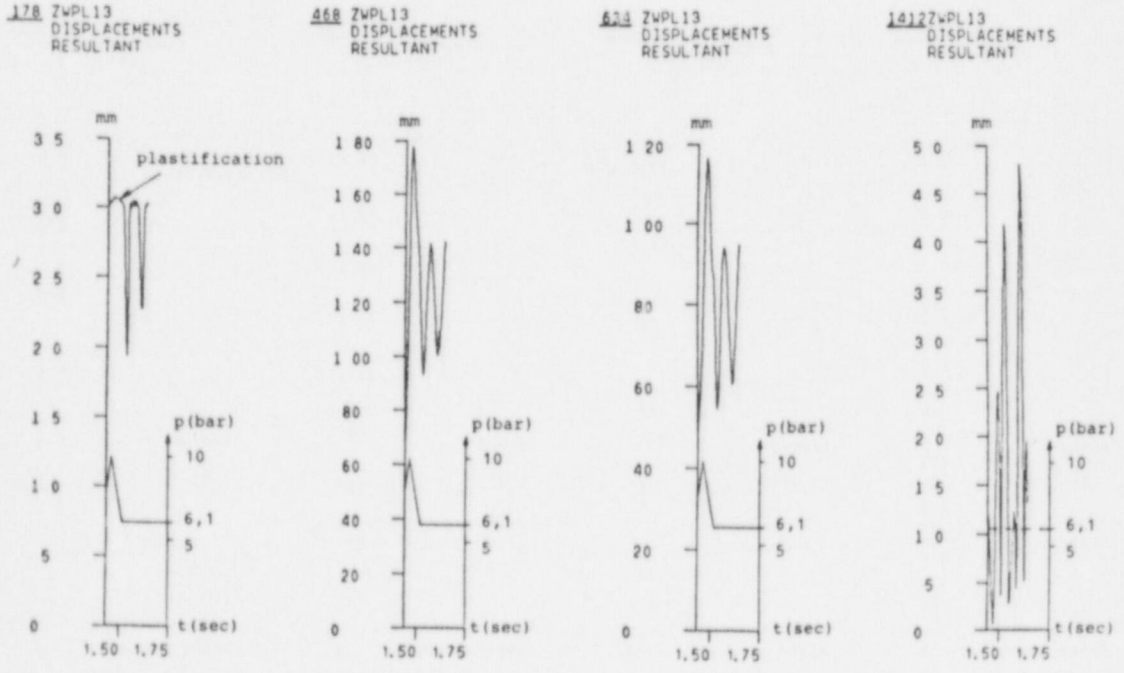


Figure 16. Dynamic Displacements for H_2-Loading at Annular Channel

SMALL SCALE MODEL FOR EXPERIMENTAL INVESTIGATIONS OF THE DYNAMIC BEHAVIOUR OF SPHERICAL STEEL CONTAINMENTS

E. Wolf, B. Göller
Kernforschungszentrum Karlsruhe GmbH
Institut für Reaktorentwicklung
Projekt Nukleare Sicherheit
Postfach 3640, D-7500 Karlsruhe

ABSTRACT

In order to study the influence of imperfections on the earthquake response of spherical steel containments corresponding theoretical and experimental investigations were started. The experimental investigations will be performed with a small scale model with a diameter of 1.3 m and a wall thickness of about 1 mm.

The necessary high precision of the spherical model required a complicated manufacturing process. The steps of this process and the resulting tolerances of the model are discussed in this paper.

1. INTRODUCTION

The containment of the standard pressurized water reactor in Germany consists of a free standing spherical shell with a diameter of 56 m and a wall thickness of 38 mm. It is clamped to the basement at an opening angle of 130° (fig. 1). Theoretical investigation of the containment response due to dynamic earthquake loading is common licensing practice. However, these computations are based on simplified models; deviations from the ideal spherical geometry caused by a number of different nozzles with reinforced sections or due to inevitable manufacturing tolerances are usually not considered.

However, from experiments with thin cylindrical shells /1/ it is known that small deviations from the ideal geometry may have significant influence on the dynamic response. For instance a cylindrical shell under earthquake excitation should oscillate only in modes with first circumferential order. In reality, inevitable small imperfections give rise to oscillations in modes with higher circumferential order. Since the stiffness of thin cylindrical shells against such modes is rather low, the amplitudes of such modes can reach rather large values.

Similar phenomena might also occur in thin spherical shells. However, no corresponding investigations are known so far. Therefore theoretical and experimental investigations will be carried through in which the influence of imperfections on the dynamic response of spherical containment shells will be determined /2/. The experimental investigations will be performed with a small scale model of the contain-

ment, the manufacturing process of which has just been finished. The steps of this process and the resulting accuracy of the model will be discussed in this paper.

2. CRITERIA FOR THE DESIGN OF THE MODEL

The large dimensions and the high manufacturing standard of real containments lead to very small relative tolerances. But the containment model should reveal even smaller tolerances in order to provide the reference results for an almost ideal geometry. This means that as far as possible the global shape should be perfect, the wall thicknness should be uniform and the material should be homogeneous and isotropic. If, additionally, the model material would be the same as that of the real containment, then any experimental finding could be directly transfered to the real containment by simply applying appropriate scale factors: if length scale and time scale have the same value λ , then the three governing mechanical equations for kinematic (1), material behaviour (2) and equilibrium (3)

$$\varepsilon = \frac{d(\lambda u)}{d(\lambda x)} \quad (1); \qquad \sigma = \sigma(\varepsilon) \quad (2); \qquad \frac{d\sigma}{d(\lambda x)} = \rho^* \frac{d^2(\lambda x)}{d(\lambda t)^2} \quad (3);$$

are satisfied for any value of λ . For simplicity, here only the equations for a single dimension are shown, in which σ and ε are stress and strain, u und x are deformation and coordinate, t is time and ρ is density of the material, respectively. Consequently, the eigenfrequencies of the model grow with the same degree as the size of the model is reduced. For ease of excitation and measurement the eigenfrequencies should be low, i.e. the model should be large, while for reasons of lower manufacturing effort the model should of course be small.

3. MANUFACTURING PROCESS

The required high precision of the model excluded manufacturing processes as deep drawing or welding from several sheets. The size of the model and the desired material excluded as well a process of electro plating as used in /3/.

Finally, it turned out that manufacturing the containment model by turing from a thicker piece using a numerical controlled lathe would provide the best results. The dimensions of the available lathe allowed for the machining of a model with a diameter of about 1.3 m. The wall thickness of the model then ought to be a little bit smaller than 1 mm. These dimensions correspond to a scale factor of 1:43.

The starting piece was welded together from two hemispherical deep drawn shells of 38 mm thickness. The material was the containment steel 15MnNi63. The pole region of the lower half was cut away at an angle of 40 degrees below the equator. A flange was welded to this location, by means of which the shell model will be fixed to its clamping plate. The weldings were investigated by intense ultrasonic

and x-ray screening. Some faults were detected and had to be repaired. In order to reduce the residual stresses the model was then annealed by heating to 560 ^{o}C for 1.5 hours with temperature rates of less than 180 ^{o}C/hour.

Then the machining of the model could start on the numerically controlled lathe. First the external shape of the model was finished (fig. 2a and fig. 3), reducing the wall thickness from initial 38 mm to approximately 11 mm. Thus a sufficient stiffness was left in order to withstand the cutting forces without undue deformations. Because of some faults on the finished surface at the first design diameter of 1300 mm, it was decided to reduce the shell diameter to 1296 mm. Indeed, an excellent surface could be machined there. Fig. 4 shows the polar diagramme of the measured deviations from the ideal meridian. The largest deviations lie within a band of $\pm$0.045 mm, what demonstrates the high quality of the machining process.

The next step consisted of machining the supporting casing (fig. 2b and fig. 5), into which later the containment model is to be clamped (fig. 2c) in order to maintain a sufficient stiffness for finishing of the model from inside (fig. 2d). There must be no gap between model and casing, as otherwise the cutting forces could locally deform the model when its wall thickness became smaller. As a consequence the surface quality would not be good and the tolerances for the wall thickness could not be maintained. On the other hand, there must be a clearance for insertion of the spherical model into the casing. That is why the casing was made of Aluminium. It could easily be heated to such a degree that the steel sphere could just be inserted. Due to the different coefficients of thermal expansion then there existed a press fit between both components at room temperature. Additional evacuation of the gap between the components intensified the press fit and acted against a danger of buckling of the model due to the shrink pressure and the local cutting forces.

Special care must be taken that no excentricity between the axis of the machine and the axis of the casing occured. Otherwise, a variation in the wall thickness along the circumference of the model with a size of twice the excentricity would occur. That is why the clamping between the casing and the machine could not be loosened during the complicated step of inserting the spherical model into the supporting casing.

In the last step the model was finished by machining the inner surface in order to reduce the wall thickness from 11 mm to its final value of 0.96 mm (fig. 2d). The correctness of the decrease of the wall thickness was controlled by an ultrasonic sensor. Thus, undue deviations of the wall thickness along the meridian could be detected and corrected by an appropriate adjustment of the path of the cutting tool.

4. THE FINISHED MODEL

After the machining was done the encasing was heated again so that its upper part could be removed and the spherical model could be taken out. It was turned over in a special device and was then fixed to its stiff clamping plate in order to provide for rigidly clamped boundary conditions. Rather large meridional forces may occur at clamped shell boundaries which - on the other hand - may induce bending deformations of the clamping plate. This, however, would violate the clamped boundary conditions and would significantly influence the eigenfrequencies of the model /4, 5/. The clamping plate used here was designed to withstand such deformations (fig. 6).

Fig. 7 shows the clamped containment model put on a turning table for measurement of its geometry. The meridional shape was measured by a dial gauge at the end of the curved beam whose axis of rotation was adjusted pointing to the center of the sphere. The azimuthal deviations were measured by a fixed dial gauge during the turning table revolved. Finally the wall thickness was measured at discrete points with an ultrasonic sensor.

The measurements yielded an outer diameter of the sphere of 1296 mm, and a wall thickness of 0.96 mm. Figs. 8 and 9 show the deviations from these ideal values. The meridian has a tolerance of +0.28 and -0.12 mm. Compared with the state after the first machining step at a wall thickness of 11 mm (fig. 4) the deviations now were larger by a factor of five. This indicates that the model slightly deformed due to residual stresses when it was removed from the casing. The deviations of the shape along the circumference are smaller than ± 0.02 mm. Only in a very small region at the equator ($\varphi = 90^{\circ}$) the deviations are considerably higher at values of ± 0.08 mm. The wall thickness along a meridian varies within ± 0.03 mm. Its variations along the circumference are much smaller again, they are in the range of ± 0.015 mm.

For completeness, the dead weight of the spherical model allone is 81 kg, the dead weight of the clamping plate is 1000 kg.

5. CONCLUSIONS

The presented process of machining a spherical containment model from a thick starting sphere was rather complicated. But the efforts were worth while yielding a model of high quality with relative tolerances in the radius of $4 \ 10^{-4}$ and in the wall thickness of $3 \ 10^{-2}$.

Thus, the experiments for modal analysis, using contactless displacement transducers, can start and will probably yield a lot of interesting results. Preliminary computations indicated that eigenfrequencies of the shell modes are concentrated at 1250 Hz with a large modal density of more than 10 Modes/Hz.

6. REFERENCES

/1/ R.W. Clough, A. Niwa, D.P. Clough: Experimental Seismic Study of Cylindrical Tanks. J. of the Structural Division, Proceedings of the ASCE, Vol. 105, No. ST9, Dec. 79, 2565-2590

/2/ R. Krieg, F. Eberle, B. Göller, J. Kadlec, G. Messemer, E. Wolf, W. Gulden, St. Müller: Investigation Program on PWR-Steel-Containment Behaviour under Accident Conditions. KfK-Bericht 3589, 1983

/3/ J.M.T. Thompson: Making of Thin Metal Shells for Model Stress Analysis. Journal of Mechanical Engineering Science, Vol. 2, No. 1, 1960, 105-109

/4/ F. Eberle, B. Göller, G. Hailfinger, J. Kadlec: Eigenoscillations of a Fluid Filled Cylindrical Shell. Proceedings of SMIRT 6, Paris 1981, paper B5/4, 1-8

/5/ M. Chung, P. Turula, H. Chung, J.A. Jendrzejczyk: Analytical and Experimental Study of Two Concentric Cylinders Coupled by a Fluid Gap. Proceedings of SMIRT 3, London 1975, paper F2/7, 1-7

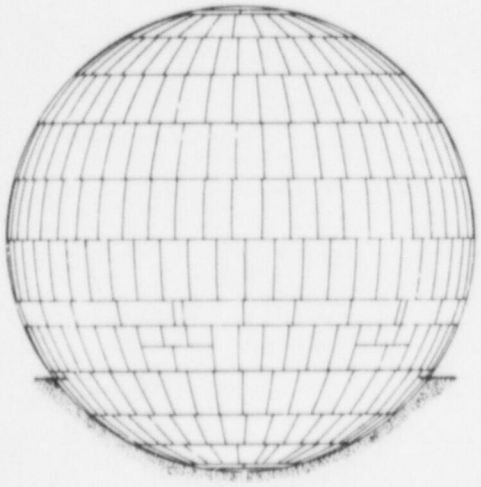


Fig. 1:
Containment of a PWR,consisting of a thin spherical shell.

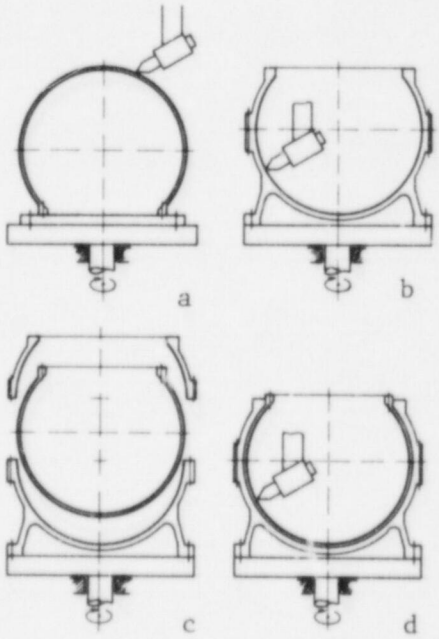


Fig. 2:
Machining the spherical model on a numerically controlled lathe:
a) Machining the outer surface of the model,
b) Machining the inner surface of the casing,
c) Clamping the model into the casing,
d) Finishing the model from inside.

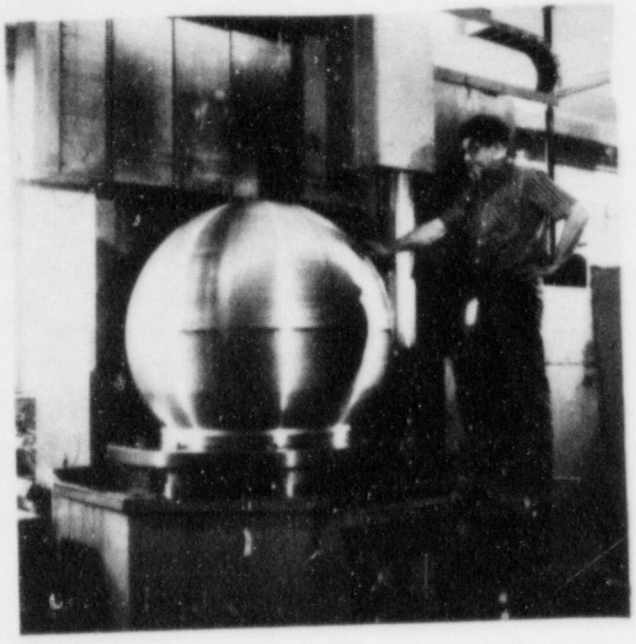


Fig. 3:
Machining the outer surface of the sphere on a lathe, reducing the wall thickness to 11 mm

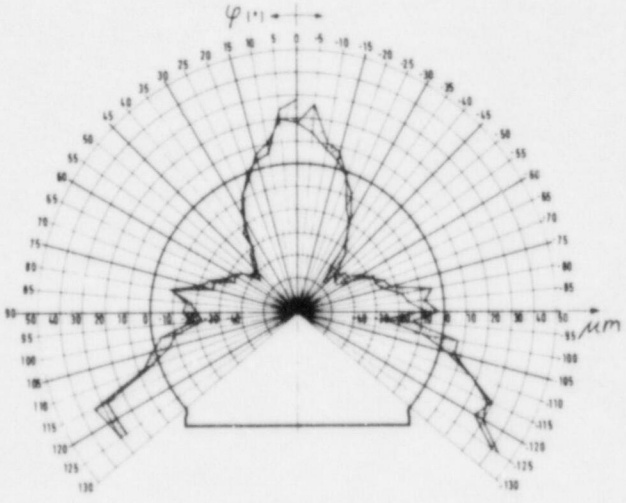


Fig. 4:
Deviations of the meridian from the ideal shape at the finished wall thickness of 11 mm



Fig. 5:
The supporting casing

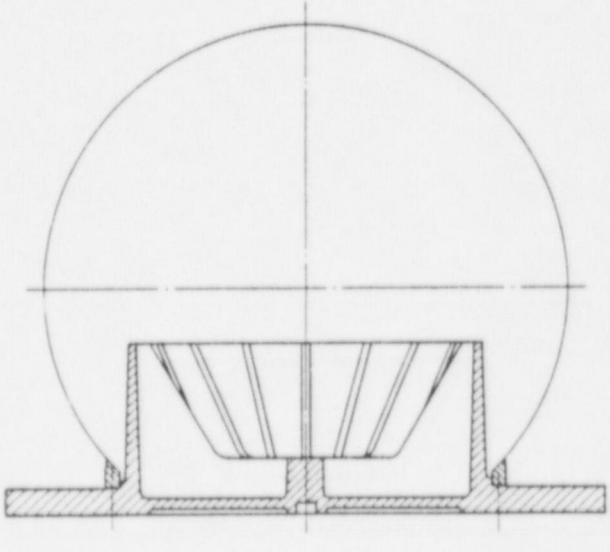


Fig. 6:
The clamping plate of the containment model for clamped boundary conditions

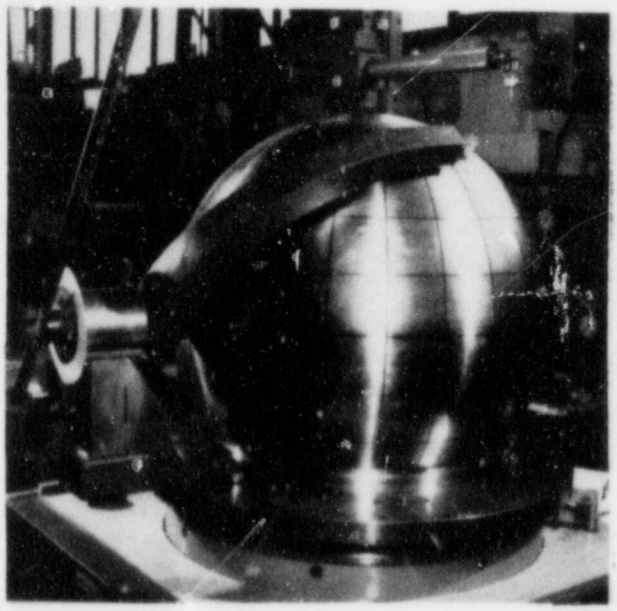


Fig. 7:
Finished model prepared for measurement of its shape.

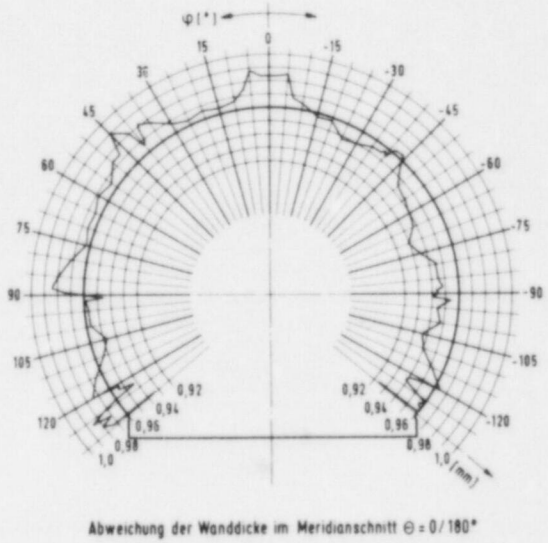
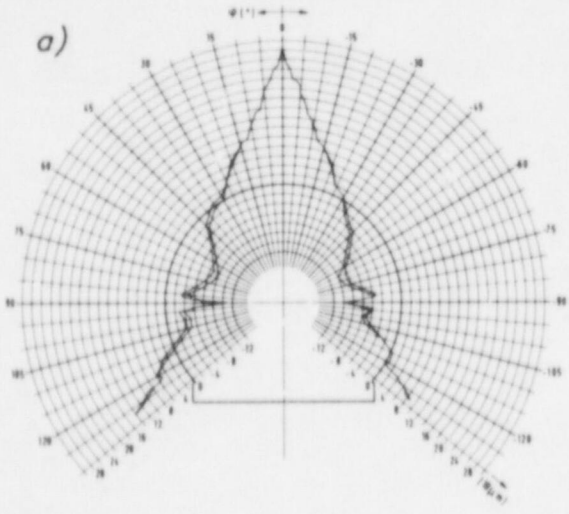


Fig. 9:
Deviations of the wallthickness from the ideal value of 0.96mm along a meridian.



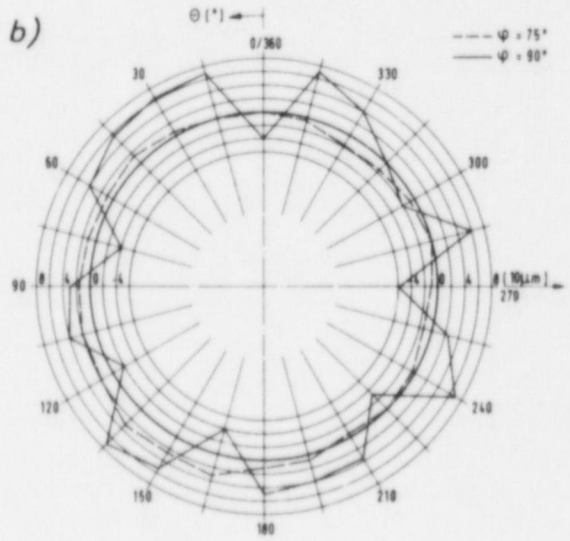


Fig. 8:
Deviations of the model from the ideal shape with a diameter of 1296mm.
a) along a meridian in 10μm.
b) along the circumference at the meridional angles of $\varphi=90°$ and $\varphi=75°$ in 10μm.

LEAKAGE POTENTIAL THROUGH MECHANICAL PENETRATIONS IN A SEVERE ACCIDENT ENVIRONMENT*

L. N. Koenig
Sandia National Laboratories

ABSTRACT

This paper reviews the findings of an ongoing program, "Integrity of Containment Penetrations Under Severe Accident Loads." The program is concerned with the leakage modes as well as the magnitude of leakage through mechanical penetrations in a containment building subject to a severe accident. Seal and gasket tests are used to evaluate the effect of radiation aging, thermal aging, seal geometry, and seal squeeze on seals and gaskets subjected to a hypothesized severe accident. The effects on leakage of the structural response of equipment hatches, personnel airlocks, and drywell heads subjected to severe accident pressures are studied by experiments and analyses. The data gathered during this program will be used to develop methodologies for predicting leakage.

1.0 INTRODUCTION

The U.S. Nuclear Regulatory Commission (USNRC) is sponsoring a set of programs to examine the failure modes of light-water reactor (LWR) containments that could result in the release of radioactive material as a result of a severe accident. These environments, which were not considered in the design of containments, result in temperature and pressure above "design-bases" conditions. Under such conditions, radioactive material could escape as a result of one or more of the following events:

- Tear or breach in the containment building
- Catastrophic rupture of the containment building
- Degradation of seal and gasket materials
- Deformations of sealing surfaces

We are studying the likelihood and consequences of these events in several programs. Under one program, "Experiments on Containment Models Under Extreme Loading Conditions," we are conducting high-pressure tests on models of steel containment buildings. In the future, a 1/6-scale model of a reinforced concrete containment building will be tested.[1] In another program, "Containment Integrity Under Extreme Loads," we compare experimental results with analytical predictions in an effort to formulate a methodology for predicting containment performance.[2] The behavior of electrical

*This work supported by the United States Nuclear Regulatory Commission and performed at Sandia National Laboratories, which is operated for the U.S. Department of Energy under contract number DE-AC04-76DP00789.

penetration assemblies is examined in a third program, "Electrical Penetration Assembly Severe Accident Test."[3] This paper focuses on a fourth program, "Integrity of Containment Penetrations Under Severe Accident Conditions," in which we study the potential for leakage through mechanical penetrations in containments subjected to severe accident environments.

In this program we are conducting experiments that evaluate the potential for leakage resulting from the degradation of seals and gaskets and from pressure-induced deformations of the sealing surfaces. Seal and gasket tests are used to evaluate the effects of radiation aging, thermal aging, seal geometry, and seal squeeze on the performance of seals in a hypothesized severe accident. The deformations of personnel airlocks, equipment hatches, and piping penetrations are studied in conjunction with tests on scale models of containment buildings. Incorporating the mechanical penetrations in models makes it possible to measure not only the effect of direct pressure on the mechanical penetration but also the effect of the interaction between the penetration and the containment shell. Completed tests include 1/32- and 1/8-scale models of steel containment buildings. A 1/6-scale model of a reinforced concrete containment building is to be tested in 1987. In addition to scale-model testing, a full-size personnel airlock is to be tested in late 1986. No testing is planned on a drywell head, because we believe that conclusions can be drawn from established analysis techniques and from comparisons with pressure-unseating equipment hatches in the 1/6-scale concrete model, which have a similar geometry.

2.0 SEALS AND GASKETS

2.1 Testing Methodology

Parameters that affect seal performance in a severe accident are material type, seal geometry, thermal aging history, radiation aging history, squeeze and temperature of the severe accident. These factors are incorporated in a "living" test matrix from which we judiciously select or omit tests, based on information gained from earlier testing. The current test matrix is shown in Table 1.

The materials being tested include silicone rubber and ethylene propylene (EPM/EPDM), both of which are used in mechanical penetrations. Silicone and EPM/EPDM are also used in electrical penetration assemblies. Seal geometries included in the test matrix are O-ring, tongue-and-groove, double-dog-ear, gumdrop, and inflatable. These geometries are used in equipment hatches, personnel airlocks or drywell heads. O-rings are also used in some electrical penetration assemblies.

Squeeze is defined as the percent reduction in seal dimension normal to the sealing surface. We tested seals at squeezes between 5%, and 30%, where 30% squeeze corresponds to metal-to-metal contact. Shims

Table 1 Seal and Gasket Test Matrix
(as of October 1985)

MATERIAL	GEOMETRY*	AGING	ENVIRONMENT	NUMBER OF TESTS PLANNED/COMPLETED
Silicone rubber	4OR	none	steam	5/5
	4OR	none	air	1/1
	4OR	rad/therm	steam	3/3
	4OR	thermal	steam	1/1
EPM/EPDM	4OR	none	steam	3/3
	4OR	none	air	1/1
	4OR	rad/therm	steam	3/3
	4OR	thermal	steam	1/1
	2OR	none	steam	1/0
	DGD	none	steam	1/1
	DDE	none	steam	1/1
	DTG	none	steam	1/0
	INF	none	steam	3/0
	INF	rad/therm	steam	3/0

*
4OR - double 1/4-inch O-ring
2OR - double 1/2-inch O-ring
DGD - double gumdrop
DDE - double dog-ear
DTG - double tongue-and-groove
INF - inflatable

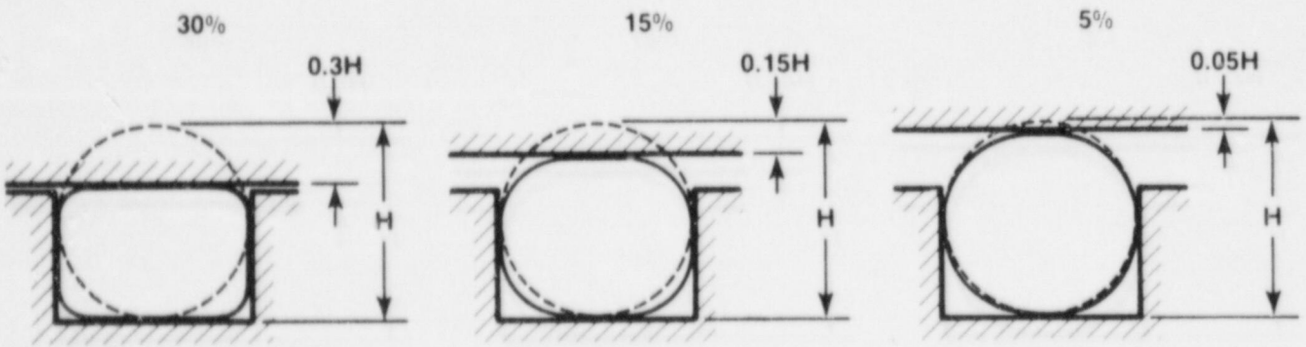


Figure 1. Percent Squeeze

are placed between the sealing surfaces of the test fixture to achieve squeezes of less than 30%, where the size of the shim depends on the dimension of the seal in the direction normal to the sealing surface (see Figure 1).

We tested seals and gaskets under three aging conditions:

- Radiation aging (200 Mrd ± 20% at <1 Mrd/h) followed by thermal aging (300°F for 168 h). The radiation aging corresponds to service life plus a loss-of-coolant accident. Thermal aging corresponds to service life only. No simultaneous radiation and thermal aging was done.
- Thermal aging only at 300°F for 168 h.
- No aging.

In all tests seals were removed from the fixture after aging to be compression checked.

We conducted tests in nitrogen, air, and steam atmospheres at temperatures up to 700°F at 155 psia. Both pressurized-water reactor (PWR) and boiling-water reactor (BWR) severe accident profiles, which are discussed in [4], are enveloped by this environment.

The environmental test chamber is shown in Figure 2. The test fixture, installed inside the chamber, is completely surrounded by the test environment to minimize temperature gradients. The fixture shown in Figure 3 is used for 1/4-inch O-rings and is multilayered so that three sets of rings can be tested simultaneously. A set consists of three rings. Leakage is measured through ports between the inner and middle gaskets on each level of the fixture except for the middle set which vents to ports in the inner cavity. The other "non-inflatable" seal geometries are tested in the same chamber but in different fixtures.

In a seal test, the initial temperature and pressure are raised to 360°F and 155 psia. We hold these conditions overnight before raising the temperature to 500°, 600°, and 700°F and holding for 2 h on successive days. Tests are terminated before 700°F is reached only if a seal fails and leaks. For safety reasons we lower the temperature to 360°F overnight after each temperature step. A temperature history from an actual test is shown in Figure 4.

Inflatable seals will be tested in a separate test chamber and fixture. Because these seals are installed only in PWR and BWR Mark III-type containments, we will test both aged and unaged inflatable seals to pressure and temperature profiles for both PWR and BWR Mark III severe accident environments. Pressure inside the inflatable seals will be based on a survey of industry practices.

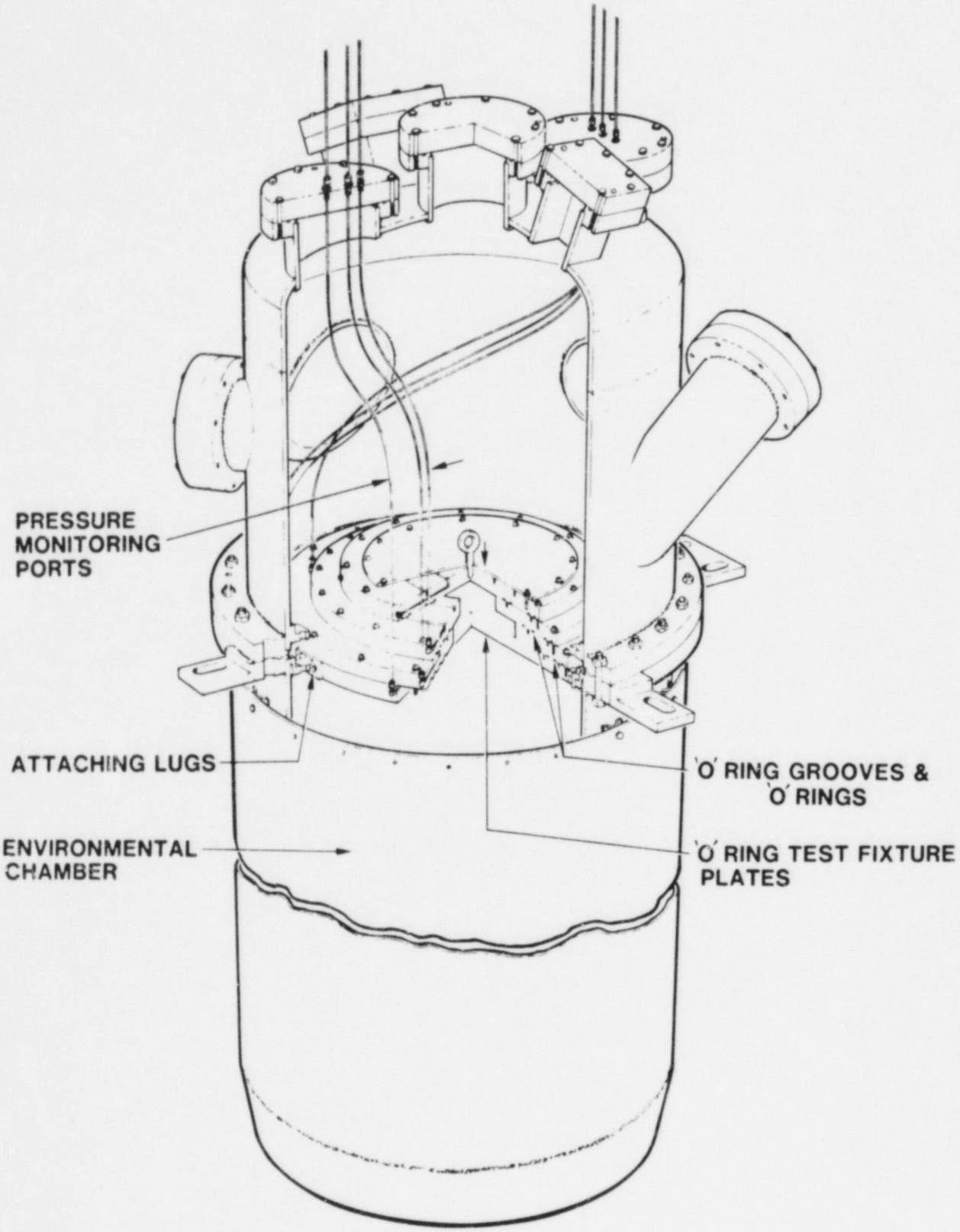


Figure 2. Environmental Test Chamber

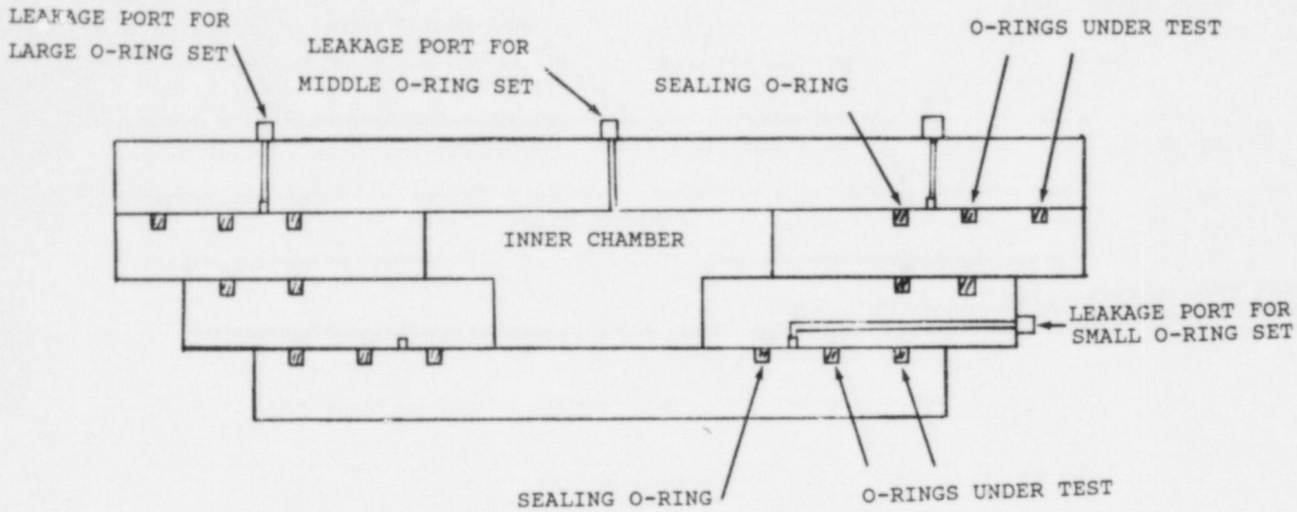


Figure 3. Test Fixture

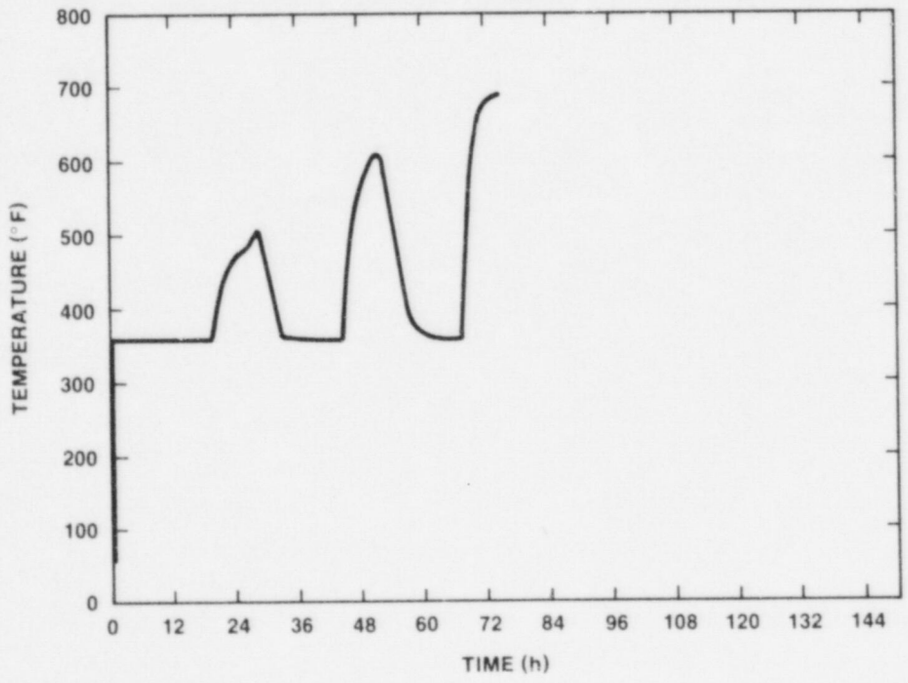


Figure 4. Typical Test Temperature History

2.2 Seal and Gasket Test Results

As of April 1986, we had completed testing of the 1/4-inch O-rings. We have also completed testing of unaged EPDM double dog-ear and double gumdrop seals. Our findings to date are:

- Seal materials degrade as a function of time and temperature. Depending on the seal material and environment, degradation took the form of melting, charring, brittleness, powder, etc.

- Leakage is limited or prevented when metal-to-metal contact is maintained at the sealing surface. In actual mechanical penetrations, the magnitude of leakage under these conditions may be higher because the surface finish and flatness of the sealing surfaces is probably not as good as in our test fixtures.

- The amount of squeeze has no apparent effect on the degradation of the seal. Metal-to-metal contact (30% squeeze) masks seal degradation by preventing or significantly limiting leakage.

- The degradation of silicone rubber under extreme environments is affected by its aging history. In a steam atmosphere, silicone rubber gaskets that were both radiated and thermally aged performed slightly better than unaged silicone rubber. Unaged silicone rubber gaskets typically failed to maintain a seal at about 500°F in a steam atmosphere. Aged silicone rubber failed to maintain a seal at about 550°F. In both cases squeeze was fixed. A decrease in squeeze during the test would probably result in leakage at lower temperatures.

- One-quarter-inch EPM/EPDM seals maintain a seal up to 650°F, regardless of aging history. As expected, the double dog-ear and double gumdrop EPDM unaged seals we tested began leaking at a lower temperature (600°F) than the 1/4-inch seals. [Typically the physical properties of a given material are degraded as cross-section increases].

- Samples are aged in a fixture at the same percent squeeze that is used during the severe accident test. When subjected to aging, either thermal or radiation, all materials retain a permanent set. As a result, any subsequent decrease in squeeze (i.e., any increase in gap size) would result in leakage depending on the degree to which resiliency is lost.

- Silicone rubber degrades at a significantly lower temperature in a steam environment than in either an air or a nitrogen environment (500°F versus 700°F). No

silicone rubber seals other than 1/4-inch O-rings have been tested.

- The degradation of EPM/EPDM is not affected by the atmosphere. One-quarter-inch EPM/EPDM O-rings typically did not leak at temperatures up to 650°F in nitrogen, air, or steam atmospheres.

- The effect of pressure on seal degradation was not investigated, but it is believed to be insignificant. Leak rate obviously depends on pressure. Higher pressures may also be more effective in eroding seal material, thus increasing leakage area.

- Leakage typically occurs over less than 30% of the seal length. It is reasonable to expect that, given time, erosion of the seal material would cause the leakage area to increase.

During posttest examinations, we found that seal material was extruded into the gaps between the sealing surfaces. We hypothesized that this material could prevent or delay leakage if the gaps were sufficiently small. This hypothesis was examined by testing two sets of unaged silicone 1/4-inch O-rings in a steam atmosphere at 0.012 and 0.006 inch gap (19% and 21% squeeze).

At 0.012 inch gap, we found that two of the three seal sets leaked after 2 h at 500°F. At 0.006 inch gap, no leakage occurred in any of the sets after 2 h at 500°F. No EPDM seals were tested at small gaps, but we would expect that they would exhibit a similar behavior.

Based on experimental observations, we conclude that seal degradation alone is not sufficient to permit significant leakage, provided continuous metal-to-metal contact is maintained at the sealing surfaces. Similarly, a loss of seal resilience alone is not sufficient to cause leakage unless accompanied by an increase in gap at the sealing surface. The increase in gap that will cause leakage is dependent on the degree to which the resilience of the seal is lost. Future tests will study the degree to which resilience is compromised due to radiation and thermal aging.

3.0 MECHANICAL PENETRATIONS

In the seal and gasket tests, we demonstrated the degradation of elastomeric materials resulting from severe accident environments. But degradation alone does not assure leakage; in most cases, loss of metal-to-metal contact at the sealing surface is also necessary for leakage to occur. For this reason, rotation, separation, and slip at the sealing surfaces of a mechanical penetration are important in assessing the potential for leakage. In a pressure-unseating configuration the loss of metal-to-metal contact results from direct pressure loading of the hatch. Mismatched bending response of a bulkhead and a door can cause gaps between the sealing surfaces in personnel airlocks. Differential diameter changes between a sleeve

and a hatch can also result in leakage if the mismatch is so large that a seal traverses from inside to outside the containment boundary. We have completed or are planning a number of tests to measure the deformation of sealing surfaces under severe accident pressures.

3.1 Personnel Airlock

To measure the deformation at the sealing surface, and to determine the environment that seals and gaskets would actually be subjected to during a severe accident, we plan to test a full-scale airlock in late 1986. The overall dimensions of the airlock are given in Figure 5. It consists of a cylindrical sleeve almost 20 ft long and 10 ft in diameter with a bulkhead near each end. A pressure-seating rectangular door 3 ft 6 inches by 6 ft 8 inches is mounted in each bulkhead and is sealed with a double dog-ear seal.

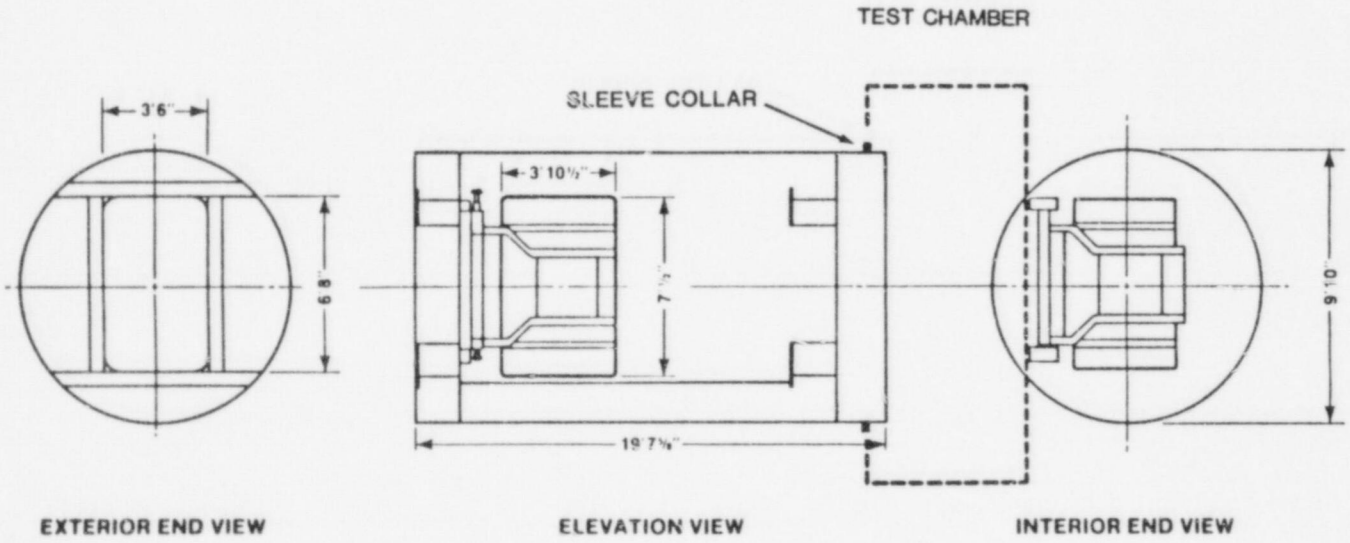


Figure 5. Personnel Airlock

The airlock will be mounted in an environmental chamber and subjected to a BWR Mark I postulated severe accident temperature and pressure profile. We will measure temperature, rotation, slip, and separation at the sealing surfaces of the doors and diameters along the axis of the sleeve, as well as leakage past both doors. The airlock doors are not initially in metal-to-metal contact, but because they are pressure-seating, metal-to-metal contact may be achieved as pressure increases if uniform (or approximate) squeeze occurs. We expect that

leakage (if any) will result from a combination of seal degradation and deformation of the sealing surfaces due to pressure loading.

3.2 Equipment Hatches

We tested two pressure-seating equipment hatch representations in a 1/8-scale steel containment model. Measurements of sleeve diameter, hatch diameter and slip, rotation, and separation at the sealing surface of the equipment hatches were made at each pressure step. Leakage for the whole model was monitored during hold periods when the model was isolated from the pressure system. Measurements showed that the equipment-hatch-sleeve diameter increased in the horizontal direction and decreased in the vertical direction. The change in diameter of the hatch was not significant compared to the change in diameter of the sleeve. The resulting mismatch at the sealing surfaces, however, did not result in leakage. The displacement histories of the sleeve and hatch diameters for one of the equipment hatches are shown in Figure 6. The shaded area between the curves represents slippage at the sealing surface. Only small rotations were measured at the sealing surface (<4° at 12 and 6 o'clock and <1° at 3 and 9 o'clock), and no leakage resulted. The hatch covers used in the 1/8-scale large steel model were stiffer than scaling laws would have dictated, but measurements from this test can still be used to qualify analytical predictive techniques. A more detailed discussion of the 1/8-scale model test results is contained in [5]; comparisons with analysis can be found in [6].

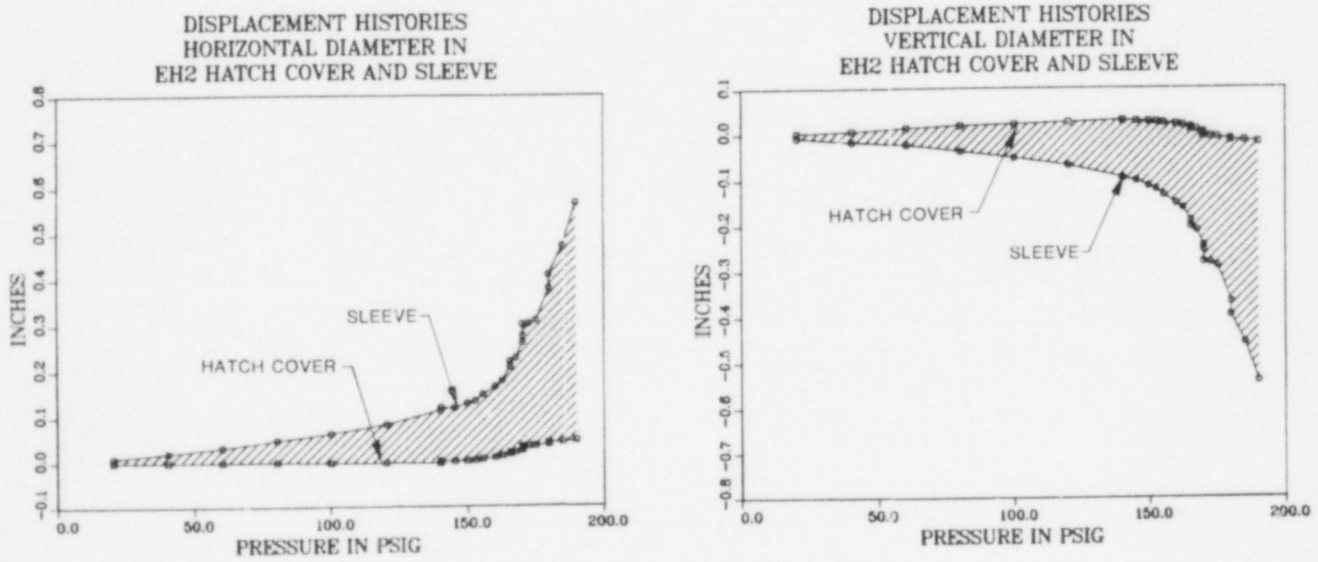


Figure 6. Diameters at Sealing Surface, 1/8-Scale Steel Model Equipment Hatch

Three equipment hatch designs will be tested in a 1/6-scale reinforced concrete model. Two of these hatch representations, one a pressure-seating and one a pressure-unseating, are installed at one opening. The pressure-unseating door is installed in the outside end of the sleeve and will be loaded first. A system of electrically actuated valves will allow us to remotely select which door is loaded. A second pressure-seating hatch representation of a different design is located in a separate penetration. The sealing surfaces and sleeves of both penetrations will be instrumented to measure deformation and strain.

3.3 Drywell Head

Drywell heads are large pressure-unseating covers (25 to 40 ft diameter) used in BWR Mark I, and II containments. The geometry of a drywell head is such that simple analytical methods can be used to predict structural response to pressure and temperature. In a BWR Mark I and II-type containments, accident temperatures are sufficient to degrade the seal, but loss of metal-to-metal contact in addition to seal degradation is necessary for leakage to occur. Independent analyses performed by Argonne National Laboratory [7] and SNLA [2] show that the temperature differential between the drywell head tie-down bolts and the drywell head flanges has the effect of additional preload which delays separation of the sealing surfaces. Possible exceptions are poor flatness or a rough surface finish such that metal-to-metal contact is not achieved.

Further insight into the behavior of a drywell head will be gained from the 1/6-scale reinforced concrete model to be tested in 1987.[1] A pressure-unseating equipment hatch in this model has a geometry similar to that of a drywell head. Data gathered during the test can be compared with analytical predictions to verify their accuracy.

4.0 SUMMARY

Several programs are being conducted by Sandia for the Nuclear Regulatory Commission to examine the failure modes of nuclear reactor containment buildings that are subjected to a severe accident environment. This paper discusses a program that is evaluating leakage through mechanical penetrations. Tests on seal and gasket materials are determining what effect factors such as aging, atmosphere, squeeze, and seal material and geometry have on seal performance during a severe accident. Leakage through mechanical penetrations is also dependent, in general, upon mechanical deformations at the sealing surfaces. Tests are being conducted on mechanical penetrations in conjunction with tests on scale models of containment buildings, so that mechanical deformations can be measured. In addition, a full-scale personnel airlock will be tested to severe accident conditions, including temperature and pressure. No test of a drywell head is planned, but conclusions can be drawn

based on analytical predictions and comparisons with the performance of the pressure unseating equipment hatch in the 1/8-scale reinforced concrete model test. Results from all tests in the program will be used to develop methodologies for predicting containment performance in a severe accident.

ACKNOWLEDGMENTS

The author acknowledges Bob Padilla, Pat Drozda, Stella St. Clair, George Dibisceglie, John Lewin, Bob Ayers and Dwight Lambert for their efforts in planning and executing the seal and gasket tests. Thanks are also given to Dan Horschel for his assistance in testing mechanical penetrations in the scale containment models and to Dave Clauss for his input into establishing test parameters.

References

[1] D.S. Horschel, J. Jung, "Construction and Analysis of a 1/6th-Scale Concrete Containment Model," 3rd Containment Workshop on Containment Integrity, Washington D. C., May 21-23, 1986.

[2] D.B. Clauss, "Failure Mechanisms for LWR Steel Containment Buildings Subject to Severe Accident Loadings," 3rd Containment Workshop on Containment Integrity, Washington D. C., May 21-23, 1986.

[3] J. Keck, F. Thome, "Leak Behavior Through EPAs Under Severe Accident Conditions," 3rd Containment Workshop on Containment Integrity, Washington D. C., May 21-23, 1986.

[4] C.V. Subramanian, "Integrity of Containment Penetrations Under Severe Accident Conditions," Proc. 8th SMiRT Conf., Brussels, Belgium, August 19-23, 1985, Paper J 4/2.

[5] L.N. Koenig, "The Test of a Large Steel Containment Model," NUREG/CR-4216, SAND85-0790, Sandia National Laboratories, Albuquerque, NM, to appear.

[6] D.B. Clauss, "Comparison of Analytical Predictions and Experimental Results for a 1:8-Scale Steel Containment Model Pressurized to Failure," NUREG/CR-4209, SAND85-0679, Sandia National Laboratories, Albuquerque, NM, July 1985.

[7] R.F. Kulak et al., "Structural Response of Large Penetrations and Closures for Containment Vessels Subjected to Loadings Beyond the Design Basis," ANL-84-41, July 1984.

Leak Behavior Through EPAs Under Severe Accident Conditions*

by
J. D. Keck and F. V. Thome
Sandia National Laboratories
Albuquerque, New Mexico

Abstract

The leakage behavior of electrical penetration assemblies (EPAs) is being evaluated by varying the penetration type, manufacturer, and hypothetical temperature and pressure accident profile. Nuclear qualified EPAs were procured from D. G. O'Brien, Westinghouse, and Conax. Severe-accident-sequence-analysis was used to generate the severe-accident-conditions (SAC) for a large dry PWR, a BWR Mark I drywell, and a BWR Mark III wetwell. The EPA manufacturers were matched to the reactor type based on a survey of EPAs used in reactors. The D. G. O'Brien EPA was chosen for the PWR SAC, the Westinghouse was chosen for the BWR Mark III, and the Conax was chosen for the BWR Mark I. The EPAs were radiation and thermal aged to a 40 year service life before the SAC test was conducted. For the D. G. O'Brien EPA SAC test, while there was no detectable leakage during the SAC test, there was a 0.13 scc/sec leak measured during the posttest inspection. For the Westinghouse EPA SAC test, there was no detectable leakage during or after the SAC test. The Conax EPA SAC test is scheduled for completion in July, 1986.

1.0 INTRODUCTION

Electrical penetration assemblies (EPAs) allow electrical energy to pass through the containment building while maintaining a pressure boundary. The electrical energy can be for instrumentation, control, or power applications. EPAs have evolved into a basic design that consists of modules containing electric feedthroughs that are sealed into a modified blank flange called a header-plate (Figure 1). The modules can be sealed into the header-plate in a variety of ways, that include glass-to-metal seals, O-ring seals, and metal-to-metal compression seals.[1] The header-plate is either bolted to a flange on the sleeve or welded to the sleeve directly. All of the EPAs tested in this program are bolted to a flange and sealed with double O-rings. An enclosure box is attached to the header-plate to protect the electrical connections made to the EPA wiring.

* This paper was supported by the U.S. Nuclear Regulatory Commission, Office of Reactor Safety Research, as part of the Electrical Penetration Assemblies (EPA) Program (FIN #A-1364) being conducted by Sandia National Laboratories, under Interagency Agreement DOE-40-550-75.

As part of an effort to evaluate "containment integrity" under severe accident conditions, EPAs were singled out as having "One of the largest uncertainties associated with predicting the amount of radionuclides released"[2]. This potential led to a study of EPAs by Sebrell[1] to assess the leak paths and potential for leakage through EPAs in Light Water Reactor (LWR) containment buildings. Some examples of maximum permissible leak-rates for nuclear plants[3], assuming 10% of the primary-containment volume per day for the severe accident condition (SAC), are:

Nuclear Plant	Number of EPAs	Leak-rate/EPA (scc/sec)
Browns Ferry	30	328
Watts Bar	53	740
Bellefonte	69	1610

At the same time there were severe-accident-sequence-analysis studies conducted at Sandia National Laboratories (SNL) and Oak Ridge National Laboratories (ORNL) that predicted temperature and pressure accident profiles for various reactor and containment types. These studies indicated that the inside containment temperature could go to 700°F (one study predicted even higher). SAC temperature/pressure profiles were developed from these studies for large PWR, BWR Mark I drywell, and BWR Mark III wetwell containments[3].

Another aspect of the Sebrell study was to identify the different EPA vendors in addition to the designs and materials for EPAs. In a review of 65 nuclear plants, 18 different vendors were identified with only 3 still in business: D. G. O'Brien, Westinghouse, and Conax. This translated to 2700 EPAs of which 650 are from current suppliers. Many of the early EPAs were constructed in-place and were not subject to stringent nuclear testing standards. Early EPA designs that are not available for testing would have to be evaluated as best as possible based on the materials and type of construction. Many of the EPAs were and are still made using epoxies and other plastics that cannot withstand high temperatures; i.e., 400 to 500°F. Some EPAs are installed utilizing pipe-type flanges and O-rings. These O-rings are elastomeric and are either silicone, EPR, or Viton rubber with the same range of temperature limitations as the plastics.

An ORNL study for a severe accident case at Browns Ferry I (BWR Mark I) indicated that high temperatures in the dry well area would result in high EPA seal temperatures that could soften and blow-out EPA seals[4]. Some basic modeling was undertaken to predict EPA seal temperatures for various temperature/pressure profiles. However, the uncertainties associated with the models resulted in the testing program described in this report. The objectives of this program are to:

1. evaluate the performance of and determine the leak rates through 3 current EPA designs,
2. use PWR and BWR profiles,
3. provide test data on material performance under SAC profiles,
4. provide test data that is useful for predicting the onset of leakage, and
5. measure electrical performance.

2.0 TEST PROGRAM

As a result of the Sebrell study, EPA designs were selected and matched with SAC profiles based on several criteria. Not all available EPA designs would be tested for all possible SAC temperature/pressure profiles. The criteria for the EPA design and SAC test profile were:

1. EPA design with highest potential for leakage,
2. EPA availability,
3. nuclear power plants near large population centers, and
4. matched EPA design with respective SAC profile for reactor type.

The selection and matching process resulted in the following test program:

1. D. G. O'Brien for a large PWR SAC.
   From ambient temperature and pressure, rise to 293°F and 60 psia steam in 30 seconds and then to 361°F and 155 psia in 12 hours, the steam pressure will follow the temperature to maintain a saturated state. The temperature and pressure will then be held at 361°F and 155 psia for the remainder of the 10 day test (Figure 2).

2. Westinghouse for a BWR Mark III SAC.
   From ambient temperature and pressure, rise to 250°F and 30 psia steam (saturated steam) in 2 hours, and then to 400°F and 75 psia steam (superheat) in 12 hours. The temperature and pressure will then be held at 400°F and 75 psia for the remainder of the 10 day test (Figure 3).

3. Conax for a BWR Mark I SAC.
   From ambient temperature and pressure, rise to 700°F and 85 psia steam in 25 minutes, and then to 135 psia steam at 700°F in 200 minutes under superheated steam. The temperature and pressure will then be held at 700°F and 135 psia for the remainder of the 10 day test (Figure 4).

There were other considerations for the test program, most of which are listed below.

1. Aged to the end of "Service Life".
   Radiation (aged and accident), 200 Mrad (air).
   Thermal, D. G. O'Brien: 275°F for 168 hours.
   Westinghouse and Conax: 300°F for 100 hours.
2. No separate LOCA steam (initial portion of SAC test includes LOCA).
3. No chemical spray.
4. No movement of EPA or cables between thermal age and SAC test except for visual examination.
5. No fault current testing.
6. Circuit continuity and insulation resistance will be measured during the SAC test.
7. No pressure cycle testing of the EPA by "pre-loading" at 100 to 115 % of the design pressure.
8. No effort to duplicate containment-shell/EPA-sleeve deformation test program.
9. Monitor leakage through O-ring seal between EPA header-plate and the containment sleeve (nozzle).
10. All EPAs will be tested with the junction (enclosure) box installed.
11. All purchases are for nuclear-qualified components built to IEEE 317-1976 and 323-1978 standards.
12. Each EPA will be tested in a pressure vessel that simulates the power plant sleeve and containment building interface. This simulation will approximate the sleeve and containment building heat sink during the SAC test.
13. These SAC tests are to collect engineering data and are not Qualification Tests.

3.0 EXPERIMENTAL

EPAs were procured as nuclear-qualified components built to IEEE 317-1976 and 323-1978 standards from the three suppliers. The D. G. O'Brien EPA was built to the same design as Duke Power's McGuire 1 and 2 and Catawba 1 and 2 stations. The Westinghouse EPA was built to the same design as Phibbs Bend and Stride stations. The Conax EPA was built to the same design as TVA's Browns Ferry 1 and 2 and Detroit Edison's Fermi 2 stations. The EPAs were built with a mix of instrumentation, control, and low voltage power penetrations (the D. G. O'Brien also had a medium voltage power penetration).

Pressure vessels were constructed to approximate the EPA-sleeve and containment building interface. This arrangement reproduces the heat source for the EPA from the SAC and the heat sink of the reactor containment building. The sleeve/pressure-vessel also serves as a collection vessel for leakage condensation. The same pressure vessel was used for both the D. G. O'Brien and Westinghouse EPA tests because the EPA installations are nearly the same at the McGuire/Catawba and Stride/Phibbs Bend power stations. The pressure vessel for the Conax EPA test simulates the EPA installation at Browns Ferry/Fermi 2.

Before conducting the SAC tests, the EPAs were both radiation and thermal aged, in that order, to the end of a 40 year "service life". The EPAs were irradiated to 200 Mrad (air) at 0.5 to 1.0 Mrad/hour. The 200 Mrad total dose included both radiation from aging and the postulated accident sequence. The Conax and Westinghouse EPAs were heated to 300°F for 100 hours and the D. G. O'Brien EPA was heated to 275°F for 168 hours. The time and temperature conditions were based on the suppliers qualification procedures for the materials used in the EPAs to meet the IEEE standards.

In order to accomplish the major objective of evaluating leak-rates through EPAs, an extensive leak-rate measuring system was developed. All calibrations were done using air, at various temperatures and pressures, directed through calibrated orifices to conventional air-flow measuring instruments. Steam flow through the same orifice arrangement was then measured at various temperatures and pressures by collecting the condensate and comparing the steam flow to the air flow on a mass flow basis. This system proved accurate and reliable for the range of less than 1 scc/sec to greater than 10,000 scc/sec[5].

After closing the pressure vessel and prior to starting the SAC test, a leak test was performed at room temperature with air. The pressure was 155 psia for the D. G. O'Brien EPA and 75 psia for the Westinghouse EPA. The Conax EPA has not been tested at this time. This leak test was to establish a baseline leak-rate through the EPA after aging and to check the pressure vessel for leaks. For both the D. G. O'Brien and Westinghouse EPA tests, there were no detectable leaks through the EPA or pressure vessels prior to the SAC tests. The same leak test was made after the SAC test was completed and the pressure vessel and EPA had cooled to room temperature.

During the SAC test, the insulation resistance of each cable circuit was monitored with an individual electrical power supply and monitoring circuit. A DC power supply provided about 0.5 amps of continuous current to each cable circuit. In addition, the monitoring circuit determined the insulation resistance to ground for a range of 25E+06 to 50E+03 ohms. The output from the monitoring circuit was recorded on an automatic datalogger. In addition, the insulation resistance was measured at 50 to 500 VDC several times a day with a Hippotronics Megohm Meter to backup and check the continuously recorded data.

4.0 RESULTS

4.1 D. G. O'Brien PWR SAC Test

The D. G. O'Brien SAC test was completed according to the temperature/pressure accident conditions. There were no detectable leaks through the EPA during the steam pressurized portions, including none through the header plate O-ring seals also called the aperture seal. A posttest air leak-rate

measurement at ambient temperature and 155 psia produced a leak on the order of 0.13 scc/sec. The electrical system on the EPA for all modules degraded over the first 2 days to the point that all modules measured <1E+06 ohms to ground at 50 volts, and 5 out of the 8 circuits were passing 0.5 amp to ground after 10 days. One-half amp is the maximum current permissible in the circuit we designed for monitoring the current to ground. The posttest inspection showed all but one module to be electrically faulty and the preliminary indication is that moisture traveled through the connector (also referred to as a plug) and grounded out between the module pin and the metal "mask" that surrounds each pin. It is this bridging with moisture or contaminates that cause the short to ground. There was posttest evidence of significant corrosion and chemical attack during this test. There was also a large amount of polysulfone expansion out from inside the plug bonnets and in some cases seizing between the plug and receptacle. It is important to recognize that this was a test that exceeded the design of the EPA. It was designed for 65 psig and 330°F. Our test had a pressure as high as 155 psia and a temperature as high as about 390°F.

4.2 Westinghouse BWR Mark III SAC Test

The Westinghouse SAC test was completed according to the temperature/pressure accident conditions. There were no detectable leaks through the EPA including the header-plate O-ring seals during the steam pressurized portions of the test and during the posttest air leak-rate measurement at 75 psia.

The electrical performance of the EPA during the steam test was more a function of the EPA cables used rather than the EPA design. The first low resistance between an EPA cable and ground occurred in one of the ITT Suprenant thermocouple cables at 64 hours after the start of the SAC test. The resistance to ground of one conductor dropped from 3E+06 ohm at 500V to 1.5 Kohm. The insulator was probably damaged by the 500V potential of the Megohm meter because the resistance dropped so quickly and then slowly recovered to 1E+06 ohm at 500V. All of the EPA thermocouple insulators failed in a similar manner, the resistance dropped suddenly from a value greater than 1E+05 ohm to less than 3E+04 ohm after an IR measurement with the Megohm meter. The use of the 50V to 500V potential to measure the insulation resistance of a thermocouple cable is a severe test, considering that the cable will only see a potential of less than 0.1V. The measurement probably overstressed the cable and accelerated the degradation.

For the Rockbestos 2 conductor, #16 AWG, each individual conductor had a resistance to ground through the conductor-insulator and jacket to ground of greater than 1E+06 ohm at 500V for 4 days and of greater than 4E+05 ohm at 100V at the end of the test. However, at 24 hours, the resistance between the conductors through the conductor-insulators dropped to 15K ohm and then recovered to 6E+05 ohm at 100V by 48 hours.

Even though the individual conductors had good insulation resistance to ground, the resistance between conductors periodically dropped to 10K to 50K ohm.The Okonite #2 AWG cable insulation resistance gradually degraded from 1E+07 ohm at 500V at 6 hours to 2E+05 ohm at 100V in 64 hours and down to 10K - 50K ohm at the end of the test. The Raychem #14 AWG cable gradually degraded from 3E+07 ohm at 500V at 6 hours to 3E+05 ohm at 100V at the end of the test. All of the cables recovered significantly during cooling.

4.3 Conax BWR Mark I SAC Test

The Conax SAC test is scheduled for completion in July 1986.

5.0 CONCLUSIONS

Both the D. G. O'Brien and Westinghouse EPAs did not leak during their respective 10 day SAC tests. The D. G. O'Brien did develop a small leak, 0.13 scc/sec, after the SAC test was completed and the EPA had cooled to room temperature. The Westinghouse did not leak after cooling to room temperature.

The electrical systems of both EPAs would probably have functioned as designed for the first 24 hours of the SAC tests. After that time, the performance of the electrical system would be dependent on the specific voltage, current, and impedence requirements for a given cable or feedthrough.

REFERENCES

1. W. A. Sebrell, The Potential for Containment Leak Paths Through Electrical Penetration Assemblies Under Severe Accident Conditions, NUREG/CR-3234, SAND83-0538, Sandia National Laboratories, Albuquerque, New Mexico, July 1983.

2. Technical Basis for Estimating Fission Product Behavior During LWR Accidents, NUREG-0772, Office of Nuclear Regulatory Research, USNRC, June 1981.

3. C. V. Subramanian and W. A. Sebrell, Test Plan for Evaluating Leak Behavior Through Electrical Penetration Assemblies Under Severe Accident Conditions,Sandia National Laboratories, Albuquerque, New Mexico, February 1984.

4. D. H. Cook et al, Station Blackout at Browns Ferry Unit One - Accident Sequence Analysis, NUREG/CR-2182, ORNL/NUREG/TM-455/V1, Oak Ridge National Laboratories, Oak Ridge, Tennessee, November 1981.

5. J. W. Grossman, F. V. Thome, and G. M. Dibisceglie, Flow Measurement Techniques For Evaluating Leak Behavior Through Electrical Penetration Assemblies Under Severe Accident Conditions, SAND 86-0756 Sandia National Laboratories, Albuquerque, New Mexico, March 1986.

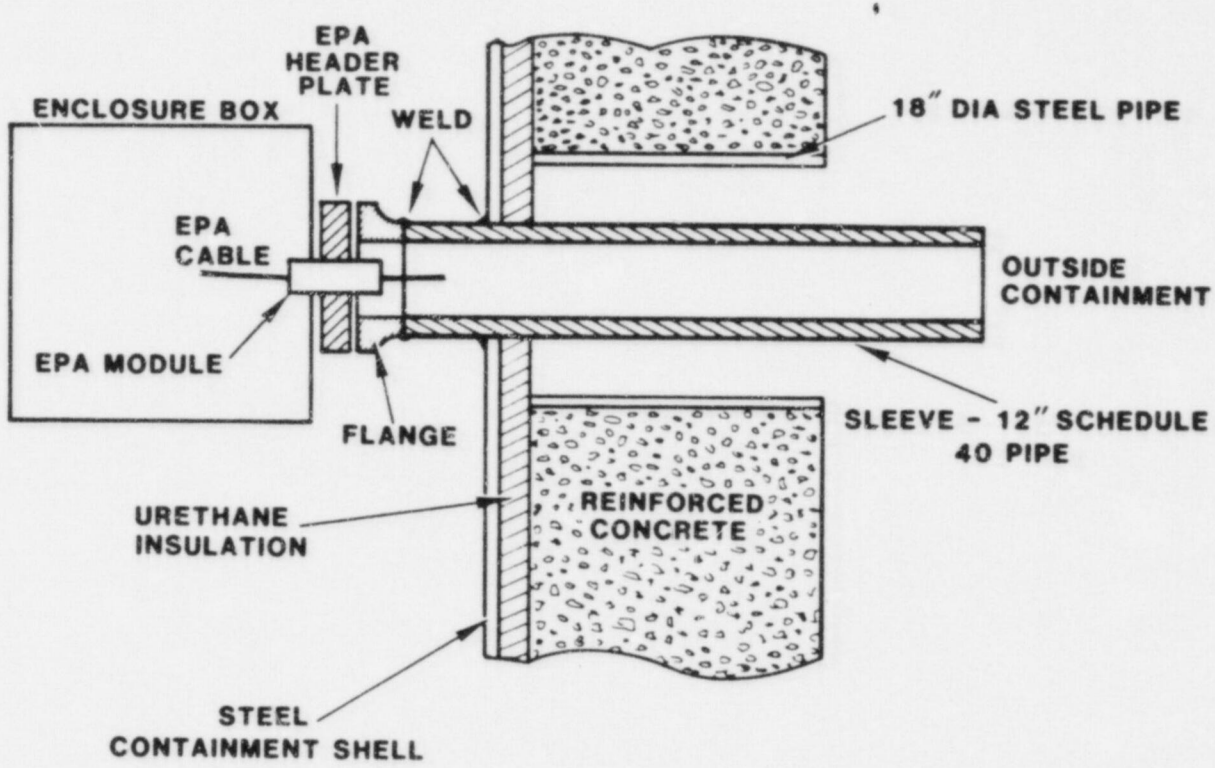


Figure 1: EPA Installed in Sleeve.

TEST PROFILES FOR PWRs

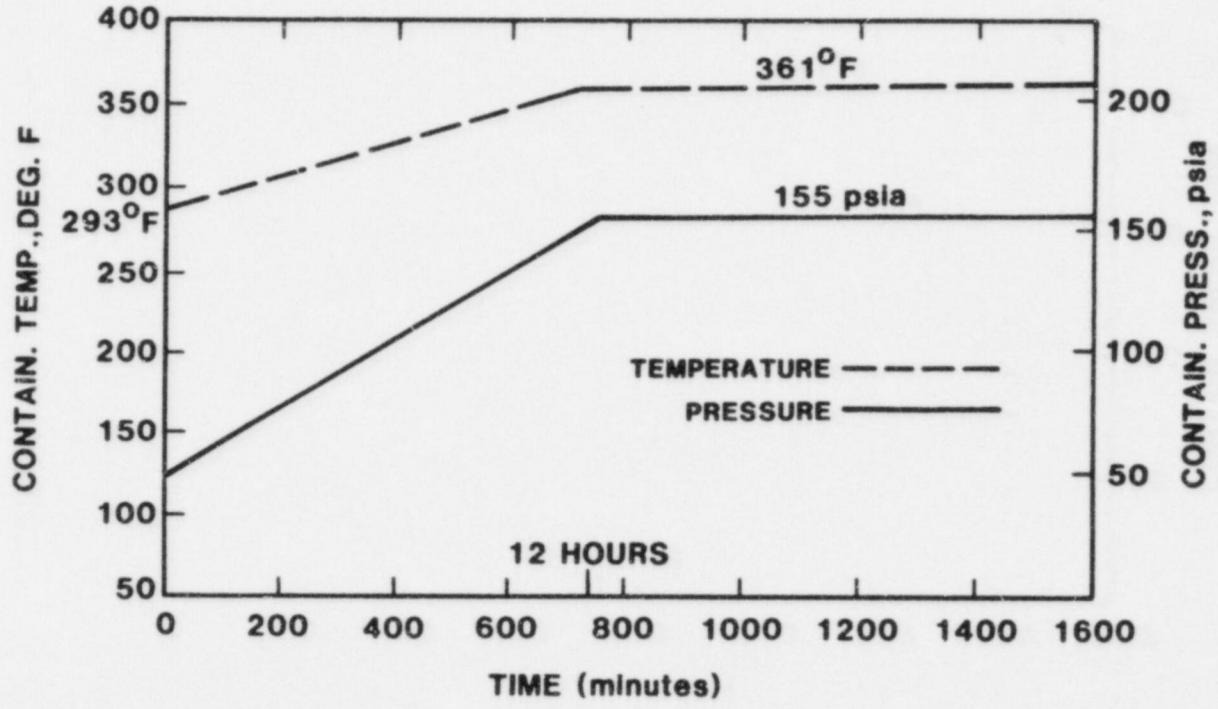


Figure 2.

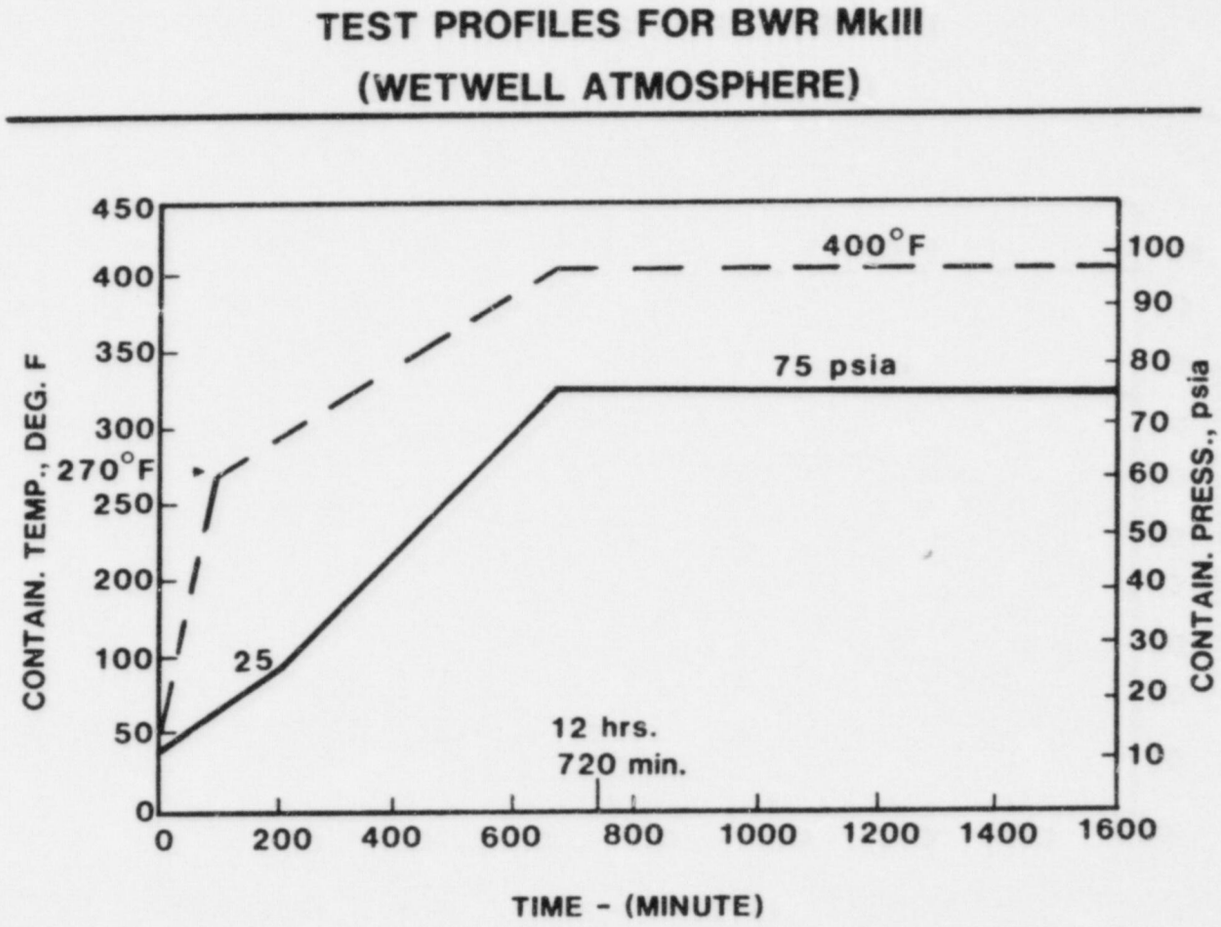

TEST PROFILES FOR BWR MkIII
(WETWELL ATMOSPHERE)
CONTAIN. TEMP., DEG. F
CONTAIN. PRESS., psia
400°F
75 psia
270°F
25
12 hrs.
720 min.
TIME - (MINUTE)
0
50
100
200
250
300
350
400
450
10
20
30
40
50
60
70
80
90
100
0
200
400
600
800
1000
1200
1400
1600

Figure 3.

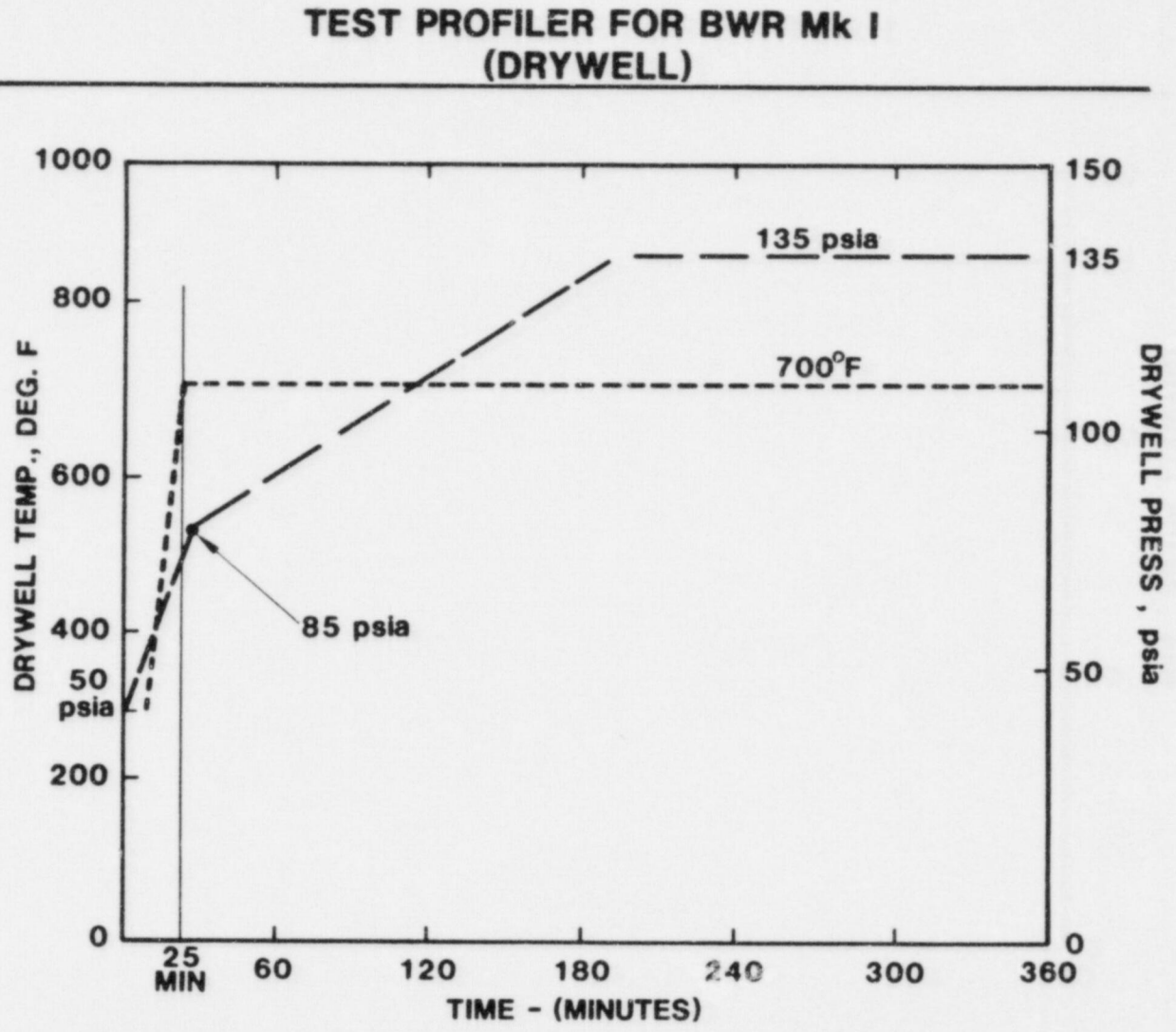

TEST PROFILER FOR BWR Mk I
(DRYWELL)
1000
800
600
400
50
psia
200
0
DRYWELL TEMP., DEG. F
150
135
100
50
0
DRYWELL PRESS , psia
135 psia
700°F
85 psia
25
MIN
60
120
180
240
300
360
TIME - (MINUTES)

Figure 4.

Distribution:
U. S. Government Printing Office
Receiving Branch (Attn: NRC Stock)
8610 Cherry Lane
Laurel, MD 20707
535 copies for R1, RD, RM

List of Attendees (137 copies)

US Nuclear Regulatory Commission
Division of Engineering Technology
5650 Nicholson Lane
Rockville, MD 20852
Attn: Hans Ashar (10 copies)

US Nuclear Regulatory Commission
Mechanical/Structural Engineering Branch
5650 Nicholson Lane
Rockville, MD 20852
Attn: J. F. Costello (10 copies)

US Department of Energy
Office of Nuclear Energy
Washington, DC 20545
Attn: A. Millunzi, D. Giessing
D. Harrison, C. Thompson
Bernard J. Rock (5 copies)

NUTECH
225 W. Michigan Ave.
16th Floor
Chicago, Illinois 60601
Attn: John Clauss

TVA
400 Commerce Ave.
Knoxville, TN 37902
Attn: D. Denton, W9A18

Los Alamos National Laboratories
PO Box 1663
Mail Stop N576
Los Alamos, NM 87545
Attn: C. Anderson
T. Butler (2 copies)

EQE Inc.
3300 Irvine Aveune
Suite 345
Newport Beach, CA 92660
Attn: M. K. Ravindra

EBASCO Services, Inc.
Two World Trade Center
New York, NY 10048
Attn: R. C. Iotti

HM Nuclear Installation Inspectorate
Thames House North
Millbank, London, SW1
UNITED KINGDOM
Attn: R. J. Stubbs,
T. Currie (2 copies)

Dept. of Energetic Systems
Southwest Research Institute
6220 Culebra Rd.
PO Drawer 28510
San Antonio, TX 78284
Attn: Wilfred E. Baker
P. A. Cox (2 copies)

William C. Black
2650 Woodside Road
Bethlehem, PA 18017

Battelle Columbus Laboratories
505 King Avenue
Columbus, Ohio 43201
Attn: Richard Denning

Bechtel Power Corp.
15740 Shady Grove Rd.
Location 1A-7
Gaithersburg, MD 20877
Attn: T. E. Johnson
K. Y. Lee (2 copies)

Dept. of Civil Engineering
University of Illinois
503 W. Michigan
Urbana, IL 61801
Attn: Mete A. Sozen

EG&G Idaho
Willow Creek Bldg. W-3
PO Box 1625
Idaho Falls, ID 83415
Attn: B. Barnes, T. L. Bridges
(2 copies)

Sargent & Lundy Engineers
55 E Monroe St.
Chicago, IL 60603
Attn: A. Walser

General Electric Company
175 Curtner Ave.
San Jose, CA 95125
Attn: R. Gou, MC 754
K. Stalter, MC 755
M. Larsen, MC 528
(3 copies)

R. F. Reedy, Inc.
236 N Santa Cruz Ave.
Los Gatos, Ca 95030

Quadrex Corporation
1700 Dell Ave.
Campbell, CA 95008
Attn: Quazi A. Hossain

Chiapetta, Welch & Associates. Ltd.
9748 Roberts Rd.
Palos Hills, IL 60465
Attn: R. L. Chiapetta

Martin Marietta Energy Systems, Inc.
Building 9108
PO Box Y
Oak Ridge, TN 37831
Attn: Steve Hodge

Brookhaven National Laboratory
Upton, NY 11973
Attn: Trever Pratt, Morris Reich
Charles Hofmayer, Ted Ginsberg
(4 copies)

Electrical Power Research Institute
3412 Hillview Avenue, PO Box 10412
Palo Alto, CA 94304
Attn: Y. K. Tang, Ian Wall
Raf Sehgal, W. Loewenstein
J. J. Taylor (5 copies)

School of Civil & Environ. Engr.
Hollister Hall Cornell University
Ithaca, NY 14853
Attn: Richard N. White

Argonne National Laboratory
9700 South Cass Avenue
Argonne, IL 60439
Attn: T. R. Bump, B. J. Hsieh,
J. M. Kennedy, R. F. Kulak
R. W. Seidensticker,
G. A. McLennan (6 copies)

Tennessee Valley Authority
400 Summit Hill Rd.
W9D24C-K
Knoxville, Tennessee 37902
Attn: Nathaniel Foster

University of Wisconsin
Nuclear Engineering Dept.
Madison, WI 53706
Attn: Michael Corradini

Dept. of Chemical & Nuclear Engineering
University of California Santa Barbara
Santa Barbara, CA 93106
Attn: T. G. Theofanous

Institut für Mechanik
Universität Innsbruck
Technikerstr 13
A-6020 Innsbruck
Austria
Attn: G. I. Schuëller

Nuclear Studies & Safety Dept.
Ontario Hydro
700 University Avenue
Toronto, Ontario
M5G 1X6
Canada
Attn: W. J. Penn

University of Alberta
Dept. of Civil Engineering
Edmonton, Alberta, CANADA T6G 2G7
Attn: D. W. Murray

Commissariat a L'Energie Atomique (CEA)
Centre d'Etudes Nucleaires de Saclay
F-91191 Gif-Sur-Yvette Cedex
France
Attn: M. Livolant, P. Jamet
A. Hoffmann (3 copies)

Staatliche Materiapruefungsanstalt (MPA)
University of Stuttgart
Pfaffenwaldring 32
D-7000 Stuttgart 80
Federal Republic of Germany
Attn: K. F. Kussmaul

Gesellschaft fuer Reaktorsicherheit (GRS)
Schwertnergasse 1
D-5000 Köln 1
Federal Republic of Germany
Attn: H. Schulz

Ente Nazionale per l'Energia Elettrica
v. le Regina Margherita, 137
Rome
Italy
Attn: Francesco L. Scotto

MPR Associates, Inc.
1050 Connecticut Ave. NW
Washington, DC 20036
Attn: William R. Schmidt

Nuclear Equipment Design Dept.
Hitachi Works, Hitachi, Ltd.
3-1-1 Saiwai-Cho
Hitachi-Shi
Ibaraki-ken
Japan
Attn: O. Oyamada

University of Tokyo
Institute of Industrial Science
22-1, Roppongi 7
Minatu-ku
Tokyo
Japan
Attn: H. Shibata

Civil Engineering Laboratory
Central Research Institute of
Electric Power Industry
1646 Abiko Abiko-Shi Chiba
Japan
Attn: Yukio Aoyagi

Kajima Corporation
No. 1-1, 2-Chome Nishishinjuku
Shinjuku-ku
Tokyo 160
Japan
Attn: K. Umeda

Nuclear Power Engineering Test Center
6-2, 3-Chome, Toranomor
Minatoku
Tokyo 105
Japan
Attn: Yoshio Tokumaru

Studsvik Energiteknik AB
S-611 82 Nyköping
Sweden
Attn: Kjell O. Johansson

Swedish State Power Board
Nuclear Reactor Safety
S-162 87 Vällingby
Sweden
Attn: Hans Cederberg
Per-Eric Ahlström
Wiktor Frid (3 copies)

Swiss Federal Institute of Technology
Institute of Structural Engineering
ETH-Hoenggerberg, HIL
CH-8093 Zurich
Switzerland
Attn: W. Ammann

Motor-Columbus Consulting Engineers, Inc.
Parkstrasse 27
CH-5401 Baden
Switzerland
Attn: K. Gahler, A. Huber
A. Schopfer (3 copies)

EIR (Swiss Federal Institute for
Reactor Research)
CH-5303 Wuerlingen
Switzerland
Attn: O. Mercier

Swiss Federal Nuclear Safety Inspectorate
Federal Office of Energy
CH-5303 Wuerenlingen
Switzerland
Attn: S. Chakraborty

Taylor Woodrow Construction Limited
345 Ruislip Road
Southall, Middlesex
UB1 2QX
United Kingdom
Attn: Carl C. Fleischer
Richard Crowder (2 copies)

Central Electricity Generating Board
Barnett Way
Barnwood, Gloucester
GL4 7RS
United Kingdom
Attn: J. Irving

Librarian
Earthquake Engineering Res. Ctr. Library
University of California/453 R.F.S.
1301 South 46th St.
Richmond, CA 94804

S.P.S.B.
P. O. Box 11113
Albuquerque, NM 87192
Attn: Terry Horn

Empresa Nuclear Argentina de
Centrales Electricas S.A.
Av. Leandro N. Alem 712
1001 Buenos Aires
Argentina
Attn: G. Sanchez Sarmiento

Southwest Center of the Nuclear
Reactor Engineering Research & Design
Ministry of Nuclear Industry
P. O. Box 291
Chengdu, Sichuan
P. R. of China
Attn: Fang-yu Gu

Kraftwerk Union AG
Berliner str. 295-299
Postfach 962
6050 Offenbach/Main
Federal Republic of Germany
Attn: Axsel Andersen

Oral Buyukozturk
Dept. of Civil Engineering
Mass. Institute of Technology
Cambridge, MA 02139
Attn: Michael Fardis

Pickard, Lowe and Garrick, Inc.
17840 Skypark Blvd.
Irvine, CA 92714
Attn: A. Torri

Laboratory for Building Materials
Swiss Federal Institute of Technology
Chemin de Bellerive 32
CH-1007 Lausanne
Switzerland
Attn: Folker H. Wittmann

Nuclear Research Development
DG XII-JRC
Commission of the European Communities
200 rue de la Loi
B-1049 Brussels
Belgium
Attn: Sergio Finzi

Commission of the European Communities
Applied Mechanics Division
JRC, Ispra Establishment
I-21020 Ispra
Italy
Attn: Jean Donea
L. Hannes Larsson (2 copies)

Universidad Politecnica
Laboratorio de Tecnologia Nuclear
El Catedratico
28006 Madrid
Spain
Attn: A. Alonso

Muto Institute of Structural Mechanics
Shinjuku-Ku
Tokyo 160
Japan
Attn: Norihide Koshika

Japan Atomic Energy Research Institute
Tokai-mura
Ibaraki-ken 319-11
Japan
Attn: Kunihisa Soda

Elektrowatt Ingenieurunternehmung AG
CH-8022 Zürich
Switzerland
Attn: John P. Wolf

URS/BLUME Engineers
150 Fourth St.
San Francisco, CA 94103
Attn: Ronald P. Gallagher

Departamento Sequridad Nuclear
Junta de Energia Nuclear
Avda. Complutense, 22
Madrid-3
Spain
Attn: B. G. del Valle

Imatran Voima Oy
P. O. Box 138
00101 Helsinki 10
Finland
Attn: J. Ikänen

Isa Sihweil
c/o CCC
P. O. Box 61092
Amaroussion 15110
Athens, GREECE

Westinghouse Electric Corporation
P. O. Box 79
BAT 33 NN
West Misslin, PA 15122

Sen-I Chang
Institute of Nuclear Energy Research
P. O. Box 3
Lung-Tan, Taiwan 325
Republic of China

Pilsoon Han
Korea Advanced Energy Research Institute
P. O. Box 7 Cheong Ryang
Seoul, Korea

1520 D. J. McCloskey
1523 C. Conley
1833 G. A. Knorovsky
3141 S. A. Landenberger (5)
3151 W. L. Garner
6400 A. W. Snyder
6410 J. W. Hickmann
6412 A. L. Camp
6415 F. E. Haskin
6420 J. V. Walker
6425 K. Matsumoto
6427 M. Berman
6427 M. Sherman
6442 W. A. von Riesemann (20)
6442 D. L. Lambert
6442 T. D. Molina (5)
6442 J. J. Westmoreland
6444 L. D. Buxton
6447 D. L. Berry
8024 P. W. Dean

NRC FORM 335 (2-84) NRCM 1102, 3201, 3202

U.S. NUCLEAR REGULATORY COMMISSION

BIBLIOGRAPHIC DATA SHEET

SEE INSTRUCTIONS ON THE REVERSE

1 REPORT NUMBER (Assigned by TIDC, add Vol. No., if any)
NUREG/CP-0076
SAND86-0618

2 TITLE AND SUBTITLE
PROCEEDINGS OF THE THIRD WORKSHOP ON CONTAINMENT INTEGRITY

3 LEAVE BLANK

4 DATE REPORT COMPLETED
MONTH: May YEAR: 1986

5 AUTHOR(S)
Ruby Cochrell and Toni Molina, Editors

6 DATE REPORT ISSUED
MONTH: July YEAR: 1986

7 PERFORMING ORGANIZATION NAME AND MAILING ADDRESS (Include Zip Code)
Sandia National Laboratories
Albuquerque, NM 87185

8 PROJECT/TASK/WORK UNIT NUMBER

9 FIN OR GRANT NUMBER
A1249

10 SPONSORING ORGANIZATION NAME AND MAILING ADDRESS (Include Zip Code)
Division of Engineering Technology
Office of Nuclear Regulatory Research
U.S. Nuclear Regulatory Commission
Washington, DC 20555

11a TYPE OF REPORT
Proceedings

b PERIOD COVERED (Inclusive dates)

12 SUPPLEMENTARY NOTES

13 ABSTRACT (200 words or less)

The Third Workshop on Containment Integrity was held in Washington, DC, on May 21-23, 1986. The workshop provided a forum for exchanging information on the integrity of containments at nuclear power plants. The behavior of containments during severe accidents was of primary interest to the over 140 participants. Thirty-seven oral presentations were made at the workshop. Written contributions that correspond to each of the presentations make up the body of this report. Sessions were held on (A) Containment Integrity as a Part of Risk Assessment, (B) Operational Experience and Its Relationship to Containment Performance During Accident Conditions, (C) Containment Environment and Loading Conditions During Severe Accidents, (D) Analysis/Testing of Containment Systems, Part I, and (F) Analysis/Testing of Containment Systems, Part II.

The workshop was hosted by Sandia National Laboratories under the sponsorship of the U.S. Nuclear Regulatory Commission. Principal organizers for the workshop were W. A. von Riesemann of Sandia, T. D. Molina of Technadyne, and J. F. Costello of the U.S. Nuclear Regulatory Commission.

14 DOCUMENT ANALYSIS - a KEYWORDS/DESCRIPTORS

b IDENTIFIERS/OPEN ENDED TERMS

15 AVAILABILITY STATEMENT
Unlimited

16 SECURITY CLASSIFICATION
(This page) Unclassified
(This report) Unclassified

17 NUMBER OF PAGES

18 PRICE

☆ U.S. GOVERNMENT PRINTING OFFICE: 1986—676-049/41007

120555078877 1 1AN1R11RD1RM
US NRC
ADM-DIV OF TIDC
POLICY & PUB MGT BR-PDR NUREG
W-501
WASHINGTON DC 20555